DEPARTMENT OF THE INTERIOR
U. S. GEOLOGICAL SURVEY

PROCEEDINGS OF
CONFERENCE XLV

Fault Segmentation and Controls of Rupture Initiation and Termination

Palm Springs, California

Sponsored by

U.S. GEOLOGICAL SURVEY
NATIONAL EARTHQUAKE-HAZARDS REDUCTION PROGRAM

Editors and Convenors

David P. Schwartz
U.S. Geological Survey
Menlo Park, California 94025

Richard H. Sibson
Department of Geological Sciences
University of California
Santa Barbara, California 93106

Organizing Committee

John Boatwright, U.S. Geological Survey, Menlo Park, California
Hiroo Kanamori, California Institute of Technology, Pasadena, California
Chris H. Scholz, Lamont-Doherty Geological Observatory, Palisades, New York

Open-File Report 89-315

1989

TABLE OF CONTENTS

INTRODUCTION TO WORKSHOP ON FAULT SEGMENTATION AND CONTROLS OF RUPTURE INITIATION AND TERMINATION

David P. Schwartz
U.S. Geological Survey
Menlo Park, CA 94025

Richard H. Sibson
Department of Geological Sciences
U.C. Santa Barbara
Santa Barbara, CA 93106

On March 6-9, 1988, a USGS workshop on Fault Segmentation and Controls of Rupture Initiation and Termination was held in Palm Springs, California. The purpose of the workshop was to bring together a diverse group of geologists, seismologists and geophysicists to discuss the status and future direction of fault segmentation, an emerging interdisciplinary field of earthquake research based on the observation that fault zones, particularly long ones, do not rupture along their entire length during a single earthquake. Increasingly, geological and seismological studies are indicating that the location of rupture is not random, that there are recognizable physical properties of fault zones that control the nucleation point and lateral extent of rupture and divide a fault into segments, that ruptures with the same characteristics often repeat in the same location, and that independent rupture segments can persist through several seismic cycles.

The workshop was attended by 51 geologists, seismologists, and geophysicists representing Federal and state agencies, universities, and the private sector. The two days of presentations and panel discussions focused on three major topics: *a)* observations of segmentation including the extent of historical ruptures, geology and seismology of rupture end points, and scale; *b)* mechanical, structural, and rheological controls of segmentation and rupture; and *c)* long-term segmentation and seismic hazards. A one-day field trip to view deformation associated with compressional stepovers in the Ocotillo Badlands and the surface faulting from the November 22-23, 1987 Superstition Hills earthquake sequence was sandwiched between the two days of presentations. The field trip provided an important hands-on focus for many of the discussion topics.

Historically the first fault-specific segmentation model can be traced to Allen (1968). He suggested a division of the San Andreas fault zone into five major segments (Figure *1a*) on the basis of differences in historical seismic behavior and on the distribution of different rock types that could affect fault mechanics. Without the benefit of paleoseismicity data, but with strong geologic intuition, he suggested that the historical behavior remains relatively constant with time. Wallace (1970) defined seven San Andreas segments (Figure *1b*). This segmentation model was also based on differences in the historical behavior of the fault, particularly seismicity and creep. Wallace (1970) suggested that these might be permanent segments. Using the very preliminary

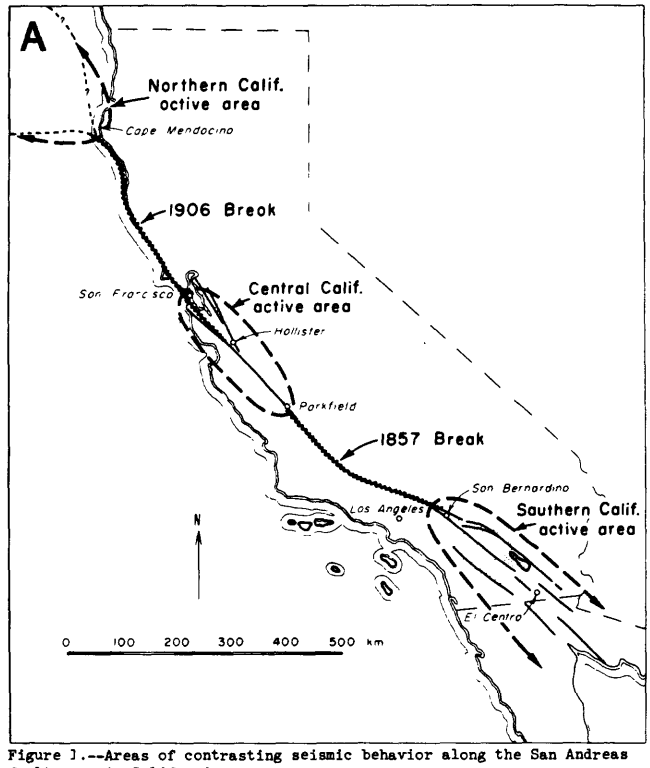

Figure 1.--Areas of contrasting seismic behavior along the San Andreas fault zone in California.

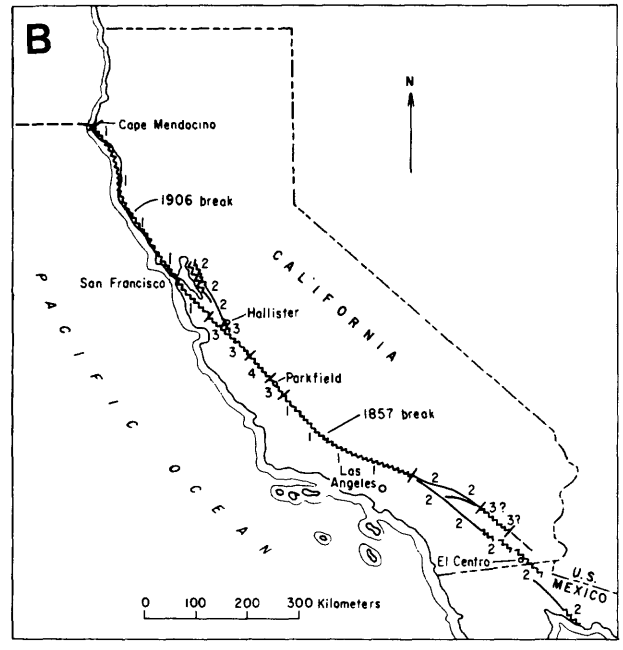

BEHAVIOR CATEGORY	1	2	3	4
MAXIMUM MAGNITUDE	7-8+	6-7	5-6	<5
MAXIMUM STRIKE SLIP (m)	1.2-10	0.3-1.2	0.1-0.3	<0.1
RECURRENCE INTERVAL (yrs)	100-1000	10-100	<10	>10
CREEP RATE, PERCENT OF SECULAR	<10	10-30	30-50	>50
SURFACE BREAK				

Figure 6. Map of California showing behavior of different segments of San Andreas system.

Figure 1. Initial segmentation models of the San Andreas fault. A) Allen (1968). B) Wallace (1970).

data on plate tectonic rates available at that time, he estimated recurrence intervals, slip per event, and maximum earthquakes for each segment. Also, fundamental ideas relating earthquake rupture to the occurrence of persistent structural or geometric features of fault zones, either barriers to rupture propagation (Aki, 1979) or heterogeneities (asperities) that nucleate rupture (Kanamori, 1978), form an important part of the foundation for present research.

Fault segmentation can provide an important framework for increasing our understanding of the mechanics of earthquake generation and for quantifying seismic hazards. During the past decade the growth of paleoseismology, the use of both strong motion seismology and improved geodetic modeling to quantify the amount and distribution of coseismic slip, high precision microearthquake monitoring to image fault planes and define the locations of locked and creeping patches, and an increasing knowledge of physical and chemical conditions and processes at seismogenic depth have all been providing new observations and techniques for better understanding the deep structure of fault zones and how faults work in space and time. Ideally, we would like to look at a fault zone prior to an earthquake and be able to identify the part of the fault that will rupture as an independent segment and, within the segment, identify the nucleation point of the earthquake. This has implications for: *a)* short-term earthquake prediction experiments, particularly in selecting sites of potential rupture nucleation for deployment of instrument arrays; *b)* long-term earthquake forecasting, especially probabilistic hazard assessment, which requires a fault segmentation model as well as information on recurrence interval, elapsed time, slip per event, and slip rate for a specific fault segment; *c)* estimates of ground motion that reflect the relationship between dynamic rupture propagation, including directivity effects, and fault zone structure; and *d)* constraints on parameters such as fault rupture length that are used in estimates of maximum or characteristic earthquakes.

Where do we stand in the quest? Where do we go from here? There was general consensus at the end of the workshop that faults are geometrically and mechanically segmented at a variety of scales. Segments may represent the repeated coseismic rupture during a single event on a long fault and may be tens to hundreds of kilometers in length, they may represent a part of the rupture associated with an individual faulting event and be only a few kilometers long, or they may represent local inhomogeneities along a fault plane and be only a few tens or hundreds of meters in length. From the perspective of hazards the large rupture segments are most important. From the point of view of earthquake mechanics the fundamental contribution from all scales of segmentation requires much further investigation. There was agreement that segmentation modeling for individual faults is extremely desireable. It was acknowledged that this can be difficult and that the methodology for segmentation modeling is in the early stages of development. Uncertainty was also expressed about the longevity or persistence of segments in time and space, the continuity of structures at the surface with structures at seismogenic depth, and the general nature of segmentation for different fault types.

A number of research topics and areas, both general and specific, were considered as being especially important for pursuing our understanding of fault segmentation and controls of rupture initiation and termination. These included: *a)* increasing the level of post-earthquake investigations; *b)* dynamic properties of earthquake rupture; *c)* physical properties of zones of

high moment release at depth; *d)* development of an integrated catalog of surface slip, geodetically determined slip, and slip from strong motion data for individual earthquakes; *e)* rupture mechanics and long-term geologic expression for different fault types; *f)* focused geologic mapping as a framework for a surface data base, especially physical rock properties and the structure at rupture endpoints and epicenters; *g)* depth extent of surface features using seismologic imaging; *h)* long-term space-time recurrence patterns from paleoseismology; *i)* fault zone evolution including the age of fault zones, times of inception, and total displacement; *j)* study of exhumed fault zones; *k)* the fluid pressure regime of active fault zones; *l)* creep studies; *m)* the time dependent behavior of, and the nature of the medium around, fault plane heterogeneities; *n)* bends--observations and theory; *o)* correlation of properties of surface rocks vs depth; *p)* rotation-induced fault patterns; *q)* longevity of fault irregularities, and *r)* loading effects and interaction between adjacent segments.

ACKNOWLEDGMENTS

The success of any meeting depends on the cooperation and effort of many people. The organizing committee of Jack Boatwright (USGS, Menlo Park), Hiroo Kanamori (CalTech) and Chris Scholz (Lamont-Doherty) was vital to planning the workshop program. We thank Wanda Seiders for her efforts in ensuring that all ran smoothly at the meeting site. Norm Brown provided invaluable logistical and technical assistance at the workshop and on the field trip. We also thank the U.S. Nuclear Regulatory Commission for a grant used for travel assistance for many of the workshop participants.

REFERENCES CITED

Aki, K., 1979, Characterization of barriers on an earthquake fault: *Journal of Geophysical Research*, v. 84, p. 6140-6148.

Allen, C. R., 1968, The tectonic environments of seismically active and inactive areas along the San Andreas fault system, in Dickinson, W. R., and Grantz, A., eds., Proceedings of the Conference on Geologic Problems of the San Andreas Fault System, *Stanford University Publications, Geological Sciences*, v. 11, p. 70-82.

Kanamori, H., 1978, Use of seismic radiation to infer source parameters: *U.S. Geological Survey Open-File Report 78-380*, p. 283-318.

Wallace, R. E., 1970, Earthquake recurrence intervals on the San Andreas fault: *Geological Society of America Bulletin*, v. 81, p. 2875-2890.

List of Participants

Clarence R. Allen
Seismological Laboratory
California Institute of Technology
Pasadena, CA 91125

Keiiti Aki
Dept. of Geological Sciences
University of Southern California
Los Angeles, CA 90089

Joe Andrews
U.S. Geological Survey
345 Middlefield Road, MS 977
Menlo Park, CA 94025

Atilla Aydin
Dept. of Applied Earth Sciences
Stanford University
Stanford, CA 94305

William H. Bakun
U.S. Geological Survey
345 Middlefield Road, MS 977
Menlo Park, CA 94025

Aykut Barka
Dept. of Earth, Atmosphere,
and Planetary Sciences
Massachusetts Institute of Technology
Cambridge, MA 02139

Norm Brown
Dept. of Geological Sciences
U.C. Santa Barbara
Santa Barbara, CA 93106

Robert D. Brown, Jr.
U.S. Geological Survey
345 Middlefield Road, MS 977
Menlo Park, CA 94025

Ronald L. Bruhn
Dept. of Geology and Geophysics
University of Utah
Salt Lake City, UT 84112

Lloyd S. Cluff
Pacific Gas and Electric Co.
77 Beale Street
San Francisco, CA 94106

Kevin J. Coppersmith
Geomatrix Consultants
1 Market Plaza, Spear St. Tower
San Francisco, CA 94105

Anthony J. Crone
USGS, MS 966
Box 25046 Federal Center
Denver, CO 80225

James F. Davis
California Dept. of Conservation
Division of Mines and Geology
P.O. Box 2980
Sacramento, CA 95812

Renata Dmowska
Dept. of Earth & Planetary Sciences
Harvard University
Cambridge, MA 02138

William Ellsworth
U.S. Geological Survey
345 Middlefield Road, MS 977
Menlo Park, CA 94025

Diane Doser
Dept. of Geological Sciences
University of Texas at El Paso
El Paso, TX 79968

Thomas C. Hanks
U.S. Geological Survey
345 Middlefield Road, MS 977
Menlo Park, CA 94025

Katherine Kadinsky-Cade
Dept. of Earth, Planetary, & Atmospheric Sciences
Massachusetts Insititute of Technology
Cambridge, MA 02139

Hiroo Kanamori
Seismological Laboratory
California Institute of Technology
Pasadena, CA 91125

John E. Kelleher
Seismology
National Science Foundation
Washington, D.C. 20550

Geoffrey C. P. King
U.S. Geological Survey
MS 966, Box 25046
Denver, Colorado 80225

Ann S. Kiremidjian
Department of Civil Engineering
Stanford University
Stanford, California 94305

Peter Kneupfer
Dept. of Geological Sciences
SUNY at Binghamton
Binghamton, NY 13901

Allan G. Lindh
U.S. Geological Survey
345 Middlefield Road, MS 977
Menlo Park, CA 94025

Michael N. Machette
U.S. Geological Survey, MS 966
Box 25046, Federal Center
Denver, Colorado 80225

Steven Martel
Bureau of Economic Geology
University of Texas at Austin
University Station, Box
Austin, Texas 78713

Richard McMullen
U.S. Nuclear Regulatory Commission
MS 244
7920 Norfolk Ave.
Bethesda, MD 20814

John Nabelek
Dept. of Geology
Oregon State University
Corvallis, Oregon 97331

Craig Nicholson
Dept. of Geological Sciences
U.C. Santa Barbara
Santa Barbara, CA 93106

Paul Okubo
U.S. Geological Survey
345 Middlefield Road, MS 977
Menlo Park, CA 94025

David Oppenheimer
U.S. Geological Survey
345 Middlefield Road, MS 977
Menlo Park, CA 94025

Elaine R. Padovani
U.S Geological Survey
MS 905, National Center
Reston, VA 22092

Leon Reiter
U.S. Nuclear Regulatory Commission
MS 244
7920 Norfolk Ave.
Bethesda, MD 20814

James R. Rice
Dept. of Earth & Planetary Sciences
Harvard University
Cambridge, MA 02138

Thomas K. Rockwell
Dept. of Geology
San Diego State University
San Diego, CA 92182

Gary Rogers
Geological Survey of Canada
Pacific Geoscience Center
P.O. Box 6000
Sidney, B.C.
V8L 4B2 Canada

Chris Sanders
U.S. Geological Survey
345 Middlefield Road, MS 977
Menlo Park, CA 94025

Chris H. Scholz
Lamont-Doherty Geological Observatory
Columbia University
Palisades, NY 10964

Richard Schultz
Dept. of Earth and Atmospheric Science
Purdue University
West Lafayette, IN 47907

David P. Schwartz
U.S. Geological Survey
345 Middlefield Road, MS 977
Menlo Park, CA 94025

Leonardo Seeber
Lamont-Doherty Geological Observatory
Columbia University
Palisades, NY 10964

Paul Segall
U.S. Geological Survey
345 Middlefield Road, MS 977
Menlo Park, CA 94025

Richard H. Sibson
Dept. of Geological Sciences
U.C. Santa Barbara
Santa Barbara, CA 93106

David B. Slemmons
Center For Neotectonics
University of Nevada
Reno, Nevada 89557

Mark T. Swanson
Department of Geology
University of Southern Maine
96 Falmouth Street
Portland, Maine 04103

Wayne Thatcher
U.S. Geological Survey
345 Middlefield Road, MS 977
Menlo Park, CA 94025

Eugenio Turco
University of Calabria
Calabria, ITALY

Robert E. Wallace
U.S. Geological Survey
345 Middlefield Road, MS 977
Menlo Park, CA 94025

Steven Wesnousky
Tennessee Earthquake Information Center
Memphis State University
Memphis, TN 38152

Rob Wesson
U.S. Geological Survey
MS 905, National Center
Reston, VA 22092

Russel Wheeler
U.S. Geological Survey, MS 966
Box 25046, Federal Center
Denver, CO 80225

Geometric Features of a Fault Zone Related to the Nucleation and Termination of an Earthquake Rupture

By

Keiiti Aki

Department of Geological Sciences

University of Southern California

Los Angeles, California 90089-0740

INTRODUCTION

The idea of a characteristic earthquake proposed by Schwartz and Coppersmith (1984) suggests that the rupture on a given segment of a fault may repeat many times with the same slip pattern characteristic to the segment. Aki (1979, 1984) attributed the physical basis for the characteristic earthquake to the presence of asperities and barriers which exist more or less permanently at fixed locations over many repeated earthquakes, and emphasized the importance of identifying asperities and barriers for strong ground motion prediction for future earthquakes.

As a first step toward the identification of asperities and barriers, we made a literature search for which the starting and stopping points of rupture propagation are known from seismological studies and maps of fault traces are available from geological studies. We found 23 such earthquakes as listed in Table 1.

Table 1. List of Earthquakes

Name of Earthquake	Date	Starting point Type	Stopping point Type	Reference
1. Fort Tejon	9 Jan 1857	1.	2.	Sieh (1978a, b)
2. San Francisco	18 Apr 1906	2.	1.	Bolt (1968) Boore (1977)
3. North Anatolia	26 Dec 1939	1.	2.	Dewey (1976)
4. Imperial	18 May 1940	1.	2.	Richter (1958)
5. North Anatolia	26 Nov 1943	1.	2.	Dewey (1976)
6. North Anatolia	1 Feb 1944	1.	2.	Dewey (1976)
7. Alaska	28 Mar 1964	2.	2.	Burk (1965) Kanamori (1970) Kelleher and Savino (1975)
8. Parkfield	28 Jun 1966	1.	2.	Lindh and Boore (1981) Aki (1979)
9. Borrego Mountain	9 Apr 1968	1.	1.	Clark (1972) Allen and Nordquist (1972)
10. Guatemala	4 Feb 1976	1.	2.	Kanamori and Stewart (1978) Plafker et al. (1976)
11. Gazli	8 Apr 1976	1.	2.	Hartzell (1980)
12. Gazli	17 May 1976	2.	1.	Hartzell (1980)
13. Tangshan	27 Jul 1976	1.	2.	Butler et al. (1979)
14. Izu-Oshima	14 Jan 1978	1.	2.	Shimazaki and Somerville (1979)

15.	Coyote Lake	6 Aug 1979	1.	2.	Bouchon (1982) Reasenberg and Ellsworth (1982)
16.	Imperial Valley	15 Oct 1979	1.	2.	Sharp et al. (1982) Archuleta (1984)
17.	Ghaenat	14 Nov 1979	2.	1.	Haghipour and Amidi (1980)
18.	Ghaenat	27 Nov 1979	2.	1.	Haghipour and Amidi (1980)
19.	El Asnam	10 Oct 1980	1.	2.	Deschamps et al. (1982) Yielding et al. (1982)
20.	Southern Italy	23 Nov 1980	2.	1.	Crosson et al. (1986) Deschamps and King (1983) Del Pezzo et al. (1983)
21.	Borah Peak	28 Oct 1983	2.	2.	Bruhn et al. (1988)
22.	Morgan Hill	24 Apr 1984	2.	?	Hartzell and Heaton (1986)
23.	Superstition Hills	25 Nov 1987	2.	1.	Nicholson (1988)

THE PARKFIELD CHARACTERISTIC EARTHQUAKE AS A PROTOTYPE

There is one segment of the San Andreas fault for which the idea of characteristic earthquake may be supported from the evidence available from historic data (Bakun and McEvilly, 1984). That is the segment where the Parkfield earthquake of 1966 originated. It is widely accepted that the rupture for this characteristic earthquake nucleated near the Middle Mountain where the fault trace shows a slight bend of 3° to 5°. The bend is very subtle, and there is no step or branching associated with it.

The stopping point of the Parkfield earthquake of 1966 is believed by some (e.g. Lindh and Boore, 1981) to be the right step in the Cholame Valley. We believe, however, that the rupture skipped the step in the manner similar to that found in the numerical simulation of Das and Aki (1977) because there were aftershocks along the segment south of the step (Eaton et al., 1970) and the displacement recorded at Station 2 of the Cholame strong motion seismograph array near the segment indicated strong evidence for the passage of a rupture front near the station (Aki, 1968, 1979; Bouchon, 1979). We believe that the Cholame Valley step decelerated the rupture, but the final stopping of the rupture occurred at the branching point at which the San Juan fault (a Quarternary fault according to Jennings, 1975) meets the San Andreas fault.

In either case, we identify the stopping point with a step or a branch point.

CLASSIFICATION OF FAULT GEOMETRY INTO TWO TYPES

In order to make a systematic survey of geometric features of faults associated with the starting and stopping of rupture, we shall classify the geometry of a fault zone into the following two types guided by the prototype example of the Parkfield earthquake.

Type 1 : The fault trace is straight with or without a slight bend.

Type 2 : The fault is significantly bent (10° or more), stepped, or branched.

Obviously, the starting point of the Parkfield earthquake belongs to Type 1, and the stopping point to Type 2.

For the other 22 earthquakes, we are able to classify the starting and stopping points into the above two types from the information available in the references listed in Table 1, except for the stopping point of the Morgan Hill earthquake.

The resultant statistics is as follows: a) in 14 out of 23 cases the starting point is associated with the type 1 feature; and b) in 15 out of 22 cases the stopping point is associated with the type 2 feature. In other words, we find a straight fault trace with or without a slight bend at about 60% of the starting points, and a significantly bent, stepped or branched fault trace at about 70% of the stopping points.

As mentioned earlier, the Parkfield earthquake is the prototype case in which the starting point is of type 1 and the stopping point is of type 2.

We found that 3 North Anatolian earthquakes, 2 Imperial Valley earthquakes, Fort Tejon, Guatemala, the first shock of Gazli, Tangshan, Izu-Oshima, Coyote Lake and El Asnam are of the same type. Including the Parkfield earthquake, this type occurs in 13 out of 23 cases.

The majority case noted above can be explained in terms of fracture mechanics. The fault trace of type 1 is simpler than that of type 2. The fracture energy required per unit area of the fault plane is expected to be less for the former than the latter. When a fault is under stress, the failure would initiate at the weakest part of the fault, namely, at a point of type 1. When the rupture encounters a point of type 2, which acts as a strong barrier, it will be stopped.

On the other hand, a significant bend, step or branch classified as type 2 can act as a stress concentrator. In this case, the rupture may nucleate at a point of type 2. The nucleation of rupture seems to have occurred in this manner for the 1906 San Francisco earthquake (near the branch point of the Palo Colorado San Gregorio fault), the 1974 Alaska earthquake (a corner of a plate boundary), Morgan Hill, Borah Peak, the second shock of Gazli, two Ghaenat earthquakes, Southern Italy, and Superstition Hills. The latter five earthquakes are quite similar to each other in that the rupture nucleated near the crossing point of a conjugate fault.

The termination of rupture occurs at a point of type 1 for the 1906 San Francisco earthquake, Borrego Mountain, the second shock of Gazli, two Ghaenat earthquakes, Southern Italy, and Superstition Hills earthquakes. In these cases, the rupture seems to stop because of running out of gas (driving stress).

CONCLUSION

Motivated by the geometric features of fault zones at the nucleation and termination points of the Parkfield earthquake of 1966, we classified the geometry of a fault into two types: a

simple trace with or without a slight bend (type 1) and a complex trace with a significant bend (10° or more), step or branch (type 2).

We found that the nucleation point is associated with the feature of type 1 in 14 out of 23 earthquakes, and the termination is associated with the feature of type 2 in 15 out of 22 earthquakes. The majority of earthquakes are similar to the Parkfield earthquake, namely, the starting point is of type 1 and the stopping point is of type 2. This case may be explained in terms of the fracture energy barrier. The failure would initiate at the weakest part of the fault, and be stopped at the strongest part.

The starting at a point of type 2, on the other hand, may be explained by a stress concentration near a bend, step or junction of branch. The stopping at a point of type 1 may be explained by the disappearance of driving stress.

ACKNOWLEDGMENT

This work was partially supported by the National Science Foundation under grant ECE-8616457. A part of this work was done at the National Research Center for Disaster Prevention, Tsukuba, Japan under the support of the project of the Science and Technology Agency of Japan entitled "Study of earthquake rupture and seismic wave propagation in inhomogeneous structure of the earth".

REFERENCES

Aki, K., Seismic displacements near a fault, J. Geophys. Res., 73, 5359-5376, 1968.

Aki, K., Characterization of barriers on an earthquake fault, J. Geophys. Res., 84, 6140-6148, 1979.

Aki, K., Asperities, barriers, characteristic earthquakes and strong motion prediction, J. Geophys. Res., 89, 5867-5872, 1984.

Allen, C. R. and J. M. Nordquist, Foreshocks, mainshock and larger aftershocks of the Borrego Mountain earthquake, U. S. Geol. Surv. Prof. Paper, 787, 16-23, 1972.

Archuleta, R. J., A faulting model for the 1979 Imperial Valley earthquake, J. Geophys. Res., 89, 4559-4585, 1984.

Bakun, W. H. and T. V. McEvilly, Recurrence models and the Parkfield, California, earthquakes, J. Geophys. Res., 89, 3051-3058, 1984.

Boore, D. M., Strong-motion recordings of the California earthquake of April 18, 1906, Bull. Seis. Soc. Am., 67, 561-577, 1977.

Bolt, B. A., The focus of the 1906 California earthquake, Bull. Seis. Soc. Am., 58, 457-471, 1968.

Bouchon, M., Predictability of ground displacement and velocity near an earthquake fault: An example: The Parkfield earthquake of 1966, J. Geophys. Res., 84, 6149-6156, 1979.

Bouchon, M., The rupture mechanism of the Coyote Lake earthquake of 6 August 1979 inferred from near-field data, Bull. Seis. Soc. Am., 72, 745-757, 1982.

Bruhn, R. L., W. A. Yonkee, and W. T. Parry, Rupture properites of geometrical boundaries in extensional faults systems, this volume, 1988.

Burk, C. A., Geology of the Alaska Peninsula: Island arc and continental margin, Geol. Soc. Am. Mem., 99, 147, 1965.

Butler, R., G. S. Stewart and H. Kanamori, The July 27, 1976 Tangshan, China earthquake: A complex sequence of interplate events, Bull. Seis. Soc. Am., 69, 207-220, 1979.

Clark, M. M., Surface rupture along the Coyote Creek fault, U. S. Geol. Surv. Prof. Paper 787, 55-86, 1972.

Crosson, R. S., M. Martini, R. Scarpa and S. C. Key, The southern Italy earthquake of 23 November 1980: An unusual pattern of faulting, Bull. Seis. Soc. Am., 76, 381-394, 1986.

Das, S. and K. Aki, Fault planes with barriers: a versitile earthquake model, J. Geophys. Res., 82, 5648-5670, 1977.

Del Pezzo, E., G. Iannaccone, M. Martini, and R. Scarpa, The 23 November 1980 Southern Italy earthquake, Bull. Seis. Soc. Am., 73, 187-200, 1983.

Deschamps, A., Y. Gaudemer and A. Cisternas, The El Asnam, Algeria, earthquake of 10 October 1980: multiple-source mechanism determined from long-period records, Bull. Seis. Soc. Am., 72, 1111-1128, 1982.

Deschamps, A. and G. C. P. King, The Campania-Lucanic (Southern Italy) earthquake of 23 November 1980, Earth Planet. Sci. Letters, 62, 296-304, 1983.

Dewey, J. W., Seismicity of Northern Anatolia, Bull. Seis. Soc. Am., 66, 843-868, 1976.

Eaton, J. P., M. E. O'Neill, and J. N. Murdock, Aftershocks of the 1966 Parkfield-Cholame, California earthquake: A detailed study, Bull. Seis. Soc. Am., 60, 1151-1197, 1970.

Haghipour, A. and M. Amidi, The November 14 to December 25, 1979 Ghaenat earthquakes of Northeast Iran and their tectonic implications, Bull. Seis. Soc. Am., 70, 1751-1757, 1980.

Hartzell, S. H. and T. H. Heaton, Rupture history of the 1984 Morgan Hill, California, earthquake from the inversion of strong motion records, Bull. Seis. Soc. Am., 76, 649-674, 1986.

Jennings, C. W., Fault map of California, Williams and Heintz Map Corp., Capitol Heights, MD, 1975.

Kanamori, H., The Alaska earthquake of 1964: Radiation of long period waves and source mechanism, J. Geophys. Res., 75, 5029-5040, 1970.

Kanamori, H. and G. S. Stewart, Seismological aspects of the Guatemala earthquake of 4 February 1976, J. Geophys. Res., 83, 3427-3434, 1978

Kelleher, J. and J. Savino, Distribution of seismicity before large strike-slip and thrust-type earthquakes, J. Geophys. Res., 80, 260-271, 1975.

Lindh, A. G. and D. M. Boore, Control of rupture by fault geometry during the 1966 Parkfield earthquake, Bull. Seis. Soc. Am., 71, 95-116, 1981.

Nicholson, C., Fault interaction and segmentatuion along the San Andreas fault system, Southern California, Proc. of the present conference, 1988.

Plafker, G., M. G. Bonilla and S. B. Bonis, Geologic effects, The Guatemala earthquake of 4 February 1976, U. S. Geol. Surv. Prof. Paper, 1002, 38-51, 1976.

Reasenberg, P. and W. L. Ellsworth, Aftershocks of the Coyote Lake, California, earthquake of 6 August 1979: A detailed study, J. Geophys. Res., 87, 10637-10655, 1982.

Richter, C. F., Elementary Seismology, 487-495, W. J. Freeman and Co., San Francisco, 1959.

Schwartz, D. P. and K. J. Coppersmith, Fault behavior and characteristic earthquakes: examples from the Wasatch and San Andreas Fault zones, J. Geophys. Res., 89, 5681-5698, 1984.

Sharp, R. V., J. J. Lienkaemper, M. G. Bonilla, D. B. Burke, B. F. Fox, D. G. Herd, D. M. Miller, D. M. Morton, D. J. Ponti,

M. J. Rymer, J. C. Tinley, J. C. Yount, J. E. Kahle, E. W. Hart, and K. E. Sieh, Surface faulting in the central Imperial Valley, The Imperial Valley, California, earthquake of 15 October 1979, U. S. Geol. Surv. Prof. Paper 1254, 119-144, 1982.

Shimazaki, K. and P. Somerville, Static and dynamic parameters of the Izu-Oshima, Japan earthquake of 14 January 1978, Bull. Seis. Soc. Am., 69, 1343-1378, 1979.

Sieh, K. E., Central California foreshocks of the great 1857 earthquake, Bull. Seis. Soc. Am., 68, 1731-1749, 1978a.

Sieh, K. E., Slip along the San Andreas fault associated with the great 1857 earthquake, Bull. Seis. Soc. Am., 68, 1421-1448, 1978b.

Yielding, G., J. A. Jackson, G. C. P. King, H. Sivhal, C. Bita-Ginzi and R. M. Wood, Relations between surface deformation, fault geometry, seismicity and rupture characteristics during the El Asnam earthquake of 10 October 1980, Earth Planet, Sci. Letters, 56, 287-304, 1982.

SEGMENTATION AND RECENT RUPTURE HISTORY OF THE XIANSHUIHE FAULT, SOUTHWESTERN CHINA

Clarence R. Allen[1], Luo Zhuoli[2], Qian Hong[2], Wen Xueze[2], Zhou Huawei[1], and Huang Weishi[3]

[1]Seismological Laboratory, California Institute of Technology, Pasadena, California 91125, USA
[2]Seismological Bureau of Sichuan Province, Chengdu, China
[3]State Seismological Bureau, Beijing, China

ABSTRACT

The left-lateral Xianshuihe fault, which traverses the eastern margin of the Tibetan Plateau in western Sichuan Province, China, is one of the world's most active faults, having produced at least 8 earthquakes of $M \geq 7$ since 1725 on a 350-km-long segment of the fault. In the more limited 150-km-long northern segment including Luhuo and Daofu, 5 earthquakes of $M \geq 6.9$ have occurred during the past 100 years alone, with well documented overlapping surface ruptures. Some of these events were remarkably similar in magnitude and location to earlier historic events, suggesting that the characteristic earthquake model may apply here. No obvious geometric segmentation characterizes the smoothly curving Luhuo-Daofu sector, although its ends are marked by major left-stepping en echelon offsets that have also been the terminating points of individual earthquake ruptures. Minor en echelon offsets and bends within this segment are associated with local vertical relief, and one 9° bend is located close to the epicenter of the 1973 Luhuo earthquake ($M = 7.6$).

In the southern sector of the Xianshuihe fault, south of Qianning, the faults splits into several branches, one of which broke over its entire 27-km length during the 1955 Kangding earthquake ($M = 7.5$). The main fault near Kangding is characterized by a series of restraining and releasing bends, associated with corresponding topography, and these bends may be related to the fact that this southern segment of the fault seems to be characterized by infrequent great earthquakes (e.g., $M = 7\text{-}3/4$ in 1786) rather than by more frequent moderate earthquakes ($M = \pm 7$) such as those that characterize the straighter and more continuous Luhuo-Daofu sector to the north.

Continuing creep has been documented along some segments of the fault, and this, together with its high degree of activity, superb high-altitude exposures, and other unique attributes, make the Xianshuihe fault one of the most promising sites in the world for earthquake-prediction, hazard-evaluation, and segmentation studies.

INTRODUCTION

The Xianshuihe fault of southwestern China (Fig. 1) is one of the world's most active faults, and it is particularly suitable for studies of segmentation because of (1) the superb high-altitude exposures along the eastern margin of the Tibetan Plateau, and (2) the occurrence of numerous historic large earthquakes, many associated with well-documented overlapping

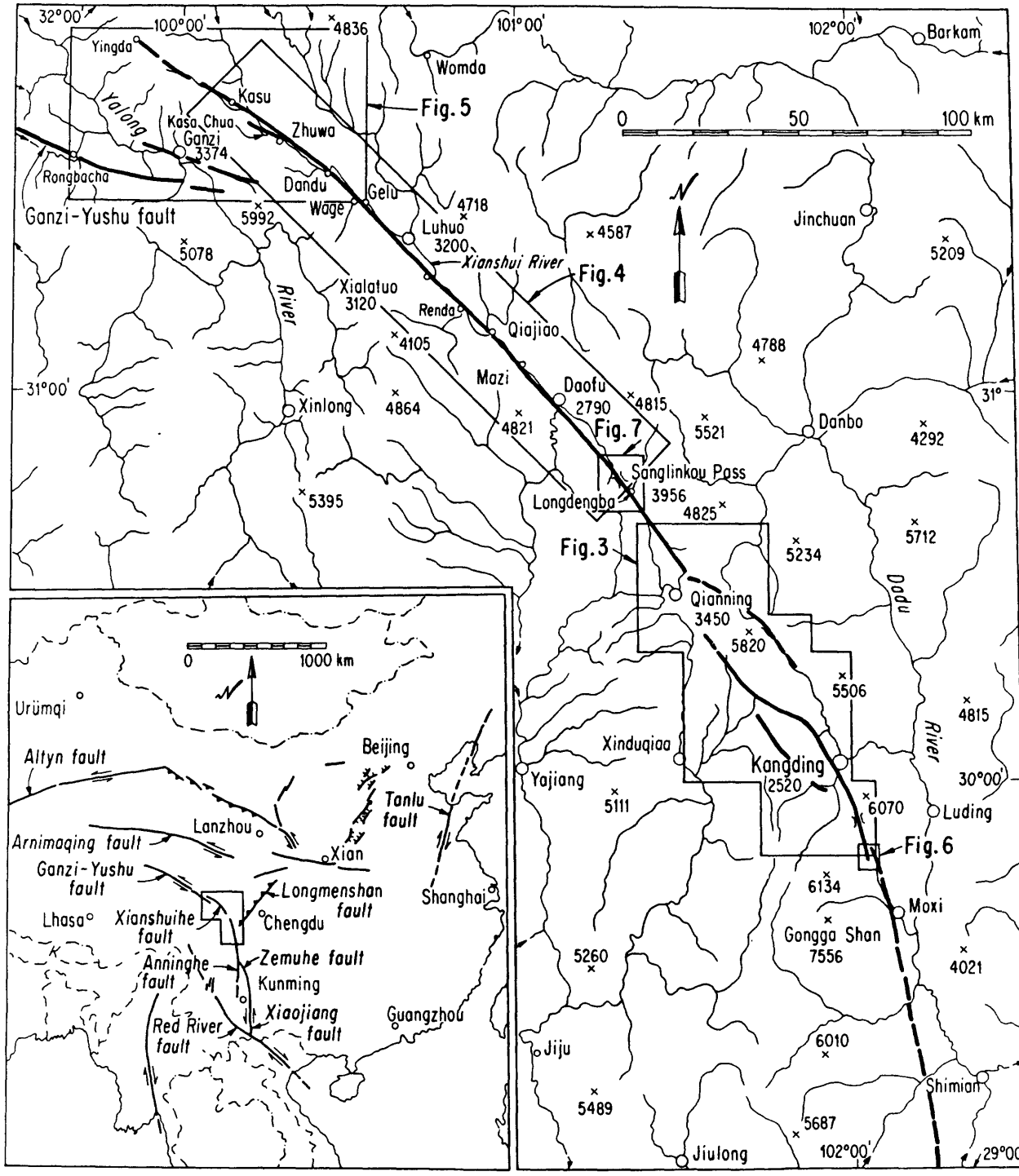

Fig. 1.--Map of Xianshuihe fault in area of this study. Boxes within map indicate areas of more detailed sketch maps herein. Inset at lower left shows location of study area and regional relationship between Xianshuihe fault and some other major active faults of China and adjacent areas. All elevations are in meters.

surface ruptures. During the present century, four earthquakes of magnitude 7 or greater have occurred along a 350-km segment of the fault, and at least eight such events have occurred here since 1725 (Fig. 2; Table 1). Five events exceeding magnitude 6.8 have occurred during the past 100 years along a single 150-km-long segment of the fault. Field study of this fault by the authors in 1986 were directed primarily toward slip-rate and seismic-hazard determinations, but segmentation was also a subject of interest. These wider studies have been reported in Wen et al. (in press) and Allen et al. (1988; in press); this paper summarizes some of the conclusions given therein.

The Xianshuihe fault zone is part of a much more extensive left-lateral fault system of at least 1,400-km length, extending from southern Yunnan Province northwest through Sichuan into Qinghai Province (Fig. 1, insert)(Ding, 1984). Almost all segments of the system have been the loci of major earthquakes within the historic record (Fig.2), and it currently constitutes probably the most active fault system within China. It clearly deserves comparison with other highly active strike-slip fault systems worldwide, such as the San Andreas fault of California, the North Anatolian fault of Turkey, and the Alpine fault of New Zealand.

Following recent Chinese practice, we differentiate herein between the Xianshuihe fault zone, extending some 350 km northwest from near Shimian to Kasu (Fig. 1), and the more restricted Xianshuihe fault itself, which is only one of five individual segments within the overall zone. These five segments (Fig. 3) are the Moxi fault, Selaha (Kangding) fault, Zheduotang fault, Yalahe fault, and the restricted Xianshuihe fault, extending northwest from Laoqiann-ing. The type area of the restricted Xianshuihe fault is the 150-km-long segment between Songlinkou Pass and Kasu (Fig. 1), where its trace is rela-tively simple and continuous, and where it controls the course of the Xianshui River and its tributaries.

At its northwestern end, the Xianshuihe fault overlaps the south-eastern end of the Ganzi-Yushu fault, with a left en echelon stepover of about 40 km. At its southeastern extremity, the Xianshuihe fault zone connects with the Anninghe fault in a complex and little-studied area near Shimian. Still farther southeast, a significant en echelon offset occurs between the Anninghe and Xiaojiang fault (Fig. 2), with the very active Zemuhe fault in the transition area. All of these individual fault zones, on the other hand, must be considered parts of the same overall left-lateral fault system. The entire system lies along the northeast boundary of a large rhomb-shaped block, or miniplate, that is bounded on the opposite southwest side by the right-lateral Red River fault system (Allen et al., 1984), and the apparent southeastward movement of this relatively stable block relative to its neighbors has been the subject of much tectonic discussion (e.g., Li and Wang, 1975; Kan et al., 1977). It is admittedly somewhat surprising that two major fault systems that are almost parallel and only 200 km apart should have opposing current senses of lateral slip, although this has been explained, at least in principle, by the mechanics of the impingement of India into Eurasia and the consequent block rotations (Molnar and Tapponnier, 1975; Tapponnier and Molnar, 1976, 1977; Tapponnier et al., 1986).

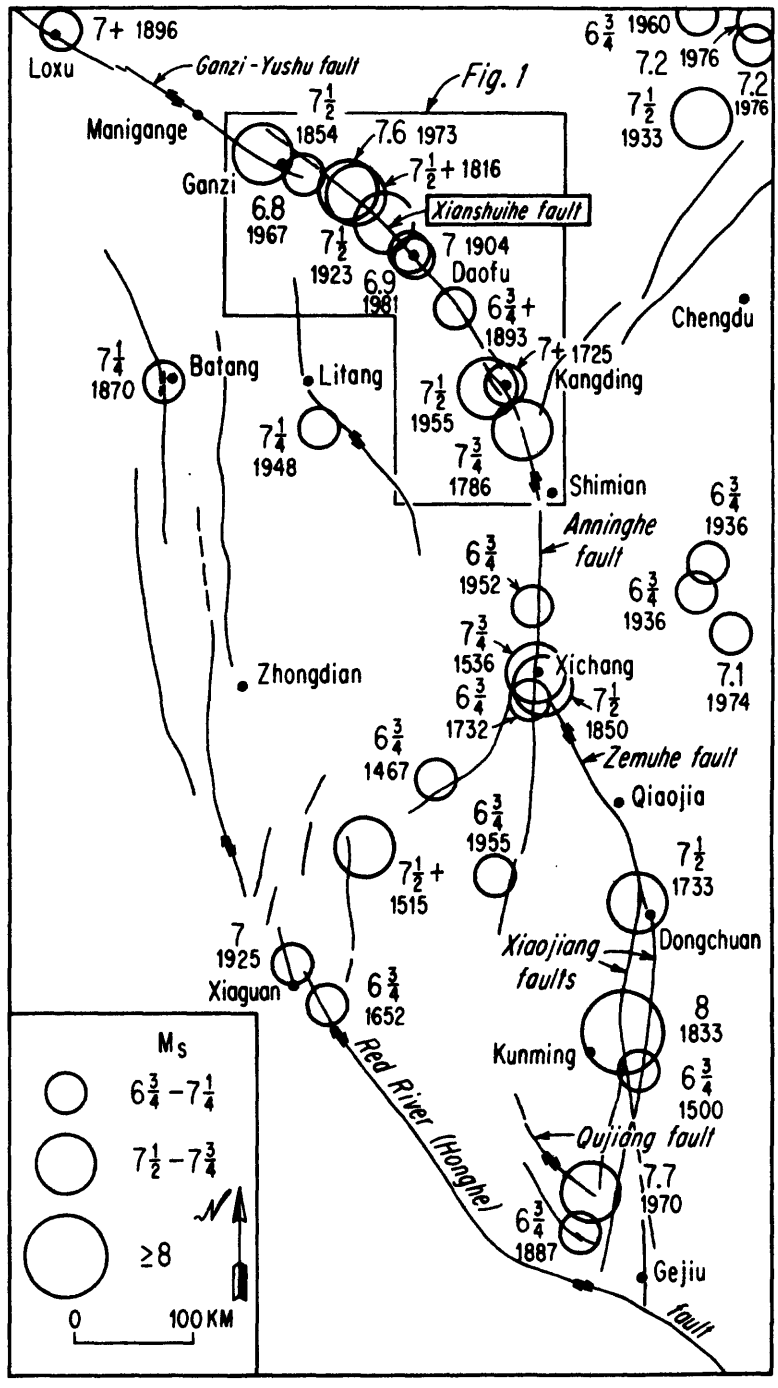

Fig. 2.--Map showing epicenters of earthquakes of magnitude (M_S) 6-3/4 and greater in the Chinese catalog (Luo, 1980), with relation to major faults in the Sichuan-Yunnan region. Box shows location of Fig. 1, the area of this study.

HISTORIC EARTHQUAKES AND SEISMICITY

Regional activity and historic events

Figure 2 shows historic large earthquakes on the Xianshuihe and associated faults of southwestern China. It should be noted that the historic record in this part of China, which is very sparsely populated (mainly by Tibetan people), is short as compared to those of the more heavily populated areas to the north, east, and south. The earliest large earthquake of record on the Xianshuihe fault itself is that of 1725. The overall pattern of epicenters clearly indicates that major earthquakes have tended to occur on major faults of the region, and the Xianshuihe fault is currently the most active of these.

Table 1

Historic earthquakes of M ≥ 6.9 on the Xianshuihe fault zone

Date	Location	Mag	Fault	Rupture Length (km)	Max Displacement (m)
1725	N. Kangding	≥7	Selaha?	?	?
1786	S. Kangding	7-3/4	Moxi-Selaha	≥70	?
1816	Luhuo	≥7-1/2	Xianshuihe	?	?
1893	Laoqianning	≥7	Xianshuihe	≥40	?
1904	Daofu	7	Xianshuihe	?	?
1923	Renda	7-1/2	Xianshuihe	>60	3+
1955	Kangding	7-1/2	Zheduotang	27	1+
1973	Luhuo	7.6	Xianshuihe	90	3.6
1981	Daofu	6.9	Xianshuihe	44	1-

1725 M ≥7 earthquake north of Kangding.--Sparse historic records of the 1725 event indicate that it was centered somewhere between Kangding and Qianning (Figs. 1, 3). No specific fault or rupture zone has been unequivocally identified in the field.

1786 M = 7-3/4 earthquake south of Kangding.--The 1786 earthquake was clearly a very large event, causing minor damage even as far away as Chengdu, more than 200 km from Kangding. Wang Xinmin (personal communication) has recently identified detailed features of very recent displacement which indicate that the surficial fault rupture extended for at least 70 km from south of Moxi nearly to Mugochuo Lake, north of Kangding (Fig. 3). Indeed, the dilatational double bend between Mugochuo and Selaha Pass (el. 4245 m, Fig. 3) may have served to terminate the rupture in this direction.

1816 M ≥ 7-1/2 earthquake near Luhuo.--The 1816 event was most damaging in the Xialatuo-Luhuo area (Fig. 1) and appears to have been remarkably similar in both location and magnitude to the subsequent 1973 event. Features related to this event have been found in trenches excavated across the Xianshuihe fault at Xialatuo (Huang et al., 1982). The edge of a cultivated field at Dandu (Figs. 1, 4), which was offset 3.6 m in 1973 (Tang et al.,

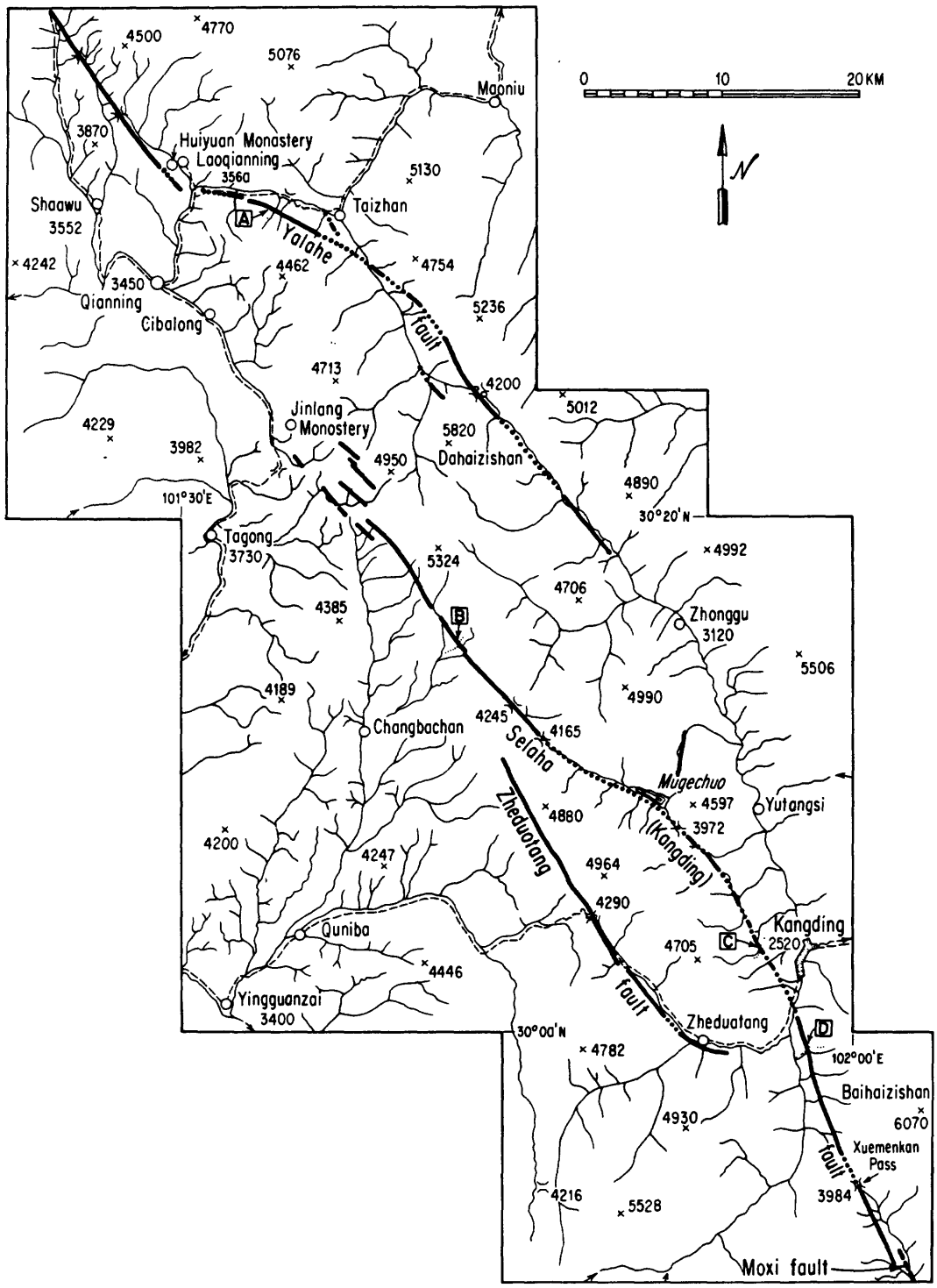

Fig. 3.--Sketch map of Xianshuihe fault zone in Laoqianning-Kangding area. Heavy solid line indicates fault where clearly represented by Holocene scarps. Heavy dotted line indicates segment where Holocene displacements are probably continuous but are not obvious on aerial photographs due to active river erosion or other causes. Dashed lines are major roads. Localities A-D are places where fault offsets of latest Pleistocene glacial moraines have been measured.

1976), has a total offset of 7.2 m, suggesting similar displacements during the two events.

1893 M ≥ 7 earthquake near Qianning.--Heavy damage in the Qianning area (Fig. 1) suggests that this event was centered along the segment of the Xianshuihe fault extending from Laoqianning northwest to Daofu. Indistinct right-stepping en echelon fissures could still be identified in 1986 along the fault 10 km northwest of Laoqianning, probably resulting from the 1893 rupture (Allen et al., in press). A trench excavated across the fault at Songlinkou Pass likewise revealed offset features probably of 1893 origin. It is noteworthy that this segment of the Qianning-Kasu sector of the Xianshuihe fault is currently the longest-lasting one without a major earthquake, and it has been identified as a temporal seismic gap (Han and Huang, 1983).

1904 M = 7 earthquake near Daofu.--This earthquake, previously thought to be of magnitude 6, has recently been reinvestigated and assigned a higher magnitude of 7 (Huang, 1985), partly on the basis of Gutenberg's unpublished notes filed in Pasadena. And recently Abe (1988) suggested a magnitude of 6.9 based on Milne seismograph records. The intensity and felt area of the 1904 event seem to have been very similar to those of the 1981 Daofu earthquake, and a very old resident of a village near Daofu reported to us in 1986 that the Xianshuihe fault ruptured along exactly the same line in both 1904 and 1981.

1923 M = 7-1/2 earthquake near Renda.--The faulting associated with the 1923 earthquake was documented by Heim (1934), although he surprisingly failed to recognize its strike-slip nature. The fissures photographed by Heim at Changcu Pass (Fig. 4) are still clearly recognizable today (Allen et al., in press). A few hundred meters southeast of the photo locality, a cultural berm or retaining wall crossing the fault at right angles is clearly offset 3 m, although it is not known whether this offset results solely from the 1923 event. Two old people living near Renda reported that their mothers had spoken of an earlier earthquake similar in destruction to that of 1923, possible referring to the 1816 event.

Heim's map shows the rupture extending as far northwest as Xialatuo, but the fault leaves the valley floor (and main trail) at this point and may not have been searched for by Heim and his local informants. Strangely, Heim concentrated his attention not on the principal fault within the valley, but instead on the many linear ravines on the adjacent mountain sides, which he thought were eroded "earthquake cracks." We doubt his interpretation. Southeast of Changcu Pass, Heim's map is not clear with regard to possible 1923 fault rupture, and his traverse was along the main trail on the opposite (north) side of the river from that of the fault trace in this area. We identified en echelon cracks similar to those at the Changcu Pass 20 km farther southeast near Mazi (Fig. 4). And at the same place, the edge of a cultivated field is left laterally offset about 2 m along the line of the cracks, presumably resulting from the 1923 event. We conclude that the 1923 earthquake was associated with a maximum left slip of about 3 m, which is consistent with strike-slip earthquakes of this magnitude (Bonilla et al., 1984), and that the rupture extended at least 36 km from Xialatuo to Mazi. But because the displacement was 2 m at Mazi, the rupture must have extended a considerable distance still farther southeast, and it is not clear that anyone at that time looked for the fault trace either here or northwest of Xialatuo.

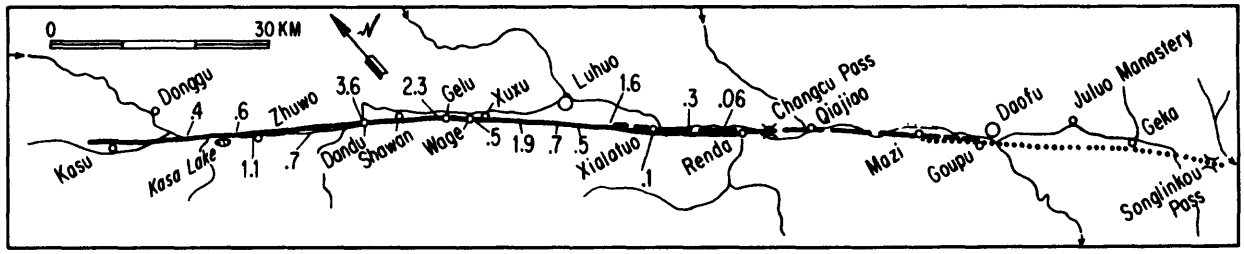

Fig. 4.--Map of ground ruptures associated with the M = 7.6 Luhuo earthquake of 1973 (heavy solid line), the M = 7½ "Sharato" earthquake of 1923 (dashed line), and the M = 6.9 Daofu earthquake of 1981 (dotted line). Note overlapping ruptures. See Fig. 1 for location. Numbers show left slip (in meters) in 1973, from Tang et al. (1976). 1923 data are partly from Heim (1934), and 1981 data are from Tang et al. (1984).

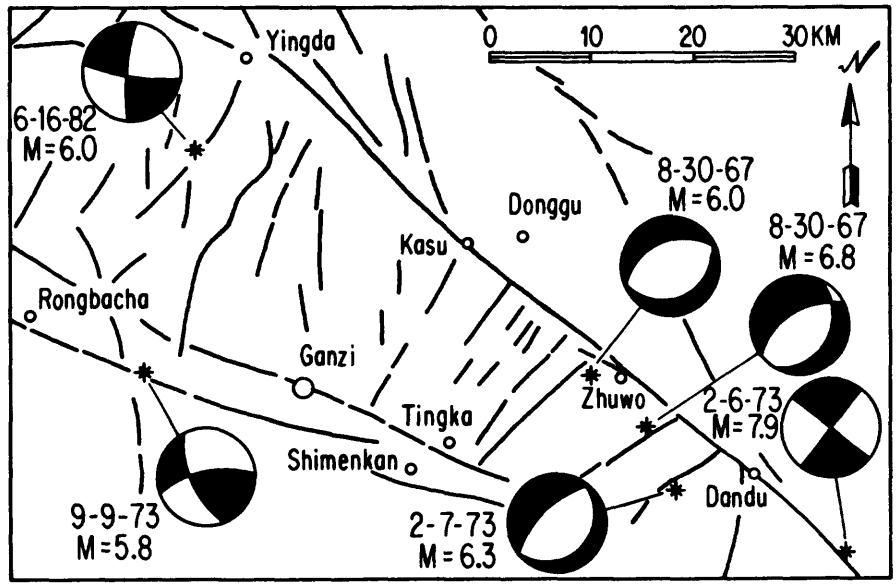

Fig. 5.--Map showing fault pattern in area of en echelon overlap between Xianshuihe fault and Ganzi-Yushu fault. See Fig. 1 for location. Most northwest-trending faults are left slip, whereas most northeast-trending faults are normal. Focal mechanisms are shown for six of the larger earthquakes in this area since 1967. Modified from Wen and Bai (1985).

Therefore, we estimate that the rupture was at least 60 km in total length, which is again consistent with faulting associated with other earthquakes of this magnitude (Bonilla et al., 1984). There can be no question, on the other hand, but that the rupture of the 1923 event overlapped on the northwest with that of the subsequent 1973 event by at least 10 km (Fig. 4), as well as with that of the 1981 event to the southeast.

1955 M = 7-1/2 Kangding earthquake.--The 1955 earthquake was associated with rupture along the entire 27-km length of the Zheduotang fault (Fig. 3). Although not documented at the time, fissures still easily visible in 1986 suggest at least 1 m of left-lateral offset. The rupture length is remarkably small for an earthquake of this magnitude (Bonilla et al., 1984).

1973 M = 7.6 Luhuo earthquake.--Faulting associated with the 1973 earthquake was unusually well described by Tang et al. (1976), with the rupture extending from near Renda to Kasu (Figs. 1, 4), a distance of about 90 km. Damage was extensive throughout this interval. Faulting clearly overlapped the rupture of 1923 by at least 10 km at the southeast end. Although listed in the Chinese earthquakes catalogs (e.g., Luo, 1980) as being of magnitude 7.9, recent re-evaluation by Chinese seismologists has placed the magnitude at 7.6. Many of the surface features of faulting associated with the Luhuo earthquake are almost as fresh today as they were in 1973 (Allen et al., in press).

Seismological studies of the Luhuo earthquake are remarkably consistent with the geological observations (Zhou et al., 1983a; Zhou et al., 1983b). The source mechanism indicates almost pure left slip on a vertical fault striking N 55° W, and the source-time function suggests greater slip northwest of the epicenter than to the southeast. The slip at depth extended some 15 km farther northwest than did the surface rupture, and this is consistent with the aftershock distribution.

Because 1/30,000 aerial photographs of the fault were taken only two weeks following the 1973 earthquake, some of the details of the fault rupture are easily discernible. For example, the fault generally broke in distinct en echelon segments that averaged a few hundred meters in length, and in some places the stepover between segments was as much as 1/2 km. But at any given point along the fault, there was typically only one fracture zone; an exception was southeast of Dandu, where three parallel traces can be seen over a width of about 200 m. Individual fracture zones themselves almost invariably consisted of smaller en echelon fractures averaging a few meters in length, separated by distinct pressure ridges at right angles, in the classic manner described by Richter (1958) and elucidated by Deng and Zhang (1984), Qian (1983), and others. In China, such features have been termed "anti-xi" type fractures, and many of these diagrammatic features near Luhuo are exceptionally well illustrated in Institute of Geology, State Seismological Bureau (1983). In only a few places was the displacement concentrated along a simple single shear surface such as has been observed more often in other strike-slip earthquakes such as that of 1906 in California (Lawson, 1908). Probably a significant contributing cause to this difference was the fact that the 1973 earthquake occurred in midwinter, and the ground was frozen to a depth of several tens of centimeters. Consequently, the soil behaved in brittle fashion and in some areas tended to break into massive tilted blocks. Indeed, some of the resulting local micro-physiography along the fault trace is truly

spectacular and is quite unlike that seen along most other major strike-slip faults. It is interesting to note that not only did the 1973 earthquake occur in midwinter, but also the last similar event here in 1816, thus serving to amplify the local topography.

1981 M = 6.9 Daofu earthquake.--The most recent significant earthquake on the Xianshuihe fault was that of 1981, centered near Daofu, which suffered considerable damage. M_S (China) was 6.9, and M_S (USGS) was 6.8. Zhou et al. (1983b) determined from surface-wave inversion that the earthquake was caused by pure left-lateral displacement on a vertical fault striking N 41° W, which agrees well with the local trend of the fault as observed in the field. Surface ruptures were much less obvious for this earthquake than for the 1923 and 1973 events, which is consistent with its lower magnitude. Scattered fissures occurred in many places in the alluviated valley floor near Daofu, but the most consistent en echelon cracks occurred squarely along the trace of the Xianshuihe fault near Goupu (Fig. 4) and clearly indicated left-lateral displacement (Deng and Zhang, 1984). En echelon cracks were observed intermittently along the fault from Songlinkou Pass northwest to Mazi, a distance of some 44 km (Tang et al., 1984). Worldwide fault rupture lengths for strike-slip earthquakes of M_S = 6.9 average about 27 km, with associated displacements of about 1 m (Bonilla et al., 1984).

CHARACTERISTIC EARTHQUAKES?

The fact that a number of large earthquakes along the Xianshuihe fault appear to have been remarkably similar to earlier events lends support to the concept of the "characteristic earthquake" (Aki, 1984; Schwartz and Coppersmith, 1984). This hypothesis holds that a given segment of a fault may break repeatedly with earthquakes of essentially the same size and fault parameters, perhaps controlled by permanent asperities on the fault plane. Thus the 1816 and 1973 events along the Xianshuihe fault are perhaps characteristic earthquakes, as well as the 1904 and 1981 events. And the projected earthquake within the Daofu-Qianning seismic gap would presumable be similar to the one which ruptured much of this same segment in 1893.

SLIP-RATE DETERMINATIONS

Slip-rate determinations represented a primary objective of our field effort and are discussed at length in Allen et al. (in press); they are only summarized herein. Along the restricted Xianshuihe fault, from Songlinkou Pass to Kasu, several lines of evidence suggest that the long-term slip rate is 15 ± 5 mm/yr. This figure is based on offset terrace risers, stream channels, and valley walls, for some of which Carbon 14 dates were obtained. For the southern sector of the fault zone, south of Qianning, four offset glacial moraines of latest Pleistocene age (Fig. 3) yield an average slip rate of about 5 mm/yr. It is interesting that Molnar and Deng (1984) obtained a slip rate of 15 mm/yr simply using assumed moments of earthquakes during the past 80 years. On a somewhat similar basis, Tang et al. (1984) suggested 9 mm/yr. A principal conclusion is that the high seismicity of the historical record is typical of the fault's long-term late Quaternary behavior, and we are not witnessing a temporal burst of activity such as that seen since 1939 along the North Anatolian fault of Turkey (Allen, 1975). It should be noted that a long-term slip rate of 15 mm/yr is very high by worldwide standards, being exceeded only by such faults as the San Andreas fault of California, the

Alpine fault of New Zealand, the Fairweather fault of Alaska, and a few other faults in China (Ding, 1984; Molnar et al., 1987). Slip rates of 1-5 mm/yr are perhaps more typical of earthquake-producing faults the world over, and very infrequent large earthquakes have sometimes occurred on faults with slip rates as low as .02 mm/yr (Cluff et al., 1982).

FAULT SEGMENTATION

Regional fault geometry

The Xianshuihe fault is only part of a much longer left-lateral fault system extending at least 1,400 km from southern Yunnan northwest through western Sichuan into southern Qinghai Province (Fig. 1, insert). The two most obvious points of segmentation along this entire system are (1) the en echelon stepover between the Xianshuihe fault and the Ganzi-Yushu fault (Wen et al., 1985; Wen and Bai, 1985), and (2) the branching point between the Anninghe and Zemuhe-Xiaojiang faults near Xichang (Huang and Tang, 1982). Both areas have been the locus of considerable historic earthquake activity (Fig. 2). The dilatational nature of the stepover between Ganzi and Zhuwo is demonstrated by the presence of northeast-trending normal faults, as well as by normal-fault focal mechanisms of recent earthquakes within the stepover (Fig. 5), and, as predicted by Sibson (1985, 1986), the zone appears to have marked the terminations of ruptures both on the Xianshuihe fault to the southeast (e.g., in 1973) and on the Ganzi-Yushu fault to the northwest (e.g., in 1854).

The very uniform curvature of the Xianshuihe fault between Kasu and Shimian (Fig. 2) is intriguing, suggesting block rotation about a pole somewhere near the Burmese border. And the gentle curvature of the Xiaojiang fault, farther south, suggests rotation about the same pole but with a larger radius. This geometry is surprisingly similar to that of members of the San Andreas fault system in southern California, where Weldon and Humphreys (1986) recently pointed out the remarkable concentric arcs of different segments of the fault, again emphasizing the rotation of mini-blocks caught within the plate boundary structure. Departures from the smooth arcs, not departures from linearity, represent the principal asperities.

En echelon offsets

The most obvious interruption in the continuity of the Xianshuihe fault itself in the region of this study is the abrupt termination of active strike-slip faulting near Laoqianning, together with the commencement farther south of normal faulting of different strike (Figs. 1, 3). No detailed geologic mapping has been done in this area, but it is clear from aerial photographs that active strike-slip faulting along the restricted Xianshuihe fault does not extend more than a few kilometers southwest of Huiyuan Monastery, at least as a single well-defined rupture similar to that to the northeast. And the Yalahe fault, as traced southeastward from the Laoqianning area, initially trends east as a normal fault before it gradually returns to the regional southwest strike; where a glacial moraine is cut by the east-trending fault at Gedalianzi Pass (A, Fig. 3), the ratio of Holocene vertical to horizontal slip is about 2:1. The broad valley of Laoqianning is itself a very unusual feature in this otherwise mountainous area and presumably owes its existence to the dilatational fault jog, analogous to those represented by many other sedimentary basins along dominantly strike-slip faults (e.g.,

Crowell, 1974; Rodgers, 1980; Sibson, 1985, 1986). Other features marking this first-order segmentation point are (1) the much higher relief to the south than to the north, (2) the current seismic gap along the Xianshuihe fault whose southern termination is near Laoqianning (Han and Huang, 1983), and (3) the much more distributed, net-like fault pattern to the south. Although little is known about historic large earthquakes in this area, strike-slip rupture associated with the M ≥ 7 event of 1893 apparently terminated on the south within a few kilometers of Laoqianning.

The next most obvious en echelon offset along the Xianshuihe fault is that between the Selaha and Moxi fault segments near Yajiagen (Fig. 6), although the separation between overlapping segments here is considerably less than that at Laoqianning, and there is no clear structural contrast to the northwest and southeast of the jog. This area was not visited in the field, but photo analysis reveals the presence of a lake in the jog area, and it appears to represent a typical pull-apart. The M = 7-3/4 earthquake of 1786 is thought by Wang Xinmin (personal communication) to have been associated with rupture through, rather than terminating at, this discontinuity, although reported intensities were highest in this area and could have been related to the presence of the asperity.

En echelon offsets of still lower order are common along the fault trace but do not appear to have been significant in the termination or initiation of fault rupture. A possible exception is the left stepover of about 1 km near Renda (Fig. 4), which is at about the southern termination of rupture in 1973. The report by Heim (1934), however, indicates that the 1923 rupture progressed through this same area, overlapping the area of subsequent 1973 rupture. Other low-order offsets are discussed by Wen et al. (in press).

Fault bends

King and Nabelek (1985) pointed out that the epicenter of the 1973 Luhuo earthquake was near a distinct bend in the fault trace near Gelu (Fig. 4). Careful tracing of the fault on Landsat images indicates a bend of about 9° over a distance of 12 km, and we agree that this may represent an important mechanical discontinuity. An even more abrupt deflection is that 115 km southeast at Longdengba (Fig. 7), where the fault bends 10° in less than 2 km, as traced on aerial photographs. Local vertical displacement associated with this bend is demonstrated by a 15-m-high, northeast-facing scarp cutting the broad post-glacial terrace at this locality. This segment of the fault is currently a conspicuous seismic gap (Han and Huang, 1983), and the Longdengba asperity may play an important role in initiating the next event. It clearly represents a promising area for instrumentation.

The gentle double curvature of the Selaha fault in the vicinity of Kangding (Fig. 3) is similar to situations along California's San Andreas fault described by Crowell (1974), with basins in the releasing bends and mountains in the restraining bends. In the Kangding area, the basin of Mugechuo Lake represents a releasing double bend, and, as mentioned above, this area is near the northwestern termination of the 1786 rupture--consistent with the hypothesis of Sibson (1985, 1986). Trenches excavated across the fault south of Kangding support the compressional nature of the faulting there, at the base of a 6070-m peak. The occurrence of these gentle bends in the Kangding region, and their possible "locking" effect on fault slip, may be

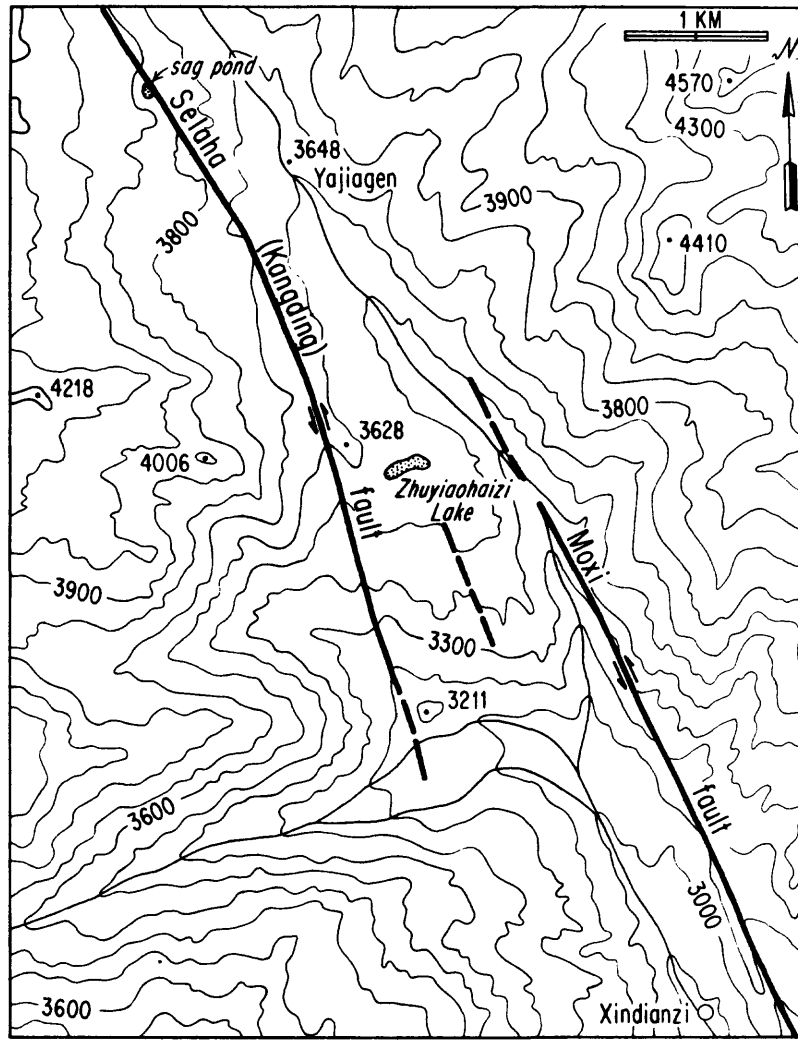

Fig. 6.--Map of area of en echelon offset between Selaha (Kangding) and Moxi members of the Xianshui fault zone, 15 km northwest of Moxi. For location, see Fig. 1.

related to the fact that this segment of the Xianshuihe fault seems to be characterized by infrequent large earthquakes rather than more frequent moderate ones. Similarly, the great earthquakes on the San Andreas fault in 1906 and 1857 have been related to major bends in those specific areas (Allen, 1967).

Surface rupture during the 1955 Kangding earthquake (M = 7-1/2) was limited, insofar as is known, to the gently curving Zheduotang fault (Fig. 3), although the entire fault segment apparently broke during this one event. Since the Selaha and Zheduotang branches of the Xianshuihe fault system are, at most, only 10 km apart in this area, and they converge toward their ends, it is possible that they dip steeply toward each other and merge at depth. This might help explain the unusually short surface rupture length of 27 km in 1955 for an earthquake of magnitude 7-1/2; fault rupture at depth may have been more complicated, with accompanying slip on the Selaha or other branches that either did not reach the ground surface or went unnoticed in this remote, mountainous region.

Other localities

Other than the few examples mentioned in the preceding sections, it is difficult to identify asperities associated with the terminations of ruptures during historic earthquakes on the relatively continuous restricted Xianshuihe fault between Qianning and Yingda (Fig. 1). Indeed, the continuity of the fault in this region is so great that, in the absence of the historical record, one could not preclude a single large earthquake rupturing the entire 220-km-long segment. Yet this has not happened in several hundred years, and the historic record instead suggests that earthquakes of shorter rupture length occur repeatedly as smaller "characteristic" events (Schwartz and Coppersmith, 1984). While it is tempting to identify more obscure geologic features such as alleged cross structures, small basins, and minor bends as asperities controlling these events, we hesitate to do so in the absence of more detailed geologic mapping and more detailed seismographic coverage. This does, however, remain a very promising area of field investigation.

FAULT CREEP

Background

Continuous or episodic surficial slip on a fault, known as fault creep, was first recognized on the San Andreas fault in California (Steinbrugge and Zacher, 1960). This behavior is now known to characterize several segments of the San Andreas fault at average rates varying from < 1 mm/yr to as much as about 30 mm/yr, and the highest rate effectively represents the total local long-term strain-accumulation rate (Savage and Burford, 1973; Thatcher, 1979). But despite intensive searches along active faults elsewhere in the world, fault creep was until recently recognized only at a single locality on the North Anatolian fault of Turkey, discovered in 1969 (Aytun, 1982). Thus the recent documentation of creep on the Xianshuihe fault is of particular scientific interest.

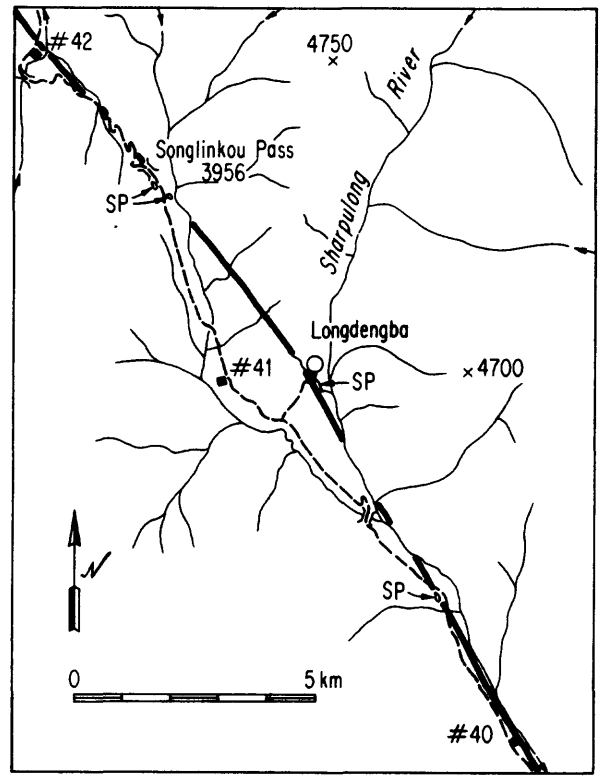

Fig. 7.--Sketch map of most active trace of Xianshuihe fault in Songlinkou-Longdengba area (Fig. 1). Dashed line represents Kangding-Lhasa highway. Four conspicuous sag ponds are indicated by "SP". Numerals indicate road maintenance stations. Note sharp 10° bend in fault at Longdengba, associated locally with a 15-m-high northeast-facing fault scarp.

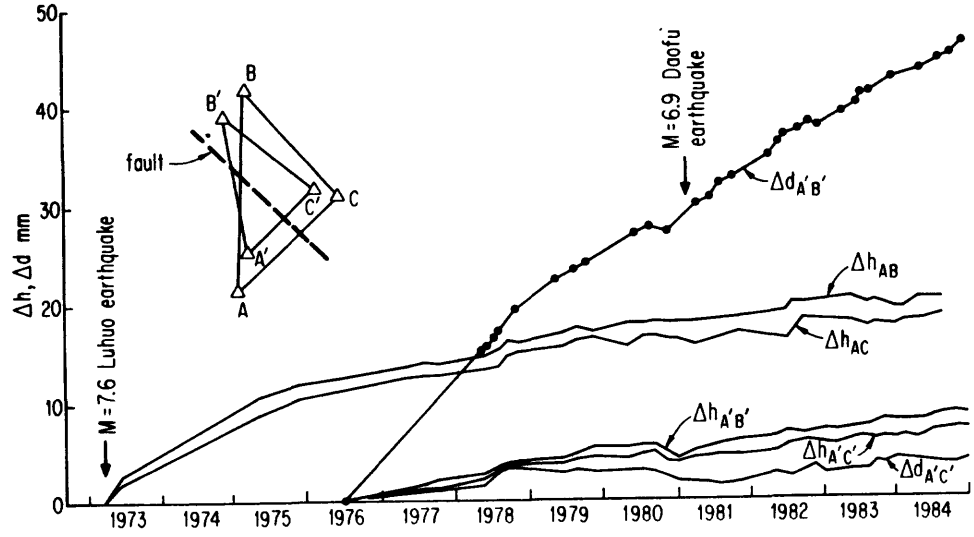

Fig. 8.--Creep measurements across the Xianshuihe fault at Xialatuo (Fig. 1). Solid circles on uppermost line (horizontal slip) represent times of individual measurements; readings were generally more frequent on the other lines (vertical slip). Inset shows arrangement of monuments. Line A'-B' is 133 m long and comprises 8 monuments. Modified from Ge (1985).

Observations

Following the 1973 Luhuo earthquake, geodetic resurveys indicated that both horizontal and vertical displacements were continuing to occur within a few hundred meters of the fault trace at several localities. These changes were particularly well documented at Xialatuo, where vertical uplift of the southwest block averaged 4.4 mm/yr between 1973 and 1975 but has subsequently decreased markedly (Ge, 1985). Probably more tectonically significant is the horizontal motion at this site, surveyed some 26 times since 1976 along a 133-m-long line of 9 monuments. These surveys (Fig. 8) show an almost steady left-lateral creep of about 6 mm/yr, most of which is concentrated within a few meters of the fault trace. From the measurements of Figure 8, one could argue either that the horizontal creep rate is relatively constant with time, or that a very long and gentle decay is following the 1973 earthquake, which was associated with 10 cm of left slip at this locality (Tang et al., 1976). Thirteen years is admittedly a long time for post-seismic creep to persist at such a high rate, and there are few other earthquakes of this magnitude for which data exist with which to compare. Exponential decay of creep following recent California earthquakes has been much faster, but the earthquakes have also been much smaller (e.g., Smith and Wyss, 1968; Cohn et al., 1982; Louie et al., 1985). It is significant, nevertheless, that post-seismic creep in California has occurred only on faults that also display continuing or episodic slip between major events. An earthquake more comparable in magnitude to that of the Luhuo event was the M_S = 7.5 Guatemala earthquake of 1976, where left afterslip on the Motagua fault continued at least through 1977 (Bucknam et al., 1978), but at a very rapidly decaying rate--quite unlike that at Xialatuo. Both in Guatemala and at Xialatuo, alluvial thicknesses at the measurement sites are small (± 10 m at Xialatuo), suggesting that whatever creep is occurring cannot be attributed solely to delay in upward propagation of slip through thick alluvium, as has been proposed for some California sites (e.g., Burford, 1972). On neither the Motagua or Xianshuihe faults is there good evidence indicating whether or not significant creep was occurring in the years before the recent earthquakes.

At other locations along the Xianshuihe fault, only sparse data of horizontal slip are available, and for much shorter time periods than that of the Xialatuo record (Ge, 1985). The survey site near the northwest end of the 1973 rupture at Zhuwo (Fig. 4), showed consistent left-lateral slip of about 1.5 mm/yr in 12 resurveys from mid-1980 through 1984. The next survey site southeast, at Dandu, showed essentially no horizontal displacement during the same period. The site at Shawan (Fig. 4) showed questionable right-lateral slip of about 1 mm/yr, but other nearby sites at Geluohazi and Xuxu showed no significant horizontal slip. No other survey sites exist along the fault except near Daofu, where some post-seismic creep following the 1981 earthquake is suggested, and near Laoqianning (Fig. 3), where no significant horizontal slip has occurred during the 1979-1984 period. Similarly, no discernible slip has occurred across the Zheduotang fault during the 1975-1984 period.

There is a strong suggestion in California that the distribution of the creeping and "locked" segments of the San Andreas fault is related to basement rock types, with creep occurring primarily in areas of abundant serpentinite and Franciscan basement on at least one side of the fault (Allen, 1967; Irwin and Barnes, 1975). We are not aware of any such relationship

along the Xianshuihe fault, although detailed geologic mapping has yet to be carried out in most of this region.

At many of the survey sites along the Xianshuihe fault, continuing vertical displacements have taken place following the Luhuo earthquake, but their tectonic significance is more debatable than that of the horizontal movements owing to the topographic relief along the fault trace, ground water changes, etc.

Summary of Creep Observations

There is no question but that significant horizontal creep has occurred along some segments of the Xianshuihe fault during the 1976-1986 time period, but not along other segments. The highest creep rate measured, about 6 mm/yr at Xialatuo, may be post-seismic creep related to the 1973 Luhuo earthquake, but the fact that it still continues at a high rate 13 years following the event suggests that other processes are also involved. Too little is known about the spatial distribution of creep along the fault, and its relationship to microseismicity, to draw conclusions of a predictive nature, but the analogy to the Parkfield, California, situation is intriguing (Bakun and Lindh, 1985). The repetition of seemingly "characteristic" historic earthquakes along the Xianshuihe fault, taken together with spatial and temporal discontinuities in creep rates, surely indicate that this is a feature worthy of further detailed studies in connection with earthquake-prediction efforts and segmentation studies.

ACKNOWLEDGMENTS

This study was carried out under the protocol for scientific and technical cooperation in earthquake studies between the State Seismological Bureau of the People's Republic of China and the U.S. Geological Survey and the National Science Foundation. The field study was sponsored by the Seismological Bureau of Sichuan Province. American participation was supported by U.S. Geological Survey Grant No. 14-08-0001-G1088. Contribution No. 4612, Division of Geological and Planetary Sciences, California Institute of Technology.

REFERENCES

Abe, K., 1988, Magnitudes and origin times from Milne seismographic data: Earthquakes in China and California, 1898-1912: p. 37-50 in Lee, W. H., Meyers, H., and Shimazaki, K., eds., Historical seismograms and earthquakes of the world, London, Academic Press.

Aki, K., 1984, Asperities, barriers, characteristic earthquakes, and strong motion prediction: Jour. Geophys. Research, v. 89, p. 5867-5872.

Allen, C. R., 1967, The tectonic environments of seismically active and inactive areas along the San Andreas fault system: Stanford Univ. Pubs. Geol. Sciences, v. 11, p. 70-82.

Allen, C. R., 1975, Geological criteria for evaluating seismicity: Geol. Soc. America Bull., v. 86, p. 1041-1057.

Allen, C. R., Gillespie, A. R., Han Yuan, Sieh, K. E., Zhang Buchun, and Zhu Chengnan, 1984, Red River and associated faults, Yunnan Province, China: Quaternary geology, slip rates, and seismic hazard: Geol. Soc. America Bull., v. 95, p. 686-700.

Allen, C. R., Luo Zhuoli, Qian Hong, Wen Xueze, Zhou Huawei, and Huang Weishi, in press, Field study of a highly active fault zone: The Xianshuihe fault of southwestern China.

Allen, C. R., Luo Zhuoli, Qian Hong, Wen Zueze, Zhou Huawei, and Huang Weishi, 1988, Seismic hazard evaluation of a highly active fault--The Xianshuihe fault of southwestern China: Proc. Internatl. Seminar on Seismic Zonation, Guangzhou, China, 6-10 Dec. 1987.

Aytun, A., 1982, Creep measurements in the Ismetpasa region of the North Anatolian fault zone, p. 279-292 in Isakara, A. M., and Vogel, A., eds., Multidisciplinary approach to earthquake prediction, v. 2: Braunschweig/Wiesbaden, Friedr. Vieweg & Sohn, 578 p.

Bakun, W. H., and Lindh, A. G., 1985, The Parkfield, California, earthquake prediction experiment: Science, v. 229, p. 619-624.

Bonilla, M. G., Mark, R. K., and Lienkaemper, J. J., 1984, Statistical relations among earthquake magnitude, surface rupture length, and surface fault displacement: Seismol. Soc. America Bull., v. 74, p. 2379-2411.

Bucknam, R. C., Plafker, G., and Sharp, R. V., 1978, Fault movement (afterslip) following the Guatemala earthquake of February 4, 1976: Geology, v. 6, p. 170-173.

Burford, R. O., 1972, Continued slip on the Coyote Creek fault after the Borrego Mountain earthquake: U.S. Geol. Survey Prof. Paper 787, p. 105-111.

Cluff, L. S., Coppersmith, K. J., and Kneupfer, P. J., 1982, Assessing degrees of fault activity for seismic zonation: Proc. 3rd Internatl. Microzonation Conf., v. 1, p. 113-118.

Cohn, S. N., Allen, C. R., Gilman, R., and Goulty, N. R., 1982, Preearthquake and postearthquake creep on the Imperial fault and the Brawley fault zone: U.S. Geol. Survey Prof. Paper 1254, p. 161-167.

Crowell, J. C., 1974, Origin of late Cenozoic basins in southern California: Soc. Econ. Paleontologists and Mineralogists Spec. Pub. 22, p. 190-204.

Deng Qidong, and Zhang Peizhen, 1984, Research on the geometry of shear fracture zones: Jour. Geophys. Research, v. 89, p. 5699-5710.

Ding Guoyu, 1984, Active faults of China, p.225-242 in A Collection of Papers of International Symposium on Continental Seismicity and Earthquake Prediction: Beijing, Seismological Press, 867 p.

Ge Peiji, 1985, Analysis of the geodetic measurements across the Xianshuihe rupture zone [in Chinese], p. 158-165 in Sichuan Seismological Bureau, Proceedings of the conference on the Xianshuihe fault zone: Beijing, Seismological Press, 254 p.

Han Weibin, and Huang Shengmu, 1983, A seismic gap on the Xianshuihe fault, Sichuan Province [in Chinese]: Acta Seismologica Sinica, v. 5 (3), p. 280-286.

Heim, A., 1934, Earthquake region of Taofu: Geol. Soc. America Bull., v. 45, p. 1035-1049.

Huang Shengmu, 1985, A preliminary discussion on seismic episodes of the Xianshuihe seismic zone, p. 88-93 in Sichuan Seismological Bureau, Proceedings of the conference on the Xianshuihe fault zone: Beijing, Seismological Press, 254 p.

Huang Shengmu, Liu Benpei, Jiang Zaixiong, and Li Dinfu, 1982, Seismic faults of Xialatuo, Luhuo County, Sichuan Province [in Chinese]: Seismology and Geology, v. 4 (1), p. 67-71.

Huang Zuzhi and Tang Rongchang, 1982, A preliminary study of the seismo-geological characteristics of the Zemuhe fault [in Chinese], p. 251-261 in The active faults of China: Beijing, Seismological Press, 337 p.

Institute of Geology, State Seismological Bureau, 1983, The photo album of eight strong earthquake disasters in China: Beijing, Seismological Press, 434 figs.

Irwin, W. P., and Barnes, I, 1975, Effect of geologic structure and metamorphic fluids on seismic behavior of the San Andreas fault system in central and northern California: Geology, v. 3, p.713-716.

Kan Rongju, Zhang Sichang, Yan Fengtong, and Yu Linsheng, 1977, Present tectonic stress field and its relation to the characteristics of recent tectonic activity in southwestern China [in Chinese]: Acta Geophysica Sinica, v. 20 (2), p. 96-109.

King, G., and Nabelek, J., 1985, Role of fault bends in the initiation and termination of earthquake rupture: Science, v. 228, p. 984-987.

Lawson, A. C., ed., 1908, The California earthquake of April 18, 1906: Carnegie Inst. Washington Pub. 87, 3 vols.

Li Ping, and Wang Liangmou, 1975, Exploration of the seismo-geological features of the Yunnan-West Sichuan region [in Chinese]: Scientia Geologica Sinica, 1975 (4), p. 308-326.

Louie, J. N., Allen, C. R., Johnson, D. C., Haase, P. C., and Cohn, S. N., 1985, Fault slip in southern California: Seismol. Soc. America Bull., v. 75, p. 811-833.

Luo Zhuoli, ed., 1980, Seismic History of Sichuan Province [in Chinese]: Chengdu, People's Press, 2 vols.

Molnar, P., Burchfiel. B. C., Liang K'uangyi, and Zhao Ziyun, 1987, Geomorphic evidence for active faulting in the Altyn Tagh and northern Tibet and qualitative estimates of its contribution to the convergence of India and Eurasia: Geology, v. 15, p. 249-253.

Molnar, P., and Deng Qidong, 1984, Faulting associated with large earthquakes and the average rate of deformation in central and eastern Asia: Jour. Geophys. Research, v. 89, p. 6203-6227.

Molnar, P., and Tapponnier, P., 1975, Cenozoic tectonics of Asia: Effects of a continental collision: Science, v. 189, p. 419-426.

Qian Hong, 1983, On the mechanism of the formation of anti xi-type ground crack zones along the Xianshuihe fault [in Chinese]: Seismology and Geology, v. 5 (3), p.75-79.

Richter, C. F., 1958, Elementary seismology: San Francisco, W. H. Freeman, 768 p.

Rodgers, D. A., 1980, Analysis of pull-apart basin development produced by en echelon strike-slip faults: Internatl. Assoc. Sedimentologists Spec. Pub. 4, p. 27-41.

Savage, J. C., and Burford, R. O., 1973, Geodetic determination of the relative plate motion in California: Jour. Geophysical Research, v. 78, p. 832-845.

Schwartz, D. P., and Coppersmith, K. J., 1984, Fault behavior and characteristic earthquakes: Examples from the Wasatch and San Andreas fault zones: Jour. Geophys. Research, v. 89, p. 5681-5696.

Sibson, R. H., 1985, Stopping of earthquake ruptures at dilatational fault jogs: Nature, v. 316, p. 248-251.

Sibson, R. H., 1986, Rupture interaction with fault jogs: Am. Geophys. Union Geophys. Mon. 37, p. 157-167.

Smith, S. W., and Wyss, M., 1968, Displacement on the San Andreas fault subsequent to the 1966 Parkfield earthquake: Seismol. Soc. America Bull., v. 58, p. 1955-1973.

Steinbrugge, K. V., and Zacher, E. G., 1960, Creep on the San Andreas fault--fault creep and property damage: Seismol. Soc. America Bull., v. 50, p. 389-396.

Tang Rongchan, Qian Hong, Chang Wenfu, Chang Chengqui, Cao Yangguo, and Liu Shengli, 1984, On the seismogeological setting and conditions of seismogenic structures of 1981 Daofu earthquake [in Chinese]: Seismology and Geology, v. 6 (2), p. 33-40.

Tang Rongchang, Wen Dehua, Deng Tiangang, and Huang Shengmu, 1976, A preliminary study of the characteristics of the ground fractures during the Luhuo M = 7.9 earthquake, 1973 and the origin of the earthquake [in Chinese]: Acta Geophysica Sinica, v. 19 (1), p. 19-27.

Tapponnier, P., and Molnar, P., 1976, Slip line field theory and large-scale continental tectonics: Nature, v. 264, p. 319-324.

Tapponnier, P., and Molnar, P., 1977, Active faulting and tectonics in China: Jour. Geophys. Research, v. 82, p. 2905-2930.

Tapponnier, P., Peltzer, G., and Armijo, R., 1986, On the mechanics of the collision between India and Asia, p. 115-157 in Coward, M. P., and Ries, A. C., eds., Collision tectonics: Geol. Soc. Spec. Pub. 19.

Thatcher, W., 1979, Systematic inversion of geodetic data in central California: Jour. Geophys. Research, v. 84, p. 2283-2295.

Weldon, R., and Humphreys, E., 1986, A kinematic model of southern California: Tectonics, v. 5, p. 33-48.

Wen Xueze, and Bai Lianxiang, 1985, The crustal fracture pattern and seismogenic structure of the northwestern segment of the Xianshuihe fault zone [in Chinese], p. 33-40 in Sichuan Seismological Bureau, Proceedings of conference on Xianshuihe fault zone: Beijing, Seismological Press, 254 p.

Wen Xueze, Huang Shengmu, and Jiang Zaixiong, 1985, Neotectonic features of the Ganzi-Yushu fault zone and assessment of its earthquake risk [in Chinese]: Seismology and Geology, v. 7 (3), p. 23-34.

Wen Xueze, Luo Zhuoli, Qian Hong, Zhou Huawei, Huang Weishi, and Allen, C. R., in press, Segmentation, geometric features, and their seismotectonic implications for the Holocene Xianshuihe fault zone [in Chinese]: Seismologica Sinica.

Zhou Huilan, Allen, C. R., and Kanamori, H., 1983a, Rupture complexity of the 1970 Tonghai and 1973 Luhuo earthquakes, China, from P-wave inversion, and relationship to surface faulting: Seismol. Soc. America Bull., v. 73, p. 1585-1597.

Zhou Huilan, Liu, H.-L., and Kanamori, H., 1983b, Source processes of large earthquakes along the Xianshuihe fault in southwestern China: Seismol. Soc. America Bull., v. 73, p. 537-551.

MECHANICS OF FAULT JUNCTIONS

D. J. Andrews
U. S. Geological Survey, Mail Stop 977
345 Middlefield Road
Menlo Park, California 94025

ABSTRACT

In order to avoid an unphysically large stress singularity, a sharp bend in a fault must be part of a triple junction, and local deformation at the junction must be rigid-body displacement. Accompanying the displacement, a volume change occurs at a junction; either a void opens or intense local deformation is required to avoid material overlap. The energy absorbed due to the volume change is proportional to the slip increment times the total past slip accumulated at the junction. At a new junction the energy absorbed is a small fraction of the energy released by slip on the fault system, but after a number of earthquakes the junction becomes a strong barrier to further slip. Although slip occurs more easily on old rupture surfaces than on fresh fractures, the changing strength of junctions requires that there be some fresh fracture in earthquakes. Fresh fracture on a small fraction of the surface that slips could provide the instability needed to explain earthquakes. The junctions that determine a characteristic strike-slip earthquake will be completely changed after 50 recurrences.

A numerical model in two-dimensional static plane strain shows, even without accounting for energy absorbed at the junction, that a bend in a fault acts as a barrier if slip is impeded on the associated fault spur. The stress concentration at the bend will tend to induce slip on the spur. Slip occurring on the spur unstably (with a drop in coefficient of friction) can induce increased slip on the main fault segments with no change in the coefficient of friction. A fault junction provides a natural realization of barrier and asperity models without appealing to arbitrary variations of fault strength.

The location of the fresh fracture that occurs after a junction becomes a strong barrier remains an unanswered question. It is likely to be initiated near the stress concentration at the old junction. A model simulating the effect of fresh fracture near old junctions might explain earthquakes without appealing to an unstable friction law anywhere.

INTRODUCTION

Researchers in earthquake mechanics have recognized for more than a decade that fault heterogeneity determines the number-size distribution of earthquakes, initiation and termination of rupture, source complexity, and random high-frequency radiation. Although most would agree that irregular fault geometry is the basis of this heterogeneity, the available computational methods have impelled more modeling of heterogeneous strength on a planar fault than of nonplanar fault geometry.

Segall and Pollard (1980) modeled the elastic stress field of *en echelon* cracks governed by a frictional sliding law, and their work has been extended by Aydin and Schultz (1988). Mavko (1982) calculated quasistatic frictional sliding in a two-dimensional

model of faults near Hollister, California. Sibson (1986) considered nonelastic void opening at a dilatational fault step and showed that the energy absorbed is sufficient to stop an earthquake rupture. In this paper I will examine energy absorbed at fault branches, rather than steps.

King (1983) pointed out that to accommodate a general finite deformation there must be sets of faults with several different orientations. Such faults will meet at triple junctions. McKenzie and Morgan (1969) show that a fault-fault-fault triple junction is unstable, meaning that it does not maintain its geometry. When slip occurs a void must open. Pressure in the earth resists void opening. King (1983) suggested that slip is zero at junctions and that large finite deformation is accommodated on a fractal array of subfaults around each junction. In this paper I will show that the energy required to open a void at a junction in a single earthquake is a small fraction of the energy released. Therefore, slip can accumulate at a triple junction in a limited number of earthquakes, but the junction progressively becomes a stronger barrier, so that eventually a fresh fracture must occur to bypass the old junction. These considerations provide a bridge between small strain, as usually considered in seismology, and large deformation accumulating in many earthquakes.

For the sake of simplicity the modeling work of this paper is restricted to static two-dimensional plane strain. This geometry is applicable to strike-slip earthquakes that rupture through the entire seismogenic depth. I first show that the stress concentration at a sharp bend in a fault requires that a third fault segment join at the bend and that deformation near the junction is approximated by rigid-block displacement. Then I examine the energetics of slip at a triple junction. Finally, faults meeting at a triple junction are modeled numerically with slip subject to a frictional sliding law.

JUNCTION KINEMATICS

Consider the simplest geometric irregularity, a bend in a fault, a point where two straight fault segments meet at a point. Suppose that slip at the bend is nonzero. Then the local stress field is the sum of two dislocation solutions, one dislocation solution for each fault segment, with the Burger's vector of each being the limiting value of slip as the bend is approached. If the two fault segments form a straight line and have equal values of slip, the stress fields cancel. If the two fault segments do not form a straight line, however, the stress fields of the two dislocation solutions will not cancel. Their sum, the local stress field due to the bend, will have a singularity proportional to $1/r$, where r is distance from the bend. This is stronger than the $1/\sqrt{r}$ singularity at a crack tip, which, at macroscopic length scales, is the strongest singularity that can exist in a real material.

The stress singularity at a fault bend can be cancelled by slip on a third fault segment at the junction. The condition for this cancellation is that the slip vectors on the three segments must form a closed triangle. The reason is that the stress field of a dislocation is proportional to its Burger's vector (the displacement vector). The sum of solutions for a number of dislocations at the same point with zero net Burger's vector has a zero stress field. Therefore the $1/r$ singularity is avoided if a fault bend is really a triple junction. If the slip vectors form a closed triangle, the three blocks bounded

by the fault segments displace as rigid bodies in the neighborhood of the junction.

Figure 1, top, shows a triple junction labelled with the notation that will be used in this paper. The three fault segments are labeled A, B, and C, and the angles opposite these segments are labeled α, β, and γ respectively. Each of the angles is less than 180° in the case shown. In the bottom of the figure the three blocks bounded by the fault segments are displaced as rigid bodies. Displacement on each fault segment is assumed to be pure slip, that is, there is no opening displacement. Slip displacements u_A, u_B, and u_C on the three segments are defined to be positive for right-lateral slip. The requirement of rigid body displacement is equivalent to the statement that the ratio of slip to the sine of the opposite angle is the same for all three segments,

$$\frac{u_A}{\sin\alpha} = \frac{u_B}{\sin\beta} = \frac{u_C}{\sin\gamma} = U\,, \tag{1}$$

and this common ratio is designated by U in the following equations. In the case shown in figure 1, the sines of all the angles are positive, so slip is in the same sense (right lateral) on all segments.

Figure 1, bottom, shows that a void opens at the junction as a result of the rigid body displacement. The volume of the void per unit length out of the paper, the area of the triangle in the figure, can be written in a symmetric form

$$V = \frac{1}{2}\,U^2\,\sin\alpha\sin\beta\sin\gamma\,, \tag{2}$$

or in terms of slip on one of the segments,

$$V = \frac{1}{2}\,u_A^2\,\frac{\sin\beta\sin\gamma}{\sin\alpha}\,. \tag{3}$$

If the medium were not subject to any confining stress, the rigid body displacement could occur with no stress change. Where there is a confining stress, however, such as in the earth, there must be a stress change in the vicinity of the void in order to satisfy the boundary condition of zero normal stress at the void surface.

The sum of the dislocation solutions of the fault segments predicts that there is no stress change associated with the rigid body displacement. The solution for the stress field of a dislocation is based on the assumptions of linear elasticity, including the assumption that displacements are small compared to the length scales of interest, so that the configuration does not change. The opening of the void at the junction and the stress change around the void are not accounted for in linear elasticity.

At a dilatational junction, where a void opens, the three angles α, β, and γ are all less than 180°. Figure 2, top, shows a compressive triple junction where one of the angles γ is greater than 180°. Since $\sin\gamma$ is negative, (1) predicts that u_C has an opposite sign from u_A and u_B, and (2) predicts a negative void volume. In the displaced configuration, figure 2, bottom, slip on segment C is left lateral, and there is an overlap of material at the junction. The overlap must be accommodated by deformation and compression in a region around the junction.

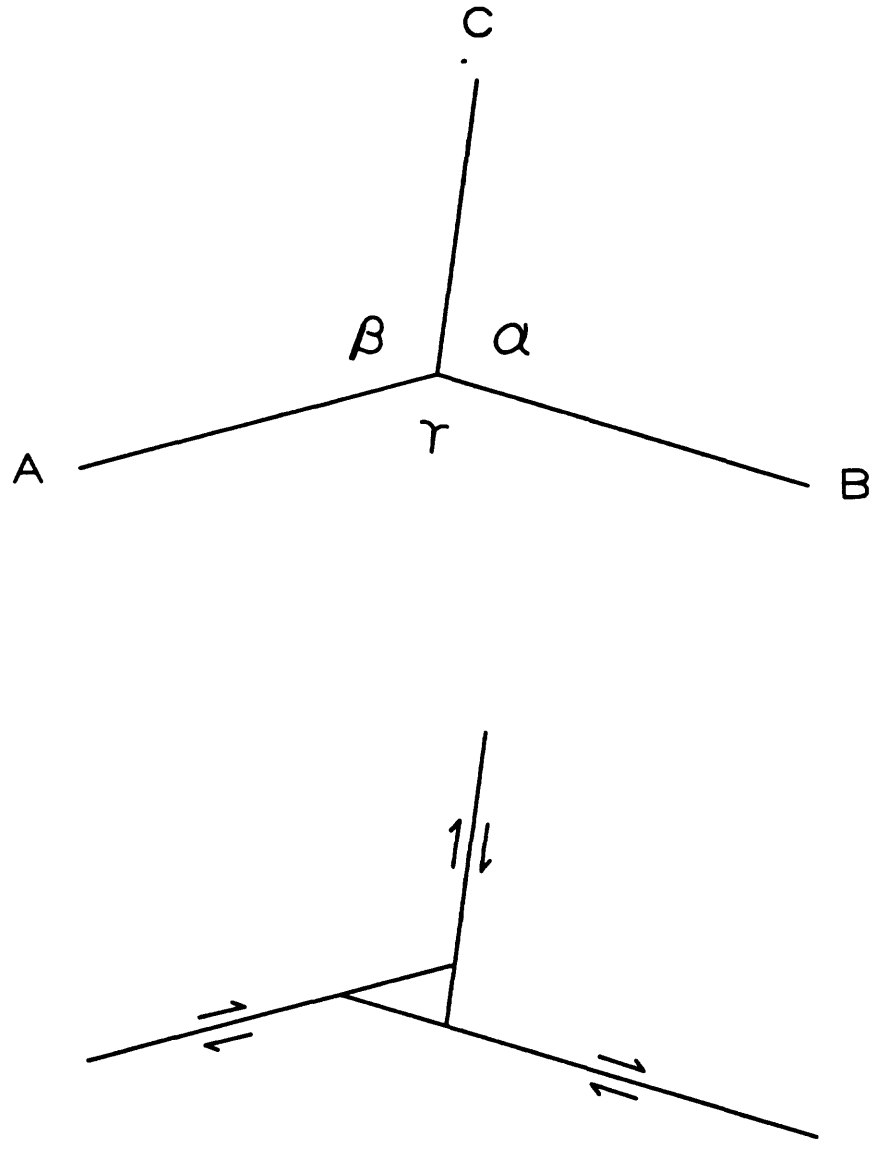

FIGURE 1. Top: A junction of fault segments A, B, and C. The opposite angles α, β, and γ are each less than 180°. Bottom: Rigid body displacement at the junction consists of slip in the same sense on the three fault segments, and a void opens.

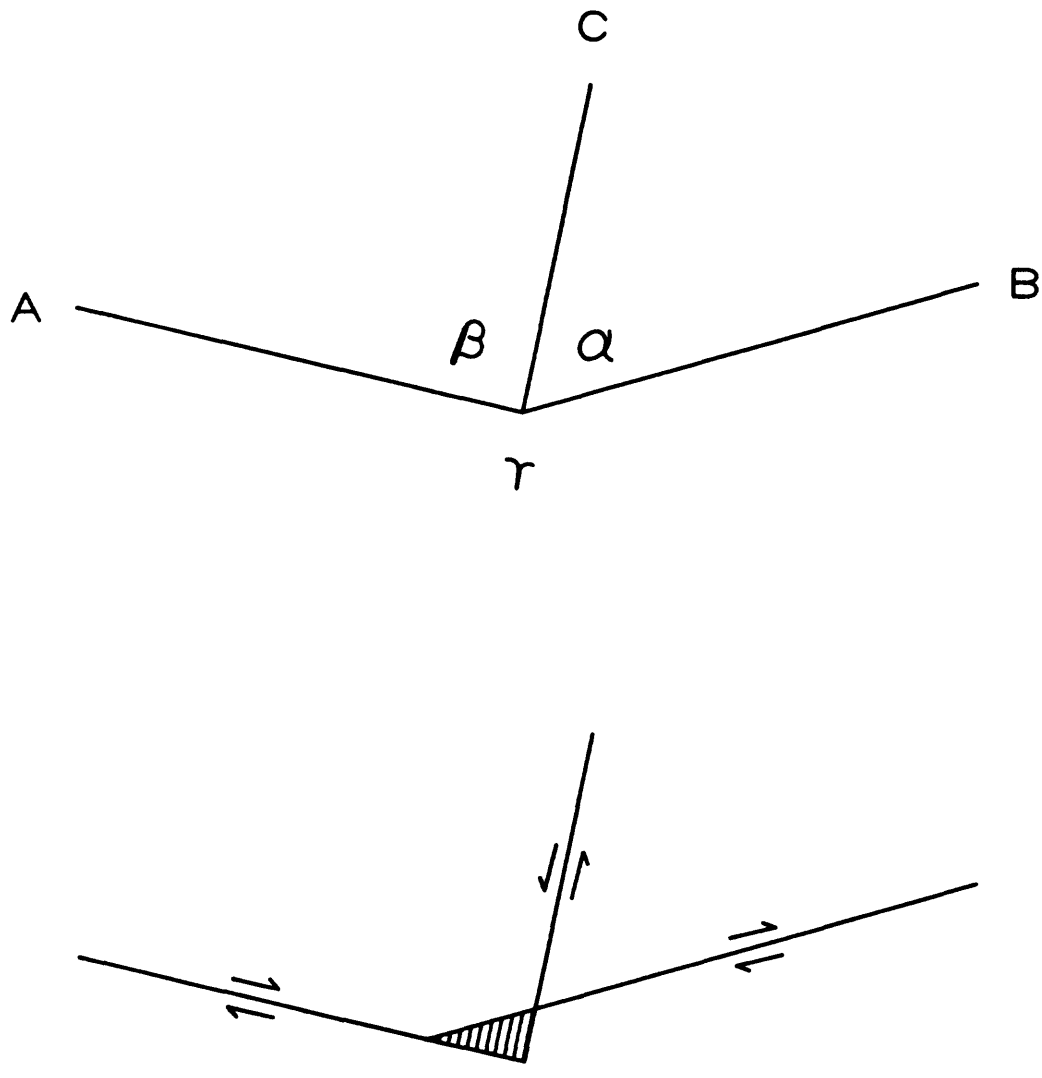

FIGURE 2. Top: A junction of fault segments A, B, and C. One of the angles γ is greater than 180°. Bottom: In rigid body displacement slip on segment C is opposite in sense from slip on segments A and B. Material overlap requires deformation and compression in the neighborhood of the junction.

THE ENERGETICS OF SLIP AT A JUNCTION

Consider first a dilatational junction. Because the material near the triple junction is displaced, to a first approximation, as rigid blocks, the net expansion of the region containing the junction is V, given by (2), and work is done against the confining stress. For the sake of an order of magnitude estimate, ignore the dependence on orientation in an anisotropic stress field. The work done against the mean compressive stress P is

$$PV = \frac{1}{2} P U^2 \sin\alpha \sin\beta \sin\gamma . \tag{4}$$

This estimate of the work required to open the void needs to be corrected by the frictional work associated with the altered stress field in the immediate vicinity of the void. Nevertheless, (4) will be taken as an estimate of the energy absorbed at a dilatational junction, and it will be compared below with an estimate of energy released by slip on the fault system.

At a compressive junction a volume V_0, larger than the overlap V, must be compressed and deformed, perhaps by intense microcracking. The stress needed to accomplish this compression is kV/V_0, where k is bulk modulus. The deformed volume V_0 will be large enough that this compressive stress is resisted by the yield stress of the material, which for a brittle rockmass is proportional to the mean compressive stress P. Therefore the volume of the intensely deformed region is $V_0 \propto (k/P)V$, and its radius is of the order of $\sqrt{k/P}$ times displacement at the junction. The work required to accommodate the overlap, then, is estimated as

$$c P |V|$$

where c is some number larger than 1 to account for work done in shear displacement on microcracks in addition to the work of compression.

In general the energy absorbed at the junction may be estimated as

$$\frac{1}{2} c P U^2 |\sin\alpha \sin\beta \sin\gamma| = \frac{1}{2} c P u_A^2 |\sin\beta \sin\gamma / \sin\alpha| \tag{5}$$

where c is of order 1 for $0 < \alpha, \beta, \gamma < 180°$, and c is larger if one of the angles is greater than 180°. The essential feature of the estimate is that energy absorbed is proportional to the square of slip at the junction.

Energy absorbed at a junction will now be compared to energy released by slip on the fault system in an earthquake. For this purpose the earthquake is approximated as a simple plane-strain shear crack. The elastic strain energy released by a crack with length $2L$ and stress drop $\Delta\tau$ minus the work done against the sliding friction stress is

$$U - W = \frac{3\pi}{8\mu}(\Delta\tau)^2 L^2 \tag{6}$$

where μ is shear modulus. A formula more useful for the present purpose expresses this quantity in terms of the maximum slip on the crack u_m,

$$U - W = \frac{\pi}{6} \mu u_m^2 . \tag{7}$$

This equation shows that the available energy released is proportional to the square of slip on the crack.

The ratio of energy absorbed at the junction (5) to the available energy released (7) is

$$c\left(\frac{P}{\mu}\right)\left|\frac{\sin\beta\sin\gamma}{\sin\alpha}\right|\left(\frac{u_A}{u_m}\right)^2 \tag{8}$$

If the triple junction is near the center of the fault system ruptured in a earthquake, the last factor, the ratio of junction slip to maximum slip, will be near 1. Near the ends of rupture or on subsidiary branches the ratio is smaller. If u_A is the largest of the set u_A, u_B, u_C at a junction, the combination of trigonometric factors lies between 0 and 1. Aside from these geometric factors, the magnitude of (8) depends on P/μ. This dimensionless ratio of mean compressive stress to shear modulus is zero at the surface, is 0.01 at 10 km depth, and ranges up to 0.2 at 650 km, the depth of the deepest earthquakes. Therefore, energy absorbed at the junction is less than the available energy released, so it is possible for slip to occur at a triple junction in an earthquake. A fault branch may branch in turn, and because of the diminishing size of the slip (the last factor in (8)), branching may continue down to an infinitesimal scale, yielding a fractal structure.

A fresh fracture propagating in virgin rock at a velocity near the shear wave speed has a stress intensity factor stronger in off-crack directions, so branching is favored. After a branch is initiated, slip may grow at the junction with little impediment in a single earthquake at shallow depths.

At shallow depths the frequency of branching may be large, but a deep-focus earthquake cannot branch as much. The relative energy cost of branching (8) constrains the frequency of branching, and hence the fractal dimension, to decrease with increasing depth. This may be the reason that deep-focus earthquakes have fewer aftershocks.

In the remainder of this discussion it is assumed that it is easier for slip to occur on an old rupture surface than to form a fresh fracture. Therefore an earthquake rupture will tend to follow old slip surfaces, and it is necessary to consider triple junctions at which slip has accumulated in earlier events. For this purpose adopt the characteristic earthquake model: after neighboring earthquakes have occurred to reset the stress state, an identical earthquake recurs. The available energy released by the earthquake (7) is the same, but the energy absorbed at the triple junctions is larger, because it depends on the total accumulated slip. Figure 3 shows a triple junction at which previous slip has opened the dark-shaded void, which is now filled with fluid or remineralized. If the previous slip is U_A, the volume of this filled void is

$$V = \frac{1}{2}U_A^2 \sin\beta\sin\gamma/\sin\alpha$$

Because of the previous displacement, the three fault segments no longer intersect at a single point, and for this reason an increment in slip will produce a larger increment in void opening. An additional earthquake with slip u_A will increment the void volume by

$$V = \frac{1}{2}\left[(U_A+u_A)^2 - U_A^2\right]\frac{\sin\beta\sin\gamma}{\sin\alpha} = (U_A + u_A/2)\,u_A\,\frac{\sin\beta\sin\gamma}{\sin\alpha}$$

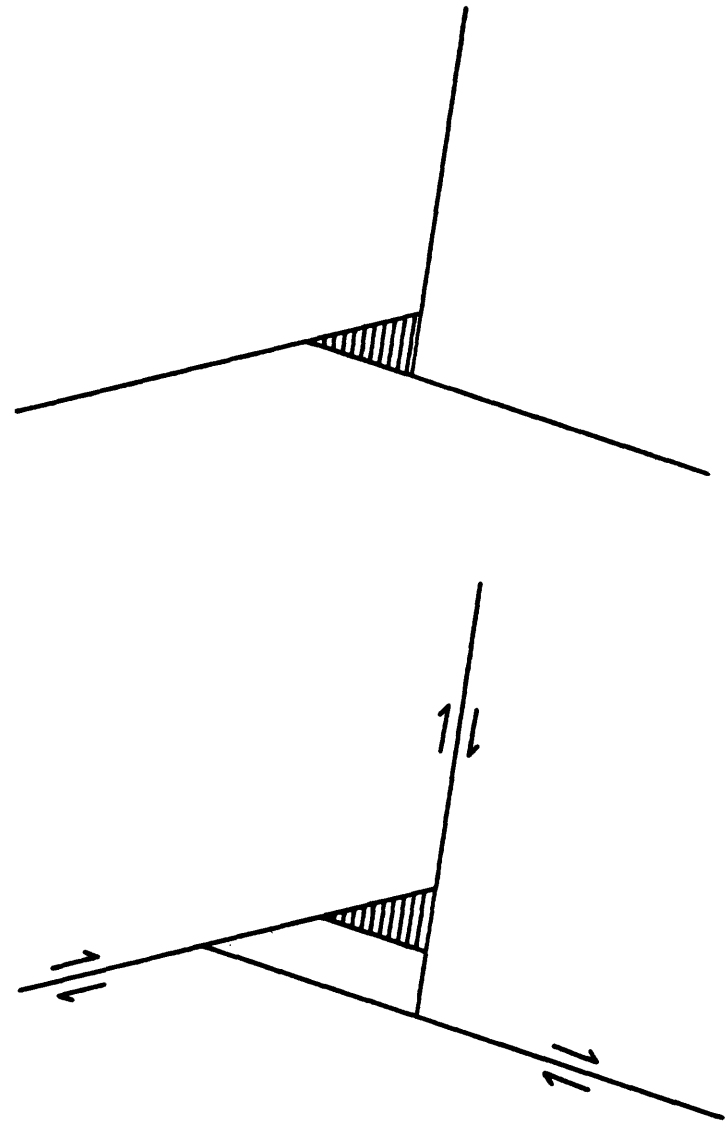

FIGURE 3. Top: The triple junction shown in the bottom of figure 1 with the void filled with fluid or remineralized. Bottom: Another increment of slip produces a larger increment of void volume.

Note that this volume increment is proportional to the product of the slip increment times the total slip that has occurred at the junction. If the current earthquake is a repeat of n identical previous events, the ratio of energy absorbed at the junction to available energy released, equation (8), is modified to become

$$(2n+1)\,c\left(\frac{P}{\mu}\right)\left|\frac{\sin\beta\sin\gamma}{\sin\alpha}\right|\left(\frac{u_A}{u_m}\right)^2 \tag{9}$$

The relative energy cost of slip at a junction increases as slip accumulates at the junction. At 10 km depth (9) becomes of order 1 after about 50 earthquakes.

As slip accumulates at a junction, the junction becomes a stronger barrier to slip. An earthquake is determined by the collective effect of many barriers. The barriers that define a characteristic earthquake become a bit stronger with each recurrence. Therefore each occurrence of a characteristic earthquake on a strike-slip fault must be slightly different from the previous one. Although most of the rupture occurs on old slip surfaces, a small fraction of the rupture area must consist of fresh fracture surface, in order to bypass old junctions that have become strong barriers. The maximun lifetime of a strike-slip junction is 50 events. Therefore, after 50 recurrences or less a characteristic strike-slip earthquake will have evolved into a completely different event.

NUMERICAL MODELING

In order to avoid an unphysically large stress singularity, it was concluded above that rigid-block displacement occurs in the neighborhood of a triple junction. At a larger scale one cannot expect slip to be constant along a fault segment. A discrete numerical method is used here to investigate stress interaction of fault segments that meet at a junction.

Method

The method, based on dislocation theory, does not account for the nonlinear effect of energy absorbed at a junction. Fault segments are divided into small elements. Stress at each element is found by summing the stress fields produced by slip on all elements plus a remotely-applied stress field. Slip on each element is adjusted iteratively until shear traction is equal to the coefficient of friction times normal traction if slip is nonzero, or shear traction is smaller and slip is zero. The relaxation method converged about as rapidly for this nonlinear problem as it would have for a linear problem of the same size, a phenomenon that has not been addressed, to my knowledge, in the numerical analysis literature.

I have performed these calculations by the boundary integral method in both first-order and second-order numerical approximations. I first used the method of Crouch (1976), in which slip is constant across an element, and stress is calculated at element centers. The method is nominally of first order, meaning that in a smooth problem the error would be proportional to the first power of the element size. Convergence with respect to element size is less rapid in these problems, however, because there are stress singularities. An advantage of the method is that each element is an independent

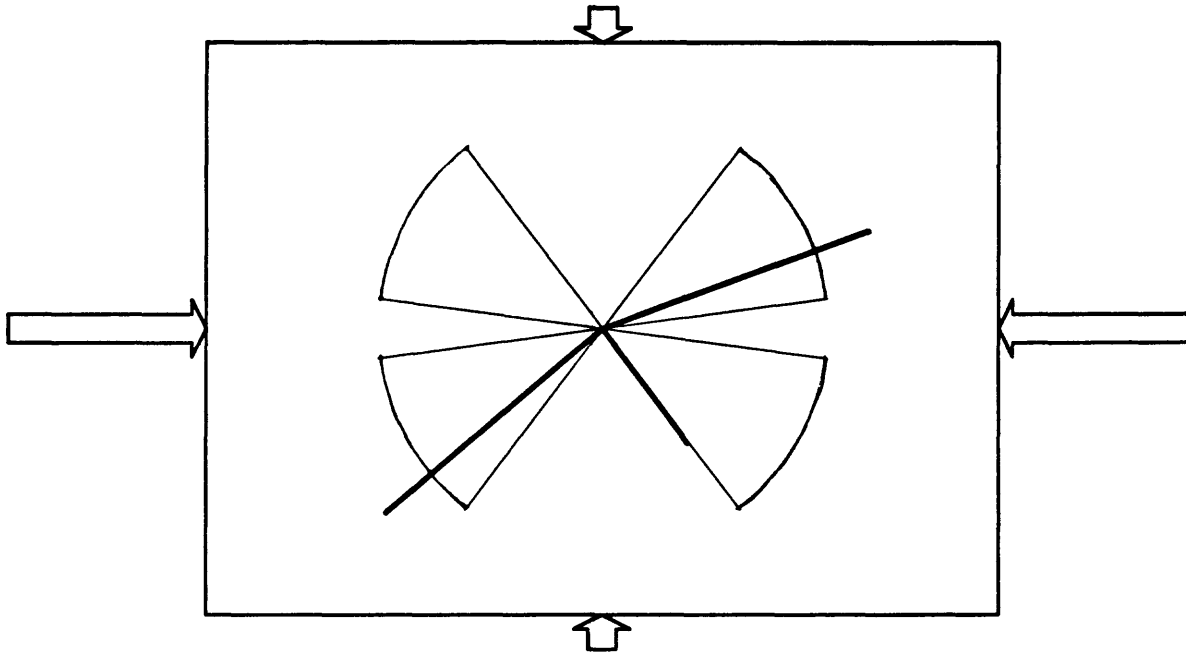

FIGURE 4. Fault segments (heavy lines). The remotely-applied stress (arrows) will cause slip on faults with azimuths lying in the sectors shown (light lines) for coefficient of friction of 0.577.

calculational unit, so no constraint need be imposed at a fault junction. A sequence of first-order solutions with decreasing element size seemed to indicate that slip at a junction was approaching the rigid-block relation (1). This supports the analysis of the first section, in which stress variation near the junction was not accounted for. I abandoned the first-order method for these junction problems, because the differences between solutions found with different element size are large. The first-order method is satisfactory, however, for *en echelon* cracks.

A nominally second-order method was used to calculate the results shown below. Slip is assumed to vary linearly across an element and is continuous between elements. Stress is calculated at the points between elements and slip is iteratively adjusted at these points. The junction point requires special logic; it was constrained by the rigid-block relation (1). The second-order method gives results consistent with the first-order method at extremely fine resolution, and reasonable results are obtained at coarser resolution.

Results

The problem geometry is shown in figure 4. The remotely applied principal compressive stress components differ by a factor of 5.8. The heavy lines indicate fault segments that meet at a triple junction. The two longer segments have a coefficient of friction of $1/\sqrt{3} = 0.577$. They are most likely to slip if their azimuths are adjusted to 30° with respect to the most compressive principal stress direction, but with this applied stress they will slip at any azimuth within the sectors indicated by light lines. Their azimuths are chosen to be 20° and 220°, both within sectors where right lateral slip will occur, forming a bend of 20°. The azimuth of the third fault segment is chosen to be −53°. It will not slip in the applied stress field for a coefficient of friction of 0.577 or larger.

The coefficient of friction on the short fault segment, the spur, is chosen to be 0.85 in the first simulation. The converged solution for slip is shown in a perspective view in figure 5, top, with right slip plotted up and left slip down. The fault bend is a barrier; slip is not as large as it would be on a straight crack with the same total length. The stress concentration at the bend induces left slip on the fault spur, but this effect has a short range.

The coefficient of friction on the spur is reduced to 0.577 in the second simulation, shown in figure 5, bottom. The larger amount of left slip on the spur allows larger right slip on the main fault segments.

The solutions shown in the top and bottom of figure 5 may be considered to be static states before and after an earthquake. The difference between these solutions, plotted at an expanded scale in figure 6, is a quasi-static approximation of slip in an earthquake in which the coefficient of friction drops from 0.85 to 0.577 on the fault spur, and slip occurs with no change in coefficient of friction on the main fault segments. The moment of the right slip on the main segments is 6 times the moment of the left slip on the spur. This is a variant of an asperity model, in which a stress drop on a small patch, the asperity, induces slip over a larger area with no change in coefficient of friction. (Shear traction changes somewhat on the main fault segments here, because there is a change in normal stress, but the slip occurs with a stable friction law.)

Slip

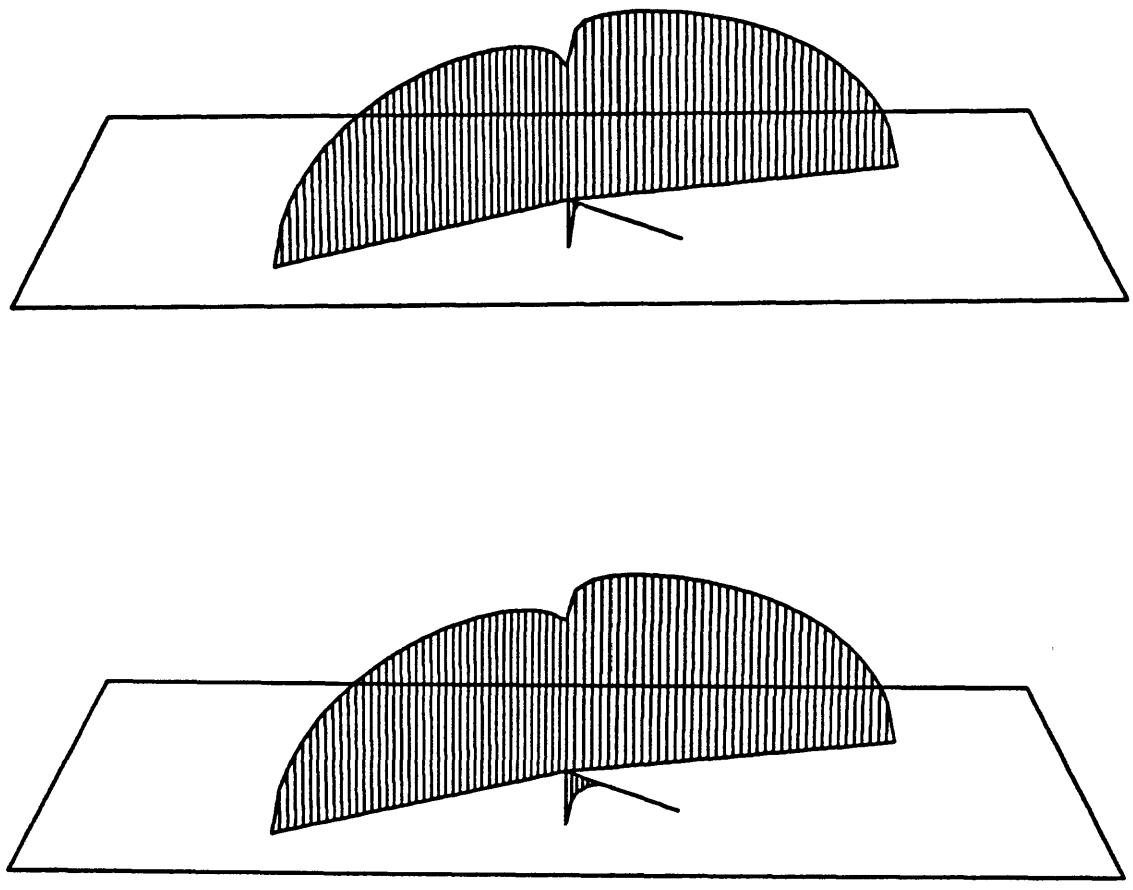

FIGURE 5. Top: Perspective view of static slip solution with coefficient of friction of 0.577 on the long fault segments and 0.85 on the short fault segment. Right slip is plotted up, left slip down. Bottom: Solution with friction of 0.577 on the short fault segment.

Slip increment

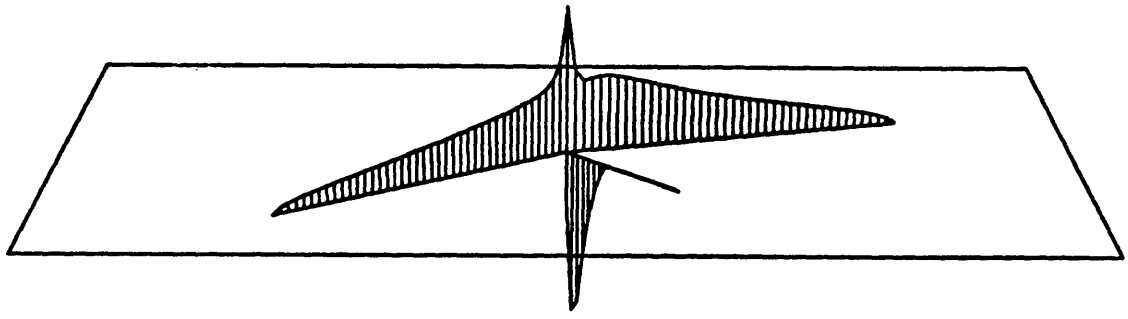

FIGURE 6. Difference between the solutions shown in figure 5. This is slip in an earthquake caused by a drop in the coefficient of friction on the fault spur.

Although a drop in stress on the spur is the active agent initiating the event in this case, note that stress sufficient to drive slip on the spur arises from the other segments, not from the remotely-applied stress. From the radiated seismic waves it would be difficult to distinguish the event in figure 6 from an event in which the asperity was a strong patch on the main fault.

Discussion

Fault junctions provide a natural model of barriers and asperities on a fault without appealing to arbitrary distributions of fault strength. The bend in the main fault is a barrier to slip in the static state shown at the top of figure 5. Slip on the spur is equivalent to breaking an asperity, and it produces the event shown in figure 6. If unstable friction were added to the model, then slip on a fault spur might trigger an even larger event on the main fault. If an earthquake has any observable precursors, such as foreshocks or accelerated creep, they might be found on a fault spur rather than on the main throughgoing fault.

The modeling in this section has ignored the energy absorbed at junctions. As discussed in the last section, after sufficient slip has accumulated, a junction will become a strong enough barrier to require that slip bypass it on a fresh fracture. The fresh fracture could be the initiating event of an earthquake. The location of the fresh fracture remains an unanswered question. The most highly stressed region will be the neighborhood of the old junction, so the fracture is likely to be initiated there. A local change in configuration is not sufficient, however. The fact that the three fault segments at an old junction no longer meet at a single point is the reason that there is a large increment of volume change accompanying a slip increment. (See figure 3.) At least one of the fault segments must jump to an alignment such that the junction is again a single point. Alternatively, slip might be taken up on surfaces distant from the old junction, but the initiation of the changed configuration would not be the stress concentration at the old junction.

The numerical method used here can easily accommodate loading by semi-infinite dislocations joined to the fault segments of interest, in addition to remotely-applied stress. More complicated fault networks can be modeled. I hope to extend the method in the future to account for energy absorbed at junctions by incorporating an effective generalized concentrated force proportional to accumulated displacement. When a junction is sufficiently stressed, the effective force restraining the junction might be reset to zero, representing a local adjustment of the junction by fresh fracture. Slip events could be initiated by this mechanism without appealing to a change of friction on any fault segment.

SUMMARY AND SPECULATIONS

Slip cannot occur across a sharp bend in a fault unless the bend is part of a triple junction. When slip occurs at a triple junction there is a change of configuration at the length scale of the displacement, either a void opens or material overlap requires local compression. The theory of linear elasticity does not account for this change of configuration, nor for energy absorbed at the junction. The energy absorbed does not

prevent slip at the junction, but as slip accumlates in a number of events the energy cost becomes larger. The nonlinearity at a junction eventually enforces a changed fault geometry. A strike-slip junction at 10 km depth can remain active for at most 50 events.

This work has addressed the question of how long a junction can remain active before becoming a strong barrier. From the point of view of fault segmentation the relevant question is: how long can a junction that has become a strong barrier remain a boundary between fault segments? It will remain a boundary until a new fracture bypasses it, and I make no prediction of how long that will be. This work does not necessarily support the characteristic earthquake model. Assuming earthquakes recur as characteristic events, this work says that the junctions that determine a characteristic stike-slip earthquake will be completely changed after 50 recurrences. The minimum modification of the characteristic earthquake model required by this work is that characteristic strike-slip events evolve gradually and have a lifetime of 50 events or less.

One might speculate that earthquakes can be modeled with a stable frictional constitutive law, with the instability provided by the fresh fracture that occurs on a small fraction of the fault surface. Stress concentrations will occur at junctions that have accumulated slip in past events. Fresh fracture is likely to occur near these locations, so an earthquake is likely to start near a junction. This variant of the asperity model suggests that the mechanism essential in modeling earthquakes is geometric irregularity of the fault, not an unstable frictional constitutive relation. In such a model, however, each event would be initiated differently from its predecessor.

There is no preferred length scale in these considerations, so fault branching may be expected to occur at all scales. Slip in a typical earthquake is 10^{-4} times the rupture length, and accumulated slip at a junction that has become a strong barrier is of the order of 10^{-2} times the rupture length. The change in configuration at triple junctions may constrain the overall mechanics of a rupture, which implies a link between length scales differing by a factor of 10^2 or μ/P. A tantalizing unanswered question is: Is it a coincidence that strain in a single earthquake is of the order of $(P/\mu)^2$?

Because slip can occur at a triple junction in only a limited number of events before at least one of the fault segments moves to a different location, one cannot expect to find distinct fault traces at a junction. Indeed, there is little geologic expression of fault junctions (Robert Sharp, personal communication). A fault trace need jump only a small distance, however, to reactivate a junction, so a large displacement and large void opening may accumulate at a diffuse junction. Some of the largest gravity and magnetic anomalies in the San Francisco Bay Region are found at the junction of the Hayward and Calaveras Faults (Allan Lindh, personal communication) and at the junction of the Calaveras and San Andreas Faults (Robert Burford, personal communication), suggesting that there are holes through the crust at these junctions.

This modeling work, while not making any specific predictions, may be important in terms of the concepts with which we interpret observations. When it was recognized that an earthquake arises from slip on a fault, modelers idealized the fault to be a plane. The concept of planar faults has dominated our thinking, and, I believe, has restricted our ideas. I believe that the essential mechanics of faulting may be determined by the

fault's geometric complexity.

ACKNOWLEDGMENTS

These thoughts have grown from discussions with Geoffrey King and Richard Sibson over a number of years. I appreciate reviews of the manuscript by John Boatwright and Geoffrey King. I thank Richard Schultz for suggesting we compare our numerical results for *en echelon* cracks and am glad to have cooperated with him.

REFERENCES CITED

Aydin, A. and Schultz, R., 1988, The effect of fault interaction on the stability of echelon strike-slip faults: this volume.

Crouch, S. L., 1976, Solution of plane elasticity problems by the displacement discontinuity method: International Journal of Numerical Methods in Engineering, v. 10, p. 301–343.

King, G., 1983, The accommodation of large strains in the upper lithosphere of the earth and other solids by self-similar fault systems: the geometrical origin of b-value: Pure and Appl. Geophys., v. 121, 761–815.

Mavko, G. M., 1982, Fault interaction near Hollister, California: J. Geophys. Res., v. 87, p. 7807–7816.

McKenzie, D. P. and Morgan, W. J., 1969, Evolution of triple junctions: Nature, v. 224, p. 125–133.

Segall, P. and Pollard, D. D., 1980, Mechanics of discontinuous faults: J. Geophys. Res., v. 85, p. 4337–4350.

Sibson, R. H., 1986, Rupture interaction with fault jogs, *in* Das, S., Boatwright, J., and Scholz, C. H., eds., Earthquake source mechanics: American Geophysical Union Monograph 37, p. 157–167.

THE EFFECT OF FAULT INTERACTION ON THE STABILITY OF ECHELON STRIKE-SLIP FAULTS

by

Atilla Aydin and Richard A. Schultz*
Dept. of Earth and Atmospheric Sciences
Purdue University
W. Lafayette, IN 47907

ABSTRACT

The overlapping geometry of echelon strike-slip faults is well known. We have quantified this observation by measuring the amount of overlap and separation and plotting them against each other for over 120 examples. Although there is large scatter, the data show a linear trend suggesting that the overlap increases proportionally with separation up to a limiting value. This conspicuous relationship has been analyzed in terms of fault interaction by using a numerical model based on displacement discontinuity. The results show that fault interaction is, in fact, an important factor in contributing to the overlapping geometry of echelon strike-slip faults.

INTRODUCTION

It is well known that map traces of strike-slip faults are characteristically discontinuous and fault segments or strands are noncolinear (Wallace, 1973; Sharp, 1979; Bonila, 1979; Allen, 1981). Adjacent discrete segments step aside and overlap slightly to form what is commonly known as an echelon fault geometry. There has been an increasing number of studies on the nature of deformation and the associated structures at stepovers between echelon strike-slip faults (see Ballance and Reading, 1980; Biddle and Christie-Blick, 1985; Aydin and Nur, 1985). A few recent publications (e.g. Aydin and Nur, 1982; Mann et al., 1983; Bahat, 1984) provide extensive surveys of previously recognized stepovers as well as a number of new ones and describe their prominent features. Theoretical stress and displacement fields at stepovers were investigated by Segall and Pollard (1980), Rodgers (1980) and Mavko (1982). The effects of interaction between colinear strike-slip faults on stress drop, seismic moment and strain energy release were explored by Rudnicki and Kanamori (1981). However, the origin of echelon patterns of strike-slip faults and the reasons for their conspicuous geometry were essentially left untouched. This paper represents an effort to fill this gap by assessing the effects of

* Now at Geodynamics Branch, Code 621
NASA Goddard Space Flight Center
Greenbelt, MD 20771

interaction on the geometry of strike-slip faults. The stabilizing effect of interaction on the propagation of closely spaced echelon faults was previously suggested by Aydin et al. (1985) and Ma et al. (1986). A similar mechanism was proposed for echelon extensional fractures (Pollard et al., 1982; Pollard and Aydin, 1984; Sempere and Macdonald, 1986).

FIELD DATA

We used both existing data available in the literature and some new data that we collected in the field. In using the existing data, we were faced with two problems in quantifying the geometric characteristics of echelon strike-slip faults. First, the published maps lack a uniform accuracy. In dealing with the uniformity problem, we considered data from California (U.S.A.), Turkey and Israel. The data from California's faults come chiefly from geologists with the United States Geological Survey (Wallace, 1973; Clark, 1973; Sharp, 1979) where strict mapping and publication guidelines and an internal review system assure uniformity. The data on the major faults in Turkey and Israel are obtained primarily from single authored documentary papers, e.g., Ketin (1969) and Garfunkel (1981). Second, many faults or fault segments are linked by cross fractures, introducing a certain degree of ambiguity in the determination of individual strike-slip fault ends. In this case, we relied upon the interpretations by the original authors or compilers.

Figures 1-4 include almost all the strike-slip faults in California, Turkey and Israel, which were used in this study. These examples alone capture the dominant geometric features which are common to all strike-slip faults. In order to characterize the echelon nature of the faults, we measured the overlap (2o) and separation (2s) of echelon fault segments (Fig. 6B, Table 1) and plotted them against each other in Fig. 5. The measurement was straight-forward when fault traces are parallel. For those cases in which fault traces are curved or nonparallel, the chord length and average separation were taken as the overlap and separation, respectively. The log-log scale used for Fig. 5 makes it possible to compare measurements with a scale differential of several orders of magnitude, at the expense of an apparent compression of the spread of the data in the plot.

Figures 1-5, and Table 1 show the following features of the echelon arrays of the strike-slip fault systems. (1) The majority of adjacent faults overlap. About 10 percent of steps have underlap configuration (negative 2o in Table 1 and Fig. 5 inset), reflecting cases in which the inner fault tips do not pass each other. (2) The overlap is roughly proportional to the separation (Fig. 5). There appears to be no such relation between the underlaps and the corresponding separations (Fig. 5 inset). The overlap-separation ratios for compressional steps (full symbols in Fig. 5) tend to be slightly smaller than those for extensional steps (empty symbols in Fig. 5). (3) Large

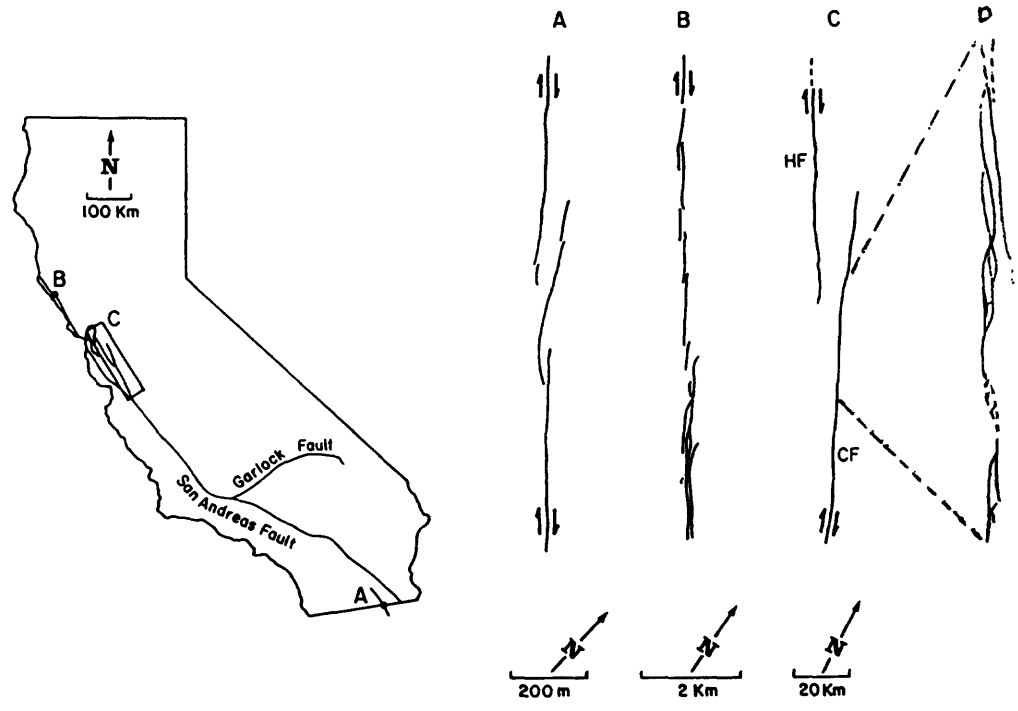

FIGURE 1. Echelon steps along the San Andreas fault system. A. Imperial fault (from Sharp, 1979). B. San Andreas fault proper (from Wallace, 1973). C. Hayward-Calaveras fault (simplified from Aydin and Page, 1984). D. Central Calaveras fault (from Aydin and Page, unpublished fault map).

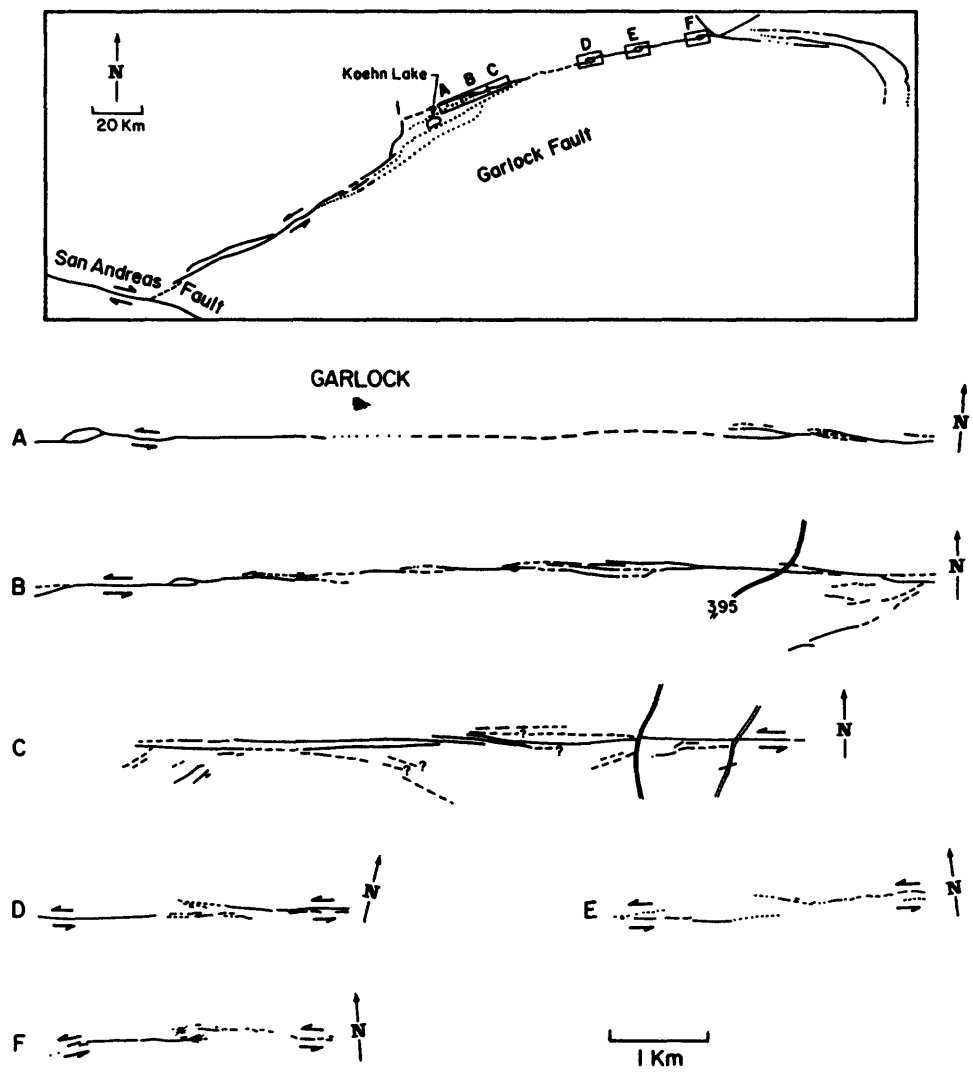

FIGURE 2. Echelon steps along the Garlock fault, California. Koehn Lake pull-apart from Aydin and Nur (1982). A, B, and C from Aydin (unpublished map). D, E, and F from Clark (1973).

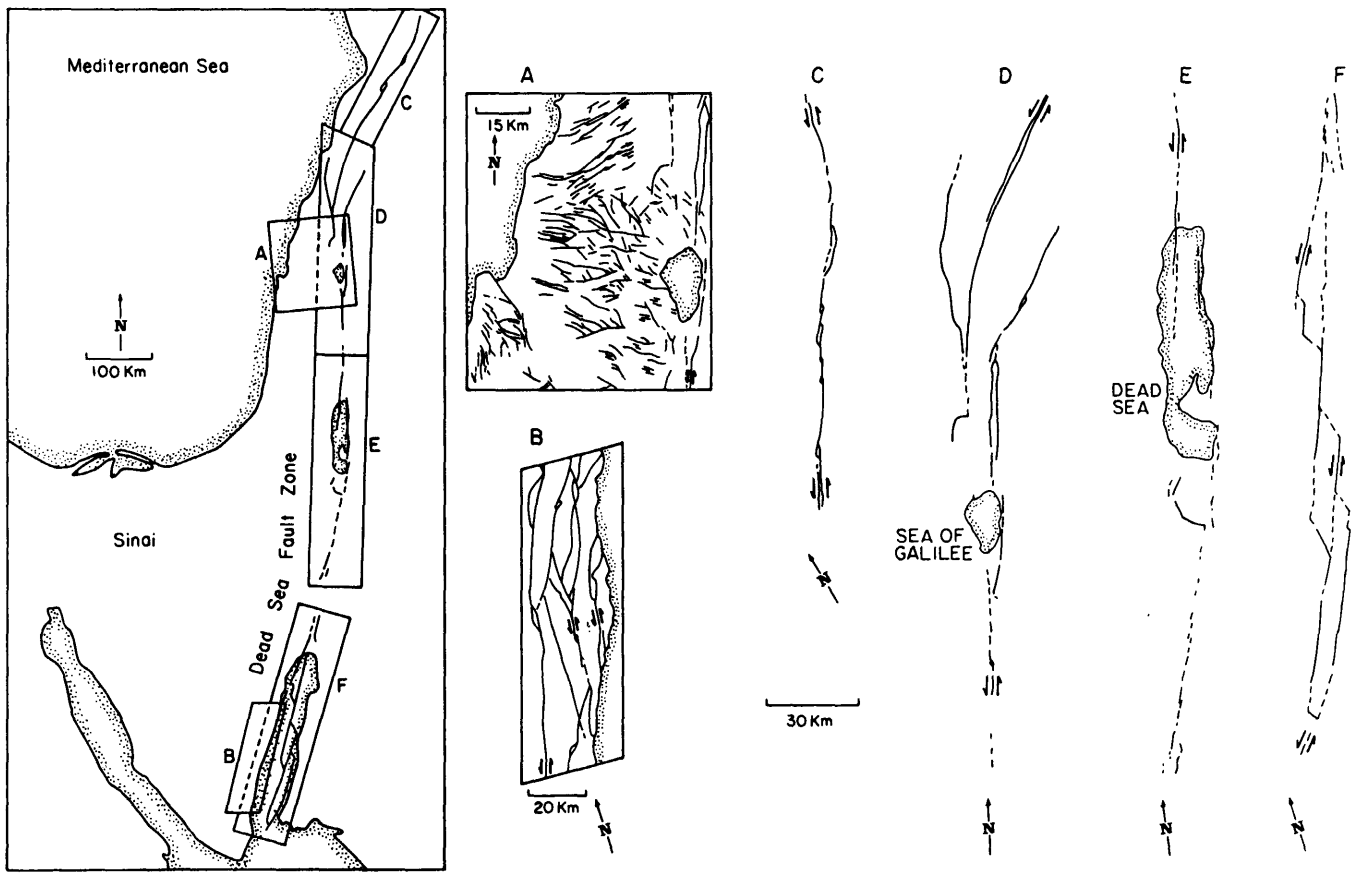

FIGURE 3. Echelon arrangement of faults along the Dead Sea system and other faults in Israel. A and B from Ron and Eyal (1985); C-F from Garfunkel et al. (1981) and Garfunkel (1981).

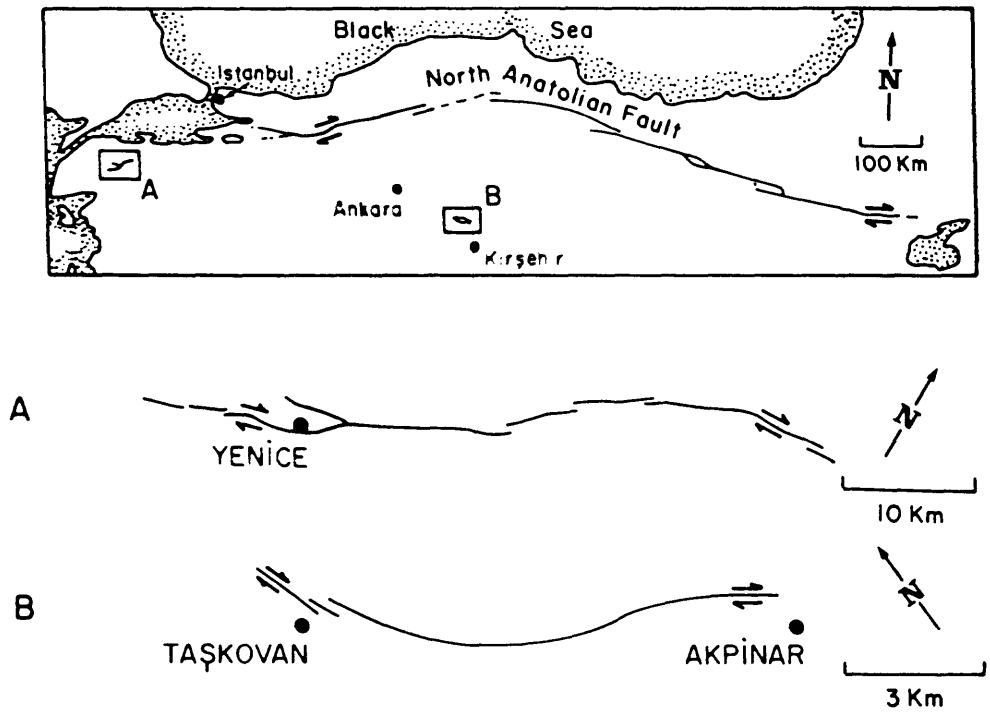

FIGURE 4. Echelon steps along strike-slip faults in Turkey (from Ketin, 1969).

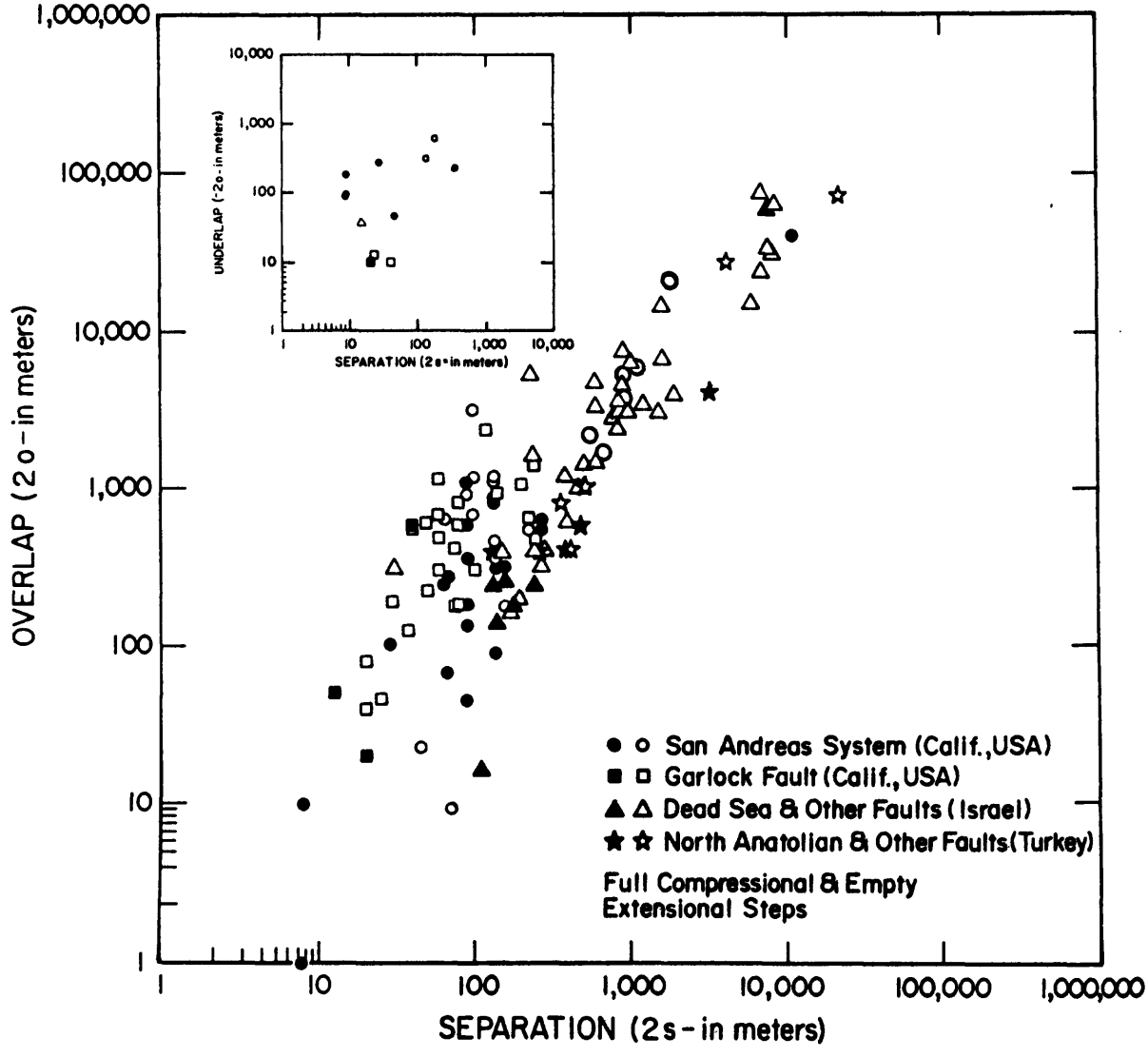

FIGURE 5. Plot of overlap vs. separation of echelon faults shown in figures 1-4 and listed in table 1. Inset shows underlap vs. separation for these faults.

TABLE 1: OVERLAP-SEPARATION DATA

Fault System	Location	Sense of Displ.	Step	Overlap (2o)m Underlap (-2o)m	Separation (2s)m	Reference
San Andreas		R	L	900	135	Wallace (1973)
		R	L	-90	9	
		R	L	810	135	
		R	L	45	90	
		R	L	540	270	
		R	L	-180	9	
		R	L	-90	9	
		R	L	-270	27	
		R	L	90	135	
		R	L	630	270	
		R	L	315	135	
		R	L	-225	360	
		R	R	-630	180	
		R	L	-45	45	
		R	L	585	90	
		R	L	67.5	67.5	
		R	L	180	90	
		R	L	270	67.5	
		R	L	135	90	
		R	L	315	157.5	
		R	R	900	90	
		R	R	630	67.5	
		R	R	1,125	99	
		R	R	675	99	
		R	L	1,080	90	
		R	R	22.5	45	
		R	R	3,060	99	
		R	R	360	135	
		R	R	540	225	
		R	R	-315	135	
		R	R	180	157.5	
		R	L	360	90	
		R	R	9	72	
		R	R	1,170	135	
		R	R	450	135	
		R	R	1,080	135	
	Imperial Fault	R	L	240	64	Sharp (1979)
		R	L	10	8	
		R	L	1	8	
		R	L	104	28	
	Hayward-Calaveras	R	L	39,900	11,200	Aydin & Page (1984)
Calaveras		R	R	16,200	1,800	Aydin & Page
	Halls Valley	R	R	4,500	900	(unpublished map)
	San Felipe Valley	R	R	1,700	700	
		R	R	5,700	1,100	
		R	R	2,100	500	
	Coyote Lake	R	R	2,700	900	

TABLE 1 CONTINUED:

Fault System	Location	Sense of Displ.	Sense of Step	Overlap (2o)m Underlap (-2o)m	Separation (2s)m	Reference
Garlock		L	L	300	100	This study
		L	L	580	80	
		L	L	480	60	
		L	L	180	80	
		L	L	220	50	
		L	R	20	20	
		L	L	1,140	60	
		L	L	40	20	
		L	L	300	60	
		L	L	80	20	
		L	L	190	30	
		L	R	-10	20	
		L	R	580	40	
		L	L	660	60	
		L	L	1,020	200	
		L	L	600	50	
		L	L	800	80	
		L	L	2,260	120	
		L	L	560	40	
		L	L	920	140	
		L	L	-10	40	
	Christmas Canyon	L	L	1,350	237.5	Clark (1973)
		L	L	425	75	
		L	R	50	12.5	
		L	L	-12.5	22.5	
		L	L	175	75	
		L	L	125	37.5	
		L	L	650	225	
		L	L	475	250	
		L	L	47.5	25	
Dead Sea	Arava Fault	L	L	385	290	Garfunkel et al.
		L	L	385	150	(1981)
		L	L	385	240	
		L	L	6,730	2,310	
		L	L	1,400	510	
		L	L	7,360	920	
		L	L	32,200	7,600	
		L	L	3,200	600	
		L	L	1,200	400	
		L	L	1,200	400	
		L	L	1,000	500	
		L	L	3,400	1,200	
		L	L	1,400	600	
		L	L	6,400	1,000	
		L	L	600	400	
		L	L	14,800	1,600	
		L	L	4,600	600	
	Hula Basin	L	L	23,200	6,800	
		L	L	4,400	880	

TABLE 1 CONTINUED:

Fault System	Location	Sense of Displ.	Step	Overlap (2o)m Underlap (-2o)m	Separation (2s)m	Reference
Dead Sea		L	L	14,700	5,900	
		L	L	2,900	1,500	
		L	R	56,400	7,880	
		L	L	3,500	850	Garfunkel (1981)
		L	L	2,700	770	
		L	L	3,100	960	
		L	L	3,900	1,900	
		L	L	6,600	1,600	
		L	L	3,100	850	
		L	L	2,300	850	
	Gulf of Elat	L	L	61,600	8,500	
		L	L	29,300	8,090	
		L	L	72,400	6,930	
		R	R	160	170	Ron & Eyal (1985)
		R	L	16	110	
		R	L	140	140	
		R	R	1,580	240	
		L	R	240	240	
		L	R	240	130	
		L	L	320	270	
		L	L	-400	16	
North Anatolian	Yenice	R	R	400	400	Ketin (1969)
		R	L	400	400	
		R	L	560	480	
		R	R	800	360	
		R	R	1,000	520	
	Kargi	R	R	27,000	4,100	
	Erbaa	R	L	4,000	3,240	
		R	R	70,200	21,600	
	Kirsehir	R	L	390	130	
		R	L	390	113	

scale echelon faults have smaller steps within themselves, suggesting that longer faults with larger separations do not feel smaller discontinuities within themselves. For example, the Calaveras fault in Fig. 1C has several smaller steps as shown in the enlargement in Fig. 1D. A similar situation occurs also in the Imperial fault in Fig. 1A.

The field data presented in Fig. 5 are compelling enough to conclude that echelon strike-slip faults tend to overlap slightly. Although the data are scattered, their approximately linear trend indicates that echelon fault patterns are self similar to a first order approximation. This generalization is consistent with that reached by Tchalenko (1970) that the geometries of shear zones in various scales are similar.

ANALYSIS

The persistence of the echelon pattern of strike-slip faults over a broad range of scales motivates an investigation of the processes that may control the geometry of strike-slip faults. One of these processes is fault interaction, which undoubtedly occurs among nearby faults or fault segments (Segall and Pollard, 1980). In order to assess the importance of fault interaction on the geometry of echelon strike-slip faults, we analyze the enhancing and impeding effect of interaction on the propagation of echelon faults. We use a special boundary element method called displacement discontinuity (Crouch, 1976, 1979; and Crouch and Starfield, 1983), which is based on a solution for a single dislocation with constant displacement. We divide echelon faults into a number of boundary elements, each of which has uniform slip. Slip on each element is driven by remote stress and adjusted iteratively until shear and normal tractions satisfy the Coulomb frictional slip criterion. Interaction between elements on nearby, echelon faults is calculated during the solution procedure.

Although many physical aspects of shear fracture propagation are not well understood, it is reasonable to assume that near tip stress concentration plays an important role in fracture growth. For mode II fractures, the stress intensity factor (K^i_{II}) that characterizes the near tip stresses for an isolated single fracture (Fig. 6A) is given in terms of the shear component of the displacement discontinuity (Ds) as

$$K^i_{II} = \frac{-\mu}{4\pi(1-\upsilon)} \left(\frac{2\pi}{d}\right)^{1/2} Ds$$

(Schultz, 1988; Sempere and Macdonald, 1986; Lin and Parmentier, 1988) where d is the distance from fault tip to the midpoint of the nearest element. The propagation energy, G^i_{II}, which is the energy available for a unit growth of an isolated mode II fracture, is given by (Lawn and Wilshaw, 1975).

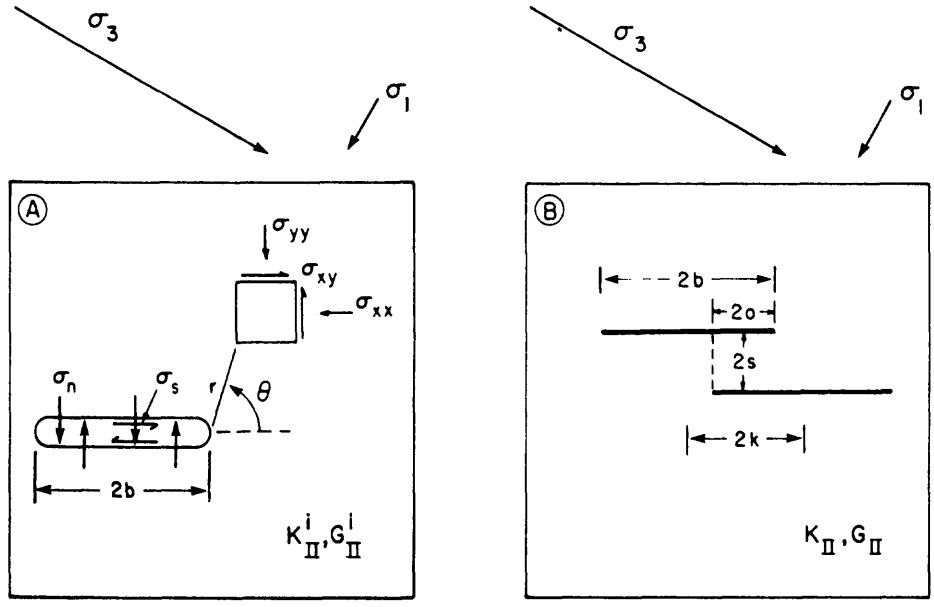

FIGURE 6. Analysis of echelon faults. A. Remote principal stresses and boundary tractions along fault. B. Geometric parameters for echelon faults. Fault length 2b, center distance 2k, overlap 2o, separation 2s.

$$G^{i}_{II} = \frac{(K^{i}_{II})^2 \ (1-\upsilon)}{2\mu}$$

Fault propagation energies at the inner tips of echelon faults are calculated for a suite of fault geometries (see Fig. 6B for the definition of overlap, 2o, separation, 2s, and center length, 2k). For each s/k, fault lengths are increased incrementally to simulate growth of the faults. For each case, the values of G_{II} for echelon faults are normalized by those for an isolated single fault (G^{i}_{II}) in order to focus on the effect of the interaction between echelon faults. For example, if $G_{II}/G^{i}_{II} = 1$, there is no interaction between the faults. On the other hand, ratios of $G_{II}/G^{i}_{II} \neq 1$ reflect fault interaction either enhancing (>1) or impeding (<1) the propagation of echelon faults.

Shear modulus, μ, and Poisson's ratio, υ, are chosen to be 1 and 0.25, respectively. Note that these values have no effect on the normalized propagation energies. Fault elements in the model are defined as thin zones with specific normal and shear stiffness. Especially useful is the normal stiffness, which can be so adjusted that the fault walls are prevented from physically interpenetrating for echelon geometries with large overlaps. We have set the stiffness ratio of fault zone material to surrounding rock at 100 to limit interpenetration. Use of high fault-zone normal stiffness gives the same results as cases in which interpenetration is prohibited as a boundary condition. The remote stress state is defined by using a ratio of principal stresses of 5 with the maximum compressive stress inclined 30^{o} to the faults. The effects of different stiffness ratios and remote stresses are discussed in the next section.

We have considered a broad range of models, only three of which are presented in this paper. The first one assumes a frictionless fault zone in order to avoid nonlinearity introduced by the dependence of fault slip on normal stress. For this case the results from both extensional (the sense of step is the same as the sense of displacement) and compressional (the sense of step is the opposite of the sense of displacement) steps are almost the same, so only the extensional case is presented in Fig. 7. The curves of fault propagation energy for five geometric cases (s/k = 0.05, 0.1, 0.25, 0.5 and 1.0) clearly show that the propagation energy for closely spaced echelon faults (s/k = 0.05 and 0.1) increases as the inner fault tips approach each other and decreases sharply beyond zero overlap (b/k=1). In contrast, the propagation energy for widely spaced echelon faults (s/k>1) shows little change.

The second model includes two cases, extensional (Fig. 8A) and compressional (Fig. 8B) steps using a Coulomb slip criterion with a friction coefficient of 0.6 (Byerlee, 1978). In both cases,

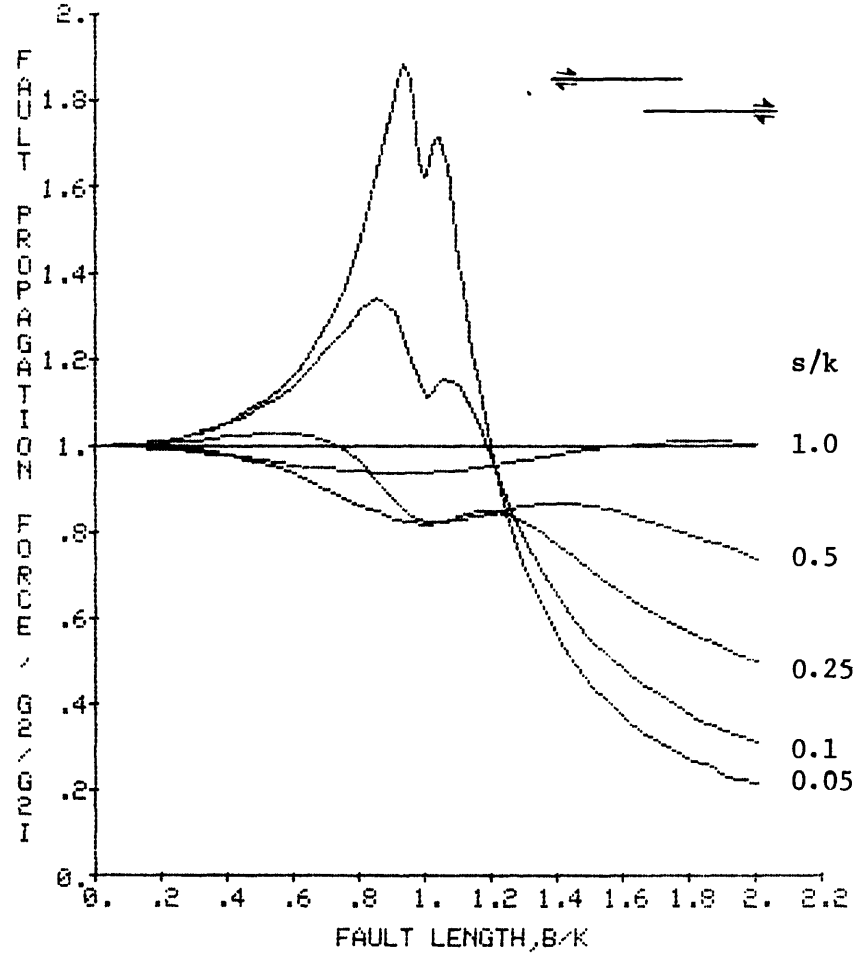

FIGURE 7. Fault propagation energy for frictionless faults in extensional step.

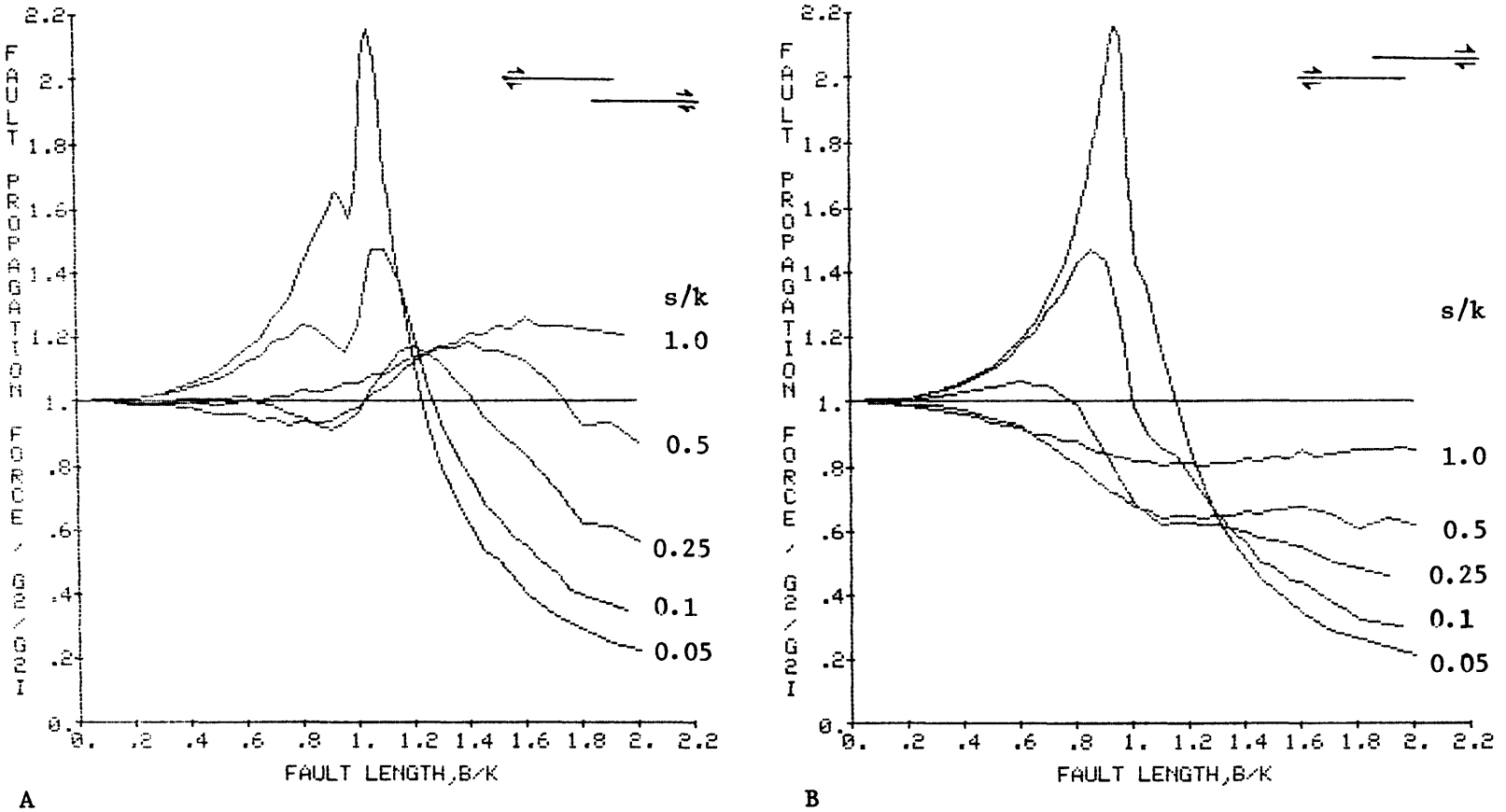

FIGURE 8. Influence of friction and step sense on fault propagation energy. Friction coefficient f=0.6. A. Extensional step. B. Compressional step.

the effect of fault interaction is generally similar to the frictionless fault cases. The difference between the compressional and the extensional cases is that the decrease of fault propagation energy for overlapped faults is much sharper for the compressional case.

Ideally, a fault would propagate when the propagation energy reaches a critical value G^c_{II}, which is dependent on material properties and the geometric parameters of a fault. We illustrate the propagation and termination of a pair of echelon faults with s/k=0.05, using an arbitrarily chosen normalized critical propagation energy curve as shown in Fig. 9. Fault growth due to the interaction between the echelon faults will occur at the geometry corresponding to b/k = 0.8 (point A) and the growth will terminate when b/k = 1.2 (point B). Unfortunately very little is known about the critical value of the mode-II propagation energy for rocks. Hence, the arguments in this paper have to be rather qualitative. By noting that an increase (or decrease) in the fault propagation energy enhances (or impedes) the fault growth, the interaction between neighboring faults favors a slightly overlapped fault pattern. The exact amount of the overlap cannot be calculated. However, the forms of normalized fault propagation energy curves (Figs 7 and 8) together with possible normalized critical fault propagation energy curves (for simplicity only one curve is shown in Fig. 9) suggest that amount of overlap (b/k) increases with amount of fault separation (s/k). Furthermore, the separation limit for significant interaction appears to be on the order of the center distance (s/k~1.0).

DISCUSSION AND SUMMARY

We have quantified the well known observation that strike-slip faults the world over occur in echelon patterns with some overlap. The overlap is generally larger as the spacing of the neighboring faults increases. The results from our numerical analysis indicate that fault interaction enhances the growth of echelon faults as the inner tips pass each other and impedes their growth after some degree of overlap. Thus, we suggest that fault interaction is one of the processes responsible for the commonly observed echelon geometry of strike-slip faults.

The frictionless and frictional slip criteria produce similar curves of fault propagation energy for the underlap configurations. Differences become pronounced as the amount of overlap increases. The frictionless case lies in between the extensional and the compressional cases, as expected from the role of fault normal stresses on fault slip. The difference between the extensional and the compressional propagation energy curves may suggest greater overlaps for the extensional steps. Although not conclusive, the field data may lend some support for this argument (see the generally lower ratios for the compressional steps, full symbols, in Fig. 5).

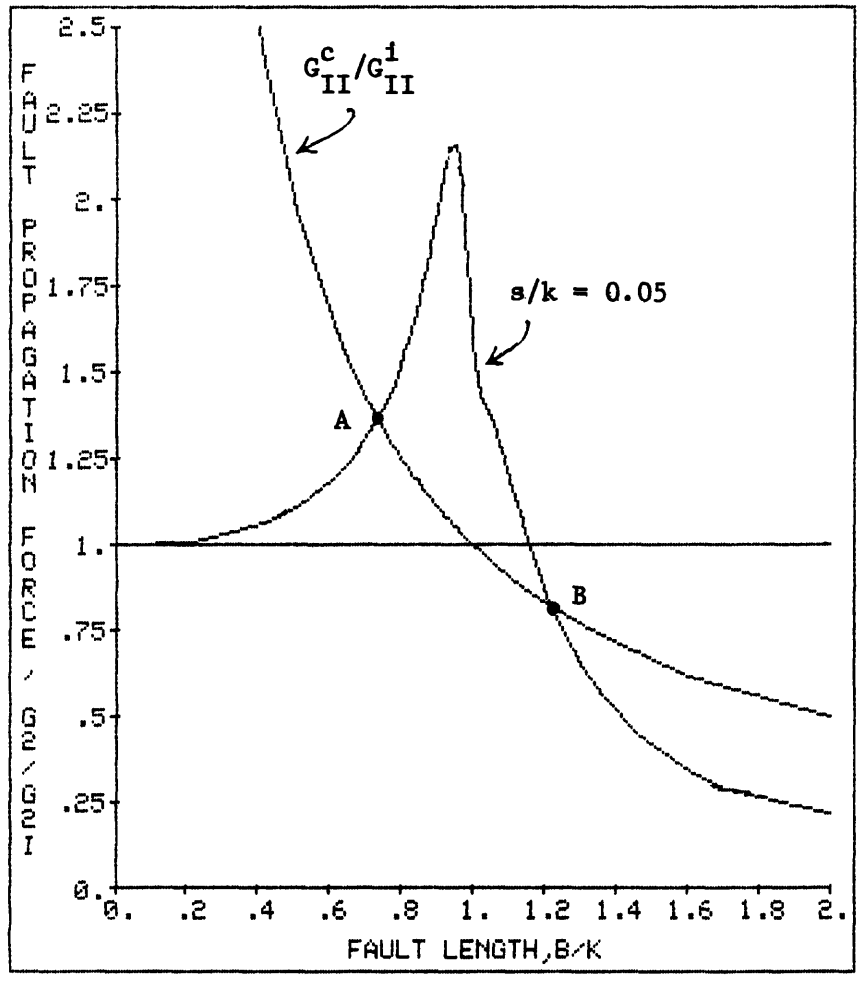

FIGURE 9. Comparison of normalized fault propagation energy (G_{II}/G^i_{II}) to normalized critical propagation energy (G^c_{II}/G^i_{II}). Faults would start to propagate at A and terminate at B producing an overlap geometry of about b/k = 1.25..

We have tested the influence of the orientation and magnitude of remote stresses on fault propagation energy due to fault interaction. Interestingly, we have found that as long as there is slip along the echelon faults the normalized propagation energy curves are the same, regardless of remote stress state.

The results reported in this paper are relevant also to the self-similarity of pull apart basins and push up ranges (Aydin and Nur, 1982) that form at extensional and compressional steps, respectively along strike-slip faults. Although the length parameters for the basins and ranges are different (usually larger) than the overlap parameters of the strike-slip faults considered in this paper, the role of fault interaction is likely to be similar in the evolution of the geometry of pull apart basins and push up ranges.

ACKNOWLEDGEMENTS

This study has been supported in part by the U.S. Geological Survey, Award number 14-08-0001-G1084. R.A.S. gratefully acknowledges support from a David Ross Fellowship (Purdue University) and from a National Research Council-NASA Goddard Space Flight Center Resident Research Associateship. Discussions with D. Pollard, S. Nemat-Nasser and P. Segall were quite helpful. Thoughtful comments by J. Andrews improved the manuscript.

REFERENCES

Allen, C.R., 1981, The modern San Andreas Fault, In The Geotectonic Development of California (edited by Ernst, W.G.), Prentice-Hall, Inc., Englewood Cliffs, New Jersey, 511-534.

Aydin, A. and Nur, A., 1982, Evolution of pull-apart basins and their scale independence, Tectonics v. 1, 91-105.

Aydin, A. and Nur, A., 1985, The types and role of stepovers in strike-slip tectonics, In Strike-Slip Deformation, Basin Formation, and Sedimentation (edited by Biddle, K.T. and Christie-Blick, N.), Soc. Econ. Paleon. Miner., Spec. Publ. 37, 35-44.

Aydin, A. and Page, B.M., 1984, Diverse Pliocene-Quaternary tectonics in a transform environment, Geological Society of America Bulletin, v. 95, p.1303-1317.

Aydin, A., Schultz, R.A., and Pollard, D.D., 1985, Why do strike-slip faults overlap?, (Abstract), EOS (Trans. Am. Geophys. Union) 66, 1067-1068.

Bahat, D., 1984, New aspects of rhomb structures, Journal of Structural Geology, v. 5, 591-601.

Ballance, P.F. and Reading, H.G. (editors), 1980, Sedimentation in Oblique-Slip Mobile Zones, Int. Assoc. Sediment., Spec. Publ. 4.

Biddle, K.T. and Christie-Blick, N. (editors), 1985, Strike-Slip Deformation, Basin Formation, and Sedimentation, Soc. Econ. Paleon. Miner., Spec. Publ. 37.

Bonilla, M.G. 1979, Historic faulting- map patterns, relation to subsurface faulting and relation to pre-existing faults, in Proceedings of Conference VIII: Analysis of Actual Fault Zones in Bedrock, USGS Open File Report, 79-1239, 36-65.

Byerlee, J., 1978, Friction of rocks, Pure and Applied Geophysics, v. 116, 615-626.

Clark, M.M., 1973, Map showing recently active breaks along the Garlock and associated faults, California, USGS Misc. Geol. Invest. Map I-741.

Crouch, S.L., 1976, Solution to plane elasticity problems by the displacement discontinuity method, International Journal of Numerical Methods in Engineering, v. 10, 301-343.

Crouch, S.L., 1979, Computer simulation of mining in faulted ground, Journal of South African Institute of Mining and Metallurgy, v. 79, 159-173.

Crouch, S.L. and Starfield, A.M., 1983, Boundary Element Methods in Solid Mechanics, George Allen & Unwin, London, 322 p.

Garfunkel, Z, 1981, Internal structure of the Dead Sea leaky transform (rift) in relation to plate kinematics, Tectonophysics, v. 80, 81-108.

Garfunkel, Z, Zak, I. and Freund, R., 1981, Active faulting in the Dead Sea rift, Tectonophysics, v. 80, 1-26.

Ketin, I, 1969, Kuzey Anadolu fayi hakkinda (in Turkish and German), Maden Tetkik Arama Enstitusu, Dergisi, No. 72, 1-27.

Lawn, B.R. and Wilshaw, T.R., 1975, Fracture of Brittle Solids, Cambridge University Press, Cambridge, 204 pp.

Lin, J. and Parmentier, E.M., 1988, Quasistatic propagation of a normal fault: A fracture mechanics model, Journal of Structural Geology, v. 10, 249-262.

Ma, J., Du, Y., and Liu, L. 1986, The instability of en-echelon cracks and its precursors, Journal Physics of the Earth, v. 34, Suppl., S141- S157.

Mann, P, Hempton, M.R., Bradley, D.C., and Burke, K., 1983, Development of pull-apart basins, Journal of Geology, v. 91, 529-554.

Mavko, G.M., 1982, Fault interaction near Hollister, California, Journal Geophysical Research, v. 87, 7807-7816.

Pollard, D.D., Segall, P., and Delaney, P.T., 1982, Formation and interpretation of dilatant echelon cracks, Geological Society of America Bulletin, v. 93, 1291-1303.

Pollard, D.D. and Aydin, A., 1984, Propagation and linkage of oceanic ridge segments, Journal Geophysical Research, v. 89, 10,017-10,028.

Rodgers, D.A., 1980, Analysis of pull-apart basin development produced by en-echelon strike-slip faults, In Sedimentation in Oblique-Slip Mobile Zones, (edited by Ballance, P.F. and Reading, H.G.), Int. Assoc. Sediment., Spec. Publ. 4, 27-41.

Ron, H. and Eyal, Y, 1985, Intraplate deformation by block rotation and mesostructures along the Dead Sea tansform, northern Israel, Tectonics, v. 4, 85-105.

Rudnicki, J.W. and Kanamori, H., 1981, Effects of fault interaction on moment, stress drop, and strain energy release, Journal Geophysical Research, v. 86, 1785-1793.

Schultz, R.A., 1988, Stress intensity factors for curved cracks obtained with the displacement discontinuity method, International Journal of Fracture, v. 37, R31-R34.

Segall, P. and Pollard, D.D., 1980, Mechanics of discontinuous faults, Journal Geophysical Research, v. 85, 4337-4350.

Sempere, J.-C. and Macdonald, K.C., 1986, Overlapping spreading centers: Implications from crack growth simulation by the displacement discontinuity method, Tectonics, v. 5, 151-163.

Sharp, R.V., 1979, The implication of surficial strike-slip fault patterns for simplification and widening with depth, In Proceedings of Conference VIII: Analysis of Actual Fault Zones in Bedrock, USGS Open File Report 79-1239.

Tchalenko, J.S., 1970, Similarities between shear zones of different magnitudes: Geological Society of America Bulletin, v. 81, p. 1625-1640.

Wallace, R.E., 1973, Surface fracture patterns along the San Andreas Fault, In Proceedings of the Conference on Tectonic Problems of the San Andreas Fault System (edited by Kovach, R.L. and Nur, A.), School of Earth Sciences, Stanford University, Stanford, Calif., 248-250.

EFFECTS OF RESTRAINING STEPOVERS ON EARTHQUAKE RUPTURE

A. Aykut Barka and Katharine Kadinsky-Cade

Earth Resources Laboratory, Department of Earth, Atmospheric and Planetary Sciences, Massachusetts Institute of Technology, Cambridge, MA 02142.

ABSTRACT

Four restraining stepovers of varying size located within strike-slip fault zones are examined in order to understand how restraining stepovers affect earthquake rupture. It appears that the width (d) of the stepover is a controlling factor in determining whether a single rupture can propagate through the stepover. When d is small (< 5 km) the stepover appears to be only a shallow structure, as in the case of the Ocotillo Badlands stepover within the 1968 Borrego Mountain, California, earthquake rupture zone. If d is large (> 5 km) the stepover area may have independent rupture characteristics. For example, during the 1976 Songpan, China, earthquake sequence three separate mainshocks occurred along three adjoining segments: two strike-slip earthquakes separated by a thrust event, the latter within the 12 km wide stepover area. Two other examples of large stepovers that have experienced earthquakes historically are the Çelikhan and Erzurum stepovers in Turkey. Although none of the large stepovers described here can support a great earthquake restricted to the stepover area (because the stepover width is less than 20 km), stress drops within the stepover may be higher than those along the adjacent strike-slip fault segments. This would result from the structural characteristics of the stepover area, where shortening is taken up mostly by thrusting and folding. The high stress drops could result in high accelerations, with important implications for earthquake hazard studies.

INTRODUCTION

Restraining features along the strike-slip fault zones can be divided into two categories: bends and stepovers. Restraining bends separate two fault segments characterized primarily by strike-slip motion, with one segment having a higher thrust component than the other. Restraining bend angles are less than 30° - 35° (Barka and Kadinsky-Cade, 1988). When the bend angle increases beyond 30°, predominantly compressional features occur within the restraining area. We refer to the resulting structure as a restraining stepover

(Fig. 1). The restraining stepover is the geometric discontinuity which causes most difficulty for motion along strike-slip faults. The stepover area is mostly characterized by complex compressional structures including thrusts, folds, conjugate strike-slip faults, uplifting etc. These structures are quite common on a small scale. For example, surface breaks of large strike-slip earthquakes often include pressure ridges and thrust faults (Fig. 2). However restraining stepovers with width greater than 1 km are not very common. The smaller stepovers may only affect the uppermost part of the crust, and may result from a decrease of confining pressure at shallow depths. The wider stepovers probably extend deeper into the crust as the stepover width increases.

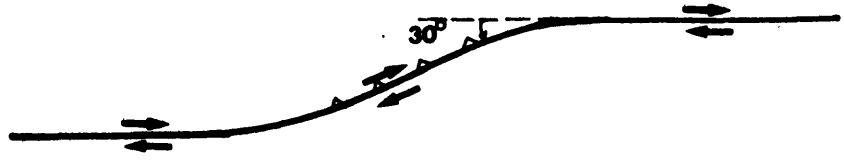

(a) Restraining Double Bend

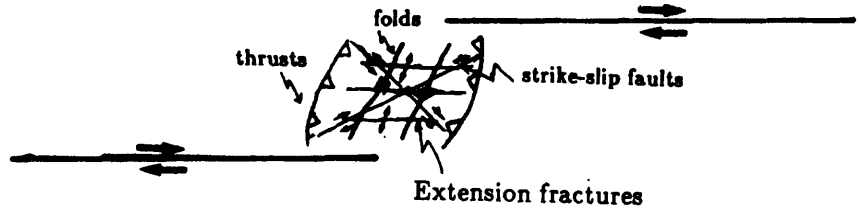

(b) Restraining Stepover

Figure 1. Two most common types of restraining discontinuities: a) Restraining double bend, where the bend angle does not exceed 30° and the dominant motion along the bend is still strike-slip but accompanied by a thrust component, and b) restraining stepover, where the stepover area is predominantly characterized by thrusting and folding.

In this short note, four examples of restraining stepovers with width > 1 km are reviewed in order to investigate earthquake rupture characteristics in restraining stepover areas.

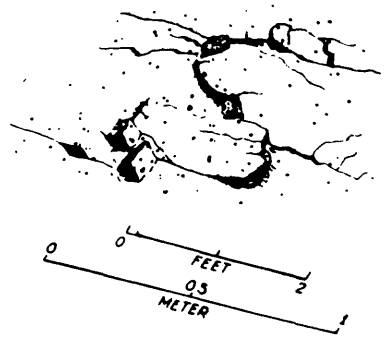

(a) 1968 Borrego Mountain Earthquake, California

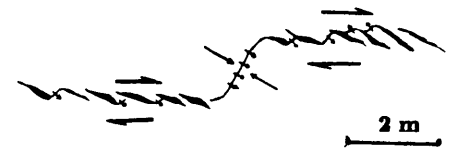

(b) 1976 Caldiran earthquake, Turkey

(c) 1983 Horasan-Narman earthquake, Turkey

Figure 2. Three examples of small-scale restraining stepovers associated with large earthquake surface ruptures (after (a) Clark, 1972, (b) Arpat et al. 1977, and (c) Barka, 1983, unpublished field notes). The shortening in the stepover is primarily taken up by thrusting.

EXAMPLES OF RESTRAINING STEPOVERS

Coyote Creek Fault, California

The first well-known example is the Ocotillo Badlands situated along the Coyote Creek fault, southern California. The restraining area is 1.5 km wide and strongly folded, and forms an anticlinal dome consisting of parasitic folds (Fig. 3a & b) (Sharp and Clark, 1972, Brown, 1987). Additionally, intrabed shearing and hinge thrusts are common structures in the stepover area (Brown, 1987). The epicenter of the 1968 Borrego Mountain earthquake (M_L = 6.4) was located near the middle of the northern segment (Fig. 3c). The rupture propagated to the south through the stepover and the amount of displacement at the surface decreased remarkably from north to south through the stepover (Clark, 1972). Aftershocks were mostly concentrated near and south of the stepover area. Sibson (1986) has concluded that, although the mainshock rupture propagated through the stepover,

rupture was at least partly arrested by the restraining area. However, geodetic measurements have revealed that fault slip was approximately constant along the entire ruptured

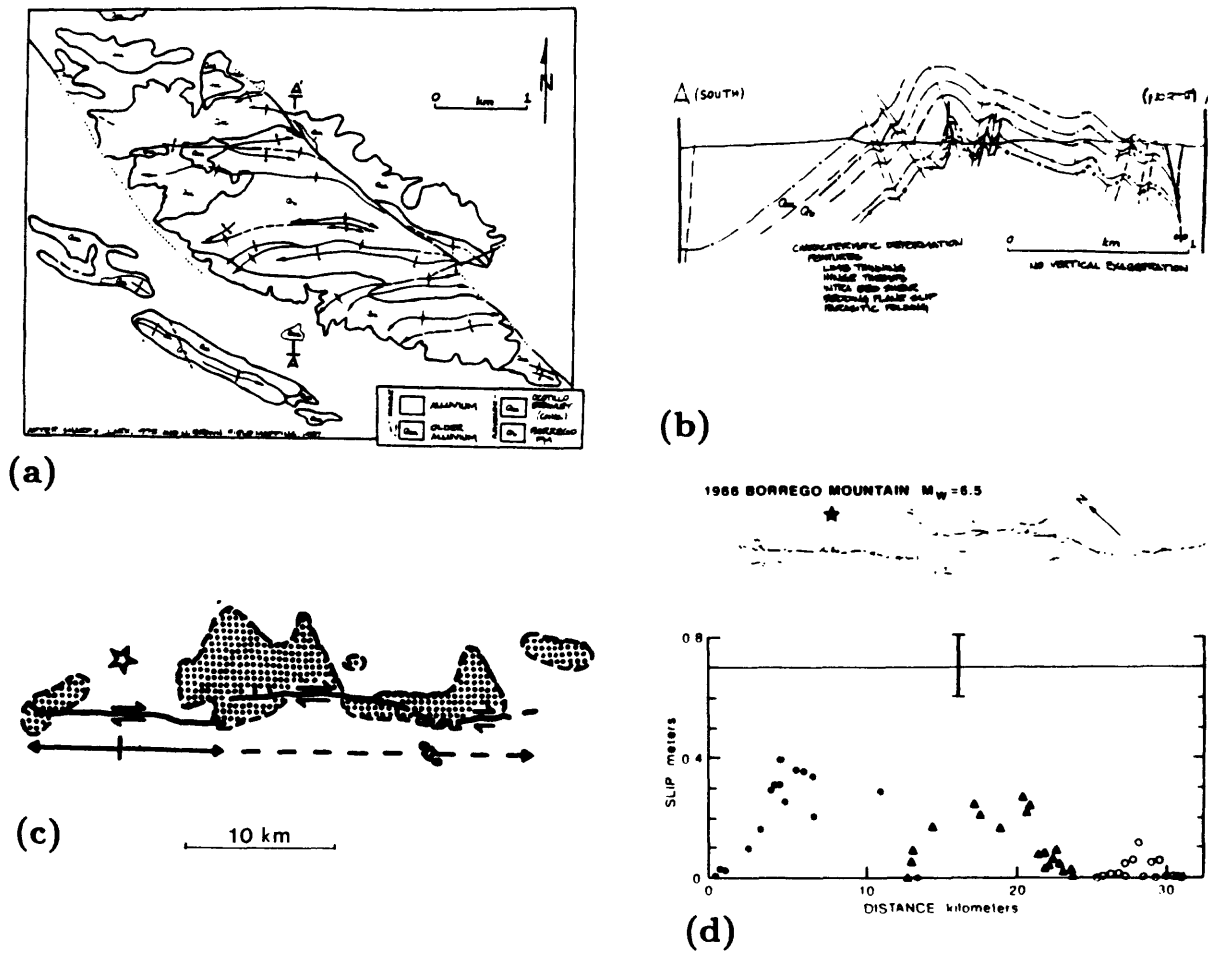

Figure 3. Structural and rupture characteristics of the Ocotillo Badlands. a) Simplified geological map of the Ocotillo Badland stepover (from Sharp and Clark, 1972, and Brown, 1988; taken from the Field Trip Guide accompanying this USGS Workshop), b) Schematic structural N-S cross-section of the Ocotillo Badlands (Brown, 1988; taken from the Field Trip Guide accompanying this USGS Workshop), c) Rupture characteristics of the 1968 Borrego Mountain earthquake. Star is the location of the epicenter, arrows indicate bilateral rupture and dotted areas illustrate the main concentrations of aftershocks (after Sibson, 1986, and Hamilton, 1972). d) Slip distribution along the Coyote Creek fault after the 1968 Borrego Mountain earthquake. The symbols represent the three main segments of the fault. A map view of the surface breaks is shown above the graph. The geodetic estimate of the slip is indicated as a straight line. This figure is from Thatcher and Bonilla (1988).

segment (Fig. 3d; Thatcher and Bonilla, 1988). These observations suggest two possibilities: (1) that the restraining stepover is only a shallow structure and the geodetic data reflect coseismic slip at depth, or (2) that afterslip on the fault evened out the final observed geodetic slip distribution.

Huya Fault, China

The second example, from China, is taken from Jones et al. (1984). The Huya fault, shown schematically in Figure 4a, is primarily a left-lateral strike-slip fault with a 12 km wide restraining stepover in its central part. The Songpan earthquake sequence was made up of three successive events (M_s = 7.2, 6.7 and 7.2) which occurred within the period of a week (an unusually rapid migration velocity). Based on fault plane solutions the second

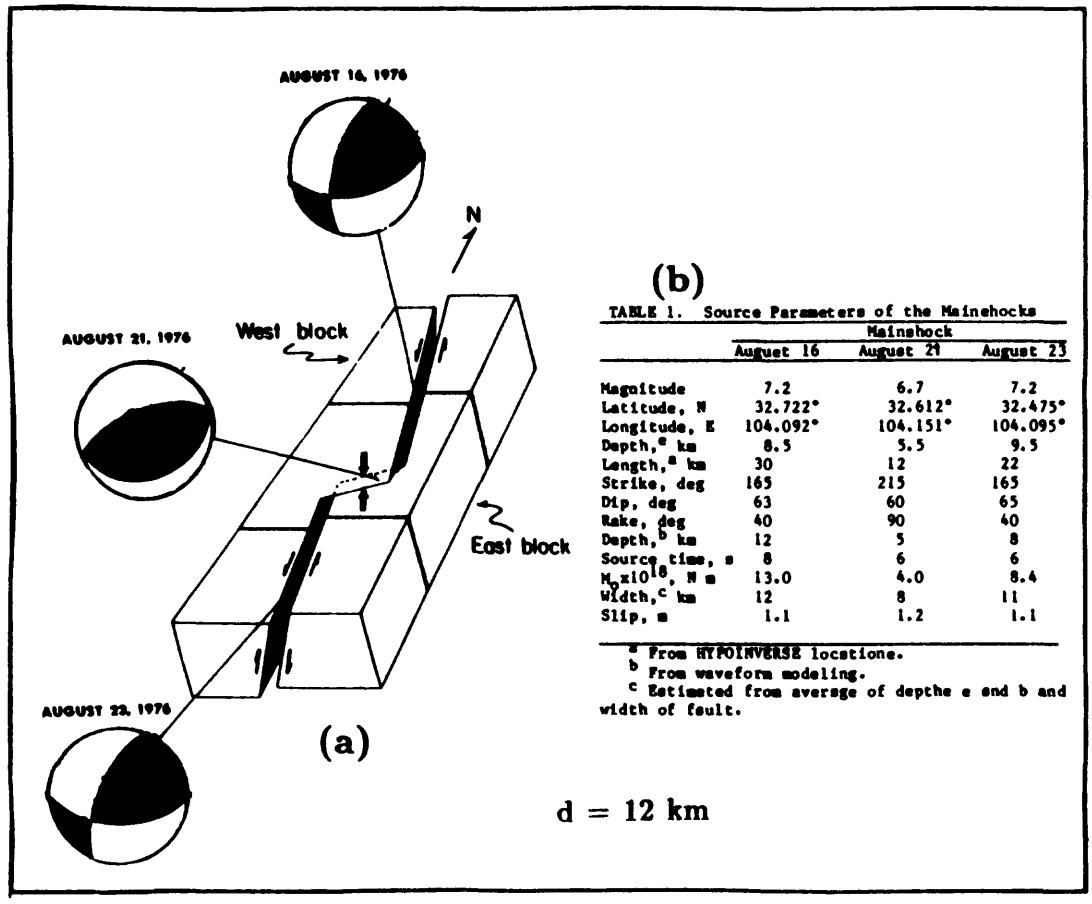

(b)

TABLE 1. Source Parameters of the Mainshocks

	Mainshock		
	August 16	August 21	August 23
Magnitude	7.2	6.7	7.2
Latitude, N	32.722°	32.612°	32.475°
Longitude, E	104.092°	104.151°	104.095°
Depth,[a] km	8.5	5.5	9.5
Length,[a] km	30	12	22
Strike, deg	165	215	165
Dip, deg	63	60	65
Rake, deg	40	90	40
Depth,[b] km	12	5	8
Source time, s	8	6	6
$M_o \times 10^{18}$, N m	13.0	4.0	8.4
Width,[c] km	12	8	11
Slip, m	1.1	1.2	1.1

[a] From HYPOINVERSE locations.
[b] From waveform modeling.
[c] Estimated from average of depths a and b and width of fault.

Figure 4. 1976 Songpan earthquake sequence, China, and summary of source parameters of the mainshocks (after Jones et al., 1984).

event, which is located in the restraining area, was characterized by reverse faulting whereas the other two were associated with a combination of left-lateral strike-slip and reverse faulting. From an inversion of teleseismic waveforms, the same amount of slip occurred during all three mainshocks (Fig. 4b). There was only a 20° difference between the slip vector orientation of the second shock and that of the first and third shocks. However, fault dimensions were smaller for the second mainshock than for the other two as evidenced both from waveform inversions and from aftershock locations using regional stations . These observations suggest that the second event had a higher stress drop than the other two events. No field measurements of surface displacement or surface fault geometry are available.

Çelikhan, Turkey

The third example, from Turkey, is the Çelikhan restraining stepover (Fig. 5). It is situated along the left-lateral East Anatolian fault zone. The stepover is approximately 5-7 km wide, and is characterized by extensive thrusting (Fig. 5). In the area of the stepover the East Anatolian fault zone intersects the older Bitlis suture zone. Thus, the the Bitlis thrust zone may have given rise to the stepover. The total displacement along the East Anatolian fault zone is about 20±5 km. We assume that the restraining stepover area has accommodated more shortening than that due to the East Anatolian fault because of the initial thrusting component. The fault strand northeast of the stepover consists either of two branches or of a new branch developing to avoid the stepover. According to Ambraseys (in press) the 1905 earthquake coincided with the NE segment. He also has documentation suggesting that the 1893 earthquake (M_s = 7.1) might have affected all segments of the stepover (Ambraseys, in press; see Figure 5). Since 1905 the area has been characterized by low to moderate seismic activity. Figure 5 includes fault plane solutions for three moderate size earthquakes that have occurred in the area.

Erzurum Fault Zone, Turkey

The final example is the Erzurum basin, in Eastern Turkey (Fig. 6). Although reliable historic records go back more than 2000 years in Eastern Turkey, no historical seismic activity is recorded in Erzurum before 1200 A.D. (Sipahioğlu, 1983). The stepover area is 15 km wide and includes a 23 km long thrust zone that forms the southern margin of the Erzurum ramp basin. This thrust zone appears to be migrating northward into the basin, and recent field observations have revealed that thrusts cut the most recent alluvial fan deposits in the basin (Barka and Bayraktutan, 1985). As in the previous example the

thrusting in this region is considered to be older than the strike-slip faults of the Erzurum fault zone. The NE segment consists of several parallel faults forming a 10 km wide left-lateral fault zone. The 1859 earthquake (I=IX-X) caused extensive damage in the basin and killed more than 15,000 people (Karnik, 1971). Most of the damage was associated with the southern margin of the basin. Seismic activity in this century has been low to moderate.

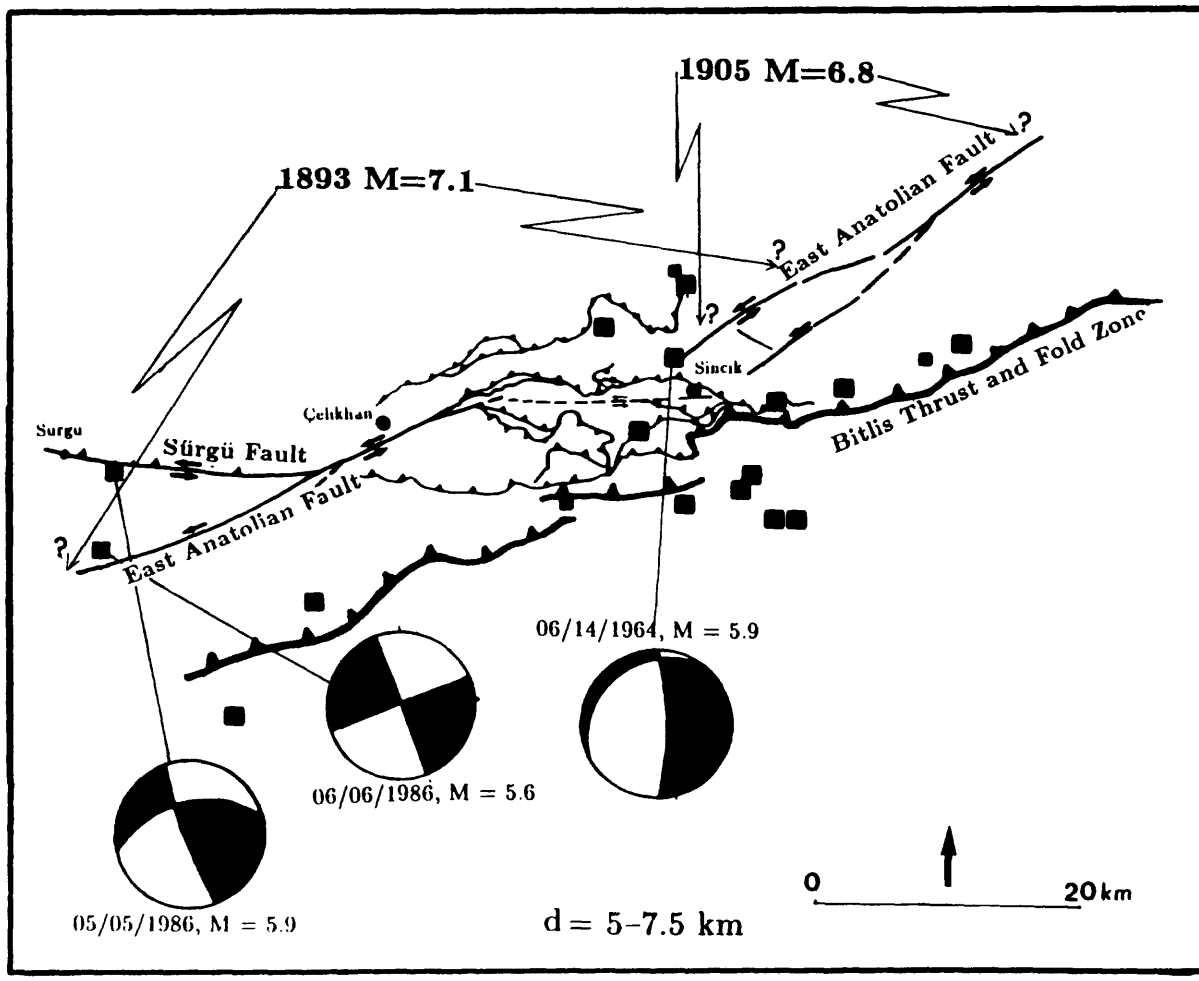

Figure 5. Çelikhan restraining stepover, East Anatolian fault zone, Turkey. Solid squares are epicenters of earthquakes that occurred between 1964 and 1984 (International Seismological Center data). Fault plane solutions of recent moderate earthquakes are from Jackson and McKenzie (1984) and from the International Seismological Center. Historical earthquake information is obtained from Ambraseys and Finkel (1987), and Ambraseys (in press). Geological data are derived from Arpat and Şaroğlu (1975), Perinçek et al. (1987) and Şaroğlu et al.(1987). The extent of these historical ruptures is not well known.

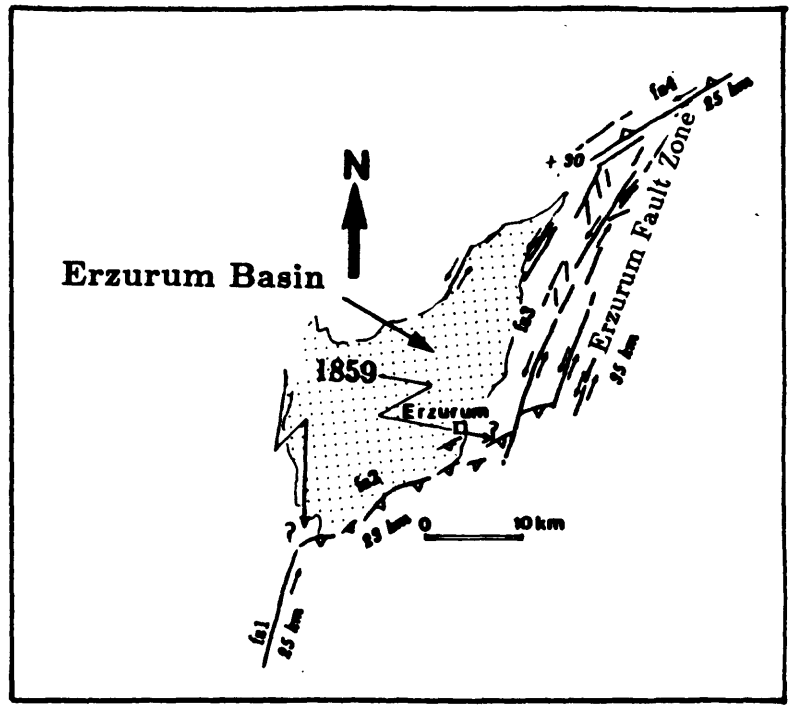

Figure 6. Simplified structural map of the Erzurum basin. The basin is a ramp basin associated with the thrust zone of the stepover area. From Karnik's (1971) description of the extent of damage the 1859 earthquake is interpreted to have occurred along the stepover thrust zone. Fault segments fs1-fs4 are 25, 23, 35 and 25 km long respectively (fs1 and fs4 are only partially shown in figure). A 30° restraining bend separates fs3 from fs4.

INTERPRETATION AND CONCLUSIONS

In Figure 7 we plot interpretive slip models for the four examples discussed above. From this figure and the preceding discussion, it appears that the size of the restraining stepover (d) is an important factor in determining whether a single earthquake rupture can propagate through the stepover, or if the stepover ruptures independently. In the latter case, the size of the earthquake that occurs within the stepover area may increase with d. From the first example it appears that when d is small (< 5 km) the stepover is a shallow structure. The exact width/depth ratio is difficult to determine without accurate knowledge of the thickness and rheology of the sedimentary layer, and knowledge of the orientation of the principal stresses relative to the fault plane. The influence of these two factors is suggested, respectively, by seismic reflection profiles of Harding (1985) and by the discussion of stresses in Naylor et al. (1986). Although small stepovers can arrest the slip at the surface, they may have little effect at depth. At shallow depths they may be responsible for delayed slip, as expressed by creep or by aftershock activity such as was observed after

after the 1968 Borrego Mountain earthquake (Clark, 1972; Thatcher and Bonilla, 1988). The Çelikhan stepover (d=5-7 km) is slightly wider. From the historical earthquake data it appears that the 1893 earthquake was a stepover earthquake affecting both strike-slip segments and the stepover area. The 1905 earthquake can be interpreted as making up

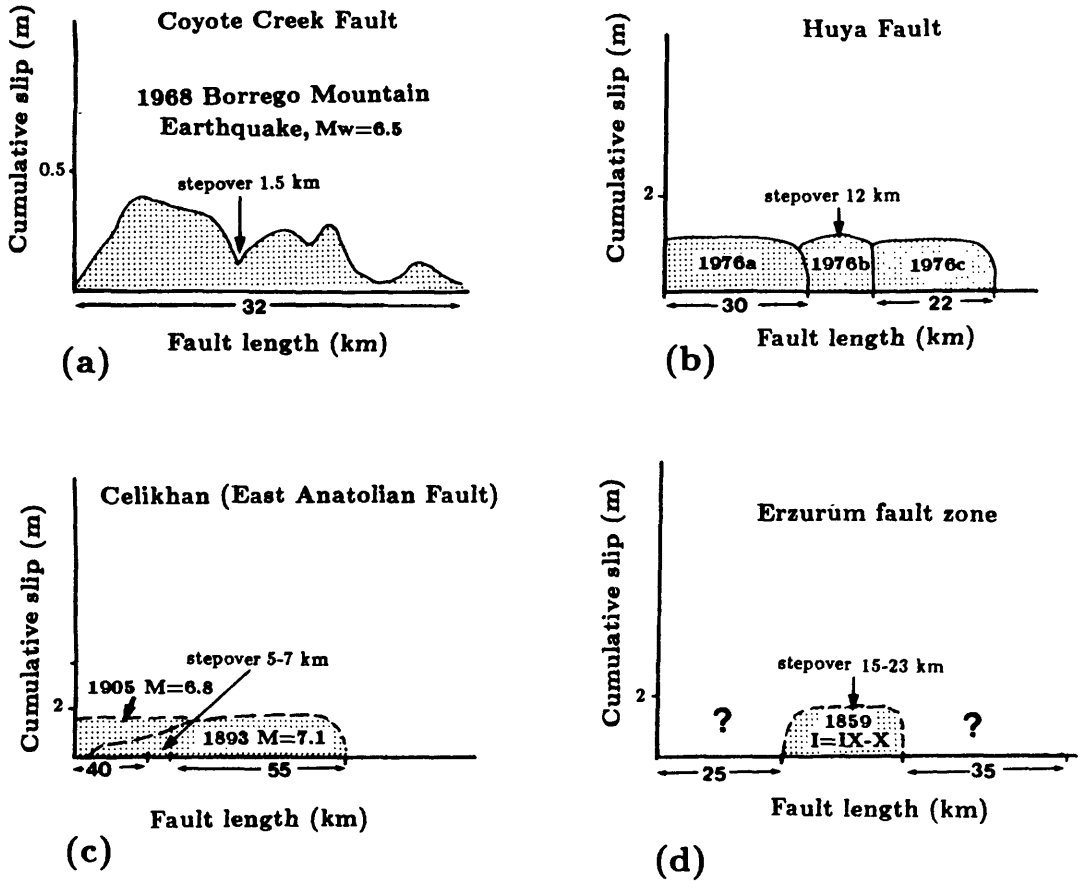

Figure 7. Summary of rupture characteristics of four restraining stepovers discussed in the text. The diagrams are set up according to the slip model suggested by Schwartz and Coppersmith (1984). (a)The surface slip is partly arrested by by the Ocotillo Badland stepover during the 1968 Borrego earthquake. (b) The Songpan earthquake sequence appears to consist of three distinctly separate events, although there is a lack of surface observations. (c) From intensity maps of the 1893 and 1905 earthquakes (Ambraseys, in press) we derive the interpretation shown here: that the 1905 earthquake made up a deficiency of slip at one end of the 1893 rupture zone. We speculate that the slip in 1893 may have been arrested by the stepover . (d) The strike-slip segments on each side of the Erzurum stepover are expected to rupture sometime in the future.

the slip deficiency at the northeastern end of the 1893 rupture zone. This interpretation results from the Borrego Mountain analogy, in which slip decreased south of the stepover (compare Fig. 7a and c). The Erzurum stepover situation is different in that the stepover area may already be ruptured, whereas the strike-slip segments appear to be unruptured. However, the data for the historical earthquakes in Figures 7c and 7d are not complete enough to draw any clear conclusions.

From the examples reviewed in this study we have been unable to resolve the issue of the relationship between stepover width and (1) stepover behavior at depth or (2) the depth of the seismogenic zone. Along the Coyote Creek fault (Borrego Mountain earthquake) the seismogenic zone extends to a depth of 12 km (aftershock distribution; Hamilton, 1972). The stepover is only 1.5 km wide at surface. In the case of the Huya fault (Songpan sequence) the seismogenic zone extends to a depth of 20 km (aftershock distribution; Jones et al., 1984). Here the stepover is 12 km wide at the surface. Jones et al. (1984) pointed out that the second mainshock of the sequence and its immediate aftershocks (in the stepover zone) are shallower than the first and third mainshocks (activity in the stepover mostly shallower than 10 km). The crust is appoximately 40 km thick in this area, although this thickness is not very well constrained (Jones et al. 1984). We do not know the depth of the seismogenic zone in the case of the Turkish stepovers (Çelikhan and Erzurum), however we can estimate it from other studies. The crust in Eastern Turkey is roughly 40-50 km thick from regional seismic and gravity data (Canitez and Toksöz, 1980; or interpretation of refraction data from Kadinsky-Cade et al., 1981). The seismogenic zone in the area of the 1983 Narman-Horasan earthquake (M_s = 6.9 strike-slip earthquake located near the Erzurum fault zone) extends to a depth of 20 km (based on Toksöz et al., 1984). The depth extent of the fault planes found by modelling waveforms of earthquakes in Eastern Turkey is less than 20 km for the 1975 Lice earthquake (M_s = 6.7 ; Nábělek, 1984) the 1976 Çaldiran earthquake (M_s = 7.4; Nábělek and Toksöz, 1984) and the 1983 Narman-Horasan earthquake mentioned earlier (Shortt, 1985). By comparison with these, results crustal thickness of 40-50 km and a seismogenic zone of thickness 20 km are probably reasonable estimates for both the Erzurum and Çelikhan fault zones. We have no evidence, however, for the depth extent of the stepovers themselves. In conclusion the differences in stepover width observed in this study may have more to do with sedimentary cover thickness and rheology, with the orientation of regional stresses relative to fault plane or with structures that predate the initiation of strike-slip faulting than with the thickness of the crust or seismogenic zone.

The large stepovers have the appearance of complex thrust zones. As the total displace-

ment within the stepover area increases, the stepover widens and more complex structures are formed. In the stepover area the displacement is taken up by a combination of many structures. This gives rise to crustal thickening and shortening. It also appears that, since d is less than 20 km in most cases, single very large earthquakes restricted to the stepover area should not occur. However, stress drops associated with stepover earthquakes may be equal to or higher than those on either side of the stepover due to the type of faulting (thrusts versus strike-slip fault, see, e.g., Sibson, 1984). This difference could be very important for earthquake hazard studies.

Another characteristic of restraining stepovers, supported by the above data, is that they may act as barriers rather than as asperities (e.g. 1968 Borrego Mountain earthquake, 1976 Songpan sequence and the Çelikhan stepover earthquakes of 1893 and 1905).

ACKNOWLEDGEMENTS

We would like to thank to Prof. N. N. Ambraseys for his comments on the historical earthquakes in the vicinity of the Çelikhan stepover and Prof. R. Sibson for helpful comments on an earlier draft. This work was supported by U.S. Geological Survey contract 14-08-0001-G1151, and NASA grant NAG5-753.

REFERENCES

Ambraseys, N. N., in press. Temporary seismic quiescence: SE Turkey, Geophysical Journal.

Ambraseys, N. N. and Finkel, C. F., 1987, The seismicity of the northeast Mediterranean region during the early twentieth century, Ann. Geophys., v. 5B(6), p. 701-726.

Arpat, E. and Şaroğlu, F. 1975, Some recent tectonic events in Turkey, Bull. Geol. Soc. Turkey, v. 18, p. 91-101

Arpat, E., Şaroğlu, F. and İz, H. B., 1977, 1976 Çaldiran earthquake, Yeryuvari ve Insan, v. 2, p. 29-41.

Barka, A. A. and Bayraktutan, S., 1985, Active fault patterns in the vicinity of the Erzurum basin (abstract), paper presented at the 39th Annual Geological Congress, Geological Society of Turkey, Ankara.

Barka, A. A. and Kadinsky-Cade, K., 1988, Strike-slip fault geometry in Turkey and its influence on earthquake activity, Tectonics, v. 7, p 663-684.

Brown, N., 1988, Structural summary map and cross-section, Ocotillo Badlands. In: Field trip guide. USGS Workshop on Fault segmentation and controls of rupture initiation

and termination, March 6-9, 1988, Palm Springs, California.

Canitez, N. and Toksöz M. N., 1980, Crustal structure in Turkey, M. I. T. Earth Resources Laboratory Internal Report.

Clark, M., 1972, Surface rupture along the Coyote Creek fault. U.S. Geol. Surv. Prof. Pap. 787, p. 55-86.

Hamilton, R. M., 1972, Aftershocks of the Borrego Mountain earthquake from April 12 to June 12, 1968, U.S. Geol. Surv. Prof. Pap. 787, p. 31-54.

Harding, T. P., 1985, Seismic characteristics and identification of negative flower structures and positive flower structures, and positive structural inversion, Am. Assoc. Pet. Geol. Bull., v. 69, p. 582-600.

Jackson, J. and McKenzie, D., 1984, Active tectonics of the Alpine-Himalayan Belt between western Turkey and Pakistan, Geophys. J. R. Astron. Soc., v. 77, p. 185-265.

Jones, L. M., Han, W., Hauksson, E., Jin, A., Zhang, Y. and Luo, Z., 1984, Focal mechanisms and aftershock locations of the Songpan earthquakes of August 1976 in Sichuan, China, J. Geophys. Res., v. 89, p. 7689-7697.

Kadinsky-Cade, K., Barazangi, M., Oliver, J. and Isacks, B., 1981, Lateral variations of high frequency seismic wave propagations at regional distances across the Turkish and Iranian plateaus, J. Geophys. Res., 86, p. 9277-9396.

Karnik, V., 1971, Seismicity of the European area, Part 2, D. Reidel, Hingham, Mass., 218 pp.

Nábělek, J., 1984, Determination of earthquake source paramaters from inversion of body waves, Ph.D. Thesis, M. I. T., Cambridge, Mass., 361 pp.

Nábělek, J. and Toksöz, M. N., 1984, The November 26, 1976 M_s = 7.4 Çaldiran earthquake, M. I. T., Earth Resources Laboratory Internal Report.

Naylor, M. A., Mandl, G. and Siypestieyn, C. H. K., 1986, Fault geometries in basement-induced wrench faulting under initial stress states, J. Struct. Geol., v. 8, 737-752.

Perinçek, D., Günay, Y. and Kozlu, H., 1987, New observations on strike-slip faults in east and southeast Anatolia, 7th Petroleum Congress of Turkey, Ankara, p. 89-103.

Şaroğlu, F., Emre, O. and Boray, A., 1987, Active faults of Turkey and their earthquake activity, Unpubl. Rep. of Mineral Research and Exploration Institute of Turkey, 394 pp.

Sharp, R. V. and Clark, M., 1972, Geologic evidence for previous faulting near the 1968 rupture on the Coyote creek fault, U.S. Geol. Surv. Prof. Pap., 787, p. 5-14.

Schwartz, D. P. and Coppersmith, K. J., 1984. Fault behavior and characteristic earthquakes: Examples from Wasatch and San Andreas faults, J. Geophys. Res., v. 89, p.

5681-5698.

Shortt, E., 1985, Source characterization of the October 30, 1983 Narman-Horasan earthquake, M.S. Thesis, M. I. T. Cambridge, Mass., 81 pp.

Sibson, R. H., 1984, Roughness at the base of the seismogenic zone: Contributing factors, J. Geophys. Res., v. 89, p. 5791-5800.

Sibson, R. H., 1986, Earthquakes and lineament infrastructure, Philos. Trans. R. Soc. London, v. 317, p. 63-79.

Sipahioğlu, S., 1984, A study of earthquake activity along the North Anatolian fault and its vicinity, Bull. Earthq. Res. Inst. of Turkey., v. 45, p. 5-139.

Soysal, H., Sipahioğlu, S., Kolçak, D. and Altınok, Y., 1981, Historical earthquake catalogue of Turkey and its vicinity. Turk. Sci. Res. Found. TBAG, 341, 122 pp.

Thatcher, W. and Bonilla, M. G., 1988, Earthquake fault slip estimation from geologic, geodetic and seismologic observations: Implications for earthquake mechanics and fault segmentation. In abstract from USGS Workshop on Fault segmentation and controls of rupture initiation and termination, March 6-9, 1988, Palm Springs, California.

Toksöz, M. N., Guenette, M., Gülen, L., Keough, G. and Pulli, J. J., 1984, Source mechanism of the Narman-Horasan earthquake of 30 October 1983 in northeastern Turkey (in Turkish), Yeryuvari ve Insan, v. 8, p. 47-52.

Slip Distribution on Oblique Segments of the San Andreas Fault, California: Observations and Theory

Roger Bilham
CIRES and Department of Geological Sciences
University of Colorado, Boulder, CO, 80309-0449

Geoffrey King
U. S. Geological Survey, MS 966
DFC Box 25046 Denver, CO 80225

ABSTRACT

The active trace of the San Andreas fault is treated as a geometric surface defined by 68 contiguous, straight, vertical fault segments with lengths of 2-38 km. A slip vector for each segment is inferred from global plate motions. An approximately gaussian distribution of obliquity centered at 6°-8° convergent with the slip vector is evident. The distribution of segment lengths is strongly peaked at 12 km. A mechanism for the persistence or creation of 12-km-long segments appears to exist.

It is necessary that slip along a plate boundary is uniform over geologic time. However, during individual earthquakes slip is non uniform. The identification of characteristic earthquakes is based on the observation that slip appears to reproduce the irregular slip distribution of previous earthquakes. A possible reason for non uniform slip is the segmented geometry of the fault zone. We present observational data from the 1906 and 1857 earthquakes that suggest that the slip on oblique fault segments is reduced compared to segments parallel to an applied slip vector. Slip velocities along the creeping zone of central California appear to attain a maximum velocity at inferred obliquities of 8°.

In an attempt to reconcile the long-term behaviour of the San Andreas fault, and the short-term observed behaviour of the fault, we focus on the slip behaviour of a single element of a segmented plate boundary. Using frictionless boundary-element models we show that slip is reduced at a transpressional offset on a vertical fault. We show that this reduction of slip may be made arbitrarily large by permitting fault-normal displacements near the fault zone. Finally we examine the distribution of slip on the geometrically complex 1906 rupture. A reasonable fit to the observed coseismic-slip data is obtained by permitting free strike-slip and fault-normal displacements along the fault zone.

We conclude that slip is reduced at an oblique fault segment compared to slip on contiguous slip-parallel segments. Slip that does not appear on the fault is manifest as off-fault deformation. Our findings are consistent with geodetic and geological observations of fault-normal displacements surrounding active faults and provide a physical basis for the recurrence of characteristic earthquakes on faults of complex geometry.

INTRODUCTION

In one of the earliest publications on plate-tectonics, Morgan (1968) articulates the consequences of oblique slip on a transform plate boundary: "The tensional or compressional features of California are qualitatively explained by the difference in strike of a feature and the average strike of the region. The Salton Trough (general strike 150°) is a depressed region; the Salton Sea is 75 meters below sea level. ....In contrast the Transverse Range (general strike 110°) reaches an altitude of 3 km."

Oblique slip results in deformation near a fault zone. This may be manifest in the morphology of the fault zone and its surroundings (Bilham and King, 1989) and as fault-normal displacement (Hurst and Bilham, 1986, Minster and Jordan 1987, Segall and Harris, 1987). A reduction of surface area arises from slip at an convergent oblique fault (Bilham and Hurst, 1988) for the same reason that a reduction in surface area accompanies subduction. A third result may be that the magnitude of slip on oblique segments differs from that on contiguous slip-parallel segments. In examining this possibility we present observational data and theoretical models that support the hypothesis that slip on an oblique fault reduces as its strike increases relative to the applied slip vector.

SEGMENT IDENTIFICATION AND GEOMETRICAL CHARACTERISTICS

The fault trace of the San Andreas system may be reduced to a series of contiguous straight segments with lengths 2-35 km. Data were obtained from the following sources: Clarke (1984), Dibblee (1973), Lawson (1908), Brown (1970), Vedder and Wallace (1970), Brown and Wolfe (1972), and Sarna-Wojcicki et al. (1975). Figure 1 illustrates a map view of the San Andreas Fault projected onto a mercator projection centered on the RM2 pole of rotation between the Pacific and North American plates. In this figure and in later views of detailed parts of the fault the projection has been expanded normal to the slip vector. The kinematic problem associated with plate boundary slip is clearly evident in these projections. Only the main trace of the San Andreas system is examined. The fault trace has been reduced to 68 contiguous segements.

The identification of the segments in figure 1 is in many cases unequivocal. A segment is always terminated by a bend or an offset. These bends and offsets are often clear features on the fault zone. They may not, however, be obvious on detailed strip maps of the fault zone because printed fault zone maps are frequently segmented at precisely those locations identified as bends between segments. Minor changes in strike sometimes result in uncertain lengths to the segments selected. In such cases unmarked maps of the fault zone were prepared and presented to several investigators who were asked to identify bends in the fault zone. In many of these cases the same locations were picked as bends in the fault zone. Remaining ambiguities do not alter the conclusions of this article.

In southern California, surface scarps and fissures between the Salton Sea and the Mission Creek fault are found within a fault zone whose width is less than 1 percent of the length of the segment. In other places where the width of the fault zone is large compared to segment length, segments have been delineated by the manifestation of a significant change in the characteristics of the fault zone along strike. An example of the latter is the San Andreas fault between Black Mountain and San Juan Bautista in central California. In this area, changes in the style and

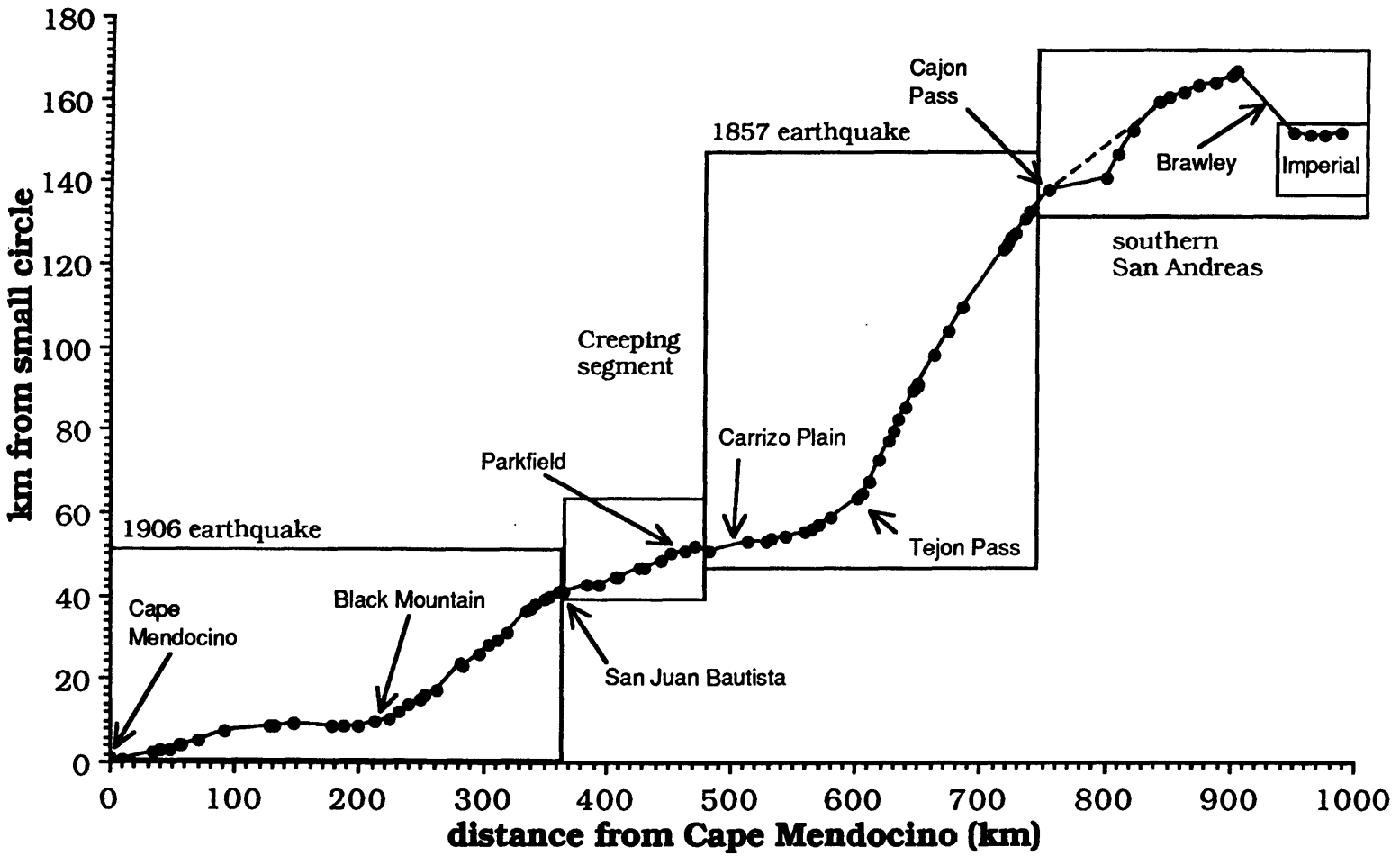

Figure 1 Transverse mercator projection of the San Andreas Fault between Cape Mendocino and the Mexican Border. Each dot signifies a bend between two straight segments. The boxed areas outline regions discussed in the text.

width of faulting within the fault zone suggest differences in fault behavior along strike.

Histograms summarizing the properties of 68 segments (Bilham and Hurst, 1988) are shown in Figure 2. Each segment has length and obliquity (the difference between the strike of the fault and the local slip vector inferred from the RM2 pole of rotation). The approximately gaussian histogram of segment obliquity shows the dominant strike of the fault to be 4°-6° resulting in overall compression. This corresponds to the mean strike of the fault in California. However, the histogram of segment length reveals a peak at 12 km. This was first noted by Wallace (1969), who drew attention to the correspondence between this length and the depths of the deepest earthquakes on parts of the San Andreas system. In a statistical analysis of segment length in the Coachella valley a segment length of 12.15 ± 0.15 km was found to best characterize five contiguous segments (Bilham and Williams, 1985).

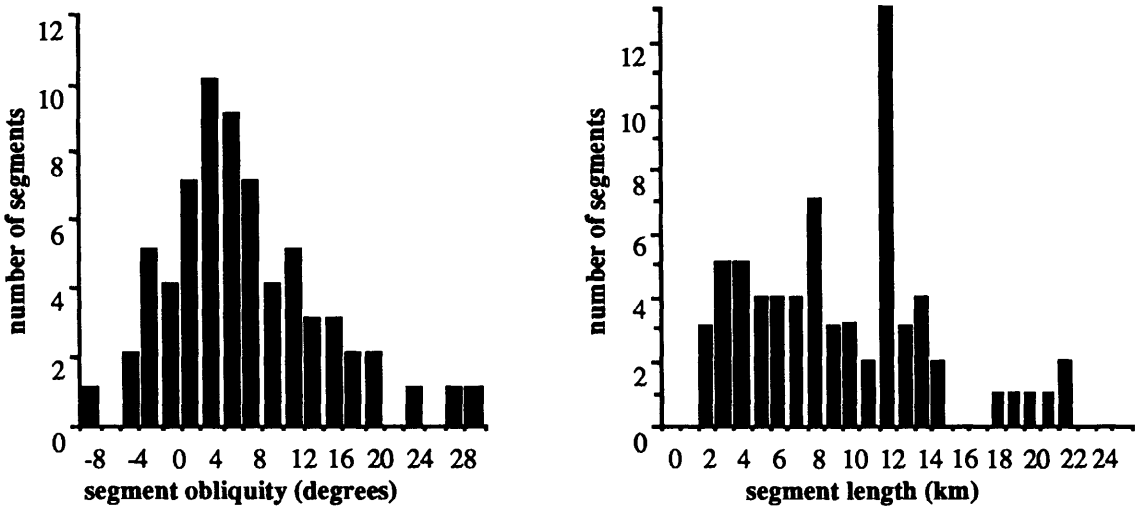

Figure 2. Distribution of length and obliquity for segments of the San Andreas fault shown in figure 1.

Unless it is a coincidence, the significance of *any* dominant segment length on the San Andreas fault is that it must represent a kinematically stable condition for the fault zone. To understand why this should be so, consider a fault which consists entirely of a saw-tooth arrangement of segments of length, say, 12 km. After a few million years and many earthquakes the boundary will have slipped, say, 4 km. The fault will now look different. A future geologist might map the fault as an equal number of 4- and 8-km segments. Thus, the observation that there is a dominant segment length implies that one or more of three mechanisms maintains their existence:

1. 12 -km segments have recently been created and have not yet been destroyed by fault slip.
2. 12-km segments are in some way favored by fault zone processes. Smaller and larger segments are less stable.
3. 12 km represents the maximum growth length for a stable fault segment. Segments start smaller and fail to grow larger.

MORE OR LESS SLIP AT AN OBLIQUE SEGMENT?

Few of the 68 segments in figure 1 are parallel to the slip vector. Is slip reduced or

increased at an oblique segment? Two descriptions for slip at the oblique segment may be forwarded based on an intuitive understanding of fault kinematics (see fig. 3).

Hypothesis (i) Since particles adjacent to the fault must move further on an oblique segment than on a slip-parallel part of the plate boundary, slip should be larger at an oblique offset. *Thus, slip on an oblique fault segment is always larger than slip on segments parallel to the slip vector.*

Hypothesis (ii) Since material near the oblique segment must deform, slip on nearby faults may occur. Slip along the fault itself is effectively reduced. *Thus slip is reduced on an oblique segment, compared to slip on a segment parallel to the slip vector.*

Which of these models for oblique slip occurs in nature? The apparent problem with hypothesis (ii) is that if slip is reduced at an oblique segment during every earthquake, then a slip deficit will accumulate at this location. This appears to conflict with common-sense. In the long term, slip must be uniform along a fault. At a convergent plate boundary this concept forms the basis of seismic-gap theory. However, advocates of (ii) include those who seek a physical basis for the recurrence of characteristic earthquakes. A characteristic earthquake (Schwartz and Coppersmith, 1984) is one that repeatedly exhibits the same slip distribution along a certain segment of a fault, apparently defying the uniformity of along-fault slip demanded over geologic time.

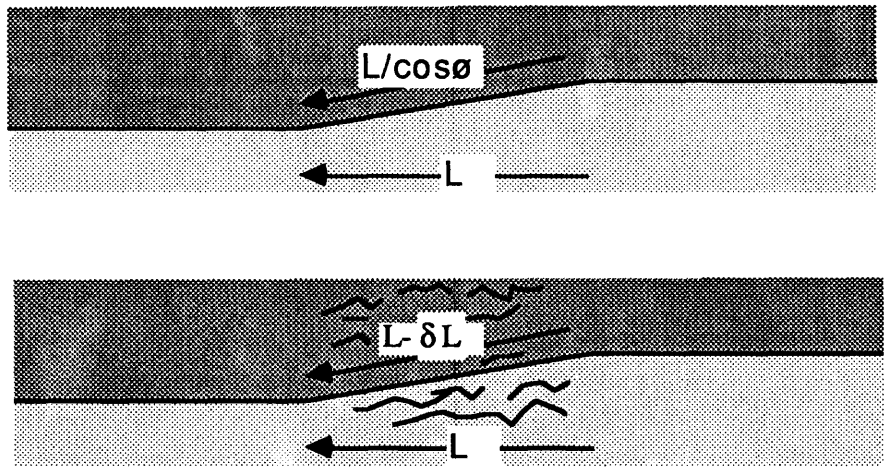

Figure 3. Two views of slip along an oblique segment. In the upper figure slip is greater at an oblique segment in order to keep up with motion on adjacent parts of the fault. In the lower figure slip is less along the oblique segment because deformation occurs within the surrounding medium.

It is believed that the reason for this apparent paradox is the false assumption that fault geometry is constant over geologic time. A slip-deficit can indeed occur for small amounts of slip. Twenty or more earthquakes cumulatively result in slip that is small compared to typical segment lengths. However, after several thousand earthquakes a substantial slip deficit will accumulate. This slip-deficit will ultimately result in stresses large enough to create new fractures that permit the fault to move more easily, or will deform the region surrounding and including the fault. Prolonged slip must inevitably change the geometry of the fault zone through either or both of these mechanisms.

In the next section we present observations of slip, or slip rate, related to the obliquity of fault segments. The observational data appear to favor hypothesis (ii) in that slip appears to decrease with increasing obliquity. In the following section we present two theoretical models that emulate these observations. Finally, we compute a synthetic slip distribution for a complex fault zone of irregular geometry and finite slip distribution.

OBSERVATIONS OF SLIP ON OBLIQUE SEGMENTS

Slip during the 1906 earthquake.

Table 1 lists seismic slip recorded along San Andreas fault in 1906 (Lawson and others, 1908). Values for slip were obtained for only 12 of the 26 segments identified along the 1906 rupture. In some cases cases several observations of slip were recorded. These are not always identical for a given segment. The obliquity of each segment was calculated from the RM2 pole of rotation (Bilham and Hurst 1988, Minster and Jordan, 1984). The use of revised pole of rotation (Minster and Jordan, 1987) reduces the obliquity of most of the segments by approximately 2° which does not alter the substance of the conclusions in this analysis. In figure 4, the obliquity of each segment is plotted as a function of slip. There is a clear reduction in slip with increasing segment obliquity. Maximum slip occurs on the Tomales Bay segment which is within 3° of the RM2 slip-vector and within 1° of the revised slip vector.

Table 1. Segments associated with slip during the 1906 earthquake.
(Segments are named for reference only. Obliquity of each segment is relative to the RM2 slip vector)

Segment	Length (km)	Strike NW	Obliquity degrees	1906 slip (m)
Arena	≥8.7	30	-2.2	4.86, 4.87,4.72
Garcia	25.9	35.4	3.2	3.1
Gualala	5.4	39	6.3	
Miller	7.3	36.5	3.8	
S.Fork	8.1	39	6.2	2.44
Plantation	2	33	0	
Fort Ross	13.1	39	6.1	2.44, 2.29, 3.5, 3.73
Ocean	21.5	38.5	5.5	
Tomales	36.5	35	1.9	6.1
Olema	4.2	31	-2.2	4.57
Bolinas	15.8	36	2.7	4.1, 4
Golden Gate	30	32	-1.3	
Mussel Rock	>10	36	1.6	
San Andreas L	12	33	0	5.1, 2.4, 4
Menlo Park	12	38.5	5	3.1, 2.4
Stanford	12.5	35.5	2	
Black Mtn.	6.7	49	15.5	
Montebello	8.3	47	14.5	0.9
Congress	9.3	41	7	
Lower Dam	5.6	48	14	
Wright	8.2	42	8	1.52
Landslide	20.4	52	18	
Loma	3.1	33	-1.8	
Next	12.4	47	12.8	
Chittenden	7.7	51	16.5	0.94, 1.3
San Juan	8. 5	46	11.5	

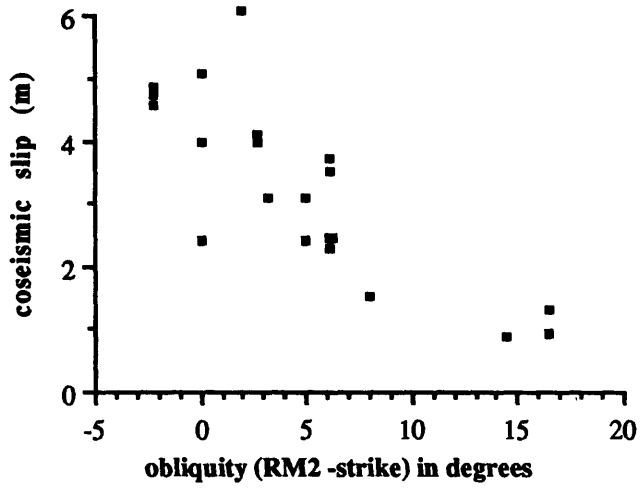

Figure 4. Observed relationship between segment obliquity and slip during the 1906 San Francisco earthquake.

Observations of 1906 slip are neither complete nor totally reliable. For example, the timing of the measurements is poorly known. Fault afterslip could have resulted in the observation of inappropriately small values for slip if the investigations of fault slip were made within a few days of the earthquake. In some California earthquakes, afterslip more than doubles the apparent coseismic signal. If afterslip occurred and the investigations were spread over several months then the documented coseismic slip signal could be misleading. At a location near Wright Tunnel left-lateral slip is recorded. Thatcher and Lisowski (1987) discuss several of the shortcomings inferred to exist in the coseismic slip data. Given these uncertainties, it is perhaps unwise to draw too great a significance from the approximately linear slip/obliquity relationship manifest in 1906. Yet it is clear that the data *do not* support hypothesis (i).

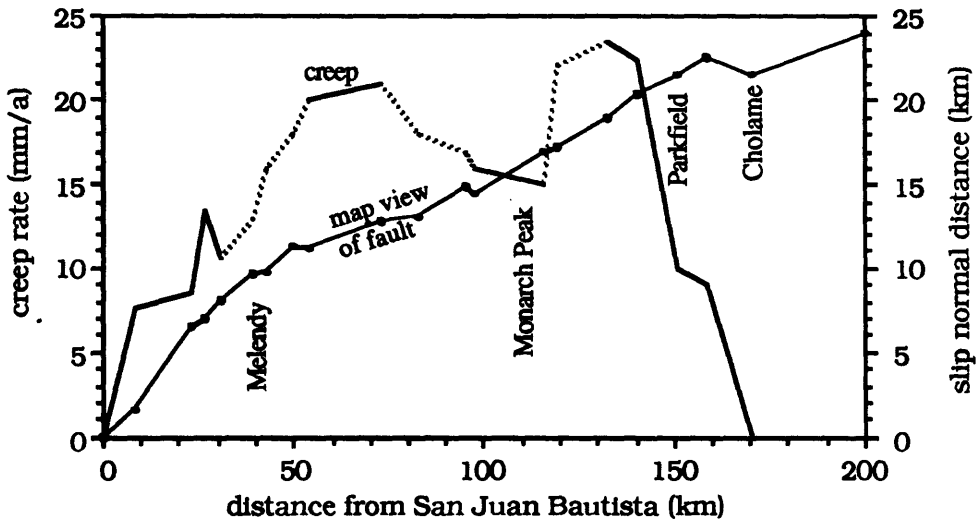

Figure 5. Distribution of creep rates on segments of the San Andreas fault in central California. The geometry of the fault is shown in map view as the solid line in the Figure. Creep data are interpolated for 7 of the 19 segments (dotted lines). Slip data from Schulz et al. (1984) .

Aseismic Slip in Central California

Nineteen segments are identified in the creeping section of the San Andreas Fault between

San Juan Bautista and the Cholame Valley. A plan view of these segments and their associated slip velocities are shown in fig. 5. A clear relationship between segment obliquity and slip velocity is not evident (fig. 6), although there is weak evidence for faster slipping segments to be at obliquities near 8 degrees to the applied slip vector.

The obliquity/velocity sample is clearly influenced by the tapered distribution of slip near the ends of the creeping zone where 50 percent of the data are obtained. We have attempted to normalize the data by computing a synthetic slip distribution assuming that all the segments in Fig. 5 are vertical, contiguous, frictionless dislocations. We have ignored creep on the Calaveras fault in this model, which may introduce errors near the northern end of the creeping zone where it interacts with the San Andreas fault (Mavko 1982). The difference between observed creep and synthetic slip is indicated by solid dots in Fig. 6 (right). The difference between the observed and synthetic slip also suggests that maximum slip occurs at an obliquity of 8° to the inferred RM2 slip vector, and is reduced on segments with smaller and greater obliquity.

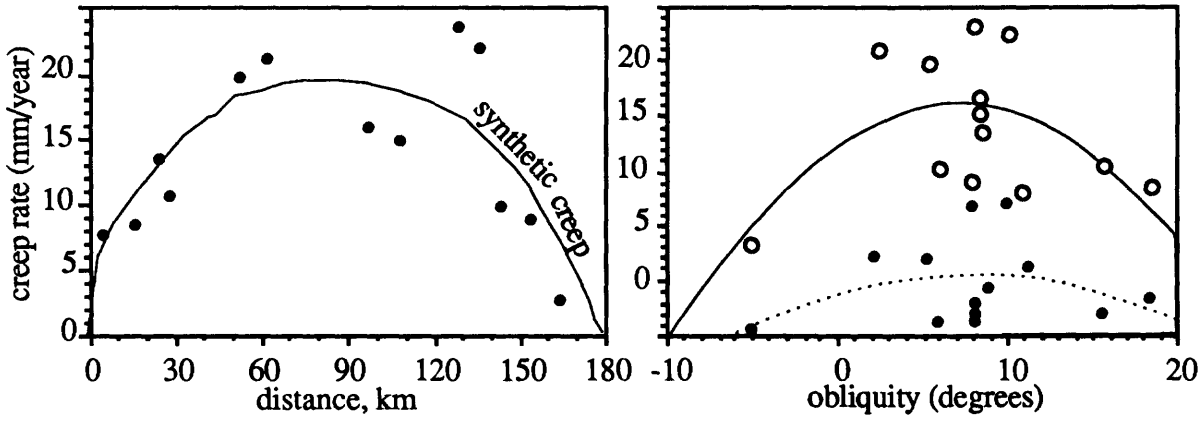

Figure 6. The left figure shows observed creep (1974-1986) in central California compared to synthetic slip calculated for a freely-slipping fault with the geometry of Fig. 5, and an applied RM2 slip vector. The applied boundary shear has been scaled to best fit the observed creep data. Fig. 6 right shows the distribution of observed creep, and observed-synthetic creep compared to segment obliquity. The two curves at right are least-squares cubic fits to the observed data (solid) and to the difference between the observed data and synthetic slip (dotted).

Characteristic Earthquakes between Cajon pass and the Carrizo plain

Geological investigations in the region of the 1857 San Andreas Fort Tejon earthquake reveal that earthquakes recur with a slip distribution that mimics the previous event at that location (Sieh 1981). This characteristic slip is plotted in figure 7. The data are sparse but suggest that slip on segments with large obliquity is smaller than on segments with small obliquity. The difficulty with this data set is that the effects of subsidiary faults (for example, the Garlock fault) is presumably substantial. Moreover, motion of the Mojave block results in an uncertain local slip vector for this part of the fault zone.

The northern Carrizo Plain is apparently anomalous in that a segment of small obliquity is associated with small slip. One explanation for low slip in this region is that it is close to the end of the 1857 rupture and coseismic slip tapers to low values in such locations. A second reason is that the area is believed to have a shorter recurrence time than 1857-type events. The data set presented in figure 7 is thus less homogeneous than data presented in figures 4-6.

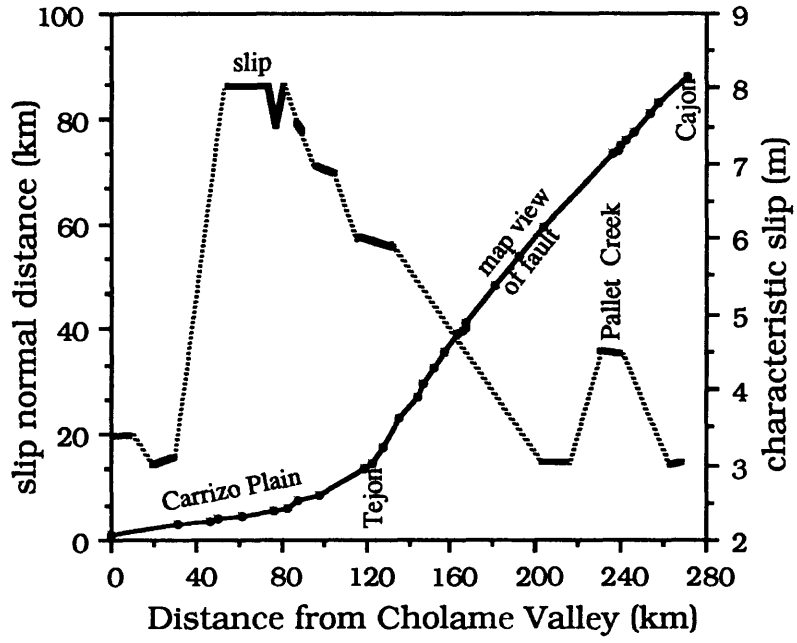

Figure 7. Fault geometry (solid line) and characteristic slip (broken line, from Fig. 15, Sieh 1981) on the San Andreas in the region of the 1857 earthquake. Distance is plotted along the RM2 slip vector. Slip normal distance is foreshortened to exaggerate the geometry of the fault.

BOUNDARY ELEMENT MODELS FOR OBLIQUE SLIP ON A VERTICAL SEGMENT

A simple estimate for the magnitude for slip on an oblique segment can be derived from elastic modeling. Consider the 12-km-long restraining (transpressional or antidilational) offset in a fault zone shown in figure 8. The restraining offset consists of an oblique segment separating two infinitely-long, contiguous, slip-parallel segments. A boundary element model was computed (Crouch and Starfield, 1983) in which shear was applied to the region and the oblique segment permitted to slide freely. The resulting dilatational strainfield shown in figure 8 is similar to models discussed by Bilham and King (1989).

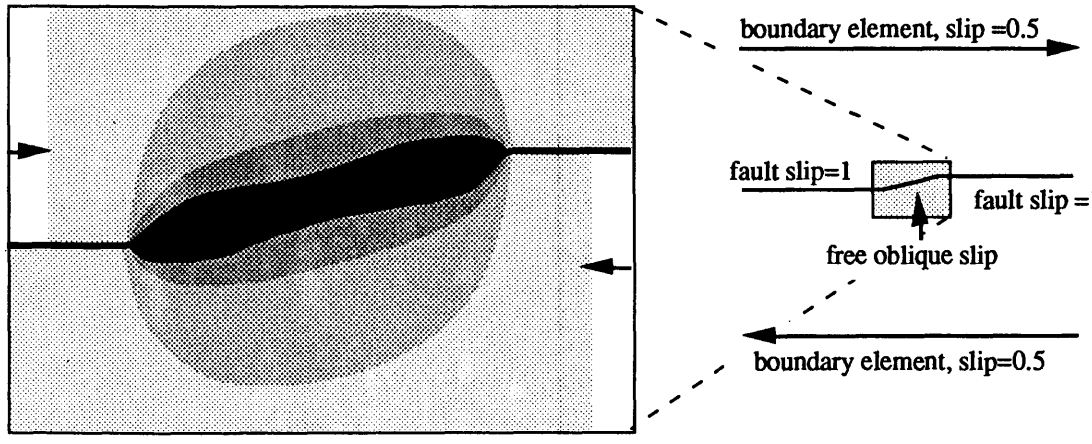

Figure 8. Compression at an oblique segment between two infinitely long segments parallel to the slip vector (sketch of geometry on right). Compression dilatational strain in the figure on the left is represented by shading. The model is used to examine the reduction of slip on the freely slipping oblique segment.

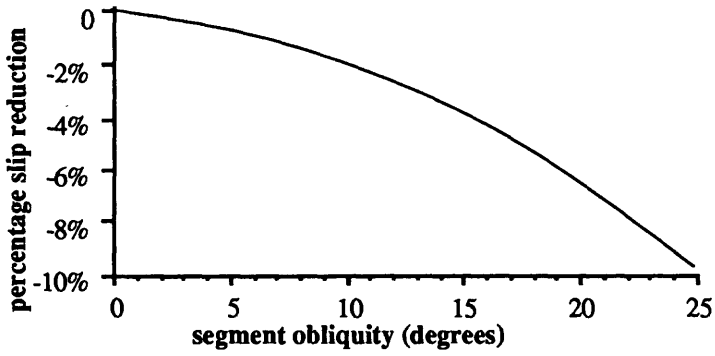

Figure 9. Reduction in slip with increasing segment obliquity. The slip is that measured at the center of a freely slipping (frictionless) segment in response to boundary-element geometries shown shown in Figure 8.

The slip along the oblique segment predicted by the model reduces with increasing segment obliquity (figure 9). Slip at the center of a 25° segment is reduced by up to 10 percent. Numerous tests of numerical stability were conducted. It was possible to partly suppress this reduction in slip by introducing boundary elements at the ends of the contiguous slip-parallel faults. However, it was not possible to increase slip at the oblique segment to a value larger than slip on the slip-parallel segments by any combination of elements with the geometry shown in figure 8. This simple frictionless model appears to support hypothesis (ii) but the reduction of slip at the offset in the fault zone is always smaller than that suggested by observational data. Accordingly a more complex boundary element model was constructed (Fig. 10). This model includes two elements parallel to the oblique segment that were permitted to move freely both in strike-slip and in a fault-normal sense. These additional faults may be considered to represent thrust faults parallel to the oblique segment. Alternatively, they can be considered to represent a compliant fault zone. Four types of boundary elements were used in the model. External boundary conditions were imposed outside the zone of interest to simulate the applied plate-boundary shear strain. These are indicated in figure 8 but are not shown in figure 10. The three boundary elements shown in figure 10 include slip-parallel elements of essentially infinite length on which unit slip is imposed. These are linked to elements that are permitted one degree of (strike-slip) freedom only. The third type of element is permitted two degrees of freedom - strike-slip and fault-normal slip. In the boundary element model, all the faults were subdivided into various combinations of sub elements to test for the stability of the resulting solutions. The maximum number of sub elements in each fault segment was 19. Stable solutions for slip were obtained for models that included five or more sub elements.

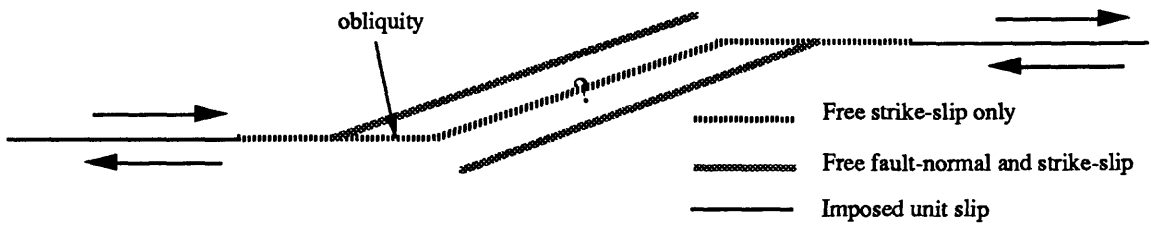

Figure 10. Boundary-element geometry used to obtain slip data illustrated in figure 11.

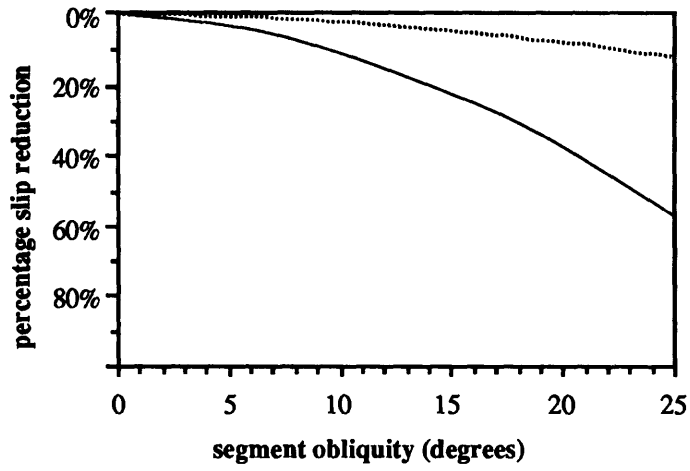

Figure 11. Reduction of slip with increasing segment obliquity for the model shown in figure 10. The reduction of slip is approximately a factor of 4 larger than that shown in figure 9 (dotted line above).

As in the simple model shown in figures 8 and 9, slip is reduced at the central oblique segment. However, the reduction of slip predicted by the model is less than 20 percent at 10° obliquity compared to a 60 percent apparent reduction in slip manifest in the 1906 slip data. By extending existing freely-slipping elements, or by adding additional freely slipping elements it is possible to reduce further the slip on the throughgoing oblique segment.

SLIP DISTRIBUTION ON A COMPLEX SEGMENTED FAULT

The analyses presented above for slip on a single oblique segment provide a basic understanding of the process of slip suppression on segments of a fault zone that are not parallel to an applied slip vector. We next consider the effects of applied shear on a group of segments of varying obliquity. We choose as our example the surface rupture of the 1906 San Francisco earthquake. The boundary element model consisted of the 26 segments between Cape Mendocino and San Juan Bautista listed in table 1, and one additional 100-km segment north of Cape Mendocino approximately parallel to the slip vector to compensate for the absence of submarine slip data. The length of this segment was derived by adjusting its length until the maximum slip predicted by the model became a maximum near Tomales Bay (≈6 m). The length and obliquity of this submarine segment has little effect on the distribution of slip at the southern end of the rupture with which we shall be primarily concerned.

In the first model, we applied a plate-boundary shear strain to a series of contiguous vertical elements with the geometry of the fault zone and allowed them to slip freely. The resulting "elliptical" slip distribution is similar to that observed for a dislocation in a half-space although it is possible to see irregularities caused by the geometry of the fault (upper line in fig. 12). The irregularities are caused by the mechanism discussed in figures 8 and 9. In the second model we permitted each fault segment to not only slip freely, but to open or close depending on the local stress distribution resulting from slip on the given geometry. The resulting synthetic slip distribution is shown as the lower curve in figure 12. The slip distribution is significantly more irregular and represents, in a simplified way, the effects of off-fault deformation that we discuss in the models of figures 10 and 11. The model predicts the general features of the slip

distribution reasonably well given the possible inadequacies in the observational data. The incorporation of fault-parallel thrusts and other compliant fault-normal features southeast of Black Mountain (Scholz, 1985) permits a more rapid decrease in slip in this region. However, the data do not appear to warrant closer modeling. If the model is correct in its present form the data suggest that more than 2 m of slip was undetected in many locations within the fault zone at the time that the fault-offset measurements were undertaken. This is consistent with the finding by Thatcher and Lisowski (1987) that in some locations less than 70 percent of the observed slip occurred on the main surface break, the remainder being distributed within 600 m of the fault.

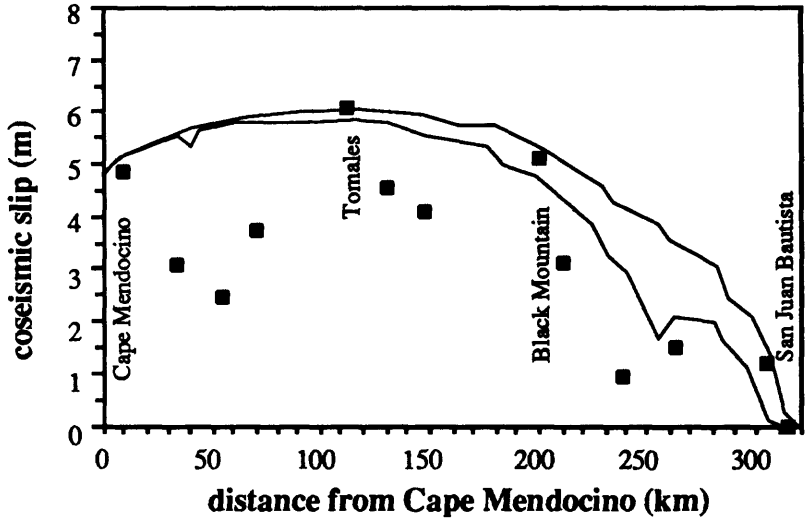

Figure 12. Distribution of slip predicted by boundary-element models with the geometry of the 1906 rupture zone as input. The upper curve is the synthetic slip predicted from a fault zone that can slip freely but is not permitted fault-normal slip. The lower curve is the synthetic slip distribution that results from a fault zone that is permitted fault-normal and fault-parallel slip. The dots are the maximum observed slip (table 1).

CONCLUSIONS

Theoretical models suggest that reduced slip should occur along fault segments that are not parallel to the applied slip vector. These boundary- element models predict reduced slip whether the offset results in contraction or extension. None of our models result in enhanced slip at an oblique segment.

Two sets of observational data suggest that slip is reduced along a fault when the strike of the fault is not parallel to the applied slip vector. However, creep rates in central California appear to attain a maximum velocity on segments that are 8° oblique to the inferred plate slip vector.

In modeling the complex geometry of the 1906 rupture, we find that a simple boundary-element model in which the fault zone can both slip and absorb fault-normal displacements can emulate the essential features of the 1906 slip distribution. Superimposed on the expected theoretical "elliptical" slip distribution is an irregular distribution of slip resulting from the geometry of the fault. It appears then that the physical basis for the slip distribution observed in characteristic earthquakes is the geometry of the fault. Slip along the main fault may be suppressed locally by the manifestation of slip on fault-parallel structures near the main rupture zone, however, in the case of the 1906 rupture the data do not appear to demand significant slip outside the fault zone.

REFERENCES CITED

Bilham, R. and K. Hurst, 1986, A Linear Relationship between Fault Slip and Segment Strike during the 1906 San Francisco Earthquake, EOS Trans American Geophysical Union [abs] No. 67, 16, p. 308.

Bilham R. and K. Hurst, 1988, Relationships Between Fault Zone Deformation and Segment Obliquity on the San Andreas fault, California. in Proc. China-U. S. Symp. on Crustal Deformation and Earthquakes, Wu Bing, ed., Seismological Press, Beijing, p. 510-524.

Bilham R. and P. Williams, 1985, Sawtooth Segmentation and Deformation Processes on the San Andreas Fault, California. Geophysical Research Letters, No. 12, p. 557-560.

Bilham, R. and G. King, 1989, The influence of fault zone geometry and non-uniform slip on the morphology of strike slip faults: examples from the San Andreas Fault, California. Journal of Geophysical Research, Journal of Geophysical Research, in the press 1989.

Brown R. D., and E. W. Wolfe, 1972, Map showing recently active breaks of the San Andreas fault between the Point Delgada and Bolinas Bay. Misc. Geol. Investigations U. S. Geological Survey Map I-692. Scale 1:24000.

Clarke, M. M., 1984, Map showing recently active breaks of the San Andreas fault between Salton Sea and Whitewater River, Mission Creek, California. Misc. Inv. Ser. U. S. Geological Survey Map I-1483, Scale 1:24000.

Crouch, S. L. & A. M. Starfield, 1983, Boundary Integral Methods in Solid Mechanics, Geo. Allen & Unwin, Lond., 322 pp.

Dibblee T.W., 1973, Regional Geology of San Andreas and related faults in Carrizo plain, Temblor, Caliente, and La Panza ranges and vicinity, California. U. S. Geological Survey, Miscellaneous Geologic Investigations Map I-757.

Hurst, K. and R. Bilham, 1986, A geodetic test for the local slip vector on creeping section of the San Andreas Fault in central California. EOS Trans American Geophysical Union [abs], No. 67, p. 16, 358.

Lawson A. C. (ed) 1908, The California earthquake of April 18 1906, in the Report of the State Earthquake Inv. Commission, Vol. 1. pp. 114-145, Carnegie Institution of Washington, Washington D. C.

Mavko G.M., 1982, Fault interaction near Hollister, California. Journal of Geophysical Research, No. 87, p. 7807-7816.

Minster, J. B., and T. H. Jordan, 1978, Present day tectonic motions, Journal of Geophysical Research,, No. 83, p. 5331-5354.

Minster, J. B., and T. H. Jordan, 1987, Vector constraints on Western U. S. Deformation from Space Geodesy, Neotectonics and Plate Motions, Journal of Geophysical Research,, No. 92, p. 4798-4804.

Morgan, J, 1968, Rises, trenches great faults and crustal blocks. Journal of Geophysical Research,, No. 73, p. 1959-1982.

Sarna-Wojcicki, A. M., E. H. Pampeyan, and N. T. Hall, 1975, Map showing recently active breaks of the San Andreas fault between the central Santa Cruz Mountains and the southern Gabilan Range, California. Misc. Field Studies U. S. Geological Survey Map MF 650 Scale 1:24000.

Schwartz, D. P. and K. J. Coppersmith, 1984, Fault behaviour and characteristic earthquakes: Examples from the Wasatch and San Andreas zones. Journal of Geophysical Research, No. 89, p. 5681-5694.

Scholz, C. H., 1985, The Black Mountain asperity: Seismic Hazard of the San Francisco Peninsula, California, Geophysical Research Letters, No. 12, p. 717-719.

Schulz S. S., G. M. Mavko, R. O. Burford and W. D. Stuart, 1982, Long term creep observations in Central California. Journal of Geophysical Research, No. 87, p. 6977-6982.

Sieh, K. E. , 1981, A review of Geological Evidence for recurrence times of large earthquakes, 181-207, in Earthquake Prediction, a review, ed. D. Simpson and P. Richards, M. Ewing Vol. 4.

Thatcher W. and M. Lisowski, 1987, Long term seismic potential of the San Andreas Fault southeast of San Francisco, California. Journal of Geophysical Research, No. 92, p. 4771-4784 .

Vedder and Wallace, R. E. , 1970 , Map showing recently active breaks of the San Andreas fault and related faults between Chalome Valley and the Tejon Pass, California. Misc. Geol. Inv., U. S. Geological Survey Map I-574.

Wallace, R. E. Surface fracture patterns along the San Andreas fault, 1973, in Proc. Conf. on the tectonic problems of the San Andreas Fault System, Stanford Univ. Pub. Geol. Sci. No. 13, p. 248-250.

STRUCTURAL GEOLOGY OF THE OCOTILLO BADLANDS ANTIDILATIONAL FAULT JOG, SOUTHERN CALIFORNIA

Norman N. Brown and Richard H. Sibson,

Department of Geological Sciences, University of California,
Santa Barbara, California 93106

ABSTRACT

Slip transfer across a left step on the Coyote Creek fault (the southernmost portion of the dextral San Jacinto fault zone in southern California) has produced a localized area of uplift and deformation called the Ocotillo Badlands. The eroded core of this 2 km wide "fault jog" contains a deformed sedimentary sequence made up of the lacustrine Borrego Formation (~200 m) and the overlying alluvial Ocotillo Formation (~100 m). The claystones, siltstones, and sandstones of these formations have been folded about east-west trending hinge lines as a result of slip transfer across the jog. Presumably this shortening has occurred incrementally in response to slip episodes on the Coyote Creek fault. Assuming rigid body translation away from the fault jog, the folding has accommodated shortening equivalent to ~800 meters of fault-parallel slip. This amount is significantly less than the 2.5 km of total right slip on the Coyote Creek fault, measured 25 km to the northwest at Coyote Ridge.

Shortening within the jog region is also constrained from the volume of locally updomed strata which, allowing for erosion, amounts to some 0.7 km^3. For the estimated strike-slip rate of 3-5 mm/yr, the sedimentary sequence has been updomed at an average rate of 9-15 mm/yr . On the assumption of constant volume deformation and a jog linking parallel echelon fault segments throughout the seismogenic zone (to ~12 km depth), this small volume of updomed material limits the slip transferred across the jog to $\leq$60 meters. Reconciliation of these disparate estimates for the total slip transferred across the jog could be achieved: (i) by allowing the fault segments to merge at a depth of ~0.5 km; (ii) by changes in the position of the principal slip surfaces with time; or, (iii) by removal of material from within the jog at depth by processes of diffusive mass transfer. Note, however, that the distribution of aftershocks following the 1968 Borrego Mountain earthquake suggests that the jog structure probably does extend to at least several kilometers depth.

The presence of an angular unconformity within the upper portion of the exposed stratigraphy indicates that deformation within the Ocotillo Badlands began during deposition of the Ocotillo Formation. A date of 0.73 Ma has been obtained for the boundary between the Borrego and Ocotillo Formations from magnetostratigraphy. If the total slip on the Coyote Creek fault at the Ocotillo Badlands is greater than 800 m, it appears that the fault jog has been a transitory feature within the fault zone, with slip alternately bypassing it or being transferred across it. Such *switchyard* behavior has important implications for understanding structural controls on rupture propagation.

INTRODUCTION

Fault jogs linking echelon fault segments (figures 1 and 2) may play a role in the arrest, and perhaps also the nucleation of earthquake rupture (Sibson, 1986). If such cross-strike irregularities on strike-slip faults are responsible for *characteristic* earthquake behavior (Schwartz and Coppersmith, 1984), it becomes important from the viewpoint of hazard assessment to know how long such structural controls persist in a particular configuration.

Study of a well-exposed antidilational fault jog at the Ocotillo Badlands in southern California (figure 3) reveals that the structure may have been intermittently active during the last 0.7 million years. Furthermore, the excellent exposure within the core of this locally updomed area allows an understanding of how incremental slip on the Coyote Creek fault has been transferred across the Ocotillo Badlands fault jog. The jog is formed by a 2 km wide left step on the Coyote Creek fault, and the updoming results from folding on E-W hingelines and probable thrusting (figure 4). This deformation has occurred in mostly unconsolidated sandstones, siltstones, and claystones of the Pleistocene Borrego and Ocotillo formations; altogether, approximately 200 m of the lacustrine Borrego Formation and 100 m of the overlying alluvial Ocotillo conglomerate are exposed in the Ocotillo Badlands.

The purpose of the study was to address: (1) the structure and style of deformation within the antidilational jog; (2) the depth to which the fault irregularity persists; (3) the longevity of the structure relative to the slip history on the Coyote Creek fault; and, (4) the mechanism forming the Ocotillo Badlands antidilational jog.

Slip and Slip Rates Along the San Jacinto Fault Zone

From the viewpoint of this analysis, it is important to appreciate that the Coyote Creek fault is the southernmost strand within the entire San Jacinto fault zone. Geologic mapping (Sharp, 1967; 1981) shows that this fault zone has been active during at least the latter half of the Quaternary. Total strike-slip across the fault zone is estimated to be ~20 km in its middle reaches (60 km NW of the Ocotillo Badlands; Sharp, 1967). Along the southern fault segments, the Coyote Creek fault has 2.5 km total right-lateral strike-slip (at Coyote Ridge, 25 km NW of the Ocotillo Badlands), and the Clark fault has ~24 km cumulative right slip (Sharp, 1967). To determine long-term slip rates, Sharp (1981) studied two sites along the San Jacinto fault zone. Along the Clark fault northeast of Anza, he estimated an average slip rate of 8-12 mm/yr since the late Pleistocene (based on a total slip of 5.7-8.6 km).

Of relevance to this study are estimates for slip rate along the Coyote Creek strand of the fault zone. Southeast of the Ocotillo Badlands, Sharp's (1981) trenching study revealed a slip rate of 2.8-5.0 mm/yr from 275-510 yrs B.P. to the present. He estimated a more modest rate of 1-2 mm/yr for the period 400 to 6000 yrs B.P. (approximate potential error in dating is ±20%). In terms of present-day slip rates, it is interesting to note that summation of seismic moments over the time period 1890-1973 yields an average seismic slip rate of ~8 mm/yr for the entire fault zone (Thatcher et al.,1975). Allowing for differences in total slip, it therefore appears that slip rates along the San Jacinto fault zone have not always been constant.

STRUCTURAL GEOLOGY

Surface geology in the Borrego Basin is dominated by Pliocene or younger processes. The dominant structure in the Borrego Basin has been produced by right-lateral

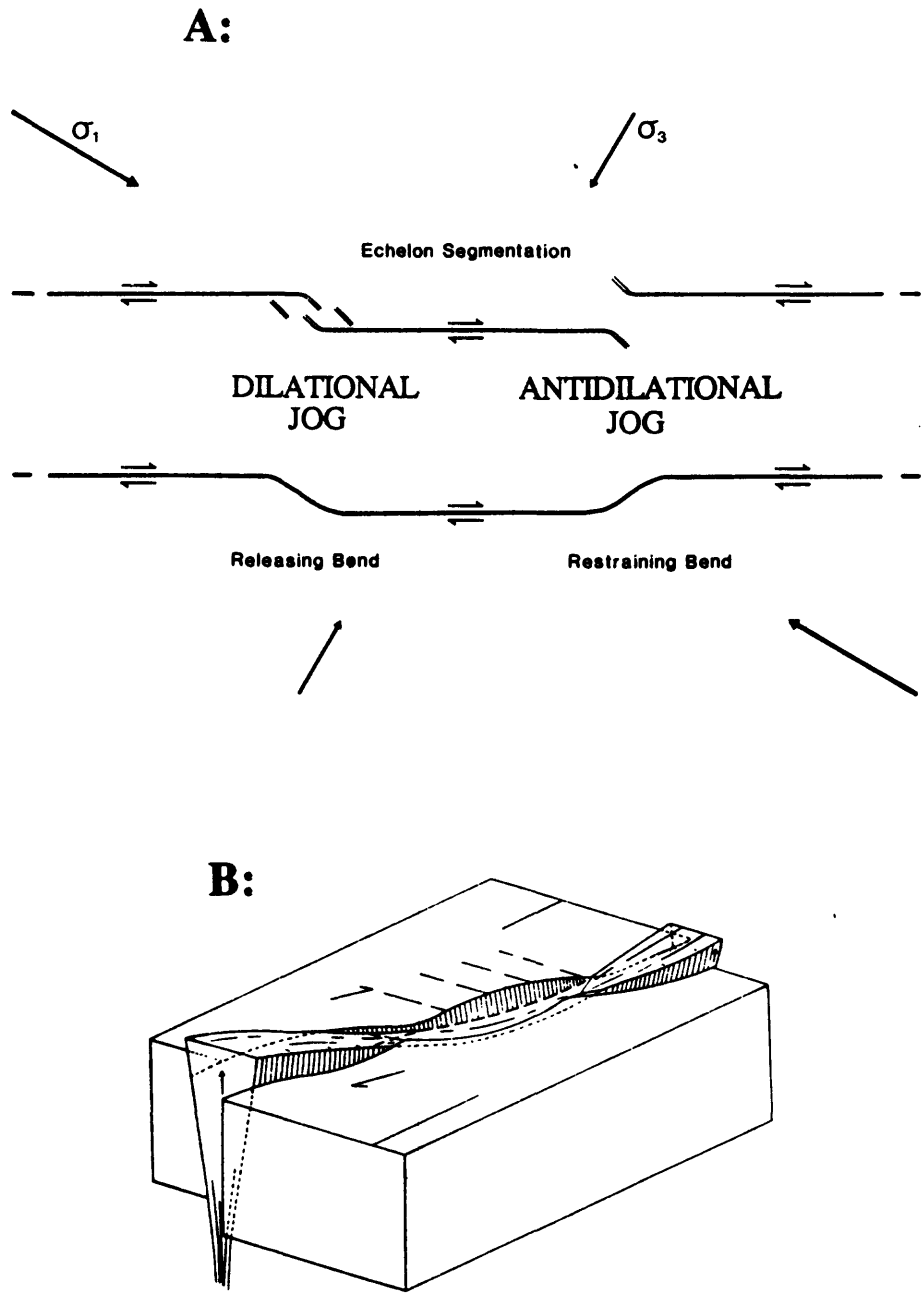

FIGURE 1. **A:** Strike-slip fault irregularities. The strike-slip fault step-overs called dilational and antidilational fault jogs are analagous to throughgoing faults with releasing and restraining bends. After Sibson, 1986. **B:** A schematic drawing of how such irregularities along fault strike may produce local regions of contraction (uplift) or extension (basin formation); from Kingma, 1958.

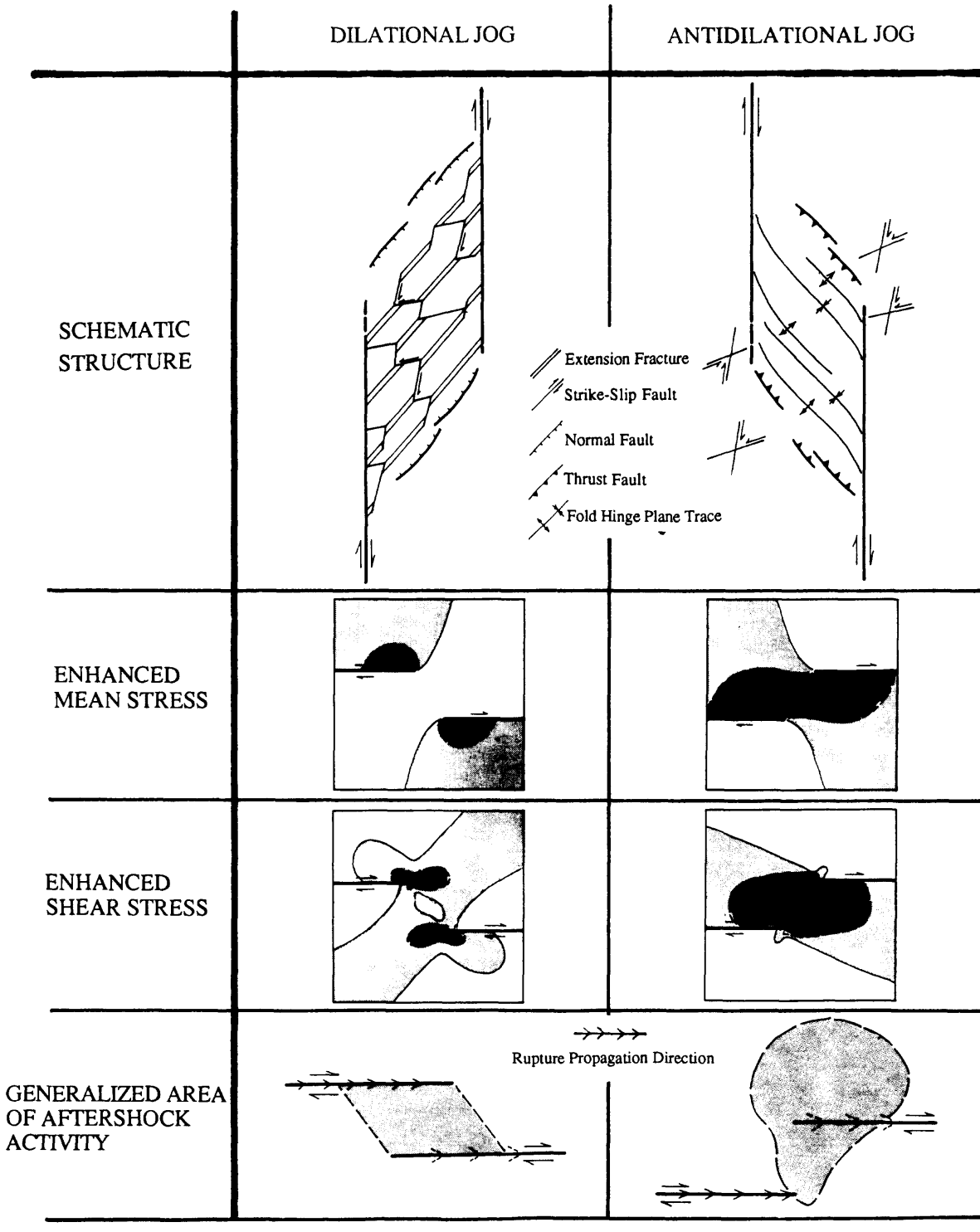

FIGURE 2. Schematic diagrams illustrating various aspects of strike-slip fault jogs. Illustrations depicting areas of enhanced stress are based on quasi-static elastic analysis (after Segall and Pollard, 1980). Shaded areas represent regions where the stress magnitude exceeds the far-field value; darker shading corresponds to greater stress increase above background values.

faulting on the Coyote Creek and Clark faults. Consequently, much of the regional structural grain follows the NW San Andreas orientation. However, a number of NE-trending strike-slip faults are also present. There is some evidence for left-lateral slip on these structures, perhaps indicative of a complicated tectonic history involving block rotation (Seeber and Nicholson, 1986). Local regions of relative uplift or subsidence are also prevalent. These features, such as at the Ocotillo Badlands, provide windows into the Borrego Basin structure and stratigraphy.

The Ocotillo Badlands were mapped on a scale of 1:4500 in an attempt to understand the history of the Coyote Creek fault and the Ocotillo Badlands antidilational jog, as well as to shed light on more general questions concerning the nature of fault jogs (a simplified version of this map is shown in figure 4). In its record of the larger structures, the map does not differ significantly from that previously published by Sharp and Clark (1972). The map presented here does, however, utilize a number of marker beds or bed packets recognized in the stratigraphy. The study also seeks to define the deformation mechanisms associated with folding and faulting in the jog. These added considerations allow more confident construction of a balanced cross section through the jog structure, and a more thorough understanding of the strain history recorded by the deformed sediments.

Style of Deformation

Shortening deformation within the Ocotillo Badlands is accommodated largely by folding of the strata. Also present, however, are faults, local zones of cataclasis or shearing, joints, and minor fractures of inconsistent orientation. In the core of the badlands faulting is sparse and is mostly restricted to: (1) N-S normal faults with less than a few meters of normal separation; and, (2) E-W hinge plane thrust faults which are sometimes found in the cores of tight to isoclinal folds. These hinge plane thrusts typically have less than a meter of separation. They are particularly important as they indicate the possibility of more pronounced thrust faulting at greater depth within the fault jog.

The tightness of the folds within the Ocotillo Badlands ranges from gentle to isoclinal, with hinge lines mostly subhorizontal to gently plunging, and hinge planes mostly upright to steeply inclined. Overall, the structure may be likened to an open, doubly subhorizontally plunging, upright anticlinal dome.

On a scale of a hundred meters or more, the strike of individual fold hinge planes is approximately east-west. In two significant instances, however, the hinge planes depart from this generalization. First, within approximately a hundred meters of the Coyote Creek fault strands, the hinge planes curve toward the trend of the faults, probably as a result of local fault *drag* (figure 4). Second, over along-strike distances less than a hundred meters, hinge planes may be sinuous. Because no field evidence for multiphase folding is seen within the Ocotillo Badlands, and because total strain appears to be somewhat heterogeneous, it seems probable that the folds initiated obliquely and amplified under conditions of progressive non-coaxial strain (Treagus and Treagus, 1981).

Fold Deformation Mechanisms

Regardless of how the folds initiated, their subsequent growth must be accommodated by mechanisms such as intra-bed strain (by shearing, for example), or bedding plane slip. At the Ocotillo Badlands, flexural slip along bedding planes does not appear as a predominant fold mechanism. Locally, small amounts of gypsum or occasionally calcite may be seen growing along bedding planes. Typically, such mineral growths are found close to the hinge regions of folds, where small inter-bed separations and void spaces occur. Rarely are the separations more than a few millimeters. The mineralization is not

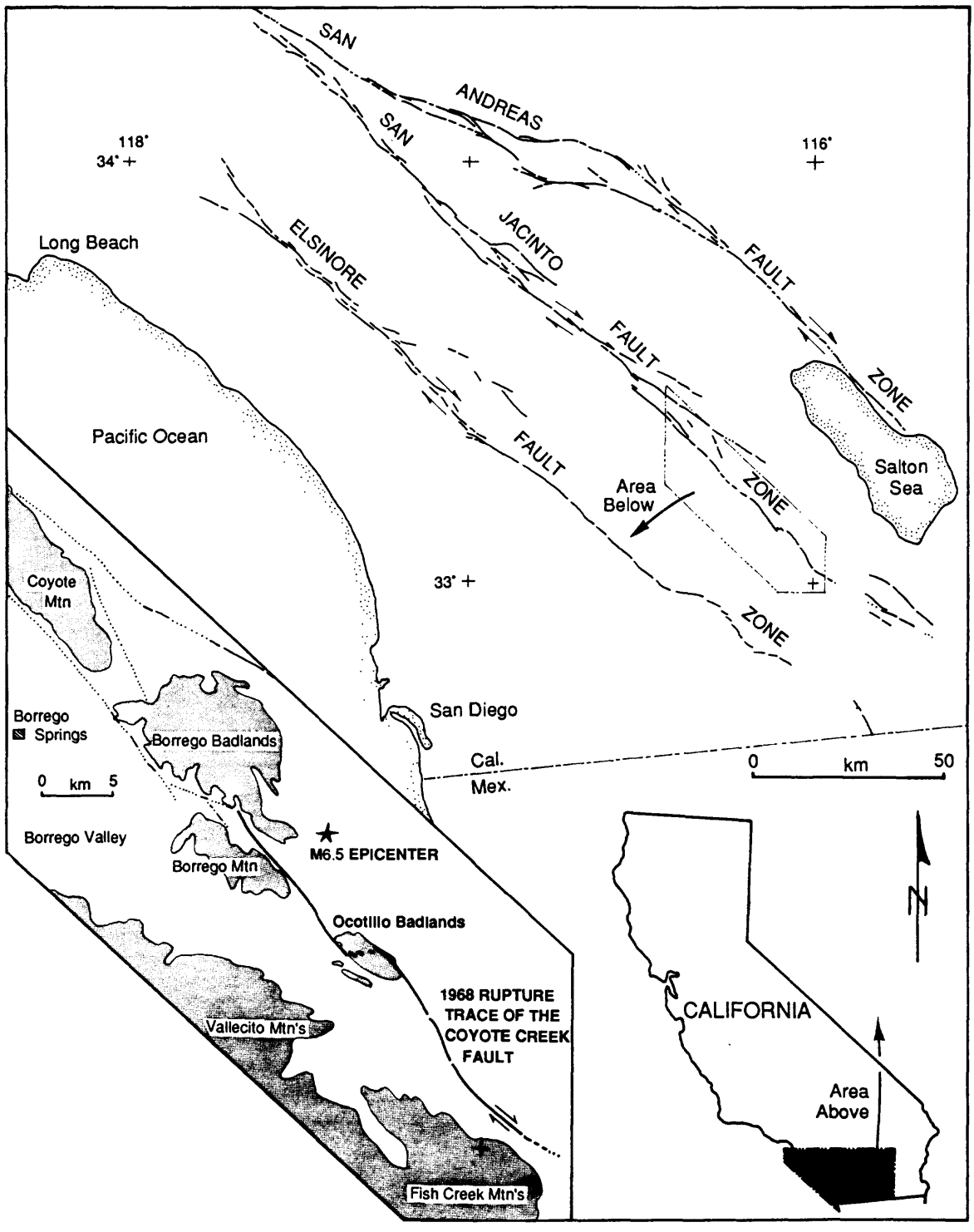

FIGURE 3. Map of southern California and selected dextral strike-slip fault systems. At the lower left is the Coyote Creek fault region with the bold line showing the 1968 rupture trace caused by the Borrego Mountain earthquake (M=6.5).

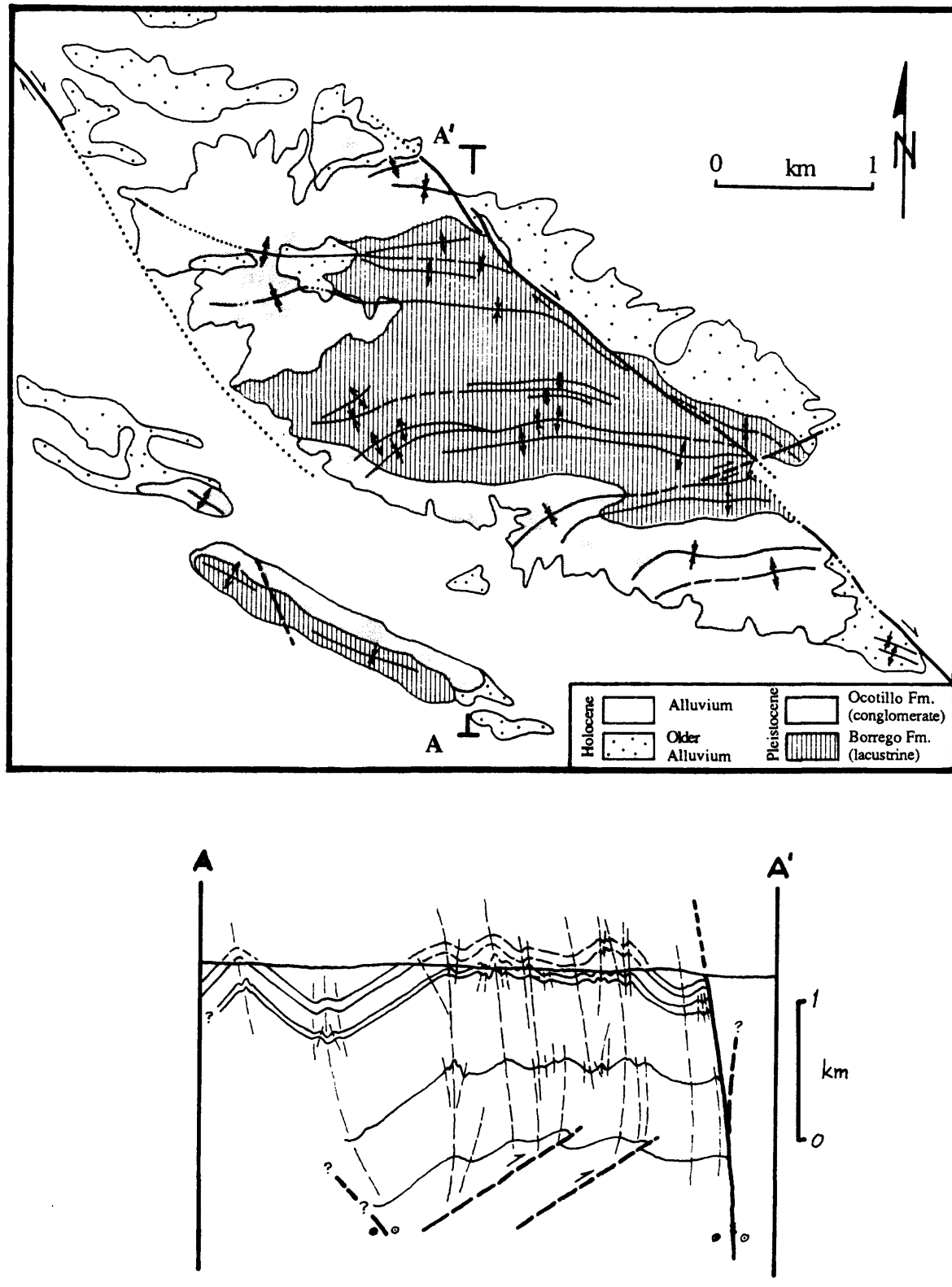

FIGURE 4. Simplified structural map and cross section of the Ocotillo Badlands.

pervasive along bedding planes and does not clearly show the fibrous growth characteristic of bedding plane slip.

Macroscopic analysis of folded beds shows that internal strain within the beds is the principal way in which fold deformation is accommodated. This deformation is found in the form of small intra-bed shear zones which persist laterally for several centimeters to a meter or more, and in which cataclasis is the dominant grain deformation mechanism. In some sandstone beds, these shear zones are only a few millimeters wide, and are recognized by grain crushing and locally reduced bed porosity. This particular feature of the intra-bed shearing implies that volume loss accompanies deformation.

Shortening

To determine the amount and style of shortening accommodated by folding within the Ocotillo Badlands, a balanced cross section was constructed along a line crossing the overall structure (schematically represented in figure 4). The solution is not unique. The construction attempts, however, to make the most reasonable use both of deformation features observed at the surface, and of the aftershock distribution from the 1968 Borrego Mountain earthquake.

As an initial approximation, the internal strain within the beds is ignored, and the simple change in line-length resulting from the folding is used to estimate shortening. Individual areas of tight to isoclinal folds are shortened approximately 30%, perpendicular to the strike of the hinge planes, and the entire structure within the jog area is shortened 18% (figure 4). These estimates of shortening correspond to 600-800 m of fault slip transferred through the jog, assuming rigid body translation outside the area of the fault jog. These estimates must, however, be regarded as minimum values because of the possibilities of layer-parallel shortening prior to folding and of volume loss accompanying deformation. The construction makes some highly speculative assumptions about subsurface geometry. Thrusting at depth is suggested because: (1) hinge plane thrusting occurs at the surface; and, (2) some thrust-style focal mechanisms exist for 1968 aftershocks in the vicinity of the Ocotillo Badlands, at depths of 3 to 6 kilometers (Hamilton, 1972). The geometry shown is perhaps representative of what happens near the boundary between the overlying sediment and the crystalline basement. This boundary may lie at greater depths (~4 km depth) than depicted in the cross section.

These geometric speculations are hampered by the possibility of significant volume reduction within the jog. Reduction of volume within the Ocotillo Badlands appears to be primarily deformation-related, although there is the possibility of some pre-tectonic compaction. Tectonic volume loss might involve local crushing and compaction of sand grains leading to reduction of porosity, recrystallization and dehydration of clay-rich materials (Ramsay and Wood, 1973), or by water-assisted diffusive mass transfer. Note that while pressure solution processes would be enhanced by the fine grained material in fault zones and might occur at nearly all depths within the seismogenic regime (Rutter, 1983), only very shallow deformation is observed at the Ocotillo Badlands. The nature of deep deformation within the jog thus remains inherently speculative. However, indirect evidence for volume reduction at depth within the jog comes from comparison of the structurally obtained shortening with that inferred from volumetric analysis (below).

VOLUMETRIC ANALYSIS

From analysis of present and inferred pre-erosional topography, the volume of updomed sedimentary rock at the Ocotillo Badlands is ~0.7 km^3. This volume may be directly correlated with shortening across the jog provided: (1) the localized folding and

uplift results from slip on the Coyote Creek fault; and, (2) deformation occurs with little or no volume change. Thus, if the cross-sectional geometry of the jog is known, one may calculate the expected amount of uplift for a given amount of slip transfer, assuming rigid block motion away from the jog. If shear strain is also accommodated by rotation of material near the fault (e.g., Salyards et al., 1987), then the total fault-parallel shortening observed in the jog region will tend to overestimate slip on the fault planes. It is implicit in the analysis that the material under compression in the jog is mobile, and moves vertically upwards rather than squeezing laterally into the country rock.

For the purpose of this analysis, the cross-section of the fault jog is modeled as a rectangle or a triangle (figure 5). In order to estimate shortening from the volume of updomed sediment, three possible subsurface configurations are considered: (1) the jog-bounding faults persist as discrete, vertical slip planes to the base of the seismogenic zone (assumed from local and regional seismicity to be 12 km (Hamilton, 1972; Sanders and Kanamori, 1984), thus creating a rectangular cross section; (2) the jog-bounding faults join at the base of the seismogenic layer, forming a triangular cross section; and, (3) the jog-bounding faults join at 5 km depth, below which the Coyote Creek fault exists as a single strike-slip plane oriented like other continuous and linear segments of the Coyote Creek fault (such a geometry was first proposed by Sharp and Clark (1972)). In all these models, the surface distance between the two fault strands bounding the antidilational jog is 2 km, which corresponds to the overlap observed in the 1968 rupture trace. The surface geology indicates that this amount of overlap has been constant for much of the jog's active history. Note that a restraining bend in a fault is, in terms of potential uplift, equivalent to a discontinuous overlap between parallel and straight segments (figure 1).

For the three jog models described above, fault-parallel shortening of 29, 58, and 140 meters respectively is needed to produce the 0.7 km^3 of updomed strata (figure 5). The rate of uplift within the jog may also be calculated using the long-term average strike-slip rate of 3 to 5 mm/yr estimated for the Coyote Creek fault by Sharp (1981). Using model 1 of figure 5, the change in updomed volume per year is

$$\Delta V = wvz \qquad \ldots\ldots (1)$$

where w is the width of the jog (~2 km), v is the average strike-slip rate, and z is the depth of the seismogenic zone. The rate of uplift, dh/dt, averaged over the map area of the fault jog (wL) is therefore

$$dh/dt = (vz)/L \qquad \ldots\ldots(2)$$

where L is the length of the jog (4 km) (c.f. Woodcock and Fischer, 1986). For the values v = 3-5mm/yr, z = 12 km, and L = 4 km, the average rate of uplift at the Ocotillo Badlands is 9-15mm/yr.

Shortening predicted by the volumetric analysis is up to 95% less than that derived from the structural analysis. The volumetrically-derived shortening could be increased to agree with the structurally-derived result of 800 m if the jog-bounding faults merge at only 0.5 km depth, but this would imply that the faults dip inwards at 30°! Moreover, the distribution of aftershocks following the 1968 Borrego Mountain earthquake suggests that the fault jog at the Ocotillo Badlands is a structure which persists to at least several kilometers depth.

The discrepancy between the structurally- and the volumetrically-derived estimates of shortening could be explained by changes in the position of the principal slip surfaces through time, or as a remote possibility, by removal of material from the within the jog through diffusive mass transfer. Compaction within the jog region is likely to be relatively insignificant.

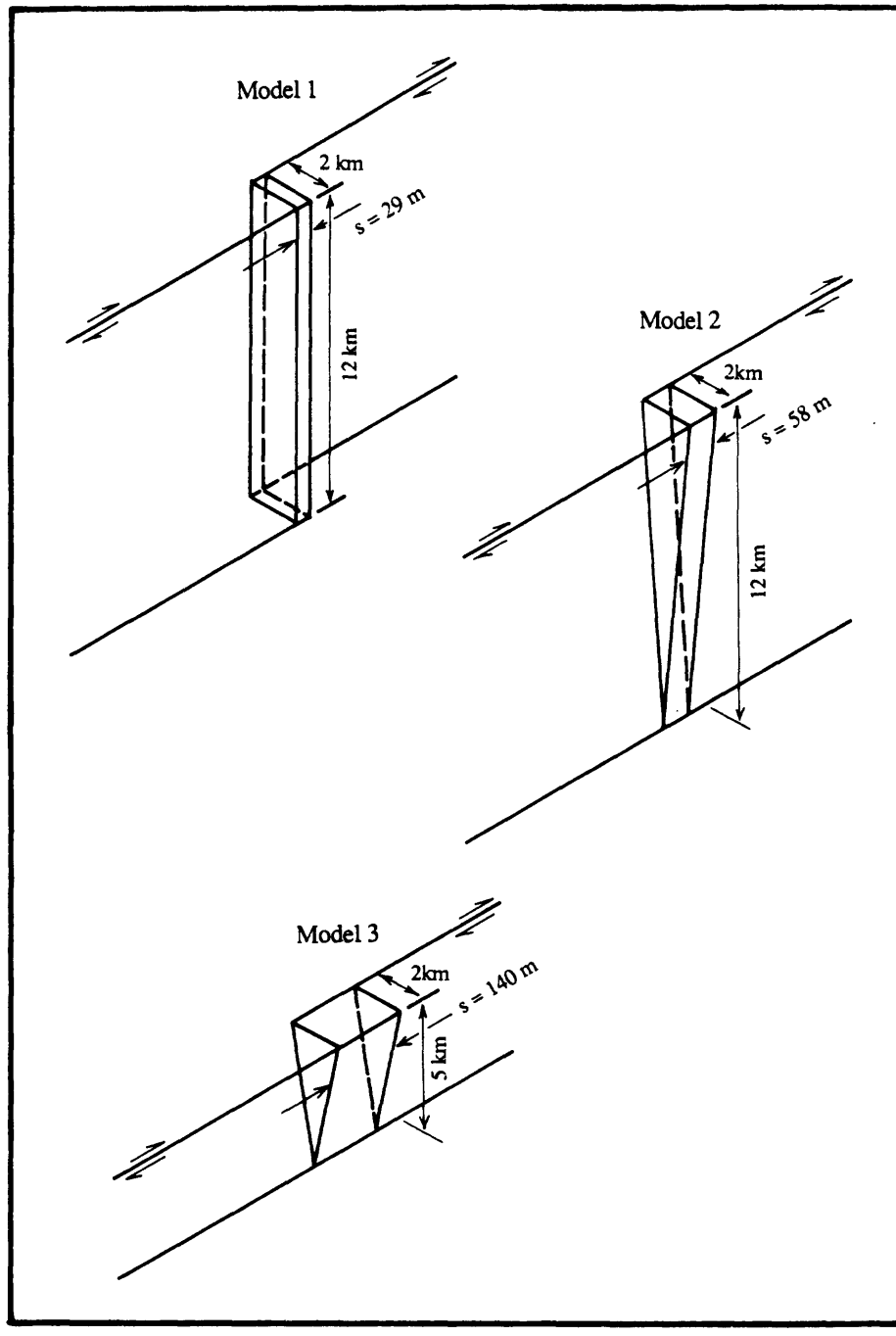

FIGURE 5. Three models for the cross-section geometry of the Ocotillo Badlands fault jog; note that the scale for shortening values (s) is exaggerated.

HISTORICAL SEISMICITY

To some extent, the geometry of the Coyote Creek fault below ground surface may be inferred from the pattern of 1968 aftershock foci. For example, when projected onto a vertical plane perpendicular to the surface rupture, aftershocks located 7 km northwest of the Ocotillo Badlands (section B-B', figure 7) cluster reasonably well along a plane dipping steeply to the northeast. Note that the surface rupture here is fairly straight and continuous (figure 6).

By comparison, at the Ocotillo Badlands, the distribution of aftershocks is more dispersed (section A-A', figure 7). At the surface, where rupture traces indicate two discrete fault planes bounding the jog, the aftershock distribution in cross-section is scattered. Significantly, this diffuse pattern continues to at least 8 km depth, and could be caused by two jog-bounding faults which persist as discrete slip surfaces through most of the seismogenic zone. If so, the data indicate that the faults have a northeasterly dip (c.f. Allen and Nordquist (1972) who estimated an 83° NE dip for the mainshock rupture plane). Note further that some of the focal mechanisms for aftershocks within the Ocotillo Badlands region involve thrust faulting on east to northeast striking planes. Some of these thrust solutions occur as deep as 6 km, indicating that the discontinuity may persist to at least this depth.

The idea that the jog-bounding faults at the Ocotillo Badlands extend to depths ≥8 km is also supported by the distribution of aftershock epicenters in the area immediately adjacent to the jog. Just to the northeast, a large cluster of aftershocks extending to 8 km depth occurred just to the side of the fault trace (figure 6), in a region where mean stress would likely have been reduced as a result of slip transfer across the jog (Segall and Pollard, 1980). A similar diffuse pattern of aftershocks occurred some 10 km to the southeast of the Ocotillo Badlands at an apparent dilational jog in the rupture trace (figures 6 and 7). Here, however, microseismicity was largely confined to the stepover region between the echelon fault segments.

Two kilometers southeast of the Ocotillo Badlands near Bailey's Well (figure 6) an alinement array on the Coyote Creek fault recorded dextral aseismic creep of 5.2 mm/yr between June, 1971 and March, 1984 (Louie et al., 1985). This is the fastest recorded aseismic slip in southern California. Louie et al. (1985) argue that this creep is not well explained as afterslip from the 1968 Borrego Mountain earthquake. Thus, some of the folding within the Ocotillo Badlands may occur as an accompaniment to aseismic creep on the fault. However, the presence of sandstone injection veins cross-cutting strata within the jog suggests that some, if not most, of the fold amplification occurred in association with seismic slip increments on the bounding faults.

INITIATION AND DURATION OF SLIP TRANSFER

Regardless of the explanation used to equate the structurally- and volumetrically-derived shortening results, both show that contraction within the fault jog is much less than the total slip of 2.5 km estimated for the Coyote Creek strand of the San Jacinto fault zone (Sharp, 1967). It is possible that the distribution of slip along the Coyote Creek fault tapers from its northwestern reaches (where 2.5 km of strike-slip was observed) toward the southeast. On the other hand, it is also possible that the antidilational jog at the Ocotillo Badlands has not always been an active feature along the fault and that, from time to time, slip has been transferred alongside the jog rather than through it.

The onset of deformation at the Ocotillo Badlands may be marked by a 20° angular unconformity which appears within the upper portion of the Ocotillo Formation. From

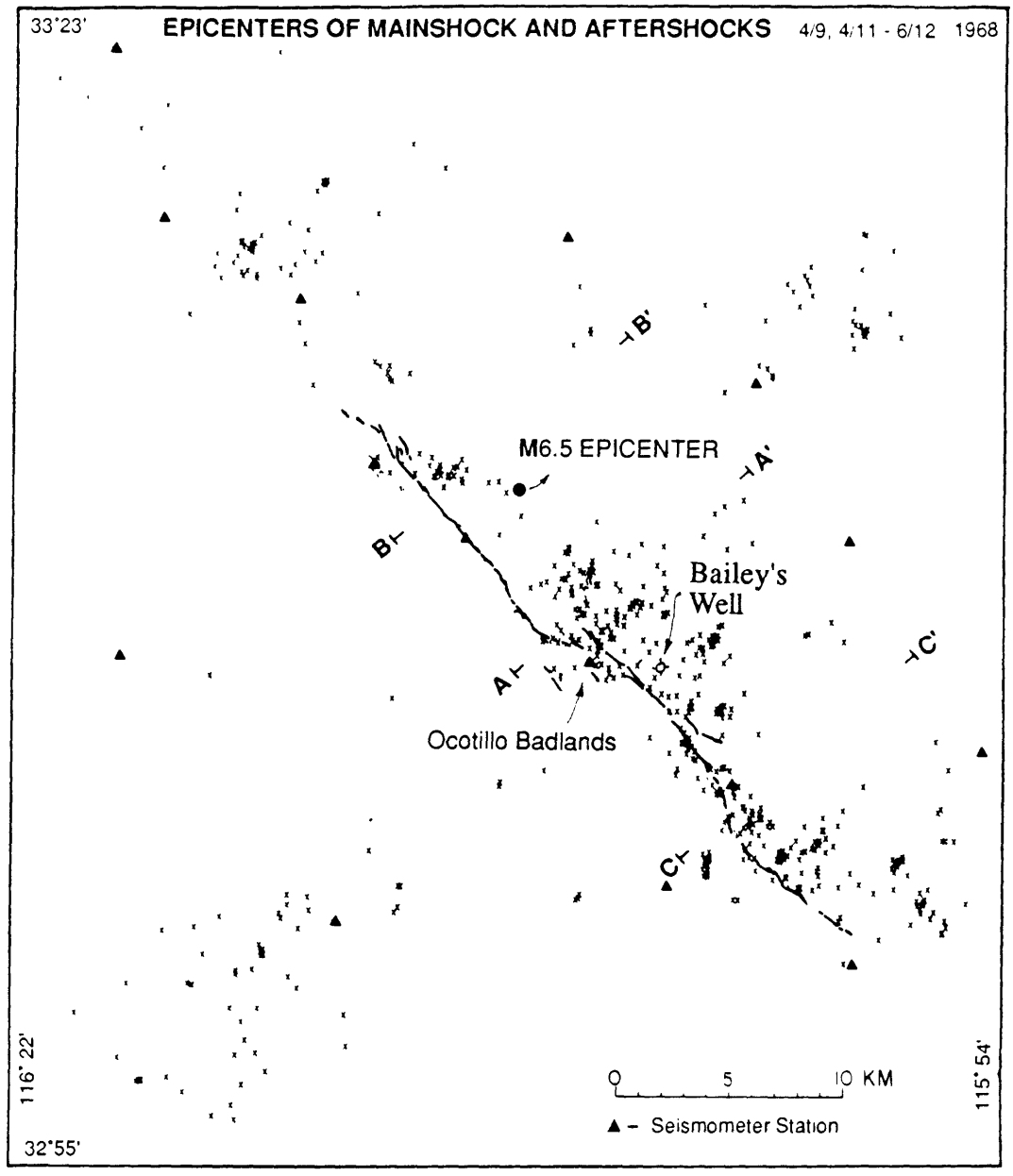

FIGURE 6. Epicenters of the mainshock and aftershocks of the 1968 Borrego Mountain earthquake. The heavy line corresponds to the surface rupture trace, and the three cross sections are shown in figure 7. After Hamilton, 1972.

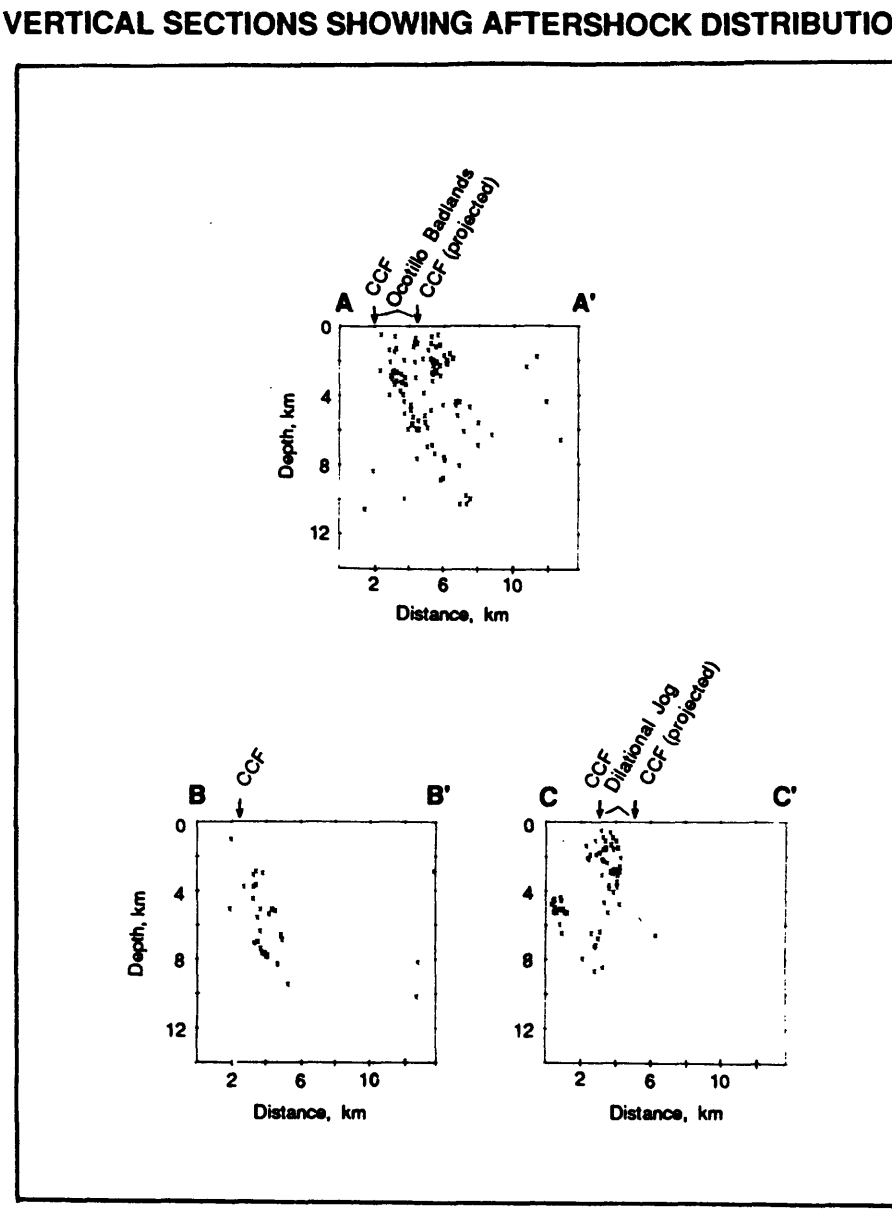

FIGURE 7. Cross sections of the 1968 Borrego Mountain aftershock sequence for the three sections shown in figure 6. After Hamilton, 1972.

magnetostratigraphy, a provisional date of 0.73 Ma has been obtained for the boundary between the upper, conglomeratic Ocotillo Formation and the stratigraphically lower Borrego Formation. Given fault parallel shortening of 800 m, and a long term slip rate on the Coyote Creek fault of 1 to 10 mm/yr, it would take between 80,000 and 800,000 years to produce the deformation observed at the Ocotillo Badlands assuming rigid body translation outside the jog region. Thus if deformation indeed began about 700,000 years ago, the fault jog at the Ocotillo Badlands has probably been active only on an intermittent basis. One of the two jog-bounding faults may have an along-strike extension which is occasionally active in accommodating the ongoing displacement and shunts the antidilational jog along strike (c.f. Woodcock and Fischer, 1980). The transitory nature of slip transfer across the antidilational fault jog at the Ocotillo Badlands reveals the danger of viewing such irregularities on strike-slip faults as constant features affecting rupture propagation.

ACKNOWLEDGEMENTS

This work was supported by National Science Foundation Grant EAR 86-07445 and U. S. Geological Survey Grant 14-08-0001-G1331. We thank Alan Hull, Tom Blenkinsop, Nano Seeber, Ed Keller, and Dave Schwartz for helpful discussion.

REFERENCES CITED

Hamilton, R. M., 1972, Aftershocks of the Borrego Mountain earthquake from April 12 to June 12, 1968, *in* The Borrego Mountain earthquake of April 9, 1968, U.S.G.S. Prof. Paper, 787, p. 31-54.

Kingma, J. T., 1958, Possible origin of piercement structures, local unconformities, and secondary basins in the eastern geosyncline, New Zealand: N. Z. Jour. Geol. Geophys., 1, p. 269-274.

Louie, J. N., C. R. Allen, D. Johnson, P. Haase, and S. Cohn, 1985, Fault slip in southern California: Seismol. Soc. Amer. Bull., 75, p. 811-833.

Ramsay, J. G., and D. S. Wood, 1973, The geometrical effects of volume change during deformation processes: Tectonophysics, 16, p. 263-277.

Rutter, E. H., 1983, Pressure solution in nature, theory, and experiment: Jour. Geol. Soc. London, 140, p. 725-740.

Salyards, S. L., K. E. Sieh, and J. L. Kirschvink, 1987, Paleomagnetic measurement of dextral warping during the past three large earthquakes at Pallett Creek, southern California (abs.): Geol. Soc. Amer. Abs. with Programs, p. 828.

Sanders, C. O., and H. Kanamori, 1984, A seismotectonic analysis of the Anza seismic gap, San Jacinto fault zone, southern California: Jour. Geophys. Res., 89, p. 5873-5890.

Schwartz, D. P., and K. J. Coppersmith, 1984, Fault behavior and characteristic earthquakes: examples from the Wasatch and San Andreas fault zones: Jour. Geophys. Res., 89, p. 5681-5698.

Seeber, L., and C. Nicholson, 1986, Block/fault rotation in geologic and interseismic deformation, *in* National Earthquake Prediction Evaluation Council, Special Report I: U.S.G.S. Open File Report, 86-580, p. 185-203.

Segall, P., and D. D. Pollard, 1980, Mechanics of discontinuous faults: Jour. Geophys. Res., 85, p. 4337-4350.

Sharp, R. V., 1981, Variable rates of late Quaternary strike slip on the San Jacinto fault zone, southern California: Jour. Geophys. Res., 86, p. 1754-1762.

Sharp, R. V., 1967, San Jacinto fault zone in the Peninsular Ranges of southern California: Geol. Soc. Amer. Bull., 78, p. 705-730.

Sharp, R. V., and M. M. Clark, 1972, Geologic evidence of previous faulting near the 1968 rupture on the Coyote Creek fault, *in* The Borrego Mountain earthquake of April 9, 1968, U.S.G.S. Prof. Paper, 787, p. 131-140.

Sibson, R. H., 1986, Rupture interactions with fault jogs, *in* Earthquake Source Mechanics, Geophysical Monographs, Maurice Ewing Series, 6, American Geophysical Union, p. 157-167.

Thatcher, W., J. Hileman, and T. Hanks, 1975, Seismic slip distribution along the San Jacinto fault zone, southern California, and its implications: Geol. Soc. Amer. Bull., 86, p. 1140-46.

Treagus, J. E., and S. H. Treagus, 1981, Folds and the strain ellipsoid: Jour. Struc. Geol., 3, p. 1-17.

Woodcock, N. H., and M. Fischer, 1986, Strike-slip duplexes: Jour. Struc. Geol., 8, p. 725-735.

SEGMENTATION OF BASIN-AND-RANGE NORMAL FAULTS: EXAMPLES FROM EAST-CENTRAL IDAHO AND SOUTHWESTERN MONTANA

by

Anthony J. Crone and Kathleen M. Haller
U.S. Geological Survey
Denver, Colorado 80225

ABSTRACT

The range-front normal faults of the Lost River and Lemhi Ranges, and the Beaverhead and Tendoy Mountains in east-central Idaho and southwestern Montana have well preserved fault scarps on Quaternary deposits along much of their lengths. Fault-scarp morphology, the age of deposits displaced by the faults, and the geomorphology of the range fronts provide a basis for dividing the faults into segments. The Lost River, Lemhi, and Beaverhead fault zones are 141-151 km long, and each contains six segments. The Red Rock fault, the range-front fault of the Tendoy Mountains, is divided into two segments that span 27 km of the central part of the 60-km-long fault. Individual segments that we describe here are typically 20-25 km long.

We identify four kinds of features that serve as guides to identifying segment boundaries: (1) major en echelon offsets or pronounced gaps in the continuity of the fault scarps, (2) distinct, persistent, along-strike changes in fault-scarp morphology that indicate different ages of faulting, (3) major salients in the range front, and (4) transverse bedrock ridges where the cumulative throw is low compared to other places along the fault zone. Only features whose size is measured on the scale of kilometers are regarded as significant enough to define segment boundaries.

The ability to accurately subdivide faults into segments can contribute to better seismic-hazard assessments. However, these assessments should not assume that the barriers which segment faults are completely effective at stopping every rupture. The topographic expression of mountain ranges indicates that, at times during their history, all barriers must fail. Some barriers apparently create "leaky" segment boundaries that impede propagating ruptures but do not completely prevent faulting on adjacent segments.

INTRODUCTION

Accurate seismic-hazard assessments rely heavily on a basic understanding of the coseismic behavior of potentially seismogenic faults. For example, the ability to estimate the length of surface faulting, the amount of displacement, and the thickness of the seismogenic layer permits magnitude estimates for possible future earthquakes and helps define the nature of the hazards associated with those events. The concept of fault segmentation has important implications to hazard assessments because, if we can identify and define the segments of a hazardous fault, we can constrain the location, length, and area of the fault that will likely rupture during a single earthquake.

The idea of fault segmentation is based on observations that only part of long fault zones rupture during large earthquakes (Schwartz and Coppersmith, 1984, 1986). Recent studies of historical earthquakes and paleoseismic investigations of major fault zones suggest that specific geologic features form barriers on fault planes that physically divide faults into segments

(Bruhn and others, 1987; Crone and others, 1987; Fonseca, 1988; King and Yielding, 1984; Machette and others, 1987; Wheeler and Krystinik, 1987). Barriers can slow or stop propagating coseismic ruptures, and, in some cases, the barriers apparently persist through several earthquake cycles (Wheeler, 1987).

The 1983 Borah Peak earthquake is a well-documented example of how barriers can affect a propagating rupture on a segmented normal fault. Geologic, seismologic, and geodetic data show that both ends of the 1983 rupture are delimited by barriers on the Lost River fault, and that apparently, those barriers have also affected earlier ruptures (Crone and others, 1987). The behavior of the Lost River fault during the 1983 earthquake may typify the coseismic behavior of many normal faults in the Basin and Range province. Thus studies of the segmentation of the Lost River and similar nearby faults may have widespread applications throughout the province.

The range-front faults of the Lost River Range and adjacent mountain fronts in east-central Idaho and southwestern Montana provide an unusually good opportunity to study segmented normal faults because scarps along these faults are well preserved and generally, are modified minimally by cultural activity. Furthermore, the Borah Peak earthquake is a thoroughly documented example of the coseismic failure of a range-front normal fault.

This report summarizes the geologic evidence and characteristics used to define segments on the range-front faults of the Lost River and Lemhi Ranges, and the Beaverhead and Tendoy Mountains in Idaho and Montana (fig. 1). We also describe some general characteristics of segment boundaries based on regional studies (Haller, 1988a, 1988b) and on detailed studies of the Lost River fault (Crone and others, 1987; Schwartz and Crone, 1988). Our efforts to examine the segmentation of faults in a broad region have two important advantages to studies of a single fault. First, the regional approach provides a more complete inventory of the kinds of features that may form segment boundaries. Secondly, it provides insight into the regional distribution of spatial and temporal patterns of surface faulting in an extensional tectonic setting. The general similarities between the faults in our study area with other Basin and Range normal faults suggests that the segment-boundary characteristics we describe here might be applied throughout the province.

Segmented Behavior of the Lost River Fault During the Borah Peak Earthquake

On October 28, 1983, the M_s 7.3 Borah Peak earthquake ruptured part of the 141-km-long Lost River fault. The total length of surface faulting along the Lost River fault was about 36 km (fig. 2) but geologic, seismologic, and geodetic data show that the primary rupture was confined to the 22-km-long Thousand Springs segment (Crone and others, 1987). The main shock nucleated near the base of the seismogenic layer close to or within the geometric barrier that separates the Thousand Springs segment from the Mackay segment to the southeast. The Thousand Springs-Mackay segment boundary coincides with a major salient in the range front; at this salient the range front changes strike by 55° within a distance of a few kilometers. The rupture propagated upward and unilaterally to the northwest on a planar fault dipping about 45° to the southwest and continued along the entire length of the Thousand Springs segment (Crone and others, 1987). The main zone of surface faulting was confined to the Thousand Springs segment (fig. 2). On this segment, the

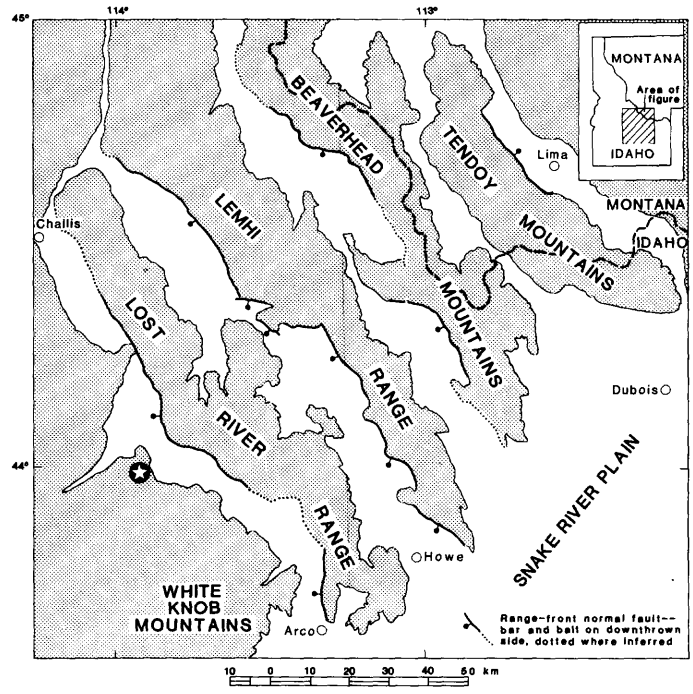

FIGURE 1.--Generalized map of major range-front normal faults in east-central Idaho and southwestern Montana. Cross-hatched areas are mountainous regions. Segmentation of individual faults is shown in figures 3 and 4. Star is epicenter of 1983 Borah Peak earthquake.

tectonic throw reached a maximum of 2.5-2.7 m, individual scarps are nearly 5 m high, and the zone of ground breakage is as wide as 140 m. En echelon scarps with synthetic and antithetic displacements are common.

At the northwestern end of the Thousand Springs segment, the rupture encountered a barrier at the junction of the Willow Creek hills and the Lost River Range (fig. 2). This barrier either completely stopped the primary rupture or deflected it away from the Lost River fault and onto a network of smaller faults within the barrier. At the southern end of this barrier, the 1983 scarps divide into two splays, a minor splay that continues along the Lost River fault for about 1-2 km before it ends, and a western splay composed of discontinuous ruptures that extends across the crest and down the north flank of the Willow Creek hills. Along the Lost River fault at the barrier, there is a 4.7-km-long gap in 1983 surface faulting. Northwest of this gap, small scarps and cracks formed along the Warm Spring segment in 1983. Geologic (Crone and others, 1987), seismologic (Boatwright, 1985; J. Nabelek, 1988, written commun.), and geodetic (Stein and Barrientos, 1985) data all indicate that the Willow Creek hills barrier effectively stopped the primary rupture on the range-front fault, however, severe shaking and the directivity of the rupture triggered some secondary slip on the Warm Spring segment northwest of the barrier.

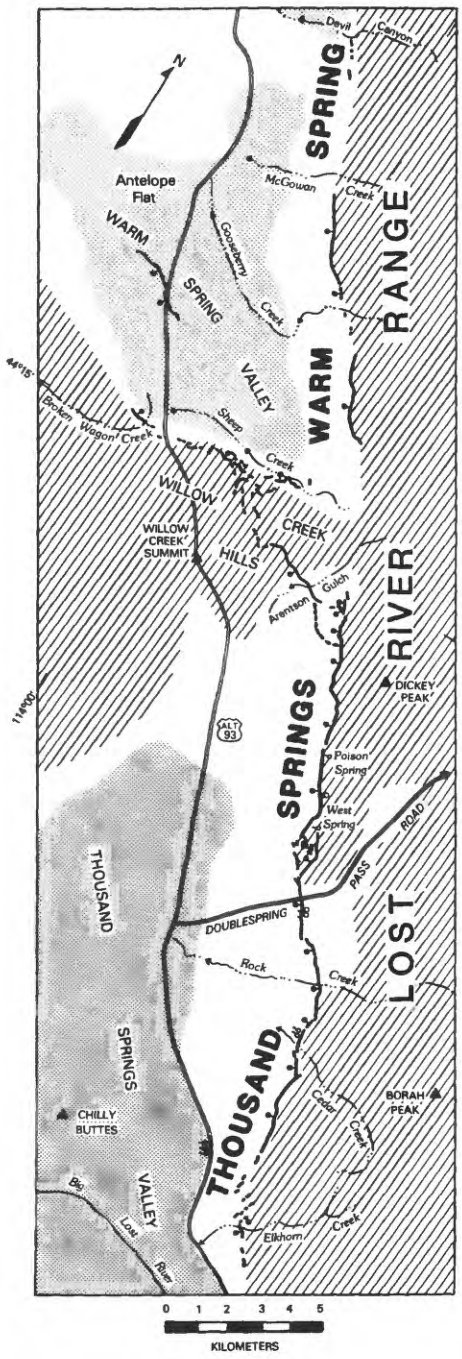

FIGURE 2.--Generalized map of fault scarps and ground ruptures associated with the Borah Peak, Idaho, earthquake (from Crone and others, 1987). Heavy lines are prominent scarps, bar and ball symbol is on downthrown side of fault; dashed lines are poorly defined scarps or cracks. Stippled areas are valley bottoms; hachured areas are mountainous parts of the Lost River Range and Willow Creek hills. The Thousand Springs segment extends from just south of Elkhorn Creek to the junction between the Willow Creek hills and the Lost River Range.

SEGMENTATION OF THE RANGE-FRONT FAULTS

Prominent fault scarps on the southwest flanks of the Lost River and Lemhi Ranges, the Beaverhead Mountains, and the northeast flank of the Tendoy Mountains can be used to identify segments on these range-front normal faults and provide insight into the history of late Quaternary faulting. The Lost River, Lemhi, and Beaverhead faults are named for their respective ranges, and the Red Rock fault bounds the northeast side of the Tendoy Mountains. The morphology, continuity, and size of fault scarps vary along strike on these faults; we use these variations to subdivide the faults into segments. Fault-scarp morphology and the geomorphic relations between scarps and Quaternary deposits of different ages provide a basis for estimating the age of the most recent movement on individual segments.

We recognize that using morphologic data from multiple-event scarps to estimate the age of faulting is plagued by problems (see Crone and Omdahl, 1987, p. 359). Age estimates derived from these data have large uncertainties and must be viewed cautiously. Nevertheless, being fully aware of these major limitations, we use morphologic data from some multiple-event scarps to make broad, general age estimates. We emphasize that these estimates are used only to compare the general age of the scarps, and thus age of faulting, on different segments.

Regional Geologic Setting

The structural style and topographic expression of the mountains and valleys in east-central Idaho are generally similar to other parts of the Basin and Range province (Reynolds, 1979). The ranges are composed of allochthonous Paleozoic and Precambrian rocks that were thrust northeastward starting in Cretaceous and continuing into Eocene time. Subsequent tectonism included the formation of northeast-striking normal faults in the Eocene, Eocene and Oligocene volcanism, and, during the late Cenozoic, regional uplift, volcanism, and the development of northwest-striking normal faults that control modern topography. The topographic relief between the range crests and the adjacent valleys is generally about 1.5 km with maxima of about 1.9 km. The cumulative structural relief on the range-front normal faults is poorly known but locally is probably 3-4 km (Scott and others, 1985), and may be as much as 6.1 km on the Lost River fault (Skipp and Hait, 1977).

The Lost River Fault

Scott and others (1985) divided the 141-km-long Lost River fault into six segments (fig. 3) based on estimated age of the youngest surface faulting, and the geomorphic expression and structural relief of the range. From northwest to southeast the segments are named the Challis, Warm Spring, Thousand Springs, Mackay, Pass Creek and Arco segments (Scott and others, 1985; Crone and others, 1987). The segments average 23 km in length with a minimum of 18 km for the Warm Spring and a maximum of 29 km for the Pass Creek segments, respectively (table 1).

Studies of faulting on the Arco segment show that the last surface faulting occurred about 30,000 yr ago (Pierce, 1985). Progressively higher scarps on older Quaternary deposits indicate recurrent faulting that has displaced 160,000-yr-old deposits 19 m (Pierce, 1985).

The Pass Creek segment, the longest segment of the Lost River fault, spans a major embayment in the Lost River Range, and is characterized by a

TABLE 1.--Segmentation of the Lost River, Lemhi, Beaverhead, and Red Rock faults, east-central Idaho and southwestern Montana

[Abbreviations for age of youngest movement are: MH, middle Holocene; P, Pleistocene, LP, late Pleistocene. Ages are queried where poorly known. Segment names are listed from northwest to southeast]

Segment name	Length (km)	Age Estimate	Segment name	Length (km)	Age Estimate
LOST RIVER FAULT			**LEMHI FAULT**		
Challis	25	P?	May	23	LP
Warm Spring	18	MH	Patterson	23	MH
Thousand Springs	22	1983	Goldburg	12	LP
Mackay	22	MH	Sawmill Gulch	43	MH
Pass Creek	29	LP?	Fallert Springs	29	LP
Arco	25	LP	Howe	20	LP
Average	23		Average	25	
BEAVERHEAD FAULT			**RED ROCK FAULT**		
Lemhi	20	LP?/P	Timber Butte	11	LP
Mollie Gulch	20	LP	Sheep Creeks	16	MH
Leadore	23	MH			
Baldy Mountain	21	LP?			
Nicholia	42	LP			
Blue Dome	25	LP?/P			
Average	25		Average	14	

general absence of fault scarps on Quaternary deposits. The oldest alluvial deposits along this part of the range front are latest Pleistocene (~15,000 yr old) in age (Pierce and Scott, 1982). Thus, there has been no surface faulting on the Pass Creek segment in the past 15,000 yr and the last surface faulting may be as much as 30,000-50,000 yr old (Scott and others, 1985).

Prominent, geomorphically young fault scarps occur along the entire length of the Mackay segment. Trenches excavated at both ends of the segment have exposed faulted Mazama ash (Scott and others, 1985; Schwartz and Crone, 1988) indicating that faulting is younger than about 6800 yr old. Additional evidence from the trench at the southern end suggests that the youngest faulting event on this segment may be slightly more than 4000 yr old (Scott and others, 1985).

The Thousand Springs segment ruptured in 1983. Although the exact age of the surface-faulting event prior to 1983 is not well constrained, several lines of evidence suggest that it probably occurred in middle to early Holocene time (Scott and others, 1985; Vincent, 1985; Hanks and Schwartz, 1987). Limited evidence suggests that surface displacement during the pre-1983 event was similar to that produced by the Borah Peak earthquake (Schwartz and Crone, 1985; Vincent, 1985).

Minor surface faulting occurred on the Warm Spring segment during the 1983 earthquake, but, as already discussed, it is probably secondary surface faulting. Pre-1983 fault scarps as much as 5.7 m high are formed on latest Pleistocene alluvial fans of this segment (Crone and others, 1987). Radiocarbon dates from two trenches 7.5 km apart on this segment indicate that

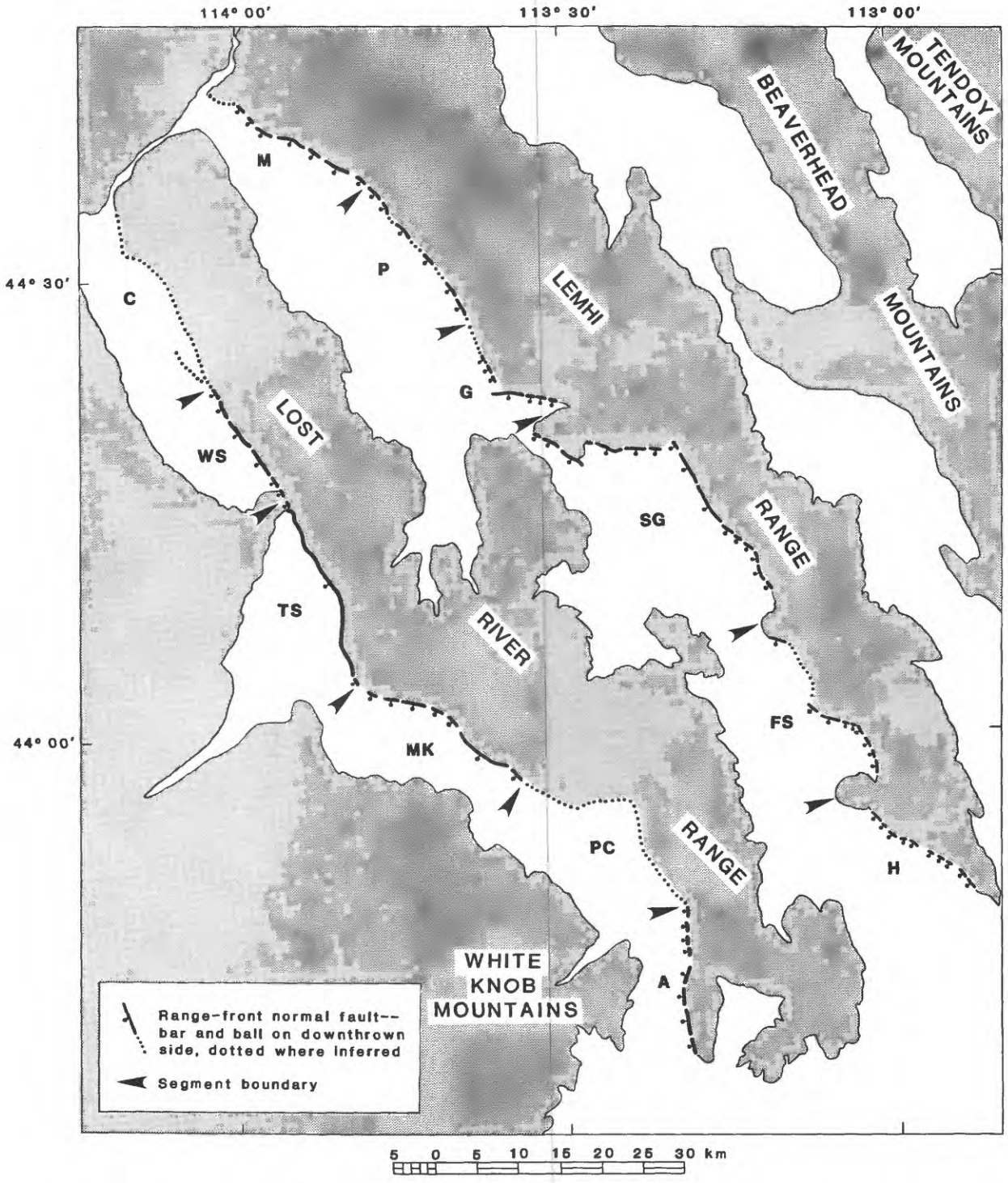

FIGURE 3.--Generalized map of Lost River and Lemhi Ranges showing segments of the Lost River and Lemhi faults; arrows identify segment boundaries. Segment names for the Lost River fault are: C, Challis; WS, Warm Spring; TS, Thousand Springs; MK, Mackay; PC, Pass Creek; A, Arco (Scott and others, 1985; Crone and others, 1987). Segment names for the Lemhi fault are: M, May; P, Patterson; G, Goldburg; SG, Sawmill Gulch; FS, Fallert Springs; H, Howe (Haller, 1988b). See table 1 for information about individual segments.

the youngest major surface faulting occurred shortly before 5500-6200 yr ago (Schwartz and Crone, 1988).

The history of faulting on the Challis segment is poorly known, but reconnaissance studies have revealed little evidence of late Quaternary faulting. The range-front geomorphology along the Challis segment is much more subdued than it is along adjacent segments to the southeast, suggesting a lower long-term slip rate. In addition, the geomorphic expression of the valley and range along the Challis segment suggests that the Lost River fault may separate into two diverging strands (fig. 3). Perhaps the generally subdued range-front morphology is the result of displacements being distributed between two major strands of the fault combined with relatively low slip rates.

The Lemhi Fault

The Lemhi fault is 150 km long and consists of at least six segments (Haller, 1988b). From northwest to southeast the segments are named May, Patterson, Goldburg, Sawmill Gulch, Fallert Springs, and Howe (fig. 3). The segments average 25 km in length with a minimum of 12 km for the Goldburg and a maximum of 43 km for the Sawmill Gulch segments, respectively (table 1). Higher scarps on increasingly older deposits indicate recurrent late Quaternary movement on all segments of the Lemhi fault.

Trenching studies on the Howe segment document at least five surface-faulting events in the past 600,000 yr with the most recent event older than 15,000 yr (Malde, 1987). The scarp height-slope angle relation of scarps on the Howe segment are similar to those for scarps on the Arco segment of the Lost River fault; this implies a similar age of late Pleistocene for the youngest surface faulting.

The morphology and continuity of scarps on the Fallert Springs segment suggest that the most recent surface faulting is also late Pleistocene in age. However, slightly steeper maximum slope angles for scarps of similar size suggests that the most recent faulting on this segment may be slightly younger than that on the Howe segment.

The Sawmill Gulch segment is the longest segment of the Lemhi fault (43 km) and includes a major embayment in the range. On this segment, single-event fault scarps are formed on latest Pinedale-age[1] terraces (Pierce and Scott, 1982), but fault-scarp morphology suggests that the scarps are probably middle Holocene in age. Progressively higher scarps on older terraces indicate recurrent late Pleistocene surface faulting. Early Pinedale-age terraces have been displaced by two faulting events. Bull Lake-age [2] (Pierce and Scott, 1982) deposits have been faulted as many as six times based on the

---

[1] The Pinedale Glaciation spans a considerable amount of time in the late Pleistocene. Some Pinedale deposits indicative of full glacial conditions may be as old as 45,000 yr B.P. (Porter and others, 1983), but most are thought to be considerably younger. Extensive deglaciation in the Rocky Mountain region occurred by about 14,000 yr B.P. For the purposes of this discussion, we consider Pinedale deposits to be 30,000-15,000 yr old.

---

[2] The Bull Lake Glaciation is late Pleistocene in age and is widely accepted to be about 140,000 yr old (Pierce and others, 1976).

presence of scarps that are three times as high as those on early Pinedale terraces.

The variable character and orientation of the scarps within the Goldburg segment suggest that, with further study, the extent of this segment may be substantially revised. This is the shortest segment on the fault and spans a salient in the range front. South of the salient, the morphology of east-west-trending, multiple-event scarps suggests that the youngest surface faulting was about 15,000 yr ago; near the salient, the youngest scarps diverge away from the range front and extend farther downslope on the alluvial fans than scarps from the older events. North of the salient, scarps trend northwest-southeast and are formed primarily on bedrock. A small gap in the youngest scarps, less than 1 km long, occurs at the salient where the scarps change trend; however, the morphology of this single-event scarp suggests that it is more than 30,000 yr old (Haller, 1988b).

Single-event scarps are formed on all Pinedale-age (latest Pleistocene) terraces on the Patterson segment, but their morphology suggests a middle Holocene age for the youngest faulting event. The longer-term history of faulting is difficult to evaluate because few multiple-event scarps are preserved on this segment.

Scarps on the May segment are morphologically indistinguishable from those on the Arco segment of the Lost River fault, thus, like the Howe segment, we infer a late Pleistocene age for the last surface faulting. By analogy, the faulting is considered to be on the order of 30,000 yr old.

The Beaverhead Fault

The 151-km-long Beaverhead fault is also composed of six segments, but unlike the Lemhi fault, not all segments have scarps on Quaternary deposits (Haller, 1988b). From northwest to southeast, the segments are named Lemhi, Mollie Gulch, Leadore, Baldy Mountain, Nicholia, and Blue Dome (fig. 4). The segments average 25 km in length with a minimum of 20 km for the Mollie Gulch and Lemhi, and a maximum of 42 km for the Nicholia segments, respectively (table 1).

The subdued morphology and low topographic relief of the range front along the Blue Dome segment suggest that the Quaternary slip rate on this part of the Beaverhead fault is low relative to other segments to the northwest. Our interpretation of aerial photographs suggests that the fault may divide into several strands. No alluvial deposits extend across the fault on this segment. Along parts of the Blue Dome segment, Paleozoic limestone is exposed on both sides of the most prominent scarp, suggesting that the cumulative Quaternary throw on the strand that defines the modern range front is low relative to other segments of the fault.

Single- and multiple-event scarps on Quaternary deposits extend nearly continuously along the entire length of the Nicholia segment. This segment, the longest on the Beaverhead fault, spans a large embayment in the range front. On the Nicholia segment, alluvium estimated to be 15,000 yr old has been faulted once, and alluvium thought to be about 30,000 yr old has higher scarps that are the product of two or more events. However, many of the single-event scarps on this segment are morphologically similar to the approximately 30,000-yr-old scarps on the Arco segment. Thus, the geologic relations indicate two faulting events younger than about 30,000 yr old, and, because of the relatively degraded character of the youngest scarps, we

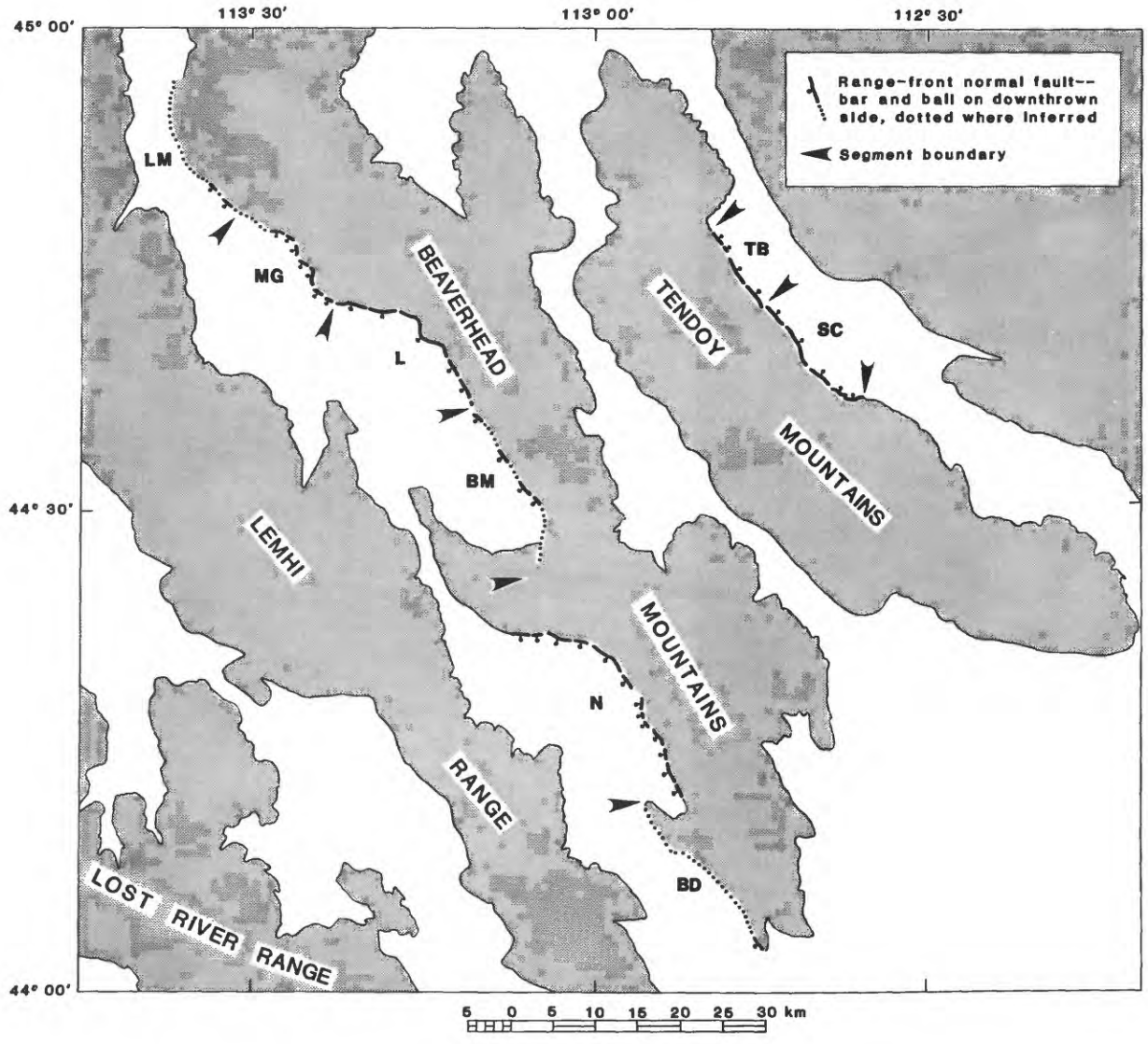

FIGURE 4.--Generalized map of the Beaverhead and Tendoy Mountains showing segments of the Beaverhead and Red Rock faults (Haller, 1988b); arrows identify segment boundaries. Segment names for the Beaverhead fault are: LM, Lemhi; MG, Mollie Gulch; L, Leadore; BM, Baldy Mountain; N, Nicholia; BD, Blue Dome. Segment names for the Red Rock fault are: TB, Timber Butte; SC, Sheep Creeks (Stickney and Bartholomew, 1987). See table 1 for information about individual segments.

believe that the most recent surface faulting occurred shortly after deposition of the 15,000-yr-old alluvium.

The Baldy Mountain segment has no scarps on Quaternary alluvium, indicating no surface faulting since onset of the last major episode of alluviation about 25,000 yr ago (Pierce and Scott, 1982). However, using the criteria of Bull (1987), the general morphology of the mountain front indicates that late Quaternary uplift, and, thus faulting, has occurred on this segment. Along the Baldy Mountain segment, the junction between the range front and the piedmont is generally straight and unembayed, and major streams that emerge from the mountains have V-shaped to U-shaped cross-valley profiles. From the characteristics of these landforms (see fig. 1 in Bull, 1987), we infer that the length of time since uplift (and thus, recurrent faulting) has occurred on this segment is no more than 100,000-150,000 yr.

The Leadore segment, which spans a prominent range-front embayment, is marked by generally continuous, morphologically young scarps on alluvium along its length. Two surface-faulting events have ruptured the Leadore segment in the past 25,000 yr. The most recent faulting is probably middle Holocene in age based on comparing single-event fault scarps on this segment with the scarps on the Mackay segment of the Lost River fault.

Scarps on the Mollie Gulch segment are poorly preserved and generally are located high on the colluvial slopes of the mountain front. The age of faulting is poorly constrained by the available data but, because scarps are still-recognizable on steep (>25°) slopes of the range front, we believe that the youngest surface faulting is probably late Pleistocene in age.

The Lemhi segment is the northernmost segment of the Beaverhead fault. The range front is less precipitous and more subdued along this part of the fault than elsewhere to the south. On the Lemhi segment, the high part of the range is separated from the adjacent valley by an area of relatively low hills as wide as 5 km. This suggests a generally slower rate of tectonic uplift on this segment compared to adjacent segments. The absence of scarps on alluvial deposits along this segment suggests the youngest surface faulting is older than latest Pleistocene (~25,000 yr) and may be more than 100,000 yr old.

The Red Rock Fault

The 60-km-long Tendoy Mountains are bounded on the northeast by the Red Rock fault (fig. 4). Quaternary deposits are not faulted along the northern 23 km or southern 10 km of the range front, so we discuss only the central part of the fault where alluvium is faulted. Changes in fault-scarp morphology along the 27-km-long central part suggests two segments (fig. 5), the 16-km-long Sheep Creeks segment on the southeast and the 11-km-long Timber Butte segment on the northwest (Stickney and Bartholomew, 1987).

Multiple-event scarps are present on upper Pleistocene terraces on the Sheep Creeks segment. The relation of these scarps to various Quaternary deposits, scarp-morphology data, and trenching studies near the southern end of the segment by Bartholomew and Stickney (1987) all indicate two faulting events in the last 10,000-15,000 yr. The most recent event is probably middle Holocene in age.

The youngest scarps on the Timber Butte segment are more degraded than those on the Sheep Creeks segment (fig. 5); their morphology suggests an age of 15,000 yr for the youngest faulting event. Multiple-event scarps are also present on this segment but we cannot estimate the age of the older event(s).

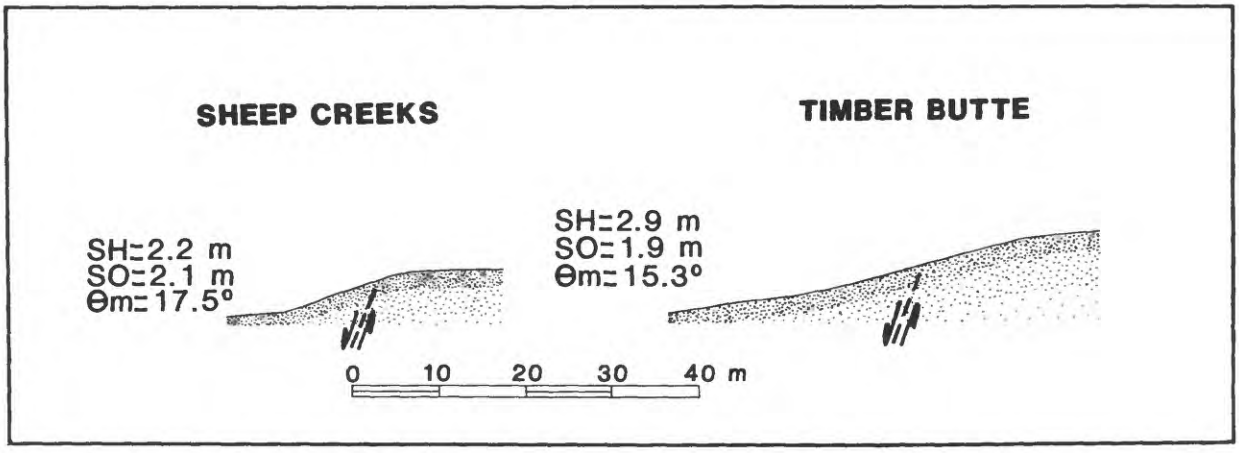

FIGURE 5.--Comparison of typical morphology of single-event scarps on the Timber Butte (TB) and Sheep Creeks (SC) segments of the Red Rock fault. SH is scarp height, SO is surface offset, and θm is maximum slope angle of the scarp. Horizontal and vertical scales are equal. Dashed line with arrow shows inferred location of fault. Fault scarps are nearly continuous across the segment boundary; the boundary is located at a distinct change in the morphology of the scarps.

In summary, the size, morphology, and relation of fault scarps to Quaternary deposits of different ages provide a basis for subdividing the Lost River, Lemhi, Beaverhead, and Red Rock faults into individual segments. In general, segments along the central parts of the faults have the youngest surface faulting and the clearest evidence of recurrent latest Quaternary faulting. In contrast, the ends of the faults are characterized by more subdued mountain-front morphology and, where present, more degraded fault scarps, both of which suggest relatively slow rates of tectonic uplift.

The average length of the segments for the Lost River, Lemhi, Beaverhead, and Red Rock faults is 23 km, 25 km, 25 km, and 14 km, respectively. For comparison, the average segment lengths for the Wasatch (Machette and others, 1987), East Cache (McCalpin, 1987), and Bear Lake (Crone, unpublished mapping 1982) faults in Utah and Idaho are 30 km, 18 km, and 18-21 km, respectively. Thus, if coseismic ruptures are typically confined to one segment and if the segment lengths on all of the faults discussed are generally correct, then the average length of surface faulting associated with large earthquakes on these faults would be in the range of 20-25 km.

Statistical relations between surface-rupture length and magnitude (Bonilla and others, 1984) suggest that surface ruptures 20-25 km long are associated with earthquakes of magnitude (M_s) less than 7. The two historic surface-faulting earthquakes in the region had magnitudes greater than 7 but the length of surface rupture was less than that which would be predicted from the statistical relations. The M_s 7.3 Borah Peak, Idaho, earthquake produced a maximum of 36 km of surface rupture but only 22 km from the primary rupture (Crone and others, 1987), and the M_s 7.5 Hebgen Lake, Montana, earthquake (Doser, 1985) produced about 26 km of surface rupture (from Bonilla and others, 1984). This emphasizes the need to apply the statistical relations

between rupture length and magnitude cautiously when considering faults in the northern Basin and Range province.

IDENTIFYING SEGMENT BOUNDARIES

Four geologic characteristics of segment boundaries that we recognize from our studies in the Idaho-Montana area are: (1) prominent en echelon offsets or gaps in continuity of fault scarps, (2) distinct, persistent changes in fault-scarp morphology along strike that probably indicate different ages of faulting, (3) major salients in the range front, and (4) transverse bedrock ridges that indicate a local decrease in the cumulative throw on the fault. Individually, these characteristics do not uniquely define a segment boundary, but collectively, we believe that the spatial coincidence of several of these characteristics on a fault is good evidence of a tectonically significant segment boundary. A scaling factor is involved when applying these characteristics; for example, en echelon offsets or gaps of a several tens of meters or even hundreds of meters are common within a segment. Similarly, bends or small salients commonly occur within segments. The en echelon offsets, gaps, and salients we consider as indicators of segment boundaries are features whose size is measured on the scale of kilometers.

En Echelon Offsets or Gaps in Scarps

Major en echelon offsets and gaps in the continuity of fault scarps are useful indicators of segment boundaries, especially where the fault scarps on one side of the offset or gap diverge away from the mountain front (fig. 6). Major en echelon offsets or gaps in scarp continuity must be clearly related to tectonic causes and thus reflect along-strike discontinuities or geometrical irregularities in the subjacent fault that would inhibit slip propagation (Sibson, 1987). Obviously, gaps caused by post-faulting erosion or deposition are the result of surficial processes unrelated to the geometry of the fault.

Gaps and en echelon offsets mark several segment boundaries on the faults we studied. On the Lost River fault, a 1.4-km-long gap in late Pleistocene scarps and a 4.7-km-long gap in 1983 scarps separate the Warm Spring and Thousand Springs segments. Also, a 3-4-km-long gap in scarps along the range front separates the Thousand Springs and Mackay segments. None of the segments on the Lost River fault are separated by en echelon offsets. On the Lemhi fault, a 2.5-km-long gap separates the Fallert Springs and Howe segments, and en echelon offsets define both ends the Goldburg segment. At the northwestern end of the Goldburg segment, the offset to the Patterson segment is 1.4 km, and, at the southeastern end, the offset to the Sawmill Gulch segment is 3.8 km. On the Beaverhead fault, a 6-km-long gap separates the Baldy Mountain and Nicholia segments, and a 5.5-km-wide en echelon offset separates the Nicholia and Blue Dome segments (fig. 6).

Persistent Changes in Fault-Scarp Morphology

Pronounced, persistent, along-strike changes in fault-scarp morphology usually indicate that the age of surface faulting is significantly different on adjacent parts of the fault. Fault-scarp morphology provides a simple, efficient way to broadly categorize the age of scarps, and thus identify parts of a fault with distinctly different rupture histories. Several segment

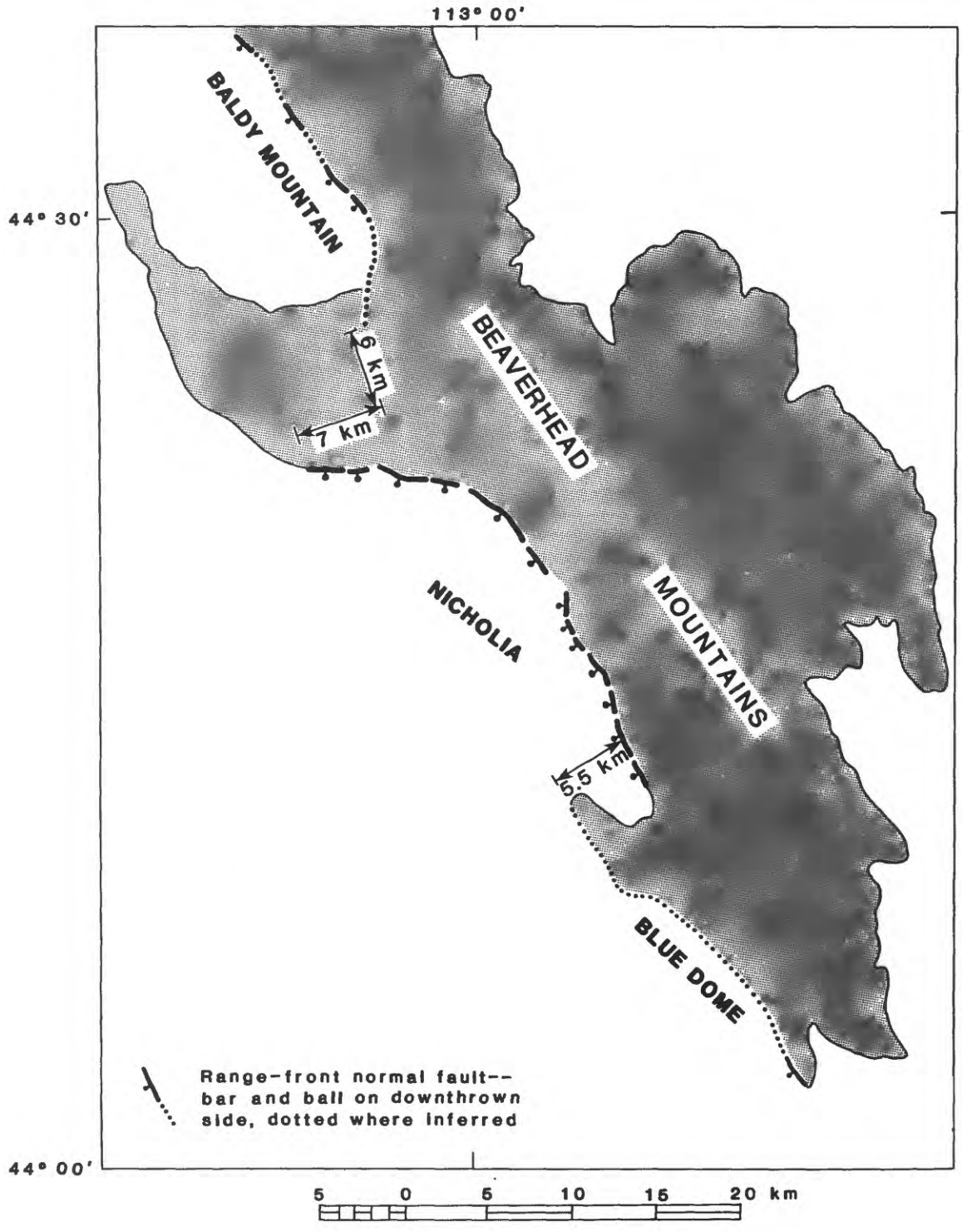

FIGURE 6.--Schematic map of fault scarps along part of the Beaverhead fault, east-central Idaho, showing gap between Baldy Mountain and Nicholia segments, and en echelon offset between Nicholia and Blue Dome segments.

boundaries coincide with significant changes in scarp morphology, including the Timber Butte-Sheep Creeks segment boundary on the Red Rock fault (fig. 5).

Major Salients

Studies of the Borah Peak earthquake and the Wasatch fault zone show that segment boundaries commonly coincide with major salients in the range front. The Borah Peak earthquake nucleated at a segment boundary that is marked by a salient where the range front changes strike by 55° (Crone and others, 1987). Four major salients on the Wasatch fault zone identify persistent segment boundaries that are likely to control future coseismic ruptures (Machette and others, 1987; Wheeler and Krystinik, 1987). On the Beaverhead fault, the boundary between the Leadore and Mollie Gulch segments coincides with a major salient in the range front (fig. 4).

In contrast to the apparent correlation between segment boundaries and major salients, we found no correlation between segment boundaries and major embayments in our study area. The Pass Creek segment of the Lost River fault (fig. 3), the Sawmill Gulch segment of the Lemhi fault (fig. 3), and the Leadore and Nicholia segments of the Beaverhead fault (fig. 4) span major embayments in the range fronts.

Transverse Bedrock Ridges

Some segment boundaries are defined by transverse ridges of bedrock expressed either at the surface or in the subsurface. At these ridges, the cumulative throw on the fault is significantly less than it is along the interior of the adjacent segments. Less throw at these types of segment boundaries indicates that they are long-lived features that have persisted through many earthquake cycles (Wheeler and Krystinik, 1987).

A transverse bedrock ridge forms the barrier at the northwestern end of the Thousand Springs segment that stopped the primary rupture of the Borah Peak earthquake. This ridge is expressed topographically as the Willow Creek hills, a group of intra-valley hills on the southwest flank of the Lost River Range (fig. 2). Intra-valley hills on the southwest flanks of both the Lemhi Range and Beaverhead Mountains presumably identify similar transverse ridges. These ridges mark the Goldburg-Sawmill Gulch segment boundary of the Lemhi fault (fig. 3) and the Baldy Mountain-Nicholia segment boundary of the Beaverhead fault (fig. 4).

Some transverse bedrock ridges have no surface expression but can be identified with gravity, magnetic, and (or) seismic-reflection data. Gravity data are especially helpful in identifying transverse ridges buried by basin fill. Typically, the basin fill is thin over transverse ridges because of the small cumulative throw on the fault. Thus, buried transverse ridges should be expressed as gravity saddles where relatively dense bedrock is covered by a thin veneer of less-dense basin fill.

We find a good correlation at most locations between the segment boundaries we describe and gravity saddles in the adjacent valleys (fig. 7). For many segments, especially along the Lemhi fault, closed gravity lows correspond to the interiors of segments where throw on the fault is greatest, and thus, the basin fill is thickest. Although not all gravity saddles correlate with the boundaries identified from surficial geologic data, the combined analysis of bouguer gravity and surficial geology provide a very good basis for recognizing segment boundaries on normal faults.

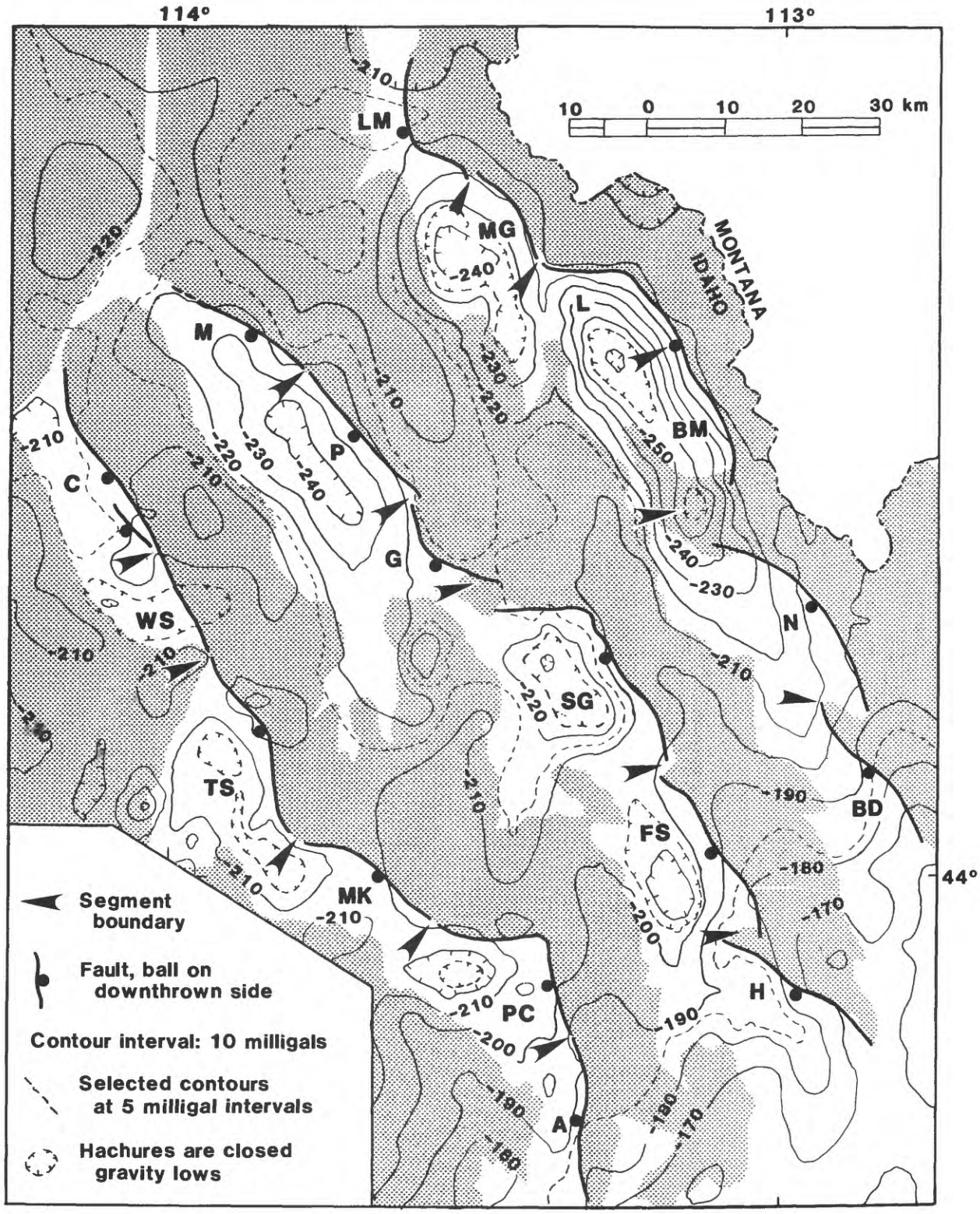

FIGURE 7.--Bouguer gravity anomaly map (from Bankey and others, 1985) and segmentation of range-front faults in east-central Idaho. Upper-case letters for segment names are explained in figures 3 and 4. From southwest to northeast, the faults are the Lost River, Lemhi, and Beaverhead faults.

SEGMENTATION AND SEISMIC-HAZARD ASSESSMENTS

Accurate seismic-hazard assessments rely on defining fault-zone segments and evaluating the reliability of individual segment boundaries to stop propagating ruptures. Segment boundaries that completely stop ruptures allow adjacent segments to behave independently during individual earthquakes. An important objective of future studies in paleoseismology should be to evaluate the behavior of different kinds of segment boundaries through several seismic cycles. This evaluation is best achieved by determining the timing of successive events on several adjacent segments. If adjacent segments have distinctly different temporal histories of surface faulting, then the boundary between those segments has probably halted propagating ruptures repeatedly in the past, and will likely do so in the future.

The above description of the behavior of segment boundaries is obviously simplistic. The segment boundaries we have identified in this study are actually just small areas of a fault (called barriers) that is consistently more resistant to rupturing, and therefore, break less frequently (or as frequently but with less throw each time) than other adjacent parts of the fault. Presumably, the past behavior of these barriers is a reasonable guide to their behavior in the future. However, at some times during their history, all segment boundaries must rupture otherwise mountain fronts would not develop into generally continuous topographic escarpments. Thus, ultimately, no segment boundaries are truly persistent throughout the entire history of the fault.

An important complication to our simplistic description of segment-boundary behavior is that some boundaries may best be described as "leaky" boundaries. In these cases, the boundary severely impedes a propagating rupture, but is not completely effective at preventing displacement on adjacent segments. The boundary of the northwestern end of the Thousand Springs segment exhibited this type of behavior during the Borah Peak earthquake. At the Willow Creek hills barrier, the primary rupture was arrested or deflected away from the Lost River fault, but enough seismic energy leaked through the barrier to trigger minor surface faulting on the Warm Spring segment. This type of "leaky" behavior may be a function of the amount of strain that has accumulated on adjacent segments of a fault and the direction of rupture propagation.

The morphology of the scarps near the Timber Butte-Sheep Creeks segment boundary of the Red Rock fault suggests that this boundary may have been a "leaky" boundary during the youngest faulting on the Sheep Creeks segment. Typically, scarps on the Timber Butte segment are more degraded with more rounded crests and lower maximum slope angles than scarps on the Sheep Creeks segment. However, a prominent, steep bevel, approximately 0.5 m high, is superimposed on the degraded scarps of the Timber Butte segment located adjacent to the segment boundary (Haller, 1988b). This bevel suggests that the youngest rupture on the Sheep Creeks segment extended across the segment boundary and produced minor surface faulting on the Timber Butte segment. Determining if this style of behavior is typical of some segment boundaries has important implications to hazard assessments and to our understanding of the long-term behavior of seismogenic faults.

REFERENCES CITED

Bankey, Viki, Webring, Michael, Mabey, D.R., Kleinkopf, M.D., and Bennett, E.H., 1985, Complete Bouguer gravity anomaly map of Idaho: U.S. Geological Survey Miscellaneous Field Studies Map MF-1773, scale 1:500,000.

Bartholomew, M.J., and Stickney, M.C., 1987, Late Quaternary faulting in southwest Montana [abs.]: Geological Society of America Abstracts with Programs, v. 19, no. 5, p. 258-259.

Boatwright, John, 1985, Characteristics of the aftershock sequence of the Borah Peak, Idaho, earthquake determined from digital recordings of the events: Bulletin of the Seismological Society of America, v. 75, no. 5, p. 1265-1284.

Bonilla, M.G., Mark, R.K., and Lienkaemper, J.J., 1984, Statistical relations among earthquake magnitude, surface rupture length, and surface fault displacement: Bulletin of the Seismological Society of America, v. 74, no. 6, p. 2379-2411.

Bruhn, R.L., Gibler, P.R., and Parry, W.T., 1987, Rupture characteristics of normal faults--An example from the Wasatch fault zone, Utah, in Coward, M.P., Dewey, J. F., and Hancock, P.L., eds., Continental extensional tectonics: Geological Society Special Publication No. 28, p. 337-353.

Bull, W.B., 1987, Relative rates of long-term uplift of mountain fronts, in Crone, A.J., and Omdahl, E.M., eds., Proceedings of conference XXXIX-Directions in paleoseismology: U.S. Geological Survey Open-File Report 87-673, p. 192-202.

Crone, A.J., Machette, M.N., Bonilla, M.G., Lienkaemper, J.J., Pierce, K.L., Scott, W.E., and Bucknam, R.C., 1987, Surface faulting accompanying the Borah Peak earthquake and segmentation of the Lost River fault, central Idaho: Bulletin of the Seismological Society of America, v. 77, no. 3, p. 739-770.

Crone A.J., and Omdahl, E.M., eds., 1987, Proceedings of conference XXXIX-Directions in paleoseismology: U.S. Geological Survey Open-File Report 87-673, 456 p.

Doser, D.I., 1985, Source parameters and faulting processes of the 1959 Hebgen Lake, Montana, earthquake sequence: Journal of Geophysical Research, v. 90, no. B9, p. 4537-4555.

Fonseca, Julia, 1988, The Sou Hills--A barrier to faulting in the central Nevada seismic belt: Journal of Geophysical Research, v. 93, no. B7, p. 475-489.

King, Geoffrey, and Yielding, Graham, 1984, The evolution of a thrust fault system--processes of rupture initiation, propagation and termination in the 1980 El Asnam (Algeria) earthquake: Geophysical Journal of the Royal Astronomical Society, v. 77, p. 915-933.

Haller, K.M., 1988a, Proposed segmentation of the Lemhi and Beaverhead faults, Idaho, and Red Rock fault, Montana--Evidence from studies of fault-scarp morphology: Geological Society of America Abstracts with Programs, v. 20, no. 6, p. 418.

------ 1988b, Segmentation of the Lemhi and Beaverhead faults, east-central Idaho, and Red Rock fault, southwest Montana, during the Quaternary: unpublished M.S. thesis, University of Colorado, 141 p., 10 pl.

Hanks, T.C., and Schwartz, D.P., 1987, Morphologic dating of the pre-1983 fault scarp on the Lost River fault at Doublespring Pass road, Custer County, Idaho: Bulletin of the Seismological Society of America, v. 77, no. 3, p. 837-846.

Machette, M.N., Personius, S.F., and Nelson, A.R., 1987, Quaternary geology along the Wasatch fault zone--Segmentation, recent investigations, and preliminary conclusions, in Gori, P.L., and Hays, W.W., eds., Assessment of regional earthquake hazards and risk along the Wasatch Front, Utah: U.S. Geological Survey Open-File Report 87-585, v. I, p. A1-A72.

Malde, H.E., 1987, Quaternary faulting near Arco and Howe, Idaho: Bulletin of the Seismological Society of America, v. 77, no. 3, p. 847-867.

McCalpin, James, 1987, Late Quaternary tectonics and earthquake hazard in Cache Valley, Utah: U.S. Geological Survey Final Technical Report, Contract No. 14-08-0001-G1091, 187 p., 2 pl.

Pierce, K.L., 1985, Quaternary history of faulting on the Arco segment of the Lost River fault, central Idaho, in Stein, R.S., and Bucknam, R.C., eds., Proceedings of workshop XXVIII-On the Borah Peak, Idaho, earthquake: U.S. Geological Survey Open-File Report 85-290, p. 195-206.

Pierce, K.L., Obradovich, J.D., and Friedman, Irving, 1976, Obsidian hydration dating and correlation of Bull Lake and Pinedale Glaciations near West Yellowstone, Montana: Geological Society of America Bulletin, v. 87, no. 5, p. 703-710.

Pierce, K.L., and Scott, W.E., 1982, Pleistocene episodes of alluvial-gravel deposition, southeastern Idaho, in Bonnichsen, Bill, and Breckenridge, R.M., eds., Cenozoic geology of Idaho: Idaho Bureau of Mines and Geology Bulletin 26, p. 685-702.

Porter, S.C., Pierce, K.L., and Hamilton, T.D., 1983, Late Wisconsin mountain glaciation in the Western United States, in Wright, H.E., ed., Late Quaternary environments of the United States: Minneapolis, Minnesota, University of Minnesota Press, v. 1, p. 71-111.

Reynolds, M.W., 1979, Character and extent of Basin-Range faulting, western Montana and east-central Idaho: Rocky Mountain Association of Geologists and Utah Geological Association, 1979 Basin and Range Symposium, p. 185-193.

Schwartz, D.P., and Coppersmith, K.J., 1984, Fault behavior and characteristic earthquakes--Examples from the Wasatch and San Andreas fault zones: Journal of Geophysical Research, v. 89, no. B7, p. 5681-5698.

_____ 1986, Seismic hazards--New trends in analysis using geologic data, in Active tectonics, Studies in geophysics: Washington, D.C., National Academy Press, p. 215-230.

Schwartz, D.P., and Crone, A.J., 1988, Paleoseismicity of the Lost River fault zone, Idaho--Earthquake recurrence and segmentation: Geological Society of America Abstracts with Programs, v. 20, no. 3, p. 228.

_____ 1985, The 1983 Borah Peak earthquake--A calibration event for quantifying earthquake recurrence and fault behavior on Great Basin normal faults, in Stein, R.S., and Bucknam, R.C., eds., Proceedings of workshop XXVIII-On the Borah Peak, Idaho, earthquake: U.S. Geological Survey Open-File Report 85-290, p. 153-160.

Scott, W.E., Pierce, K.L., and Hait, M.H., Jr., 1985, Quaternary tectonic setting of the 1983 Borah Peak earthquake, central Idaho: Bulletin of the Seismological Society of America, v. 75, no. 4, p. 1053-1066.

Sibson, R.H., 1987, Effects of fault heterogeneity on rupture propagation, in Crone, A.J., and Omdahl, E.M.. eds., Proceedings of conference XXXIX-Directions in paleoseismology: U.S. Geological Survey Open-File Report 87-673, p. 362-373.

Skipp, Betty, and Hait, M.H., Jr., 1977, Allochthons along the northeast margin of the Snake River Plain, Idaho: Wyoming Geological Association 29th Annual Field Conference Guidebook, p. 499-515.

Stein, R.S., and Barrientos, Sergio, 1985, Planar high-angle faulting in the Basin and Range--Geodetic analysis of the Borah Peak, Idaho, earthquake: Journal of Geophysical Research, v. 90, no. B13, p. 11,355-11,366.

Stickney, M.C., and Bartholomew, M.J., 1987, Seismicity and late Quaternary faulting of the northern Basin and Range province, Montana and Idaho: Bulletin of the Seismological Society of America, v. 77, no. 5, p. 1602-1625.

Vincent, K.R., 1985, Measurement of vertical tectonic offset using longitudinal profiles of faulted geomorphic surfaces near Borah Peak, Idaho--A preliminary report, in Stein, R.S., and Bucknam, R.C., eds., Proceedings of workshop XXVIII on the Borah Peak, Idaho, earthquake: U.S. Geological Survey Open-File Report 85-290, p. 76-96.

Wheeler, R.L., 1987, Boundaries between segments of normal faults--Criteria for recognition and interpretation, in Crone, A.J., and Omdahl, E.M., eds., Proceedings of conference XXXIX-Directions in paleoseismology: U.S. Geological Survey Open-File Report 87-673, p. 385-389.

Wheeler, R.L., and Krystinik, K.B., 1987, Persistent and nonpersistent segmentation of the Wasatch fault zone, Utah--Statistical analysis for evaluation of seismic hazard, in Gori, P.L., and Hays, W.W., eds., Assessment of regional earthquake hazards and risk along the Wasatch Front, Utah: U.S. Geological Survey Open-File Report 87-585, v. 1, p. B1-B124.

HISTORICAL BASIN AND RANGE PROVINCE SURFACE FAULTING AND FAULT SEGMENTATION

by

Craig M. dePolo[1], Douglas G. Clark[2], D. Burton Slemmons[2], and William H. Aymard[3]

1 Nevada Bureau of Mines and Geology
2 Center for Neotectonic Studies
3 Cooperative Institute for Aerospace Science and Terrestrial Applications

Mackay School of Mines
University of Nevada - Reno
Reno, Nevada 89557

ABSTRACT

Seventeen historical Basin and Range earthquakes associated with surface faulting provide a data base for evaluating the relation between surface rupture and fault zone structure in an extensional tectonic setting. Several of these events had widely distributed surface rupture patterns, ruptured in complex manners, or extended beyond mapped lengths of faults. Eleven of the seventeen events were divided into geometric or structural segments. Moderate magnitude ($M<7$) events ruptured individual geometric or structural segments (three events) and were associated with sympathetic or secondary surface faulting (at least three events). All of the earthquakes with magnitude ≥ 7 (eight events) ruptured multiple geometric or structural segments. Approximately half of the surface rupture end-points coincided with identifiable fault zone discontinuities. The results of this study suggest that inferred geometric or structural segments do not always represent earthquake segments in the Basin and Range province. Further, some earthquake discontinuities may be difficult to identify and significant faulting may occur beyond postulated discontinuities. Multiple geometric or structural segments should be considered and several lines of physical and paleoseismic evidence are needed to delineate earthquake segments in the Basin and Range province.

INTRODUCTION

The division of faults into earthquake segments is becoming a widely used technique for determining potential earthquake sizes for seismic hazard analyses. One reason is that segmentation techniques attempt to incorporate more physical and paleoseismic information than more arbitrary techniques (e.g. assumed half lengths).

Application of the concept of fault segmentation has been proposed for a number of faults, including the San Andreas fault system and the Wasatch fault system (Allen, 1968; Schwartz and Coppersmith, 1984; Schwartz, 1988). At the present time there are not enough well-documented examples of fault segmentation to assess the extent of the applicability of segmentation models for different types of faults and in different tectonic settings. This study provides observations of seventeen historical earthquakes associated with surface faulting within the Basin and Range extensional province. Normal, normal-oblique, and strike-slip senses of displacement are represented. We summarize the events and discuss segmentation of the larger surface ruptures. The amount of available data and first-hand experience with each of the events varies to some degree. In each case a comprehensive literature review has been conducted and most of the surface ruptures have been visited in the field by at least one of the authors. Unfortunately, there is only a limited amount of paleoseismic data available for incorporation into this study.

FAULT SEGMENTATION

Fault segments have been identified at a wide range of scales and with different criteria. This has led to many different definitions of the term "segment", making it particularly important to define or understand a specific author's usage of the term. This study examines historical "earthquake segments" or parts of a fault or faults that rupture as a unit during an earthquake. Earthquake segments have been referred to as "earthquake rupture segments" and "rupture segments" by other authors. Large earthquake segments may comprise one or more fault segments as defined in other ways, such as by fault geometry or structure (geometric or structural segments, respectively).

Earthquake segmentation involves the identification and substantiation of "earthquake discontinuities" along faults which may potentially act as barriers to earthquake ruptures. Several compilations of the characteristics of fault zone discontinuities have been presented (Schwartz and Coppersmith, 1984, 1986; Slemmons and dePolo, 1986; Knuepfer, 1987; Wheeler and Krystinik, 1988; Barka and Kadinsky-Cade, 1988). Indicators of fault zone discontinuities fall into several categories: geometric, structural, behavioral, paleoseismic, geomorphic, geological, geophysical, and rheological heterogeneities. Several lines of evidence are needed to confidently identify an earthquake

discontinuity and evaluate its persistence or non-persistence through time.

Geometric discontinuities include changes in fault orientation (bends), step-overs, and separations or gaps in a fault zone. Wheeler (1987) points out that geometric discontinuities in map view may not have a significant effect on earthquake ruptures with a normal sense of displacement. An abrupt bend in a normal fault in map view, for example, can accommodate a vertical slip vector, and would not necessarily inhibit a propagating rupture. Thus, the sense of displacement needs to be understood to evaluate geometric data.

Structural discontinuities include branches and intersections with other faults and folds or terminations at cross structures. Since the ends of a fault zone can be considered structural discontinuities, distinct or individual faults can be considered structural segments.

Behavioral discontinuities include changes in complexity or pattern of surface faults, slip-rates, interseismic intervals, senses of displacement, or creeping versus locked behavior.

Paleoseismic data help to constrain the rupture histories of earthquake segments and discontinuities. In this paper, paleoseismicity refers specifically to prehistoric earthquakes. Determining the history and extent of paleoearthquake segments along a fault zone can provide direct spatial and/or temporal evidence of previous segmentation behavior.

Geomorphic data can fall into geometric, behavioral and paleoseismic categories, but because geomorphology is a common tool used in the study of faults, it warrants its own category. Geomorphic indicators occur at many scales (e.g. large salients in range fronts and smaller scale features such as differences in the morphology of fault scarps related to differences in the timing of discrete events).

Geological indicators of discontinuities include Quaternary basins and young volcanic fields. These features are commonly associated with local tectonic extension along a fault zone, which can influence rupture behavior. Abrupt changes in geologic units, particularly where these units have crustal scale dimensions, can also be potential fault zone discontinuities.

Geophysical data can help image subsurface characteristics and geologic structures that can act as discontinuities to faulting. The occurrence of seismicity has also been used as an indicator of discontinuities.

Rheological heterogeneities, which can be important in the physics of discontinuities, include large variations in fault width, crustal type (continental vs. oceanic), thermal gradient, and geologic materials.

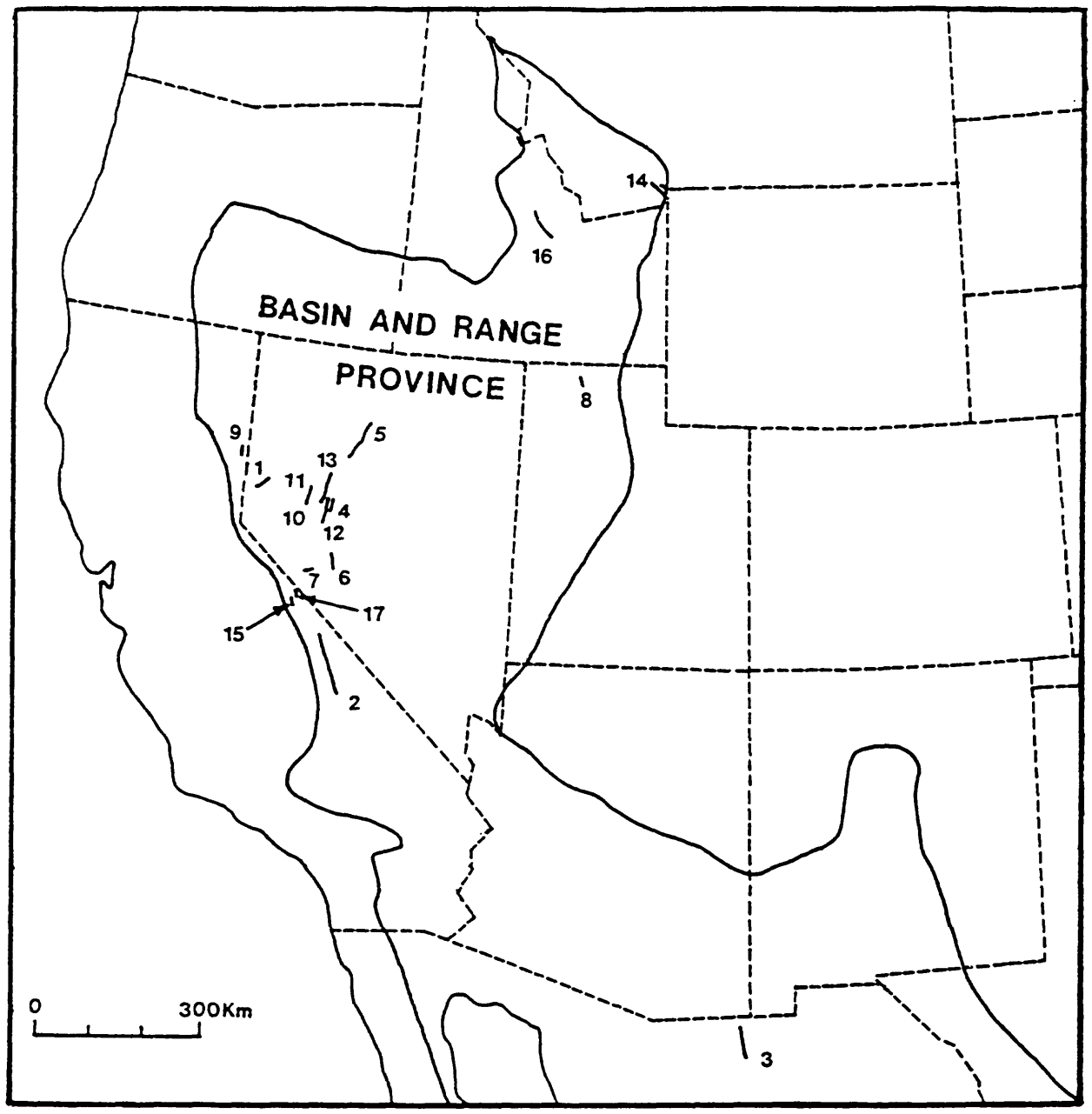

Figure 1. Location map of Basin and Range province surface faulting earthquakes discussed in text. 1, 1869 Olinghouse; 2, 1872 Owens Valley; 3, 1887 Sonora, Mexico; 4, 1903 Wonder; 5, 1915 Pleasant Valley; 6, 1932 Cedar Mountain; 7, 1934 Excelsior Mountain; 8, 1934 Hansel Valley; 9, 1950 Fort Sage Mountain; 10 and 11, 1954 Rainbow Mountain; 12, 1954 Fairview Peak; 13, 1954 Dixie Valley; 14, 1959 Hebgen Lake; 15, 1980 Mammoth Lakes; 16, 1983 Borah Peak; 17, 1986 Chalfant Valley. Base map modified from Stewart (1978, Fig 1-2) and Renyolds (1977).

BASIN AND RANGE PROVINCE

The Basin and Range province of the western United States and northern Mexico is a Cenozoic extensional province that is actively deforming (fig. 1). The province encompasses the extensional areas between the Rocky Mountains on the east and the Sierra Nevada on the west, and from the Lewis and Clark Line in Montana (Reynolds, 1979) south into northern Mexico (fig. 1). Spatial and temporal variations in the rates of activity have occurred within the province throughout the Cenozoic. Today, higher rates of tectonic activity occur in the northern Basin and Range province and along the province's east and west margins than in the southern half of the province.

Most of the active extensional region is marked by high heat flow, thin crust, sparsely distributed, bimodal volcanic activity, and generally shallow earthquakes with focal depths of 10 to 15 km or less. Geomorphic, geophysical, and topographic information indicates widespread domains of tilted fault blocks and horst and graben development. Historical seismic activity in the Basin and

TABLE 1. HISTORICAL SURFACE FAULTING EVENTS IN THE BASIN AND RANGE PROVINCE

No.	Date	Magnitude	Earthquake, or Fault	Main Style of Surface Faulting
1	12-27-1869	6.7	Olinghouse, NV	Strike-slip, normal-oblique?
2	03-26-1872	M_W = 7.8-8.0	Owens Valley, CA	Strike-slip
3	05-03-1887	M_W = 7.2-7.4	Sonora, Mexico	Normal
4	1903?	5.5-6.5?	Wonder, NV	Normal, normal-oblique?
5	10-03-1915	M_S = 7.6	Pleasant Valley, NV	Normal
6	12-21-1932	M_S = 7.2	Cedar Mtn., NV	Strike-slip
7	01-30-1934	6.3	Excelsior Mtn, NV	Normal-oblique?
8	03-14-1934	6.6	Hansel Valley, UT	Normal-oblique?
9	12-14-1950	M_L = 5.6	Ft. Sage Mtn., CA	Normal
10	07-06-1954	M_S = 6.3	Rainbow Mtn., NV	Normal
11	08-24-1954	M_S = 7	Rainbow Mtn., NV	Normal
12	12-16-1954	M_S = 7.2	Fairview Peak, NV	Normal-oblique
13	12-16-1954	M_S = 6.8	Dixie Valley, NV	Normal
14	08-17-1959	M_S = 7.5	Hebgen Lake, MT	Normal
15	05-25-1980-05-27-1980	M_L = 6.0-6.3	Mammoth Lakes, CA	Strike-slip & Normal-oblique
16	10-29-1983	M_S = 7.3	Borah Peak, ID	Normal-oblique
17	07-21-1986	M_S = 6.2	Chalfant Valley, CA	Strike-slip

Range province is concentrated in three major belts: 1) along the western margin of the province, 2) within the western part of the province, along the Central Nevada-Eastern California seismic belt, and 3) along the eastern margin of the province, along the Intermountain seismic belt.

HISTORICAL SURFACE FAULTING EVENTS

Seventeen events are reviewed in this paper that have been associated with surface rupture in the Basin and Range province (table 1, and fig. 1).

Historical surface ruptures are not uniformly distributed throughout the Basin and Range province, but rather, occur in discrete spatial/temporal groupings (Wallace, 1987). Eleven of the seventeen events (Events 2,4-7,10-13,15 and 17) occurred within the northeast-trending Central Nevada-Eastern California seismic belt (Wallace, 1984b). Events 8, 14 and 16 occurred in the Intermountain seismic belt.

1869 Olinghouse, Nevada Earthquake

The December 27, 1869 Olinghouse earthquake is believed to have ruptured a portion of the arcuate east to northeast-trending Olinghouse fault zone in west-central Nevada (fig. 1). Displacement was primarily left-lateral (D_{max}= 3.7 m), with additional dip-slip (up to 0.9 m) offsets locally (Sanders and Slemmons, 1979). Toppozada and others (1981) question the location of the 1869 event and instead prefer an epicenter located farther south, based on an isoseismal map of the event. The seismic parameters of this pre-instrumental event are poorly known; the isoseismal pattern and maximum intensities, however, suggest an estimated 6.7 magnitude (Slemmons, 1977).

Length of the 1869 surface rupture is not well constrained but may have ruptured a maximum of 23 km from the southwestern edge of the Pyramid Lake fault zone and late Cenozoic basin to where the Olinghouse fault dies out or splays about 3 km northwest of Clark Station. Bell (1984) indicates 5 to 12 km of historical surface rupture. The uncertainties of the event location and rupture extent make it difficult to evaluate the relation between surface rupture and fault zone structure.

1872 Owens Valley, California Earthquake

The March 26, 1872 Owens Valley earthquake is the largest historical event in the Basin and Range province, both in apparent size and rupture parameter measurements. It had an estimated magnitude of M_w=7 3/4 to 8, and was felt strongly over an area of 324,000 km^2 (Beanland and others, in review; Coffman and von Hake, 1973).

The 1872 earthquake caused 100 to 110 km of surface faulting along the Owens Valley fault zone (OVFZ) in the westernmost Basin and Range province (fig. 1). Surface displacements were dominantly right-lateral strike-slip, with a maximum lateral offset of 7 m, an average lateral offset of 6 m, a maximum vertical offset of 4.4 m, and an average vertical offset of 1 m (Beanland and others, in rev.). The surface rupture consisted of a relatively straight central section located in the middle of a large graben (Owens Valley) and more distributed, non-linear northern and southern sections (fig. 2).

Both the north and south ends were at or near extensional basins. The north end of the rupture zone appears to step and distribute slip into northern Owens Valley, forming small depressions within the valley such as Klondike and Warren Lakes. The OVFZ at this location has complex intersections or stepping relationships with other fault zones.

The exact position of the southern end of the 1872 surface rupture is less certain. Faults that ruptured in 1872 clearly offset the shorelines at the northern end of Owens Lake, whereas at the southern end there was extensive liquefaction and the tectonic component is less clear. The southern end of the rupture can be estimated with an uncertainty of <10 km, however, and probably terminated near Olancha, where the basin ends at the south against a northeast-trending fault zone and the Coso Range.

The OVFZ can be divided from south to north into four geometric segments (fig. 2): the Owens Lake segment, the Lone Pine segment, the Independence segment, and the Poverty Hills - Klondike Lake segment. The Owens Lake segment extends about 25 km from Olancha to the northern edge of Owens Lake and has a slightly more northerly trend than the rest of the OVFZ. Both segment ends may be at cross-fault intersections. The OVFZ is difficult to delineate along this segment due to the presence of young lake bed sediments and liquefaction features. The Lone Pine segment is up to 2.5 km wide and includes a number of faults between the northern edge of Owens Lake, northward for about 27 km to a 1.5 km right-step (approximate cross-strike distance) between the Lone Pine and Independence segments, which ruptured through in 1872.

The Independence segment (35 km length) is a remarkably linear, narrow fault zone (up to 0.5 km wide), with sag ponds and small left-stepping en echelon patterns. At the northern end of the Independence segment, the Poverty Hills form a distinct discontinuity in the OVFZ. A discontinuity is interpreted here based on several factors: change in fault geometry and distribution, fault intersections, a postulated left step in the fault zone (Martel, 1984), a bedrock high between the Owens Lake and Bishop basins and associated geophysical anomalies, and Quaternary volcanism. This discontinuity appears to have deflected the 1872 rupture's orientation and displacement, but did not terminate the rupture. The Poverty Hills - Klondike Lake segment extends 23 km north of the Poverty Hills. This segment trends

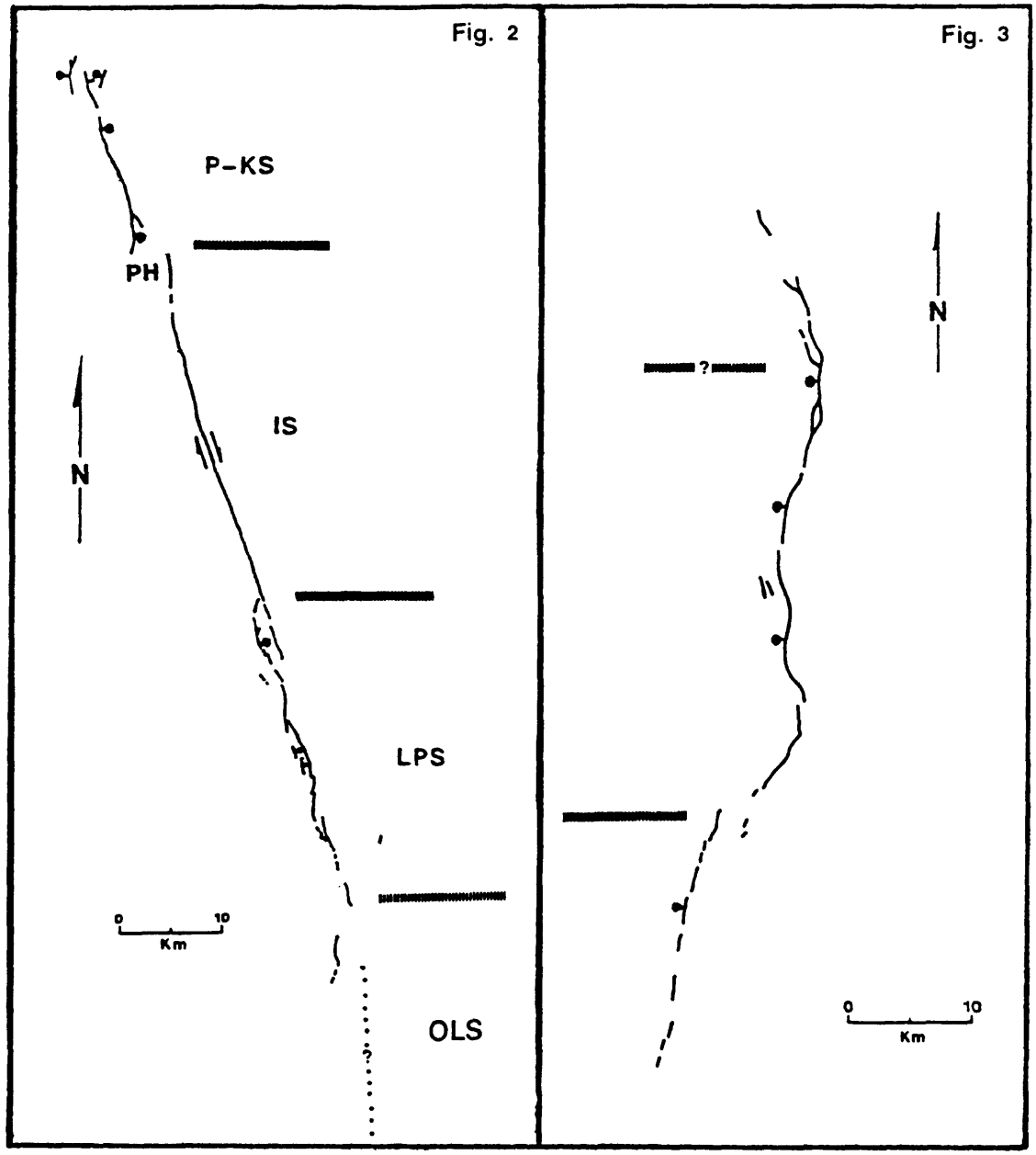

Figures 2 - 11. Selected Basin and Range province historical surface ruptures. Solid lines denote simplified surface ruptures. Balls on downthrown side of fault. Bold lines denote segment boundaries discussed in text.

Figure 2. 1872 Owens Valley (from Beanland and others, in prep.), IS=Independence segment, LPS=Lone Pine segment, OLS=Owens Lake segment, PH=Poverty Hills, P-KS=Poverty Hills-Klondike Lake segment.

Figure 3. 1887 Sonora, Mexico (from Bull and Pearthree, 1988).

slightly more westerly and exhibits a complex pattern with several secondary faults.

The 1872 event ruptured four geometric segments along the OVFZ. The OVFZ shows evidence of at least two prior Holocene events which may have ruptured the same reach as in 1872 (Beanland and Clark, 1987). Determination of the extent of paleoseismic events may result in a fairly accurate delineation of the 1872 earthquake segment.

1887 Sonora, Mexico Earthquake

The May 3, 1887 Sonora earthquake, in the southern Basin and Range province, had a moment magnitude of M_w=7.2 to 7.4 and an estimated felt area of nearly two million square kilometers(DuBois and Sbar, 1981; Herd and McMasters, 1982; DuBois and Smith, 1980). Surface faulting (fig. 3) occurred along the Pitaycachi fault for a distance of 75 km (Bull and Pearthree, 1988). The displacement was dominantly normal, with scarp heights of 0.5 to 4 m (Bull and Pearthree, 1988).

Surface faulting occurred along a mountain front - alluvium contact for much of the rupture length (Goodfellow, 1888; Bull and Pearthree, 1988). Surface faulting at the northern end of the rupture splayed from the range front, bordered a pediment for several kilometers, and extended 5 km into the San Bernardino Valley basin; at the southern end, surface faulting appears to have died out in bedrock, along a range front (Dubois and Smith, 1980; Bull and Pearthree, 1988). The 1887 earthquake segment consisted of at least two and possibly three structural segments (Pearthree, pers. comm., 1988). The southern segment had less than 1 m of vertical displacement and was separated from the northern ruptures by a right step with a cross-strike distance of about 2 km. A northern segment is considered where the fault enters a pediment or structural bench.

The total length of the fault that ruptured in 1887 may have been difficult to identify prior to 1887. Although pre-existing fault scarps are present in older alluvium, much of the fault was covered by Holocene and late Pleistocene deposits, and the continuity along this zone may have been difficult to assess (Bull, pers. comm., 1988). Bull and Pearthree (1988) suggest that about 200,000 years have elapsed since the event prior to 1887.

1903(?) Wonder, Nevada Earthquake

The Wonder earthquake occurred along a fault which was re-ruptured during the 1954 Fairview Peak - Dixie Valley earthquake sequence (fig. 1). Information about this event is incomplete and comes principally from an investigation by Slemmons and others (1959) and unpublished research by Peizhen Zhang and Slemmons. No historical earthquake was recorded for this area, so the timing of

this event is uncertain.

Surface faulting from this event occurred on the Gold King fault on the eastern side of Dixie Valley, near the mining town of Wonder. An unpublished map by F. C. Schrader in 1911 indicates 5 or more kilometers of surface rupture (Slemmons and others, 1959). Personal interviews conducted by Slemmons and others (1959) of a cattleman and miners indicated that surface fractures probably extended a significant distance to the south (potentially as much as 16 km further south). Schrader noted, "the fissure is marked by an open cleft or crack 3 to 5 feet wide, particularly in alluvium, which in places was open to depths of about 5 feet." Slemmons and others (1959) measured 0.15 to 0.6 m vertical offsets produced by the 1954 event, and speculated that the 1903(?) surface ruptures were similar. Recent field work by Peizhen Zhang and Slemmons suggests that the vertical offsets from 1903(?) were closer to 10-30 cm. No earthquake size has been estimated for this event. Because the earthquake was not recorded at the town of Fallon, it is assumed to have been a moderate event, perhaps of magnitude 5.5 to 6.5. The paucity of data on this earthquake rupture makes it difficult to evaluate its potential segmentation.

1915 Pleasant Valley, Nevada Earthquake

The October 2, 1915 Pleasant Valley earthquake, in north-central Nevada, had a surface-wave magnitude of 7.6 (Bonilla and others, 1984), and was felt between southern Washington and the Mexican border and from western Colorado to the Pacific coast. Four major fault scarps formed in a right-stepping en echelon pattern (fig. 4) for a combined, end-to-end rupture distance of 60 km (Wallace, 1984a). From northeast to southwest the major 1915 earthquake scarps are: China Mountain (10 km; D_{max}=1.5 m), Tobin (8.5 km; D_{max}=4.7 m), Pearce (30 km; D_{max}=5.8 m), and Sou Hills (10.5 km; D_{max}=2.7 m). Cross-strike distances between the en echelon steps ranged from 3.5 to 6 km. A fifth scarp near the crest of the Stillwater Range (1.5 km; D_{max}=1.2? m) has been attributed to gravitational spreading (Wallace, 1984a). However, its position as a potential fifth right-step to a zone of faulting with a similar spacing, orientation and west-side-down character suggests a tectonic origin. If this scarp was tectonic, then the total rupture zone length would have been 74 km.

The four major ruptures occurred near the base of west-facing range blocks and mainly followed pre-existing late Quaternary fault scarps. In detail, ruptures formed branching, discontinuous scarps, some of which included abrupt changes in strike and gaps of hundreds of meters. Faulting was predominately dip-slip, with maximum vertical displacement of 5.8 m on the Pearce scarp and an average vertical displacement of 2 m (Wallace, 1984a). Up to 2 m of right-lateral offset occurred locally.

Surface rupture took place on what might be considered four or five individual faults or structural segments, based on the

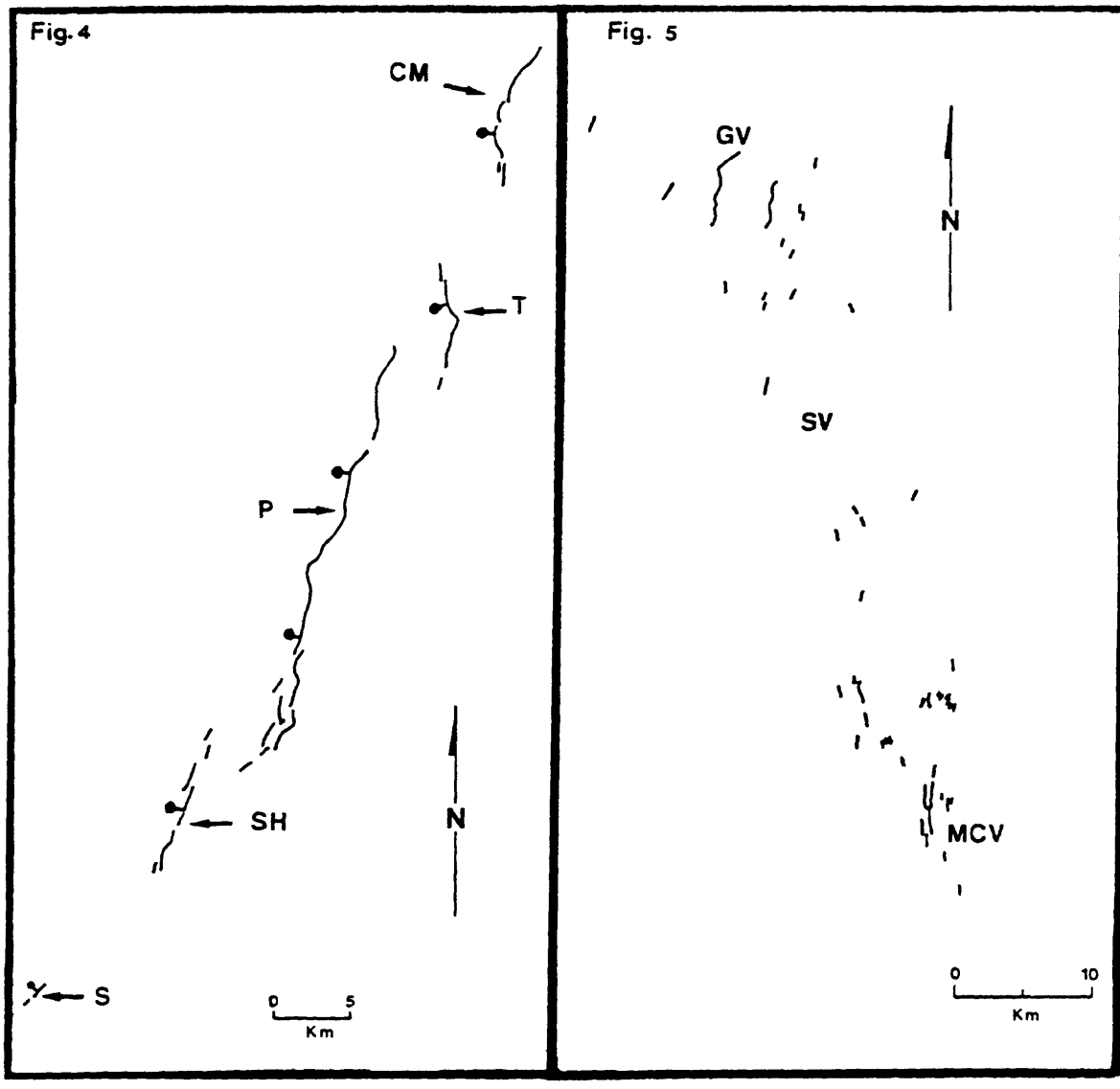

Figure 4. 1915 Pleasant Valley (from Wallace, 1984), CM=China Mountain scarp, P=Pearce scarp, S=Stillwater scarp, SH=Sou Hills scarp, T=Tobin scarp.

Figure 5. 1932 Cedar Mountain (from Gianella and Calleghan, 1934), GV=Gabbs Valley, MCV=Monte Cristo Valley, SV=Stewart Valley.

continuity of horst blocks and the pattern of late Quaternary fault scarps. The Pearce scarp, for example, broke the entire length of the west-dipping Pearce fault (Page, 1934). The Tobin and Sou Hills scarps broke sections of longer, discrete faults that can be mapped several kilometers beyond the 1915 breaks (Wallace, 1984a).

The southern end of 1915 surface faulting (excluding the 1.5 km failure at the crest of the Stillwater Range) coincides with the Sou Hills transverse bedrock zone. Fonseca (1988) used geologic, geomorphic and paleoseismic data to show that the Sou Hills have acted as a profound barrier to the propagation of surface ruptures throughout the Quaternary. The southern end of surface faulting also coincides with aeromagnetic and gravity cross-structures, and a pronounced change in the tilt directions of range blocks north and south of the approximate latitude of the Sou Hills (Stewart, 1980).

The northernmost surface rupture crossed the Tobin Range with a 6 km step (cross-strike distance) in surface faulting between the Tobin and China Mountain scarps (Wallace, 1984a). The north end of the Tobin scarp is aligned with conspicuous late Quaternary fault scarps that continue tens of kilometers to the northwest along the west flank of the Tobin and Sonoma Ranges, which did not rupture in 1915 (Wallace, 1984a).

The 1915 earthquake segment consisted of four and possibly five discrete, structural segments. A notable feature of this surface rupture is the step distances between the segments of up to 6 km. Paleoseismic investigations of the faults involved in this event will be important for assessing whether past earthquakes duplicated the faulting pattern of the 1915 event.

1932 Cedar Mountain, Nevada Earthquake

The December 20, 1932 earthquake in the Cedar Mountain area was a strike-slip event with a wide distribution of scattered surface ruptures (Gianella and Callaghan, 1934). The magnitude of this event was M_s=7.2, with a felt area of 850,000 km^2 (Abe, 1981; Coffman and von Hake, 1973).

The 1932 earthquake involved the rupturing of several faults (fig. 5), including the Stewart-Monte Cristo Valley fault zone (SMCFZ), and several shorter, unnamed faults in Stewart and Gabbs Valleys (Molinari, 1984a, 1984b; dePolo and others, 1987b). Modeling of body waveforms of the main shock from regional and teleseismic seismograms (Doser, in review [a]) also suggests that the main event consisted of multiple earthquakes.

The epicenter of the 1932 earthquake was located in or near Gabbs Valley, near the north end of the rupture zone (Gianella and Callaghan, 1934). The zone of surface ruptures was approximately 60 km in length and 6-14 km wide, and generally trends southeast from the epicentral area. Surface ruptures were not confined to

a mountain front or a single topographic feature, but rather were distributed broadly across three valleys, involving short parts of adjacent mountain fronts. At the northern part of this zone, ruptures were mapped by Gianella and Callaghan as widely spaced, short breaks.

At the southern end of the rupture zone, surface breaks were longer and more narrowly confined. The longest and most continuous surface faulting occurred near the southern end of the rupture zone, along the SMCFZ. Surface faulting occurred discontinuously along the SMCFZ for a distance of about 17 km, with average right-lateral displacements of several tens of centimeters and maximum lateral displacements of 1-2 m (Molinari, 1984a; dePolo and others, 1987a). Normal displacements for the overall rupture zone ranged from 0-0.5 m. The southern end of surface faulting occurred in the vicinity of cross-faults and an extensional basin. The northern termination of surface faulting is indistinct and consisted of several small ruptures in Gabbs Valley. The northernmost 1932 rupture occurred along the southern end of a fault that had small displacements along its northern end during the 1954 Fairview Peak earthquake.

The extent of surface rupture associated with the 1932 earthquake would have been difficult or impossible to predict due to the widespread pattern of many small surface ruptures. This widespread surface rupture pattern has been attributed to possible detachment and folding of Tertiary lake bed and ash flow deposits (Molinari, 1984a). The event may have been composed of several faults (structural segments) failing in sequence, leading to a larger earthquake size than if these faults had failed separately.

1934 Excelsior Mountains, Nevada Earthquake

A magnitude 6.3 earthquake occurred in the Excelsior Mountains area on January 30, 1934 (Slemmons and others, 1965). A northeast-trending surface rupture 1.4 km long was identified by Callaghan and Gianella (1935) near the crest of the Excelsior Mountains. The surface rupture had dominantly down-to-the-north normal displacement (D_{max}=13 cm), with a small en echelon pattern on its western end suggestive of a slight left-lateral component (Callaghan and Gianella, 1935).

Doser (in review [a]) inverted the body waveforms from this event and suggests a dominantly normal focal mechanism. The earthquake's epicenter, originally located 20 km southwest of the surface ruptures, has been relocated by Doser (in review [a]) to about 5 km west of the surface rupture.

There are several possibilities for what this surface rupture may represent: primary, secondary, sympathetic, or non-tectonic rupture. Primary and secondary surface faulting are not likely, if the epicenter located well into the footwall, south or west of the north dipping surface rupture. This surface rupture may

represent sympathetic displacement, which has been observed in several earthquakes in the nearby Mammoth Lakes and Chalfant earthquake sequences. Non-tectonic movement, such as slope failure, has been proposed for this rupture, but this is not apparent from aerial reconnaissance. The rupture lies proximal and subparallel to a small group of faults that separate Tertiary volcanic deposits from metamorphic basement (Garside, 1982). The back-facing character of the fault and the left-lateral component suggests a tectonic, rather than gravitational origin.

1934 Hansel Valley, Utah Earthquake

The Hansel Valley earthquake occurred on March 12, 1934, in the eastern Basin and Range province (fig. 1). The earthquake is located immediately north of the Great Salt Lake, within the Intermountain seismic belt. It had a magnitude of 6.6 and was felt over an area of 440,000 km^2 (Gutenberg and Richter, 1954; Shenon, 1936). Surface ruptures consisted of at least four subparallel, northerly-trending zones, the longest being slightly over 10 km. These zones consist of short breaks, with en echelon patterns, small grabens and extension fractures (Shenon, 1936; McCalpin and others, 1987). The maximum reported displacements were 50 cm vertical (Shenon, 1936) and 25 cm horizontal (Walter, 1934). Liquefaction occurred during this event, which may have caused or enhanced many of the surface ruptures and displacements.

The inversion of regional and teleseismic body waveforms suggests a focal mechanism with nearly pure left-lateral strike-slip displacement occurring on a N38-48°E, vertical fault (Doser, in review [b]). This plane of the solution was chosen because it matches regional structures and, in general, the orientation of surface faulting. Although Shenon (1936) reports that Prof. Reed Bailey observed no lateral offset on a small scarp and Prof. F.J. Pack observed no lateral offset of the road, some aspects of the surface faulting are consistent with a strike-slip earthquake at depth. For example, en echelon patterns were noted (Shenon, 1936) and a horizontal offset of 25 cm was reported (Walter, 1934).

The 1934 earthquake occurred on the west side of Hansel Valley, possibly along southern extensions of several faults, including the eastern frontal fault of the Hansel Mountains (Robison, 1986; McCalpin and others, 1987). McCalpin and others (1987) identified an earlier fault scarp which ruptured along its southern end in 1934. Gully exposures of this scarp suggest that the last event had significantly larger single event offsets than in 1934 (McCalpin and others, 1987). Most of the surface expression of the 1934 event has been eroded or buried in the last 50 years (McCalpin, pers. comm., 1988).

The lack of available data and the effects of liquefaction make it difficult to evaluate fault segmentation for this event.

1950 Fort Sage, California Earthquake

The Fort Sage earthquake occurred on December 14, 1950, had a magnitude of M_L=5.6, and was felt over an area of 52,000 km^2, (Bonilla and others, 1984; Coffman and von Hake, 1973). A 9 1/2 km long scarp formed at the western base of the Fort Sage Mountains along the Fort Sage fault (Gianella, 1951 and 1957). The rupture was composed of two distinct, continuous breaks, separated by a 320 m left-step. The maximum offset at the surface was 20 cm, however, the surface displacement may have been as much as 60 cm if folding of alluvium is considered (Gianella, 1957). Offsets at the surface were normal, with no evidence of lateral offset (Gianella, 1957).

The Fort Sage Mountains, the Fort Sage Mountains fault and the 1950 surface ruptures are all ostensibly terminated at their northern end by the Warm Springs fault system, which bounds the northeastern side of the Fort Sage Mountains (Bonham, 1969; Lydon and others, 1960). The southern end of surface faulting is only 2 km short of a 38° bend in the fault and in the mountain front (broad salient). Surface ruptures from the 1950 earthquake appear to be confined to a single geometric segment.

1954 Rainbow Mountain, Nevada Earthquakes

The Rainbow Mountain earthquakes of July 6 and August 24, 1954 (Ms = 6.3 and 7, respectively; Bonilla and others, 1984) were the first of four closely spaced surface rupturing earthquakes in west-central Nevada over a six month period. The July 6 event was accompanied by 18 km of surface faulting (fig. 6). Extensive fractures and small east-facing scarps up to 30 cm in height formed in a north-northwest-trending zone across the eastern base of Rainbow Mountain and adjacent Quaternary basins (Tocher, 1956). The August 24 earthquake reactivated and increased the heights of fault scarps on the northern end of the July 6 rupture (fig. 6 and 7) and broke an additional 23 kilometers northwards across the Stillwater Refuge playa to the Carson Sink (Tocher, 1956; Bell, 1984). The August 24 earthquake produced scarp heights of up to 75 cm. Neither of the Rainbow Mountain earthquakes produced measurable lateral offsets (Tocher, 1956). Focal mechanisms, however, indicate significant strike-slip components (Doser, 1986).

Approximately 10 km of the July rupture occurred near the eastern base of west-tilted Rainbow Mountain. The northern end of the July rupture and most of the August rupture broke the valley floor north of Rainbow Mountain, where no recognizable fault scarps existed prior to 1954 (Slemmons, unpub. research; Bell and others, 1984). The August event was associated with two distinct surface rupture zones, which are separated by approximately 7 km gap in surface faulting (fig. 7). These two rupture zones can be considered at least two geometric segments.

Bell (1981) noted that the Rainbow Mountain surface ruptures occurred along a fault zone that had not ruptured the surface since

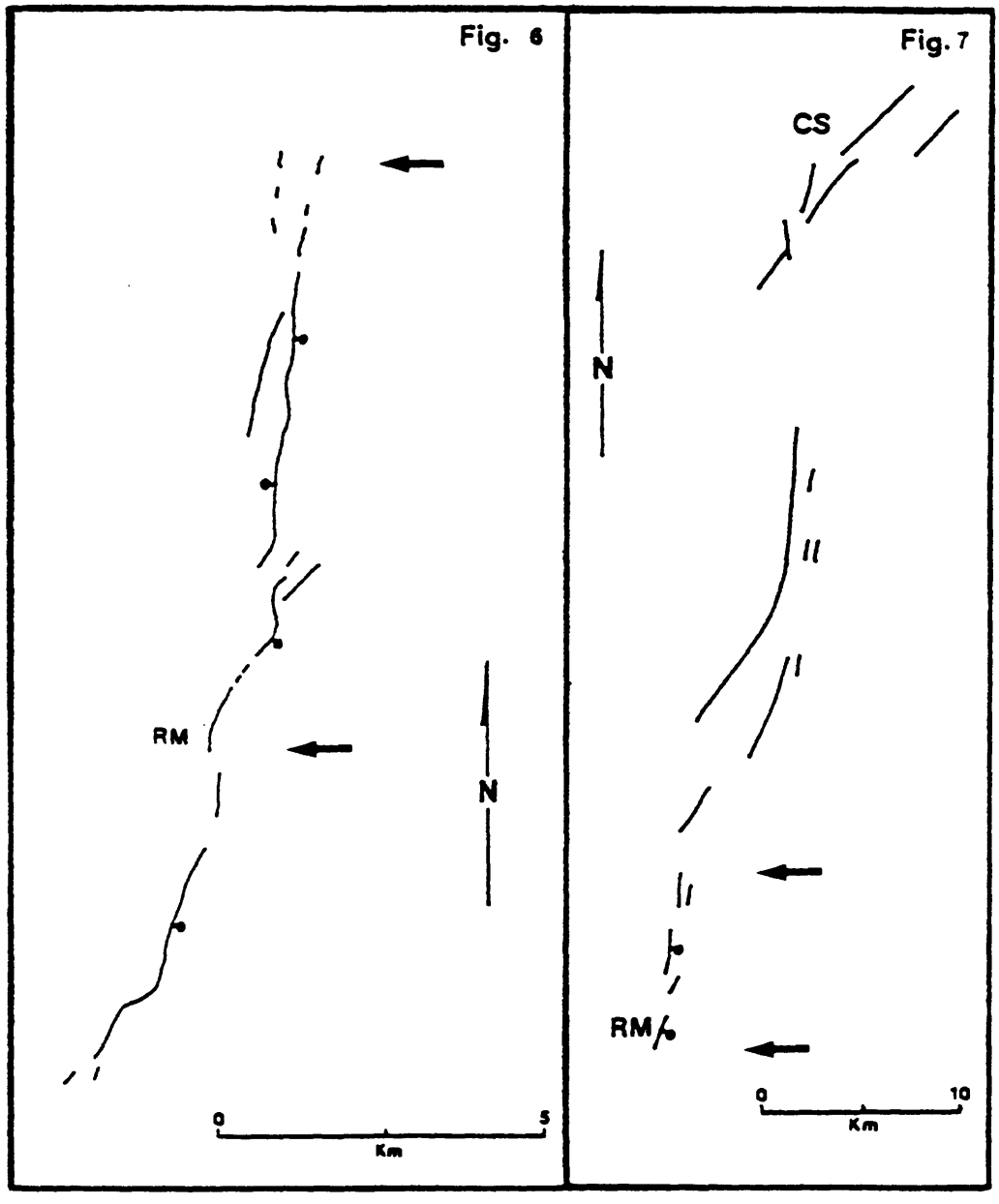

Figure 6. July 6, 1954 Rainbow Mountain (from Tocher, 1956 and Bell, 1984), RM=Rainbow Mountain. Arrows in Fig.6 and Fig.7 denote zone of overlapping surface rupture.

Figure 7. August 24, 1954 Rainbow Mountain (from Tocher, 1956 and Bell, 1984), CS=Carson Sink, RM=Rainbow Mountain.

the Lake Lahontan high stand, 12.5 ka ago. Burial by Holocene sediments and an interseismic interval of greater than 12.5 ka have combined to obscure surficial evidence of this fault zone.

1954 Fairview Peak - Dixie Valley, Nevada Earthquakes

The Fairview Peak and Dixie Valley earthquakes of December 16, 1954 (Ms = 7.2 and 6.8 respectively; Bonilla and others, 1984; Doser, 1986) produced a complex set of surface ruptures in a 102 km by 32 km north-trending belt in west-central Nevada (fig. 1). The Fairview Peak earthquake produced a 67 km north-trending zone of normal-right oblique slip on three primary traces (fig. 8): the Fairview, Gold King and Westgate faults. A fault plane solution by Doser (1986) has a preferred nodal plane that strikes N10°W, dips 60° NE, and has a significant right-lateral component. The Dixie Valley earthquake followed four minutes later with surface rupture along the eastern flank of the Stillwater Range (fig. 9). Displacements were dominantly normal. Fault plane solutions have not been constructed, as this event lies in the coda of the Fairview Peak event.

The Fairview Peak fault ruptured for approximately 32 km at the eastern base of Slate Mountain, Fairview Peak and Chalk Mountain. Normal-right oblique slip dominated, with maximum displacements of 3.7 m right-lateral, and 3.1 m normal (Slemmons, 1957). The southern end of surface faulting breaks into multiple discontinuous ruptures south of Bell Flat and continues south of Mount Anna. The Fairview fault follows the Fairview Peak range front north to near Highway 50, where it branches into a series of northeast-trending en echelon ruptures, then continues as a range-front fault at Chalk Mountain and across an alluviated gap south of Louderback Mountain.

Surface rupture continued to the north on the west-dipping Gold King fault, partly along the western edge of Louderback Mountain and partly in bedrock within the range. Normal displacements of up to 0.6 m may have been similar to surface displacements on the Gold King fault during the 1903(?) Wonder earthquake (Slemmons and others, 1959). This is one of the few cases of recurrent surface faulting within historical times in the United States. Recent field work indicates a significant right-lateral component along this trace (Peizhen Zhang and Slemmons, unpub. research). The northern end of surface faulting attributed to the Fairview Peak earthquake is near a small salient in Louderback Mountain. The Westgate fault on the west edge of the Clan Alpine Mountains parallels and is 2 to 4 km east of the Fairview and Gold King faults. It had a maximum of approximately 1 m of normal and 0.5 m of right-lateral displacement.

The Dixie Valley earthquake ruptured a zone of at least 43 to 47 km on the west side of Dixie Valley. Rupture during this event probably did not cross a 10 km en echelon left-step across Dixie Valley to the Fairview Peak rupture, although the limits of surface

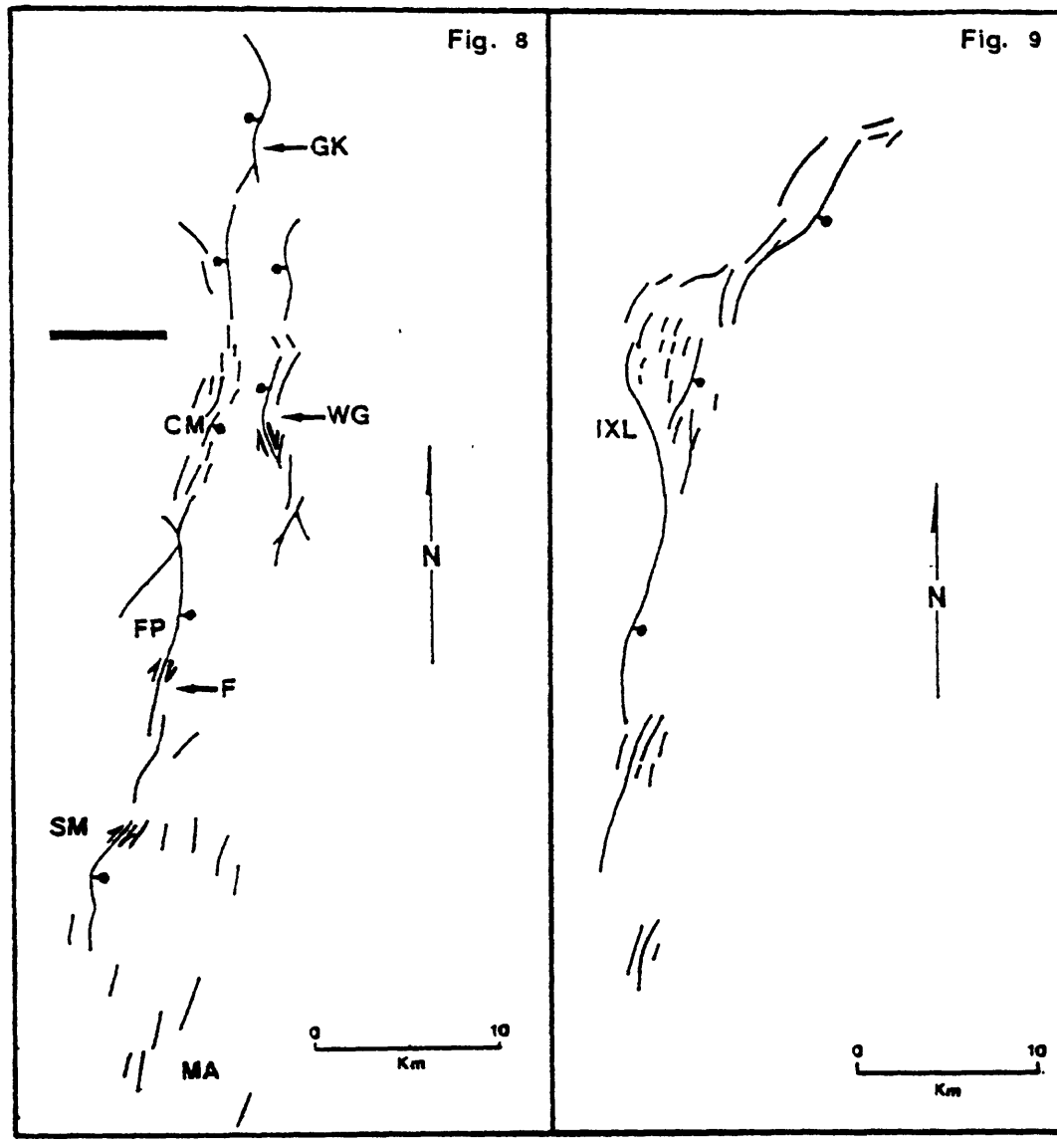

Figure 8. 1954 Fairview Peak (from Slemmons, 1957), CM=Chalk Mountain, F=Fairview scarp, FP=Fairview Peak, GK=Gold King scarp, MA=Mount Anna, SM=Slate Mountain, WG=West Gate fault.

Figure 9. 1954 Dixie Valley (from Slemmons, 1957), IXL=IXL Canyon.

faulting produced by the two closely-spaced earthquakes is conjectural. Normal displacements of more than 2 m were measured (Slemmons, 1957). The southern end of surface faulting coincides approximately with the southeastern end of the Stillwater Range, and has complex, branching relationships.

At the north end, the rupture propagated through "the Bend", a large range-front reentrant north of IXL Canyon, and continued for about 12 km after a change in the strike of the range front of about 38°. A magnetic anomaly associated with the Humboldt lopolith crosses the Dixie Valley fault in the general vicinity of the northern end of the 1954 rupture. Speed (1976) used gravity and geologic data to estimate a thickness of just over 1 km for the Humboldt lopolith. This shallow crustal depth probably would not have affected the subsurface rupture, but may have influenced the surface rupture.

The range front and paleoseismic scarps are essentially continuous across the northern limit of the 1954 rupture. To date, offset Holocene deposits, mathematical modeling of scarps, and analysis of soils and geomorphic surfaces have not allowed a determination of the timing of the last paleoseismic event between the historically ruptured and unruptured portions of the Dixie Valley fault (Wallace and Whitney, 1984; Hecker, 1985; Bell and Katzer, 1987).

In summary, surface faulting during the 1954 Fairview Peak-Dixie Valley earthquakes occurred mainly at or near the alluvium/bedrock range front boundary and nearly always followed prehistoric fault scarps (Slemmons, 1957). At least three complex structural segments failed during the Fairview Peak earthquake: the Fairview segment (approx. 32 km), the Gold King segment (approx. 16 km), and the West Gate segment (approx. 18 km). A more complicated segmentation model, involving as many as seven segments, can also be considered, with segments defined by geometric, behavioral, and geological (changes in bedrock) criteria. The Dixie Valley earthquake may have ruptured only one structural segment. However, the northern end of the surface rupture does not coincide with a well defined discontinuity.

1959 Hebgen Lake, Montana Earthquake

The August 17, 1959 Hebgen Lake earthquake (Ms = 7.5; Doser, 1985a) developed a 26 km long (end-to-end distance) complex pattern of normal faults near the southern end of the Madison Range in southwestern Montana. The event was felt over 870,000 km^2 (Stover, 1985), and produced dramatic fault scarps, landslides and major basin subsidence. The main shock is the largest recorded earthquake in the Intermountain seismic belt. Seismic data indicate a double rupture 5 seconds apart on one or more west-northwest-trending fault planes dipping 45°-60° S, with pure dip-slip motion (Doser, 1985a).

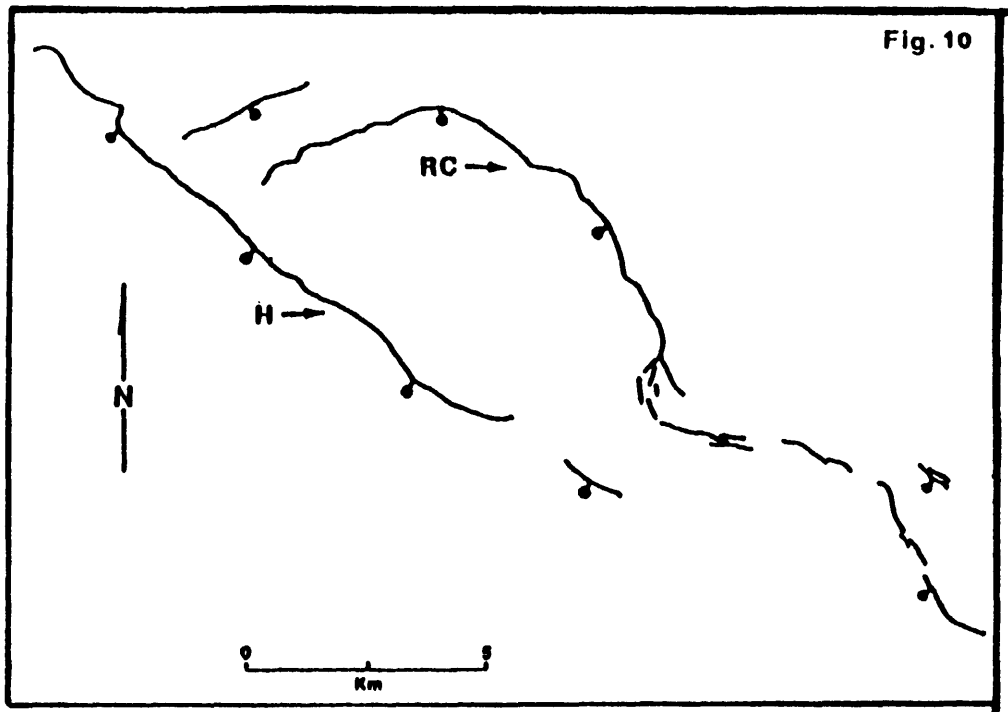

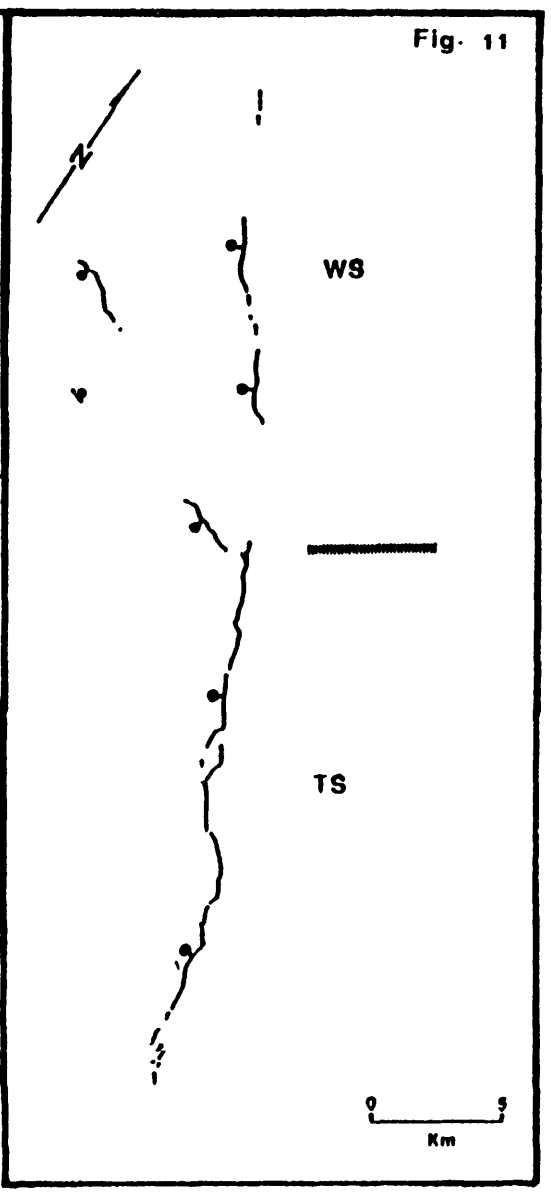

Figure 10. 1959 Hebgen Lake (from USGS, 1964), H=Hebgen scarp, RC=Red Canyon scarp.

Figure 11. 1983 Borah Peak (from Crone and others, 1985), TS=Thousand Springs segment, WS=Warm Springs segment.

Pronounced normal surface displacement occurred on the Red Canyon and Hebgen faults, with minor displacement on several additional faults (fig. 10). The trends of these faults and the style of faulting was somewhat atypical of Basin and Range faulting (Hall and Sablock, 1985). The Red Canyon and Hebgen faults strike chiefly west to northwest, discordant to the north-northwest trend of the prominent Madison Range. The Red Canyon fault ruptured for 23 km in a complex curving trace that closely paralleled Laramide age fold axes and thrust fault surfaces (Witkind and others, 1962). Maximum vertical displacement (D_{max}= 6.7 m) occurred where bedding and pre-existing fault planes were favorably oriented for south to southwest-dipping normal slip (Myers and Hamilton, 1964). The 12 km Hebgen fault rupture (D_{max}= 6.1 m) similarly appears to have been controlled by Laramide structures (Witkind and others, 1962).

The Red Canyon and Hebgen faults may have been delineated on the basis of preexisting fault scarps along much of their lengths, despite their positions internal to the main range and their relatively subdued geomorphic expression (Witkind and others, 1962; Hall and Sablock, 1985).

Fault zone discontinuities at the endpoints of the 1959 ruptures are not well defined. The Red Canyon and Hebgen faults appear to be controlled more closely by Laramide anisotropies than by decoupling at discrete cross-structures. Myers and Hamilton (1964) interpreted these ruptures as part of a developing west-trending zone of deformation superimposed upon Laramide structures and north-northwest-trending Basin and Range style block faulting. At least two large structural segments failed during this event, the Red Canyon and Hebgen faults.

1980 Mammoth Lakes, California Earthquake Sequence

On May 25 and 27, 1980, four earthquakes of $M_L \geq 6$ occurred within the Sierra Nevada - Great Basin Boundary Zone, near Mammoth Lakes. Three of these events occurred within the Sierran mountain block. A fourth event occurred immediately northwest of the other earthquakes, in the southern part of a resurgent dome graben complex, within the Long Valley caldera (Lide and Ryall, 1985). Aftershock studies by Lide (1984) suggest that the main events within the mountain block may have ruptured northeast-trending left-lateral faults. Magmatic intrusion has also been suggested for these events, both as the direct cause of the earthquakes, and/or as part of the overall tectonic episode (Savage and Clark, 1982; Julian and Sipkin, 1985).

A 20 km long zone of surface fractures associated with this event was mapped (Taylor and Bryant, 1980; Clark and others, 1982). Fractures were confined to the northern Hilton Creek fault in the southern part of the zone, and splayed and were distributed across a zone up to 6 1/2 km wide in the north, within the caldera. Maximum measured offsets (both right lateral and normal) were approximately 20 cm (Clark and Yount, 1981; Clark and others,

1982). Most of the surface faulting appears to have been secondary or sympathetic in nature. Sympathetic displacement is suggested along the Hilton Creek fault, as the epicenters located significantly behind the fault zone, well into the footwall (Clark and Yount, 1981).

1983 Borah Peak, Idaho Earthquake

The M_s=7.3 Borah Peak earthquake of October 28, 1983 produced about 36 km of surface rupture at the western base of the Lost River Range in east-central Idaho (Crone and Machette, 1984). The event was felt over 670,000 km^2 of the United States plus a large part of western Canada (Stover, 1985) and produced surface faulting on two well-defined segments of the 140 km Lost River fault and a branch fault (Scott and others, 1985). Doser and Smith's (1985) preferred fault plane solution of N48°W, 45°SW, with approximately 5:1 normal to left-lateral displacement, agrees closely with surface measurements. Rupture is believed to have propagated to the northwest from a point 15-16 km deep near the southern end of surface faulting (Doser and Smith, 1985).

Surface rupture (fig. 11) occurred on three main traces (geometric segments): from south to north, a 20.8 km section of the Lost River fault that constitutes the main rupture and includes the maximum vertical displacement of 2.8 m and a maximum left-lateral offset of 0.7 m; a 14.2 km west-northwest trending discordant break across a series of bedrock hills and out onto Antelope Flat (D_{max}=1.6 m); and an 7.9 km northern rupture (D_{max}=1 m) that also coincides with the Lost River fault (Crone and Machette, 1984; Crone and others, 1987). The Lost River fault has been divided into six or seven discrete fault segments based on differing geomorphic expression, structural relief, and ages of most recent fault displacement (Scott and others, 1985). The southern and northern 1983 ruptures correspond, respectively, to the Thousand Springs segment and the central portion of the Warm Spring segment.

The southern boundary of the Thousand Springs segment south of Elkhorn Creek is marked by transverse faults in bedrock and an abrupt change in the strike of the range front forming a salient. Rupture appears to have propagated northwestward from near this point about 20 km to a transverse bedrock ridge between Thousand Springs and Warm Spring Valleys, where it was partially deflected west-northwest (Crone and others, 1985). Faulting on the range front continued to the northwest on the Warm Spring segment after a gap of 4.8 km (Crone and Machette, 1984).

The style and amount of displacement of the 1983 rupture was similar to a mid-Holocene(?) event documented on the Thousand Springs segment (Hait and Scott, 1978; Schwartz and Crone, 1985; Hanks and Schwartz, 1987). Similarities between the two most recent events on this segment support the earthquake segmentation and characteristic earthquake model (Schwartz and Coppersmith, 1984). The most recent paleoseismic event along the Warm Spring

segment occurred just prior to 5.5-6.2 ka (Schwartz and Crone, 1988), about the same age as the mid-Holocene event on the Thousand Springs segment. However, surface displacements from this paleoearthquake were twice that of the 1983 event along the Warm Spring segment, and surface ruptures were much more extensive (Schwartz, pers. comm., 1988). The mid-Holocene event may have been similar to the 1983 event, but with larger displacements at its northern end. Alternatively, a second earthquake may have occurred along the Warm Spring segment relatively close in time to the mid-Holocene event on the Thousand Springs segment or following a prior "1983 type" event (Schwartz, pers. comm., 1988).

Earthquake magnitude estimates for the Lost River fault based solely on relatively short individual segments are significantly lower than the 1983 M_s=7.3 event (Freeman and others, 1986). Rupture of the 22 km Thousand Springs segment alone yields an estimated magnitude M_s=6.7-6.8 event, using magnitude versus fault-length relations from Slemmons (1982), Bonilla and others (1984) and Slemmons and others (1987). A 36 km rupture length yields an estimated magnitude of M_s=6.9-7.1.

1986 Chalfant Valley, California Earthquake Sequence

The Chalfant Valley earthquake sequence consisted of six earthquakes of about magnitude 5 and greater occurring over a period of 11 days, with a main shock of M_s=6.2 (National Earthquake Information Service, 1986; Cockerham and Corbett, 1987). Focal mechanism and aftershock studies indicate that the main shock was dominantly a strike-slip event occurring along a northwest-trending, southwest dipping fault (Cockerham and Corbett, 1987; dePolo, unpub. research). The southern end of the fault containing the main shock intersects the White Mountains fault zone (WMFZ).

Many surface fractures and offsets were discovered after the main shock. These were scattered in and north of the aftershock area (volcanic tablelands) and along the adjacent WMFZ (Lienkaemper and others, 1987; dePolo and Ramelli, 1987). Surface fractures in the tablelands occurred discontinuously over a 26 km distance, with a maximum width of 7 km. Surface faulting and fracturing occurred along the WMFZ for 15.5 km and had normal-right oblique offsets with maximum displacements of 5 cm (dePolo and Ramelli, 1987).

Primary rupture for this event is difficult to discern. Most of the surface ruptures appeared to have been secondary or sympathetic in nature. The main event occurred along a fault which does not have identified surface expression. Significant minor detachment may have occurred below the welded Bishop tuff, which blankets the surface and forms the volcanic tableland in the epicentral area.

DISCUSSION

The seventeen events associated with surface faulting in the Basin and Range province exhibit a large degree of variability in their faulting styles. Some events are predictable range-front fault ruptures (e.g. 1954 Dixie Valley and 1983 Borah Peak earthquakes), whereas others occurred in widely distributed fashions or along faults that lacked identified surface expression (e.g. 1980 Mammoth Lakes and 1986 Chalfant Valley earthquake sequences). Eleven of the seventeen events have sufficient data and the surface ruptures were extensive enough that geometric and structural segments could be identified.

The moderate magnitude earthquakes included in this study ($M < 7$) were less complex when primary tectonic ruptures occurred on single faults or along parts of fault segments (e.g. 1950 Fort Sage, July 1954 Rainbow Mountain earthquake, 1954 Dixie Valley). Several of the moderate magnitude events were associated with sympathetic or secondary surface faulting in widely distributed patterns and on adjacent fault zones (e.g. 1980 Mammoth Lakes and 1986 Chalfant Valley earthquake sequences).

All of the earthquakes with magnitude ≥ 7 (eight events) ruptured multiple geometric or structural segments. Examples are: the 1872 Owens Valley earthquake, which ruptured four geometric segments; the 1915 Pleasant Valley earthquake, which ruptured four to five structural segments; and the 1983 Borah Peak earthquake, which ruptured three geometric segments. Failure of multiple segments may be responsible for the multiple ruptures often observed by seismologists for large events in the Basin and Range province.

Many of the largest events ($M \geq 7.2$) involved complex, widely distributed rupture patterns (e.g. 1915 Pleasant Valley, 1932 Cedar Mountain, and 1954 Fairview Peak earthquakes). These events ruptured consecutive and parallel structural segments along range fronts and across ranges and valleys in complicated fashions. Extensive paleoseismic and structural data would have been required to have predicted these complex patterns, if they were at all predictable.

Some of the possible reasons for the complex and widely distributed surface ruptures in the Basin and Range province include: decoupling and detachment faulting in the mid- to upper crust (Burchfiel, 1965; Hardyman, 1978, 1984; Wallace, 1979; Molinari, 1984a), occurrence in highly tectonized crust with pre-existing structures and fabrics and varying lithologies, triggering of ruptures either by exceedence of seismic failure thresholds of adjacent faults or through sympathetic displacement, significant or dominant strike-slip displacement components, and long interseismic intervals, which allow removal of surficial evidence of faulting by erosion and burial by younger alluvium.

Approximately one half of the endpoints on the eleven segmented historical surface ruptures ended at discontinuities that could have been identified using indicators of fault zone discontinuities and existing data. Characteristics of the identified discontinuities include cross-faults, branch faults, extensional basins, ends of mountain ranges, topographic barriers, and salients. The other half were either widely distributed with indistinct end points or ended at locations at the surface that did not coincide with clear indicators of fault zone discontinuities.

For many of the events, successful paleoseismic studies may have revealed that multiple geometric or structural segments had failed during individual paleoseismic events. This input of timing is an important element of a successful segmentation model as pointed out by Schwartz and Coppersmith (1984, 1986) and Schwartz (1988). In some cases, where paleoearthquakes have clustered spatially and temporally, it may be difficult to delineate individual earthquake segments. For example, the paleoseismic record of the future will have difficulty distinguishing between the 1954 Fairview Peak and Dixie Valley earthquakes, or distinguishing between these and other historical ruptures in the Central Nevada seismic belt. For some events, such as the 1915 Pleasant Valley, the 1932 Cedar Mountain, and the 1954 Fairview Peak earthquakes, paleoseismic investigations will be important for determining whether complex historical events were characteristic events, with similar multiple geometric and structural segment ruptures during past events.

The results of this study suggest that failure of multiple geometric and structural segments should be considered in seismotectonic investigations in the Basin and Range province. Further, some earthquake discontinuities may be difficult to identify and significant faulting may occur beyond postulated discontinuities.

CONCLUSIONS

Historical surface faulting earthquakes in the Basin and Range province below magnitude 7 generally occurred along single structural or geometric segments, along parts of faults, or in areas with previously unidentified faults. In some cases surface faulting associated with moderate events was secondary and sympathetic in nature. Earthquakes of magnitude 7 and greater have involved the failure of multiple geometric or structural segments. Many of the events larger than magnitude 7.2 had complex, widespread rupture patterns.

Approximately half of the endpoints of the historical Basin and Range province surface ruptures coincided with identifiable discontinuities. The other half ended in either widespread distributions and/or did not coincide with clear indicators of discontinuities. Historical surface faulting has commonly ruptured through geometric, geomorphic and structural discontinuities.

Thus, several lines of evidence are required to evaluate earthquake discontinuities.

These observations suggest that earthquake segmentation models need to be applied with caution in the Basin and Range province and should consider multiple geometric or structural segments, different types of data, and large uncertainties in earthquake segment lengths and earthquake size estimations. Further studies of historical earthquakes and faults,. and the development of new data, such as geophysical and paleoseismic data, will help in understanding some of the complexities of earthquakes in extensional provinces.

ACKNOWLEDGMENTS

We would like to thank Sarah Beanland, John Bell, William Bull, Malcolm Clark, Kevin Coppersmith, Diane dePolo, Peter Kneupfer, Dick Meeuwig, James McCalpin, Phil Pearthree, Alan Ramelli, Woody Savage, Tom Sawyer, Bert Swan and especially Bill Lettis and David Schwartz for many useful discussions, comments, and reviews which improved the manuscript. We are responsible for all statements in the text and do not imply that these are the views of the reviewers. We would also like to thank Roger Laurence for drafting the figures. This study was supported in part by a grant from the Nevada Nuclear Waste Project Office.

REFERENCES CITED

Allen, C. R., 1968, The tectonic environments of seismically active and inactive areas along the San Andreas fault system, in Dickinson, W. R. and Granz, A., eds., Proceedings of the conference on geological problems of the San Andreas system: Stanford University Publications Geological Sciences, v. 11, p. 70-82.

Abe, K., 1981, Magnitudes of large shallow earthquakes from 1904 to 1980: Physics of the Earth and Planetary Interiors, v. 27, p. 72-80.

Barka, A. A. and Kadinsky-Cade, K., 1988, Strike-slip fault geometry in Turkey and its influence on earthquake activity: Tectonics, v. 7, p. 663-684.

Beanland, S. and Clark, M., 1987, The Owens Valley fault zone, and surface rupture associated with the 1872 earthquake: Seismological Society of America, Seismological Research Letters, v. 58, p. 32 (abstract).

Beanland, S., Clark, M., and Slemmons, D. B., in review, The Owens Valley fault zone and surface rupture in the 1872 Inyo County, California, earthquake: U. S. Geological Survey Bulletin.

Bell, J. W., 1981, Quaternary fault map of the Reno 1° by 2° quadrangle: U. S. Geological Survey Open-File Report 81-982.

Bell, J. W., 1984, Quaternary fault map of Nevada-Reno sheet: Nevada Bureau of Mines and Geology Map 79.

Bell, J. W., Slemmons, D. B., and Wallace, R. E., 1984, Roadlog: Reno to Dixie Valley-Fairview Peak earthquake areas, field trip 18: Geological Society of America 1984 Annual Meeting, Western Geological Excursions, v. 4, p. 425-472.

Bell, J. W. and Katzer, T., 1987, Surficial geology, hydrology, and late Quaternary tectonics of the IXL Canyon area, Nevada, as related to the 1954 Dixie Valley earthquake: Nevada Bureau of Mines and Geology, Bulletin 102, 52 p.

Bonilla, M. G., Mark, R. K., and Lienkaemper, J. J., 1984, Statistical relations among earthquake magnitude, surface rupture length, and surface fault displacement: Seismological Society of America Bulletin, v.74, p. 2379-2422.

Bonham, H. F., 1969, Geology and mineral deposits of Washoe and Storey Counties, Nevada: Nevada Bureau of Mines and Geology, Bulletin 70, 140 p.

Bull, W. B. and Pearthree, P. A., 1988, Frequency and size of Quaternary surface ruptures of the Pitaycachi fault, northeastern Sonora, Mexico: Seismological Society of America Bulletin, v. 78, p. 956-978.

Burchfiel, B. C., 1965, Structural geology of the Specter Range quadrangle, Nevada, and its regional significance: Geological Society of America Bulletin, v. 76, p. 175-192.

Callaghan, E. and Gianella, V. P., 1935, The earthquake of January 30, 1934, at Excelsior Mountains, Nevada: Seismological Society of America Bulletin, v. 25, p. 161-168.

Clark, M. M. and Yount, J. C., 1981, Surface faulting along the Hilton Creek fault associated with Mammoth Lakes, California, earthquakes of May 1980: Seismological Society of America, Earthquake Notes, v. 52, p. 45-46 (abstract).

Clark, M. M., Yount, J. C., Vaughan, P. R., and Zepeda, R. L., 1982, Map showing surface ruptures associated with the Mammoth Lakes, California, earthquakes of May 1980: U. S. Geological Survey, Miscellaneous Field Studies Map MF-1396.

Cockerham, R. S. and Corbett, E. J., 1987, The July 1986 Chalfant Valley, California, earthquake sequence: preliminary results: Seismological Society of America Bulletin, v. 77, p. 280-289.

Coffman, J. L. and von Hake, C. A., 1973, Earthquake history of the United States, revised edition (through 1970): U. S. Dept. of Commerce, publication 41-1, 208 p.

Crone, A. J., and Machette, M. N., 1984, Surface faulting associated with the Borah Peak earthquake, central Idaho: Geology, v. 12, p. 664-667.

Crone, A. J., Machette, M. N., Bonilla, M. G., Lienkaemper, J. J., Pierce, K. L., Scott, W. E., and Bucknam, R. C., 1985, Characteristics of surface faulting accompanying the Borah Peak earthquake, central Idaho: U.S. Geological Survey Open-File Report 85-290, p. 43-58.

Crone, A. J., Machette, M. N., Bonilla, M. G., Lienkaemper, J. J., Pierce, K. L., Scott, W. E., and Bucknam, R. C., 1987, Surface faulting accompanying the Borah Peak earthquake and segmentation of the Lost River fault, central Idaho: Seismological Society of America Bulletin, v. 77, p. 739-770.

dePolo, C. M. and Ramelli, A. R., 1987, Preliminary report on surface fractures along the White Mountains fault zone associated with the July 1986 Chalfant Valley earthquake sequence: Seismological Society of America Bulletin, v. 77, p. 290-296.

dePolo, C. M., Bell, J. W., and Ramelli, A. R., 1987a, Geometry of strike-slip faulting related to the 1932 Cedar Mountain earthquake, central Nevada: Geological Society of America, Abstracts with Programs, v. 19, p. 371 (abstract).

dePolo, C. M., Ramelli, A. R., and Bell, J. W., 1987b, Visit to trenches along the southern part of the 1932 Cedar Mountain earthquake ruptures, Monte Cristo Valley, Nevada: Nevada Bureau of Mines and Geology, unpublished field guide.

Doser, D. I., 1985a, Source parameters and faulting processes of the 1959 Hebgen Lake, Montana earthquake sequence: Journal of Geophysical Research, v. 90, p. 4537-4555.

Doser, D. I., 1985b, The 1983 Borah Peak, Idaho and 1959 Hebgen Lake, Montana earthquakes: models for normal fault earthquakes in the Intermountain seismic belt: U.S. Geological Survey Open-File Report 85-290, p. 368-384.

Doser, D. I., 1986, Earthquake processes in the Rainbow Mountain-Fairview Peak-Dixie Valley, Nevada, region 1954-1959: Journal of Geophysical Research, v. 91, p. 12,572-12,586.

Doser, D. I., in review (a), Source mechanisms of earthquakes in the Nevada seismic zone (1915-1943) and implications for deformation in the western Great Basin: submitted to Journal of Geophysical Research.

Doser, D. I., in review (b), Extensional tectonics in northern Utah - southern Idaho, U. S. A., and the Hansel Valley sequence: submitted to Physics of the Earth and Planetary Interiors.

Doser, D. I., and Smith, R. B., 1985, Source parameters of the 28 October 1983 Borah Peak, Idaho, earthquake from body wave analysis: Seismological Society of America Bulletin, v. 75, p. 1041-1051.

Dubois, S. M. and Smith, A. W., 1980, The 1887 earthquake in San Bernardino valley, Sonora: Historical accounts and intensity patterns in Arizona: Arizona Bureau of Geology and Mineral Technology, Special Paper No. 3, 112 p.

Dubois, S. M. and Sbar, M. L., 1981, The 1887 earthquake in Sonora: Analysis of regional ground shaking and ground failure, in Proceedings of conference XIII, Evaluation of regional seismic hazards and risk: U. S. Geological Survey, open-file report 81-437.

Fonseca, J., 1988, The Sou Hills: a barrier to faulting in the central Nevada seismic belt: Journal of Geophysical Research, v. 93, p. 475-489.

Freeman, K. J., Fuller, S., and Schell, B. A., 1986, The use of surface faults for estimating design earthquakes; implications of the 28 October 1983, Idaho earthquake: Association of Engineering Geologists, v. 23, p. 325-332.

Garside, L. J., 1982, Geologic map of the Moho Mountain quadrangle, Nevada: Nevada Bureau of Mines and Geology, Map 74.

Gianella, V. P., 1951, Fort Sage Mountain, California, earthquake of December 14, 1950: Geological Society of America Bulletin, v. 62, p. 1502.
Gianella, V. P., 1957, Earthquake and faulting, Fort Sage Mountains, California, December, 1950: Seismological Society of America Bulletin, v. 47, p. 173-177.
Gianella, V. P. and Callaghan, E., 1934, The Cedar Mountain, Nevada, earthquake of December 20, 1932: Seismological Society of America Bulletin, v. 24, p. 345-377.
Goodfellow, G. E., 1888, The Sonora earthquake: Science, v. 11, p. 162-166.
Gutenberg, B. and Richter, C. F., 1954, Seismicity of the earth and associated phenomena: Hafner Publishing Company, 310 p.
Hait, M. H., Jr., and Scott, W. E., 1978, Holocene faulting, Lost River Range, Idaho: Geological Society of America Abstracts with Program, v. 10, p. 217 (Abstract).
Hall, W. B., and Sablock, P. E., 1985, Comparison of the geomorphic and surficial fracturing effects of the 1983 Borah Peak, Idaho earthquake with those of the 1959 Hebgen Lake, Montana earthquake: U.S. Geological Survey Open-File Report 85-290, p. 141-152.
Hanks, T. C. and Schwartz, D. P., 1987, Morphologic dating of the pre-1983 fault scarp on the Lost River fault at Doublespring Pass Road: Seismological Society of America Bulletin, v. 77, p. 837-846.
Hardyman, R. F., 1978, Volcanic stratigraphy and structural geology of the Gillis Canyon quadrangle, northern Gillis Range, Mineral County, Nevada: University of Nevada - Reno, PhD Thesis, 248 p., unpublished.
Hardyman, R. F., 1984, Strike-slip, normal, and detachment faults in the northern Gillis Range, Walker Lane of West Central Nevada: Geological Society of America 1984 Annual Meeting, Western Geological Excursions, v. 4, p. 184-199.
Hecker, S., 1985, Timing of Holocene faulting in part of a seismic belt, west-central Nevada: University of Arizona, Masters thesis, 42 p.
Herd, D. G. and McMasters, C. R., 1982, Surface faulting in the Sonora, Mexico, earthquake of 1887: Geological Society of America, Abstracts with Program, v. 14, p. 172 (abstract).
Julian, B. R. and Sipkin, S. A., 1985, Earthquake processes in the Long Valley Caldera area, California: Journal of Geophysical Research, v. 90, p. 11,155-11,169.
Knuepfer, P. L. K., Bamberger, M. J., Turko, J. M., and Coppersmith, Kevin J., 1987, Characteristics of the boundaries of historical surface fault ruptures: Seismological Society of America, Seismological Research Letters, v. 58, p 31 (abstract).
Lide, C. S., 1984, Aftershocks of the May, 1980 Mammoth Lakes, California earthquakes: University of Nevada - Reno, Masters thesis, 78 p.
Lide, C. S. and Ryall, A. S., 1985, Aftershock distribution related to the controversy regarding mechanisms of the May 1980 Mammoth Lakes, California, Earthquakes: Journal of Geophysical Research, v. 90,p. 11,151-11,154.

Lienkaemper, J. J., Pezzopane, S. K., Clark, M. M., and Rymer, M. J., 1987, Fault fractures formed in association with the 1986 Chalfant Valley, California, earthquake sequence: preliminary report: Seismological Society of America Bulletin, v. 77, p. 297-305

Lydon, P. A., Gay, T. E., Jr., and Jennings, C. W., 1960, Geologic map of the Westwood Sheet: California Division of Mines and Geology, Geologic map of California, Olaf P. Jenkins edition.

Martel, S. J., 1984, Structure of the Owens Valley fault zone near Poverty Hills, Owens Valley, California: Geological Society of America, Abstracts with program, v. 16, p. 585 (Abstract).

Molinari, M. P., 1984a, Late Cenozoic geology and tectonics of Stewart and Monte Cristo Valleys, west-central Nevada: University of Nevada - Reno, Masters thesis, 122 p.

Molinari, M. P., 1984b, Late Cenozoic structural geology of Stewart and Monte Cristo Valleys, Walker Lane of west-central Nevada, in Western Geological Excursions: Guidebook, Geological Society of American, Annual Meeting, v. 4, p. 219-231.

McCalpin, J., Robison, R. M., and Gan, J. D., 1987, Neotectonics of the Hansel Valley - Pocatello Valley corridor, northern Utah and southern Idaho, in Assessment of regional earthquake hazards and risk along the Wasatch Front, Utah: U. S. Geological Survey, open-file report 87-585, v. 1, p. G1-G44.

Myers, W. B., and Hamilton, W., 1964, Deformation accompanying the Hebgen Lake earthquake of August 17, 1959: U.S. Geological Survey Professional Paper 435-I, p. 55-98.

National Earthquake Information Service, 1986, Preliminary determination of epicenters: U. S. Geological Survey, no. 31-86.

Page, B. M., 1934, Basin-range faulting of 1915 in Pleasant Valley, Nevada: Journal of Geology, v. 43, p. 690-707.

Reynolds, M. W., 1979, Character and extent of basin-range faulting, western Montana and east-central Idaho, in Newman, G. W. and Goode, H. D., eds., Basin and range symposium and Great Basin field conference: Rocky Mountain Association of Geologists

Robison, R. M., 1986, The surficial geology and neotectonics of Hansel Valley, Box Elder County, Utah: Utah State University, Masters thesis, 120 p.

Sanders, C. O., and Slemmons, D. B., 1979, Recent crustal movements in the central Sierra Nevada-Walker Lane region of California-Nevada-part III, the Olinghouse fault zone: Tectonophysics, v. 52, p. 585-597.

Savage, J. and Clark, M., 1982, Magmatic resurgence in Long Valley caldera, California: Possible cause of the 1980 Mammoth Lakes earthquakes: Science, v. 217, p. 531-533.

Schwartz, D. P., 1988, Geology and seismic hazards: moving into the 1990's, in Von Thun, J. Lawrence, edt., Earthquake engineering and soil dynamics II - recent advances in ground motion evaluation: American Society of Civil Engineers, Geotechnical Special Publication No. 20, p. 1-42.

Schwartz, D. P., and Coppersmith, K. J., 1984, Fault behavior and characteristic earthquakes: examples from the Wasatch and San Andreas fault zones: Journal of Geophysical Research, v. 89, p. 5681-5698.

Schwartz, D. P., and Crone, A. J., 1985, The 1983 Borah Peak earthquake: a calibration event for quantifying earthquake recurrence and fault behavior on Great Basin normal faults: U.S. Geological Survey Open-File Report 85-290, p. 153-160.

Schwartz, D. P. and Coppersmith, K. J., 1986, Seismic hazards: new trends in analysis using geological data, in Active tectonics: National Academy Press, p. 215-230.

Schwartz, D. P. and Crone, A. J., 1988, Paleoseismicity of the Lost River fault zone, Idaho: earthquake recurrence and segmentation: Geological Society of America, Abstracts with Programs, v. 20, p. 228.

Scott, W. E., Pierce, K. L., and Hait, M. H., 1985, Quaternary tectonic setting of the 1983 Borah Peak earthquake, central Idaho: Seismological Society of America Bulletin, v. 75, p. 1053-1066.

Shenon, P. J., 1936, The Utah earthquake of March 12 1934, in Neumann, F., United States earthquakes, 1934: U. S. Department of Commerce, Serial No. 593., p. 43-48.

Slemmons, D. B., 1957, Geological effects of the Dixie Valley-Fairview Peak, Nevada, earthquakes of December 16, 1954: Seismological Society of America Bulletin, v. 47, p. 353-375.

Slemmons, D. B., 1977, State-of-the-art for assessing earthquake hazards in the United States: Report 6, Faults and Earthquake Magnitude: U.S. Army Engineers Waterways Experiment Station, Miscellaneous Paper S-73-1, Report 6, 166 p.

Slemmons, D. B., 1982, Determination of design earthquake magnitudes for microzonation, in Third international earthquake microzonation conference proceedings, p. 119-130.

Slemmons, D. B., Steinbrugge, K. V., Tocher, D., Oakeshott, G. B. and Gianella, V. P., 1959, Wonder, Nevada, earthquake of 1903: Seismological Society of America Bulletin, v. 49, p. 251-265.

Slemmons, D. B., Jones, A. E., and Gimlett, J. I., 1965, Catalog of Nevada earthquakes, 1852-1960: Seismological Society of America Bulletin, v. 55, p. 519-565.

Slemmons, D. B. and dePolo, C. M., 1986, Evaluation of active faulting and associated hazards, Active tectonics: National Academy Press, p. 45-62.

Slemmons, D. B., Bodin, P., and Zhang, X., in press, Determination of earthquake size from surface faulting events, in Proceedings of the international seminar on seismic zonation: Guangszhou, China, 12 p.

Smith, R. B. and Sbar, M. L., 1974, Contemporary tectonics and seismicity of the western United States with emphasis on the Intermountain seismic belt: Geological Society of America Bulletin, v. 85, p. 1205-1218.

Speed, R. C., 1976, Geologic Map of the Humboldt lopolith and surrounding terrane, Nevada: Geological Society of America, Map MC-14.

Witkind, I. J., Myers, W. B., Hadley, J. B., Hamilton, W., and Fraser, G. D., 1962, Geologic features of the earthquake at Hebgen Lake, Montana, August 17, 1959: Seismological Society of America Bulletin, v. 52, p. 163-180.

THE CHARACTER OF FAULTING PROCESSES OF EARTHQUAKES IN THE INTERMOUNTAIN REGION

by

Diane I. Doser

Department of Geological Sciences
University of Texas at El Paso
El Paso, Texas 79968-0555

ABSTRACT

Source parameters collected for 47 earthquakes have been used to examine the faulting characteristics of magnitude $\geq$ 5.5 earthquakes within the Intermountain region. The earthquakes occurred between 1915 and 1987 in a region extending from the eastern Sierra Nevada to western New Mexico and from northwestern Montana to Trans-Pecos Texas. Source parameters used in this study include information from first motion analysis, body and surface waveform modeling, geodetic studies, and geological studies of surface faulting. Preliminary results of this analysis include: (1) All earthquakes with M $\geq$6.0 occurred on faults dipping 38° or more. (2) Average depth of rupture initiation was 10 km, with M$\geq$7.0 earthquakes occurring at depths of 15 or more. (3) Most earthquakes had unilateral ruptures. (4) Nearly 30% of the earthquakes for which source-time function information was available were complex, multiple ruptures.

INTRODUCTION

The intermountain region of the western United States is a zone of active intraplate extension located between the Sierra Nevada and Transverse Ranges on the west and the Wyoming Basin and Great Plains to the east (figure 1). The region includes the Basin and Range, the Southern, Middle and Northern Rocky Mountains, the Snake River Plain/Yellowstone system, the Colorado Plateau and the Rio Grande Rift.

Since 1900 at least ten earthquakes of M>6.5 have occurred in this region (table 1), including the two largest earthquakes to have occurred in the continental United States during the last 30 years. Most of the earthquakes have occurred in sparsely populated areas, however the presence of Holocene faulting in more densely populated areas (i.e. Utah's Wasatch Front) indicates that similar sized earthquakes have occurred in the recent past. Study of the faulting processes of large earthquakes occurring during the last 70 years within the intermountain area provides information vital to the assessment of hazards associated with large earthquakes expected to occur in these areas in the future.

In an effort to examine the faulting processes of large earthquakes within the intermountain region, source parameters were collected for 47 earthquakes of magnitude 5.5 to 7.8 occurring between 1915 and 1987. Over 35 parameters and their associated uncertainties were examined for each earthquake. The data collection process and the parameters used in this study are discussed in the following section.

Parameters obtained using different techniques such as waveform modeling, first motion analysis, geodetic analysis or the mapping of surface faulting, were compared to one another to examine the consistencies and differences between data sets. Then, relationships between individual sets of parameters were examined to determine whether earthquakes of similar magnitude or similar mechanism exhibit similar faulting processes, and whether certain

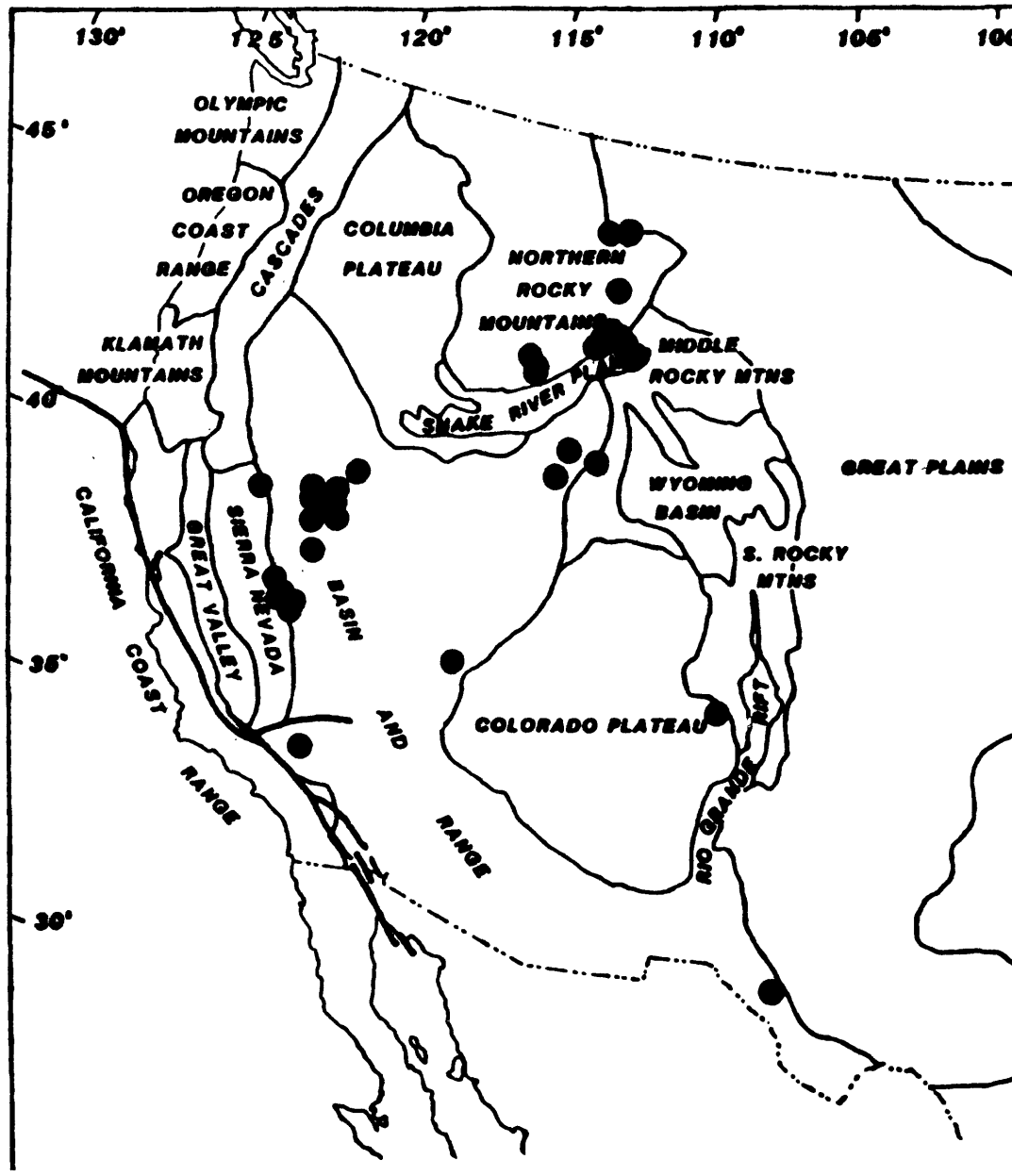

FIGURE 1. -- Earthquakes used in this study. Physiographic provinces modified from Zoback and Zoback (1980).

TABLE 1.- Earthquakes Used in This Study

Event	Date	Origin time	M	Reference[+]
Pleasant Valley, NV	151003	654	7.8	20,66,70,74
Clarkston, MT	250627	121	6.8	17,19,47,53
Valentine, TX	310816	1140	6.4	23,28,36,45,46
Cedar Mtn., NV	321221	610	7.2	16,20,32,44,66,70
Excelsior Mtn., NV	340130	2016	6.5	10,20,66
Hansel Valley, UT	340312	1505	6.6	1,17,21,30,39,41,63
Hansel Valley, UT	340312	1820	6.1	1,17,21,30,39,41,63
Helena, MT	351019	448	6.3	17,19,31,40,61
Helena, MT	351031	1837	6.0	17,19,31,40,61
Manix, CA	470410	1558	6.4	18,55,56
Virginia City, MT	471123	946	6.3	17,19,71
Rainbow Mtn., NV	540706	1113	6.6	22,24,65,66,69,72
Rainbow Mtn., NV	540706	2207	6.4	22,24,65,66,69,72
Rainbow Mtn., NV	540824	551	6.8	22,24,65,66,69,72
Rainbow Mtn., NV	540831	2220	5.8	22,24,65,66,69,72
Rainbow Mtn., NV	540901	518	5.5	22,24,65,66,69,72
Fairview Peak, NV	541216	1107	7.1	24,57,60,64,66,69
Dixie Valley, NV	541216	1111	6.8	24,57,60,64,66,69
Dixie Valley, NV	590323	710	6.3	22,24,66
Schurz, NV	590623	1435	6.1	22,24,66
Schurz, NV	590623	1504	5.5	22,24,66
Hebgen Lake, MT	590818	637	7.5	17,25,60,77
Hebgen Lake, MT	590818	756	6.5	17,25,60,77
Hebgen Lake, MT	590818	841	6.0	17,25,60,77
Hebgen Lake, MT	590818	1103	5.6	17,25,60,77
Hebgen Lake, MT	590818	1526	6.5	17,25,60,77
Hebgen Lake, MT	590819	404	6.0	17,19,25,77
Logan, UT	620830	1335	5.7	1,39,68,75
Hebgen Lake, MT	641021	738	5.8	17,19,25,77
Dulce, NM	660123	156	5.5	37,48
Southeast NV	660816	1802	5.6	8,27,68,70
Truckee, CA	660912	1641	5.8	9,42,59,73,75
Pocatello V., UT	750328	231	6.0	1,2,3,7,48,76
Norris, WY	750630	1854	6.4	3,7,50
Wheeler Crest, CA	781004	1642	5.8	29,38,58
Mammoth, CA	800525	1633	6.1	4,13,29,33
Mammoth, CA	800525	1944	6.1	4,13,29,33
Mammoth, CA	800527	1450	6.2	4,13,29,33
Mammoth, CA	810930	1153	5.8	29
Borah Peak, ID	831028	1406	7.3	6,14,26,54,62
Borah Peak, ID	831028	1951	5.8	29,49,54
Borah Peak, ID	831029	2329	5.8	29,54
Borah Peak, ID	840822	946	5.8	18,52
Round Valley, CA	841123	1808	5.9	5,12,34,52

Chalfant Vlly, CA	860720	1429	5.9	11,15,35,43,51,67
Chalfant Vlly, CA	860721	1442	6.3	11,15,35,43,51,67
Chalfant Vlly, CA	860731	722	5.7	51

+ Reference Index:

1 Arabasz and McKee (1980)
2 Arabasz et al. (1981)
3 Bache et al. (1980)
4 Barker and Langston (1983)
5 Barker and Wallace (1986)
6 Barrientos et al. (1987)
7 Battis and Hill (1977)
8 Beck (1970)
9 Burdick (1977)
10 Callaghan and Gianella (1935)
11 Cockerham and Corbett (1987)
12 Corbett (1985)
13 Cramer and Toppozada (1980)
14 Crone et al. (1987)
15 de Polo and Ramelli (1987)
16 de Polo et al. (1987)
17 Dewey et al. (1973)
18 Doser, unpublished data (1988)
19 Doser (1988a)
20 Doser (1988b)
21 Doser (1988c)
22 Doser (1987a)
23 Doser (1987b)
24 Doser (1986)
25 Doser (1985)
26 Doser and Smith (1985)
27 Doser and Smith (1982)
28 Dumas et al. (1980)
29 Ekstrom and Dziewonski (1985)
30 Engineering News Record (1935)
31 Freidline et al. (1976)
32 Gianella and Callaghan (1934)
33 Given et al. (1982)
34 Gross and Savage (1987)
35 Gross and Savage (1985)
36 Henry and Price (1985)
37 Herrmann et al. (1980)
38 Hill et al. (1985)
39 Hintze (1974)
40 Johns et al. (1982)
41 Jones (1987)
42 Kachadoorian et al. (1967)
43 Lienkaemper et al. (1987)
44 Molinari (1984)
45 Muehlberger et al. (1978)
46 Ni et al. (1981)
47 Pardee (1926)
48 Patton (1985)
49 Patton and Doser (1988)
50 Pitt et al. (1979)
51 Prelim. Determ. of Epic. (1986)
52 Prelim. Determ. of Epic. (1984)
53 Qamar and Hawley (1979)
54 Richins et al (1987)
55 Richter (1958)
56 Richter (1947)
57 Romney (1957)
58 Ryall and Ryall (1981)
59 Ryall et al. (1968)
60 Savage and Hastie (1969)
61 Schmidt (1986)
62 Scott et al. (1985)
63 Shenon (1936)
64 Slemmons (1957)
65 Slemmons (1956)
66 Slemmons et al. (1965)
67 Smith and Priestly (1988)
68 Smith and Sbar (1974)
69 Snay et al. (1985)
70 Stewart and Carlson (1977)
71 Stickney and Bartholomew (1987)
72 Tocher (1956)
73 Tsai and Aki (1970)
74 Wallace (1984)
75 Wallace et al. (1981)
76 Williams (1979)
77 Witkind (1964)

factors such as heatflow appear to influence faulting processes.

DATA COLLECTION

A wide variety of information was collected for each earthquake. Source parameter information collected included focal depth (from local network information, long period body and surface waveform modeling and geodetic studies), focal mechanism (from body and surface wave modeling, first motion analysis, geodetic studies and mapping of surface faulting), moment (from waveform modeling, geodetic and geologic estimates), magnitude (M_L, M_S, m_b), rupture length (from geodetic, geologic or waveform studies), vertical and horizontal displacement (from surface faulting, geodetic and waveform studies), and source duration (from waveform studies). If uncertainty information for a parameter was available, it was recorded. Origin time, epicenter location, magnitude, depth, and focal mechanism information was collected for the largest aftershock and/or foreshock associated with each earthquake. In addition, the regional heatflow, age and type of rock faulted, complexity of rupture, and features controlling the end point of the rupture were also noted.

About 30% of the earthquakes with published source-time function shapes were composed of source-time functions with two or more distinct peaks of moment release separated in time by 4 to 20 sec. Each of these peaks was considered a separate subevent. In a few cases, the subevents for an earthquake were best modeled as occurring at distinctly different depths along faults with different orientations, and the source properties of each subevent were listed separately.

The cut-off magnitude for this study was chosen to be 5.5. That is, if any of several magnitude values given for an earthquake was greater than or equal to 5.5, the earthquake was included in the study. This cut-off value was chosen for several reasons. First, earthquakes below a magnitude of 5.5 are not well recorded by regional networks and only limited source information is generally available. Second, earthquakes of $M < 5.5$ usually do not cause significant damage or loss of life, and are not of as great of interest in hazard assessment studies. Finally, the threshold magnitude for surface faulting in the intermountain region is about 6.0, and a cut-off magnitude of 5.5 includes all earthquakes that are associated with surface faulting or geodetic displacement.

Earthquakes examined in this study and the references used in the data collection process are listed in table 1. In addition to magnitude requirement stated above, earthquakes used in the study had a minimum of one focal mechanism determination. In cases where several researchers had determined source parameters using the same data set and had obtained different results, the average parameter value was noted, and the parameter uncertainties were chosen to encompass the range of values obtained by the different researchers.

COMPARISONS OF DATA SETS

In order to check the consistency of source parameter information comparisons were made between source information obtained from body and surface waveform modeling, geodetic analysis, first motion studies, and observed surface faulting. Space limitations do not allow for illustration of all the comparisons undertaken, however, an example of a comparison of source parameters (strike, dip, rake, rupture length) obtained from body waveform modeling to those obtained from surface faulting is shown in figure 2. The source parameters obtained from waveform modeling are reflective of faulting near the depth of rupture initiation. Comparison of these parameters with surface faulting parameters may indicate changes in the fault geometry with depth.

All of the strike values in figure 2 are within 20° of a one-to-one correspondence.

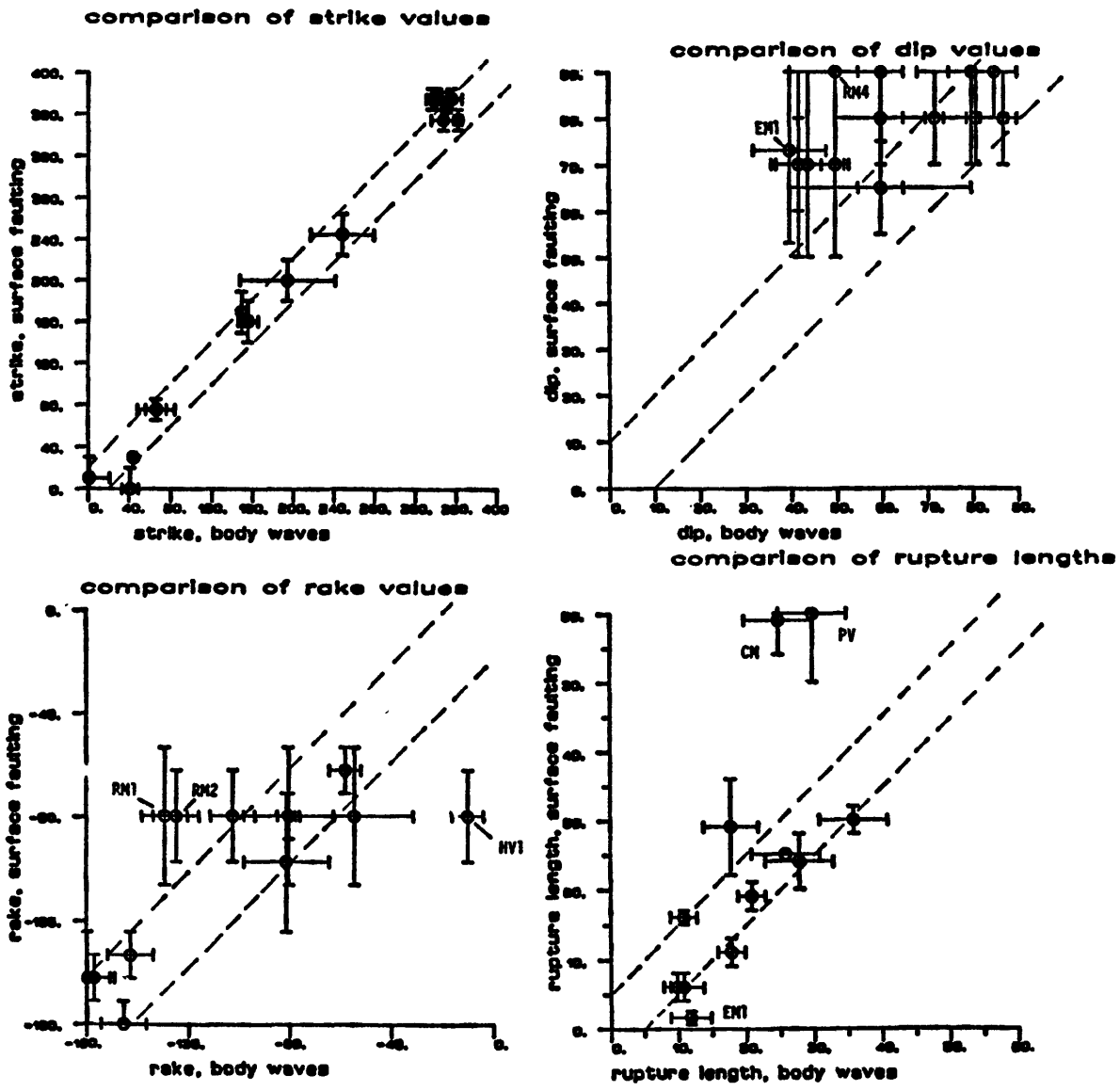

FIGURE 2. -- Comparison of strike, dip, rake, and rupture length obtained from body waveform modeling to those obtained from surface faulting. Dashed lines for strike and rake are ±20° from one-to-one correspondence, dashed lines for dip are ±10° from one-to-one correspondence, and dashed lines for rupture length are ±5 km from one-to-one correspondence. Earthquakes falling outside the dashed limits are labeled. RM1, RM2, and RM4 are the first, second, and fourth events of the Rainbow Mountain sequence. HV1, EM1, CM, and PV are the Hansel Valley, Excelsior Mountain, Cedar Mountain, and Pleasant Valley mainshocks.

Comparisons of dip values show that the dip observed at the surface is almost always greater than that obtained from body waveform modeling. This suggests a slight shallowing of dip with depth, most likely due to a change in rock properties with depth.

Although rake is often the poorest resolved focal mechanism parameter, 80% of the earthquakes have rakes within 20° of a one-to-one correspondence. Three earthquakes fall outside the 20° range. Two are the first two events of the Rainbow Mountain sequence (RM1, RM2, figure 2), the other is the Hansel Valley mainshock (HV1). Both seismic (Doser, 1986) and geodetic (Snay et al., 1985) information for the Rainbow Mountain sequence indicate that oblique normal slip occurred at depth during the sequence. Geodetic information was not sufficient for the Hansel Valley mainshock to determine whether oblique or strike-slip motion occurred at depth, however body waveform modeling of the largest aftershock of the sequence also gave a strike-slip (rake -20°) mechanism (Doser, 1988c).

Body wave rupture length, L, is estimated using the relationship $L=v\ t_c$ (Kanamori and Stewart, 1976) where t_c is the rupture time and v is the rupture velocity (3.5 km/sec). Due to the complex shape of many source-time functions, rupture time was chosen to be half the source duration and in most cases gives a minimum estimate of rupture length. In modeling body waveforms recorded by long period instruments, source duration can usually only be resolved to the nearest second, giving a minimum uncertainty of rupture length of 2 km. Note that most estimates of rupture length shown in figure 2 lie within 5 km of each other when uncertainties are included. Body wave rupture length significantly underestimates the observed surface rupture length for the Pleasant Valley (PV) and Cedar Mountain (CM) earthquakes. Both earthquakes appear to be complex, multiple ruptures (Doser, 1988b), and the moments of the subevents of the earthquakes do not equal the total moment estimated from surface faulting for each of the events. This suggests that some of the observed surface faulting could be produced by large aftershocks occurring within the coda of the mainshock. Large foreshocks could also have caused faulting in Pleasant Valley (Doser, 1988b). Faulting during the Cedar Mountain sequence is irregular and discontinuous (Gianella and Callaghan, 1934), making an accurate estimate of total surface rupture length difficult. Estimated body wave rupture length was greater than the observed surface faulting for the Excelsior Mountain (EM1) earthquake. There is some question as to whether the surface fractures observed following this earthquake represent tectonic displacement (Doser, 1988b).

SOURCE CHARACTERISTICS

The primary objective of this study was to evaluate the distribution of source parameters for intermountain earthquakes, to compare faulting processes within the region, and to determine what factors may influence the observed processes. Figures 3 through 7 illustrate some of the source parameters and faulting characteristics that have been examined in this preliminary study.

Figure 3 shows the distribution of dip (top) and rake (bottom) obtained from body waveform modeling for earthquakes where the fault plane could be selected from the two possible nodal planes using the alignment of surface faulting or aftershocks, or waveform information. Dip values shown have uncertainties of 10° or less (average value of 7°) and rake values have uncertainties of 20° or less (average value of 11°). Magnitude shown is the largest magnitude given for earthquake (M_L, M_S, or m_b).

Note that all earthquakes of this study occurred on faults dipping 30° or more. The lowest dip, 38°, is for the Pocatello Valley earthquake. There is no evidence for faulting along low angle (<30° dip) faults, although low angle faults have been observed at seismogenic depths on seismic reflection profiles throughout the intermountain west (Smith and Bruhn, 1984; Anderson et al., 1983). Most of the intermountain area is considered to be undergoing extension, however the distribution of rakes (figure 3) indicates that the amounts of normal (rakes of -60° to -120°), oblique-slip (rakes of -120° to -160° and -20° to -60°), and

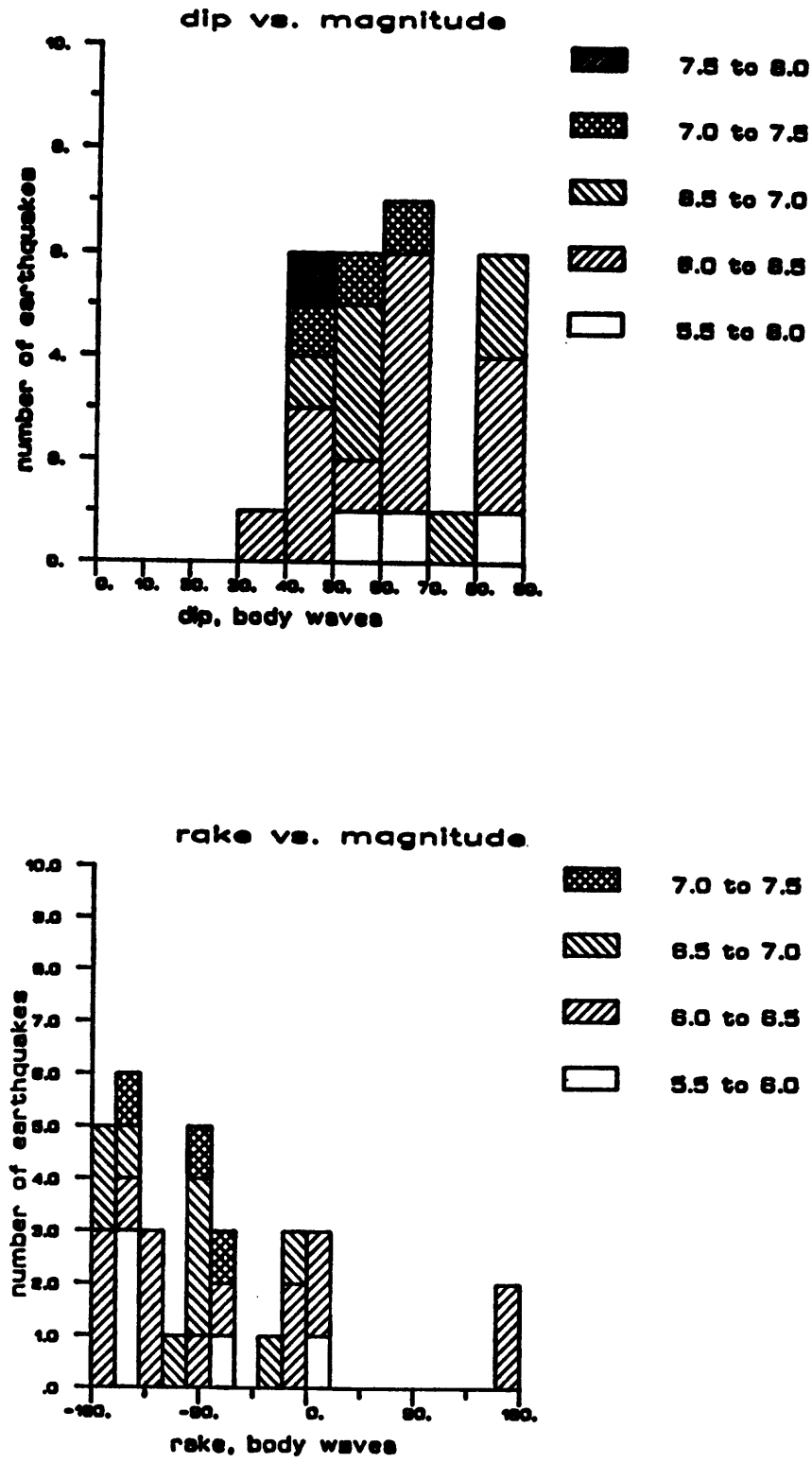

FIGURE 3. -- Dip versus magnitude (top) and rake versus magnitude (bottom).

strike-slip faulting (rakes of 0° to -20°, -160° to -180°, 0° to 20°, and 160° to 180°) are nearly equal. This relationship appears to hold true even when earthquakes are grouped into separate physiographic provinces.

Figure 4 illustrates the relationship between focal depth and several source parameters. Focal depths shown are the depths of rupture initiation determined either from body waveform modeling or from local network information. The focal depths have uncertainties of $\leq$3 km. The top histogram shows that the majority of earthquakes occur at depths of 6 to 12 km. The deepest earthquakes (15 to 18 km) have magnitudes $\geq$7.0, while earthquakes with magnitudes < 6.0 occur no deeper than 12 km. In most regions the largest earthquakes occur at the maximum depth of observed background seismicity, suggesting rupture initiation during these large earthquakes occurs near the brittle/ductile transition zone. The middle histogram in figure 4 compares focal mechanism to focal depth. Focal mechanisms are divided into the categories normal, oblique-slip, and strike-slip, using the same ranges of rake discussed previously. The rakes have uncertainties of 20° or less with an average uncertainty of 9°. There appears to be no relationship between focal mechanism and depth for the earthquakes of this study.

Regional heatflow taken from Sass et al., (1981) with estimated uncertainties of $\leq$ 20 mW/m^2, is plotted versus focal depth in the bottom histogram of figure 4. In regions of highest heatflow (110 to 130 mW/m^2), earthquakes occur no deeper than 12 km, however earthquakes in regions of high heatflow (90 to 110 mW/m^2) occur as deep as 18 km. Earthquakes in regions of lowest heatflow (50 to 70 mW/m^2) are also shallower than 12 km, but none of these earthquakes has a magnitude > 6.5. The lack of a simple correlation between heatflow and focal depth suggests that other factors such as rock type or magnitude may influence focal depth, and that these factors may not be easily separable from the effects of heatflow on focal depth.

Figure 5 compares rupture complexity (top) and rpture direction (bottom) to magnitude. As mentioned previously, about 30% of the earthquakes whose source-time function shapes have been published, consist of two or more subevents. No earthquake with magnitude < 6.0 appears to exhibit rupture complexity at the periods (0.5 to 10 sec) generally examined during body waveform modeling studies. All earthquakes with magnitude $\geq$ 7.0, except the Borah Peak mainshock (Doser and Smith, 1985; Nabelek, 1988), have complex ruptures best modeled by multiple subevents. Rupture direction was determined from the location of the mainshock with respect to surface faulting and/or aftershocks. At all magnitude levels unilateral rupture direction predominates.

Rupture lengths of intermountain earthquakes are shown in figure 6. The bottom histogram shows rupture lengths for individual subevents, and the top histogram shows total rupture length, obtained by adding the rupture lengths of subevents comprising each earthquake, versus magnitude. Recall that the minimum resolvable rupture length for body waveforms recorded on long period instruments is about 2 km. The peak in the length of individual subevent ruptures occurs at 8 to 12 km, with 92% of the subevents having a rupture length < 16 km. The peak in total rupture length also occurs at 8 to 12 km, with a sharp falloff at 16 km. Note that 80% of the earthquakes with total rupture length < 16 km have magnitudes of < 6.5 and that all magnitude $\geq$7.0 earthquakes have rupture lengths of 20 km or more.

A final figure (figure 7) illustrates the types of nucleation and termination points observed for intermountain earthquakes. The grouping of rupture termination and nucleation point into behavioral, geological, structural, and geometrical points follows the end point classification system of Kneupfer (this volume). Nucleation points appear to be almost equally distributed among behavioral, structural, and geometrical end points. It is important to note that most of the behavioral nucleation points are associated with earthquakes that are large aftershocks. Fewer termination points were identified, with slightly more behavioral termination points than structural endpoints.

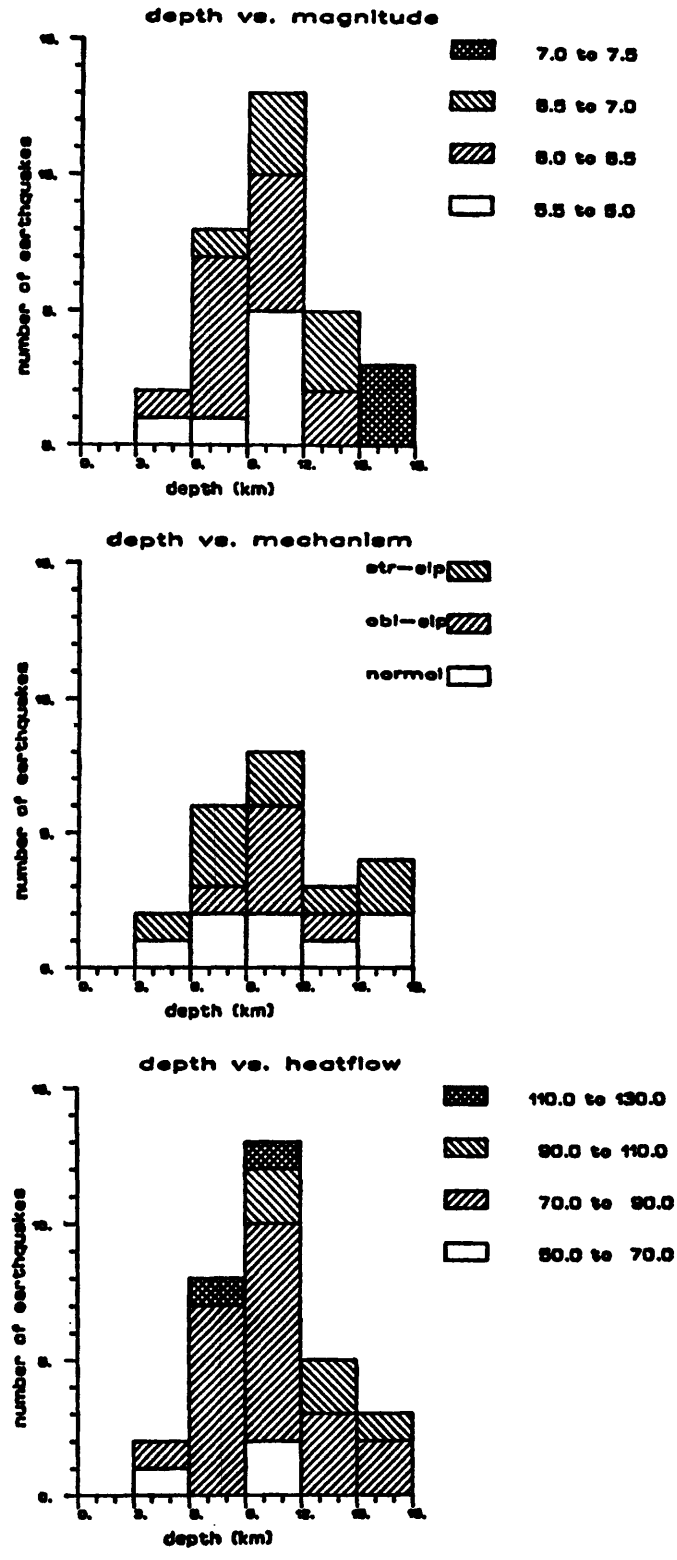

FIGURE 4. -- Depth versus magnitude (top), mechanism (middle), and heatflow in mW/m^2. See text for details.

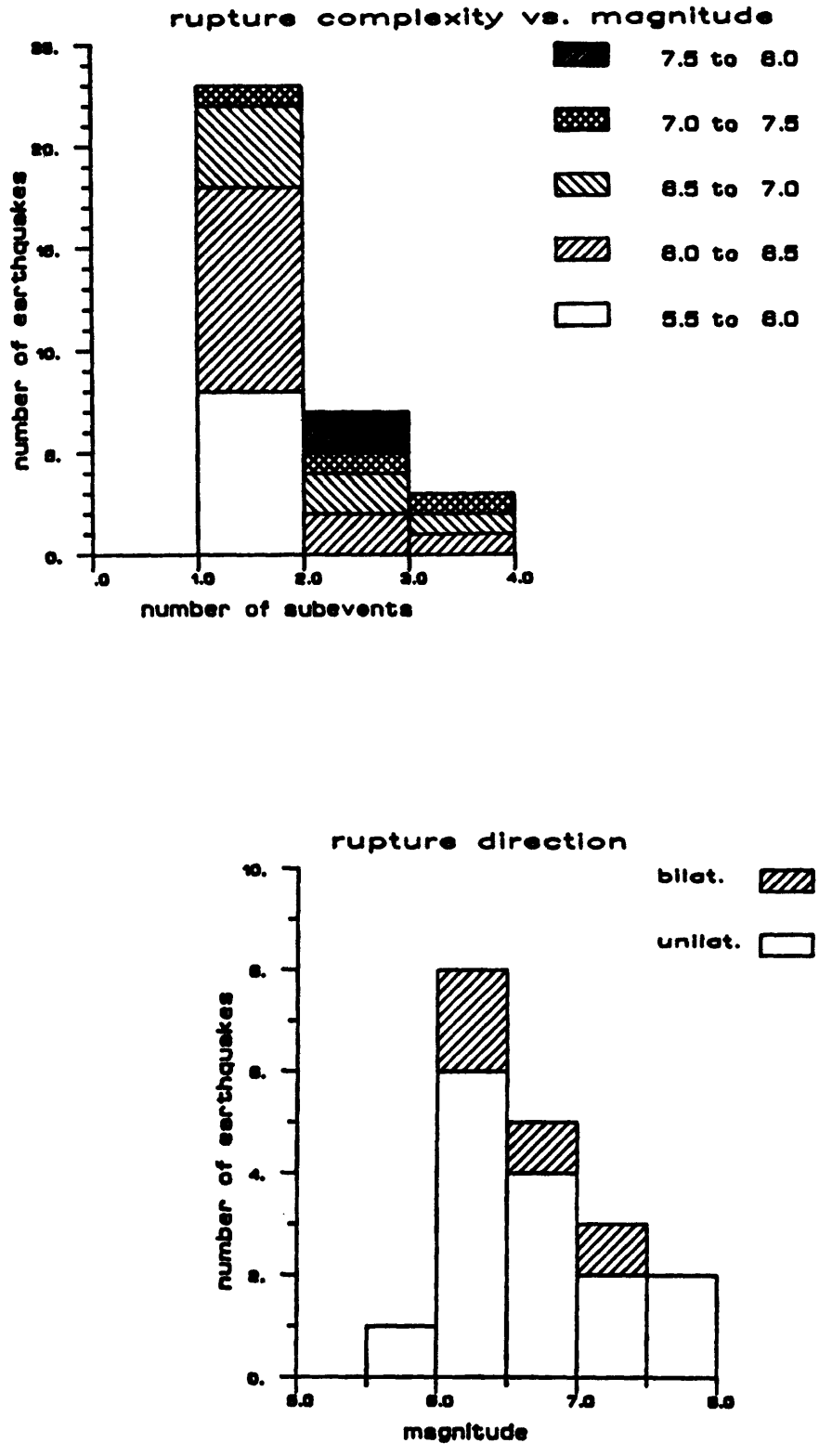

FIGURE 5. -- Rupture complexity (top) and rupture direction (bottom) versus magnitude.

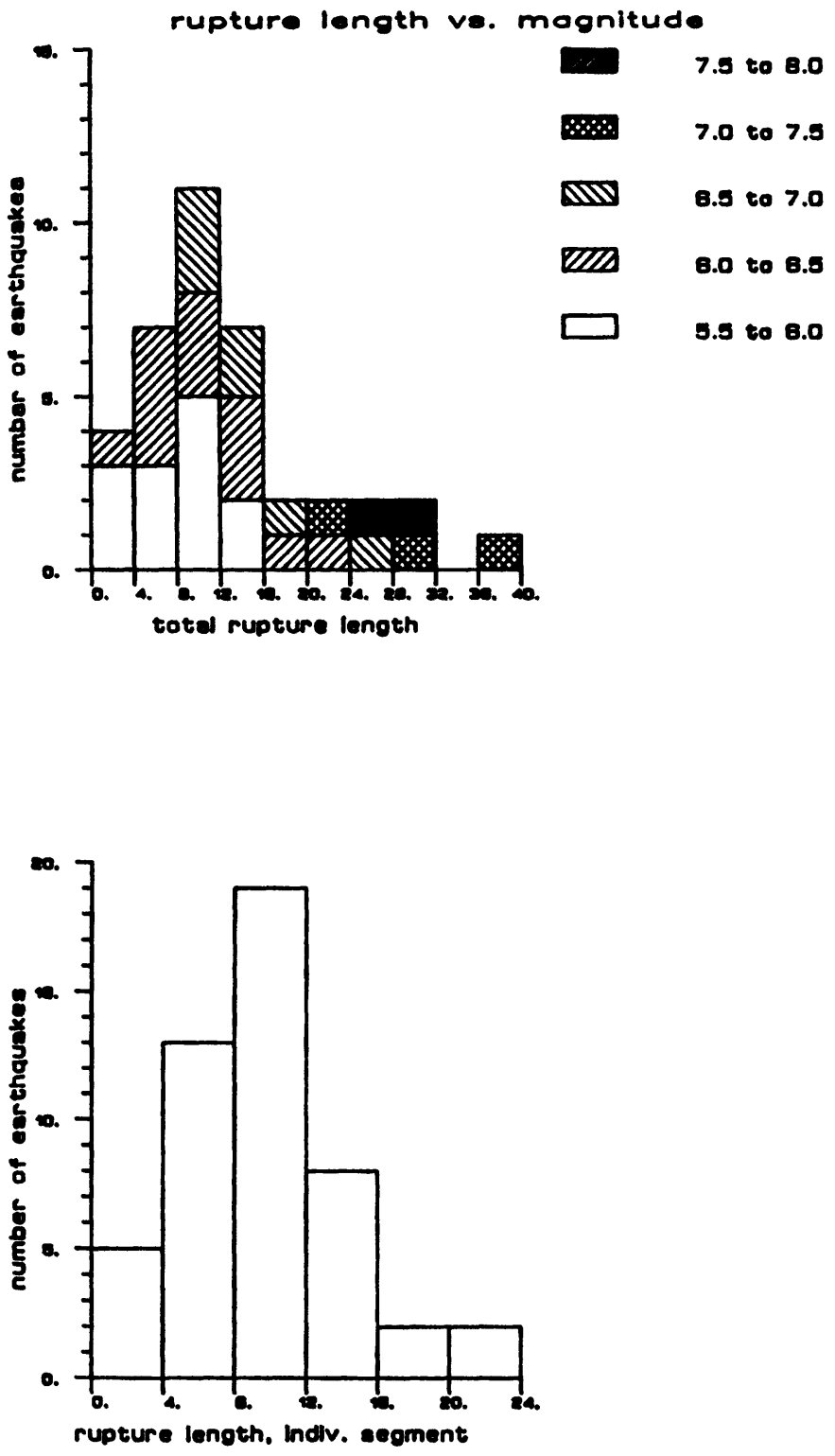

FIGURE 6. -- Total rupture length versus magnitude (top) and distribution of rupture lengths of individual subevents (bottom).

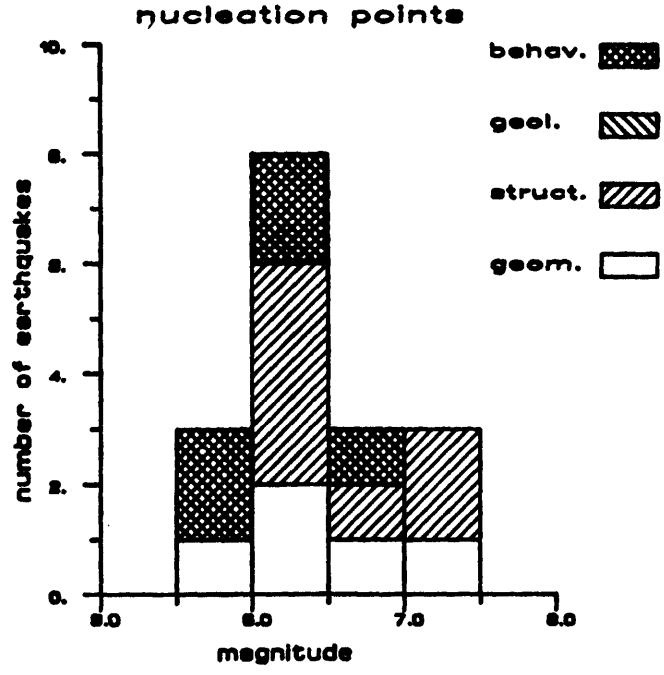

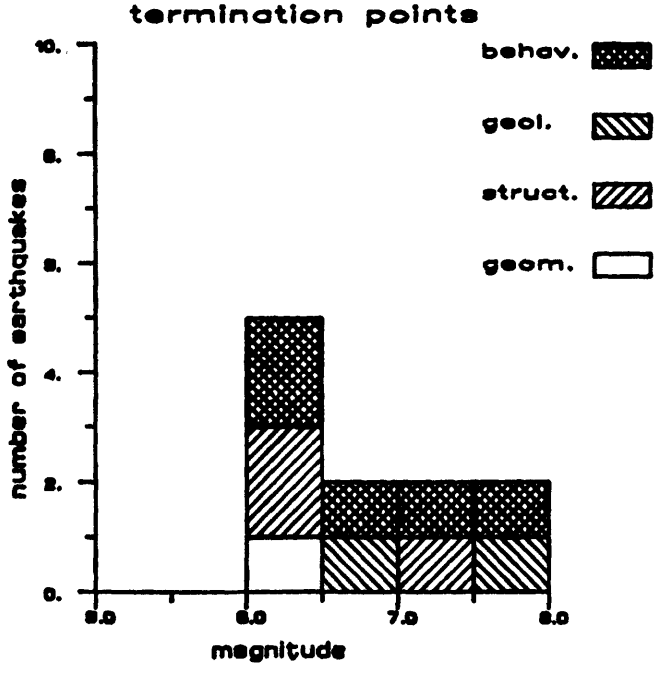

FIGURE 7. -- Nucleation points (top) and termination points (bottom) versus magnitude. End points follow the classification system of Kneupfer (this volume).

CONCLUSIONS

This paper has presented a brief overview of a larger, ongoing study of the faulting characteristics and source parameters of intermountain earthquakes. Although many results of this study are not surprising (i.e., larger earthquakes have longer rupture lengths, occur at deeper depths, and have more complex ruptures than smaller magnitude earthquakes), some results (i.e., the lack of correlation between heatflow and focal depth, the predominant unilateral nature of faulting) bear more investigation. Comparisons between source parameters and type of rock, age of rock, and physiographic province, are continuing, and may provide insight on why particular earthquakes within a similar magnitude range or geographic region may differ greatly. Studies of the mechanism and timing of foreshocks and aftershocks also may reveal important factors that control the nature of an entire earthquake sequence. It is hoped that study will ultimately lead to a better quantification of the range of source parameters that may be expected for earthquakes within a certain magnitude range or certain region, allowing for a better assessment of the hazards associated with future large magnitude earthquakes.

ACKNOWLEDGEMENTS

I would like to thank R. B. Smith for providing me with a compilation of source parameters and related references for western U.S. earthquakes that were used to supplement my compilations. M. R. Baker helped me to structure the large data set of source parameter information for easy retrieval and analysis from a data base manager system. This research was supported by National Science Foundation grant EAR-8608403.

REFERENCES CITED

Anderson, R. E., Zoback, M. L., and Thompson, G., 1983, Implications of selected subsurface data on the structural form and evolution of some basins in the northern Basin and Range Province, Nevada and Utah: Geological Society of America Bulletin, v. 94, p. 1055-1072.

Arabasz, W. J., and McKee, M. E., 1979, Utah earthquake catalog 1850-June 1962, *in* Arabasz, W. J., Smith, R. B., and Richins, W. D., eds., Earthquake studies in Utah 1850 to 1978: Salt Lake City, Utah, University of Utah, p. 119-143.

Arabasz, W. J., Richins, W. D., and Langer, C. J., 1981, The Pocatello Valley (Idaho-Utah border) earthquake sequence of March to April 1975: Bulletin Seismological Society of America, v. 71, p. 803-826.

Bache, T. C., Lambert, D. G., and Barker, T. G., 1980, A source model for the March 28, 1975 Pocatello Valley earthquake from time-domain modeling of teleseismic P waves: Bulletin Seismological Society of America, v. 70, p. 405-418.

Barker, J. S., and Langston, C. A., 1983, A teleseismic body wave analysis of the May 1980 Mammoth Lakes, California, earthquakes: Bulletin Seismological Society of America, v. 73, p. 419-434.

Barker, J. S., and Wallace, T. C., 1986, A note on the teleseismic body waves from the 23 November 1984, Round Valley, California, earthquake: Bulletin Seismological Society of America, v. 76, p. 883-888.

Barrientos, S. E., Stein, R. S., and Ward, S. E., 1987, Comparison of the 1959 Hebgen Lake, Montana, and the 1983 Borah Peak, Idaho, earthquakes from geodetic observations: Bulletin Seismological Society of America, v. 77, p. 784-808.

Battis, J. C., and Hill, K. J., 1977, Analysis of seismicity and tectonics of the central and western United States: Texas Instruments, Inc., Interim Scientific Report No. 1.
Beck, P. J., 1970, The southern Nevada-Utah border earthquakes August to December, 1966: Salt Lake City, Utah, University of Utah M.S. Thesis, 53 p.
Burdick, L. J., 1977, Broad-band seismic studies of body waves: Pasadena, Calif., California Institute of Technology Ph. D. dissertation, 254 p.
Callaghan, E., and Gianella, V. P., 1935, The earthquake of January 30, 1934, at Excelsior Mountains, Nevada: Bulletin Seismological Society of America, v. 25, p. 161-168.
Cockerham, R. S., and Corbett, E. J., 1987, The July 1986 Chalfant Valley earthquake sequence: Preliminary results: Bulletin Seismological Society of America, v. 77, p. 280-289.
Corbett, E. J., 1985, The Round Valley, California, earthquake of November 23, 1984: Earthquake Notes, v. 55, p. 30.
Cramer, C. H., and Toppozada, T. R., 1980, A seismological study of the May 1980 and earlier earthquake activity near Mammoth Lakes, California: California Division of Mines and Geology, Special Report 150, p. 91-130.
Crone, A. J., Machette, M. N., Bonilla, M. G., Lienkaemper, J. J., Pierce, K. L., Scott, W. E., and Bucknam, R. C., 1987, Surface faulting accompanying the Borah Peak earthquake and segmentation of the Lost River fault, Central Idaho: Bulletin Seismological Society of America, v. 77, p. 739-770.
de Polo, C. M., and Ramelli, A. R., 1987, Preliminary report on surface fractures along the White Mountains fault zone associate with the July 1986 Chalfant Valley earthquake sequence: Bulletin Seismological Society of America, v. 77, p. 290-296.
de Polo, C. M., Bell, J. W., and Ramelli, A. R., 1987, Geometry of strike-slip faulting related to the 1932 Cedar Mountain earthquake, central Nevada: Geological Society of America Abstracts with Programs, v. 19, p. 371.
Dewey, J. W., Dillinger, W. H., Taggart, J., and Algermissen, S. T., 1973, A technique for seismic zoning: Analysis of earthquake locations as mechanisms in northern Utah, Wyoming, Idaho and Montana: National Oceanic and Atmospheric Administration Technical Report ERL267-ESL30, p.28-48.
Doser, D. I., 1988a, Source parameters of Montana earthquakes (1925-1964) and tectonic deformation in the northern Intermountain seismic belt: in press, Bulletin Seismological Society of America.
------1988b, Source mechanisms of earthquakes in the Nevada Seismic Zone (1915-1943): in press, Journal of Geophysical Research.
------1988c, Extensional tectonics in northern Utah-southern Idaho, U.S.A., and the 1934 Hansel Valley sequence: in press, Physics of the Earth and Planetary Interiors.
------1987a, Modeling the Pnl waveforms of the Fairview Peak-Dixie Valley, Nevada, U.S.A. earthquake sequence (1954-1959): Physics of the Earth and Planetary Interiors, v. 48, p. 64-72.
------1987b, The August 16, 1931 Valentine, Texas earthquake: Evidence for normal faulting in west Texas: Bulletin Seismological Society of America, v. 77, p. 2005-2017.
------1986, Earthquake processes in the Rainbow Mountain-Fairview Peak-Dixie Valley, Nevada, region 1954-1959: Journal Geophysical Research, v. 91, p. 12,572-12,586.
------1985, Source parameters and faulting processes of the 1959 Hebgen Lake, Montana, earthquake sequence: Journal Geophysical Research, v. 90, p. 4537-4555.
Doser, D. I., and Smith, R. B., 1985, Source parameters of the 28 October, 1983, Borah Peak, Idaho, earthquake from body wave analysis: Bulletin Seismological Society of America, v. 75, p. 1041-1051.
------1982, Seismic moment rates in the Utah region: Bulletin Seismological Society of America, v. 72, p. 525-551.
Dumas, D. B., Dorman, H. J., and Latham, G. V., 1980, A reevaluation of the August 16, 1931 Texas earthquake: Bulletin Seismological Society of America, v. 70, p. 1171-1180.
Ekstrom, G. and Dziewonski, A. M., 1985, Centroid-moment tensor solutions for 35

earthquakes in western North American (1977-1983): Bulletin Seismological Society of America, v. 75, p. 23-40.
Engineering News Record, 1935, v. 114, p. 322.
Freidline, R. A., Smith, R. B., and Blackwell, D. D., 1976, Seismicity and contemporary tectonics of the Helena, Montana area: Bulletin Seismological Society of America, v. 66, p. 81-95.
Gianella, V. P., and Callaghan, E., 1934, The Cedar Mountain, Nevada, earthquake of December 20, 1932: Bulletin Seismological Society of America, v. 24, p. 345-377.
Given, J. W. Wallace, T. C., and Kanamori, H., 1982, Teleseismic analysis of the 1980 Mammoth Lakes earthquake sequence: Bulletin Seismological Society of America, v. 72, p. 1093-1109.
Gross, W. K., and Savage, J. C., 1987, Deformation associated with the 1986 Chalfant Valley earthquake, eastern California: Bulletin Seismological Society of America, v. 77, p. 306-310.
------1985, Deformation near the epicenter of the 1984 Round Valley, California, earthquake: Bulletin Seismological Society of America, v. 75, p. 1339-1347.
Henry, C. D., Price, J. G., 1985, Summary of the tectonic development of Trans-Pecos Texas: Austin, Texas, University of Texas at Austin, Bureau of Economic Geology, Miscellaneous Map 36, 8 p.
Herrmann, R. B., Dewey, J. W., and Park S-K, 1980, The Dulce, New Mexico, earthquake of 23 January 1966: Bulletin Seismological Society of America, v. 70, p. 2171-2184.
Hill, D. P., Bailey, R. A., and Ryall, A. S., 1985, Active tectonic and magmatic processes beneath Long Valley Caldera, eastern California: An overview, Journal of Geophysical Research, v. 90, p. 11,111-11,120.
Hintze, L. F., 1974, Geologic Map of Utah: Brigham Young University Geology Studies, Special Publication 2.
Johns, W. M., Straw, W. T., Bergantino, R. N., Dresser, H. W., Hendrix, T. E., McClernan, H. G., Palmquist, J. C., and Schmidt, C. J., 1982, Neotectonic features of southern Montana east of 112° 30' west longitude: Montana Bureau of Mines and Geology Open-File Report 91, 79 p.
Jones, C. H., 1987, A geophysical and geological investigation of extensional structures, Great Basin, western United States: Cambridge, Mass., Massachusetts Institute of Technology Ph. D. dissertation, 226 p.
Kachadoorian, R., Yerkes, R., and Waananen, A., 1967, Effects of the Truckee, California, earthquake of September 12, 1966: U.S. Geological Survey Circular, 537.
Kanamori, H., and Stewart, G. S., 1976, Mode of strain release along the Gibbs fracture zone, Mid-Atlantic Ridge: Physics of the Earth and Planetary Interiors, v.11, p. 312-332.
Lienkaemper, J. J., Pezzopane, S. K., Clark, M. M., and Rymer, M. J., 1987, Fault fractures formed in association with the 1986 Chalfant Valley, California, earthquake sequence: Preliminary report: Bulletin Seismological Society of America, v. 77, p. 297-305.
Molinari, M. P., 1984, Late Cenozoic geology and tectonics of Stewart and Monte Cristo Valleys, west-central Nevada: Reno, Nev., University of Nevada M. S. thesis, 124 p.
Muehleberger, W. R., Belcher, R. C., and Goetz, L. K., 1978, Quaternary faulting in Trans-Pecos Texas: Geology, v. 6, p. 337-340.
Nabelek, J., 1988, Planar vs. listric faulting: The rupture process and fault geometry of the 1983 Borah Peak, Idaho earthquake from inversion of teleseismic body waves: submitted to Journal of Geophysical Research.
Ni, J. F., Reilinger, R. E., and Brown, L. D., 1981, Vertical crustal movements in the vicinity of the 1931 Valentine, Texas, earthquake: Bulletin Seismological Society of America, v. 71, p. 857-864.
Pardee, J. T., 1926, The Montana earthquake of June 27, 1925: U.S. Geological Survey Professional Paper 147, p. 7-23.
Patton, H. J., 1985, P-wave fault plane solutions and the generation of surface waves by earthquakes in the western United States: Geophysical Research Letters, v. 12, p. 518-

521.
Patton, H. J., and Doser, D. I., 1988, Inversion of regional Pnl and surface-wave data for source parameters of a Borah Peak aftershock: Geophysical Research Letter, in press.
Pitt, A. M., Weaver, C. S., and Spence, W., 1979, The Yellowstone Park earthquake of June 30, 1975: Bulletin Seismological Society of America, v. 69, p. 187-205.
Preliminary Determination of Epicenters, July, 1986, p. 21.
Preliminary Determination of Epicenters, November, 1984, p. 18.
Qamar, A., and Hawley, B., 1979, Seismic activity near the Three Forks basin, Montana: Bulletin Seismological Society America, v. 69, p. 1917-1929.
Richins, W. D., Pechmann, J. C., Smith, R. B., Langer, C. J., Goter, S. K., Zollweg, J. E., and King, J. J., 1987, The 1983 Borah Peak, Idaho, earthquake and its aftershocks: Bulletin Seismological Society of America, v. 77, p. 694-723.
Richter, C. F., 1958, *in* Elementary Seismology: W. H. Freeman and Co., p. 516-518.
------1947, The Manix (California) earthquake of April 10, 1947: Bulletin Seismological Society of America, v. 37, p. 171-179.
Romney, C., 1957, Seismic waves from the Dixie Valley-Fairview Peak earthquakes: Bulletin Seismological Society of America, v. 47, p. 310-319.
Ryall, A., and Ryall, F., 1981, Spatial-temporal variations in seismicity preceding the May 1980 Mammoth Lakes, California, earthquakes: Bulletin Seismological Society of America, v. 71, p. 747-760.
Ryall A., Van Wormer, J. D., and Jones, A. J., 1968, Triggering of microearthquakes by earthtides, and other features of the Truckee, California earthquake sequences of September, 1966: Bulletin Seismological Society of America, v. 58, p. 215-248.
Sass, J. H., Blackwell, D. D., Chapman, D. S., Costain, J. K., Decker, E. R., Lawver, L. A., and Swanberg, C. A., 1981, Heat flow from the crust of the United States *in* Touloukian, Y. S., and Ho, C. Y., eds., Physical Properties of Rocks and Mineral, Volume II-2: McGraw-Hill, p. 503-548.
Savage, J. C., and Hastie, L. M., 1969, A dislocation model for the Fairview Peak, Nevada, earthquake: Bulletin Seismological Society of America, v. 59, p. 1937-1948.
Schmidt, R. G., 1986, Geology, earthquake hazards, and land use in the Helena area, Montana - A review: U.S. Geological Survey Professional Paper 1316, 64 p.
Scott, W. E., Pierce, K. L., and Hait, H. M., Jr., 1985, Quaternary tectonic setting of the 1983 Borah Peak earthquake, central Idaho: U. S. Geological Survey Open File Report 85-290, p. 1-16.
Shenon, P. J., 1936, The Utah earthquake of March 12, 1934 (extracts from unpublished report), *in* Neumann, F., United States earthquakes, 1934: U.S. Coast and Geodetic Survey Serial 593, p. 43-48.
Slemmons, D. B., 1957, Geological effects of the Dixie Valley-Fairview Peak, Nevada, earthquakes of December, 16, 1954: Bulletin Seismological Society of America, v. 47, p. 353-375.
------1956, Geologic setting for the Fallon-Stillwater earthquakes of 1954: Bulletin Seismological Society of America, v. 46, p. 4-9.
Slemmons, D. B., Jones, A. E., and Gimlet, J. I., 1965, Catalog of Nevada earthquakes 1852-1960: Bulletin Seismological Society of America, v. 55, p. 537-583.
Smith, K. D., and Priestley, K. F., 1988, The foreshock sequence of the 1986 Chalfant, California, earthquake: Bulletin Seismological Society of America, v. 78, p. 172-187.
Smith, R. B., and Bruhn, R. L., 1984, Intraplate extensional tectonics of the eastern Basin-Range: Inferences on structural style from seismic reflection data, regional tectonics, and thermal-mechanical models of brittle-ductile deformation: Journal of Geophysical Research, v. 89, 5733-5762.
Smith, R. B., and Sbar, M. L., 1974, Contemporary tectonics and seismicity of the western United States with emphasis on the Intermountain seismic belt: Geological Society of America Bulletin, v. 85, 1205-1218.
Snay, R. A., Cline, M. W., and Timmermann, E. L., 1985, Dislocation models for the 1954

earthquake sequence in Nevada, U. S. Geological Survey Open-File Report 85-290, p. 531-555.
Stewart, J. H., and Carlson, J. E., 1977, Million-scale geologic map of Nevada: Nevada Bureau of Mines and Geology, Map 57.
Stickney, M. C., and Bartholomew, M. J., 1987, Seismicity and late Quaternary faulting of the northern Basin and Range province, Montana and Idaho: Bulletin Seismological Society of America, v. 77, p. 1602-1625.
Tocher, D., 1956, Movement on the Rainbow Mountain fault: Bulletin Seismological Society of America, v. 46, p. 10-14.
Tsai, Y. B., and K. Aki, 1970, Source mechanisms of the Truckee, California, earthquake of September 12, 1966: Bulletin Seismological Society of America, v. 60, p. 1199-1208.
Wallace, R. E., 1984, Fault scarps formed during the earthquakes of October 2, 1915, in Pleasant Valley, Nevada, and some tectonic implications: U.S. Geological Survey Professional Paper 1274-A, 33 p.
Wallace, T. C., Helmberger, D. V., and Mellman, G. R., 1981, A technique for the inversion of regional data in source parameter studies: Journal Geophysical Research, v, 86, p. 1679-1685.
Williams, B. R., 1979, M_o calculations from a generalized AR parameter method for WWSSN instruments: Bulletin Seismological Society of America, v. 69, p. 309-351.
Witkind, I. J., 1964, Reactivated faults north of Hebgen Lake: U.S. Geological Survey Professional Paper 435, p. 37-50.
Zoback, M. L, and Zoback, M. D., 1980, State of stress in the conterminous United States: Journal of Geophysical Research, v. 85, p. 6113-6156.

EFFECTS OF RESTRAINING BENDS ON THE RUPTURE OF STRIKE-SLIP EARTHQUAKES

by

Katharine Kadinsky-Cade and A. Aykut Barka

Earth Resources Laboratory, Massachusetts Institute of Technology,
Cambridge, MA 02142

ABSTRACT

Single and double restraining bend fault geometries are examined in conjunction with associated large earthquake rupture zones. Data are mostly taken from Turkey, although supplemented by earthquakes from California and China. It is found that restraining bend angles have an upper limit of 30°-35°, in agreement with results from laboratory studies. In addition, earthquake magnitude is found to be proportional to log ($L_2 \sin \alpha$), where L_2 is the length of the restraining fault segment and α is the angle between that segment and the main trend of the rupture zone.

INTRODUCTION

From a detailed comparison between the surface geometry of strike-slip faults and the known rupture extent of associated large earthquakes in Turkey (Barka and Kadinsky-Cade, 1988) we have found that a majority (about 2/3) of these events can be associated with single or double restraining bend patterns. These geometric terms are defined schematically in figure 1.

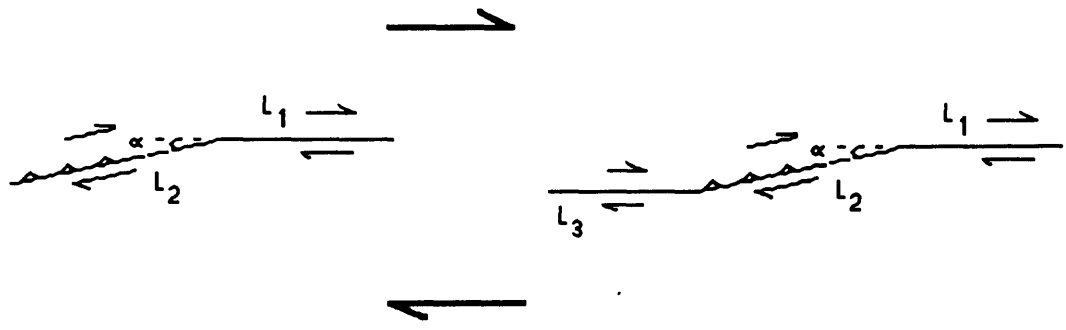

FIGURE 1.--Single and double restraining bends (left and right figures, respectively). L_2 is the restraining segment in each case. Here the direction of block motion (thicker arrows), or relative motion across the fault, is drawn parallel to L_1 and L_3. L_2 has a component of thrust faulting in addition to the strike-slip motion.

Surface fault geometry observations in Turkey are derived from several sources: published maps at scales of 1:25,000 - 1:100,000, aerial photographs at scales of 1:10,000 - 1:60,000 and fieldwork by one of the authors (A.A. Barka). In this study we have expanded

our data set by identifying similar fault geometry patterns from California and China based on published maps and reports. Relationships between fault geometry and earthquakes along the North Anatolian fault zone in Turkey, from which we have taken many of our examples, have been discussed previously by Barka and Hancock (1982) and by Barka (1983). These studies have tied bend locations and angles to earthquake magnitude and epicenter location.

From the combined data set, which includes events with magnitudes between 5.1 and 7.9, we find that restraining single and double bend angles have a maximum value of 30°-35°, and that the restraining segment length and orientation (figure 1) can be related to the earthquake magnitude. Most of the events considered in this study have magnitude > 7. We have looked at large events for practical reasons (e.g., documented surface fault geometry). Our results may hold for smaller earthquakes as well, but we do not have data available at those scales. We are restricting our observations to restraining single or double bend earthquakes because we feel that a particular fault geometry should be characterized by a particular earthquake mechanism.

The approach taken in this paper is as follows. First we describe our data set and the assumptions made in compiling the observations. Then we discuss bend angles and their relation to earthquake magnitude. Following that we compare our results to those of laboratory studies in order to seek a physical explanation for the field observations. Finally we examine the influence of the geometric fault pattern on the distribution of slip and on the epicenter location.

OBSERVATIONS AND ASSUMPTIONS

We assume that restraining bends and double bends maintain their character at least during a time period of several earthquake cycles, if not during the lifetime of the current tectonic regime. The identification of these restraining features does not depend on the direction of rupture propagation during an individual earthquake, but rather on the direction of block motion relative to the orientation of the fault (figure 2). The direction of block motion is the average direction of relative motion across the fault. Ideally the direction of block motion can be obtained from a collection of fault plane solutions or from geodetic data. In practice we have inferred its direction from surface fault morphology in most cases. Sections that have a relatively high obliquity (angle between the fault strike and the direction of block motion) can generally be identified by high topography and compressional features such as folds and thrusts (restraining segments such as L_2 in figures 1 and 2) or by low topography and extensional features (releasing segments, not discussed in this paper).

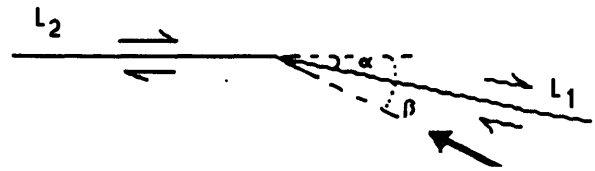

FIGURE 2.-- The direction of block motion (thick arrow) affects the identification of the bend (here shown as a restraining single bend).

In table 1 we have summarized geometric fault parameters from our data set. Sources for these parameters are listed in the Appendix. Note that in most of the Turkish cases the parameters are based not only on the listed sources, but also on field work and examination of maps and aerial photographs by one of the authors (A.A. Barka). More information on the Turkish faults can be found in Barka and Kadinsky-Cade (1988). Examples that have particular

problems have been identified by an asterisk in table 1. These include cases in which (1) well-located aftershock epicenters do not coincide with the surface trace of the fault, or (2) the earthquake was part of a sequence of events in a structurally complex area, and activation of neighboring faults makes a simple interpretation impractical. The 1979 Coyote Lake event falls into category (1), and the 1976 Tangshan earthquake falls into categories (1) and (2). For reasons of consistency we have chosen to tabulate the surface rupture trace parameters even when it is clear that the fault has a different character at depth than at the surface. Similarly we always list surface fault offsets, even though in a couple of the well-studied cases it is known that higher displacements occurred at depth (e.g., 1979 Imperial Valley earthquake). Some of the peculiarities of the individual earthquakes are described in the Appendix.

Table 1.--Summary of geometric values

	Event[1]	M[2]	α (deg)	L_2[3] (km)	L[4] (km)	u (m)	$\log(L_2 \sin\alpha)$ (km)	log L (km)	log(uL) (m^2)
1	1857 San Andreas	7.9	34	70 d	390	9	1.59	2.59	6.54
2	1906 San Andreas	7.7	14	70 d	450	5	1.23	2.65	6.35
3	1939 NAF	7.9	20	110 s	360	7.5	1.58	2.55	6.43
4	1942 NAF	7.0	14	10 s	40	1.7	0.38	1.60	4.83
5	1943 NAF	7.6	15	65 s	320	1.1	1.22	2.50	5.55
6	1944 NAF	7.4	15	10 s	150	3.5	0.41	2.18	5.80
7	1949 NAF	7.0	20	15 s	42	1.5	0.71	1.62	4.80
8	1953 NAF	7.2	17	10 d	52	4.3	0.46	1.72	5.35
9	1966 Parkfield FS	5.1	5	4.5 s	--	---	-0.41	---	---
10	1967 NAF	6.9	20	6 d	90	1.90	0.31	1.95	5.23
11	1970 Tonghai	7.5	24	10 d	50	2.70	0.61	1.70	5.13
12	1973 Luhuo	7.5	11	45 s	90	3.60	0.31	1.95	5.51
13	1976 Çaldiran	7.3	18	28 s	50	3.70	0.94	1.70	5.26
14	1976 Tangshan *	7.8	14	32 s	60	2.70	0.89	1.78	5.21
15	1979 Coyote Lake *	5.7	10	6 d	25	---	0.02	1.40	---
16	1979 Imperial Val	6.5	22	5.5 d	30	0.78	0.31	1.48	4.37

[1]NAF means North Anatolian fault, Turkey. FS means foreshock. See Appendix for details.

[2]Magnitudes are M_W for the 1857 and 1906 cases, M_L for the 1966 Parkfield foreshock, and Ms elsewhere.

[3]Double or single bends (d, s) are identified in the L_2 column.

[4]L is total rupture length observed at surface.

Two other earthquakes could have been included in table 1, however we felt that there was not enough information on them. One of these events was the 1202 Eastern Mediterranean earthquake that occurred on the Dead Sea fault, with approximate magnitude 7.5. This earthquake has been analyzed by Ambraseys and Melville (1987). Subsequent earthquakes in that region have been examined by Ambraseys and Barazangi (in preparation). This last paper includes a fault map and LANDSAT image suggesting that α has a value of about 30° and L_2 a length of about 125 km. The fault has a double bend geometry, although the total length of earthquake rupture in 1202 is not as well constrained as, for example, that of the 1857 California earthquake. If we plot this event in Figure 3, it ends up a bit too high on the vertical axis compared with the other points and regression line. It is possible that the 7.5 magnitude.

estimated from intensity data, is too low. The other event is the 1975 Ms=7.3 Haicheng, China earthquake (Jones et al., 1982). This event appears to have occurred on a fault that includes a restraining single bend with a releasing stepover (offset) right at the bend. We are lacking detailed surface fault maps for this example.

There are several problems with the inclusion in table 1 of horizontal slip at the surface as derived from field measurements. First, the slip values may vary substantially along the fault trace. Second, they may not be an accurate reflection of slip at depth. Third, it is usually not known whether the measurements represent coseismic slip alone, or also include afterslip. Fourth, the availability of slip measurements varies widely from case to case. We have chosen to include the largest value of measured horizontal surface slip in table 1, assuming that surface measurements tend to underestimate the slip at depth (e.g., Thatcher and Lisowski, 1987).

Another complication is the choice of bend angle in the double bend cases. Usually the bend angles are similar on either side of the restraining segment (as shown in figure 1). When they differ by a few degrees we have chosen to include the larger bend angle. Some of the segments are gently curved over distances of tens of kilometers. We do not include gradual bends in table 1, only sharp bends.

RESTRAINING BEND ANGLES AND EARTHQUAKE MAGNITUDE

Two main results emerge from table 1. First, the observed bend angles for single and double restraining bends seem to be restricted to values less than about 30°-35°. When the bend angle is larger than that amount, a restraining stepover tends to occur instead of the bend (lateral offset between segments with complex compressional structures at the offset; see Barka and Kadinsky-Cade, this volume). Second, the magnitude of the event appears to be related to the restraining segment length and orientation, as shown by the linear relationship in figure 3.

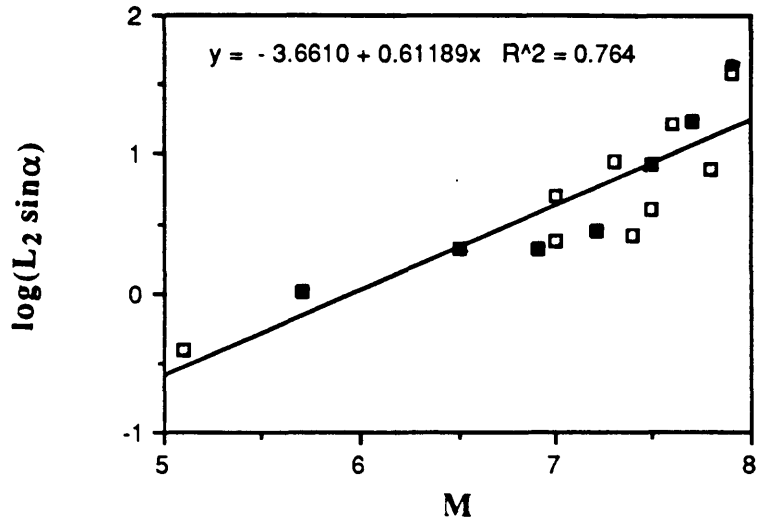

FIGURE 3.--Data from table 1. Open squares are single bends, and closed squares are double bends. The line is a simple regression fit to the data.

In figure 4a we have plotted magnitude versus log (L) as is commonly done (e.g., Slemmons, 1977). A linear relationship is obtained here as expected, with M proportional to

log L^2. Figure 4b combines the results of Figures 3 and 4a. In figure 4c we compare log (L_2 sin α) with log(uL), which should be a measure of earthquake magnitude derived from moment. Figure 4c is no improvement over 4b, possibly due to the uncertainties in estimating the correct value for u from surface measurements as discussed earlier.

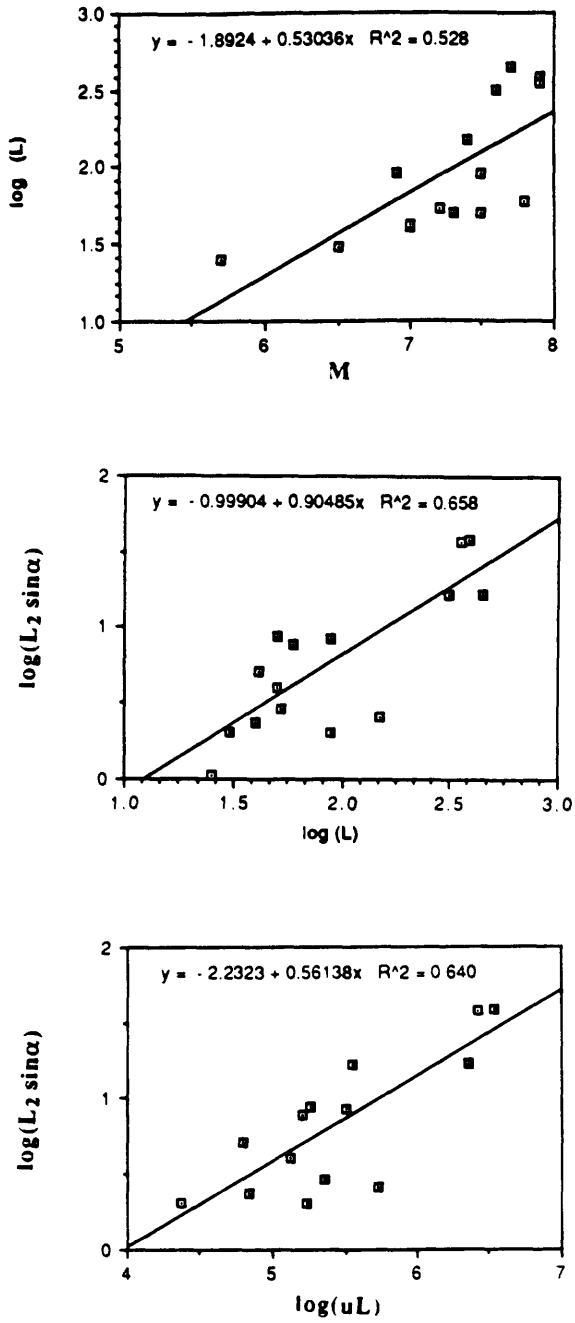

FIGURE 4.--Plots derived from table 1. Regression fits shown for each plot.

COMPARISON WITH LABORATORY RESULTS

In figure 5 we illustrate how an increase in the obliquity of the restraining (L_2) branch could cause a larger earthquake. As θ_2 increases, both normal and shear stresses (components of P_2) increase on the L_2 segment. Increases in shear stress are experimentally correlated with an increase in stress drop (Scholz et al., 1972) and should therefore result in larger moment and magnitude for a given fault size.

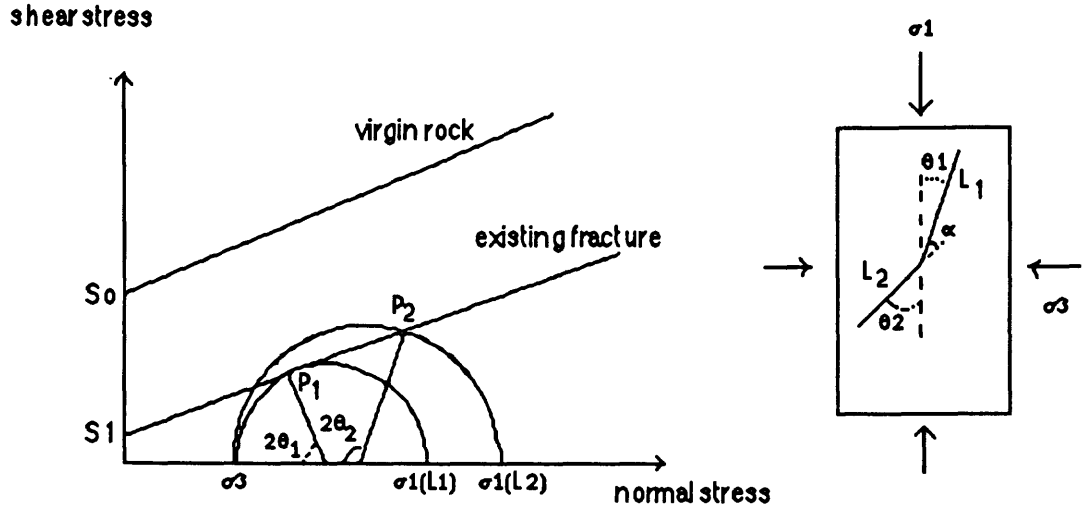

FIGURE 5. --Mohr circle representation of stress state in rock with single restraining bend. So and S1 are cohesive strength of virgin rock and existing fault, respectively. The slope of the failure lines is determined by the coefficient of friction. L_1, L_2 and α are as shown in Figure 1. $\sigma 1$ and $\sigma 3$ are the maximum and minimum compressive stresses, respectively. We increase $\sigma 1$ from $\sigma 1(L_1)$, where rupture can occur on L_1, to $\sigma 1(L_2)$.Rupture can occur simultaneously on L_1 and L_2 (angles $\theta 1$ and $\theta 2$ relative to $\sigma 1$ direction) when points P1 and P2 lie on the "existing fracture" failure line.

The upper limit of about 30°-35° on bend angles agrees well with the results of Nur et al. (1986). Based on mechanical considerations derived from laboratory studies, these authors find that there is a limit on the amount of fault rotation allowed under a stationary stress field before a new set of shear faults must form. Starting from the optimal failure direction relative to the direction of maximum stress (derived from a Mohr circle diagram and failure law), they show that a preexisting fault can only rotate up to an angle of 20°-45° before it is easier to form new faults in the initial optimal direction. The 20°-45° variation depends on the values of the coefficient of friction, cohesive strength and depth of the fault. Although their study focuses on a block rotation process, the result is applicable to our situation. Strike-slip fault rupture may not propagate through a bend if the bend angle is too high.

SLIP DISTRIBUTION AND EPICENTER LOCATION

The notion of a higher stress drop on L_2 relative to L_1 and L_3 suggests that a relatively large amount of slip should be observed on L_2. Some of the earthquakes from table 1 have a well-documented distribution of surface slip. These include the following events: 1857 San Andreas, 1906 San Andreas, 1939 North Anatolian Fault, 1967 North Anatolian Fault, 1970 Tonghai, 1973 Luhuo and 1979 Imperial Valley. In general it can be seen, however, that the maximum horizontal surface slip values are highly scattered in all cases. The maximum horizontal surface slip values do not necessarily occur along the L_2 segment (although they do in the 1939 North Anatolian Fault case). In some of the double bend cases (1857, 1906, 1979 Imperial Valley) the L_2 branch lies at a transition between regions with relatively high and relatively low values of horizontal surface slip.

The epicenter location relative to the surface fault geometry pattern is known for some of the cases in table 1 (see Appendix for references). In all of the restraining single bend cases for which the epicenter is known, it appears that the epicenter was located in the vicinity of the bend. These cases include the following: 1939 North Anatolian Fault, 1973 Luhuo, 1976 Çaldiran and 1976 Tangshan. From waveform modeling it is known that in the last three cases the L_2 segment ruptured before L_1. The epicenter of the 1939 earthquake was relocated, and is known to be near the bend because the relocation accuracy is sufficient in comparison with the very long rupture zone. We do not know, however, which side ruptured first in that case. Epicenters are known in three double bend cases: 1970 Tonghai, 1979 Coyote Lake and 1979 Imperial Valley. In all of these examples the epicenter was located away from L_2. There is some evidence to suggest that the epicenters of the 1857 and 1906 California earthquakes were also located off L_2. (see, e.g., Sieh, 1978b, or Bakun and Lindh, 1985, for an 1857 epicenter near the north end of the rupture zone; and Bolt, 1968, or Ellsworth et al., 1981, for a 1906 epicenter north of the L_2 segment). During the 1979 Imperial Valley earthquake maximum slip occurred between the epicenter and the double bend, both at the surface and at depth.

CONCLUSIONS

The slip distribution and epicenter location for earthquakes associated with restraining single or double bend surface fault geometries is not simple, and it appears that many questions are still unanswered. Two interesting conclusions remain, however. First, it appears from the examples reviewed above that there is an upper limit on the allowable bend angle for these rather common geometric patterns. Second, from Figure 3 it appears that the earthquake magnitude is related to the length and orientation of the restraining fault segment L_2. for both single and double bend earthquakes

We feel that it is important to study fault geometry patterns in order to understand the rupture processes for large earthquakes, because a particular geometric pattern (here restraining bends and double bends) should intuitively be associated with a characteristic earthquake mechanism. We have only looked at large events for practical reasons, and are not able to extrapolate our results to smaller scales at this time, even though the comparison with laboratory results has been a useful exercise.

APPENDIX

(Sources for data in table 1)

(1) January 9, 1857 San Andreas. Fault map from Clark et al. (1984), maximum slip from Sieh (1978a). Ms is not known, although estimated as larger than 8.25 (Sieh, 1978a). The moment magnitude M of Hanks and Kanamori (1979) is only 7.9. Relatively high

topography and compressional features are observed along L_2 (Highway 166 - Tejon Pass region).

(2) April 18, 1906 San Andreas. Fault map from Clark et al. (1984), maximum slip from Lawson et al. (1908). Ms is about 8.25 from Gutenberg and Richter (1954). The moment magnitude of Hanks and Kanamori (1979) is 7.7. Relatively high topography is observed along L_2 (Black Mountain - Loma Prieta region).

(3) December 26, 1939 North Anatolian Fault. Fault map is from Tatar (1978). Slip information is derived from several sources: Pamir and Ketin (1941), Parejas et al.(1942), Ambraseys and Zatopek (1969), Koçyiğit (1988) and most recently field work by A.A. Barka (unpublished data). Few slip measurements were made immediately after this earthquake. We selected L_2 as the distance from the bend to the Susehri releasing stepover west of the bend. The L_2 section of the fault has noticeable restraining features such as high topography, thrust faults and positive flower structures, mostly along its eastern half. The relocated epicenter lies near the bend (see Dewey, 1976).

(4) December 20, 1942 North Anatolian Fault. Fault map from Barka (1981), slip from Blumenthal (1943) and from Ambraseys and Zatopek (1969). Few slip measurements were made immediately after the event, so the extent to which they represent average slip along the fault is unclear. The bend area has relatively high topography.

(5) November 26, 1943 North Anatolian Fault. Fault map from Barka (1981), slip from Blumenthal (1945) and from Ambraseys and Zatopek (1969). Slip values qualified as in (4). There is a high mountainous area along the L_2 segment, near Tosya.

(6) February 1, 1944 North Anatolian Fault. Fault map from Tokay (1973), slip from Ketin (1969) and from Ambraseys and Zatopek (1969). Slip values qualified as in (4). Topography along L_2 is relatively high.

(7) August 17, 1949 North Anatolian Fault. Fault map from unpublished field work by A.A. Barka, with summary map in Barka and Kadinsky-Cade (1988). Slip from Ambraseys (1988, personal communication). Slip values qualified as in (4). The restraining section has relatively high topography.

(8) March 18, 1953 North Anatolian Fault (Western Turkey). Fault map and slip from Ketin and Roesli (1953). The highest topography is located along the L_2 segment.

(9) June 28, 1966 (04:08 UTC) M_L=5.1 Parkfield, California foreshock, 18 minutes before M_L=5.5 mainshock. L_2 is in an elevated region (Middle Mountain). Length L_2 is not well constrained. It is assumed to coincide with the short section northwest of the mainshock epicenter that is believed to have ruptured again during the mainshock. Fault map from Brown et al. (1967). Other information on foreshock from Lindh and Boore (1981). No displacements were measured at the surface that could be associated solely with the foreshock.

(10) July 22, 1967 North Anatolian Fault. Fault map and slip from Ambraseys and Zatopek (1969). Slightly higher topography along L_2, visible from the river drainage pattern.

(11) and (12) January 4, 1970 Tonghai and February 6, 1973 Luhuo, China. Fault map and slip from Zhou et al. (1983). In both cases there seems to be a slight topographic high along L_2 as evidenced by river drainage patterns. Epicenter derived from waveform modeling (Zhou et al., 1983).

(13) November 24, 1976 Çaldiran, Turkey. Fault map and slip from Arpat et al. (1977). The topography is higher on the L_2 side. The epicenter information is taken from waveform modeling (King and Nabelek, 1985).

(14) July 27, 1976 Tangshan, China. Fault map, slip and other information from Nábělek et al. (1987). The bend angle selected here is that of the mapped surface fault trace (14°). However the aftershocks define a larger bend angle (30°), and waveform modeling suggests a bend angle of 40°. The topography in the area is all low (North China Basin), and the structural complexity in the area of the earthquake is very high. Several other faults were reactivated by the sequence. The epicenter is obtained from waveform modeling.

(15) August 6, 1979 Coyote Lake, California. Fault map from Bakun (1980). The fault trace does not follow the aftershock trend. The L_2 segment here extends from the northern shore of Anderson Lake to Coyote Lake. Near the L_2 segment the aftershocks are displaced away from the fault trace (Reasenberg and Ellsworth, 1982). This example shows that matching surface information to fault geometry at depth can be quite tricky, particularly for the smaller strike-slip earthquakes where the matching uncertainty is most critical.

(16) October 15, 1979 Imperial Valley, California. Fault map and slip from Sharp et al. (1982). In this case slip was much larger at depth than at the surface, and maximum values of slip occurred between the L_2 branch and the epicenter (Archuleta, 1984; Reilinger and Larsen, 1986). The Ms magnitude is taken from Kanamori and Allen (1986).

ACKNOWLEDGEMENTS

We would like to thank Prof. N.N. Ambraseys for sending information on two of the earthquakes. This work was supported in part by U.S. Geological Survey contract 14-08-0001-G1151 and NASA grant NAG5-753.

REFERENCES

Ambraseys, N.N., and Melville, C.P., 1987, An analysis of the Eastern Mediterranean earthquake of 20 May 1202, *in* Lee, W.H.K., ed., Proceedings of the Symposium on Historical Seismograms & Earthquakes, IASPEI/UNESCO Working Group on Historical Earthquakes (Tokyo, 1985), San Francisco, p. 390-409.

Ambraseys, N.N., and Barazangi, M., in prep., The 1759 large earthquake in the Bekaa Valley: implications for earthquake hazard assessment in Lebanon and Syria.

Ambraseys, N.N., and Zatopek, A., 1969, The Mudurnu Valley, West Anatolia, Turkey, earthquake of 22 July 1967, Bull. Seismol. Soc. Am., v. 59, p.521-589.

Archuleta, R.J., 1984, A faulting model for the 1979 Imperial Valley earthquake, J. Geophys. Res., v. 89, p. 4559-4585.

Arpat, E., Şaroğlu, F., and Iz, H.B., 1977, The 1976 Çaldiran earthquake, Yeryuvari Insan, v. 2, p. 29-41.

Bakun, W., 1980, Seismic activity on the Calaveras fault in Central California, Bull. Seismol. Soc. Am., v. 70, p. 1181-1198.

Bakun, W., and A. Lindh, 1985, The Parkfield, California, prediction experiment, Earthquake Prediction Research, v. 3, p. 285-304.

Barka, A.A., 1981, Seismo-tectonic aspects of the North Anatolian fault zone, Ph.D. thesis, Univ. of Bristol, England, 335 pp.

Barka, A.A., 1983, Geological criteria for the forecasting of epicentral areas of large magnitude earthquakes (in Turkish), Bull. Geol. Soc. Turkey, v. 26, p. 21-30.

Barka, A.A., and Hancock, P.L., 1982, Relationship between fault geometry and some earthquake epicenters within the North Anatolian fault zone, *in* Isikara, A.M., and Vogel, A., eds., Multidisciplinary Approach to Earthquake Prediction, Friedr. Vieweg & Sohn, Federal Republic of Germany, p. 137-142.

Barka, A.A. and Kadinsky-Cade, K., 1988, Strike-slip fault geometry in Turkey and its influence on earthquake activity, Tectonics, v. 7(3), p.663-684.

Blumenthal, M., 1943, Zur Geologie der Landstrecken der Erdbeben con Ende 1942 in Nord Anatolien und dort ausgeführte Macro Seismische Beobachtungen (Osmancik-Erbaa), Unter Mitwirkung von H.N. Pamir und C.H. Akyol, Maden Tetkik Arama Enst. Yayin, Seri A, (29), 46 pp.

Blumenthal, M., 1945, Ladik earthquake zone, Bull. Miner. Res. Explor. Inst. Turk., v. 1, (33), p. 153-174.

Bolt, B., 1968, The focus of the 1906 California earthquake, Bull. Seismol. Soc. Am., v. 58, p. 457-471.

Brown, R.D., et al., 1967, The Parkfield-Cholame, California, earthquakes of June-August 1966 - Surface geologic effects, water-resources aspects, and preliminary seismic data, U.S. Geol. Surv. Prof. Paper 579, 66 pp.

Clark, M.M., et al., 1984, Preliminary slip-rate table and map of Late-Quaternary faults in California, scale 1:1,000, in U.S. Geol. Surv. Open-File Report 84-106.

Dewey, J.W., 1976, Seismicity of Northern Anatolia, Bull. Seismol. Soc. Am., v. 66, p. 843-868.

Ellsworth, W.L., A.G. Lindh, W.H. Prescott and D.G. Herd, 1981, The 1906 San Francisco earthquake and the seismic cycle, in Simpson, D.W. and P. G. Richards, eds., Earthquake Prediction- An International Review, Maurice Ewing Series 4, American Geophysical Union, Washington, D.C., p. 126-140.

Gutenberg, B., and Richter, C.F., 1954, Seismicity of the earth, 2nd. ed., Princeton Univ. Press, Princeton, N.J..

Hanks, T., and Kanamori, H., 1979, A moment magnitude scale, J. Geophys. Res., v. 84, p. 2348-2350.

Jones, L.M., Wang, B., Xu, S., and Fitch, T., 1982, The foreshock sequence of the February 4, 1975, Haicheng earthquake (M=7.3), J. Geophys. Res., v. 87, p. 4575-4584.

Kanamori, H., and Allen, C., 1986, Earthquake repeat time and average stress drop, *in* Das, S., Boatwright, J., and Scholz, C., eds., Earthquake Source Mechanics, AGU Geophys. Monograph 37, Maurice Ewing Vol. 6, Washington D.C., p. 227-235.

Ketin, I., 1969, Über die Nordanatolische Horizontalverschiebung, Bull. Miner. Res. Explor.Inst. Turk., v. 72, p. 1-28.

Ketin, I., and Roesli, F., 1953, Makroseismische Untersuchungen über das nordwest-anatolische Beben vom 18 März 1953, Eclogae Geol. Helv., v. 46, p. 187-208.

King, G., and Nabelek, J., 1985, Role of fault bends in the initiation and termination of earthquake rupture, Science, v. 228, p. 984-987.

Koçyiğit, A., 1988, Basic geological characteristics and total offset of North Anatolian fault zone in Susehri area, NE Turkey, Middle East Tech. Univ. Journal of Pure and Applied Sciences, v. 23, in press.

Lawson, A.C., et al., 1908, The California earthquake of April 18, 1906, Report of the State Earthquake Investigation Commission, Carnegie Inst. of Washington, Washington, D.C. (2 vols. and atlas), 461 pp.

Lindh, A., and Boore, D., 1981, Control of rupture by fault geometry during the 1966 Parkfield earthquake, Bull. Seismol. Soc. Am., v. 71, p. 95-116.

Nábělek, J., Chen, W-P., and Ye, H., 1987, The Tangshan earthquake sequence and its implications for the evolution of the North China Basin, J. Geophys. Res., v. 92, p. 12,615-12,628.

Nur, A., Ron, H. and Scotti, O., 1986, Fault mechanics and the kinematics of block rotations, Geology,v. 14, p. 746-749.

Pamir, H.N., and Ketin, I., 1941, Das Anatolische Erdbeben ende 1939, Geol. Rundsch., v. 32, p. 279-287.

Parejas, E., I.H. Akyol, and E. Altinli, 1942, Le tremblement de terre d'Erzincan du 27 decembre, 1939, Rev. Fac. Sci. Univ. Istanbul, Ser. B, 6, p. 177-222.

Reasenberg, P. and Ellsworth, W.L., 1982, Aftershocks of the Coyote Lake, California, earthquake of August 6, 1979: a detailed study, J. Geophys. Res., v. 87, p. 10,637-10,655.

Reilinger, R. and Larsen, S., 1986, Vertical crustal deformation associated with the 1979 M=6.6 Imperial Valley, California earthquake: implications for fault behavior, J. Geophys. Res., v. 91, p. 14,044-14,056.

Scholz, C., Molnar, P., and Johnson, T., 1972, Detailed studies of frictional sliding of granite and implications for the earthquake mechanism, J. Geophys. Res., v. 77, p. 6392-6406.

Sharp, R.V., et. al., 1982, Surface faulting in the central Imperial Valley, U. S. Geological Survey Prof. Paper 1254, p. 119-144.

Sieh, K.E., 1978a, Slip along the San Andreas fault associated with the great 1857 earthquake, Bull. Seismol. Soc. Am., v. 68, p. 1421-1448.

Sieh, K.E., 1978b, Central California foreshocks of the great 1857 earthquake, Bull. Seismol. Soc. Am., v. 68, p. 1731-1749.

Slemmons, D.B., 1977, State-of-the-art for assessing earthquake hazards in the United States; Report 6, Fault and earthquake magnitude, U.S. Army Eng. Waterways Experiment Station, Soils and Pavements Lab., S-73-1, 120 pp.

Tatar, Y., 1978, Tectonic investigations on the North Anatolian fault zone between Erzincan and Refahiye (in Turkish), Yerbilimleri, v. 4, p. 201-236.

Tokay, M., 1973, Geological observation on the North Anatolian fault zone between Gerede and Ilgaz, *in* Symposium on the North Anatolian fault zone, Spec. Publ., Mineral Research and Exploration Insttitute of Turkey, Ankara, Turkey.

Thatcher, W., and Lisowski, M., 1987, Long-term seismic potential of the San Andreas fault southeast of San Francisco, California, J. Geophys. Res., v. 92, p. 4771-4784.

Zhou, H-L., Allen, C.R. and Kanamori, H., 1983, Rupture complexity of the 1970 Tonghai and the 1973 Luhuo earthquakes, China, from P-wave inversion and relationship to surface faulting, Bull. Seismol. Soc. Am., v. 73, p. 1585-1597.

IMPLICATIONS OF THE CHARACTERISTICS OF END-POINTS OF HISTORICAL SURFACE FAULT RUPTURES FOR THE NATURE OF FAULT SEGMENTATION

Peter L.K. Knuepfer
Dept. of Geological Sciences
State University of New York
Binghamton, NY 13901

ABSTRACT

Most faults do not rupture their entire length during single earthquakes but break in segments, and the ends of these segments commonly occur at distinct structural, geometric, or geologic features. Similar features also characterize many rupture end-points recognized through detailed mapping of paleoseismic events, producing geologically recognizable segment boundaries. In order to evaluate the features that can form rupture end-points, and thus segment boundaries, we have examined the surface geologic, structural, and geometric characteristics of end points and features ruptured through for more than 75 historical surface fault ruptures. We assume that the surface geometry of a fault is representative of that at seismogenic depths, and we examine end-points irrespective of their behavior as nucleation or termination points for the rupture. Several clear trends emerge. Releasing bends and steps, branch or cross-cutting structures, and changes in the sense of slip along an otherwise-continuous fault most often characterize rupture ends on strike-slip faults. Restraining features, however, are only slightly less likely than releasing features to act as rupture endpoints as to be ruptured through. The patterns on reverse faults are less clear-cut; fault bends are common end-points, but they are less diagnostic. Branching and cross structures also are common characteristics. Discontinuities in surface traces, however, appear to rarely present barriers to propagation of reverse-slip ruptures. Finally, no clear patterns are visible in normal-fault ruptures; different historical events have either terminated at or ruptured through large discontinuities in fault traces and range fronts. The variety of end-point characteristics indicates that rupture ends do not follow any single, simple model of fault mechanics and rupture propagation.

INTRODUCTION

Most long faults do not rupture their entire length during single large earthquakes. Detailed studies of strike-slip, normal, and even reverse faults during the last 20 years have yielded increasing evidence that many if not most faults rupture repeatedly on discrete segments (e.g., Schwartz and Coppersmith, 1984). This behavior is clearly demonstrated by the San Andreas fault, where the large ruptures of 1906 and 1857 are separated by a section of the fault that ruptures through fault creep and smaller-magnitude earthquakes. Allen (1968) first suggested that the San Andreas fault is divided into five segments, each with its own characteristic fault and earthquake activity; subsequent work, such as that of Sieh (1981), has substantiated and refined our understanding of segmented behavior along this fault. That fault segments should be

The present study was conducted to review a larger population of historical ruptures in order to characterize the types of features that occur at the endpoints of a surface rupture, as well as those that occur within the rupture, and to determine which features are important in controlling the segmentation of active faults. One measure of the relative importance is the frequency with which individual features or combinations of features occurs at the ends of a surface rupture compared to the frequency with which they are ruptured through. This study includes strike-slip, normal, and reverse earthquakes for which rupture characteristics can be identified. The analysis is restricted to surface ruptures, despite several problems associated with such a restriction, as discussed below. The data set currently incorporates endpoint data from more than 100 events, but the present analysis considers only about 75 events for which sufficiently detailed maps have allowed the compilation of characteristics of features within ruptures. The results remain preliminary, as additional events may alter some of the patterns discussed herein.

The data set thus obtained provides the most complete compilation yet available of the characteristics not only of the endpoints of historical surface ruptures, but also of the features ruptured through. With this data set, it is possible to recognize how anomalous certain associations of geologic and geometric features are along faults. Not only do the frequencies of some geometric characteristics such as pull-apart basins at rupture endpoints emerge from the study, but also the frequencies with which such features did not occur at an endpoint are becoming clearer. Because persistent segment boundaries on faults are formed only through repeated influence of certain rupture endpoints, analysis of historical ruptures provides direct insight into the range of features that can form segment boundaries, and the likelihood that they have done so.

USE OF SURFACE FAULT STUDIES

When large earthquakes rupture to the surface, the geometric pattern of rupture traces as mapped at the surface commonly mimics the geometry of the rupture at depth as mapped by aftershock distributions. A good example of this correspondence is provided by the 1966 Parkfield rupture (Lindh and Boore, 1981); in contrast, the aftershock geometry of the 1984 Morgan Hill earthquake (which did not rupture the surface) is different from the mapped surface fault pattern (Michael, 1987). Even in events like the 1983 Borah Peak rupture the surface and subsurface patterns correspond, if the geometries of the slip vector and rupture propagation are taken into account (Bruhn, unpublished data). In general, then, surface rupture geometries are good approximations to the geometry of faulting throughout the seismogenic zone. It is important to note that surface displacements can be much less than subsurface displacements inferred from seismic and geodetic data (King, 1986; Thatcher and Bonilla, this volume), even when the rupture geometry and length are nearly identical. On the other hand, surface deformation (brittle slip and inelastic strain) often matches inferred subsurface slip on the fault (e.g. Thatcher and Lisowski, 1987).

This general correspondence between surface and subsurface rupture geometries allows the use of surface rupture patterns in assessing characteristics of rupture endpoints. Although a wealth of seismologic and geodetic data exists for some historical fault ruptures (e.g., Thatcher and Bonilla, this volume),

persistent features in the geologic record is directly implied by such fault-mechanics models as the barrier hypothesis of Aki (1979), which embraces the notion that certain geologic and geometric features of faults tend to act as barriers to the propagation of earthquake energy. Different models of rupture processes and rupture terminations suggest that releasing features, fault branches and intersections, and even restraining features may be critical in starting and stopping ruptures on strike-slip faults (e.g., Sibson, 1985, 1986). Yet, despite intensive study of the characteristics of endpoints of some ruptures, like Parkfield (e.g., Lindh and Boore, 1981) (fig. 1), our knowledge of how earthquakes have stopped (as opposed to how we expect them to) remains incomplete. In other words, we have yet to determine which features are important, and which are not, in controlling segmentation of active faults.

Up to the present time, then, no clear set of physical criteria for recognizing or evaluating segment boundaries has been proposed. Rather, several authors (notably King and Nabelek, 1985; King, 1986; and Sibson, 1985, 1987) have examined the rupture terminations and nucleation points of a few well-studied events, and Aki (this volume) has extended a similar analysis to some 25 earthquakes. These previous studies, however, have not examined a large number of events, have not presented systematic documentation of geologic characteristics associated with surface ruptures (especially the nature of features ruptured through), and thus have not provided a quantitative basis for specifying the characteristics that are most important to fault segmentation.

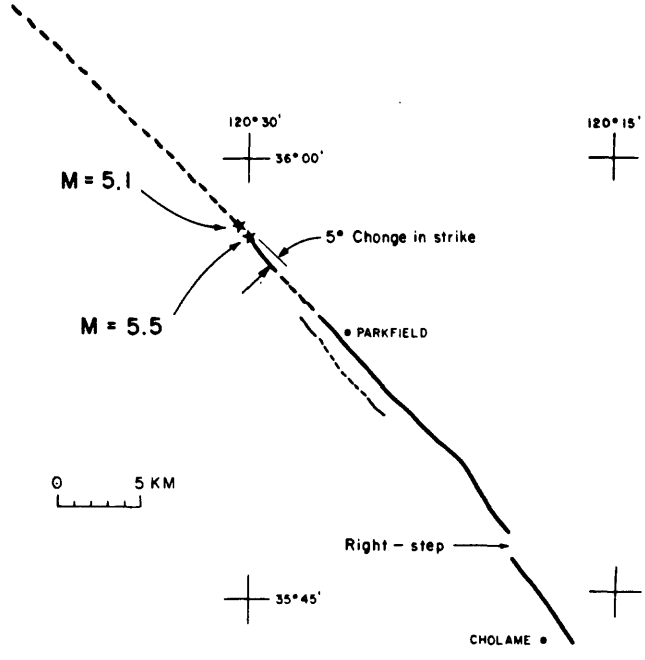

FIGURE 1.--Rupture geometry, 1966 Parkfield earthquake surface displacement. Largest foreshock and mainshock epicenter shown. Surface rupture nucleated at 5° bend in fault and extended past right-step in San Andreas fault, although the coseismic rupture may have ended at the step. From Segall and Pollard, 1980.

relatively few events have been intensively studied due to lack of instrumentation. Aftershock zones clearly define fault geometry for many subduction-zone ruptures, but it is generally very difficult to describe the geometric and/or geologic characteristics of rupture endpoints for such events due to the lack of mapping. Furthermore, only rarely is it possible to identify subsurface fault geometries for onshore events such that endpoint characteristics (let alone ruptured-through characteristics) can be classified. Thus, surface fault rupture patterns provide the most accessible and largest data set that can be compiled to examine the frequency of occurrence of rupture characteristics.

This study concentrates on documented surface ruptures from historical earthquakes, principally those of this century. Surface ruptures that were triggered by earthquakes on nearby faults (such as slip on the San Andreas fault associated with the 1979 Imperial Valley earthquake) are not included in the data set. Several earthquakes with extremely short or highly complex multiple surface ruptures also are excluded due to the difficulties in interpretation of the rupture. Finally, true coseismic rupture is not distinguished from the composite of coseismic and postseismic slip. Reasons for this approach include the lack of distinction presented in the literature for many ruptures mapped immediately after the earthquake, and the fact that most mapping of surface fault displacements occurs days, weeks, months, or even years after the rupture actually occurred. Thus, the northern termination of the 1983 Borah Peak is treated as the die-out in surface displacement about 5 km north of the Willow Creek Hills (fig. 2), even though some workers (e.g. Crone and others, 1987) argue that north end of the coseismic rupture was at the Willow Creek Hills. In the present interpretation, the branching and cross structures that occur at the Willow Creek Hills are features ruptured through by the fault.

THE HISTORICAL RUPTURE DATA SET

Patterns and locations of surface ruptures and their relationships to previously mapped (or previously unmapped) faults are described in the literature in varying levels of detail. Assessment of geologic and geometric characteristics of endpoints and along surface ruptures depends on availability and quality of regional or local geologic and tectonic maps. In many cases, the geometry of the fault rupture can be assessed, but the geologic characteristics of the nucleation point of the rupture are unknown. Thus the level of resolution is highly variable due to the inconsistencies in the availability of data for individual events.

Analysis of historical surface ruptures indicates that features that occur at endpoints and along ruptures can be classified into four groups: geometric, structural, geologic, and behavioral; in addition, in some cases no features can be identified at an endpoint. Geometric properties include fault bends; releasing features (on strike-slip faults) that include double bends, stepovers, and (if the direction of rupture propagation is known) single bends (figs. 3 and 4); similar kinds of restraining features on strike-slip faults (figs. 3 and 4); and gaps, discontinuities, or steps in fault traces (fig. 5). Structural features include branches and intersections with faults and folds (figs. 2, 3, and 4), and the termination of a fault against another cross-cutting structure. Geologic features include margins of Quaternary basins (figs. 3 and

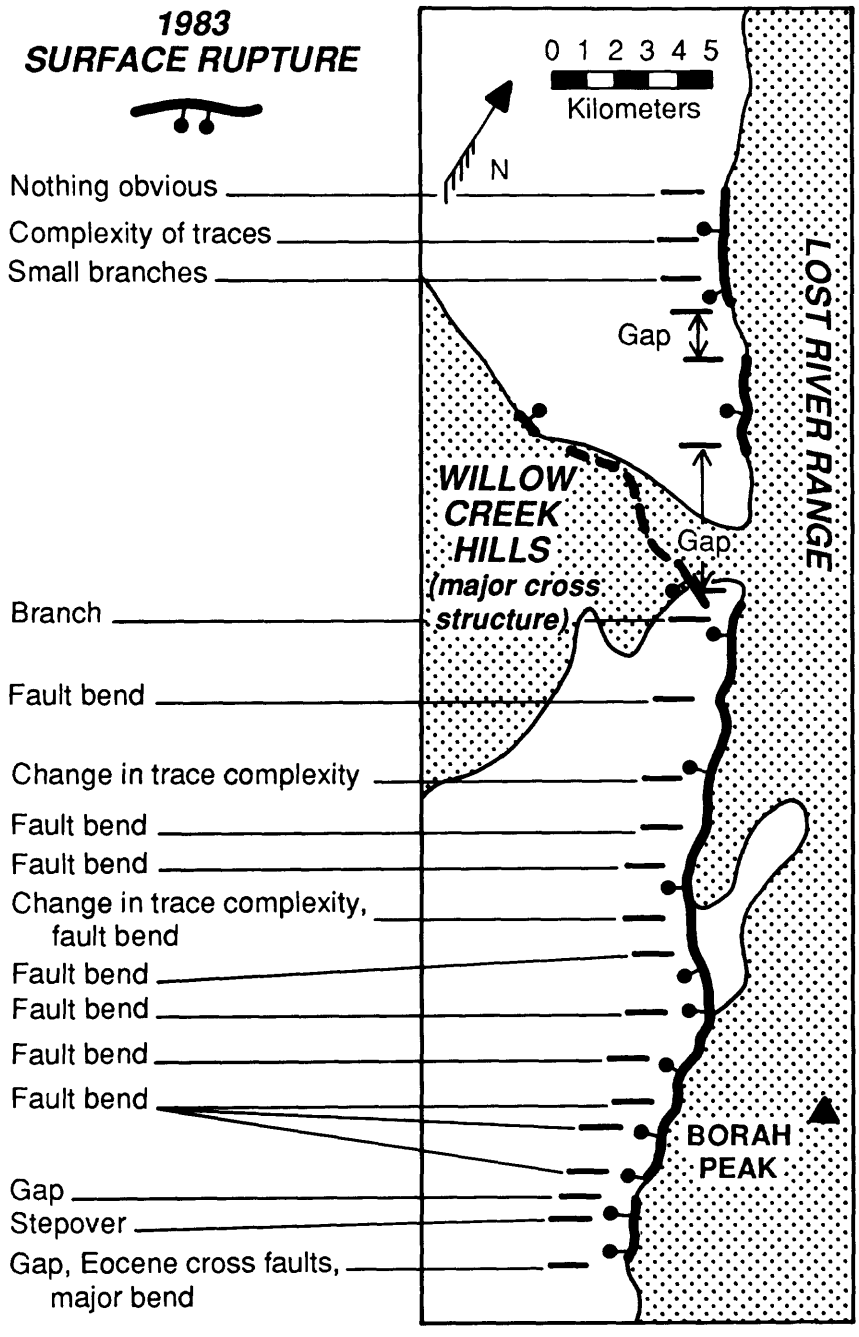

Figure 2.--Rupture details, Borah Peak earthquake, Lost River fault, Idaho. Data interpreted from maps of Crone and others, 1987. Mountain blocks stippled.

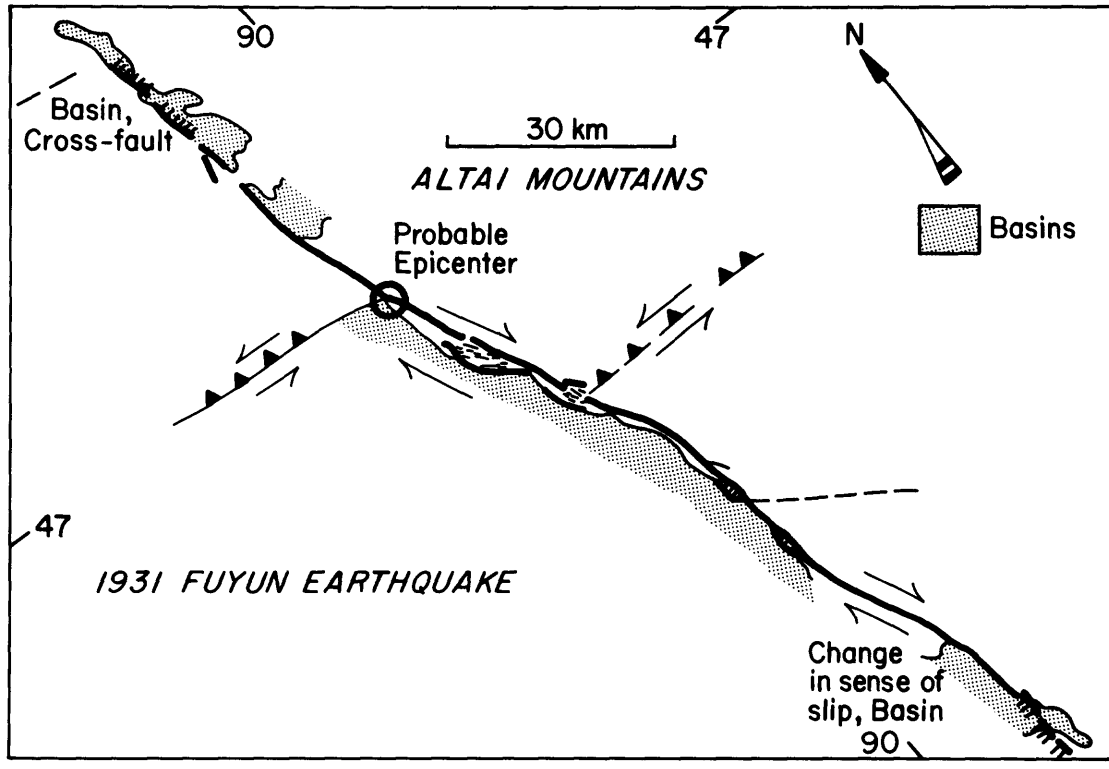

Figure 3.--General rupture (shown by heavy solid line) characteristics for 1931 Fuyun earthquake on Keketuohai-Ertai fault in northwest China. Interpreted from Shi and others, 1984. Basin margins are stippled. Note that rupture propagated past restraining bends and some releasing bends. Event also ruptured past several major cross faults, although it may have terminated at a cross fault at the north end.

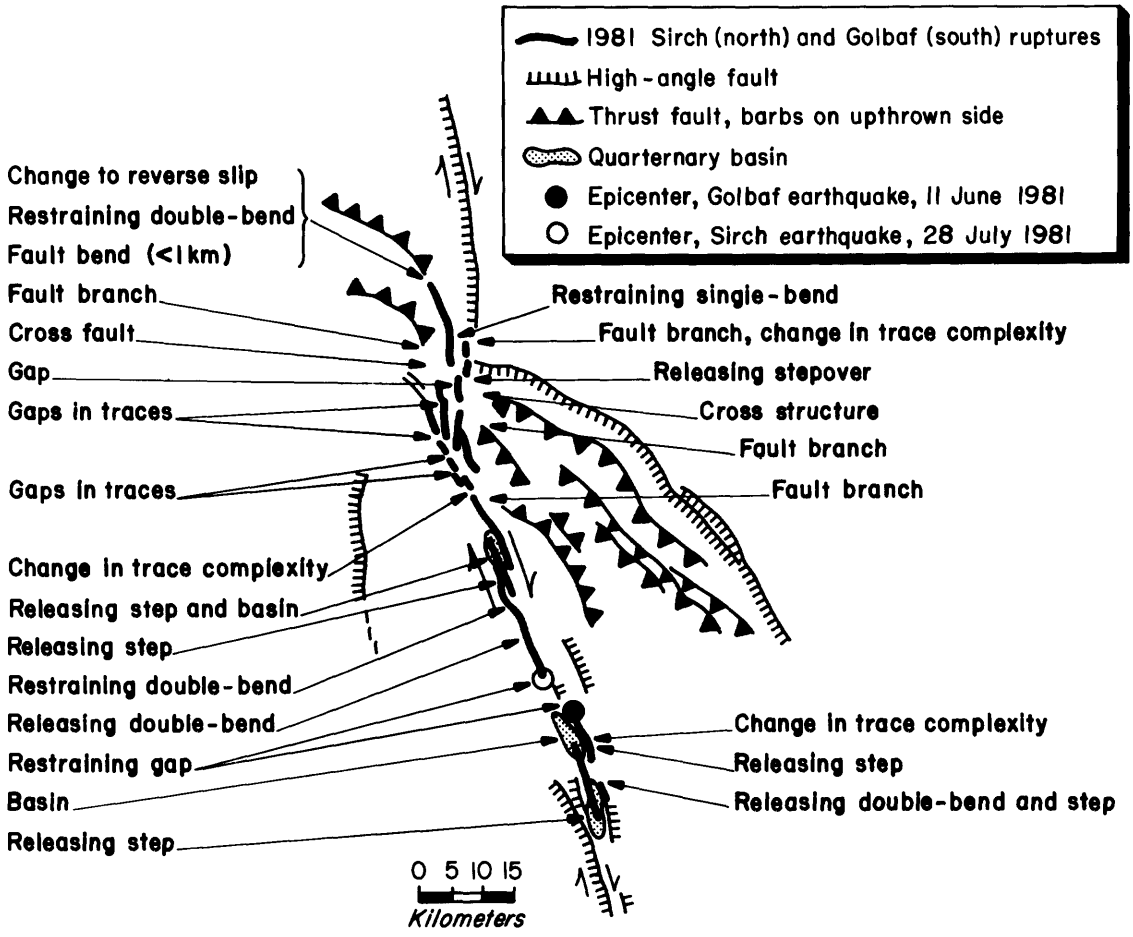

Figure 4.--Rupture details, 1981 Golbaf (southern) and Sirch (northern) ruptures on Gowk fault, Iran. Interpreted from Berberian and others, 1984. Basins are stippled.

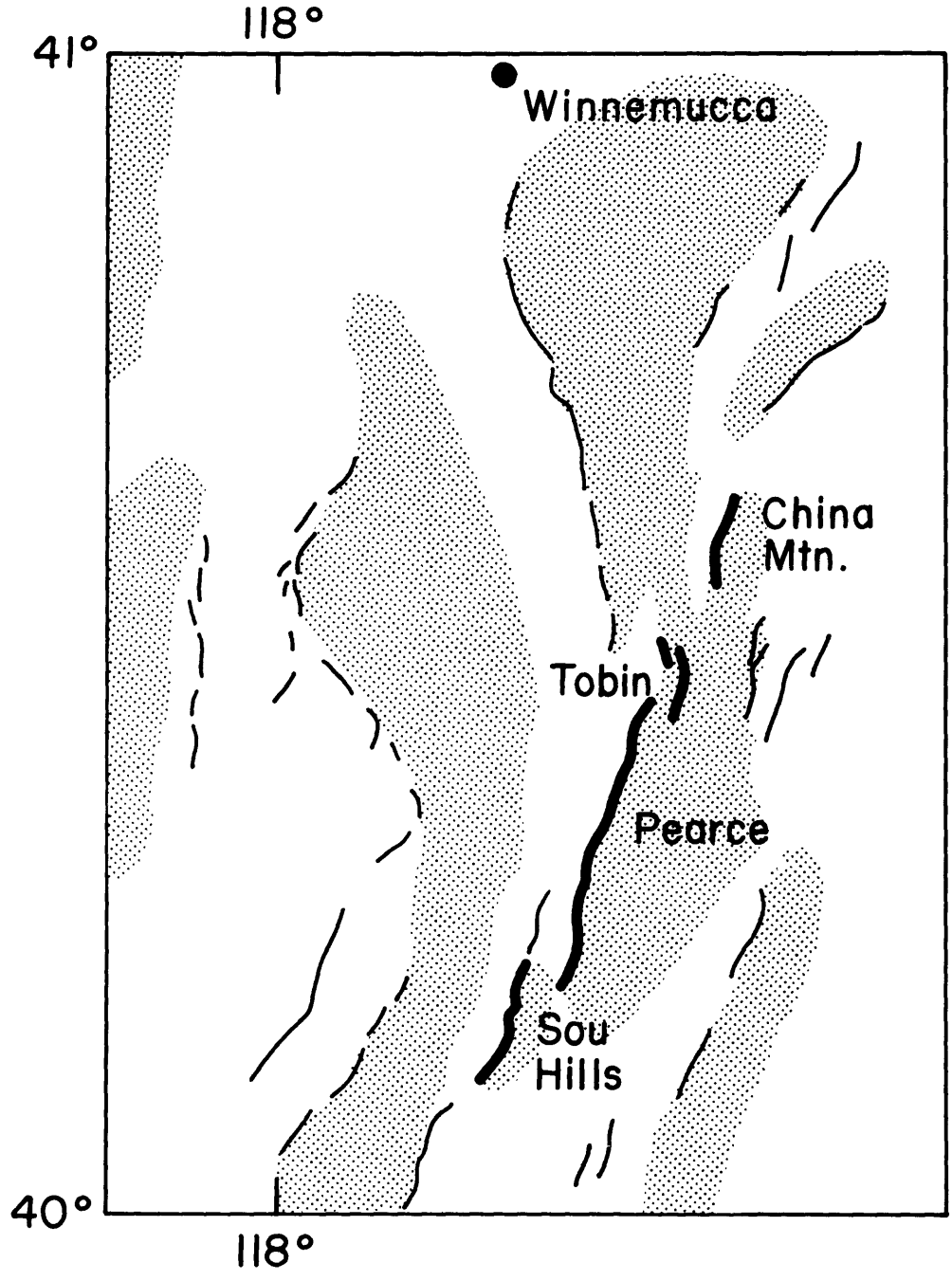

Figure 5.--Generalized surface rupture (shown by heavy solid lines) characteristics, 1915 Pleasant Valley earthquake, Nevada. Compiled from Wallace, 1979, 1984. Mountain blocks stippled. Faults with late Quaternary activity that did not rupture in 1915 shown by narrow solid lines.

5) and changes in bedrock lithology (especially those involving changes in rheologic properties of rock, such as from sandstone to serpentinite). A large variety of behavioral changes are recognized, including changes in complexity of fault traces (fig. 4), a change in the sense of slip across a fault (fig. 4), in the mechanics of slip from creeping to locked, in the recency of prior rupture on a segment (elapsed time), in the slip rate, in the displacement function of a previous fault rupture, and in the die-out of fault traces (beyond which no active faulting is mapped). The nature of each feature and general guidelines for identification of these features are given in table 1.

The reliability of the data has been subjectively evaluated by assigning a level of confidence to the interpretation for each earthquake. The level of confidence, high (H), medium (M), or low (L), indicates a general measure of the quality of data used in the identification of the endpoints and ruptured-through features. The level of confidence also depends in part on scale of the maps that were used in the analysis. In general, the high-confidence rating indicates that detailed maps of scale 1:250,000 or larger are available for surface ruptures longer than 50 km, or 1:50,000 or larger for surface ruptures shorter than 10 km; low confidence implies that only maps of scale 1:1,000,000 or smaller were available.

Table 2 presents a listing of 74 ruptures from 69 different earthquakes for which data have been compiled; the data on features at endpoints and along ruptures are compiled in the Appendix. Two distinct faults, generally conjugates, ruptured in five of the earthquakes. Note that the conjugate left-slip faults that ruptured in the Superstition Hills events of 1987 are not included on table 2 and in the Appendix because of the complexity of the rupture pattern. Several examples of the kinds of data utilized in compilation of this data set are displayed on figures 1 through 5.

In each case, the rupture length has been redetermined from measurement of ruptures on published maps. In several cases, these rupture lengths differ from those reported in the literature (even the sources from which maps were obtained) and in compilations such as those of Bonilla and Buchanan (1971), Slemmons (1977), and Bonilla and others (1984). The most common difference is that many published reports of surface ruptures list the length of the portions of the fault that actually broke the surface, others list the total length from one end of the rupture to the other (including gaps), and still others list the total length of ruptured fault traces (including overlapping rupture traces). Thus there is rarely consistency in the reported rupture length. The length employed in this study is the total map length from one end of the mapped fault rupture to the other, including any gaps, but not including duplication due to overlapping ruptures. This use of rupture length facilitates reporting the location of various ruptured-through features along a fault. Furthermore, the use of an end-to-end rupture length is consistent with the kind of rupture length normally reported in seismic or geodetic studies, in which gaps in apparent rupture generally are included in the total rupture length or area.

TABLE 1.--Characteristic Features of Surface Ruptures

	FEATURE LOCATION. All features are located by distance from either the west or north end of the surface fault rupture.
	END POINT LENGTH. Length of portion of the fault over which endpoint features are described (in km). Estimate of how accurately actual endpoint of surface rupture can be identified. **END_0** refers to west or north end of rupture; **END_X** refers to east or south end.
RLDB	RELEASING DOUBLE BEND. Applicable only to strike-slip faults. Double-bends or stepovers that act as dilational jogs (Sibson, 1985) on faults, producing local extension and pull-apart basins. Right step for right-lateral faults; left step for left-lateral faults. Data include location of midpoint of the bend or stepover, total length (range) of feature, and its width.
RSDB	RESTRAINING DOUBLE BEND. Applicable to strike-slip faults. Double-bends or stepovers that act as anti-dilational jogs on faults, producing localized compression. Left step for right-lateral faults; right step for left-lateral faults. Data as for releasing double bends.
RLSB RSSB	SINGLE BENDS. If direction of rupture propagation is known, a single fault bend on a strike-slip fault can be classified as releasing (RLSB) or restraining (RSSB) dependent on the rupture geometry. Data include location of the inflection point of the bend and the angle of the bend.
STP	STEPOVERS. These are discontinuities in faults connected by an en echelon step in map view. These include steps on reverse and normal faults, which cannot be classified as releasing or restraining unless the 3-D geometry of the fault is known. Also, when insufficient information is available on strike-slip fault geometry to classify nature of a step, the class of stepover is assigned. Data include location of the midpoint of the step, its total length (range), and the width of the step.
FB	FAULT BENDS. Bends or changes in strike on normal or reverse faults cannot be readily placed in a releasing-restraining framework unless 3-D fault geometry is known. Many single bends on strike-slip faults cannot readily be classified, especially when the nucleation point of the rupture is unknown or uncertain. These generic fault bends are described in the same manner as the single bends noted above.
GAP	GAPS AND DISCONTINUITIES. This is a non-overlapping along-strike discontinuity in surface traces along a fault (as opposed to a stepover). Data include the range of the location of the gap from beginning to end.
FTBR FDBR	FAULT AND FOLD BRANCHES. This is a structure, with documented Quaternary activity (if data available), that intersects the rupture trace at an angle of 30° or less. Data include the locations where faults (FTBR) or folds (FDBR) intersect the rupture trace and the branch angle.

TABLE 1 (Continued)

CFT CFD	CROSS FAULTS AND FOLDS. Same as branches, except that these structures intersect the main fault at angles greater than 30°. Data recorded as for branches.
RT FDO	FAULT TERMINATIONS. These are locations beyond which no surface fault traces are mapped. Two kinds of fault terminations are possible: rupture terminates but the fault trace continues (RT), and where the fault the fault appears to die out (FDO).
QB	BASIN BOUNDARIES. Note locations of Quaternary basins. Mark locations where the fault enters or exits from a basin. Note that on strike-slip faults this should be highly correlated with releasing features.
CBT	CHANGES IN BASEMENT TERRANES. If geologic or tectonic maps are available, note the locations where rock types change on a regional basis. This category does not emphasize formation contacts, only changes in rheologic properties, such as from granitics to carbonates, clastics to metamorphics, greenstones and serpentinites to shales, etc. Data include both location and type of change.
CTC	CHANGE IN TRACE COMPLEXITY. Record locations where the rupture changes from a relatively simple single surface trace at the map scale to multiple traces or anastomosing traces, and vice versa.
CSS	CHANGE IN SENSE OF SLIP. Record locations where the primary sense of slip along a fault changes, for example from right-lateral strike-slip to reverse. This category does not apply to localized changes associated with portions of a double bend on a strike-slip fault, but if does apply to changes in sense of slip that result from a single bend. These changes should not be not scaled to the rupture end length.
FC	FAULT CREEP. This category refers to locations where behavior of the surface fault changes to creeping from locked or vice versa. This is relevant mostly for the San Andreas, Hayward, and Calaveras faults in California. Note that this does not include slip on a fault triggered by an earthquake rupture on another fault.
CET	CHANGE IN ELAPSED TIME. For those faults for which paleoseismic data are available, record locations at which prehistoric ruptures terminated, i.e. locations where the time elapsed since the last rupture changes.
CSR	CHANGE IN SLIP RATE. Record locations at which changes in slip rate across a fault are reported.

TABLE 2: Listing of Studied Earthquakes

EQN	LOCATION	FAULT	EQDATE	TYPE	LENGTH	END O	END X	CONF	REFERENCES	COMMENTS
4	USA, Calif	S Andreas 1857	01/09/57	S	297.0	1.0	20.0	M	CA1,11-13,61,65	Uncertain end locations
7	USA, Calif	Owens Valley	03/26/72	S	108.0	1.0	1.0	M	CA1,21-22,58-60,G1-2	
8	Mexico	Pitaycachi	05/03/87	N	75.0	1.0	5.0	M	M1-2	Longest normal flt rupt
10	Japan	Nobi-Neodani	10/28/91	S	89.5	1.0	1.0	M	J1,6,17,19-20	
13	Japan	Rikuu-Senya	08/31/96	R	40.0	0.5	0.5	H	J1-2, G4	13a - Rikuu
13	Japan	Rikuu-Kawafune	08/31/96	R	7.0	0.5	0.5	M	J1-2	13b - Kawafune
14	Turkey	Aydin-Nazili	01/01/99	N	55.0	5.0	5.0	L	T6	Confidence: very low
17	USA, Calif	San Andreas 1906	04/18/06	S	432.0	1.0	1.0	H	CA1-5,55-57, G1,3	
19	USA, Nevada	Pleasant Valley	10/02/15	N	51.0	2.0	2.0	H	N3,12, G3-4	
20	China	Haiyuan-Kansu	12/16/20	S	200.0	10.0	10.0	M	CH8-11,16	Confid L-ends, med-mid
21	China	Xianshuihe-Qiaj.	03/24/23	S	66.0	5.0	8.0	L	CH1,3,23-24	Confid: very low
23	Japan	Yamada	03/07/27	SR	8.5	1.0	1.0	H	J1,4	One of 2 conj flts, 23b
23	Japan	Gomura	03/07/27	SR	13.9	1.0	1.0	H	J1,4	One of two conj. flts 23a
26	Kenya	Rift zone	01/06/28	N	32.0	1.0	3.0	L	K1-2, G1,3,6	Confidence: L-M
36	China	Ertai-Fuyun	08/10/31	S	171.0	1.0	1.0	M	CH4	
38	China	Changma	12/25/32	R	119.0	5.0	5.0	L	CH9,16,37, G1	Lateral component unclear
44	Taiwan	Tuntzuchio	04/21/35	S	17.3	1.0	1.0	M	CH14-15	44a Bedding-plane thrust?
44	Taiwan	Chihhu	04/21/35	SR	14.0	1.0	1.0	M	CH14-15	44b
52	Turkey	N Anat Erzincan	12/26/39	S	360.0	20.0	20.0	L	T1-2,4,8,10-11,14	Largest of Anatolian EQs
53	USA, Calif	Imperial 1940	05/19/40	S	58.0	1.0	1.0	H	CA17-18,51	
59	Turkey	N Anat Erbaa	12/20/42	S	50.0	10.0	10.0	M	T1-2,8,10-11,14	
61	Japan	Tottori-Yosioka	09/10/43	S	7.6	1.0	1.0	M	J1,5	61b Two branch faults
61	Japan	Tottori-Sikano	09/10/43	S	4.7	1.0	1.0	M	J1,5-6, G4	61a Two branch faults
62	Turkey	N Anat Kastamanu	11/26/43	S	280.0	10.0	10.0	M	T1-2,4,8,10-11	T-4 map
63	Turkey	N Anat Bolu	02/01/44	S	180.0	15.0	15.0	M	T1-2,8,10-11	
68	Japan	Fukozu-Mikawa	01/13/45	R	21.5	1.0	1.0	M	J1,8-9	Unusual Y-shaped rupture
111	USA, Calif	Fort Sage Mtns	12/14/50	N	9.2	0.8	0.5	H	CA1,61-62	
112	Taiwan	Coast R Hualien	10/22/51	S	5.9	1.0	1.0	M	CH14-15,17-19	
113	Taiwan	Coastal R Yuli	11/25/51	S	40.0	1.0	1.0	L	CH14-15,17-19	Poorly documented
118	USA, Calif	White Wolf	07/21/52	RS	52.0	1.0	1.0	M	CA1,32-35	Large gap in alluvium
150	Turkey	N Anat Yenice	03/18/53	S	60.0	2.0	2.0	M	T1-2,8,11	
158	USA, Nevada	Rainbow Mtn S	07/06/54	N	19.0	2.0	1.5	M	N2,4,9-10	
159	USA, Nevada	Rainbow Mtn N	08/24/54	N	28.0	5.0	1.0	M	N2,4,9-10	
161	USA, Nevada	Dixie Valley	12/16/54	N	61.0	2.0	2.0	H	N1-2,4,11, G4	
162	USA, Nevada	Fairview Peak	12/16/54	N	62.0	6.0	6.0	H	N1-2,4,11	
171	Mexico	San Miguel	02/09/56	S	22.0	0.2	0.5	H	M3-6	
180	Turkey	N Anat Abant	05/26/57	S	47.0	5.0	5.0	L	T1,8,10-11	
184	Mongolia	Gobi-Altai Bogdo	12/04/57	SR	245.0	3.0	10.0	H	CH13,16,34, G1,3	
199	USA, Montana	Hebgen Lake	08/18/59	N	25.0	2.5	2.5	H	MO1-3, G1,3	
207	Iran	Ipak	09/19/62	SR	99.0	2.0	5.0	M	I8-10,14-15	LL slip, 2ndary on NW flt
230	USA,Calif	S Andreas Parkfd	06/28/66	S	38.5	1.0	1.0	H	CA1,6-10	N end 3-5 km, S end 38.5?
234	Turkey	N Anat Varto	08/19/66	S	20.0	1.0	1.0	M	T1,8,10-12,15	Map T-15
242	Turkey	N Anat Mudurnu	07/22/67	S	83.0	5.0	5.0	M	T7-8,10-11	Map T-7
244	China	Xianshuihe Zhuwo	08/30/67	S	14.1	2.0	2.0	L	CH1,3,23-24	
247	Japan	Izu-Osh Inatori	01/14/78	SR	2.7	0.5	0.5	L	J1,14-15,18	Also offshore flt 247b
247	Japan	Izu-Osh Sengenya	01/14/78	S	3.2	0.5	0.5	M	J1,14-15	247a Inatori
252	USA, Calif	Coyote Cr San J	04/09/68	S	31.0	0.5	0.5	H	CA14-16,52	
277	Iran	Dasht-e-Bayaz	08/31/68	S	80.0	0.5	5.0	H	I1-3,9-10	
281	Turkey	Alasehir Valley	03/28/69	N	30.0	5.0	5.0	L	T5-6	Confidence: very low
289	Peru	Huaytapallana	10/01/69	SR	18.0	0.5	1.0	M	P1-4	
290	China	Qujiang/Tonghai	01/04/70	S	44.0	1.0	1.0	M	CH12,16	
292	Turkey	Gediz	03/28/70	NS	42.0	0.5	0.5	H	T5,7,16	Map T-16 - Complex flt NW
300	USA, Calif	San Fernando	02/09/71	R	16.0	1.0	1.0	H	CA1,24-27	
315	China	Xianshuihe Luhuo	02/06/73	S	89.0	1.0	1.0	M	CH1-3,23-24	
323	Japan	Izu-Oki Irozaki	05/08/74	SR	6.1	1.0	1.0	L	J1,7,10	Offshore faulting
337	USA, Calif	Galway Lake	05/31/75	S	8.0	0.5	0.5	H	CA39-40	
342	USA, Calif	Cleveland Hill	08/01/75	N	4.8	0.5	0.5	H	CA41-44,52	
353	Turkey	Caldiran	11/24/76	S	55.0	1.0	1.0	M	T3-4,10-11	50 km on map? T-10
358	Iran	Kuhbanan-Zarand	12/19/77	S	19.0	0.1	0.1	M	I9,11,13	Confidence: M-H
363	Iran	Tabas-e-Golshan	09/16/78	R	95.0	0.5	0.5	M	I5-6,9,11	Multi-trace rupture
368	USA, Calif	Imperial 1979	10/15/79	S	30.5	0.5	0.5	H	CA17-20	Partial rerupture of 1940
369	Iran	Abiz-Ghaenat	11/14/79	S	30.0	0.5	2.0	M	I7,9,11-12	Conjugate flt, conf M-L
370	Iran	Dasht-Ghaenat	11/27/79	S	57.5	2.0	5.0	M	I7,9,11-12	Reported RL 60 km, E/1968
372	Algeria	El Asnam	10/10/80	R	26.5	8.2	0.2	H	A1-3, G1	
373	China	Xianshuihe Daofu	01/24/81	S	49.0	1.0	1.0	L	CH1,3,23-24	
374	Iran	Gowk-Golbaf	06/11/81	S	17.0	0.2	0.5	H	I4,10-11	
375	Iran	Gowk-Sirch	07/28/81	S	66.0	2.0	0.5	H	I4,10-11	
377	USA, Idaho	Lost River (BP)	10/28/83	N	34.0	2.0	2.0	H	ID1-4	Assumes rupt. N/Willow Cr
381	USA, Calif	Homestead Valley	03/15/79	S	3.9	0.5	0.5	H	CA36-39	
384	China	Zheduotang	04/14/55	S	27.0	1.0	1.0	M	CH1,23-25	Brench of Xianshuihe flt
389	Turkey	East Anatolian	05/22/71	S	39.0	1.0	1.0	M	T4,9	Bingol-complex rep-RL=15
390	USA, Calif	White Mtns.	07/21/86	S	18.0	1.0	1.8	H	CA1,23,28-31	Chalfant Valley EQ
500	Iran	Quchan-Bakharden	01/05/29	SN	57.0	5.0	5.0	L	I8,16, G1,3	Reported RL = 60-70 km
503	USA, Calif	Superstition H.	11/24/87	S	23.1	0.1	0.1	H	CA61,63-64	Rupture on main fault

EXPLANATION, TABLE 2

EQN — Earthquake number. These events are part of a larger data set that includes rupture length and endpoint data; thus, not all earthquake numbers are listed.

TYPE — Dominant (and secondary) sense of slip. S = strike-slip; N = normal-slip; R = reverse.

LENGTH — Rupture length computed from maps of surface rupture. See text for discussion.

END 0 — Endpoint length (km) of north or west endpoint. The north or west endpoint also is the starting point for identifying feature location in The Appendix.

END X — Endpoint length (km) of east or south endpoint.

CONF — Confidence level in overall data. H = high, M = medium, L = low. See text for discussion.

REFERENCES are keyed by letter and number to reference list.

G1: Bonilla and others, 1984; G2: Slemmons, 1977; G3: Lienkaemper, 1984; G4: Wesnousky, 1986; G5: Ambraseys and Tchalenko, 1968; G6: Bonilla, 1967; G7: Bonilla and Buchanan, 1970.

CA1: Jennings, 1975; CA2: Lawson and others, 1908; CA3: Bolt, 1968; CA4: Jennings, 1977; CA5: Ellsworth and others, 1981; CA6: Archuleta and Day, 1980; CA7: Brown, 1970; CA8: Brown and Vedder, 1967; CA9: Lienkaemper and Brown, 1985; CA10: Lindh and Boore, 1981; CA11: Sieh, 1978; CA12: Weldon and Sieh, 1985; CA13: Weldon and Matti, 1986; CA14: Clark, 1972; CA15: Sharp, 1972; CA16: Wyss and Hanks, 1972; CA17: Johnson and Hill, 1982; CA18: Sharp, 1982b; CA19: Sharp and others, 1982; CA20: Kanamori and Regan, 1982; CA21: Beanland and Clark, 1987; CA22: Carver, 1969; CA23: Kahle and others, 1986; CA24: Sharp, 1975; CA25: Bull, 1978; CA26: Crook and others, 1979; CA27: Oakeshott, 1975; CA28: dePolo and Ramelli, 1987; CA29: Lienkaemper and others, 1987; CA30: Cockerham and Corbett, 1987; CA31: Gross and Savage, 1987; CA32: Buwalda and St. Amand, 1955; CA33: Stein and Thatcher, 1981; CA34: Hanks and others, 1975; CA35: Dunbar and others, 1980; CA36: Hill and others, 1980; CA37: Hutton and others, 1980; CA38: Stein and Lisowski, 1983; CA39: Dibblee, 1967; CA40: Hill and Beeby, 1977; CA41: Clark and others, 1976; CA42: Lahr and others, 1976; CA43: Buchholz, 1975; CA44: Savage and others, 1977; CA51: Anderson and Bodin, 1987; CA52: Hamilton, 1972; CA53: Akers and McQuilkin, 1975; CA54: Hart and Rapp, 1975; CA55: Pampeyan, 1979; CA56: Buchanan-Banks and others, 1978; CA57: Herd and Helley, 1977; CA58: Streitz and Stinson, 1974; CA59: Matthews and Burnett, 1965; CA60: Strand, 1967; CA61: Jennings, 1985; CA62: Gianella, 1957; CA63: Kahle and others, 1988; CA64: Sharp, 1982a; CA65: Davis and Duebendorfer, 1987.

N1: Slemmons, 1957; N2: Doser, 1986; N3: Wallace, 1984; N4: Bell, 1984a; N9: Slemmons, 1956; N10: Tocher, 1956; N11: Bell, 1984b; N12: Wallace, 1979.

EXPLANATION, TABLE 2 (Cont.)

ID1: Crone and others, 1987; ID2: Smith and others, 1985; ID3: Stein and Barrientos, 1985; ID4: Scott and others, 1985.MO1: Myers and Hamilton, 1964; MO2: Doser, 1985; MO3: Barrientos and others, 1987.

M1: Bull and Pearthree, 1988; M2: Natali and Sbar, 1982; M3: Shor and Roberts, 1958; M4: Gastil and others, 1975; M5: Gastil and others, 1979; M6: Brune and others, 1979.

J1: Research Group for Active Faults, 1980; J2: Matsuda and others, 1980; J3: Matsuda and others, 1976; J4: Yamasaki and Tada, 1928; J5: Tsuya, 1944; J6: Kanamori and Anderson, 1975; J7: Kinugasa, 1976; J8: Iida and Sakabe, 1972; J9: Tsuya, 1946; J10: Kakimi and Kinugasa, 1976; J11: Otuka, 1933; J12: Kuno, 1936; J13: Sugimura and Matsuda, 1965; J14: Murai and others, 1978; J15: Shimazaki and Somerville, 1979; J17: Matsuda, 1974; J18: Aki, 1987; J19: Research Group for Active Faults of Japan, 1980; J20: Tsukuda, 1987.

CH1: Tang and others, 1984; CH2: Tang and others, 1976; CH3: Zhou and others, 1983; CH4: Shi and others, 1984; CH8: Chen and Molnar, 1977; CH9: Tapponnier and Molnar, 1977; CH10: Zhang and others, 1987; CH11: Deng and others, 1984; CH12: Zhang and Liu, 1978; CH13: Florensov and Solonenko, 1963; CH14: Bonilla, 1975; CH15: Bonilla, 1977; CH16: Molnar and Deng, 1984; CH17: Biq, 1981; CH18: Hsu, 1962; CH19: Biq, 1965; CH23: Qian, 1986; CH24: Zhou and others, 1983; CH25: C. Allen, oral commun., 1987; CH34: Tapponnier and Molnar, 1979; CH37: Shih and others, 1978.

T1: Ambraseys and Zatopek, 1968; T2: Ketin and Roesli, 1953; T3: Toksoz and others, 1978a; T4: Dewey and others, 1986; T5: Eyidogan and Jackson, 1985; T6: Allen, 1975; T7: Ambraseys and Zatopek, 1969; T8: Geological maps of Turkey, scale 1:500,000; T9: Seymen and Aydin, 1972; T10: Toksoz and others, 1978b; T11: Barka and Kadinsky-Cade, 1988; T12: Barka and others, submitted; T13: Wallace, 1968; T14: Ambraseys, 1970; T15: Kato and Barka, 1985; T16: Tasdemiroglu, 1971.

I1: Brunol, 1968; I2: Tchalenko and Ambraseys, 1970; I3: Crampin, 1969; I4: Berberian and others, 1984; I5: Berberian, 1979; I6: Stocklin and others, 1965; I7: Haghipour and Amidi, 1980; I8: Berberian, 1976; I9: Berberian, 1981; I10: Nowroozi, 1985; I11: Nowroozi and Mohajer-Ashjai, 1985; I12: Niazi and Kanamori, 1981; I13: Berberian and others, 1979; I14: Ambraseys, 1963; I15: Ambraseys, 1965; I16: Tchalenko, 1975.

A1: Meghraoui and others, 1986; A2: Yielding, 1985; A3: Yielding and others, 1981.

P1: Blanc and others, 1983; P2: Deza, 1971; P3: Philip and Megard, 1977; P4: Suarez and others, 1983.

K1: McCall, 1967; K2: Willis, 1936.

COMMENTS Letters appended to the earthquake number identify multiple surface ruptures associated with a single earthquake.

DISCUSSION OF THE RUPTURE DATA

The primary purpose of this paper is to present a preliminary listing of characteristic features of the historical surface ruptures; compilation of the data base is an ongoing project. However, several trends (and lack of trends) emerge from the data set, and several of these trends have important implications for models of fault segmentation.

Releasing bends and steps, restraining bends, branch or cross-cutting structures, and changes in the sense of slip along an otherwise-continuous fault are the most common characteristics of rupture endpoints on strike-slip faults (table 3). The frequency with which both restraining features and releasing features occur as rupture endpoints compared to features ruptured through during an earthquake is very similar, although restraining features are slightly less likely (diagnostic) to be endpoints. This observation contrasts with the models of Sibson (1985) and King and Nabelek (1985) that releasing (or dilational) features, not restraining (or antidilational) features, control the ends of strike-slip fault ruptures. Thus the data indicate that not all strike-slip ruptures behave according to simple geometric or mechanical fault models.

A related consideration is the size of releasing and restraining double bends and stepovers. As shown in figure 6a, there is a slightly greater tendency for narrow (less than 2 km wide) releasing double-bends or steps to be ruptured through than to be endpoints. Perhaps more importantly, the only step or double-bend wider than 10 km in the historical ruptures data set acted as an endpoint. In other words, large (wide) double-bends and steps are more likely to be rupture endpoints than small steps and double-bends (consistent, this time, with King's (1986) and Sibson's (1985) models). There is a similar, indeed even more dramatic, result for the restraining features (fig. 6b). No ruptures in the data set have propagated through any restraining double-bends or steps wider than about 5 km, although several events have endpoints at wider basins. If this result is not simply an artifact of the data base, it implies that large (wide) restraining features are diagnostic segment boundaries on strike-slip faults.

One other feature appears to be diagnostic for strike-slip faults. In nine cases, historical rupture on a strike-slip fault appears to end where the primary sense of slip changes from strike-slip to dip-slip. The Sirch rupture on the Gowk fault in Iran (fig. 4) terminates where the fault bends and becomes a reverse fault (Berberian and others, 1984). Again, if the result is truly reflective of fault behavior and not an artifact of how changes in slip sense was defined in this study, then the change from strike-slip to dip-slip displacement on a fault is a diagnostic segment boundary. This change in slip sense must be a long-term behavior, as the nine cases all involve changes in long-term displacement across the faults in question.

The patterns on reverse faults are less clear-cut, perhaps because of the much smaller data set utilized. Fault bends are the most common end-points, but they are also ruptured through with a much higher frequency than comparable features on strike-slip faults. Thus, bends are much less diagnostic than along strike-slip faults. This is not surprising, as along-strike bends should have little influence on rupture propagation for a pure dip-slip displacement.

TABLE 3.—Summary of Features Identified Along Fault Ruptures and Endpoint Frequencies

FEATURE TYPE	STRIKE-SLIP			REVERSE			NORMAL			ALL EVENTS		
	Ruptured Through	At End-Point	Endpoint Frequency %	Ruptured Through	At End-Point	Endpoint Frequency %	Ruptured Through	At End-Point	Endpoint Frequency %	Ruptured Through	At End-Point	Endpoint Frequency %
RLSB	37	2	5.1	0	0	0.0	0	0	0.0	37	2	5.1
RLDB	117	42	26.4	0	0	0.0	0	0	0.0	117	42	26.4
RSSB	25	5	16.7	0	0	0.0	0	0	0.0	25	5	16.7
RSDB	105	31	22.8	0	0	0.0	0	0	0.0	105	31	22.8
FB	7	6	46.2	35	3	7.9	81	14	14.7	123	23	16.9
STP	9	2	18.2	27	1	3.7	29	4	12.1	65	7	9.7
GAP	35	3	7.9	15	1	6.7	19	2	9.5	69	6	8.0
FTBR	91	8	8.1	1	0	0.0	18	3	14.3	110	11	9.1
FDBR	1	4	80.0	0	1	100.0	0	0	0.0	1	5	83.3
CFT	68	24	26.1	8	4	33.3	9	6	40.0	85	34	28.6
CFD	1	0	0.0	0	0	0.0	0	0	0.0	1	0	0.0
RT	0	1	100.0	0	0	0.0	0	1	100.0	0	2	100.0
FDO	0	19	100.0	0	10	100.0	0	8	100.0	0	37	100.0
QB	15	9	37.5	0	0	0.0	1	1	50.0	16	10	38.5
CBT	0	0	0.0	0	0	0.0	0	0	0.0	0	0	0.0
CTC	36	9	20.0	11	2	15.4	19	4	17.4	66	15	18.5
CSS	0	9	100.0	0	0	0.0	2	0	0.0	2	9	81.8
FC	0	2	100.0	0	0	0.0	0	0	0.0	0	2	100.0
CET	0	0	0.0	0	0	0.0	9	0	0.0	9	0	0.0
CSR	1	1	50.0	0	2	100.0	3	0	0.0	4	3	42.9

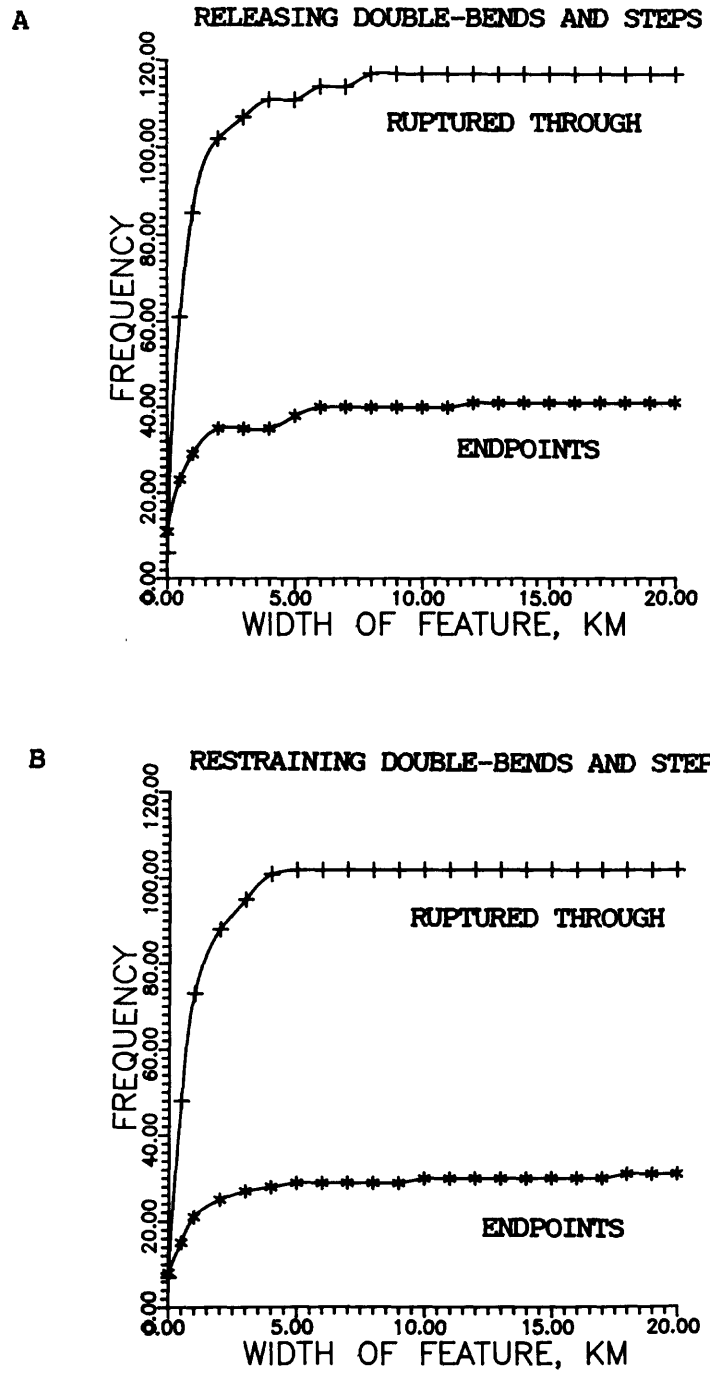

Figure 6.--Cumulative frequency graphs of widths of releasing (a) and restraining (b) double-bends and steps, strike-slip fault historical ruptures. Lower lines with asterisks show data from endpoints, upper lines with crosses show data from double-bends and steps that were ruptured through during earthquakes.

Branching and cross structures also are common characteristics on reverse faults. Indeed, cross-faults display a very high frequency of being endpoints, although the data set is too small for this to be a very meaningful conclusion. Discontinuities in surface traces, however, appear to rarely present barriers to propagation of reverse-slip ruptures. Thus, gaps apparently do not form segment boundaries on reverse fault ruptures.

Finally, most features on normal faults appear little more likely to be rupture endpoints than to be ruptured through, despite the increased size of the data set compared to that for reverse faults. The Pleasant Valley rupture (fig. 5) demonstrates the lack of control of at least one rupture by discontinuities, gaps, and steps in fault traces. The Borah Peak rupture (fig. 2) illustrates the lack of control by gaps along the rupture and the major cross structure of the Willow Creek Hills: even though the displacement decreased significantly north of the Willow Creek Hills (Crone and others, 1987), the rupture extended north of this "barrier." On the other hand, the south end of the 1983 rupture terminated in close association to hanging-wall cross faults, which may well have controlled the geometry of the rupture (Bruhn, unpublished data). The limited data set on normal faults (table 3) suggests that gaps are generally ruptured through and that cross structures have a relatively high frequency as rupture endpoints. However, different historical normal surface rupture events have either terminated at or ruptured through large discontinuities in fault traces and range fronts and cross faults, so no clear conclusions can be reached.

The variety of end-point characteristics clearly indicates that rupture ends do not follow any single, simple model of fault mechanics and rupture propagation. For example, not all releasing features of a certain size terminate strike-slip fault ruptures, nor do a large percentage of strike-slip ruptures actually terminate at releasing features. The major implication is that faults behave in complex fashions, that segment boundaries can and are caused by numerous different geologic and geometric features. Equally important, the study indicates that features that might be expected to act as segment boundaries, like steps in range fronts along normal fault, discontinuities along reverse faults, or even many releasing steps on strike-slip faults, often are ruptured through by earthquakes. This is certainly no revelation, but compilations of segment characteristics provides us with a quantification of the range of complexities, and it allows us to differentiate between those features which truly are diagnostic of rupture endpoints and segment boundaries and those features which occur only rarely. Ultimately, the study suggests that, in many cases, rupture endpoints are controlled more by the rupture dynamics than by static characteristics of the fault zone. An increased understanding and utilization of segmentation awaits more study of the role static characteristics really do play in controlling ruptures.

ACKNOWLEDGMENTS

This study represents the combined efforts of several of us at SUNY Binghamton and colleagues at Geomatrix Consultants in San Francisco. I particularly thank Julianne Turko, Anne Darling, and Mark Bamberger at SUNY and Donald Wells and Kevin Coppersmith at Geomatrix for their contributions in compiling data. The interpretations, however, are solely mine. The data compilation has been

funded principally by Pacific Gas and Electric Company as part of their ongoing Long Term Seismic Program studies for the Diablo Canyon Power Plant; discussions and permission from Lloyd Cluff and Frank Brady of PG&E are gratefully appreciated. Additional funding has been obtained from the NEHRP, USGS, Contract No. 14-08-0001-G1527. I thank Aykut Barka for providing a key preprint on Turkish ruptures. I appreciate the reviews of Wayne Thatcher and David Schwartz.

REFERENCES

Akers, R.J., and McQuilkin, M.J., 1975, Geologic investigation of the Oroville earthquake: California Division of Mines and Geology Special Report 124, p. 45-52.

Aki, K., 1979, Characterization of barriers on an earthquake fault: Journal of Geophysical Research, v. 84, p. 6140-6148.

Aki, K., 1987, How to find the nucleation point of an earthquake faulting? (abs.): Seismological Research Letters, v. 58, p. 31.

Allen, C.R., 1968, The tectonic environments of seismically active and inactive areas along the San Andreas fault system: Stanford University Publications in Geological Sciences, v. 11, p. 70-82.

Allen, C.R., 1975, Geological criteria for evaluating seismicity: Geological Society of America Bulletin, v. 86, p. 1041-1057.

Ambraseys, N.N., 1963, The Buyin-Zara (Iran) earthquake of September, 1962: a field report: Bulletin of the Seismological Society of America, v. 53, p. 705-740.

Ambraseys, N.N., 1965, An earthquake engineering study of the Buyin-Zara earthquake of September 1st, 1962 in Iran: Proceedings of the Third World Conference on Earthquake Engineering, New Zealand, v. III, p. V-7 - V-25.

Ambraseys, N.N., 1970, Some characteristic features of the Anatolian fault zone: Tectonophysics, v. 9, p. 143-165.

Ambraseys, N., and Tchalenko, J., 1968, Documentation of faulting associated with earthquakes (Part I): Unpublished report, Imperial College of Science, 35 p.

Ambraseys, N.N., and Zatopek, A., 1968, The Varto Usturkan (Anatolia) earthquake of 19 August 1966; summary of a field report: Bulletin of the Seismological Society of America, v. 58, p. 47-102.

Ambraseys, N.N., and Zatopek, A., 1969, The Mudurnu Valley, West Anatolia, Turkey, earthquake of 22 July 1967: Bulletin of the Seismological Society of America, v. 59, p. 521-589.

Anderson, J.G., and Bodin, P., 1987, Earthquake recurrence models and historical seismicity in the Mexicali-Imperial Valley: Bulletin of the Seismological Society of America, v. 77, p. 562-578.

Archuleta, R.J., and Day, S.M., 1980, Dynamic rupture in a layered medium: the 1966 Parkfield earthquake: Bulletin of the Seismological Society of America, v. 70, p. 671-689.

Barka, A., and Kadinsky-Cade, K., 1988, Strike-slip fault geometry and earthquake activity in Turkey: Tectonics, v. 7, p. 663-684.

Barka, A., Toksoz, M.N., Kadinsky-Cade, K., and Gulen, L., submitted, The segmentation, seismicity, and earthquake potential of the eastern part of the North Anatolian fault zone: in review, Journal of Geophysical Research.

Barrientos, S.E., Stein, R.S., and Ward, S.N., 1987, Comparison of the 1959 Hebgen Lake, Montana and the 1983 Borah Peak, Idaho, earthquakes from geodetic observations: Bulletin of the Seismological Society of America, v. 77, p. 784-808.

Beanland, S., and Clark, M.M., 1987, The Owens Valley fault zone, eastern California, and surface rupture associated with the 1872 earthquake (abs.): Seismological Research Letters, v. 58, p. 32.

Bell, J.W., 1984a, Guidebook for selected Nevada earthquake areas: in Lintz, J., Jr., ed., Western Geological Excursions: Guidebook, 1984 Geological Society of America Annual Meetings, v. 4, p. 387-472.

Bell, J.W., 1984b, Quaternary fault map of Nevada, Reno sheet: Nevada Bureau of Mines and Geology, Map 79, scale 1:250,000.

Berberian, M., 1976, Contribution to the Seismotectonics of Iran, Part II: Iran Geological Survey Report no. 39, 516 p.

Berberian, M., 1979, Earthquake faulting and bedding thrust associated with the Tabas-e-Golshan (Iran) earthquake of September 16, 1978: Bulletin of the Seismological Society of America, v. 69, p. 1861-1887.

Berberian, M., 1981, Active faulting and tectonics of Iran, in Zagros-Hindu Kush-Himalaya Geodynamic Evolution: American Geophysical Union, Geodynamics Series, v. 3, p. 33-69.

Berberian, M., Asudeh, I., and Arshadi, S., 1979, Surface rupture and mechanism of the Boh-Tangol (south-eastern Iran) earthquake of 19 December 1977: Earth and Planetary Letters, v. 42, p. 456-462.

Berberian, M., Jackson, J.A., Ghorashi, M., Kadjar, M.H., 1984, Field and teleseismic observations of the 1981 Golbaf-Sirch earthquake in southeastern Iran: Geophysical Journal of the Royal Astronomical Society, v. 77, p.809-838.

Biq Ch., 1965, The east Taiwan rift: Petroleum Geology of Taiwan, no. 4, p. 93-106.

Biq Ch., 1981, Collision, Taiwan-style: Geological Society of China Memoir no. 4, p. 91-102.

Blanc, J.-L., Cabrera, J., and Sebrier, M., 1983, Estudio microtectonico de la falla sismica de Huaytapallana (Andes del Peru Central): Revista Geofisica (Instituto Panamericano de Geografia e Historia), no. 18/19, p. 5-25.

Bolt, B.A., 1968, The focus of the 1906 California earthquake: Bulletin of the Seismological Society of America, v. 50, p. 457-471.

Bonilla, M.G., 1967, Historic surface faulting in continental United States and adjacent part of Mexico; a factor in nuclear facility siting and design: U.S. Geological Survey Report to U.S. Atomic Energy Commission, TID-24124, 36 p.

Bonilla, M.G., 1975, A review of recently active faults in Taiwan: U.S. Geological Survey Open File Report 75-41, 61 p.

Bonilla, M.G., 1977, Summary of Quaternary faulting and elevation changes in Taiwan: Memoir of the Geological Society of China, no. 2, p. 43-55.

Bonilla, M.G., and Buchanan, J.M., 1970, Interim report on worldwide historic surface faulting: U.S. Geological Survey Open-File Report, 32 p.

Bonilla, M.G., Mark, R.K., and Lienkaemper, J.J., 1984, Statistical relations among earthquake magnitude, surface rupture length, and surface fault displacement: Bulletin of the Seismological Society of America, v. 74, p. 2379-2411.

Brown, R.D., Jr., 1970, Map showing recently active breaks along the San Andreas and related faults between the northern Gabilan Range and Cholame Valley, California: U.S. Geological Survey Miscellaneous Geological Investigations Map I-575, scale 1:62,500.

Brown, R.D., Jr., and Vedder, J.G., 1967, Surface tectonic fractures along the San Andreas fault: U.S. Geological Survey Professional Paper 579, p. 2-23.

Brune, J.N., Simons, R.S., Rebollar, C., and Reyes, A., 1979, Seismicity and faulting in northern Baja California, in Earthquakes and Other Perils, San Diego Region: Guidebook, 1979 Geological Society of America Annual Meeting, p. 83-100.

Brunol, L., 1968, Contribution a l'Etude des gisements de plomb et zinc de l'Iran; Essais de classification pargenetique: Iran Geological Survey Report no. 11.

Buchanan-Banks, J.M., Pampeyan, E.H., Wagner, H.C., and McCulloch, D.S., 1978, Preliminary map showing recency of faulting in coastal south-central California: U.S. Geological Survey Miscellaneous Field Studies Map MF-910, scale 1:250,000.

Buchholz, P.E., 1975, Generalized geology of the Oroville earthquake area: California Division of Mines and Geology Special Report 124, p. 29-39.

Bull, W.B., 1978, Geomorphic tectonic activity classes of the south front of the San Gabriel Mountains, CA: Technical Report, U.S. Geological Survey Contract No. 14-08-0001-G-394, 59 p.

Bull, W.B., and Pearthree, P.A., 1988, Frequency and size of Quaternary surface ruptures of the Pitaycachi Fault, northeastern Sonora, Mexico: Bulletin of the Seismological Society of America, v. 78, p. 956-978.

Buwalda, J.P., and St. Amand, P., 1955, Geological effects of the Arvin-Tehachapi earthquake, in Earthquakes in Kern County, California, During 1952: California Division of Mines Bulletin 171, p. 41-56.

Carver, G.A., 1969, Quaternary tectonism and surface faulting in the Owens Lake basin, California: Master's thesis, University of Nevada, Reno, 105 p.

Chen, W., and Molnar, P., 1977, Seismic moments of major earthquakes and the average rate of slip in Central Asia: Journal of Geophysical Research, v. 82, p. 2945-2969.

Clark, M.M., 1972, Surface rupture along the Coyote Creek fault: U.S. Geological Survey Professional Paper 787, p. 55-86.

Clark, M.M., Sharp, R.V., Castle, R.O., and Harsh, P.W., 1976, Surface faulting near Lake Oroville, California in August, 1975: Bulletin of the Seismological Society of America, v. 66, p. 1101-1110.

Cockerham, R.S., and Corbett, E.J., 1987, The July 1986 Chalfant Valley, California, earthquake sequence: preliminary results: Bulletin of the Seismological Society of America, v. 77, p. 280-289.

Crampin, S., 1969, Aftershocks of the Dasht-e-Bayaz, Iran, earthquake of August, 1968: Bulletin of the Seismological Society of America, v. 59, p. 1823-1841.

Crone, A.J., Machette, M.N., Bonilla, M.G., Lienkaemper, J.J., Pierce, K.L., Scott, W.E., and Bucknam, R.C., 1987, Surface faulting accompanying the Borah Peak earthquake and segmentation of the Lost River fault, central Idaho: Bulletin of the Seismological Society of America, v. 77, p. 739-770.

Crook, R., Jr., Kamb, B., Allen, C.R., Payne, C.M., and Proctor, R.J., 1979, Quaternary geology and seismic hazard of the Sierra Madre and associated faults, western San Gabriel Mountains, California: Final Technical Report, U.S. Geological Survey Contract No. 14-08-0001-15258.

Davis, T.L., and Duebendorfer, E., 1987, Strip map of San Andreas fault western Big Bend segment: Geological Society of America Map and Chart Series MC-60, scale 1:31,682.

Deng Q., Sung F., Zhu S., Li M., Wang T., Zhang W., Burchfiel, B.C., Molnar, P., and Zhang, P., 1984, Active faulting and tectonics of the southern Ningxia-Hui Autonomous Region: Journal of Geophysical Research, v. 89, p. 4427-4445.

dePolo, C.M., and Ramelli, A.R., 1987, Preliminary report on surface fractures along the White Mountains fault zone associated with the July 1986 Chalfant Valley earthquake sequence: Bulletin of the Seismological Society of America, v. 77, p. 290-296.

Dewey, J. F., Hempton, M.R., Kidd, W.S.F., Saroglu, F., and Sengor, A.M.C., 1986, Shortening of continental lithosphere: the neotectonics of Eastern Anatolia-a young collision zone, in Collision Tectonics: Geological Society of London Special Publication No. 19, p. 3-36.

Deza, E., 1971, The Pariahuanca earthquakes, Huancayo, Peru: July-October 1969; preliminary report, in Recent Crustal Movements: Royal Society of New Zealand, Bulletin 9, p. 77-83.

Dibblee, T.W., Jr., 1967, Geologic map of Emerson Lake quadrangle, San Bernardino County, California: U.S. Geological Survey Miscellaneous Geologic Investigations Map I-490, scale 1:62,500.

Doser, D.I., 1985, Source parameters and faulting processes of the 1959 Hebgen Lake, Montana, earthquake sequence: Journal of Geophysical Research, v. 90, p. 4537-4555.

Doser, D., 1986, Earthquake processes in the Rainbow Mountain-Fairview Peak-Dixie Valley, Nevada Region 1954-1959: Journal of Geophysical Research, v. 91, p. 12,572-12,586.

Dunbar, W.S., Boore, D.M., and Thatcher, W., 1980, Pre-, co-, and postseismic strain changes associated with the 1952 M_L = 7.2 Kern County, California, earthquake: Bulletin of the Seismological Society of America, v. 70, p. 1893-1905.

Ellsworth, W.L., Lindh, A.G., Prescott, W.H., and Herd, D.G., 1981, The 1906 San Francisco earthquake and the seismic cycle, in Earthquake Prediction; an International Review: American Geophysical Union, Maurice Ewing Series 4, p. 126-140.

Eyidogan, H., and Jackson, J., 1985, A seismological study of normal faulting in the Demirci, Alasehir, and Gediz earthquakes of 1969-70 in western Turkey: implications for the nature and geometry of deformation in the continental crust: Geophysical Journal of the Royal Astronomical Society, v. 81, p. 569-607.

Florensov, N.A., and Solonenko, V.P., eds., 1963, The Gobi-Altai Earthquake (in Russian; English translation by Israel Program for Scientific Translations, 1965): Academy of Sciences, Moscow, 424 p.

Gastil, R.G., Phillips, R.P., and Allison, E.C., 1975, Reconnaissance geologic map of the State of Baja California, Mexico: Geological Society of America Memoir 140, 170 p.

Gastil, R.G., Kies, R., and Melius, D.J., 1979, Active and potentially active faults: San Diego County and northernmost Baja California, in Earthquakes and Other Perils, San Diego Region: Guidebook, 1979 Geological Society of America Annual Meeting, p. 47-60.

Gianella, V.P., 1957, Earthquake and faulting, Fort Sage Mountains, California, December, 1950: Bulletin of the Seismological Society of America, v. 47, p. 173-177.

Gross, W.K., and Savage, J.C., 1987, Deformation associated with the 1986 Chalfant Valley earthquake, eastern California: Bulletin of the Seismological Society of America, v. 77, p. 306-310.

Haghipour, A. and Amidi, M., 1980, The November 14 to December 25, 1979 Ghaenat earthquakes of northeast Iran and their tectonic implications: Bulletin of the Seismological Society of America, v.70, p. 1751-1757.

Hamilton, R.M., 1972, Aftershocks of the Borrego Mountain earthquake from April 12 to June 12, 1968: U.S. Geological Survey Professional Paper 787, p. 31-54.

Hanks, T.C., Thatcher, W., and Hileman, J.A., 1975, Seismic moments of the larger earthquakes of the southern California region: Geological Society of America Bulletin, v. 86, p. 1131-1139.

Hart, E.W., and Rapp, J.S., 1975, Ground rupture along the Cleveland Hill fault: California Division of Mines and Geology Special Report 124, p. 61-72.

Herd, D.G., and Helley, E.J., 1977, Faults with Quaternary displacement, northwestern San Francisco Bay Region, California: U.S. Geological Survey Miscellaneous Field Studies Map MF-818, scale 1:125,000.

Hill, R.L., and Beeby, D.J., 1977, Surface faulting associated with the 5.2 magnitude Galway Lake earthquake of May 31, 1975: Mojave Desert, San Bernardino County, California: Geological Society of America Bulletin, v. 88, p. 1378-1384.

Hill, R.L., Pechmann, J.C., Treiman, J.A., McMillan, J.R., Given, J.W., and Ebel, J.E., 1980, Geologic study of the Homestead Valley earthquake swarm of March 15, 1979: California Geology, v. 33, p. 60-67.

Hsu, T.L., 1962, Recent faulting in the Longitudinal Valley of eastern Taiwan: Geological Society of China Memoir no. 1, p. 95-102.

Hutton, L.K., Johnson, C.E., Pechmann, J.C., Ebel, J.E., Given, J.W., Cole, D.M., and German, P.T., 1980, Epicentral locations for the Homestead Valley earthquake sequence, March 15, 1979: California Geology, v. 33, p. 110-114.

Iida, K., and Sakabe, K., 1972, The extension of the Fukozu fault associated with the Mikawa earthquake in 1945 [in Japanese with English abstract]: Zisin (J. Seismological Soc. Japan), v. 25, p. 44-55.

Jennings, C., 1975, Fault map of California with locations of volcanoes, thermal springs, and thermal wells: California Division of Mines and Geology, Geologic Data Map No. 1, scale 1:750,000.

Jennings, C.W., 1977, Geologic map of California: California Division of Mines and Geology, Geologic Data Map No. 2, scale 1:750,000.

Jennings, C.W., 1985, An explanatory text to accompany the 1:750,000 scale fault and geologic maps of California: California Division of Mines and Geology Bulletin 201, 197 p.

Johnson, C.E., and Hill, D.P., 1982, Seismicity of the Imperial Valley: U.S. Geological Survey Professional Paper 1254, p. 15-24.

Kahle, J.E., Bryant, W.A., Hart, E.W., 1986, Fault rupture associated with the July 21, 1986 Chalfant Valley earthquake Mono and Inyo Counties, California: California Geology, v. 39, p. 243-245.

Kahle, J.E., Wills, C.J., Hart, E.W., Treiman, J.A., Greenwood, R.B., and Kaumeyer, R.S., 1988, Preliminary report, surface rupture, Superstition Hills earthquakes of November 23 and 24, 1987: California Geology, v. 41, p. 75-84.

Kakimi, T., and Kinugasa, Y., 1976, A geologic significance of the Irozaki earthquake fault, viewed from "maturity" of faulting: Journal of the Geodetic Society of Japan, v. 22, p. 278-279.

Kanamori, H., and Anderson, D.L., 1975, Theoretical basis of some empirical relations in seismology: Bulletin of the Seismological Society of America, v. 65, p. 1073-1095.

Kanamori, H., and Regan, J., 1982, Long-period surface waves: U.S. Geological Survey Professional Paper 1254, p. 55-58.

Kato, H., and Barka, A., 1985, Remarks on the tectonic features of Turkey and Japan: geology, earthquakes, earthquake faults and active faults, in Research on Earthquake Faults, Active Faults, and Earthquake Prediction: ITIT, Japan, p. 15-52.

Ketin, I., and Roesli, F., 1953, Makroseismiche Untersuchungen uber das nordwestanatolische Beben vom 18 Marz 1953: Eclogae Geologicae Helvetiae, v. 46, p. 187-208.

King, G.C.P., 1986, Speculations on the geometry of the initiation and termination processes of earthquake rupture and its relation to morphology and geological structure: Pure and Applied Geophysics, v. 124, p. 567-585.

King, G.C.P., and Nabelek, J., 1985, The role of bends in faults in the initiation and termination of earthquake rupture: Science, v. 228, p. 984-987.

Kinugasa, Y., 1976, The Izu-Hanto-oki earthquake of 1974 and Irozaki earthquake fault [in Japanese with English abstract]: Geological Society of Japan, Memoir 12, p. 139-149.

Kuno, H., 1936, On the displacement of the Tanna fault since the Pleistocene: Earthquake Research Institute (Tokyo) Bulletin, v. 14, p. 619-631.

Lahr, K.M., Lahr, J.C., Lindh, A.G., Bufe, C.G., and Lester, F.W., 1976, The August 1975 Oroville earthquakes: Bulletin of the Seismological Society of America, v. 66, p. 1085-1099.

Lawson, A.C., editor, 1908, The California Earthquake of April 18, 1906: Report of the State Earthquake Investigation Committee, Carnegie Institute, Washington, Publication 87, v. 1, 451 p.

Lienkaemper, J.J., 1984, Comparison of two surface-wave magnitude scales: M of Gutenberg and Richter (1954) and M_S of "Preliminary Determination of Epicenters": Bulletin of the Seismological Society of America, v. 74, p. 2357-2378.

Lienkaemper, J.J., and Brown, R.D., 1985, Map of faulting accompanying the 1966 Parkfield, California, earthquake: U.S. Geological Survey Open-file Report 85-0661, 8 p., scale 1:12,000.

Lienkaemper, J.J., Pezzopane, S.K., Clark, M.M., and Rymer, M.J., 1987, Fault fractures formed in association with the 1986 Chalfant Valley, California, earthquake sequence: preliminary report: Bulletin of the Seismological Society of America, v. 77, p. 297-305.

Lindh, A.G., and Boore, D.M., 1981, Control of rupture by fault geometry during the 1966 Parkfield earthquake: Bulletin of the Seismological Society of America, v. 71, p. 95-116.

Matsuda, T., 1974, Surface faults associated with Nobi (Mino-Owari) earthquake of 1891, Japan [in Japanese with English abstract]: Earthquake Research Institute Special Bulletin 13, p. 85-126.

Matsuda, T., Okada, A., and Huzita, K., 1976, Distribution map and catalogue of active faults in Japan [in Japanese with English abstract]: Geological Society of Japan, Memoir 12, p. 185-198.
Matsuda, T., Yamazaki, H., Nakata, T., and Imaizumi, T., 1980, The surface faults associated with the Rikuu earthquake of 1896 [in Japanese with English abstract]: Earthquake Research Institute (Tokyo) Bulletin, v. 55, p. 795-855.
Matthews, R.A., and Burnett, J.L., 1965, Geologic map of California, Fresno sheet: California Division of Mines and Geology, scale 1:250,000.
McCall, G.J.H., 1967, Geology of the Nakuru-Thomson's Falls-Lake Hannington area: Geological Survey of Kenya Report No. 78, 122 p.
Meghraoui, M., Cisternas, A., and Philip, H., 1986, Seismotectonics of the lower Cheliff basin: structural background of the El Asnam (Algeria) earthquake: Tectonics, v. 5, p. 809-836.
Molnar, P., and Deng Q., 1984, Faulting associated with large earthquakes and the average rate of deformation in central and eastern Asia: Journal of Geophysical Research, v. 89, p. 6203-6227.
Murai, I., Matsuda, T., and Nakamura, K., 1978, Surface ruptures in the Inatori vicinity associated with the Izu-Oshima-Kinkai earthquake of 1978 [in Japanese with English abstract]: Earthquake Research Institute (Tokyo) Bulletin, v. 53, p. 995-1024.
Myers, W.F., and Hamilton, W., 1964, Deformation accompanying the Hebgen Lake earthquake of August 17, 1959: U.S. Geological Survey Professional Paper 435, p. 37-98.
Natali, S.G., and Sbar, M.L., 1982, Seismicity in the epicentral region of the 1887 northeast Sonora earthquake, Mexico: Bulletin of the Seismological Society of America, v. 72, p. 181-196.
Niazi, M., and Kanamori, H., 1981, Source parameters of 1978 Tabas and 1979 Qainat, Iran, earthquakes from long-period surface waves: Bulletin of the Seismological Society of America, v. 71, p. 1201-1213.
Nowroozi, A.A., 1985, Empirical relations between magnitudes and fault parameters for earthquakes in Iran: Bulletin of the Seismological Society of America, v. 75, p. 1327-1338.
Nowroozi, A.A., and Mohajer-Ashjai, A., 1985, Fault movements and tectonics of eastern Iran: boundaries of the Lut plate: Geophysical Journal of the Royal Astronomical Society, v. 83, p. 215-237.
Oakeshott, G.B., 1975, Geology of the epicentral area, in San Fernando, California, Earthquake of 9 February 1971: California Division of Mines and Geology, Bulletin 196, p. 19-30.
Otuka, Y., 1933, The geomorphology and geology of northern Idu Peninsula, the earthquake fissures of Nov. 26, 1930, and the pre-and post-seismic crust deformations: Earthquake Research Institute (Tokyo) Bulletin, v. 11, p. 530-574.
Pampeyan, E.H., 1979, Preliminary map showing recency of faulting in coastal north-central California: U.S. Geological Survey Miscellaneous Field Studies Map MF-1070, scale 1:250,000.
Philip, H., and Megard, F., 1977, Structural analysis of the superficial deformation of the 1969 Pariahuanca earthquakes (central Peru): Tectonophysics, v. 38, p. 259-278.
Qian H., 1986, Recent displacements along Xianshuihe fault belt and its relation with seismic activities: Journal of Seismological Research, v. 9, p. 601-613.

Research Group for Active Faults, 1980, Active faults in Japan; sheet maps and inventory [in Japanese with English summary]: University of Tokyo Press, 363 p.

Research Group for Active Faults of Japan, 1980, Active faults in and around Japan: the distribution and the degree of activity: Natural Disaster Science, v. 2, p. 61-99.

Savage, J.C., Lisowski, M., Prescott, W.H., and Church, J.P., 1977, Geodetic measurements of deformation associated with the Oroville, California, earthquake: Journal of Geophysical Research, v. 82, p. 1667-1671.

Schwartz, D.P., and Coppersmith, K.J., 1984, Fault behavior and characteristic earthquakes: examples from the Wasatch and San Andreas fault zones: Journal of Geophysical Research, v. 89, p. 5681-5698.

Scott, W.E., Pierce, K.L., and Hait, M.H., Jr., 1985, Quaternary tectonic setting of the 1983 Borah Peak earthquake, central Idaho: Bulletin of the Seismological Society of America, v. 75, p. 1053-1066.

Segall, P., and Pollard, D.D., 1980, Mechanics of discontinuous faults: Journal of Geophysical Research, v. 85, p. 4337-4350.

Seymen, I., and Aydin, A., 1972, The Bingol earthquake fault and its relation to the North Anatolian fault zone: Bulletin of the Mineral Research and Exploration Institute of Ankara, v. 79, p. 1-8.

Sharp, R.V., 1972, Tectonic setting of the Salton Trough: U.S. Geological Survey Professional Paper 787, p. 3-15.

Sharp, R.V., 1975, Displacement on tectonic ruptures, in San Fernando, California, Earthquake of 9 February 1971: California Division of Mines and Geology, Bulletin 196, p. 187-194.

Sharp, R.V., 1982a, Tectonic setting of the Imperial Valley region: U.S. Geological Survey Professional Paper 1254, p. 5-14.

Sharp, R.V., 1982b, Comparison of 1979 surface faulting with earlier displacements in the Imperial Valley: U.S. Geological Survey Professional Paper 1254, p. 213-221.

Sharp, R.V., Lienkaemper, J.J., Bonilla, M.G., Burke, D.B., Fox, B.F., Herd, D.G., Miller, D.M., Morton, D.M., Ponti, D.J., Rymer, M.J., Tinsley, J.C., Yount, J.C., Kahle, J.E., Hart, E.W., and Sieh, K.E., 1982, Surface faulting in the central Imperial Valley: U.S. Geological Survey Professional Paper 1254, p. 119-143.

Shi J., Feng X., Ge S., Yang Z., Bo M., and Hu J., 1984, The Fuyun earthquake fault zone in Xinjiang, China, in A Collection of Papers of the International Symposium on Continental Seismicity and Earthquake Prediction: Seismology Press, p. 325-346.

Shih, C.L., Huan, W.L., Yao, K.K., and Hsie, Y.T., 1978, On the fracture zones of the Changma earthquake of 1932 and their genesis: Chinese Geophysics, v. 1, p. 17-45.

Shimazaki, K., and Somerville, P., 1979, Static and dynamic parameters of the Izu-Oshima, Japan earthquake of January 14, 1978: Bulletin of the Seismological Society of America, v. 69, p. 1343-1378.

Shor, G., and Roberts, E.E., 1958, San Miguel, Baja California Norte, earthquakes of February, 1956: a field report: Bulletin of the Seismological Society of America, v. 46, p. 101-116.

Sibson, R.H., 1985, Stopping of earthquake ruptures at dilational fault jogs: Nature, v. 316, p. 248-251.

Sibson, R.H., 1986, Rupture interaction with fault jogs, in Earthquake Source Mechanics: American Geophysical Union Monograph 37 (Maurice Ewing Symposium 6), p. 157-167.
Sibson, R.H., 1987, Effects of fault heterogeneity on rupture propagation, in Directions in Paleoseismology: U.S. Geological Survey Open-File Report 87-673, p. 362-373.
Sieh, K.E., 1978, Slip along the San Andreas fault associated with the great 1857 earthquake: Bulletin of the Seismological Society of America, v. 68, p. 1421-1448.
Sieh, K.E., 1981, A review of geological evidence for recurrence times of large earthquakes, in Earthquake Prediction: An International Review: American Geophysical Union, Maurice Ewing Series, v. 4, p. 181-207.
Slemmons, D.B., 1956, Geologic setting for the Fallon-Stillwater earthquakes of 1954: Bulletin of the Seismological Society of America, v. 46, p. 4-9.
Slemmons, D.B., 1957, Geological effects of the Dixie Valley-Fairview Peak, Nevada, earthquake of December 16, 1954: Bulletin of the Seismological Society of America, v. 47, p. 353-375.
Slemmons, D.B., 1977, Faults and earthquake magnitude: U.S. Army Waterways Experiment Station, Vicksburg, Mississippi, Miscellaneous Paper S-73-1, Report 6, 129 p.
Smith, R.B., Richins, W.D., and Doser, D.I., 1985, The Borah Peak, Idaho, earthquake: regional seismicity, kinematics of faulting, and tectonic mechanism, in Proceedings of Workshop XXVIII on the Borah Peak, Idaho, earthquake: U.S. Geological Survey Open File Report 85-290, p. 236-263.
Stein, R., and Barrientos, S., 1985, The 1983 Borah Peak, Idaho, earthquake: geodetic evidence for deep rupture on a planar fault, in Proceedings of Workshop XXVIII on the Borah Peak, Idaho, earthquake: U.S. Geological Survey Open File Report 85-290, p.459-484.
Stein, R.S., and Lisowski, M., 1983, The 1979 Homestead Valley earthquake sequence, California: control of aftershocks and postseismic deformation: Journal of Geophysical Research, v. 88, p. 6477-6490.
Stein, R.S., and Thatcher, W., 1981, Seismic and aseismic deformation associated with the 1952 Kern County, California, earthquake and relationship to the Quaternary history of the White Wolf fault: Journal of Geophysical Research, v. 86, p. 4913-4928.
Stocklin, J., Eftehar-nezhad, J., Hushmand-zadeh, A., 1965, Geology of the Shotori Range (Tabas region, east Iran): Iran Geological Survey Report No. 3.
Strand, R.G., 1967, Geologic map of California, Mariposa sheet: California Division of Mines and Geology, scale 1:250,000.
Streitz, R., and Stinson, M.C., 1974, Geologic map of California, Death Valley sheet: California Division of Mines and Geology, scale 1:250,000.
Suarez, G., Molnar, P., and Burchfiel, B.C., 1983, Seismicity, fault plane solutions, depth of faulting, and active tectonics of the Andes of Peru, Ecuador, and southern Colombia: Journal of Geophysical Research, v. 88, p. 10,403-10,428.
Sugimura, A., and Matsuda, T., 1965: Atera fault and its displacement vectors: Geological Society of America Bulletin, v. 76, p. 509-522.

Tang R., Huang Z., Qian H., Deng T., Jiang L., Ge P., Liu Sh., Cao Y., and Zhang, Ch., 1984, On the recent tectonic activity and earthquake of the Xianshuihe Fault zone, in A Collection of Papers of the International Symposium on Continental Seismicity and Earthquake Prediction: Seismological Press, p. 347-369.

Tang R.C., Wen D.H., Deng T.G., and Huang S.M., 1976, A preliminary study on the characteristics of the ground fractures during the Lu-Huo M = 7.9 earthquake, 1973 and the origin of the earthquake [in Chinese with English abstract]: Acta Geophysica Sinica, v. 19, p. 17-27.

Tapponnier, P., and Molnar, P., 1977, Active faulting and tectonics in China: Journal of Geophysical Research, v. 82, p. 2905-2930.

Tapponnier, P., and Molnar, P., 1979, Active faulting and Cenozoic tectonics of the Tien Shan, Mongolia, and Baykal regions: Journal of Geophysical Research, v. 84, p. 3425-3459.

Tasdemiroglu, M., 1971, The 1970 Gediz earthquake in western Anatolia, Turkey: Bulletin of the Seismological Society of America, v. 61, p. 1507-1527.

Tchalenko, J.S., 1975, Seismicity and structure of the Kopet Dagh (Iran, USSR): Philosophical Transactions of the Royal Society of London, v. 278A, p. 1-28.

Tchalenko, J.S., and Ambraseys, N.N., 1970, Structural analysis of the Dasht-e-Bayaz (Iran) earthquake fractures: Geological Society of America Bulletin, v. 81, p. 41-60.

Thatcher, W., and Lisowski, M., 1987, Long-term seismic potential of the San Andreas fault southeast of San Francisco, California: Journal of Geophysical Research, v. 92, p. 4771-4784.

Tocher, D., 1956, Movement on the Rainbow Mountain fault: Bulletin of the Seismological Society of America, v. 46, p. 10-14.

Toksoz, M.N., Nabelek, J., and Arpat, E., 1978a, Source properties of the 1976 earthquake in eastern Turkey: a comparison of field data and teleseismic results: Tectonophysics, v. 49, p. 199-205.

Toksoz, M.N., Shakal, A.F., and Michael, A.J., 1978b, Space-time migration of earthquakes along the North Anatolian fault zone and seismic gaps, in Methodology for Identifying Seismic Gaps and Soon-to-Break Gaps: U.S. Geological Survey Open-File Report 78-943, p. 829-856.

Tsukuda, E., 1987, Migration of historical earthquakes, central Japan, in Directions in Paleoseismology: U.S. Geological Survey Open-File Report 87-673, p. 271-284.

Tsuya, H., 1944, Geological observations of the earthquake faults (Sikano and Yosioka) of 1943 in Tottori prefecture [in Japanese]: Earthquake Research Institute (Tokyo) Bulletin, v. 22, p. 1-32.

Tsuya, H., 1946, The Fukozu fault, a remarkable earthquake fault formed during the Mikawa earthquake of January 13, 1945 [in Japanese with English abstract]: Earthquake Research Institute (Tokyo) Bulletin, v. 24, p. 59-75.

Wallace, R.E., 1968, Earthquake of August 19, 1966, Varto area, eastern Turkey: Bulletin of the Seismological Society of America, v. 58, p. 11-45.

Wallace, R.E., 1979, Map of young fault scarps related to earthquake in north central Nevada: U.S. Geological Survey Open-File Report 79-1554, scale 1:125,000.

Wallace, R.E., 1984, Faulting related to the 1915 earthquakes in Pleasant Valley, Nevada: U.S. Geological Survey Professional Paper 1274-A, 33 p.

Weldon, R., and Matti, J., 1986, Geologic evidence for segmentation of the southern San Andreas fault (abs.): EOS, v. 67, p. 905-906.

Weldon, R.J., II, and Sieh, K.E., 1985, Holocene rate of slip and tentative recurrence interval for large earthquakes on the San Andreas fault, Cajon Pass, southern California: Geological Society of America Bulletin, v. 96, p. 793-812.

Wesnousky, S.G., 1986, Earthquakes, Quaternary faults, and seismic hazard in California: Journal of Geophysical Research, v. 91, p. 12,587-12,631.

Willis, B., 1936, Studies in comparative seismology; East African plateaus and rift valleys: Carnegie Institution of Washington, Publication 470, 358 p.

Wyss, M., and Hanks, T.C., 1972, Source parameters of the Borrego Mountain earthquake: U.S. Geological Survey Professional Paper 787, p. 24-30.

Yamasaki, N., and Tada, F., 1928, The Oku-Tango earthquake of 1927: Earthquake Research Institute, Tokyo, Bulletin, v. 4, p. 159-179.

Yielding, G., 1985, Control of rupture by fault geometry during the 1980 El Asnam (Algeria) earthquake: Geophysical Journal of the Royal Astronomical Society, v. 81, p. 641-670.

Yielding, G., Jackson, J.A., King, G.C.P., Sinvhal, H., Vita-Finzi, C., and Wood, R.M., 1981, Relations between surface deformation, fault geometry, seismicity, and rupture characteristics during the El Asnam (Algeria) earthquake of 10 October 1980: Earth and Planetary Science Letters, v. 56, p. 287-304.

Zhang S., and Liu B., 1978, Seismic geological characteristics of Tonghai earthquake in 1970 [in Chinese with English abstract]: Scientia Geologica Sinica, v. 4, p. 323-334.

Zhang, W., Jiao, D., Zhang, P., Molnar, P., Burchfiel, B.C., and Deng, Q., 1987, Displacement along the Haiyuan Fault associated with the great 1920 Haiyuan, China, earthquake: Bulletin of the Seismological Society of America, v. 77, p. 117-131.

Zhou, H., Liu, H.L., and Kanamori, H., 1983, Source processes of large earthquakes along the Xianshuihe fault in southwestern China: Bulletin of the Seismological Society of America, v. 73, p. 537-551.

Zhou, H.L., Allen, C.R., and Kanamori, H., 1983, Rupture complexity of the 1970 Tonghai and 1973 Luhuo earthquakes, China, from P-wave inversion, and relationship to surface faulting: Bulletin of the Seismological Society of America, v. 73, p. 1585-1597.

APPENDIX: Features Identified from Surface Ruptures

EQN	PT	FAULT, EQ	FEATURE	DISTANCE	WIDTH	ANGLE	COMMENTS
4		San Andreas 1857	FC	0.0	0.0	0	End creeping section approx. at N end
4			FTBR	0.0	0.0	28	Cholame endpoint
							incomplete data
4			FTBR	2.0	0.0	10	
4			RSSB	2.0	0.0	5	
4			CTC	3.0	0.0	0	
4			CTC	50.0	0.0	0	
4			RSSB	82.0	0.0	10	
4			FTBR	105.0	0.0	5	
4			FTBR	110.0	0.0	10	
4			RSSB	120.0	0.0	25	
4			CFT	125.0	0.0	55	Plaito thrust
4			RSDB	150.0	2.0	0	12 km long
4			CFT	163.0	0.0	50	Pine Mtn. fault
4			CFT	168.0	0.0	80	Fraser Mountain fault
4			RSDB	168.0	2.5	0	7 km long
4			CFT	170.0	0.0	45	Garlock fault
4			RLSB	210.0	0.0	5	
4			RSDB	282.0	0.5	0	1 km long
4			RLDB	290.0	0.5	0	4 km long
4			FTBR	307.0	0.0	15	Endpoint
							San Jacinto fault branch
7		Owens Valley	CSS	0.0	0.0	0	Endpoint: at jct w/Sierra Nevada flt
7			CTC	0.0	0.0	0	Endpt: splays at jct w/Sierra Nevada flt
7			RLDB	0.0	5.0	0	Endpoint: step to White Mtns flt
7			RLDB	4.0	0.5	0	
7			CFT	15.0	0.0	30	
7			RSDB	18.0	2.0	0	
7			RSDB	36.0	0.4	0	
7			RLDB	57.0	1.6	0	Width?
7			FTBR	60.0	0.0	15	
7			RLDB	72.0	1.5	0	
7			CFT	79.0	0.0	76	
7			RLDB	84.0	1.9	0	
7			CFT	100.0	0.0	0	Endpoint:at Sierra Nevada Frontal flt
7			RLDB	108.0	4.2	0	Endpoint
8		Pitaycachi	FB	0.0	0.0	0	Endpoint: Basinward fault bend?
8			GAP	3.0	3.5	0	
8			FTBR	0.0	0.0	10	
8			FB	13.0	0.0	30	
8			FTBR	13.0	0.0	30	
8			FTBR	17.0	0.0	0	bends back into rupture
8			FB	20.0	0.0	25	
8			GAP	21.5	0.5	0	
8			FB	30.0	0.0	38	
8			FB	33.0	0.0	28	
8			FB	38.0	0.0	20	
8			STP	40.5	1.0	0	
8			FB	44.0	0.0	35	
8			CTC	48.0	27.0	0	discontinuous traces
8			STP	50.0	2.5	0	48-52 km
8			FB	58.0	0.0	10	
8			GAP	63.0	2.0	0	
8			GAP	67.0	2.0	0	
8			STP	71.0	0.0	0	minor stepover
8			QB	75.0	0.0	0	Endpoint: Southern basin margin
10		Nobi-Headant, Japan	CSS	0.0	0.0	0	Endpoint: reversal in upthrown direc.
10			FDO	0.0	0.0	0	Ends past RLDB
10			RLDB	1.9	0.0	0	
10			CFT	3.6	0.0	80	
10			CFT	7.5	0.0	30	
10			CTC	14.7	0.0	0	increase: multiple fault traces
10			RSSB	14.7	0.0	14	
10			CFT	22.0	0.0	90	
10			RSDB	22.7	2.6	0	
10			RLSB	25.5	0.0	26	
10			FTBR	31.7	0.0	10	
10			FTBR	30.0	0.0	20	
10			RLDB	43.0	2.3	0	
10			RSDB	50.0	1.9	0	
10			RLSB	64.6	0.0	25	
10			RSSB	70.3	0.0	21	
10			CTC	85.0	9.5	0	Endpt: discontinuous traces 80-90 km
10			RSDB	89.5	3.6	0	Endpoint: R.L.=88 km?
13 a		Rikuu-Senya	CTC	0.0	0.0	0	Endpt: 13A-change to simple range front
13 a			FB	0.5	0.0	40	Endpoint
13 a			FB	1.3	0.0	30	
13 a			GAP	5.0	0.0	0	
13 a			STP	14.0	4.0	0	step in range front
13 a			FB	15.2	0.0	38	
13 a			FB	15.7	0.0	63	
13 a			FB	18.1	0.0	10	
13 a			STP	20.0	0.3	0	
13 a			STP	21.0	0.2	0	
13 a			STP	23.1	2.0	0	
13 a			FB	24.1	0.0	33	
13 a			CTC	27.3	0.0	0	simple to complex range front
13 a			STP	27.3	0.0	0	
13 a			FB	30.1	0.0	33	
13 a			FB	33.4	0.0	33	
13 a			GAP	35.4	3.0	0	
13 a			FB	36.5	0.0	40	
13 a			CSR	40.0	0.0	0	Endpoint: 13A-Slip rate decr. to S.
13 a			CTC	40.0	0.0	0	Endpt: 13A-complex to simple range front
13 b		Rikuu-Kawafune Japan	FDO	0.0	0.0	0	Endpoint: 13B-1 km beyond FB
13 b			FB	1.1	0.0	54	
13 b			FB	5.5	0.0	35	
13 b			FDO	7.0	0.0	0	Endpoint: 13B-1.5 km beyond FB
14		Aytin-Hazili, Turkey	FB	0.0	0.0	15	Endpoint: Bend in fault and range frt
14			STP	0.0	0.0	0	Endpoint: Step in range front
14			FB	5.0	0.0	25	
14			FB	10.0	0.0	30	
14			FB	18.0	0.0	13	
14			FB	31.0	0.0	20	
14			FB	40.0	0.0	35	
14			FB	55.0	0.0	0	Endpoint: Bend in fault and range frt
17		San Andreas, 1906	RSDB	0.0	0.6	0	Endpoint at Pt. Delgado?
17			RSSB	0.0	0.0	25	Endpt: jct. w/ Mendocino fracture zone
17			RSSB	13.0	0.0	17	
17			RLSB	36.0	0.0	12	
17			RLSB	86.0	0.0	13	
17			RSDB	140.0	0.3	0	
17			RLDB	146.0	0.2	0	
17			RLDB	154.0	0.3	0	
17			RLDB	158.0	0.3	0	
17			FTBR	174.0	0.0	28	
17			CFT	181.0	0.0	50	
17			RSSB	215.0	0.0	5	
17			FTBR	220.0	0.0	26	
17			RLSB	241.0	0.0	3	
17			CFT	257.0	0.0	55	
17			RSDB	266.0	0.3	0	
17			CFT	275.0	0.0	37	
17			RLDB	295.0	1.2	0	step in bay?
17			RSDB	308.0	0.5	0	step on shore?
17			FTBR	316.0	0.0	20	
17			FTBR	325.0	0.0	10	
17			RSSB	328.0	0.0	4	
17			FTBR	333.0	0.0	11	
17			FTBR	353.0	0.0	10	
17			CTC	356.0	0.0	0	increase to south
17			CFT	361.0	0.0	47	
17			CFT	362.0	0.0	40	
17			CFT	366.0	0.0	77	
17			RSDB	367.0	1.8	0	
17			CFT	374.0	0.0	60	
17			FTBR	374.0	0.0	22	
17			FTBR	379.0	0.0	19	
17			FTBR	383.0	0.0	20	
17			FTBR	384.0	0.0	21	
17			RSDB	387.0	3.5	0	
17			CTC	403.0	0.0	0	decrease to south
17			RLDB	406.0	0.0	0	
17			FTBR	419.0	0.0	17	
17			RSDB	424.0	0.5	0	
17			CSS	432.0	0.0	0	Endpoint-change to creep: R.L.=444 km
17			QB	432.0	0.0	0	Endpoint 10km north of Zayante thrust
19		Pleasant Valley	FDO	0.0	0.0	0	Endpt: End of range bounding N-dip f
19			CET	4.0	0.0	0	
19			FB	6.0	0.0	45	
19			FB	7.0	0.0	30	
19			STP	12.0	0.2	0	9-14 km
19			CET	14.0	0.0	0	
19			FB	17.0	0.0	40	
19			CFT	10.5	0.0	65	
19			STP	19.0	2.7	0	18.5-20 km
10			CET	20.0	0.0	0	
19			FB	21.0	0.0	35	
19			FB	23.0	0.0	30	
19			FB	26.0	0.0	20	
19			FB	30.0	0.0	25	
19			FB	33.0	0.0	20	
19			CET	35.0	0.0	0	
19			CTC	37.0	10.0	0	several parallel traces
19			FB	41.0	0.0	40	
19			STP	42.5	3.3	0	41-46 km
19			CET	44.0	0.0	0	
19			CSR	44.0	0.0	0	
19			CFT	51.0	0.0	0	Endpoint: at cross structure
19			FDO	51.0	0.0	0	Endpoint: R.L.=59 km or 61 km
20		Kansu, China	FDO	0.0	0.0	0	Endpoint: At RLDB
20			RLDB	5.0	5.0	0	Endpoint: 0-10 km
20			FTBR	43.0	0.0	0	
20			RLDB	47.0	0.0	0	41-53 km
20			FTBR	50.0	0.0	0	
20			FTBR	60.0	0.0	0	
20			RLSB	60.0	0.0	5	
20			FTBR	69.0	0.0	0	
20			RLSB	69.0	0.0	10	
20			RLDB	81.0	1.0	0	80-82 km
20			FTBR	95.0	0.0	0	
20			RLDB	96.5	4.0	0	95-98 km
20			FTBR	98.0	0.0	0	
20			FTBR	106.0	0.0	0	
20			RLSB	116.0	0.0	0	
20			RLDB	130.0	1.0	0	126-134 km
20			RLDB	144.0	2.0	0	142-146 km
20			STP	150.0	5.0	0	
20			CSS	200.0	0.0	0	Endpoint: change to reverse or thrust
20			RSSB	200.0	0.0	40	Endpoint
21		Xianshuihe, Qiajiao	FDBR	0.0	0.0	0	Endpoint
21			RSDB	0.0	0.3	0	Endpoint
21			RLDB	10.0	0.6	0	
21			CFT	23.0	0.0	90	
21			RSSB	23.0	0.0	3	
21			RLSB	27.0	0.0	7	

APPENDIX (cont.)

EQN	PT	FAULT, EQ	FEATURE	DISTANCE	WIDTH	ANGLE	COMMENTS
21			CFT	32.0	0.0	26	
21			RSOB	36.0	0.7	0	
21			CTC	47.0	0.0	0	multiple traces: crossfaults to 66 km
21			FTBR	66.0	0.0	0	Endpoint: rupture details unknown
21			RLDB	66.0	1.0	0	Endpoint
23	a	Gomura Japan	CTC	0.0	0.0	0	Endpoint: 23A-rupture along 3 traces
23	a		RLSB	3.2	0.0	21	
23	a		RLDB	3.7	0.2	0	
23	a		RLDB	6.3	0.2	0	
23	a		CFT	8.5	0.0	00	
23	a		RLDB	0.1	0.5	0	
23	a		RLDB	10.5	0.5	0	
23	a		RLDB	12.6	0.3	0	
23	a		FDO	13.0	0.0	0	Endpoint: 23A-past RSOB: R.L.=33 km?
23	b	Yamada Japan	RSOB	0.0	1.2	0	Endpoint: 23B
23	b		RSOB	3.4	0.0	0	
23	b		RSOB	6.0	0.3	0	
23	b		RLDB	0.1	0.3	0	Endpoint: 23B-at RLDB-0.5km
26		Rift zone, Kenya	FTBR	0.5	0.0	0	Endpoint
26			FB	1.5	0.0	0	Endpoint?
26			GAP	4.0	0.6	0	
26			FB	4.5	0.0	0	
26			FTBR	4.5	0.0	0	
26			FTBR	5.0	0.0	0	
26			GAP	8.0	0.6	0	
26			FB	13.0	0.0	0	
26			FTBR	14.0	0.0	0	
26			FB	18.0	0.0	0	
26			FTBR	18.0	0.0	0	
26			CFT	22.0	0.0	0	
26			GAP	22.0	0.3	0	
26			FTBR	23.0	0.0	0	
26			CFT	25.0	0.0	0	
26			FB	25.0	0.0	0	
26			FB	29.0	0.0	0	
26			FTBR	29.0	0.0	0	
26			FDO	32.0	0.0	0	Endpoint: R.L.=287
36		Nahetuohai-Ertai	CFT	0.0	0.0	0	Endpoint
36			QB	0.0	0.0	0	Endpoint: CSS?
36			RLDB	0.0	0.0	0	Endpoint
36			RLDB	0.0	2.0	0	
36			CFT	16.0	0.0	30	
36			RLDB	16.0	0.5	0	
36			RLDB	19.0	0.5	0	
36			GAP	21.0	2.5	0	
36			RLDB	22.0	0.6	0	
36			RSOB	30.0	0.3	0	
36			RLSB	34.0	0.0	15	
36			RSOB	36.0	0.7	0	
36			RSOB	41.0	0.3	0	
36			RLSB	44.0	0.3	0	
36			RDLB	48.0	0.3	0	
36			CFT	49.0	0.0	34	
36			CTC	80.0	20.0	0	complex fault traces to 80 km
30			RSOB	80.0	1.3	0	9 km long
36			FTBR	73.0	0.0	25	
36			QB	76.0	4.0	0	
36			FB	77.0	0.0	23	
36			FB	81.0	0.0	15	
36			FTBR	90.0	0.0	25	
36			QB	103.0	3.0	0	
36			CFT	105.0	0.0	30	
36			QB	110.0	4.0	0	
36			RLDB	111.0	1.2	0	
36			RSSB	120.0	0.0	14	
36			RLDB	124.0	0.2	0	
36			RLSB	155.0	0.0	15	
36			CTC	160.0	0.0	0	multiple fault traces
36			RLDB	165.0	1.0	0	may be 1.5 km width
3E			CTC	171.0	0.0	0	Endpoint
36			RLDB	171.0	0.0	0	Endpoint at 172 km
38		Changma, China	CFT	0.0	0.0	40	Endpoint at jct. with Altyn Tagh flt
38			STP	7.0	7.0	0	
36			GAP	15.0	5.0	0	
30			GAP	24.0	0.0	0	
DB			STP	33.0	3.0	0	
36			STP	40.0	4.0	0	
30			FB	57.0	0.0	20	
36			GAP	63.0	6.0	0	
30			CFT	71.0	0.0	45	
36			STP	73.0	0.5	0	
36			STP	77.0	0.5	0	
30			GAP	86.0	3.0	0	
36			STP	87.0	1.0	0	
36			FB	103.0	0.0	24	
30			STP	110.0	1.5	0	
36			CFT	119.0	0.0	50	Endpoint: rupture length = 116 km?
30			GAP	119.0	0.0	0	Endpoint
36			STP	110.0	11.0	0	Endpoint at major step in range front
44	a	Chihhu Taiwan	CFT	0.0	0.0	0	Endpt: 44A-jct. with another fault or FB
44	a		FB	0.0	0.0	42	Endpoint: 44A
44	a		FDBR	0.0	0.0	0	Endpoint
44	a		GAP	1.7	2.9	0	
44	a		STP	5.3	0.3	0	
44	a		STP	0.0	0.2	0	
44	a		CFT	10.7	0.0	30	
44	a		STP	10.9	0.1	0	
44	a		FB	14.5	0.0	10	

EQN	PT	FAULT, EQ	FEATURE	DISTANCE	WIDTH	ANGLE	COMMENTS
44	a		GAP	16.1	1.2	0	
44	a		FDO	17.3	0.0	0	Endpoint unknown: 44A-past RSSB?
44	b	Tuntzchio Taiwan	RSOB	0.1	0.1	0	Endpoint: 44B-at minor RSOB
44	b		CFT	0.3	0.0	50	Endpoint: 44B-Reverse cross fault
44	b		CFT	0.3	0.0	00	Endpoint: 44B
44	b		FDBR	0.3	0.0	0	Endpoint: 44B
44	b		RSOB	3.6	0.2	0	
44	b		CFD	3.7	0.0	35	
44	b		GAP	5.2	1.0	0	
44	b		RLDB	6.5	0.6	0	
44	b		GAP	6.0	1.0	0	
44	b		RSOB	8.2	0.1	0	
44	b		RLDB	10.4	0.2	0	discontinuous traces
44	b		RSOB	12.1	0.3	0	
44	b		FDBR	14.0	0.0	0	Endpoint: 44B
44	b		FDO	14.0	0.0	0	Endpoint: 44B-past RSOB
52		N. Anat. Erzincan	CTC	0.0	20.0	0	Endpoint: discontinuous traces
52			RSOB	0.0	0.0	0	Endpoint: Regional scale RSOB
52			RLDB	15.0	0.0	0	10-20 km
52			FTBR	44.0	0.0	0	
52			FTBR	67.0	0.0	0	
52			QB	67.0	10.0	0	
52			RSSB	67.0	0.0	10	
52			RLDB	94.0	6.0	0	80-106 km
52			CTC	113.0	63.0	0	multiple traces not intersectng main rup
52			FTBR	113.0	0.0	0	
52			QB	204.0	65.0	0	
52			GAP	215.0	14.0	0	
52			FTBR	235.0	0.0	0	
52			RSOB	253.0	3.0	0	247-286 km
52			RLDB	270.0	4.0	0	266-275 km
52			RSOB	281.0	4.0	0	284-298 km
52			FTBR	293.0	0.0	0	
52			QB	293.0	67.0	0	
52			FTBR	300.0	0.0	0	
52			RLDB	340.0	0.0	0	Endpoint? 321-360 km
52			QB	360.0	0.0	0	Endpoint
53		Imperial 1940	RLDB	0.0	1.0	0	Endpt: regional step to San Andreas fl
53			RLSB	2.5	0.0	26	
53			RLDB	0.5	1.5	0	
53			CFT	12.5	0.0	35	
53			RSSB	12.5	0.0	10	
53			RLDB	19.0	2.5	0	
53			CSR	26.5	0.0	0	Increase in S.R. to south
53			RSOB	30.3	0.6	0	
53			RSOB	36.5	0.6	0	
53			RLDB	50.0	12.0	0	Endpoint L=62km, step to Cerro Prieto
59		N. Anatolian Erbaa	CFT	0.0	0.0	0	Endpoint: Possible cross structure
59			DB	0.0	0.0	0	Endpoint
59			RLDB	0.0	0.0	0	Endpoint: width=?
59			GAP	4.0	3.0	0	
59			CTC	11.0	10.0	0	parallel fault
59			RSOB	11.0	1.0	0	
59			RSOB	19.0	2.0	0	18-22 km
59			FTBR	20.0	0.0	20	
50			RSOB	42.5	1.0	0	41-44 km
59			RSOB	47.0	1.0	0	46-48 km
59			FB	50.0	0.0	0	Endpoint: Bend in range front
59			QB	50.0	0.0	0	
59			RLDB	50.0	0.0	0	width=?
61	a	Sikano Japan	CFT	0.0	0.0	40	Endpt: 61A-near FB 0 jct. with Sikano fl
61	a		STP	0.0	2.0	0	Endpoint: 61A-jct. with Sikano fault
61	a		RLSB	0.5	0.0	17	61A
61	a		GAP	2.0	1.0	0	61A
61	a		RSOB	3.5	0.5	0	61A
61	a		RSSB	4.7	0.0	0	Endpoint: 61A-width = ?
61	b	Yoniaka Japan	RSOB	0.0	2.0	0	Endpoint: 61B-jct. with Yoniaka fault
61	b		GAP	0.5	1.0	0	
61	b		RSOB	2.2	0.5	0	
61	b		RSOB	3.0	0.2	0	
61	b		RSSB	5.3	0.0	21	
61	b		GAP	5.7	0.7	0	
61	b		RSOB	7.2	0.1	0	
61	b		RSSB	7.6	0.0	0	Endpoint: 61B-at minor RSSB
62		N. Anatol. Kastamonu	QB	0.0	62.0	0	Endpoint: Length of basin
62			RLDB	0.0	1.5	0	Endpoint
62			RLDB	28.0	4.0	0	19-37 km
62			RLDB	81.0	4.0	0	76-88 km
62			RSOB	109.0	4.0	0	102-116 km
62			RLDB	134.0	6.0	0	120-148 km
62			RLDB	100.0	2.0	0	162-174 km
62			RSOB	105.0	4.0	0	185-204 km
62		/	RLDB	250.0	1.0	0	
62			RLDB	280.0	0.0	0	Endpoint: R.L.=280 km?
63		N. Anatolian Bolu	FB	0.0	0.0	0	Endpoint
63			QB	0.0	10.0	0	Endpoint
63			RLDB	7.5	1.0	0	Endpoint: 0-15 km
63			RSSB	710.0	0.0	7	
63			CFT	100.0	0.0	0	Endpoint
63			RLDB	100.0	1.5	0	Endpoint
60		Fukozu, Japan	FDO	0.0	0.0	0	Endpoint unknown
60			FB	2.3	0.0	36	
00			FB	3.0	0.0	32	
60			CFT	5.6	0.0	55	
60			CFT	5.6	0.0	90	7.5 km step? segment boundary?
00			FB	6.6	0.0	26	
60			STP	0.6	0.4	0	
60			FB	14.4	0.0	50	

APPENDIX (cont.)

EQ#	PT	FAULT, EQ	FEATURE	DISTANCE	WIDTH	ANGLE	COMMENTS
60			FDO?	21.5	0.0	0	Endpoint offshore: R.L.=20 km?
111		Fort Sage Mtns	FTBR	0.0	0.0	0	Endpoint
111			FB	0.3	0.0	25	Endpoint?
111			FB	1.4	0.0	15	
111			FTBR	2.5	0.0	0	
111			FB	3.6	0.0	13	
111			CFT	4.0	0.0	0	
111			STP	4.1	0.3	0	
111			FB	5.7	0.0	15	
111			FB	6.3	0.0	20	
111			FB	0.0	0.0	20	
111			FB	8.5	0.0	17	
111			FDO	9.2	0.0	0	Endpoint
112		Coastal Range Taiwan	FDO?	0.0	0.0	0	Endpt.? Rupture continued offshore
112			CFT	3.5	0.0	90	
112			FOBR	3.5	0.0	20	
112			QB	4.0	0.0	0	basin-syncline
112			RLOB	4.0	0.4	0	
112			FDO	5.9	0.0	0	Endpoint uncertain: R.L.=? km?
113		Coastal Range Taiwan	FDO	0.0	0.0	0	Endpoint past RLOB
113			RLOB	1.0	1.2	0	Endpoint
113			RLOB	10.0	2.0	0	geometry of rupture uncertain
113			FB	20.0	0.0	7	
113			RSOB	30.0	1.0	0	Endpoint
113			FDO	40.0	0.0	0	Endpoint past RSOB
110		White Wolf Calif	FDO	0.0	0.0	0	Endpoint
110			GAP	2.3	10.5	0	2.3-21.0 km, gap in alluvium
110			STP	2.7	0.0	0	
110			GAP	23.7	8.8	0	23.7-32.6 km
110			FB	33.9	0.0	20	
110			STP	35.5	0.6	0	
110			STP	38.5	0.0	0	
110			CFT	41.0	0.0	60	
110			STP	41.0	0.5	0	
110			STP	43.2	0.3	0	
110			FB	44.4	0.0	25	
110			CFT	45.0	0.0	34	
110			FB	46.5	0.0	15	
110			CTC	46.0	5.0	0	Discontinuous traces-cross faults to end
110			CFT	49.0	0.0	60	
110			CFT	50.0	0.0	55	
110			CFT	52.0	0.0	30	Endpt.: 51.6-52.4 km: angle uncertain
110			FDO	52.0	0.0	0	Endpoint: 52-57 km
150		N. Anatolian Yemies	FDO	0.0	0.0	0	Endpoint
156			QB	5.0	22.0	0	
150			RLOB	5.0	0.5	0	4-8 km
150			RLOB	11.0	0.3	0	10.5-12 km
150			RLOB	15.0	1.0	0	13-17 km
150			FTBR	16.0	0.0	0	
156			FTBR	16.5	0.0	0	
150			FTBR	19.0	0.0	0	
150			RSOB	20.5	0.0	0	19-22 km
150			FTBR	23.0	0.0	0	
150			RSOB	26.0	0.6	0	27-29 km
150			RSOB	33.0	0.5	0	32-33.5 km
150			RSOB	00.0	0.3	0	37-38 km
150			QB	42.0	14.0	0	
156			RLOB	47.0	0.0	0	45-50 km
150			RSOB	50.5	0.5	0	55-50 km
150			CSS	00.0	0.0	0	Endpoint: Change to normal slip
150			RLSB	00.0	0.0	0	Endpoint
150		Rainbow Mtn No. 1	GAP	0.0	0.0	0	Endpoint at gap?
156			STP	0.0	0.0	0	Endpoint
150			FB	0.0	0.0	20	
150			GAP	1.2	2.0	0	
150			CTC	4.0	0.0	0	
150			STP	4.0	0.6	0	
150			CTC	7.0	0.0	0	
150			STP	9.5	0.4	0	
150			CTC	10.0	0.0	0	
150			FTBR	10.0	0.0	0	
150			FB	10.2	0.0	33	
150			FB	11.0	0.0	20	
150			FB	16.0	0.0	35	
150			FB	16.6	0.0	40	
150			CTC	17.5	0.0	0	
150			FB	17.5	0.0	20	
150			FB	10.0	0.0	30	
150			CFT	19.0	0.0	0	Endpoint
150			FDO	19.0	0.0	0	Endpoint: R.L.=20km
159		Rainbow Mtn No. 2	FBO	0.0	0.0	0	Endpoint
159			FB	0.0	0.0	25	
159			STP	0.0	1.5	0	
159			FB	10.0	0.0	22	
159			GAP	10.0	2.5	0	
159			STP	11.0	0.6	0	
159			FB	10.5	0.0	25	
159			FTBR	19.0	0.0	0	
159			QB	10.0	0.0	0	
159			GAP	20.5	1.0	0	
159			GAP	23.0	3.4	0	
159			FB	20.0	0.0	30	Endpoint: R.L.=26 km?
101		Dixie Valley	CTC	0.0	2.0	0	Endpt: breakup in traces at secondary fl
101			FB	0.0	0.0	10	Endpoint
101			CTC	2.0	0.0	0	two parallel traces
101			STP	2.0	1.5	0	2.5-3.0 km
101			STP	2.0	0.5	0	2.5-3.0 km
101			FB	3.0	0.0	30	

EQ#	PT	FAULT, EQ	FEATURE	DISTANCE	WIDTH	ANGLE	COMMENTS
161			CET	7.0	0.0	0	
161			FB	7.5	0.0	90	
161			FB	0.0	0.0	25	
161			FB	13.0	0.0	55	
161			CET	17.0	0.0	0	
161			CET	25.0	0.0	0	
161			FB	31.0	0.0	35	
161			CET	30.0	0.0	0	
161			CTC	30.0	5.0	0	breakup into several parallel traces
161			STP	30.5	1.0	0	30-39 km
161			STP	53.0	3.0	0	50-56 km
161			CFT	54.0	0.0	0	possible cross fault?
161			CTC	56.0	3.0	0	multiple parallel traces
161			CFT	61.0	0.0	0	Endpoint at Walker Lane flt?
162		Fairview Peak	FB	0.0	0.0	25	Endpoint
162			STP	0.0	0.0	0	Endpoint
162			FB	3.0	0.0	50	
162			FB	6.0	0.0	10	
162			CTC	9.0	21.0	0	multiple traces
162			FB	0.0	0.0	20	
162-			FTBR	15.0	0.0	0	
102			CSS	19.0	0.0	0	Changes from up to west to down to west
162			FB	20.5	0.0	20	
162			STP	32.5	0.3	0	32-33 km
162			FB	34.0	0.0	20	
162			FTBR	30.0	0.0	0	
162			STP	30.0	1.0	0	31-30.5 km
162			FB	30.0	0.0	30	
162			FB	42.0	0.0	30	
162			CTC	42.5	3.5	0	fault breaks up
162			STP	43.0	1.0	0	42.5-44 km
162			FB	44.0	0.0	65	
162			FTBR	44.0	0.0	0	
162			FB	46.0	0.0	45	
162			FB	49.0	0.0	20	
162			CTC	50.0	0.0	0	fault breaks up
162			STP	53.0	1.0	0	52.5-53.5 km
162			STP	53.5	1.5	0	53-54 km
162			CFT	62.0	0.0	0	Endpoint: R.L.=47 km or 36 km?
162			CTC	62.0	0.0	0	Endpoint: fault breaks up
171		San Miguel Mexico	RLOB	0.0	0.2	0	Endpoint
171			RSOB	0.4	0.2	0	0.3-0.6 km (0.15 km)
171			RLOB	2.5	0.5	0	2.0-3.0 km
171			RSOB	5.0	0.0	0	4.5-5.5 km
171			FTBR	5.5	0.0	0	
171			STP	0.5	0.1	0	0.4-6.7 km
171			RLOB	7.0	0.1	0	7.5-7.7 km (0.05 km)
171			RSOB	0.9	0.0	0	0.2-9.0 km
171			FTBR	9.0	0.0	0	
171			FB	10.2	0.0	25	
171			FTBR	11.3	0.0	0	
171			RSOB	11.6	0.1	0	11.6-11.7 km
171			STP	12.0	0.2	0	12.7-12.9 km
171			FTBR	15.0	0.0	0	
171			RLOB	10.0	0.7	0	17.0-10.5 km
171			CSS	22.0	0.0	0	Endpoint? normal faulting to S
171			GAP	22.0	3.0	0	Endpoint?
100		N. Anatolian Abant	RSOB	0.0	3.0	0	Endpoint: 0-6 km
100			GAP	0.0	3.0	0	
100			CTC	17.0	0.0	0	11 traces
100			RLSB	37.0	0.0	11	30-45 km
100			RSOB	39.0	1.5	0	34-43 km
100			RSOB	47.0	2.0	0	Endpoint
100			FB	50.0	0.0	0	Endpoint
100			RLOB	50.0	0.0	0	Endpoint
104		Gobi-Altai Mongolia	CFT	0.0	0.0	0	Endpoint
104			CTC	0.0	0.0	0	Endpoint
104			RSOB	0.0	10.0	0	Endpoint
104			FTBR	5.0	0.0	0	
104			RLOB	22.5	1.0	0	20-25 km
104			FTBR	34.0	0.0	0	
104			FTBR	47.0	0.0	0	
104			RLOB	55.0	2.0	0	50-60 km
104			CTC	62.0	0.0	0	
104			FTBR	62.0	0.0	0	
104			RSOB	65.0	3.0	0	60-70 km
104			RSSB	77.0	0.0	15	
104			RSOB	94.5	1.0	0	01-90 km
104			RLOB	102.5	1.0	0	101-104 km
104			CTC	100.0	0.0	0	
104			RLOB	109.5	3.0	0	100-109 km
104			RSOB	119.5	3.0	0	119-120 km
104			CTC	120.0	0.0	0	
104			FTBR	130.0	0.0	0	
104			FTBR	130.0	0.0	0	
104			RSOB	140.0	2.0	0	130-143 km
104			CFT	160.0	0.0	0	
104			RLSB	160.0	0.0	25	
104			CTC	170.0	0.0	0	
104			FTBR	175.0	0.0	0	
104			RSOB	179.0	1.5	0	176-102 km
104			CTC	100.0	0.0	0	
104			RSSB	100.0	0.0	10	
104			CTC	195.0	0.0	0	
104			CTC	200.0	0.0	0	
104			RSSB	206.0	0.0	30	
104			FTBR	204.0	0.0	0	
104			CFT	206.0	0.0	0	

APPENDIX (cont.)

EQN	PT	FAULT, EQ	FEATURE	DISTANCE	WIDTH	ANGLE	COMMENTS
184			FTBR	200.0	0.0	0	
184			FTBR	220.0	0.0	0	
184			RSDB	225.0	5.0	0	220-231 km
184			CTC	230.0	0.0	0	
184			FTBR	231.0	0.0	0	
184			CFT	245.0	0.0	0	Endpoint: Reverse cross fault
184			CTC	245.0	0.0	0	Endpoint: R.L.=270 km?
184			RSDB	245.0	0.0	0	Endpoint
185		Hebgen Lake	CFT	0.0	0.0	0	Endpoint: Jct with Laramide Thrust
189			FB	0.5	0.0	50	Endpoint
190			STP	2.3	0.0	0	
190			CFT	3.0	0.0	70	intersecting fault?
190			CTC	3.0	13.0	0	intersecting traces, gaps
188			CFT	5.5	0.0	70	
188			FB	10.0	0.0	20	
189			FB	11.0	0.0	45	
189			GAP	13.0	3.0	0	
189			CFT	16.0	0.0	90	bends back into rupture
189			CTC	16.0	10.0	0	breaks into several smaller traces
189			FB	21.0	0.0	45	
189			FB	25.0	0.0	50	Endpoint: R.L.=28 km
207		Ipak, Iran	CFT	0.0	0.0	0	Endpoint
207			CFT	9.0	0.0	0	
207			GAP	9.0	0.0	0	
207			RSSB	0.0	0.0	45	
207			RSDB	21.0	0.5	0	20-22 km
207			GAP	22.0	12.0	0	
207			FTBR	35.0	0.0	0	
207			RSDB	37.0	1.7	0	34.5-39 km
207			RLDB	41.0	2.5	0	46.5-48 km
207			CTC	57.0	0.0	0	
207			RSDB	60.0	4.0	0	56-65 km
207			RLDB	75.0	0.3	0	74-75.5 km
207			RLDB	82.0	0.4	0	80-83.5 km
207			RSDB	87.0	0.4	0	86-88 km
207			RLDB	89.5	0.6	0	88-90 km
207			RSDB	92.0	1.5	0	90.5-93 km
207			RSDB	90.0	0.5	0	87-89 km
207			CFT	90.0	0.0	0	Endpoint: R.L.=100 or 80 km?
230		San Andr. Parkfield	GAP	0.6	3.6	0	Endpoint: 0.6-4.2 km
230			RSDB	1.7	0.1	0	Endpoint? 1.3-2.0 km: N of Middle Mtn
230			RLDB	4.7	0.2	0	4.3-5.1 km
230			GAP	4.0	0.0	0	4.0-5.7 km
230			RLSB	6.4	0.0	10	At nucleation point
230			GAP	6.0	3.0	0	6.9-10.7 km
230			RSDB	9.1	0.1	0	8.8-9.4 km
230			CTC	10.7	0.0	0	
230			RLSB	11.7	0.0	5	
230			OB	17.0	21.5	0	17-38.5 km: ends at south termination
230			CTC	19.0	0.0	0	
230			RLDB	22.1	0.2	0	21.0-22.4 km
230			RSDB	22.0	0.2	0	22.5-23.2 km
230			RLDB	26.0	0.4	0	25.4-26.6 km
230			RLSB	27.5	0.0	10	
230			RLDB	30.9	1.0	0	29.5-32.3 km
230			RLDB	37.7	0.2	0	Endpoint: 37-38.5 km
230			FC	38.5	0.0	0	Endpoint: Surface rupture "crept" south
234		N. Anatolian Yerto	RSSB	0.0	0.0	0	Endpoint
234			RSDB	3.0	2.0	0	
234			RSDB	0.0	2.6	6	
234			RSDB	20.0	1.0	0	Endpoint
242		N. Anat. Rudurnu Vly	CSS	0.0	0.0	0	Endpoint
242			FDO	0.0	0.0	0	Endpoint: Across RLDB
242			RLDB	0.0	0.1	0	Endpoint: 0-5 km
242			GAP	6.0	16.0	0	
242			GAP	23.0	3.0	0	
242			GAP	27.5	3.5	0	
242			GAP	32.0	1.5	0	
242			CTC	33.5	0.5	0	multiple traces
242			GAP	34.0	1.0	0	
242			RLDB	38.0	1.1	0	36-39.5 km
242			RLDB	42.0	0.5	0	41-43 km
242			FTBR	44.5	0.0	0	
242			RSDB	47.0	0.7	0	46-48 km
242			CTC	49.0	1.0	0	parallel faults
242			RSDB	49.0	0.0	0	48-50 km
242			RLDB	51.0	0.2	0	50.5-51.5 km
242			RSDB	54.0	0.5	0	52.5-55 km
242			RLDB	56.5	0.3	0	56-57 km
242			CTC	58.0	3.5	0	parallel faults
242			RSDB	60.0	0.9	0	58-61.5 km
242			CTC	62.5	7.5	0	break-up in traces
242			RLDB	66.0	2.2	0	62.5-70 km
242			RSDB	70.5	0.2	0	70-71 km
242			RLDB	74.0	0.4	0	72.5-75 km
242			RSDB	76.0	0.2	0	75-77 km
242			RLDB	78.0	0.2	0	77.5-79 km
242			CTC	78.3	0.7	0	parallel & orthog. flts. not intersecting
242			FTBR	78.3	0.0	0	
242			CTC	88.5	1.5	0	fault branches
242			FTBR	88.5	0.0	0	
242			FTBR	92.0	0.0	0	
242			RLDB	83.0	0.2	0	Endpoint: 82.5-84 km
244		Xianshuiha Zhuwo	FTBR	0.0	0.0	0	Endpoint
244			RLDB	0.0	0.4	0	Endpoint at RLDB
244			RLDB	5.4	0.5	0	rupture details unknown
244			CFT	14.1	0.0	10	Endpoint: rupture length = 12 km ?
244			RSDB	14.1	0.3	0	Endpoint at RSDB?

EQN	PT	FAULT, EQ	FEATURE	DISTANCE	WIDTH	ANGLE	COMMENTS
247	a	Inatori Japan	FTBR	0.0	0.0	0	Endpoint: 247A-past RLDB
247	a		RLDB	0.3	0.1	0	Endpoint? 247A
247	a		RLDB	1.2	0.3	0	A
247	a		RLSB	1.6	0.0	22	A
247	a		RSDB	1.9	0.1	0	A
247	a		RSDB	2.6	0.1	0	A
247	a		FDO?	3.2	0.0	0	Endpt? 247A-rupture continues offshore
247	b	Senganyama Japan	FDO	0.0	0.0	0	Endpoint: 247B-past minor RLDB
247	b		RLDB	0.5	0.2	0	
247	b		GAP	1.0	0.7	0	
247	b		RSDB	1.5	0.3	0	
247	b		GAP	2.2	0.3	0	
247	b		FDO?	2.7	0.0	0	Endpoint? Rupture continued offshore
252		San Jac. Borrego Mtn	CFT	0.0	0.0	52	Endpoint
252			RSDB	0.0	0.0	0	Endpoint:step to Clark fault? width=?
252			CFT	1.0	0.0	46	
252			RLSB	1.0	0.0	26	
252			RLDB	9.0	0.3	0	
252			RSDB	10.5	1.0	0	
252			RLDB	15.0	0.2	0	
252			RLDB	20.5	1.0	0	
252			RSDB	23.0	0.5	0	
252			RSDB	26.5	0.3	0	
252			RSDB	26.5	0.3	0	
252			RSDB	31.0	0.2	0	Endpoint: fault dies out?
277		Qasht-e-Bayaz Iran	CFT	0.0	0.0	0	Endpoint
277			RLDB	0.0	0.2	0	Endpoint
277			FTBR	3.2	0.0	0	
277			RLDB	5.0	0.2	0	4.0-5.2 km
277			FTBR	6.3	0.0	0	
277			FTBR	7.1	0.0	0	
277			RLDB	9.0	0.5	0	9.2-10.0 km
277			FTBR	10.0	0.0	0	
277			RLDB	24.0	1.5	0	21-27 km
277			FTBR	27.0	0.0	0	
277			RLSB	32.5	0.0	15	
277			FTBR	30.0	0.0	0	
277			FTBR	40.5	0.0	0	
277			FTBR	40.7	0.0	0	
277			FTBR	44.0	0.0	0	
277			RSDB	44.0	3.0	0	39-49 km
277			FTBR	49.5	0.0	0	
277			FTBR	54.0	0.0	0	
277			FTBR	57.5	0.0	0	
277			RSDB	58.0	2.0	0	54-61.5 km
277			CFT	60.5	0.0	0	
277			FTBR	64.5	0.0	0	
277			RSDB	66.0	0.6	0	64.5-67 km
277			RLDB	73.0	0.2	0	Endpoint: 73-80 km
277			FTBR	80.0	0.0	0	Endpoint
281		Alasehir Vly Turkey	FB	0.0	0.0	15	Endpoint - ends in basin
281			FB	10.0	0.0	25	
281			FB	15.0	0.0	15	
281			FB	20.0	0.0	25	
281			FB	25.0	0.0	20	
281			CTC	30.0	0.0	0	Endpoint: FDO in basin?
281			FB	30.0	0.0	0	Endpoint: Bend in range front
289		Huaytapallana Peru	RLSB	0.0	0.0	0	Endpoint: Regional scale bend
289			RSDB	5.6	0.3	0	
289			STP	6.3	0.3	0	RLDB?
289			GAP	9.3	3.3	0	
289			RSDB	13.2	0.4	0	
289			FB	16.8	0.0	5	
289			CTC	18.0	0.0	0	Endpoint: R.L.=16 km?
289			FB	18.0	6.6	18	Endpoint
289			RLDB	18.8	0.0	0	Endpoint: Regional scale bend
290		Qujiang/Tonghai	CFT	0.0	0.0	46	Endpoint
290			RSDB	0.0	0.4	0	Endpoint in basin
290			OB	4.0	0.0	0	
290			CFT	7.0	0.0	85	
290			RLSB	7.0	0.0	11	
290			OB	9.0	0.0	0	
290			FTBR	10.0	0.0	27	
290			RSSB	10.5	0.0	12	
290			CFT	14.5	0.0	90	
290			RSSB	10.0	0.0	0	
290			CFT	19.5	0.0	90	
290			CFT	22.0	0.0	75	
290			RSDB	24.0	0.7	0	
290			CFT	30.0	0.0	90	
290			RSDB	31.5	4.0	0	Regional step at 27-36 km
290			CFT	32.5	0.0	80	
290			RLDB	32.5	6.4	0	
290			CFT	33.0	0.0	90	
290			OB	35.0	0.0	0	
290			CFT	36.0	0.0	90	
290			RLDB	36.0	0.5	0	
290			RSDB	36.0	0.7	0	
290			CFT	40.0	0.0	90	
290			CFT	44.0	0.0	30	Endpoint at 45 km past CFT
292		Gediz Turkey	CTC	0.0	0.0	0	Endpoint - parallel fault traces
292			STP	0.0	0.1	0	Endpoint, 0-0.5 km
292			STP	1.0	0.2	0	1-1.5 km
292			STP	5.0	0.5	0	4.5-5.0 km
292			STP	7.0	0.0	0	6-6.5 km
292			FTBR	0.5	0.0	0	
292			FB	10.0	0.0	40	
292			GAP	11.0	1.5	0	

APPENDIX (cont.)

EQN	PT FAULT, EQ	FEATURE	DISTANCE	WIDTH	ANGLE	COMMENTS
292		STP	12.5	1.1	0	12-13 km
292		STP	16.0	0.2	0	15.5-16.2 km
292		STP	17.0	0.2	0	17-17.5 km
292		FB	19.5	0.0	40	
292		GAP	19.5	0.5	0	
292		GAP	20.5	0.5	0	
292		GAP	22.5	0.5	0	
292		FTBR	24.0	0.0	0	
292		STP	28.0	1.1	0	
292		FB	30.0	0.0	30	
292		GAP	31.5	3.5	0	
292		CSS	36.5	0.0	0	RL to LL slip at bend
292		FTBR	36.5	0.0	0	
292		FB	37.5	0.0	90	
292		GAP	38.5	1.0	0	
292		FB	39.0	0.0	30	
292		FB	41.0	0.0	80	
292		FTBR	42.0	0.0	0	Endpoint
300	San Fernando	CSR	0.0	0.0	0	Endpoint: chg in recency of activity
300		FB	0.0	0.0	0	Endpoint - regional bend
300		FB	0.0	0.0	25	
300		FB	2.2	0.0	21	
300		CFT	0.3	0.0	40	
300		STP	10.0	1.3	0	
300		FB	12.3	0.0	20	may be part of step
300		GAP	12.9	1.1	0	
300		STP	13.1	0.4	0	
300		GAP	14.7	1.7	0	
300		FB	16.0	0.0	0	Endpoint at regional scale bend
300		FDO	16.0	0.0	0	Endpoint - uncertain
315	Xianshuihe Luhuo	RLDB	0.0	0.0	0	Endpoint at regional scale RLDB
315		RLDB	1.0	0.2	0	
315		RSSB	7.0	0.0	0	
315		RLSB	16.5	0.0	12	
315		RLDB	20.7	0.4	0	
315		RLDB	26.1	0.5	0	
315		FTBR	36.0	0.0	19	
315		RSDB	34.0	0.3	0	
315		FTBR	41.0	0.0	26	
315		CFT	44.7	0.0	30	
315		RSDB	45.9	1.2	0	
315		CFT	48.9	0.0	40	
315		RSDB	51.6	0.3	0	
315		CFT	54.4	0.0	90	
315		CFT	57.7	0.0	70	
315		RSDB	60.3	0.3	0	
315		CFT	61.3	0.0	90	
315		CFT	66.4	0.0	80	
315		CFT	68.1	0.0	90	
315		RSDB	68.1	0.2	0	
315		RSDB	72.9	0.5	0	
315		RSDB	77.7	0.3	0	
315		RLDB	80.0	0.6	0	Endpoint: at 80-85 km
323	Irozaki Izu-oki Jap	FDO?	0.0	0.0	0	Endpoint offshore
323		CTC	1.5	0.0	0	0-1.5 km: 3 fault traces: 1.5 km: 1 flt.
323		FB	3.1	0.0	6	
323		FTBR	3.0	0.0	13	
323		RLDB	5.0	0.1	0	
323		FDO	6.1	0.0	0	Endpoint past minor restraining bend
337	Galway Lake	RLDB	0.4	0.2	0	Endpoint at 0.0-0.4?
337		GAP	1.0	1.1	0	
337		RLDB	3.7	0.3	0	
337		RLDB	5.0	0.2	0	Endpoint??
337		FDO	6.0	0.0	0	Endpoint?
337		CFT	8.0	0.0	0	Endpoint? Jct with Emerson fault
342	Oroville Cleve. Hill	FDO	0.0	0.0	0	Endpt: discontinous features to north
342		FB	2.0	0.0	30	
342		FDO	4.0	0.0	0	Endpoint- R.L.=15 km??
353	Caldiran Turkey	CFT	0.0	0.0	0	Endpoint
353		FTBR	6.0	0.0	0	
353		RSDB	10.5	1.0	0	10-11 km
353		RLDB	14.0	1.0	0	13-15 km
353		FTBR	21.0	0.0	0	
353		FTBR	22.0	0.0	0	
353		RSDB	25.5	0.5	0	25-26 km
353		RLDB	28.0	1.5	0	27-28.5 km
353		RSDB	30.0	0.5	0	29-31.5 km
353		GAP	30.0	2.5	0	
353		RLDB	39.0	1.5	0	37-41 km
353		GAP	42.5	3.5	0	
353		RSDB	46.5	1.0	0	42-47 km
353		RSDB	55.0	5.0	0	Endpoint: Possible RSDB
360	Nuhbanan-Zarand Iran	RLDB	0.0	0.2	0	Endpoint
350		RLDB	4.9	0.2	0	4.0-5.0 km
350		RSDB	7.0	0.2	0	6-8 km
350		RLDB	12.7	0.2	0	12.5-12.8 km
350		RLDB	19.0	1.0	0	Endpoint
356		STP	19.0	0.0	0	Endpoint: Range front discontinuity
383	Tabas-e-Golshan Iran	FDO	0.0	0.0	0	Endpoint or GAP
383		FB	4.0	0.0	35	
383		STP	8.0	0.0	0	
383		FB	19.0	0.0	40	
383		GAP	21.0	5.0	0	
383		CTC	30.0	6.0	0	
383		STP	30.0	0.5	0	
383		STP	30.5	2.0	0	
383		FB	39.0	0.0	30	
383		GAP	42.0	7.0	0	

EQN	PT FAULT, EQ	FEATURE	DISTANCE	WIDTH	ANGLE	COMMENTS
363		STP	42.0	2.5	6	
363		CTC	46.6	0.0	6	
363		FB	52.0	0.0	40	
363		CTC	62.0	0.0	0	
363		STP	70.0	7.5	6	
363		FB	71.0	0.0	30	
363		GAP	61.0	1.0	0	
363		CTC	82.0	0.0	0	
363		FTBR	82.0	0.0	0	
363		STP	82.0	4.0	0	
363		FB	88.0	0.0	45	Regional fault bend
363		FB	91.0	0.0	45	Regional fault bend
363		FDO	95.0	0.0	0	Endpoint: R.L.=85 km? GAP?
360	Imperial 1979	QB	0.0	0.0	0	Endpt: between San Andreas & Imperial fl
360		RLDB	0.0	0.0	0	Endpoint: Regional RLSB to San Andreas
360		RLSB	1.5	0.0	43	
360		RLDB	4.0	1.0	6	
360		RLSB	8.5	0.0	26	
360		RLDB	10.5	1.5	0	
360		CFT	16.5	0.0	35	
360		RSSB	16.5	0.0	10	
360		RLDB	23.0	0.3	0	
360		CSS	30.5	0.0	0	Endpoint: CSS of 1940 EQ
369	Abiz Ghaenat Iran	CFT	0.0	0.0	0	Endpoint
369		GAP	2.5	2.0	0	
369		RLSB	5.0	0.0	25	
369		GAP	11.0	2.0	0	
369		RLSB	17.0	0.0	20	
368		FTBR	25.0	0.0	0	?
369		RLSB	25.0	0.0	17	R.L.=20 km?
369		CFT	30.0	0.0	0	Endpoint
369		RLDB	30.0	1.5	0	Endpoint: broad releasing bend
370	Kali Ghaenat Iran	FTBR	0.0	0.0	0	Endpoint
370		RSDB	0.0	0.0	0	Endpoint
370		FTBR	3.5	0.0	0	
370		RSDB	4.0	2.0	0	Endpoint: 0-7.5 km
370		CFT	6.5	0.0	0	
370		FTBR	10.5	0.0	0	
370		RSDB	12.0	0.0	0	10.5-13 km
370		RLDB	20.0	0.2	0	19-21 km
370		RLDB	35.5	1.0	0	34-37 km
370		RSDB	39.0	2.5	0	37-42 km
370		RSDB	52.0	1.0	0	50-55 km
370		CFT	57.0	0.0	0	
370		RLDB	57.5	1.0	0	Endpoint: 55-60 km
372	El Asnam Algeria	FDO	0.0	0.0	0	Endpoint
372		FB	1.0	0.0	35	
372		STP	2.6	0.3	0	2.5-2.7 km
372		FB	3.3	0.0	35	
372		GAP	3.5	0.4	0	
372		FB	5.1	0.0	20	
372		CTC	8.2	0.0	0	
372		CTC	10.7	0.0	0	
372		FB	10.7	0.0	35	
372		CTC	12.0	0.R	0	
372		FB	13.5	0.0	30	
372		CTC	19.7	0.0	0	
372		CTC	21.0	0.0	0	
372		FB	22.0	0.0	35	
372		GAP	23.5	0.7	0	
372		CFT	28.5	0.0	0	Endpoint: SS CFT not active?
372		FDBR	26.5	0.0	0	Endpoint?
373	Xianshuihe Daofu	RSDB	0.0	0.7	0	Endpoint: 0-1 km?
373		RLDB	15.0	1.0	0	
373		CFT	17.0	0.0	70	
373		CFT	20.0	0.0	90	
373		RSSB	20.0	0.0	22	
373		CFT	21.6	0.0	85	
373		RLSB	29.0	0.0	16	
373		CFT	30.0	0.0	65	
373		CFT	33.0	0.0	85	
373		RSDB	38.0	0.7	0	
373		GAP	40.0	0.0	0	
373		RT	49.0	0.0	0	Endpoint: R.L.=48 or 49 km?
374	Gowk Golbaf Iran	CTC	0.0	0.0	0	Endpoint
374		FDO	0.0	0.0	0	Endpoint?
374		RSDB	0.0	1.0	0	Endpoint: 0-7 km
374		STP	0.2	1.0	0	
374		STP	6.0	1.5	0	
374		RLDB	6.5	0.0	0	5-0 km
374		RLDB	17.0	1.5	0	Endpoint: 15-20 km: R.L.=15 km?
375	Gowk Sirch Iran	CSS	0.0	0.0	0	Endpoint: Change to reverse slip
375		FB	0.0	0.0	0	Endpoint
375		RSDB	0.0	0.0	0	Endpoint: width < 1 km
375		RSSB	5.0	0.0	15	
375		FTBR	6.0	0.0	0	
375		CTC	10.0	0.0	0	
375		CFT	12.0	0.0	0	
375		GAP	14.0	2.0	0	
375		RLDB	15.0	0.0	0	10-30 km - near jct. with reverse flts.
375		CFT	20.0	0.0	0	
375		FTBR	20.0	6.0	0	
375		FTBR	32.0	0.0	0	
375		GAP	33.0	4.0	0	
375		CTC	38.0	0.0	0	
375		CFT	37.0	0.0	0	
375		RLDB	40.0	1.5	0	
375		RLDB	50.0	0.5	0	57.5-50.5 km

APPENDIX (cont.)

EQN	PT	FAULT, EQ	FEATURE	DISTANCE	WIDTH	ANGLE	COMMENTS
375			GAP	66.0	0.0	0	Endpoint
375			RSDB	66.0	0.0	0	Endpoint: width < 1 km
377		Lost River Borah Pk	RT	0.0	0.0	0	Endpoint: rupture terminates, no FDO
377			CTC	3.0	2.0	0	several parallel traces
377			FB	6.0	0.0	25	
377			FB	7.0	0.0	55	
377			CSR	8.0	0.0	0	
377			GAP	8.0	5.0	0	
377			CSR	13.0	0.0	0	
377			CTC	13.0	3.0	0	discontinuous curving traces
377			CFT	16.0	0.0	30	
377			FB	16.0	0.0	40	
377			FB	16.5	0.0	45	
377			CTC	19.0	4.0	0	multiple traces, various orientations
377			FB	22.0	0.0	40	
377			FB	23.0	0.0	45	
377			CTC	24.0	4.0	0	short parallel traces
377			FB	24.0	0.0	20	
377			FB	26.0	0.0	30	
377			FB	28.0	0.0	30	
377			FB	29.0	0.0	40	
377			FB	29.5	0.0	35	
377			CTC	31.0	3.0	0	gaps, parallel traces
377			STP	32.0	0.5	0	31-33 km
377			CFT	34.0	0.0	0	Endpoint: Eocene cross faults
377			FB	34.0	0.0	55	Endpoint: Regional bend in range front
377			GAP	34.0	0.0	0	Endpt: 4 km gap in late Quaternary scarp
381		Homestead Valley	RSDB	0.0	0.3	0	Endpoint: at bedrock high
381			RLDB	1.5	0.2	0	
381			RLDB	2.2	0.2	0	
381			RLDB	2.0	0.2	0	
381			CFT	3.4	0.0	50	
381			RLDB	3.4	0.1	0	
381			RSDB	3.9	0.6	0	Endpt: bedrock high, aftershock x-trend
384		Zhaduotang Xianshui	RSDB	0.0	3.0	0	Endpt. at regional RSDB - to Kangding fl
384			RLDB	7.5	0.4	0	
384			RLDB	10.6	0.0	0	rupture details unknown
384			RLDB	17.0	0.5	0	
384			RLSB	24.0	0.0	40	
384			RLDB	27.0	0.0	0	Endpt. at regional RLDB - to Selaha faul
389		E. Anatolian Bingol	CFT	0.0	0.0	0	Endpoint at cross-structure
389			QB	0.0	4.5	0	Endpoint
389			RLDB	0.0	0.3	0	Endpt. at SW end of RLDB-3.3 km long
389			FTBR	2.5	0.0	0	
389			RSDB	2.5	0.0	0	1.5-3.5 km: near endpoint
389			GAP	4.5	13.0	0	4.5-17.5 km
389			FTBR	6.5	0.0	0	
389			FTBR	7.5	0.0	0	
389			RSDB	8.5	0.5	0	7-16 km long, 0.3-0.8 km wide
389			FTBR	12.0	0.0	0	
389			CFT	14.2	0.0	0	
389			RLDB	14.0	0.0	0	13.3-16.3 km
389			RLDB	18.0	0.2	0	18-28 km
389			GAP	20.0	1.3	0	20-21.3 km
389			CTC	21.5	0.0	0	
389			RSDB	22.0	0.5	0	21.3-22.5 km
389			FTBR	24.0	0.0	0	
389			QB	24.0	11.0	0	11 km wide
389			FTBR	26.0	0.0	0	
389			RLDB	26.0	1.0	0	26-27.5 km
389			CTC	29.5	0.0	0	
389			GAP	31.5	4.3	0	31.5-35.8 km
389			CFT	34.5	0.0	0	
389			RSDB	38.0	18.0	0	Endpoint at NE end of RSDB-46 km long
398		White Mtn Chalfant	CSR	0.0	0.0	0	Endpoint: 0-2.0 discontinuous trace
398			GAP	2.0	2.2	0	
398			RSSB	5.5	0.0	20	
398			RLSB	17.3	0.0	17	
398			RLDB	14.3	0.3	0	
398			FDO?	15.0	0.0	0	Endpoint: R.L.=0.0 km?
398			RSDB	18.0	0.2	0	Endpoint?
500		Baghan-Germab Iran	FTBR	0.0	0.0	0	Endpoint
500			RSDB	0.0	0.0	0	Endpoint
500			FTBR	3.0	0.0	0	
500			CFT	5.0	0.0	0	cross faults or folds?
500			RSDB	12.0	3.0	0	
500			CFT	14.5	0.0	0	
500			FTBR	21.0	0.0	0	
500			CFT	27.0	0.0	0	
500			CFT	35.0	0.0	0	
500			CFT	45.0	0.0	0	
500			CFT	48.0	0.0	0	
500			QB	52.0	0.0	0	
500			CFT	55.0	0.0	0	
500			RLDB	57.0	6.0	0	Endpoint? R.L.=68-78 km?
503		Superstition Hills	CFT	0.0	0.0	75	Endpoint
503			RLDB	0.0	0.2	0	Endpoint: 0-0.2 km, w=.16
503			RLDB	2.7	0.1	0	2.6-2.8 km, w=.04
503			RLSB	4.0	0.0	15	
503			CFT	4.0	0.0	50	
503			RLSB	5.0	0.0	0	
503			RLDB	7.0	0.1	0	6.8-7.2 km, w=.06
503			CTC	11.2	0.0	0	Parallel fault traces
503			RLDB	14.0	0.3	0	13.2-14.8 km, w=.32
503			CTC	15.0	0.0	0	Single trace
503			CTC	17.6	1.0	0	Multiple, parallel fault traces
503			RSDB	20.0	0.1	0	19.6-20.4 km, w=.012
503			CFT	22.7	0.0	40	Endpoint
503			RLDB	23.0	0.1	0	Endpoint: 22.0-23.1 km, w=.08

EXPLANATION

EQN — Earthquake number. As in Table 2.

PT — Part of the rupture. A letter is appended for multiple surface ruptures associated with a single earthquake. Most of these parts are conjugate faults.

FAULT, EQ — Brief indicator of the earthquake being listed.

FEATURE — Type of feature. See Table 1 for list of abbreviations.

DISTANCE — Distance from the west or north end of fault to feature. For fault bends, distance is to inflection point. For basins and gaps, distance is to beginning of feature. For double bends and steps, distance is to midpoint, except when feature is located at a termination point. Distance is to beginning of feature for END 0 and to end of feature for END X.

WIDTH — Map width of double bends, or length of gaps and basins.

ANGLE — Change in strike direction for single bends, and acute angle of intersection for cross and branch faults and folds.

COMMENTS — Includes identification of features considered to form endpoints for each rupture, range (beginning and end) of double bends and steps, and other characteristics of the rupture.

SEGMENTATION MODELS AND HOLOCENE MOVEMENT HISTORY OF THE WASATCH FAULT ZONE, UTAH

by

[1]Michael N. Machette, [1]Stephen F. Personius, [1]Alan R. Nelson
[2]David P. Schwartz, and [3]William R. Lund

[1]U.S. Geological Survey, Denver, Colorado
[2]U.S. Geological Survey, Menlo Park, California
[3]Utah Geological and Mineral Survey, Salt Lake City, Utah

INTRODUCTION

The Wasatch fault zone (WFZ) is one of the longest and most active extensional fault zones in the western United States. It is the main structural component of a prominent transition zone that separates the eastern part of the Basin and Range province from the western margin of the Colorado Plateaus and middle Rocky Mountains provinces. The late Quaternary trace of the WFZ extends 343 km from Malad City, Idaho, to Fayette, Utah (fig. 1), and is marked by large scarps on glacial, lacustrine, colluvial and alluvial deposits of middle to late Pleistocene age as well as smaller scarps on Holocene deposits.

Previous studies

Although the WFZ has been the subject of scientific interest since the pioneering work of G.K. Gilbert almost 100 years ago (Gilbert, 1890, 1928; Machette, 1988), the first systematic study of the fault zone was not undertaken until the 1970's. That study was conducted by Cluff and others (1970, 1973, 1974) using low-sun-angle aerial photographs to map the surface trace of the WFZ from Malad City, Idaho, to Gunnison, Utah. As an extension of their reconnaissance, geologists at Woodward-Clyde Consultants made detailed investigations of four trench sites along the WFZ during the period 1978-1982. Their work resulted in many preliminary (contract) reports and culminated in two major synthesis reports that highlighted paleoseismological aspects of the WFZ. In the first of these reports, Swan and others (1980) speculated on the number of possible segments for the WFZ: they suggested at least 6 on the basis of modern microseismicity to as many as 10 on the basis of geometric variations along the fault zone and a common rupture length of 30-40 km for normal faults worldwide. In the second report, Schwartz and Coppersmith (1984) proposed that the WFZ is composed of six major segments; these segments were chosen on the basis of a combination of geomorphic, geophysical, paleoseismic, and geodetic data.

These two papers introduced the concept that individual slip events (surface ruptures and associated earthquakes) on a major normal fault zone (such as the WFZ) are largely confined to discrete parts that represent only a fraction of the fault's total length and whose location may be controlled by local geometric and structural properties of the fault zone. However, the term segment was not explicitly defined; the term has been used in contexts that range from "a portion" (that is, a geometric part) to "a structural entity" (that is, a structural segment). In this volume, dePolo and others discuss this problem of nomenclature and suggest that the term "earthquake segment" be used for those parts of a fault or faults that "rupture as a unit during an earthquake." We use the term segment with the same meaning,

although our determination of segments of the WFZ is based on paleoseismological data rather than historical seismological data. Nevertheless, the segments defined herein indicate the extent of surface rupturing that we would expect during large-magnitude earthquakes that nucleate on the WFZ.

Recent studies

The results of recent surficial geologic mapping by Machette, Nelson, and Personius lead them to modify some of the proposed segment boundaries, suggest several new boundaries, and subdivide four of the original segments (Machette and others, 1986). These modifications were based on perceived recency of fault movement as determined by analysis of fault-scarp morphology and relations between young surficial deposits and the WFZ. The boundaries for the Salt Lake City and Nephi segments of the WFZ were not altered from Schwartz and Coppersmith's (1984) segmentation model (see fig. 1).

In 1986 we started a cooperative USGS/UGMS program of exploratory trenching to better define the recency of faulting along several of the newly proposed segments, to determine the timing of older faulting events, to define recurrence intervals, and to gain insight into the timing of movement on adjacent fault segments. We have completed most of our dating studies at the following trenching sites: Brigham City, East Ogden, Dry Creek, American Fork Canyon, Rock Canyon, and Mapleton (see Machette and others, 1987). In addition, studies by geologists at the Bureau of Reclamation, University of Colorado, and Utah State University have augmented our findings. This recent flurry of trenching has more than tripled the original number of sites and probably increased our data on timing of faulting events by a factor of five.

This paper is our attempt to reach a consensus on a segmentation model and movement history for the WFZ based on each of our studies. We have been working on the WFZ for the past 5-10 years, somewhat independently at first, but more recently as an allied research team. We believe that major surface-rupturing events have occurred repeatedly in the Holocene--commonly 2 or 3 times over the past 6,000 years on each of the central WFZ segments from Brigham City to Nephi. In addition, one of the two southern segments has ruptured once during the past 7,300 years. Movement on the four remaining segments is dated only as pre-Holocene because we have not found exposures of faulted upper Quaternary deposits along these segments. Although we are not in complete agreement as to the persistence of some of the newly defined segment boundaries, our current hypothesis is that the WFZ is comprised of ten (or possibly eleven) segments. As we continue to work on this problem our segmentation model may change as a result of new dating or exposures; however, we are confident that the basic structural and chronologic framework presented here is scilentifically sound and relatively accurate.

SEGMENTATION OF THE WASATCH FAULT ZONE

Our studies show that segments along the central two-thirds (259 km; Brigham City to Nephi) of the 383-km-long WFZ have each ruptured two or more times in the past 6,000 years. The distal segments are shorter and have both lower slip rates and longer recurrence intervals than segments along the central part of the WFZ. In general, the distribution of WFZ segment lengths forms a broad envelope that has its maximum values in the central part and which tails off at the ends, not unlike that of the altitude of the crest of the Wasatch Range and other ranges along the WFZ (see Schwartz and Coppersmith, 1984, fig. 10). These relations indicate a strong correlation between topography (a proxy for structural offset), slip rates and recurrence intervals, and lengths of segments along the WFZ.

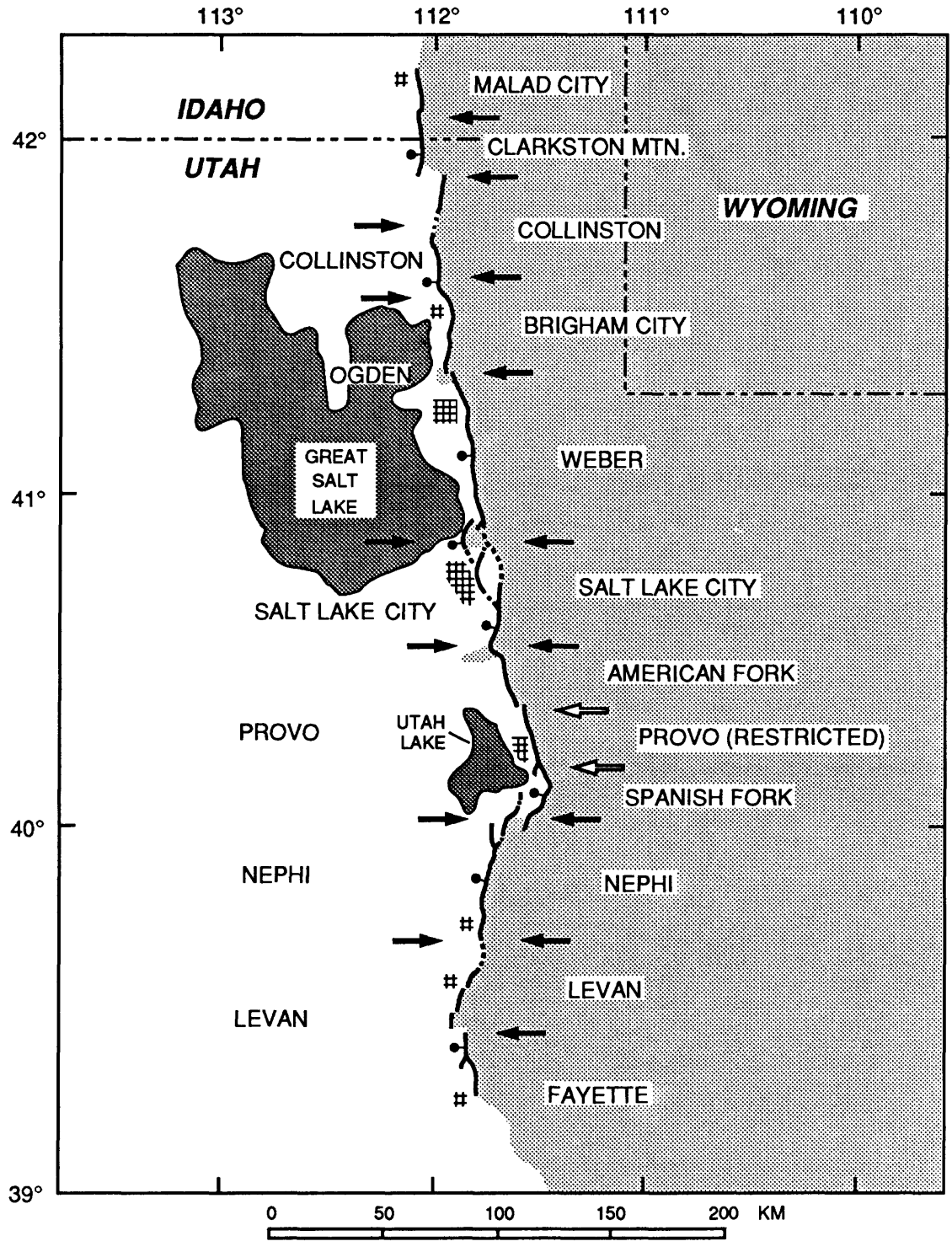

FIGURE 1.--Names and positions of Wasatch fault zone segments as proposed by Schwartz and Coppersmith (1984; left column) and by the authors of this report (right column). Solid arrows indicate segment boundaries; hollow arrows show two segment boundaries proposed by Machette and others (1986) which probably are not persistent (that is, they are subsegment boundaries). Major towns shown by cross-hachure symbol.

Table 1.--Lengths of segments and positions of boundaries on the Wasatch fault zone.
[Lengths are rounded to closest 0.5 km]

Fault segment	Length of segment (km)		Comments
	Surface trace	Straight line	
Malad City.....	17.0	16.5	No movement since 15 ka. Length does not include 6-km-wide Woodruff spur at south end.
Clarkston Mountain.....	19.0	17.0	No movement since 15 ka. Extends from Woodruff spur south to Malad River. Has 7-km left-step and 2-km overlap with Collinston segment.
Collinston.....	30.0	29.5	No movement since 15 ka. North end at Short Divide; position of fault across Bear River area uncertain.
Brigham City.....	40.0	35.5	Repeated Holocene movement. Has 1-km left step and 1.5-km overlap with Weber segment at south end: includes most of Pleasant View salient.
Weber.....	61.0	56.0	South end is on north-central flank of Salt Lake salient. Steps 2.7-km west to Warm Springs fault (Salt Lake City segment).
Salt Lake City.....	46.0	39.0	Has three left-stepping faults: Warm Springs (7.5-10 km), East Bench (13 km), and main Wasatch (23 km). South end is at Corner Canyon where WFZ steps 7.5 km east across Traverse Range. Length based on 10-km-long Warm Springs fault.
Provo segment.....	69.5	59.0	Extends from Chipman Creek (near Alpine) to Payson Canyon.
American Fork (subsegment).....	22.5	21.0	Extends from Chipman Creek south to Provo River. Steps 2-km east into bedrock at south end. No overlap at south end. Northern part of the original Provo segment.
Provo (subsegment, restricted sense).....	18.5	17.0	Extends from Provo Canyon to south end of Springville fault. Overlaps 3 km with Spanish Fork segment. Central part of original Provo segment.
Spanish Fork (subsegment).....	31.5	24.0	Major concave-to-west fault. Has 4-km west step and 5.5 km overlap with Nephi segment. Southern part of the original Provo segment.
Nephi.....	42.5	37.5	Payson to Nephi. Makes 8.5-km step to west between Santaquin Canyon and Juab Valley. Separated from Levan segment by 15-km gap in faulting. Excludes 2.5-km-long Benjamin fault, north of Payson.
Levan.....	30.0	25.5	Length includes two major gaps (6-km net) in faulting within segment. Steps 3.5 km east across bedrock and 5 km south to Fayette segment. Northern part of original Levan segment.
Fayette.....	11.0	10.5	No proven Holocene movement. Has 4-km-long western strand and range-bounding eastern strand (9-km long). Ends just west of Fayette Cemetery. Southern part of original Levan segment.
A. TOTAL LENGTH OF ALL SEGMENTS.....	366.0	326.0	Sum of lengths of all segments of the Wasatch fault zone.
B. AVERAGE LENGTH OF SEGMENTS.....	36.6 33.3	32.6 29.6	(A) divided by 10. (A) divided by 11.
C. TOTAL LENGTH OF HOLOCENE SEGMENTS..	259.0	227.0	Sum of lengths of all segments having repeated Holocene movement.
D. AVERAGE LENGTH OF HOLOCENE SEGMENTS..	51.8 43.1	45.4 37.8	(C) divided by 5. (C) divided by 6.
E. TOTAL LENGTH OF OLDER SEGMENTS.....	107.0	99.0	Sum of lengths of all segments without repeated Holocene movement.
F. AVERAGE LENGTH OF OLDER SEGMENTS.....	21.4	19.8	(E) divided by 5.
G. TOTAL LENGTH OF WASATCH FAULT ZONE.	383.0	343.0	Total length of all segments including gaps and salients, subtracting overlaps.

Types of segment boundaries

If segment boundaries are persistent and repeated barriers to lateral propagation of faults, they should cause structural anomalies along fault zones. The anomalies may present themselves as abrupt changes in structural relief along strike (owing to different long-term slip rates) or more likely as areas of less structural relief than adjacent parts of the range within a segment (see Wheeler, this volume). These changes in structural relief may be expressed as (1) subsurface ridges between deep structural basins (that is, gravity saddles), (2) depressed structural levels in the range, (3) bedrock blocks (salients) stranded at intermediate structural levels between parallel strands of a fault zone, or (4) as a combination of these. Nonpersistent structural boundaries are those that change position through time (see definition and criteria for recognition of persistent and nonpersistent boundaries in Wheeler, 1987 and this volume).

As a result our mapping along the central and southern parts of the WFZ (Honeyville to Fayette, Utah), we recognize four features that mark persistent and nonpersistent segment boundaries (see Machette and others, 1987).

1. Salients--major bedrock blocks that extend into the basin at intermediate structural levels. The salients commonly are bounded by Quaternary faults that are less active than the range-bounding faults. The bedrock spurs north of Salt Lake and Ogden, and the Traverse Range are salients. Salients can persistent as barriers for millions of years.
2. Lateral (echelon) steps in the fault zone. These steps can cross bedrock-cored ranges, such as at Dry Mountain south of Payson (a variety of a salient) and between the Levan and Fayette segments, or can be within bedrock, such as at Provo Canyon. Lateral steps may be either persistent or nonpersistent barriers; dePolo and others (this volume) found many examples of historical faulting where echelon steps in a fault failed to stop propagating ruptures.
3. T-junctions. This type of boundary involves oblique intersection of two fault traces. One of the fault traces extends either basinward (as does the Springville fault in the Utah Valley) or into bedrock (as does the northern part of the Brigham City segment). These features are classified as geometric segment boundaries by dePolo and others (this volume); they are not usually associated with reduced structural relief in either the ranges or basin and, thus, are largely nonpersistent in the geologic record. Geometric boundaries usually do not mark stopping or starting points for surface ruptures.
4. Gaps. The Nephi-Levan segment boundary is marked by an obvious gap of 15 km in Holocene and latest Pleistocene faulting, but middle(?) Pleistocene scarps in the gap attest to the presence of a through-going fault. Long gaps probably reflect the reduction of structural relief across boundaries on a time scale of hundreds of thousands of years (that is, long cycles of slip versus low or no slip). Through time, gaps may move in response to changes in stress accumulation on fault zones.

Segmentation Models

The six segments originally proposed by Schwartz and Coppersmith in 1984 are shown on the left side of figure 1. Although they ended their northernmost (Collinston) segment at the Bear River, they followed Cluff and others' (1970) belief that older movement on the Wasatch fault zone continued much farther to the north. The southern end of their Collinston segment has been moved 5 km north on the basis of mapping north of Brigham City by Personius (1988, in press) and its northern end has been extended about 11 km past the

Bear River (Machette and others, 1987). In addition, we recognize another 41 km of the Wasatch fault zone that extends north along the Malad Range to Malad City, Idaho. This extension of the WFZ is subdivided tentatively into the Clarkston Mountain and Malad City segments (fig. 1), which are separated by a 6-km-wide salient (the Woodruff spur; Machette and others, 1987). The original Ogden segment, which extended from north of Brigham City to North Salt Lake City, is now divided into the 40-km-long Brigham City segment and the 61-km-long Weber segment.

The Provo segment, which borders the eastern margin of Utah Valley, appears to be a single segment as evidenced by similarities in the timing of the most recent (500-650 years ago) and penultimate (2.6-2.9 ka) events determined from major trenching investigations at American Fork Canyon and Mapleton. Schwartz and Coppersmith (1984) originally proposed this segmentation (that is, a single Provo segment), but Machette and others (1986) subdivided the WFZ into three shorter subsegments named American Fork, Provo (restricted sense), and Spanish Fork (fig. 1, table 1). The most recent movement on the medial Provo (restricted sense) segment is poorly dated at about 1,100 years ago (Machette and others, 1987), so Lund and Schwartz trenched the Rock Canyon site (northeast of Provo) in the spring of 1988 to help resolve this apparent incongruity in timing. When completed, their radiocarbon analyses will be able to better constrain the timing of the most recent faulting event at Rock Canyon, but not the penultimate event. Thus, although we all prefer to interpret that WFZ of Utah Valley as a single segment, we still cannot preclude future surface rupturing on two discrete segments in the valley. If there are two segments, we suspect that Machette and others' (1986) Provo segment is probably a part of the Spanish Fork segment because the proposed segment boundary at Provo Canyon (table 1) appears to be the more persistent of the two problematic boundaries (marked by hollow arrows in fig. 1). As a single segment, the original Provo would to be the longest (about 70 km) and one of the most recently active segments of the WFZ.

South of Nephi, the WFZ is characterized by lower slip rates and recurrence intervals that are >6,000 to >10,000 years long. Machette's unpublished studies of fault-scarp morphology along this part of the WFZ suggests that scarps along the southern 16 km of the WFZ are clearly older than those to the north. He suggests that these scarps mark a separate distal fault segment that has not ruptured in the Holocene, whereas the 30 km of the WFZ to the north was active in the late Holocene. The name Levan has been retained for the northern (late Holocene) part of the fault zone and the older southern part has been named the Fayette segment (Machette and others, 1986).

Lengths of Wasatch fault-zone segments

The total length of the WFZ is 383 km as measured along its surface trace, which is our preferred method of reporting fault lengths. Individual lengths of segments are as short as 11-17 km (on the ends) to as long as 61 km for the centrally located Weber segment and about 70 km for a recombined Provo segment in the Utah Valley (table 1). If there are two segments in Utah Valley, the lengths of the American Fork segment (22.5 or 41 km) and Spanish Fork segment (31.5 or 47 km) segments are dependent upon which one includes the disputed 18.5-km-long Provo segment (restricted sense).

The average length along surface trace for all of the segments of the WFZ is 33 or 37 km (for 11 or 10 segments, respectively). The segments with repeated Holocene movement have an average length of about 50 km along surface trace (see table 1 for calculated range in segment lengths). The three northernmost segments and the two southernmost segments have an average length of about 20 km, with the inboard segments each being 30 km long.

ANALOGS FOR SURFACE RUPTURING AND EARTHQUAKES ON THE WASATCH FAULT ZONE

The various empirical relations that have been determined from surface ruptures associated with historic and prehistoric earthquakes in the extensional regime of the Basin and Range province (Slemmons, 1977; Bonilla and others, 1984) are our best analogs for the expected nature of future surface rupturing during large-magnitude earthquakes on the Wasatch fault zone. Although there are still some uncertainties about the Utah Valley part of the WFZ, the lengths of our proposed segments are generally comparable to the lengths of surface ruptures caused by recent, large-magnitude earthquakes in the northern part of the Basin and Range province and along the Intermountain Seismic Belt (ISB). The ISB forms an arcuate belt of pronounced seismicity that stretches 1300 km from southern Nevada and northern Arizona to northwestern Montana (see Arabasz and others, 1987). As depicted by Arabasz and Smith (1981), the ISB is the seismically active zone between the largely aseismic and structurally passive Colorado Plateaus, middle Rocky Mountains, and northern Rocky Mountains provinces to the east and the moderately seismic, extending terrain of the Basin and Range province to the west.

Historical earthquakes and surface ruptures

Large-magnitude (M 7+) earthquakes have been concentrated in two regions of the Basin and Range province in historical times: (1) an elongate northeast-trending zone named the Central Nevada-Eastern California Seismic Belt that been the locus of historical faulting (Wallace and Whitney, 1984; dePolo and others, this volume), and (2) a region along the northern part of the ISB that is characterized by abundant Holocene faulting and the regions two largest earthquakes, both of which have been associated with major surface ruptures in intermontane basins north of the Snake River Plain (Stickney and Bartholomew, 1987).

The most recent earthquake in the Central Nevada-Eastern California Seismic Belt was the 1954 Fairview Peak-Dixie Valley sequence (Slemmons, 1957; Doser, 1986). The Fairview Peak-Dixie Valley earthquake sequence produced a total of 102 km of surface ruptures (dePolo and others, this volume) from two earthquakes having discrete hypocenters and separated in time by only four minutes (Doser, 1986). Doser (this volume) reports M_w 7.1 for the Fairview Peak earthquake and M_w 6.8 for Dixie Valley earthquake (Bonilla and others, 1984, report M_s 7.2 and 6.8, respectively, for these same earthquakes). Surface ruptures of about 67 km and 45±2 km, respectively, were associated with the 1954 earthquake sequence (dePolo and others, this volume).

DePolo and others' (this volume) compilation of surface-rupture patterns and lengths for historical earthquakes in the Basin and Range province suggests that M 7+ earthquakes usually are associated with multiple ruptures (that is, several distinct but linked or echelon surface ruptures) and Doser (this volume) suggests that all of these large earthquakes are modelled best by multiple earthquake subevents. For example, dePolo and others (this volume) suggest that the normal-oblique faulting of the Fairview Peak earthquake was the result of failure along three complex structural segments (that

is, separate faults) that are 16, 18, and 32 km long. However, they also propose that the rupturing could be subdivided into as many as seven segments on the basis of different criteria such as geometry, fault behavior, scarp morphology, or geologic discontinuities. In contrast, the Dixie Valley earthquake probably ruptured along a single geometric segment (dePolo and others, this volume). In this context, geometrically defined segments (such as those proposed in 1986 by Machette and others for the Utah Valley part of the WFZ) need not be persistent rupture entities, but rather may be building blocks for long ruptures ("earthquake segments" of dePolo and others, this volume) and large-magnitude earthquakes.

In the past 30 years, there have been two M_w 7+ earthquakes in the northern Basin and Range province and the Intermountain Seismic Belt: the 1959 M_w 7.5 earthquake at Hegben Lake, Montana (Doser, 1985), and the 1983 M_w 7.3 earthquake near Borah Peak, Idaho (Doser and Smith, 1985). Doser's (1985) analysis of seismic data from the Hegben Lake earthquake indicates a double rupture (two subevents) five seconds apart on one or more fault planes having dip-slip motion (see also dePolo and others, this volume). Surface rupturing occurred on two faults during this earthquake: 23 km along the Red Canyon fault and 12 km along the Hegben fault (Witkind and others, 1962), although the reported net rupture length for this earthquake is only 26 km because the two traces overlap.

Crone and others (1987) report a total of 36 km of surface rupturing for the 1983 Borah Peak, Idaho, earthquake. Most of the rupturing occurred along the Thousand Springs segment (22 km) of the Lost River fault zone, but additional, subsidiary ruptures extended north into the Warm Springs Valley on a basinward splay and along the range-bounding Warm Spring segment of the Lost River fault zone. Of the total surface-rupture length reported for the Borah Peak earthquake only 26 km (72 percent) had a continuous offset of >25 cm (see Crone and others, 1987, fig. 4).

Prehistoric surface faulting in the region

Most of the reported lengths for historic surface ruptures in the Basin and Range province come from earthquakes of the Central Nevada Seismic Belt that often have large components of oblique slip and significant lengths of small vertical displacement (<25 cm). Therefore, for this report it is appropriate to compare the Wasatch fault zone with some prehistoric surface ruptures along late Quaternary faults in the northern part of the ISB.

The northern part of the ISB is largely coincident with a belt of Holocene faults that form a right-stepping en echelon pattern from the Brigham City segment of the WFZ northward through the Cache, Bear Lake, Star, and Teton Valleys to the Yellowstone area; from there, it turns westward into southwestern Montana and central Idaho (see Scott and others, 1985; Pierce and Scott, 1986; Smith, 1988).

Regional studies of faulting in northern Utah (McCalpin, 1987; Personius, 1988, in press; Crone and Machette, unpubl. data) suggest that Holocene movement has occurred on the West Cache and East Cache faults (due west and east of Logan, Utah) and East Bear Lake fault, the latter of which bounds the east side of Bear Lake in northern Utah and southern Idaho. The proposed segments on the East Cache fault (McCalpin, 1987) and the East Bear Lake fault (Crone and Machette, unpubl. data) average 18-21 km and $\geq$23 km in length, respectively. In addition, the northern segment of the East Bear Lake fault has ruptured in the late Holocene, as evidenced by extremely fresh-appearing fault scarps and the presence of oxbow channels of the Bear River stranded on the uplifted fault block (Crone and Machette, unpubl. data).

From Bear Lake, Holocene faulting can be traced northward discontinuously into the Star Valley of Wyoming where Piety (1987) has found evidence of two faulting events that postdate upper Pleistocene alluvial fans along the southern part of the Star Valley fault. The Star Valley fault has been divided into two segments, a 24-km-long Holocene Star Valley fault (segment) and a 16-km-long older Star Valley fault (segment) on the basis of recency of movement, geomorphic expression, and upper Quaternary slip rates (Piety and others, 1986). Further north, studies of the Quaternary geology of the Jackson Hole area by K.L. Pierce (U.S. Geological Survey, oral commun., 1989) suggests that repeated Holocene movement has occurred on two discrete segments of the range-bounding Teton fault at the western front of the Teton Range; a 34-km-long segment that extends from the north end of Jackson Lake to near Taggart Lake, and a southern segment that extends 19 km further south. Ostenna (1988) proposed a segment boundary that would subdivide Pierce's 34-km-long segment into a central segment (19 km) and a northern segment (14 km). However, this subdivision appears to be based largely on the geometry of the fault and therefore the proposed boundary is probably not a barrier to surface faulting. Ostenna (1988) argues for an average recurrence interval of about 2,000 years along the central, most active part of the Teton fault.

The zone of Holocene faulting makes a sharp bend westward at Yellowstone National Park in northwestern Wyoming, and spreads out into a wide band of late Quaternary faulting that extends about 300 km west and north of the Snake River Plain through southwestern Montana and into central Idaho (Stickney and Bartholomew, 1987). The Yellowstone area is dominated by a thermal anomaly (Quaternary volcanism, mantle upwelling, and high heat flow) that seems to have migrated to the northeast along the Snake River Plain during late Cenozoic time. According to Pierce and Scott (1986), the Yellowstone area is the tip of a northeasterly propagating v-shaped wave of Neogene tectonism that is associated with the thermal anomaly. They envision the most active tectonism (the belt of Holocene faulting previously outlined) as occupying the wave front. The proposed wave front, which includes the aforementioned Holocene faults, probably intersects the WFZ north of Brigham City, which might explain why the northern segments (Collinston, Clarkston Mountain, and Malad City) of the WFZ have been relativley inactive in the late Quaternary.

Crone and Haller's (this volume) study of some of the range-bounding fault zones in the northern Basin and Range province (north of the Snake River Plain) shows that the major fault zones have patterns of segmentation that are similar in both time and space to those recognized along the Lost River fault zone (Crone and others, 1987). Their comparative analysis of scarp morphology indicates average segment lengths of 23-25 km for the Lost River, Lemhi, and Beaverhead fault zones in Idaho, but only 14 km for the shorter, less prominent Red Rock fault in southwestern Montana (Crone and Haller, this volume, table 1).

The regional studies of paleoseismicity cited here suggest a common range of segment lengths for range-bounding faults believed to be associated with large-magnitude (M_w 7+) earthquakes in the northern part of the Basin and Range province and Intermountain Seismic Belt. Figure 2 summarizes the lengths of segments found in two classes of faults: (1) those along major range fronts (the Lost River, Beaverhead, Lehmi, and Teton faults) that are typically >100 km long; and (2) those along lesser range fronts (the Red Rock, Star Valley, East Cache, and East Bear Lake faults) that are typically <100 km long. The longer faults have proposed segments that commonly range from 20-40 km in length and average about 25 km, whereas the shorter faults with have segments that range from 15-30 km in length and average about 20 km.

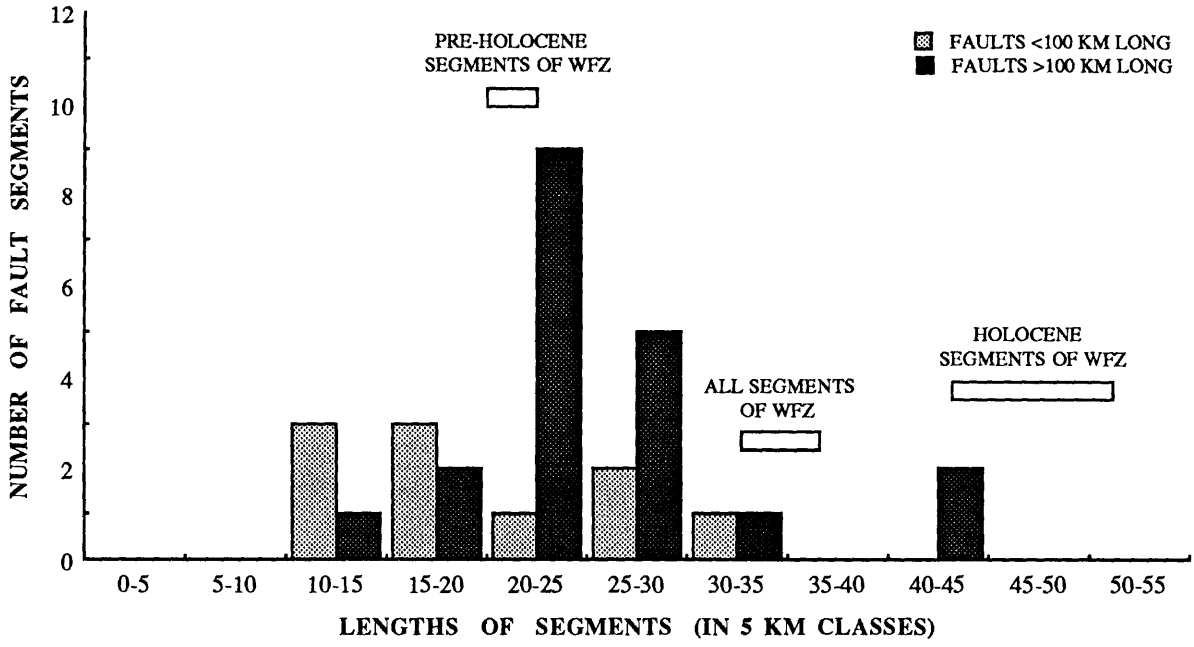

FIGURE 2. Nomograph of proposed fault segment lengths in the northeastern Basin and Range province and along the Wasatch fault zone.

Comparison of historical surface ruptures, prehistorical fault segments, and the Wasatch fault zone

Seismological and geological studies of four recent earthquakes in the northern Basin and Range province and Intermountain Seismic Belt suggest that rupture lengths ranging between 26 and 67 km (average 43 km) have been associated with historical earthquakes of M_w 6.8-7.5. In contrast, paleoseismological studies of late Pleistocene and Holocene faulting in the northeastern Basin and Range province suggest that segment lengths average about 25 km for prehistoric faulting along major uplifted ranges. The Wasatch fault zone, which is the longest fault zone in the region, is characterized by segments that are about twice as long (43-52 km in average length) along the central active part and about 20 km long on the distal, less active portions (fig. 2, table 1). The disparity between lengths of historical and prehistorical fault segments probably is best explained by differences in resolution. For example, careful mapping of modern surface ruptures, such as those that formed during the 1983 Borah Peak earthquake (Crone and others, 1987, fig. 4), shows that as much as a third of the length may be of relatively small displacement (<25 cm in this case). Small ruptures such as these might not be recognized along prehistoric faults solely on the basis of surficial geologic mapping. If small-displacement ruptures overlapped adjacent fault segments, even careful trenching may fail to detect the faulting event.

TIMING OF HOLOCENE MOVEMENT ON THE WASATCH FAULT ZONE

The WFZ has been the focus of extensive trenching efforts since the initial investigations of Cluff and others in the 1970's. Including the trench studies that were completed in 1987, 43 trenches and 3 natural exposures have been logged and described from 18 sites on 6 segments of the WFZ (see Machette and others, 1987). Most of the trench sites have provided some control on the time of most recent faulting and set limits on recurrence intervals and slip rates. In the past two years we have obtained about 50 radiocarbon dates using both conventional and accelerator-mass-spectrometry

methods on charcoal and soil organic matter and 12 experimental thermoluminescence age estimates. Although many of these dates are not yet published, they are used herein to construct a chronology of Holocene surface-faulting events and recurrence intervals along the WFZ (fig. 3). More importantly, differences in the timing of the most recent and older events along the length of the WFZ are the most diagnostic data for defining segments (that is, "earthquake segments").

Several interesting patterns evolve from the chronology depicted in figure 3. One pattern is the apparently random distribution of faulting events during the 1,500 to 6,000 year time interval. Within this time span there seems to be a spatial difference in recurrence intervals; the southern segments (Salt Lake City to Nephi) have fairly long intervals, typically 2,000-3,000 years to as much as 4,000 years, whereas the Weber and Brigham City segments have been characterized by intervals of 2,000 years or less. The second pattern is more striking. There is strong evidence for a recent period of temporal clustering of large earthquakes; that is, a strong grouping of surface-rupturing earthquakes on the WFZ over an unusally short time interval. If one assumes that the most recent event on the Salt Lake City segment occurred about 1,500 years ago (rather than closer to the 1,800 year limit shown in fig. 3), then faulting has occurred between about 400(?) and 1500(?) years ago on five of the six segments of the Wasatch that have Holocene movement. On the basis of the WFZ's behavior during the past 4,000-5,500 years, we calculate that a major earthquake occurred once every 415 years (see table 2) somewhere on the active segments of the WFZ (Brigham City to Nephi). However, the recent episode of clustering of the WFZ (six faulting events during an interval of 1,100 years) indicates that one major surface-rupturing event every 220 years--or about twice as often as we would expect from the longer (Holocene) record. In addition, we have no evidence for a major surface-rupturing earthquake on the WFZ during the past 400 years (which is the youngest time we allow for the Weber segment and our best estimate for the most recent event on the Nephi segment). Although these relations point strongly to a process of temporal clustering of large-magnitude earthquakes on the WFZ, the process seems to be intermittent through time (that is, no other strong clustering episodes between 1,500 and 5,500 years ago).

Our chronology for times of faulting demonstrates the variability in recurrence intervals on segments of the central WFZ. Figure 3 shows that recurrence intervals may vary from as little as 500 years (for the past two events on the Weber segment) to as much as 4,000 years (on the Salt Lake City segment). Conversely, data from the American Fork site shows two recurrence intervals of similar durations (2,100 and 2,650 years; see Forman and others, 1989). Of particular interest is the lack of recent movement along the Brigham City segment. There were three faulting events between about 6 ka to 8 ka and 3.6 ka (Machette and others, 1987)--and average of one event every 1,500-2,200 years--and the last two faulting events have a recurrence interval of 1,100 years (fault events at 3.6 and 4.7 ka, fig. 3). However, the most recent faulting occurred nearly 3,600 years ago. Of all the WFZ segments, only the Brigham City has an elapsed time (time since the most recent faulting) that exceeds its recurrence interval.

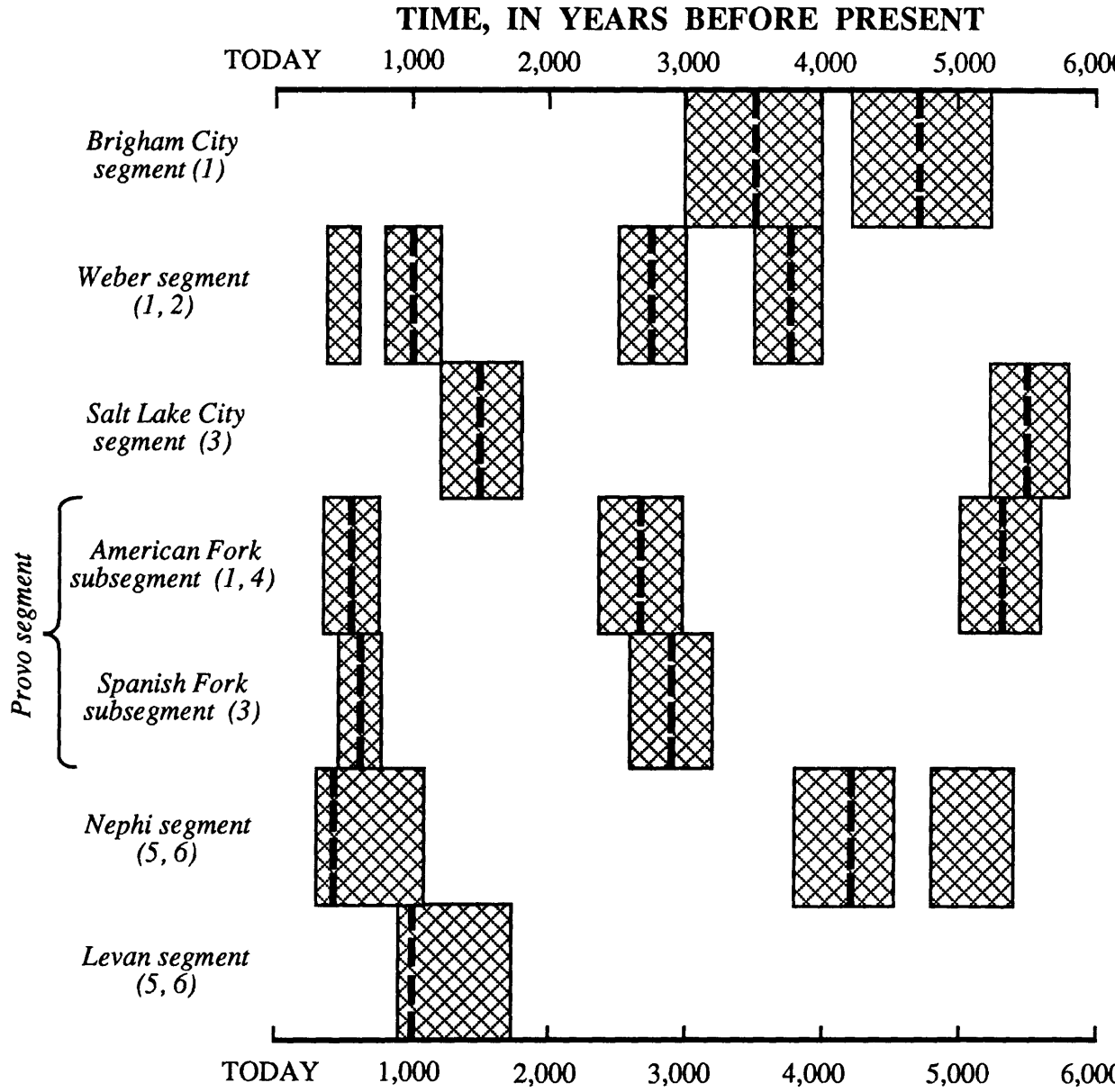

Sources of information:
(1) Machette and others (1987), modified in this report.
(2) Swan and others (1980), modified in this report.
(3) Schwartz and others (1988), modified in this report.
(4) Forman and others (1989).
(5) Schwartz and Coppersmith (1984).
(6) Jackson (1988).

FIGURE 3.--Timing of movement on segments of the Wasatch fault zone during the past 6,000 years as determined in January, 1989. Heavy-dashed lines indicate our best estimates of times of faulting and cross-hachure pattern indicates likely limits for faulting as determined from radiocarbon dates and thermoluminescence age estimates. Although the American Fork and Spanish Fork segments are shown separately, they appear to be parts of a single segment as proposed by Schwartz and Coppersmith (1984).

Table 2.—Timing, number of major surface-faulting earthquakes, and recurrence intervals for Holocene movement on the Wasatch fault zone

[All values for age and time intervals (columns A-C) are rounded to the nearest 100 years. Ages based on calendar-corrected radiocarbon dates and thermoluminescence analyses. The average recurrence interval is determined by dividing the sum of time intervals (column C) by the sum of intervals between faulting events (column D). Time intervals (column C) for some segments include time between the oldest (undated) event at a site and the age of the datum; thus, some values in column C are maximum values. N/A indicates a value that is not applicable to the calculation]

Fault segment	Trench site	A Oldest event (t) or datum (d) (years ago)	B Estimated time since most recent faulting (years)	C Time interval (A-B) (years)	D Number of faulting events (and intervals) Events	Intervals
Brigham City..	Brigham City	4,700t	3,600	1,100	2	1
Weber.....	East Ogden..	4,000t	500	3,500	4	3
Salt Lake City	Dry Creek...	5,500t	1,500	4,000	2	1
American Fork.	AF-1, AF-2..	5,300t	500	4,800	3	2
Spanish Fork..	Mapleton....	3,000t	600	2,400*	2*	1*
Nephi.....	North Creek.	5,300d	400	4,900	3	2
Levan.....	Deep Creek..	7,300d	1,000	>6,300 N/A	1	0
Totals* (based on five segments; segments 1-4, 6).....				18,300	14	9
Totals (based on six segments; segments 1-6).....				20,700	16	10

Calculated recurrence intervals (in years) for segments of the WFZ having repeated Holocene movement#	Minimum value	Maximum value
Average recurrence interval (RI) on a single segment.....	2035	2070
Average composite recurrence interval (CRI).....	340	415

Notes: t—Time of oldest well-dated faulting event.
d—Age of datum from dating, stratigraphic, or tectonic considerations (rounded to nearest 100 years).
*—For a five segment model we use only the number of events and intervals from American Fork for the Provo segment).
#—Three significant figures are used to compute average values of recurrence from the totals in columns C and D. Values are rounded to nearest 5 years. Minimum values calculated from 20,700 years, 10 intervals, and 6 segments. Maximum values calculated from 18,300 years, 9 intervals, and 5 segments. The latter model (maximum value) is based on our preferred model of segmentation.

Our calculations of the average recurrence interval for the segments having repeated Holocene movement are shown on table 2. The average recurrence interval on any single segment is about 2,050 years (for either five or six segments). However, there is so much variation between and within segments (fig. 3) that this value for recurrence is statistically meaningless. The composite recurrence interval, which is defined as the average time between two faulting events anywhere on the central part of the fault zone, ranges from a maximum of 415 years to a minimum of 340 years. We prefer the 415 year (maximum) value because it is based on our preferred simple model of a long Provo segment. Schwartz and Coppersmith (1984, table 2) reported a maximum (composite) recurrence intervals of 615-666 years, but preferred a value of 444 years. Our method of calculating composite recurrence interval differs from that of Schwartz and Coppersmiths' by (1) using the total number of intervals between events in variable time windows (column C, table 2) rather that total number of events in a set time window (8,000 years in Schwartz and Coppersmith, 1984) and by (2) using only fault segments having two or more datable faulting events and discarding unconstrained values for recurrence (open-ended intervals). Even though the two methods are significantly different, both investigations reached basically the same conclusion.

CONCLUSIONS

The Wasatch fault zone is one of the longest and most active normal faults in the Basin and Range province of the western United States. Our segmentation model suggests five or six active, medial segments that average about 50 km in length and five less active, distal segments that average about 20 km in length. The lengths of segments proposed for other prehistorically active faults in the northern Basin and Range province are 20-25 km, or about half of that proposed for the Wasatch fault zone. The central portion of the WFZ has ruptured repeatedly along five or six segments during the Holocene, and individual recurrence intervals on these segments average about 2,050 years. The record of surface-faulting along the Wasatch fault zone for the past 6,000 years indicates that a major earthquake has struck on the average of once every four hundred years somewhere along the central active portion of the fault zone. Between about 400 and 1,500 years ago, however, faulting occurred at an accelerated rate of one major surface-rupturing event every 220 years--or about twice as often as expected. The WFZ's pattern of temporal clustering is much like that of historic faulting in the Central Nevada-Eastern California Seismic Belt, where eleven major earthquakes have occurred since 1860 (dePolo and others, this volume). Although the scale of the patterns is different--120 years versus 1,100 years--we consider the Central Nevada-Eastern California Seismic Belt to be good model for future activity on the WFZ.

REFERENCES

Arabasz, W.J., and Smith, R.B., 1981, Earthquake prediction in the Intermountain seismic belt--An intraplate extensional regime, in Simpson, D.W., and Richards, P.G., eds., Earthquake Prediction--An International Review: American Geophysical Union, Maurice Ewing Series, v. 4, p. 248-258.

Arabasz, W.J., Pechmann, J.C., and Brown, E.D., 1987, Observational seismology and the evolution of earthquake hazards and risk in the Wasatch Front area, Utah, in Gori, Paula, and Hays, W.W., eds., Assessment of Regional Earthquake Hazards and Risk along the Wasatch Front, Utah: U.S. Geological Survey Open-File Report 87-585, v. I, Chapter D, p. D1-D58.

Bonilla, M.G., Mark, R.K., and Lienkaemper, J.J., 1984, Statistical relations between earthquake magnitude, surface rupture length, and surface fault displacement: Bulletin of the Seismological Society of America, v. 74, no. 6, p. 2379-2411.

Cluff, L.S., Brogan, G.E., and Glass, C.E., 1970, Wasatch fault, northern portion--Earthquake fault investigation and evaluation, prepared for the Utah Geological and Mineral Survey: Woodward-Clyde and Associates, Oakland, CA, 27 p., 21 maps, scale 1:24,000.

_____1973, Wasatch fault, southern portion--Earthquake fault investigation and evaluation, prepared for the Utah Geological and Mineral Survey: Woodward-Lundgren and Associates, Oakland, CA, 79 p., 23 maps, scale 1:24,000.

Cluff, L.S., Glass, C.E., and Grogan, G.E., 1974, Investigation and evaluation of the Wasatch fault north of Brigham City and Cache Valley faults, Utah and Idaho--A guide to land-use planning with recommendations for seismic safety, prepared for the U.S. Geological Survey, Contract No. 14-08-001-13665: Woodward-Lungren and Associates, Oakland, CA, 147 p., 35 maps, scale 1:24,000.

Crone, A.J., Machette, M.N., Bonilla, M.G., Lienkaemper, J.J., Pierce, K.L., Scott, W.E., and Bucknam, R.C., 1987, Surface faulting accompanying the Borah Peak earthquake and segmentation of the Lost River fault, central Idaho: Bulletin of the Seismological Society of America, v. 77, no. 3, p. 739-770.

Doser, D.I., 1985, Source parameters and faulting processes of the 1959 Hegben Lake, Montana, earthquake sequence: Journal of Geophysical Research, v. 90, no. B6, p. 4537-4555.

_____1986, Earthquake processes in the Rainbow Mountain-Fairview Peak-Dixie Valley, Nevada, region 1954-1959: Journal of Geophysical Research, v. 91, no. B12, p. 12572-12586.

Doser, D.I., and Smith, R.B., 1985, Source parameters of the 28 October, 1983, Borah Peak, Idaho, earthquake from body wave analysis: Bulletin of the Seismological Society of America, v. 75, p. 1041-1051.

Forman, S.L., Machette, M.N., Jackson, M.E., and Mott, Paula, 1989, An evaluation of thermoluminscence dating of paleoearthquakes on the American Fork segment, Wasatch fault zone, Utah: Journal of Geophysical Research, v. 94, no. B2, p. 1622-1630.

Gilbert, G.K., 1890, Lake Bonneville: U.S. Geological Survey Monograph 1, 438 p.

_____1928, Studies of Basin-Range structure: U.S. Geological Survey Professional Paper 153, 89 p.

Jackson, M.E., 1988, Thermoluminescence dating of Holocene paleoseismic events on the Nephi and Levan segments, Wasatch fault zone, Utah: Boulder, University of Colorado, M.S. thesis, 149 p.

Machette, M.N., editor, 1988, In the footsteps of G.K. Gilbert--Lake Bonneville and neotectonics of the eastern Basin and Range province: Utah Geological and Mineral Survey Miscellaneous Publication 88-1, 120 p.

Machette, M.N., Personius, S.F., and Nelson, A.R., 1986, Late Quaternary segmentation and slip-rate history of the Wasatch fault zone, Utah: EOS (Transactions, American Geophysical Union), v. 67, no. 44, p. 1107.

Machette, M.N., Personius, S.F., and Nelson, A.R., 1987, Quaternary geology along the Wasatch fault zone--Segmentation, recent investigations, and preliminary conclusions, in Gori, Paula, and Hays, W.W., eds., Assessment of Regional Earthquake Hazards and Risk along the Wasatch Front, Utah: U.S. Geological Survey Open-File Report 87-585, v. I, Chapter A, p. A1-A72.

McCalpin, James, 1987, Late Quaternary tectonics and earthquake hazards in Cache Valley, Utah: Final Technical Report for U.S. Geological Survey Contract No. 14-08-0001-G1091, 187 p., 7 appendices, 2 plates, scale 1:24,000.

Ostenna, D.A., 1988, Late Quaternary behavior of the Teton fault, Wyoming: Geological Society of America Abstracts with Programs, v. 20, no. 7, p. A14.

Personius, S.F., 1988, Preliminary surficial geologic map of the Brigham City segment and adjacent parts of the Weber and Collinston segments, Wasatch fault zone, northern Utah: U.S. Geological Survey Miscellaneous Field Studies Map MF-2042, scale 1:50,000.

_____Surficial geologic map of the Brigham City segment and adjacent parts of the Weber and Collinston segments, Wasatch fault zone, northern Utah: U.S. Geological Survey Miscellaneous Investigations Map I-1979, scale 1:50,000, in press.

Piety, L.A., 1987, Late Quaternary surface faulting on the Star Valley fault, west-central Wyoming: Geological Society of America Abstracts with Programs, v. 19, no. 5, p. 327.

Piety, L.A., Wood, C.K., Gilbert, J.D., Sullivan, J.T., and Anders, M.H., 1986, Seismotectonic study for Palisades Dam and Reservior, Palisades Project [Idaho]: Denver, Colorado, U.S. Bureau of Reclamation Seismotectonic Report 86-3, 198 p, 6 appendices., 2 plates.

Pierce, K.L., and Scott, W.E., 1986, Migration of faulting along and outward from the tract of thermo-tectonic activity in the eastern Snake River Plain region during the last 15 m.y.: EOS (Transactions of the American Geophysical Union), v. 67, no. 44, p. 1225.

Schwartz, D.P., and Coppersmith, K.J., 1984, Fault behavior and characteristic earthquakes--Examples from the Wasatch and San Andreas fault zones: Journal of Geophysical Research, v. 89, no. B7, p. 5681-5698.

Schwartz, D.P., Lund, W.R., Mulvey, W.E., and Buddington, K.E., 1988, New paleoseismicity data and implication for space-time clustering of large earthquakes on the Wasatch fault zone [abs.]: Seismological Research Letters, v. 59, no. 1, p. 15.

Scott, W.E., Pierce, K.L., and Hait, M.H., Jr., 1985, Quaternary tectonic setting of the 1983 Borah Peak earthquake, central Idaho: Bulletin of the Seismological Society of America, v. 75, no. 4, p. 1053-1066.

Slemmons, D.B., 1957, Geological effects of the Dixie Valley-Fairview Peak, Nevada, earthquakes of December 16, 1954: Bulletin of the Seismological Society of America, v. 47, p. 353-375.

_____1977, Faults and earthquake magnitude: U.S. Army Corp of Engineers Waterways Experiment Station, Vicksburg, Mississippi, Miscellaneous Paper S-73-2, 129 p.

Smith, R.B., 1988, Seismicity and earthquake hazards of the Borah Peak-Hegben Lake-Yellowstone-Teton region--Implications for earthquakes in extensional and active volcanic regimes: Geological Society of America Abstracts with Programs, v. 20, no. 7, p. A12.

Stickney, M.C., and Bartholomew, M.J., 1987, Seismicity and late Quaternary faulting of the northern Basin and Range province, Montana and Idaho: Bulletin of the Seismological Society of America, v. 77, no. 5, p. 1602-1625.

Swan, F.H., III, Schwartz, D.P., and Cluff, L.S., 1980, Recurrence of moderate to large magnitude earthquakes produced by surface faulting on the Wasatch fault zone, Utah: Bulletin of the Seismological Society of America, v. 70, p. 1431-1462.

Wallace, R.E., and Whitney, R.A., 1984, Late Quaternary history of the Stillwater seismic gap, Nevada: Bulletin of the Seismological Society of America, v. 74, no. 1, p. 301-314.

Wheeler, R.L., 1987, Boundaries between segments of normal faults--Criteria for recognition and interpretation, in Crone, A.J., and Omdahl, E.M., eds., Proceedings of Conference XXXXIX--Directions in Paleoseismology: U.S. Geological Survey Open-File Report 87-673, p. 385-398.

Witkind, I.J., Myers, W.B., Hadley, J.B., Hamilton, Warren, and Fraser, G.D., 1962, Geologic features of the earthquake at Hegben Lake, Montana, August 17, 1957: Bulletin of the Seismological Society of America, v. 52, p. 163-180.

FORMATION OF SEGMENTED STRIKE-SLIP FAULT ZONES MOUNT ABBOT QUADRANGLE, CALIFORNIA

by

Stephen J. Martel
Earth Sciences Division, Building 50E
Lawrence Berkeley Laboratory
University of California
Berkeley, CA 94720

ABSTRACT

Segmented strike-slip fault zones as much as several kilometers in length developed in the Sierran batholith of California from pre-existing, steeply-dipping, subparallel joints. These joints generally were less than 50 m long and usually were spaced several centimeters to a few meters apart. Some joints subsequently slipped and became small faults. *Simple fault zones* formed as oblique dilatant fractures (splay cracks) linked noncoplanar faults side-to-side and end-to-end. The intensity of fracturing within a simple fault zone is markedly greater than in the adjacent rock. Simple fault zones are as much as a kilometer long and accommodated displacements as great as 10 meters. *Compound fault zones* formed as splay cracks linked small faults and simple fault zones together. The intensity of fracturing across a compound fault zone is highly variable. Compound fault zones are as much as several kilometers long and accommodated displacements as great as 70 meters. As a result of the linking process, both types of fault zones developed segmented geometries along strike; adjacent segments join at steps or bends. The longest splay cracks occur along the longest fault zones, indicating that the size of geometric irregularities along strike increased as the fault zones lengthened. Because the lateral displacement across compound fault zones is much greater than the lateral displacement across simple fault zones, the fracturing associated with displacement past large geometric irregularities would be more widespread along compound fault zones than along simple fault zones. Other fault zones that take advantage of pre-existing fractures or anisotropies may grow in a similar manner.

INTRODUCTION

Fault zones commonly serve as long-standing zones of weakness in the earth's crust, and their initial structure is likely to influence their subsequent behavior for long periods of time. It is widely recognized that as fault zones form they take advantage of pre-existing fractures (Hobbs and others, 1976; Price, 1981; Davis, 1984; Suppe, 1985). However, because fault zones can be reactivated in different episodes of deformation under markedly different environmental conditions (Sibson, 1977; Sibson and others, 1981; McKee and others, 1984; Muehlberger, 1986; Sibson, 1986), the manner in which fault zones form from pre-existing fractures commonly is obscured.

This paper describes how large strike-slip fault zones formed from pre-existing fractures within plutons of the Mount Abbot quadrangle in the Sierra Nevada of California (Fig. 1). This area provides a rare opportunity to track the development of faults from their inception for three main reasons: 1) faulting developed to different stages in different parts of the quadrangle; 2) the effects of subsequent deformation are minimal; 3) exhumed strike-slip faults and fault zones are well displayed. The smallest faults in the area are a few meters long, a few millimeters thick, and accommodated less than a centimeter of strike-slip displacement, whereas the largest fault zones are several kilometers long, several meters thick, and accommodated as much as seventy meters of strike-slip displacement.

The study area is in the Bear Creek region and includes three adjacent NW-trending plutons (Fig. 1) mapped and described by Lockwood and Lydon (1975). Field relations show that the westernmost pluton (the Lamarck granodiorite) is the oldest, that the central pluton (the granodiorite of Lake Edison) is of intermediate age, and that the easternmost pluton (the quartz monzonite of Mono Recesses) is youngest. Based on potassium-argon dating of biotites, these plutons have ages of 79-85, 77-82, and 79-82 million years, respectively (Stern and others, 1981). These ages provide maximum ages for the fault zones. Mineralized joints, faults, and fault zones that strike ENE are abundant within the older two plutons. Mineralized joints that strike ENE are also abundant within the Mono Recesses pluton, but faults and fault zones that strike ENE appear scarce. Because of the manner by which the faults and fault zones formed (discussed below), their distribution suggests that the faulting in the older two plutons may have occurred before or during emplacement of the Mono Recesses pluton. Accordingly, the faults may have formed at the depth the plutons were emplaced. Work by Noyes and others (1983) indicates that the nearby and nearly contemporaneous Eagle Peak and Red Lake plutons were emplaced at a depth of emplacement of ~4 km.

The first three stages of faulting in the the Bear Creek area (Fig.2) have been discussed recently by Martel and others (1988). The faults and fault zones developed from steeply-dipping subparallel joints (Segall and Pollard,

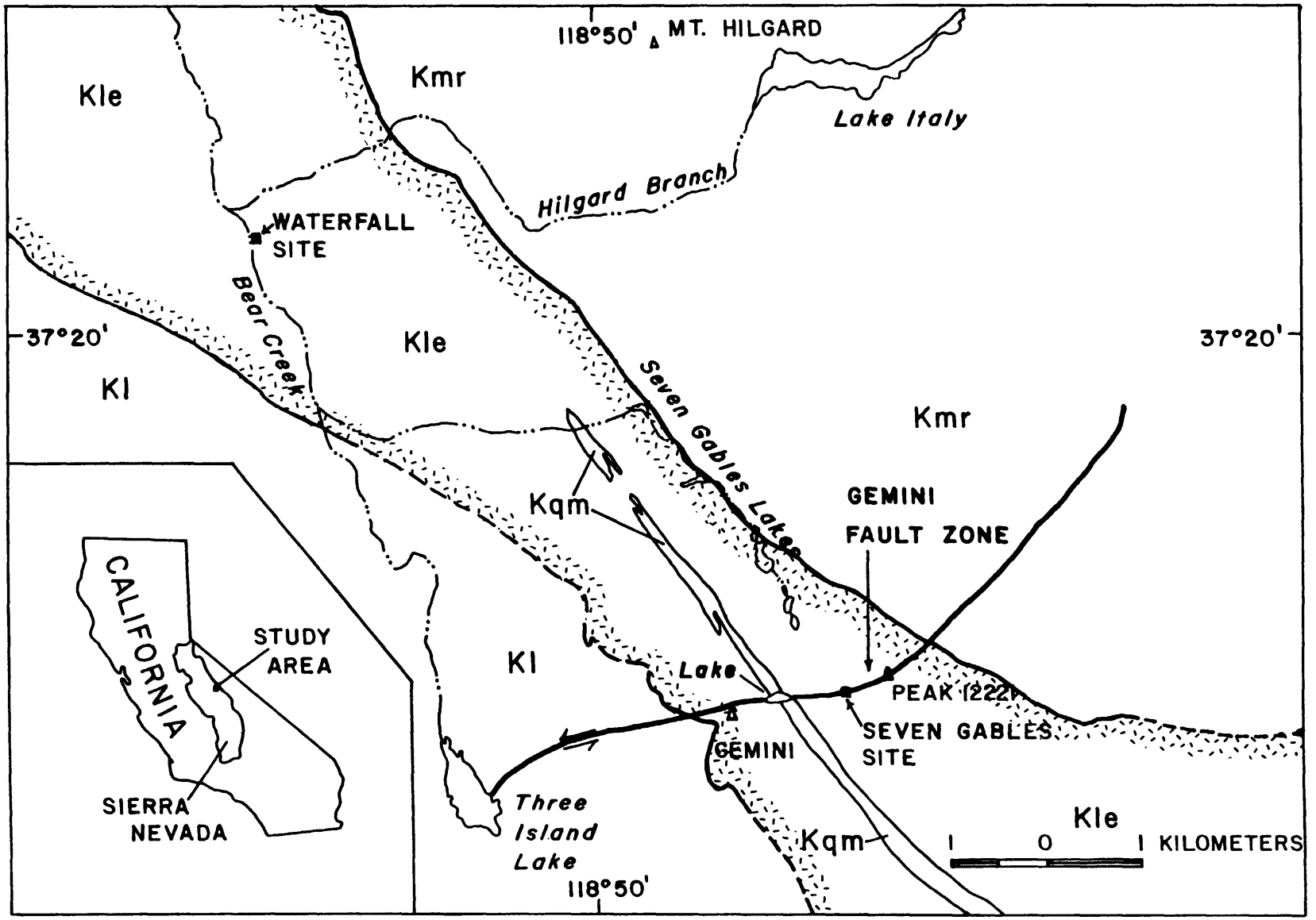

Figure 1.--Geologic map of the Bear Creek area as generalized from Lockwood and Lydon (1975). Locations of outcrop maps shown by solid squares. Kl = Cretaceous Lamarck granodiorite; Kle = Cretaceous granodiorite of Lake Edison; Kmr = Cretaceous quartz monzonite of Mono Recesses. The nearly vertical quartz monzonite body (Kqm) is displaced left-laterally approximately 70 meters across the Gemini fault zone.

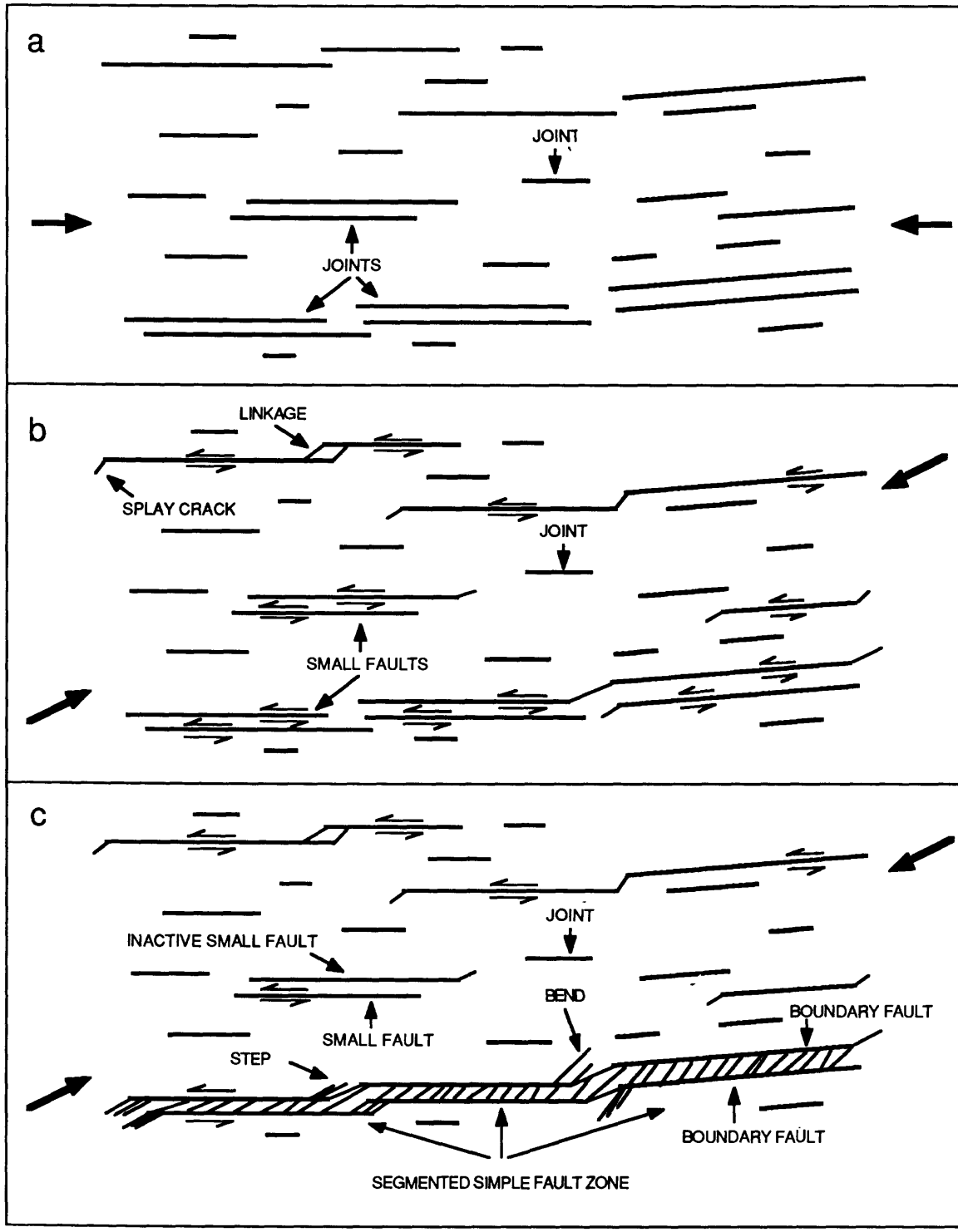

Figure 2.--The first three stages of faulting in the Mount Abbot quadrangle. Heavy arrows indicate inferred direction of maximum horizontal compressive stress. (a) Opening of joints. (b) Development of small left-lateral faults. Splay cracks form near the ends of some faults and some faults become linked. (c) Development of simple fault zones as extensive fracturing develops between some closely spaced faults.

1983a, 1983b). Hydrothermal minerals fill the joints, epidote and chlorite being particularly common. Those joints not involved in subsequent deformation contain undeformed minerals. Joint spacing and joint length range from a few decimeters to a few tens of meters. The joints typically are 0.1-10 millimeters thick.

During the second stage of deformation some joints slipped and became small left-lateral faults (Fig. 2b), offsetting xenoliths and steeply-dipping aplite dikes as much as 2 m (Segall and Pollard, 1983b; Martel and others, 1988). Not all joints in a given outcrop slipped, so unslipped joints parallel adjacent small faults. Slickenlines on the fault surfaces typically plunge less than 20°, indicating that at least the most recent displacements on the faults were dominantly strike-slip (Segall and Pollard, 1983b). As a result of slip, the material in these faults acquired mylonitic fabrics, and NNE-striking fractures (splay cracks) opened near fault ends. The splay cracks are filled primarily by epidote, chlorite, and quartz. Although some splay cracks are several meters long, they rarely extend more than a few meters away from the faults. Some originally unconnected left-stepping echelon faults were linked by splay cracks, whereas some right-stepping echelon faults were linked by ductile deformation of the intervening rock. Linked echelon faults are as much as several hundred meters in length and accommodated left-lateral displacements as great as several meters.

Larger left-lateral displacements were accommodated in the third stage of deformation (Fig. 2c) as abundant fractures linked faults side-to-side to form *simple fault zones* (Martel and others, 1988). The fractures within these zones contain epidote, chlorite, and quartz, with smaller amounts of muscovite and calcite. The most prominent fractures strike obliquely to the sharply defined faults (the boundary faults) at the edges of the zones. The rock inside a zone is highly fractured, in sharp contrast to the relatively unfractured rock immediately outside. Simple fault zones typically are half a meter to three meters thick and up to a kilometer long. Their traces consist of straight, noncolinear segments a few tens of meters long that join at steps or bends. This indicates that noncoplanar small faults linked end-to-end to form the boundary faults of simple fault zones. The maximum strike-slip displacement observed across a simple fault zone is about ten meters. The displacement is concentrated on the boundary faults.

This paper describes the structure and growth process of *compound fault zones*, the longest and structurally most complex type of fault zone in the Bear Creek area. These zones grew to lengths of several kilometers and accommodated several tens of meters of lateral displacement. Two exposures of compound fault zones were mapped in detail, one at the Waterfall site, and another at the Seven Gables site (Fig. 1). The linkage of originally discontinuous structures by fractures formed during faulting played an important role in the growth process. Accordingly, the evolution of fault zone geometry, the distribution of fault slip, and the distribution of fractures receive special attention.

STRUCTURE OF COMPOUND FAULT ZONES

Waterfall Site

The Waterfall site lies along the north edge of a network of faults and fault zones that is a few tens of meters wide and accommodates between twenty and eighty meters of left-lateral displacement. This network is well exposed over a horizontal distance of 500 meters and crops out over a vertical interval of at least 300 meters.

The site contains several groups of steeply-dipping fracture systems (Fig. 3, 4). The oldest and most prominent set consists of mineral-filled joints and small faults that strike 060-075° and two mineralized fault zones that strike 070-075°. The second set consists of mineral-filled fractures that strike NNE. They are present across the site, but are most common near the fault zones. The youngest group consists of joints that strike NNW and cut all other steeply-dipping fractures. These lack chlorite-epidote mineral fillings. They are not shown on figures 3 or 4.

The spacing between the mineralized joints and small faults generally ranges from about 20 cm to 3 m. A kink band with axial planes that strike ~010° deflects some of the joints and faults right-laterally. The spacing between the kinked joints and faults generally is less than 20 cm. Similar kink bands occur elsewhere in the Bear Creek region (Davies and Pollard, 1986; Martel and others, 1988).

The two fault zones (Fig. 3, 4) appear to offset the kink band left-laterally by several meters. They also offset prominent aplite dikes left-laterally by about ten meters each. The fault zones are 2-3 meters thick and are spaced 7-14 meters apart. The rock exposed inside the fault zones is highly fractured, whereas the rock immediately adjacent to the zones is little-fractured (Fig. 5). The topographic expression of the fault zones as shallow troughs indicates that internal fractures are abundant along the length of the fault zones. The fractures contain epidote, chlorite, quartz, calcite, and muscovite (sericite). Even the least fractured rock within the zones appears to erode more readily than the adjacent rock outside the zones, for many outcrops outside the fault zones display glacially polished surfaces, whereas outcrops within the zones have had their polish eroded.

The boundaries of the northern fault zone do not form straight traces across the Waterfall site. Instead, the fault zone is segmented along strike, making a left-step at site I of figure 4 and a bend of ~10° near dike D of figure 3. The segment defined is ~50 m long. The northern boundary fault of this zone has a maximum exposed thickness

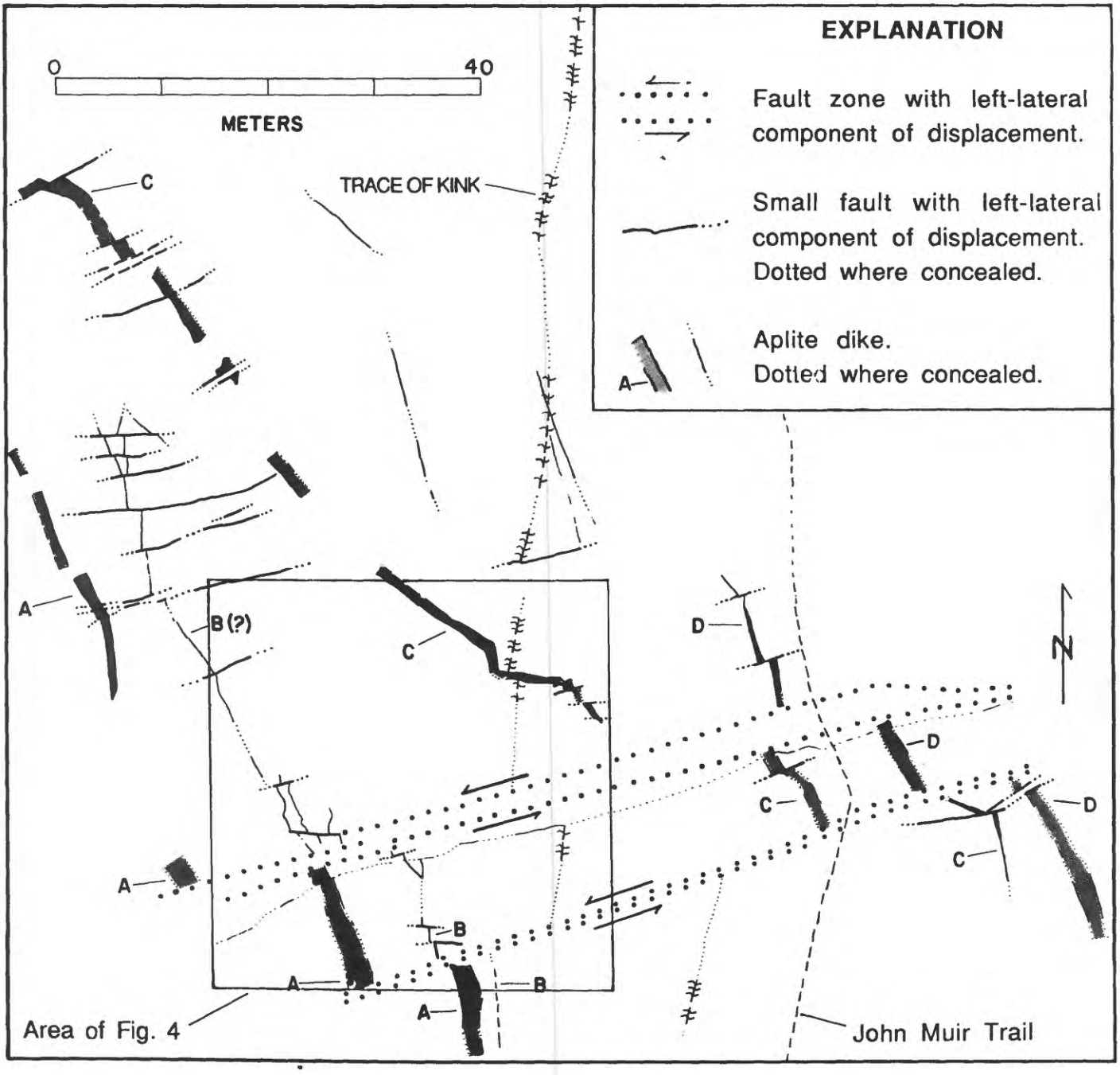

Figure 3.--Map showing displaced dikes and a displaced kink band at the Waterfall site. The dikes and the kink band are offset similar amounts across the fault zones. Note the irregularities in the along-strike trace of the northern fault zone near dikes A and D.

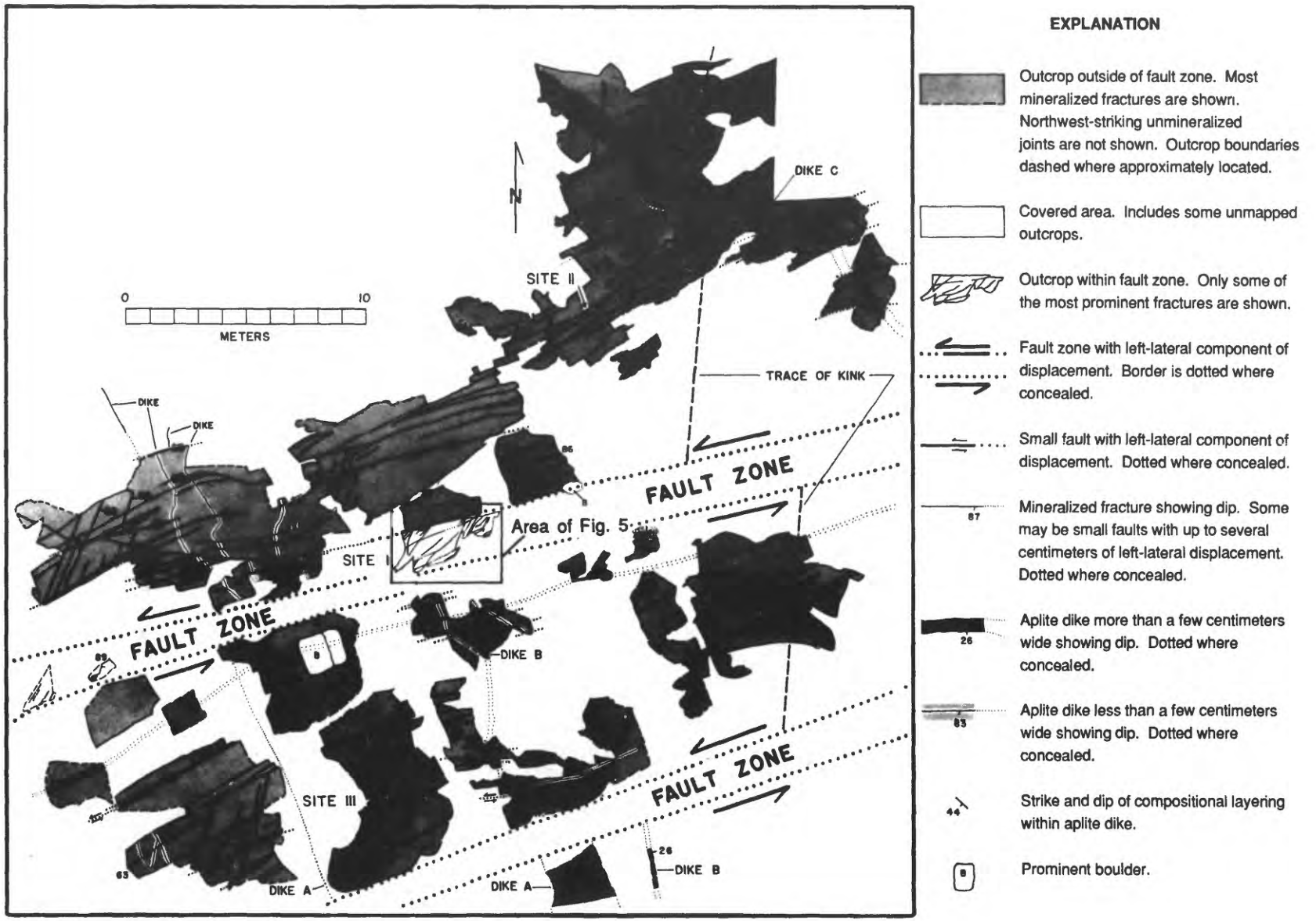

Figure 4.--Map showing joints, faults, and fault zones at the Waterfall site. Sites I, II, and III are referred to in the text. See figure 3 for location.

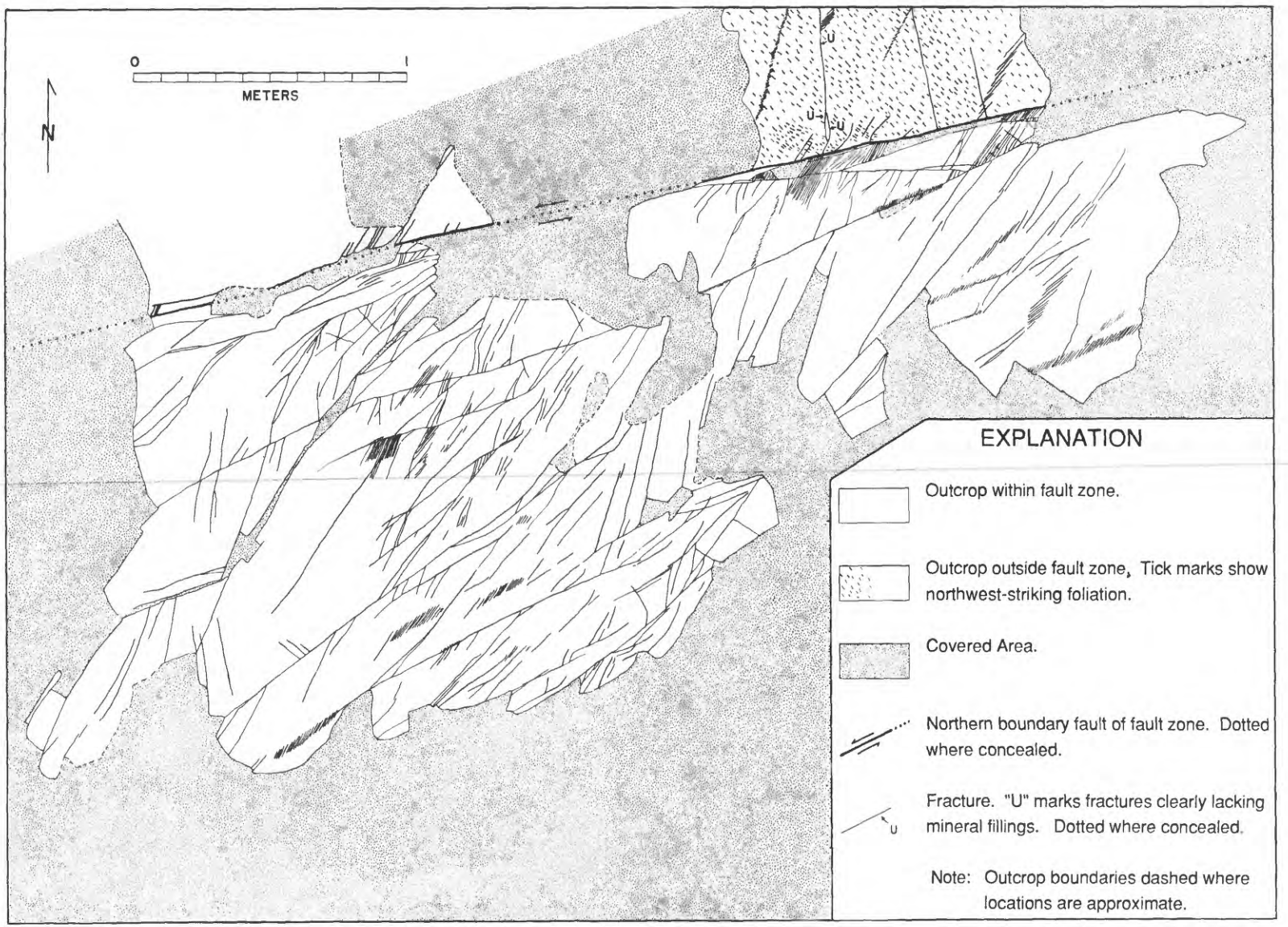

Figure 5.--Map of fractures within a small outcrop in the northern fault zone at the Waterfall site. See figure 4 for location.

of a centimeter. Like all other boundary faults sampled in the Bear Creek region, it has a cataclastic texture, with angular fragments of quartz and feldspar set in a dark green-brown, fine-grained, isotropic matrix. The cataclastic texture contrasts sharply with the mylonitic fabrics of small faults (Segall and Pollard, 1983b).

Two sets of mineral-filled dilatant fractures strike NNE at the Waterfall site. The first set comprises fractures that are no more than several decimeters long and contain epidote, quartz, and chlorite. They typically branch from small faults (site II, Fig. 4), and they most likely formed in response to slip on the small faults. Fractures of the second set typically are one to four meters long and are bordered by halos of hydrothermally altered rock (site III, Fig. 4). These long fractures are common only between or alongside the two fault zones, suggesting that they may have formed in response to slip on the fault zones. Some of the long fractures are continuous structures, whereas others are bands of short echelon cracks. Some of these fractures cross small faults; most are not offset, although some appear to be offset slightly (less than 2 mm). This implies that the long fractures formed after all or nearly all of the slip on the small faults had occurred. Long NNE-striking fractures have been observed along other fault zones in the Bear Creek area, but only along those that accommodated displacements of at least ten meters.

The Gemini fault zone and the Seven Gables site

The Gemini fault zone (Fig. 1) is the largest fault zone mapped by Lockwood and Lydon (1975) within the Mount Abbot quadrangle. The topographic trough marking the fault zone generally is about ten meters wide and extends over an elevation range of approximately 700 m. However, neither the top nor the bottom of the fault zone is exposed, so the fault zone could have a vertical extent much greater than 700 m. The zone as mapped at a scale of 1:62,500 by Lockwood and Lydon (1975) is about 10 km long, but more detailed work by the author has documented displacement across only the central 5-km-interval west of the contact between the Lake Edison and Mono Recesses plutons (Fig. 1). That contact appears to be offset laterally less than 10 m and may not be offset at all. Within the 5-km-interval, the fault zone strikes on the average 075°, dips steeply to the north, and offsets steeply-dipping markers several tens of meters left-laterally.

An exposure of the Gemini fault zone was mapped at the south end of the Seven Gables basin (Fig. 6). Half a kilometer to the west, the zone offsets a steeply-dipping quartz monzonite body ~70 m (Fig. 1). Only the northern part of the fault zone was mapped; the southern part of the zone is covered by talus. The trace of the fault zone is somewhat irregular near this exposure. The fault zone strikes approximately 080° over a 40-50 m interval and dips approximately 70° to the north. Several meters west of the outcrop, the fault zone either assumes a more southwesterly strike or steps to the south. Immediately east of the exposure, the fault zone strikes ~065°.

The rock north of the fault zone contains three major sets of fractures (Fig. 6). The first set consists of fractures that parallel the fault zone and contain epidote and chlorite. The typical spacing between these fractures is half a meter to a few meters, similar to the spacing between ENE-striking fractures at the Waterfall site. Some of the fractures appear to be joints, but others are faults with slickenlines. The second set comprises fractures that strike 010-050° and dip steeply to the east. Some are several meters long. Fractures of the second set appear to be dilatant cracks, for they cross fractures of the first set but do not offset them laterally. This set has three subsets: continuous fractures, bands of short echelon cracks, and ribs of hydrothermally altered granitic rock. These fractures resemble the long, NE-striking fractures at the Waterfall site, and by analogy may be associated with slip on the Gemini fault zone. The third and youngest set of fractures are joints that strike 330-355° and dip steeply. They are not shown on figure 6. These joints appear to lack fillings of epidote and chlorite. They cut but do not offset fractures of the first and second sets.

The Gemini fault zone is divided into bands of markedly different fracture intensity (Fig. 6). Four bands are exposed at the west end of the outcrop; additional bands might exist beneath the talus that covers the southern part of the fault zone. Only the third and fourth bands are exposed at the east end of the outcrop. The first and northernmost band is about 80 cm thick and contains highly fractured rock. The northern and southern boundaries of this band are exposed over a 3-m-long interval, and in this interval both boundaries are sharply defined. Prominent fractures in the band strike ~35° counterclockwise from the band boundaries and are coated with chlorite. These fractures cut an aplite dike but do not offset it laterally. In contrast, the rock adjacent to both sides of the band is much less fractured. Although a lack of markers prevented the displacement across this band from being documented, it appears to be a relict simple fault zone. The second band is about one meter thick and is much less fractured than the first band. This band is exposed over an interval about ten meters long. Its east end apparently pinches out beneath a large boulder. The intensity of fracturing within this band is similar to that in the rock outside the fault zone. The third and fourth bands consist of angular fragments. The third band is one to four meters thick and consists of fragments 5-25 cm long. The surfaces of the fragments are coated with chlorite. The fourth band is at least five meters thick and consists of cobble- to boulder-size blocks that generally lack chloritic coatings. A fault separates the third band from the little-fractured rock of the second band. Where exposed at the east end of the

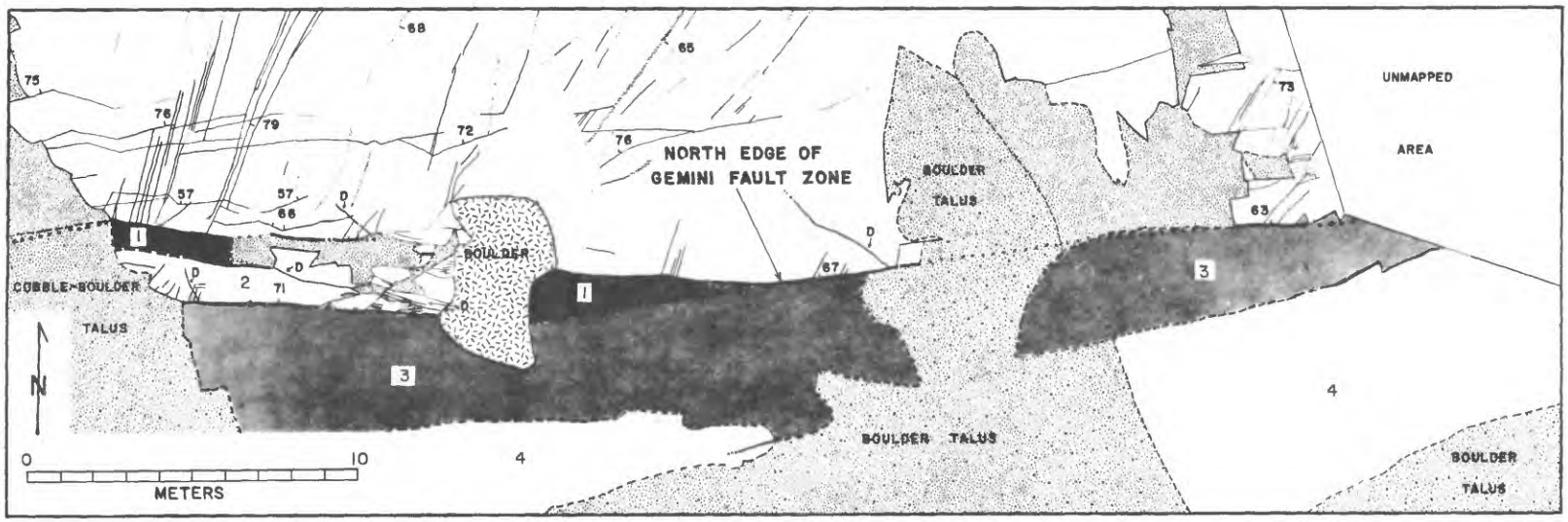

EXPLANATION

Outcrop showing mineralized fractures. Northwest-striking unmineralized joints are not shown.

Band of angular blocks mostly 5-100 cm in diameter.

Band of angular blocks mostly 5-100 cm in diameter with chlorite-coated surfaces.

Band of angular fragments mostly less than 20 cm in diameter with chlorite-coated surfaces.

Talus.

Area covered by granitic sand and angular pebble-sized fragments.

Contact, dashed where location is approximate.

Fault, showing dip. Dashed where location is approximate, dotted where concealed.

Mineralized fracture showing dip. The fractures are planar; the "staircase topography" of the outcrop causes many of the fracture traces to be nonlinear. Dotted where concealed.

Band of echelon fractures showing dip of band.

Raised rib of hydrothermally altered granodiorite showing dip.

Aplite dike. Dotted where concealed.

Prominent boulder.

Figure 6.--Map of fractures along the northern margin of the Gemini fault zone at the Seven Gables site.

outcrop, the contact between the third and fourth bands proves to be a fault with a cataclastic texture. West of that spot it strikes nearly parallel to the north edge of the fault zone.

Observations at other points along the Gemini fault zone confirm its banded across-strike structure. For example, half a kilometer east of the Seven Gables site, an outcrop of moderately fractured rock lies in the center of the trough marking the fault zone. The outcrop apparently is less fractured and hence more resistant to erosion than the rock at the edges of the fault zone. The most prominent fractures within the outcrop strike oblique to the fault zone at 037° to 058°. The outcrop also contains faults that strike subparallel to the fault zone and divide the outcrop into bands. The intensity of fracturing and the color of the rock varies from one band to another. The internal faults are spaced from several centimeters to a few meters apart, similar to the spacing of fractures that strike ENE outside the fault zone. As is typical along the Gemini fault zone, fractures striking oblique to the fault zone are scarce in the rock immediately adjacent to the zone.

GROWTH OF COMPOUND FAULT ZONES

Simple fault zones and compound fault zones

The fault zones that extend through the Waterfall and Seven Gables sites are larger and more developed than simple fault zones. For example, most simple fault zones appear to be 0.1-1 km long, less than a few meters thick, and have accommodated less than ten meters of lateral displacement. In contrast, the Gemini fault zone is 5-10 km long, approximately ten meters thick, and has accommodated ~70 m of lateral displacement. The Gemini fault zone and the network of faults at the Waterfall site are structurally more complex than simple fault zones. Within simple fault zones, two boundary faults are linked side-to-side, and faults parallel to the boundaries are rare. In contrast, the Gemini fault zone incorporates many internal faults that parallel its boundaries, and is referred to here as a *compound fault zone*. The fault network at the Waterfall site is of an intermediate nature, for small faults and simple fault zones are distinct, but long oblique fractures connect some of the simple fault zones side-to-side. The fault network at the Waterfall site can therefore be regarded as a compound fault zone deactivated at an early stage of development.

The across-strike structure of simple and compound fault zones reflects the distribution of joints in local unfaulted outcrops. Both kinds of zones are paralleled by steeply-dipping small faults and joints. ENE-striking fractures inside and outside the Gemini fault zone (Fig. 6), as well as those in the vicinity of the Waterfall site (Fig. 3, 4), generally are spaced several decimeters to a few meters apart. This is similar to the spacing of joints and the thicknesses of simple fault zones throughout the Bear Creek region (Segall and Pollard, 1983a, b; Martel and others, 1988) and indicates that compound fault zones developed from arrays of joints. The compound fault zones apparently did not develop from joints with either an unusually close or unusually wide spacing, nor did the growth of the zones involve the generation of new fractures parallel to the zone. The across-strike structure of compound fault zones also indicates that many fractures were incorporated into the fault zones as they grew in thickness.

The segmented along-strike structure of compound fault zones also reflects the distribution of joints in local unfaulted outcrops. The segment of the Gemini fault zone at the Seven Gables exposure is 40-50 m long, and the segment in the northern fault zone at the Waterfall site is ~50 m long (Fig. 3). The principal fractures in the network of faults east of the Waterfall site usually are no more than several tens of meters long. The longer joints in local outcrops also have maximum lengths of several tens of meters (Segall and Pollard, 1983a). It seems likely that the simple and compound fault zones preferentially developed from joints several tens of meters long.

Compound fault zones are larger than simple fault zones, have accommodated greater displacements, and are more complex structurally, yet both types of zones appear to have evolved from similar distributions of joints. The compound fault zone exposures appear to contain relict small faults and simple fault zones. This indicates that compound fault zones grew by the linkage of smaller faults and simple fault zones. The formation of fault zones several kilometers long apparently did not require the presence of joints several kilometers long.

Localization of Deformation

Field relations among small faults, kink bands, and simple fault zones indicate that fault slip in the Bear Creek region became localized on a decreasing number of structures through the course of time (Martel and others, 1988). At several outcrops, including the Waterfall site (Fig. 3, 4), kink bands deflect small faults. Small faults do not appear to offset kink bands significantly if at all. Thus, at least locally, kinking postdated slip on small faults. Kink bands, in turn, appear to be offset by simple fault zones. This suggests that slip on simple fault zones postdated the kinking, and therefore at least some of the slip on small faults. Structural relations at the Waterfall site and the Seven Gables outcrop suggest that slip on compound fault zones also post-dated most of the slip on adjacent small faults. Several long NE-striking fractures that splay from the fault zones at the Waterfall site cross adjacent faults without being offset visibly, although a few splay cracks are offset slightly. Long splay fractures on

the north side of the Seven Gables outcrop also cross adjacent fractures parallel to the Gemini fault zone without being offset. Assuming that the long splay fractures formed as a result of slip along large fault zones, these cross-cutting relationships indicate that slip occurred along the compound fault zones after slip had largely ceased on most adjacent small faults.

FACTORS AFFECTING SLIP AND FRACTURING ALONG FAULTS AND FAULT ZONES

The incremental and cumulative slip along faults and fault zones largely determine the nature of fracturing in the adjacent rock. Theoretical studies (Pollard and Segall, 1987) and experimental work (Brace and Bombolakis, 1963) indicate that splay fractures form along sliding surfaces where displacement gradients are sufficiently large. Therefore, in addition to using the distribution of fault slip to infer the distribution of fractures along faults and fault zones, the distribution of fractures can be used to gain insight into the factors controlling the distribution of fault slip.

Geometric Factors Affecting Fault Slip

The evolution of faulting in the Bear Creek area involved the linkage of of noncoplanar structures. As a result, faults and fault zones have irregular geometries along strike. The scale of these irregularities varied from one stage of faulting to another. Small faults evolved from joints. Detailed work (Segall and Pollard, 1983a) shows that the joints are not perfectly planar structures. Instead, they consist of numerous parallel echelon strands spaced less than a few centimeters apart. When a joint subsequently slipped and became a small fault, these strands became linked. As a result, small faults formed with slightly irregular surfaces. Irregularities along the strike of small faults have amplitudes of less than a few centimeters. Simple fault zones formed as small faults linked side to side and end to end. As a result, these zones are segmented along strike. Adjacent segments join at steps as wide as a few meters or at bends of as much as 20° (Martel and others, 1988). Irregularities along the strike of simple fault zones thus have amplitudes of a few meters at wavelengths of several tens of meters. The formation of compound fault zones involves the linkage of simple fault zones. Because the linkage process involves fracturing, and splay cracks along compound fault zones can be several meters long, the irregularities along the strike of compound fault zones probably have amplitudes of several meters. The size of along-strike geometric irregularities thus increased as faulting evolved in the Bear Creek region.

The geometric irregularities along small faults do not appear to have influenced fault slip significantly, for splay fractures are common near fault ends but are scarce elsewhere. This distribution of fractures indicates that displacement gradients were steep near the ends of small faults (steep enough to result in stress concentrations sufficient to fracture the adjacent rock), but were low elsewhere along small faults. Apparently the geometric irregularities along small faults were too small to cause displacement to be distributed in a markedly uneven manner.

The geometric irregularities along simple fault zones appear to have influenced slip to a greater extent. The rock adjacent to simple fault zones is fractured at spots other than the fault zone ends; fractures are abundant near segment ends. Apparently the geometric irregularities at segment ends were of sufficient size to cause steep displacement gradients as the boundary faults slipped. The segment end irregularities did not present permanent barriers to slip however, for the displacements across adjacent segments of some simple fault zones appear to be very similar (Martel and others, Fig. 9a, 1988). Apparently displacement was eventually transferred from one segment to another. The geometric irregularities along compound fault zones are probably at least as large as those along simple fault zones. Therefore, it seems likely that geometric irregularities at segment ends also caused subsidiary fractures to form during slip along compound fault zones.

Non-Geometric Factors Affecting Fault Slip

Factors other than geometric irregularities along the boundary faults appear to have affected the distribution of fractures along simple fault zones. Along the central portions of a simple fault zone segment, fractures that splay to the inside of the zone are abundant, whereas fractures that splay to the outside are scarce. If these fractures were produced because geometric irregularities restricted fault slip, then roughly as many external fractures as internal fractures would be expected. Something other than geometric irregularities must have caused the internally directed fractures to form. Based on elastic stress analyses, Martel (1987) suggested that the mechanical interaction of the boundary faults could cause internally directed fractures to develop preferentially along the central portions of simple fault zones.

Observations at the Waterfall site suggest that slip surfaces within compound fault zones also may interact mechanically to cause preferential development of internal fractures. The long mineralized NE-striking fractures at the Waterfall site (Fig. 4) are more common between the two simple fault zones than to the outside, and they are not

associated with any obvious geometric irregularities along the two fault zones. Perhaps the mechanical interaction of the two simple fault zones was responsible for some of those fractures.

Effect of Cumulative Slip on Fracturing Along Fault Zones

Simple and compound fault zones accommodated markedly different amounts of displacement, and the gross distributions of oblique fractures outside the zones probably differ as a result. Outside a simple fault zone abundant fractures are associated only with the large irregularities near the ends of fault zone segments. Geometric irregularities elsewhere along the boundary faults of simple fault zones apparently were too small for fault slip to cause extensive external fracturing. The oblique fractures that did develop are restricted to small areas near segment ends because the displacement across a simple fault zone is a small fraction of the length of the fault zone segments. In contrast, along a large interval of a compound fault zone the cumulative displacement reached several tens of meters, displacements comparable to the lengths of simple fault zone segments. Along that interval, the displacement of rock past large geometric irregularities must have resulted in widespread fracturing. Towards the ends of a compound fault zone the lateral displacement presumably decreases. Along some intervals the displacement must be small relative to the length of a fault zone segment. In these places, outwardly directed fractures are probably concentrated in areas near segment ends in a manner similar to that along simple fault zones. Outwardly directed fractures therefore may be widespread along the central portion of a compound fault zone and distributed in clusters nearer its ends.

DISCUSSION

Data collected from many fault zones show that thicker fault zones generally accommodate larger displacements than narrower ones (Robertson, 1983; Wallace and Morris, 1986). This relationship suggests that many fault zones have grown in thickness as they slipped. Microstructural observations suggest that the process of thickening at the grain-scale level commonly occurs by a diffuse front of brittle deformation migrating laterally into the host rock. Friction experiments with orthoquartzite (Hundley-Goff and Moody, 1980), sandstone (Engelder, 1974), and crystalline rock (Jackson and Dunn, 1974) show that artificial faults can increase in thickness as grains in the host rock adjacent to the fault become fractured and then incorporated into the fault. A similar process apparently operated over distances of a few grain diameters along the boundary faults in the Mount Abbot quadrangle (Martel and others, 1988). Such a process may also operate at a much larger scale. Within both the White Rock thrust fault in Wyoming (Mitra, 1984) and the Punchbowl fault of the San Andreas system (Chester and Logan, 1986), deformation is greatest in the middles and decreases towards the margins. The intensity of deformation in ductile shear zones also commonly decreases away from the center of the zone (Ramsay, 1980). These observations suggest that many natural fault zones and shear zones also thickened as a diffuse front of brittle or ductile deformation migrated from a central weak zone into the host rock.

The observations along Bear Creek indicate that neither the simple nor the compound fault zones in the Mount Abbot quadrangle grew in thickness by such a diffusive process. The compound zones thickened as fractures linked small faults and simple fault zones. The fault zones thickened in increments determined by the initial joint spacing and the distance splay cracks could propagate. This process of fault zone formation allows deformation to be most intense at the edges of a fault zones rather than in its center, while still enabling the zone to maintain sharp boundary faults. As the fault zones grew and displacement increased, the geometric irregularities along strike became larger, not smaller. In this sense, as displacement increased the fault zones became rougher, not smoother. This process of growth probably is not unique to the Mount Abbot quadrangle. Single systems of parallel fractures occur in a broad variety of otherwise unfractured rocks. Other kinds of planar anisotropies also may provide a mechanical foundation similar to the Mount Abbot joints. For example, Swanson (1989) has described brittle fault zones that developed in mylonitic host rocks which are strikingly similar to the compound fault zones of the Mount Abbot plutons. Conditions sufficient for compound fault zones to form elsewhere thus appear common. It seems likely that many brittle fault zones that formed in rocks with strong planar penetrative fabrics may have formed in a manner similar to the compound fault zones of the Bear Creek area.

ACKNOWLEDGEMENTS

This report is an outgrowth of my Ph.D. research at Stanford University under David Pollard. The research was supported by National Science Foundation Grants EAR8417021 and EAR8319431. I thank David Pollard and Rick Sibson for their reviews of this manuscript.

REFERENCES CITED

Brace, W.F., and E.G. Bombolakis, 1963, A note on brittle crack growth in compression: Journal of Geophysical Research, v. 68, 3709-3713.

Chester, F.M., and Logan, J.M., 1986, Implications for the mechanical properties of brittle faults from observation of the Punchbowl fault zone, California: Pure and Applied Geophysics, v. 124, p. 79-106.

Davies, R.K., and Pollard, D.D., 1986, Relations between left-lateral strike-slip faults and right-lateral monoclinal kink bands in granodiorite, Mt. Abbot quadrangle, Sierra Nevada, California: Pure and Applied Geophysics, v. 124, p. 177-201.

Davis, G.H., 1984, Structural Geology of Rocks and Regions: New York, New York, John Wiley and Sons, 492 p.

Engelder, J.T., 1974, Cataclasis and the generation of fault gouge: Geological Society of America Bulletin, v. 85, p. 1515-1522.

Hobbs, B.E., Means, W.D., and Williams, P.F., 1976, An Outline of Structural Geology: New York, New York, John Wiley and Sons, 571 p.

Hundley-Goff, E.M., and Moody, J.B., 1980, Microscopic characteristics of orthoquartzite from sliding friction experiments. I. sliding surface: Tectonophysics, v. 62, p. 279-299.

Jackson, R.E., and Dunn, D.E., 1974, Experimental sliding friction and cataclasis of foliated rocks: International Journal of Rock Mechanics and Mining Sciences and Geomechanics Abstracts, v. 11, p. 235-249.

Lockwood, J.P., and Lydon, P.A., 1975, Geologic map of the Mount Abbot quadrangle, California: U.S. Geological Survey Geologic Quadrangle GQ-1155, scale 1:62,500.

Martel, S.J., 1987, Development of strike-slip fault zones in granitic rock, Mount Abbot Quadrangle, Sierra Nevada, California: Stanford University Ph.D. thesis, 184 p.

Martel, S.J., Pollard, D.D., and Segall, P., 1988, Development of simple strike-slip fault zones, Mount Abbot quadrangle, Sierra Nevada, California: Geological Society of America Bulletin, v. 100, p. 1451-1465.

McKee, J.W., Jones, N.W., and Long, L.E., 1984, History of recurrent activity along a major fault in northeastern Mexico: Geology, v. 12, p. 103-107.

Muehlberger, W.R., 1986, Different slip senses of major faults during different orogenies: the rule?: in Proceedings, International Conference on Basement Tectonics, 6th, Santa Fe, September, 1985: Salt Lake City, Utah, International Basement Tectonics Association, p. 76-81.

Mitra, G., 1984, Brittle to ductile transition due to large strains along the White Rock thrust, Wind River Mountains, Wyoming: Journal of Structural Geology, v. 6, p. 51-61.

Noyes, H.J., Wones, D.R., and Frey, F.A., 1983, A tale of two plutons: petrographic and mineralogic constraints on the petrogenesis of the Red Lake and Eagle Peak plutons, central Sierra Nevada, California: Journal of Geology, v. 91, p. 353-379.

Pollard, D.D., and P. Segall, 1987, Theoretical displacements and stresses near fractures in rocks: with applications to faults, joints, veins, dikes, and solution surfaces, in Atkinson, B.K., ed., Fracture Mechanics of Rock: Academic Press, London, p. 277-349.

Pollard, D.D., Segall, P., and Delaney, P.T., 1982, Formation and interpretation of dilatant echelon cracks: Geological Society of America Bulletin, v. 93, p. 1291-1303.

Price, N.J., 1981, Fault and Joint Development in Brittle and Semi-brittle Rock: Oxford, England, Pergammon Press, 176 p.

Ramsay, J.G., 1980, Shear zone geometry: a review: Journal of Structural Geology, v. 2, p. 83-99.

Robertson, E.C., 1983, Relationship of fault displacement to gouge and breccia thickness: Mining Engineering, v. 35, p. 1426-1432.

Segall, P., and Pollard, 1983a, Nucleation and growth of strike-slip faults in granite: Journal of Geophysical Research, v. 88, p. 555-568.

Segall, P., and Pollard, D.D., 1983b, Joint formation in granitic rock of the Sierra Nevada: Geological Society of America Bulletin, v. 94, p. 563-575.

Segall, P., and Simpson, C., 1986, Nucleation of ductile shear zones on dilatant fractures: Geology, v. 14, p. 56-59.

Sibson, R.H., 1977, Fault rocks and fault mechanisms: Journal of the Geologic Society of London, v. 133, p. 191-213.

Sibson, R.H., 1986, Earthquakes and rock deformation in crustal fault zones: Annual Reviews of Earth And Planetary Sciences, v. 14, p. 149-175.

Sibson, R.H., White, S.H., and Atkinson, B.K., 1981, Structure and distribution of fault rocks in the Alpine fault zone, New Zealand, in McClay, K.R., and Price, N.J., eds., Thrust and Nappe Tectonics: London, Blackwell Scientific Publications, p. 197-210.

Stern, T.W., Bateman, P.C., Morgan, B.A., Newell, M.F., and Peck, D.L., 1981, Isotopic U-Pb ages of zircon from the granitoids of the central Sierra Nevada, California: U.S. Geological Survey Professional Paper 1185, 17 p.

Suppe, J., 1985, Principles of Structural Geology: Englewood Cliffs, New Jersey, Prentice-Hall Inc., 537 p.

Swanson, M.T., 1989, Psuedotachylyte-bearing strike-slip duplex structures in the Fort Foster Brittle Zone of southernmost Maine: Journal of Structural Geology, v. 11 (in press)

Wallace, R.E., and Morris, H.T., 1986, Characteristics of faults and shear zones in deep mines: Pure and Applied Geophysics, v. 124, p. 107-125.

NUMERICAL MODEL STUDIES OF DYNAMIC RUPTURE PROCESSES

by

Paul G. Okubo

United States Geological Survey
345 Middlefield Road
Menlo Park, California 94025

ABSTRACT

Motivated by laboratory model studies of both quasistatic and dynamic, or stick-slip, frictional sliding along simulated faults in rock samples, a series of numerical modeling experiments has been undertaken to simulate the full cycle of fault response. The nucleation of the rupture under quasistatic conditions is combined with the dynamic extension of fault rupture to rupture arrest. The post-seismic fault restrengthening can be simulated by resuming the quasistatic calculation.

The key element in these studies is the use of a laboratory-derived friction constitutive relation of the form proposed by Dieterich for describing frictional sliding on surfaces in rock samples and further developed by Ruina and others. As commonly used, these constitutive relations are characterized by an explicitly rate-dependent term and a fault state-dependent term which involves loading history and slip rate history. The combination of the rate- and state-dependent effects yields fault behavior following suddenly introduced increases in slip rate which resembles that associated with a slip-weakening fault response of the kind used in earlier numerical model studies of dynamic rupture propagation. Use of the state variable fault constitutive relation is preferred because it provides for both slip weakening and fault restrengthening. This formulation is also capable of accounting for a range of laboratory observations. Alternative constitutive formulations that have been used in dynamic rupture simulations do not encompass a corresponding range of laboratory-observed effects. Nor do they include a means for fault restrengthening.

The models are two-dimensional plane strain. Using a solution for relating fault stress to fault displacements using dislocation equations developed by Dieterich, the tests begin with the quasistatic sliding of a highly stressed fault patch, or asperity, surrounded by a less highly stressed region on the fault. The dislocation solution proceeds until slip rate at any position on

the fault reaches a specified maximum slip rate, in this stage of the calculation identified with the onset of fault instability. At this step, the fault state is frozen and used as the initial conditions for a boundary integral solution for the dynamic extension of a mode II shear crack. By following this procedure, the nucleation of the dynamic rupture is achieved without artificially forcing the extension of the fault failure surface.

Rupture propagation in the unstable or dynamic phase of the cycle is simulated with the boundary integral solution. For this discussion, the asperity is assigned a fixed initial stress level and different model calculations are carried out to demonstrate the effects of adjusting the initial asperity size. The rupture grows at the Rayleigh wave speed out of the nucleation configuration achieved during the quasistatic calculation. When the rupture front encounters the edge of the asperity, the rupture velocity suddenly decreases. Rupture typically extends beyond the edge of the asperity, and the dynamic overshoot, regarded here as the amount by which the rupture extends beyond the edge of the asperity, varies with the square of the initial asperity size.

INTRODUCTION

With a growing body of seismological and geological observations of earthquake rupture and fault characteristics, it is suggested that there are recognizable features of fault zones that can be related to details of the earthquake rupture process. Besides affecting radiated ground motions, some of these features may also control the starting and stopping of ruptures and define the extent of fault segments. Thus, there is obvious importance, with regard to both earthquake prediction and ground motion estimation, to developing further the methodologies for recognizing and classifying possible segment boundaries.

Theoretical models of the faulting and earthquake process can complement the observational fault studies. By including features of interest in such models it is possible to determine the expected behavior of a fault and to understand the role of these features in the rupture process. Of interest is the variability of the faulting motion due to properties of the fault. A dynamic modeling approach is required to study this behavior.

The key element in a dynamic model is the constitutive relation which is selected to characterize the material response to the applied loads and, thus, govern the manner in which the crack extends over the failure surface. Using the notion of a crack-tip cohesive zone introduced by Barenblatt [1959] for tensile cracks, Ida [1972] introduced fault slip weakening constitutive models for shear cracks. In a subsequent paper [Ida, 1973], he used this type of cohesive zone fault model to determine seismic ground motion parameters and to demonstrate the effects of fault model parameters on ground motion. The initial motivation for introducing the cohesive zone was to mathematically eliminate the singularity which characterizes the elastic-brittle crack tip stress field. Independently, Palmer and Rice [1973] proposed a slip

weakening model for the behavior of a shear band in soil. Their introduction of such a constitutive relation was prompted by soil mechanics experiments, and an important part of their analysis was the identification of size effects on the behavior of the shear band. They also derived an expression for the size of the cohesive zone along the shear band which serves as a guide for comparing laboratory to field observations [Rice, 1980].

As mentioned by Andrews [1985], the use of a slip weakening or other cohesive zone fault model has the advantage over a critical stress intensity factor model with regard to the way in which stresses at the crack tip are treated. Rather than modeling a singular elastic brittle crack solution with a discrete numerical method, the slip weakening model is associated with a finite continuous crack solution. A simple realization of a slip weakening model is presented in figure 1, featuring a linear decrease in fault strength from a peak stress to a residual stress over a slip increment d_r . As mentioned above, parameters of the slip weakening behavior can be related to ground motion parameters and tied to other aspects of the rupture process like stable fault nucleation and the formation of a critical shear crack for unstable rupture propagation [Andrews, 1976 and 1985; Day, 1982].

However, it has also been pointed out [Dieterich, 1979a; Rice, 1983] that slip weakening, with explicit fault weakening with displacement, does not by itself include a means by which a fault can regain strength. This would limit the fault's tendency to generate repeated slip events and produce sequences of events. Therefore, while simple slip weakening laws might be satisfactory for describing the fault behavior during a single earthquake, characterizing the complete cycle of fault behavior would require modifying such laws to produce the desired fault restrengthening effects. The state variable friction model is preferred as an alternative fault constitutive formulation to slip weakening. It directly allows for fault restrengthening as well as a displacement weakening-like effect and it can account for the range of rate- and time-dependent frictional sliding behavior observed in the laboratory.

In this paper, rupture models using a form of the state variable frictional constitutive relation are presented. The rupture models feature the failure of a central high-stress patch surrounded by low-stress fault regions. Rupture nucleation is achieved naturally, without artificial forcing, with a quasistatic fault model and state variable friction law.

STATE VARIABLE FRICTION MODEL

The development of the state variable friction model for the sliding of simulated fault surfaces in rock samples can be traced to the observations of the time dependence of the strength of stationary frictional contact in Dieterich [1972]. In that work, it was observed that frictional resistance or strength increased as the logarithm of the time of stationary contact. Dieterich [1978] presented additional observations that the coefficient of friction under constant velocity sliding conditions is proportional to the logarithm of the inverse of the slip rate ($1/v$). It was also observed that, following a sudden change in slip rate, a transitional

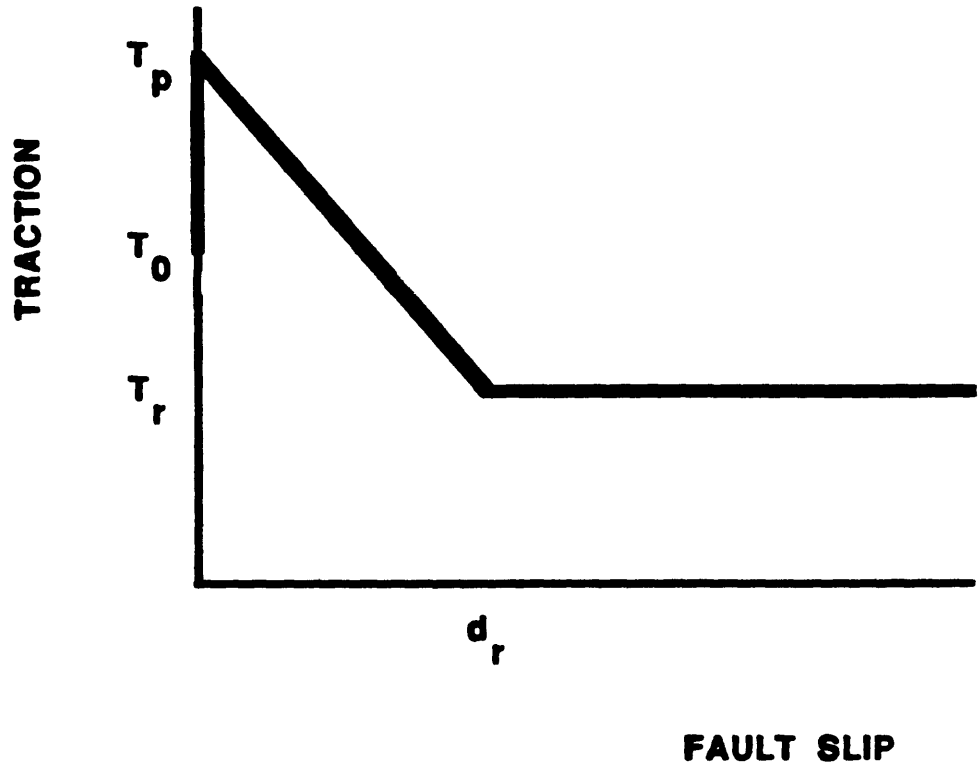

Figure 1. Idealized slip weakening fault constitutive model.

slip increment was required before a new population of contacts characteristic of the new slip rate was established. Frictional resistance during this slip increment evolves with displacement in an exponential-like way to the new steady value. Dieterich introduced the notion of average lifetime of a population of contacts at constant velocity to be compatible with the time dependence observed earlier. Additional experiments including a variety of imposed loading conditions and fault surface conditions established the rate- and state-dependencies, and the state variable friction constitutive relation was developed [Dieterich, 1979a and 1981; Ruina, 1980 and 1983].

As established from laboratory observations of the quasistatic sliding of rock surfaces under constant applied normal force, the principal features of the state variable friction model are:

(i) A steady state effect. For sliding at constant slip rate, frictional resistance mainatains a steady state value which is proportional to the logarithm of inverse slip rate.

(ii) A direct velocity effect. When a sudden change in slip rate is introduced, frictional resistance changes in the same sense. That is, suddenly imposed increases in slip rate lead to sudden increases in friction and sudden decreases in slip rate lead to sudden decreases in friction.

(iii) Characteristic slip distances. Following changes in slip rate, frictional resistance evolves toward the steady-state value for that slip rate. The evolution toward steady-state friction is controlled by an exponential decay with sliding distance. The decay constant, referred to as d_c , depends on fault surface conditions including fault roughness and, if present, fault gouge condition. For coarse fault surfaces and large gouge particle size, d_c is large; smooth fault surfaces and fine gouge particles are associated with smaller d_c .

Sliding behavior representative of that observed during these sliding tests is illustrated schematically in figure 2. From initial steady sliding rate v_1, slip rate is suddenly increased to v_2. Following the sudden increase in frictional resistance due to the increase in slip rate, friction decreases gradually through an apparent displacement weakening to a constant level associated with slip rate v_2. Note the similarities between figure 1 and the parts of figure 2 where the slip rate is increased. In general, however, both the peak frictional resistance and the residual frictional strength depend on fault slip rate in the state variable model.

When used in the theoretical analysis of frictional sliding systems, the state variable friction models have been able to produce a variety of behavior. Numerical simulations of the sliding behavior of a simple block/spring system with state variable friction reproduce in detail features of laboratory experiments [*e.g.*, Dieterich, 1979b, 1980 and 1981; Ruina, 1983]. Dieterich [1981], Ruina [1983], Rice and Ruina [1983], Gu et al. [1984], Rice and Tse [1986], and

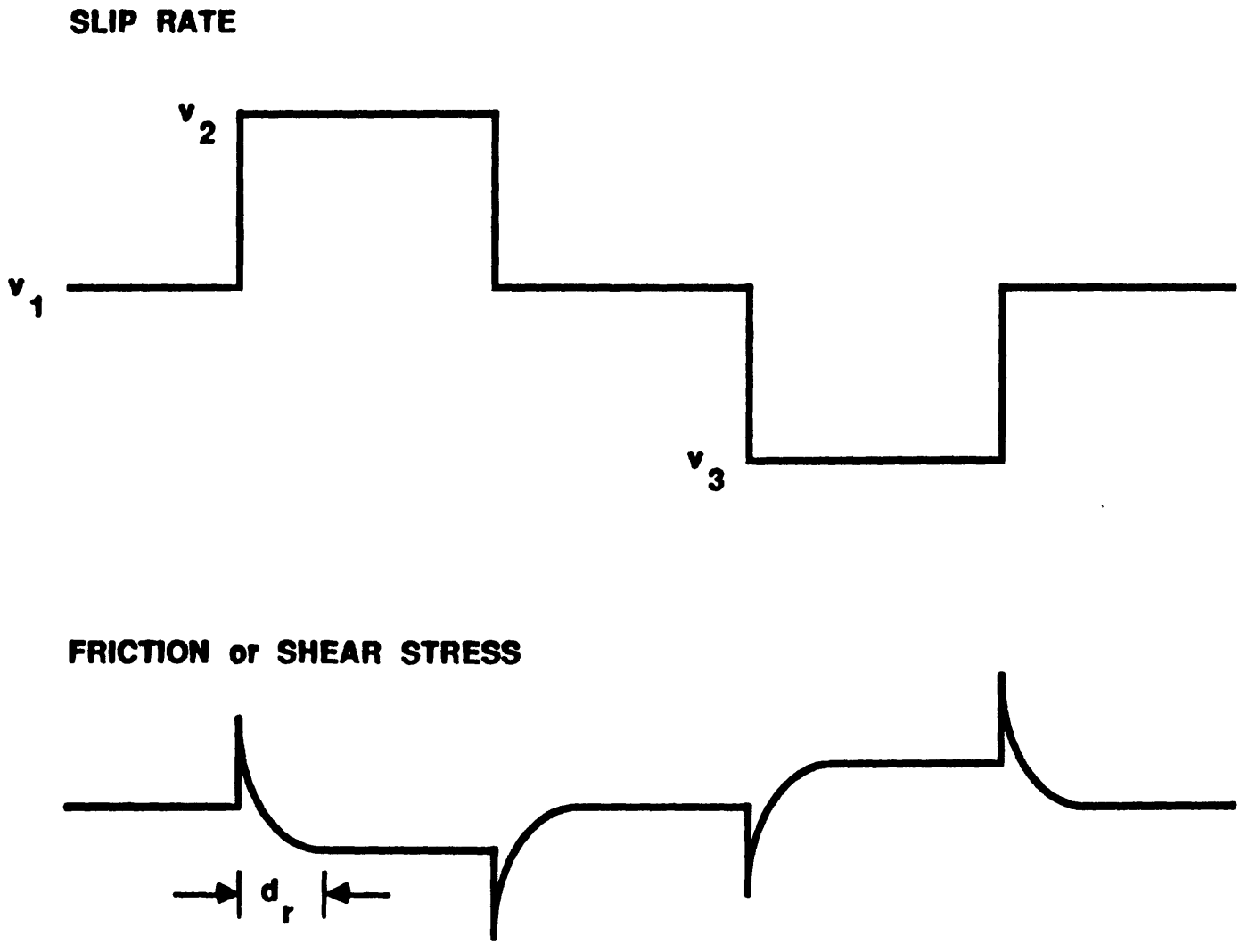

Figure 2. Schematic drawing of frictional response during velocity stepping experiment. Top curve is applied slip rate as a function of fault offset. Bottom curve is frictional resistance in response to introduced slip rate changes.

Tullis and Weeks [1986] have discussed the sliding stability of such a system. State variable models have also been used in numerical simulations of the motion along large scale, *i.e.* crustal, faults. These simulations produce earthquake sequences [Cao and Aki, 1986] and the confinement of unstable slip to the uppermost brittle crust upon appropriate specification of the friction model parameters [Mavko, 1980 and unpublished manuscript, 1983; Tse and Rice, 1986]. Further understanding of aspects of this friction constitutive description remains the object of much research.

While developed and applied to frictional sliding under quasistatic conditions, it has also been proposed that the state variable formulation is also appropriate for unstable sliding [Okubo and Dieterich, 1984 and 1986]. That suggestion is based on high frequency (200 kHz) recordings of fault displacements and fault shear strains from different transducer locations as stick-slip frictional instabilities are generated and propagate along a simulated fault. It might be somewhat intuitive that this would be the case, as the fault materials in both the quasistatic and the stick-slip tests are the same. It is important to recognize, though, that the rates and time scales relevant to stick-slip propagation, rupture velocities of 10^5 cm/s, slip speeds of 1 to 10 cm/s and stress drops occurring over 10^{-5} to 10^{-3} s intervals, are substantially different from those typically used in the quasistatic sliding tests, no rupture propagation, slip speeds of 10^{-4} to 10^{-2} cm/s and stress drop time intervals of 10^{-2} s or greater. As discussed in Okubo and Dieterich [1986], key elements in the application of the state variable models to dynamic high speed slip are cutoffs to both the rate and state dependencies at effectively high slip rates. Suggestions of the existence of the high speed cutoff to the steady state friction were presented in Dieterich [1978].

For the remainder of this paper, the specific form of state variable friction model that will be assumed is:

$$\mu = \mu_0 + b \log\left(b_1 \theta + 1\right) - a \log\left(\frac{a_1}{v} + 1\right) \qquad (1)$$

where μ_0, a, a_1, b, and b_1 are empirically determined model coefficients and fault slip rate is v. The direct velocity effect is contained in the last term on the right hand side of (1), and the state evolution including the characteristic slip distance effect is contained in the middle term. θ is the state variable for which the evolution is given by

$$\frac{d\theta}{dt} = 1 - \frac{\theta v}{d_c}. \qquad (2)$$

For sliding at constant slip rate v, the state evolution can be expressed as

$$\theta = \frac{d_c}{v} + \left(\theta_0 - \frac{d_c}{v}\right) \exp\left(\frac{u_0 - u}{d_c}\right). \qquad (3)$$

θ_0 and u_0 are the values of θ and fault displacement u at which constant velocity sliding at v is initiated. d_c is the exponential decay constant which leads to the observations of a characteristic slip displacement d_r following suddenly introduced changes in fault slip rate. For large displacement u at constant slip rate, θ approaches a steady state value $\theta_{ss} = d_c / v$. Cutoffs to the rate and state dependent behavior appear due to the inclusion of the + 1 terms in the arguments of the logarithms in equation (1). Their effects are discussed in Okubo and Dieterich [1986] and Dieterich [1986]. As velocity increases, μ increases until $v >> a_1$. Due to the slip rate cutoff, larger values of slip rate do not lead to larger values of μ. Similarly, at small θ such that $b_1\theta << 1$, the cutoff to the decrease in μ with decreasing θ is encountered.

NUMERICAL MODELING RESULTS

The rupture calculations focus on the asperity model. The notion of the asperity as used in the seismological sense is generalized somewhat from its specific application to surface roughness geometry and the theory of contact. The asperity is defined as a fault patch over which there is a relatively high stress required to sustain slip, surrounded by fault surface which slips freely. During a rupture episode, slip on the asperity is associated with a finite stress drop, while slip taking place on the fault immediately outside of the asperity is associated with zero net stress drop. The asperity model is discussed in numerous papers, including that by Rudnicki and Kanamori [1981].

The problem geometry for the asperity calculations is shown in figure 3. Friction model parameters are those listed earlier and a uniform normal stress σ of 100 bars is specified to act over the entire fault. Uniform initial values of $\theta = 10^6$ s are also specified. The high stress patch is established by specifying that an initial shear stress level of 65 bars acts over the central part of the fault. Outside of this patch, the remainder of the fault is stressed to 60 bars, equal to the frictional resistance for very high speed steady state sliding. The starting dimension of the high stress patch L_0 is varied to look at the amount of overshoot, or penetration of slip, into the less highly stressed part of the fault. Parameters of the different

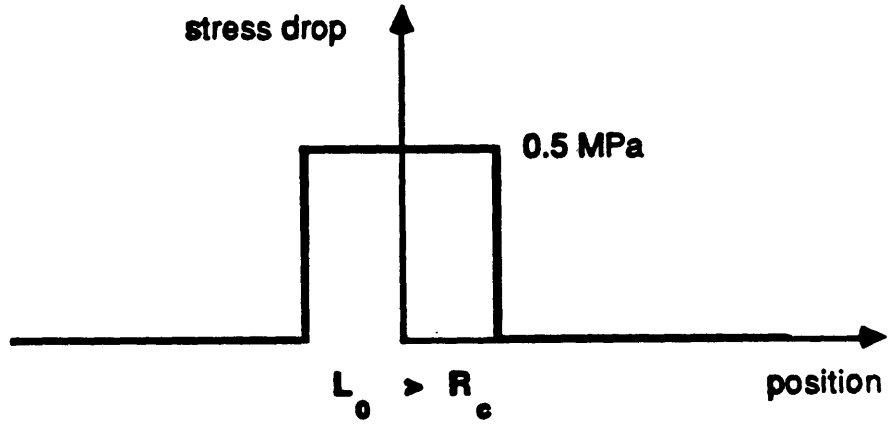

Figure 3. Sketch of initial stress distributions for asperity rupture models. Initial asperity size L_0 is varied.

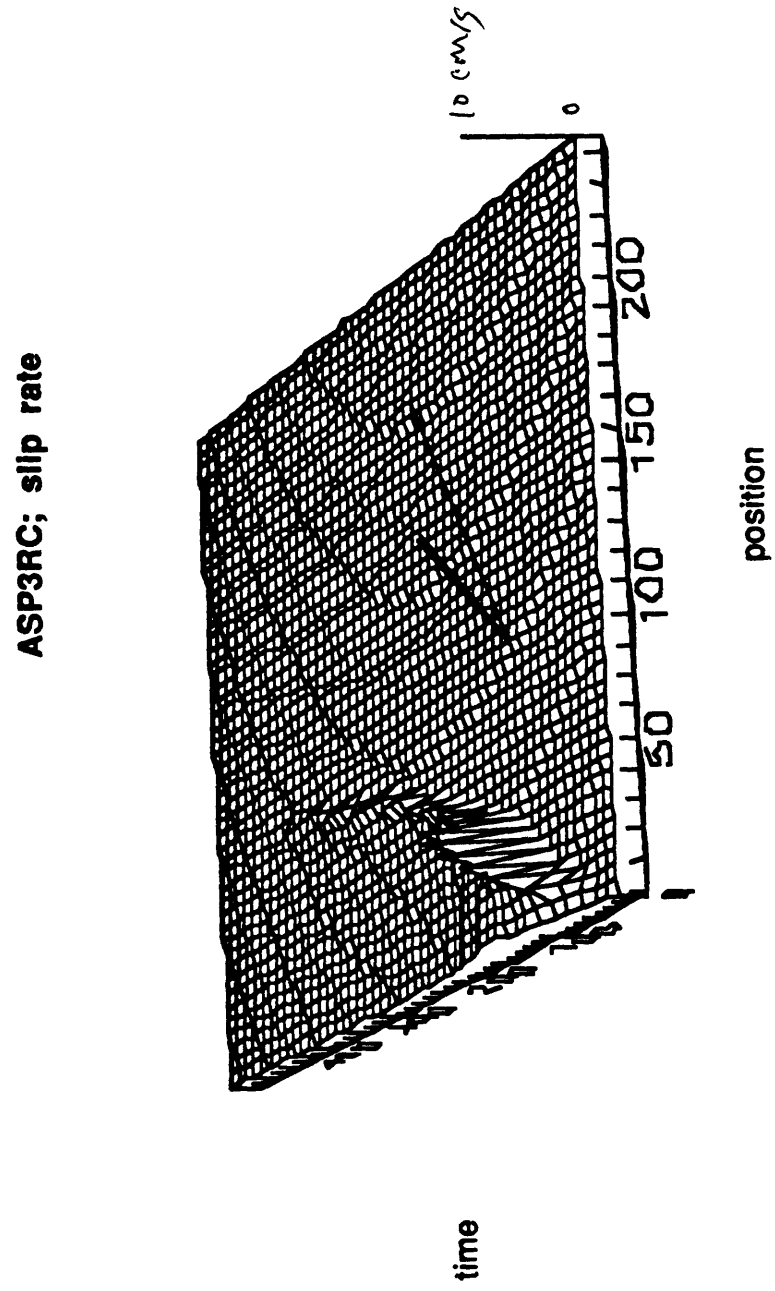

Figure 4. Rupture history for model ASP3RC. Starting size of seismological asperity is 3 times critical fault patch size. Time-space mesh perspectives for (a) fault slip rate, (b) fault slip, and (c) traction.

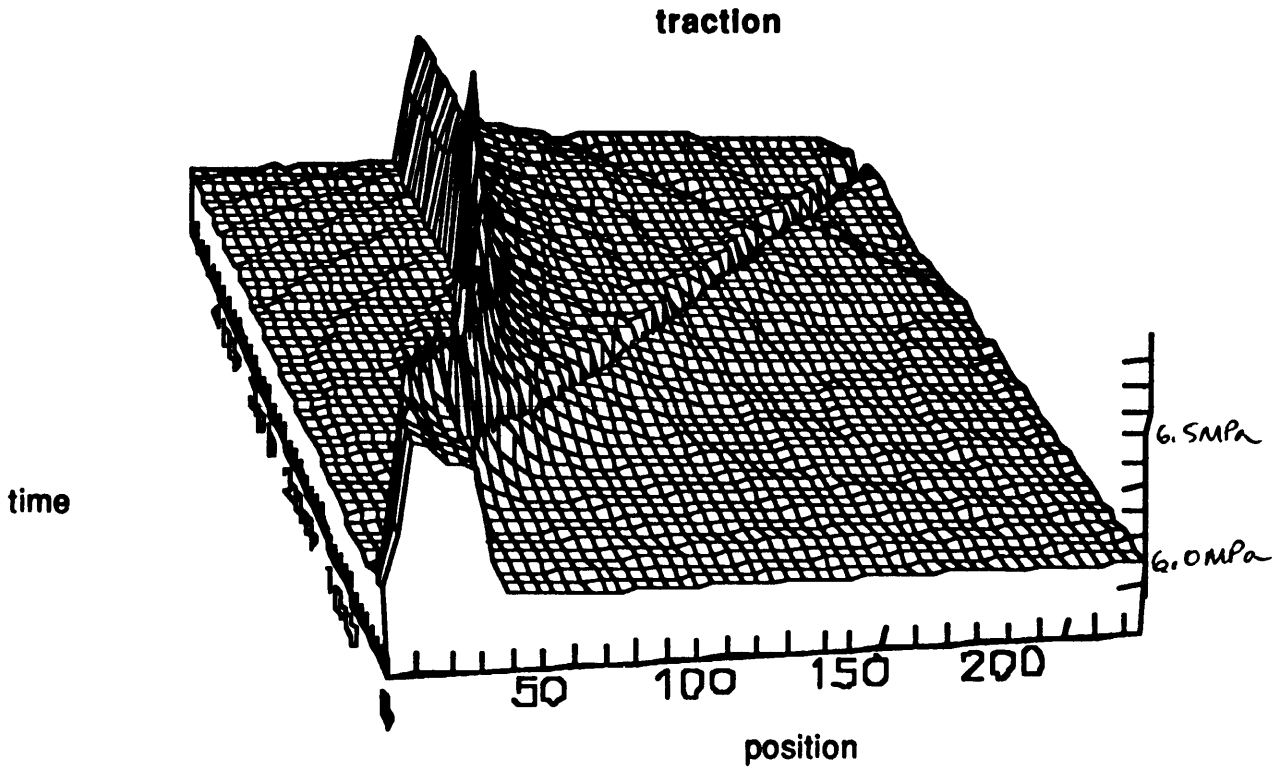
traction
time
6.5MPa
6.0MPa
50
100
150
200
position

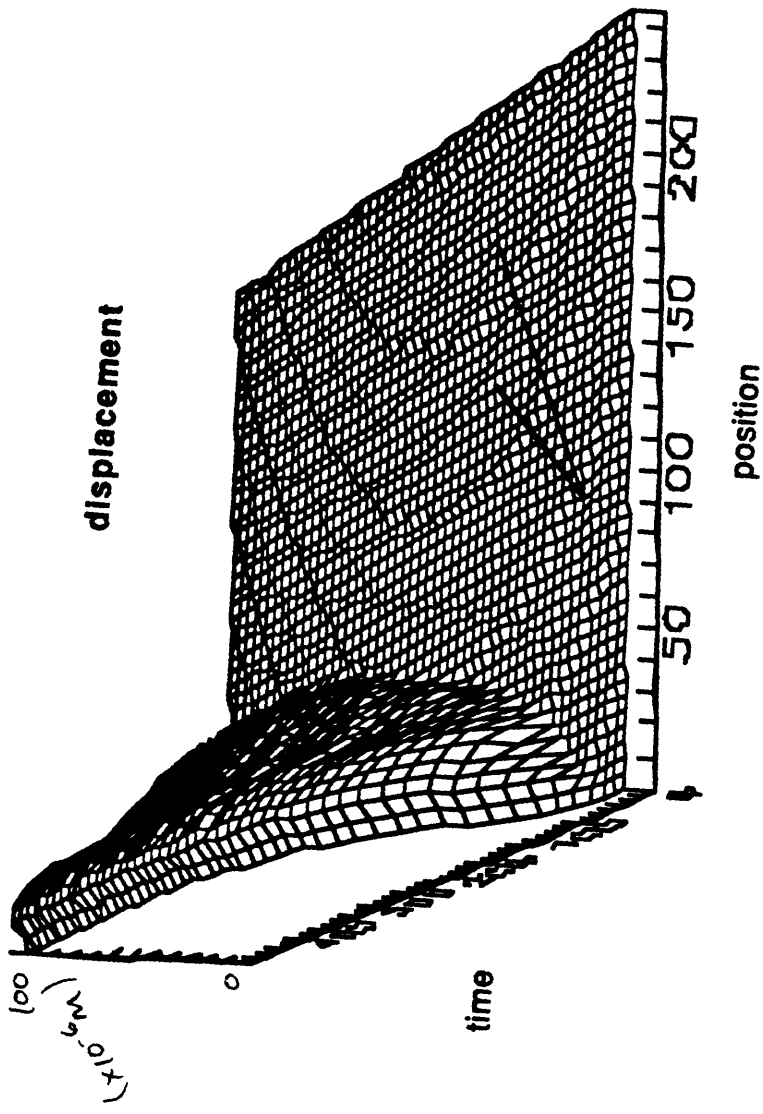
displacement
position
time
50
100
150
200
0
100
(x10^-4)

rupture models are given in Table 1.

The numerical simulations are carried out following modeling procedures presented in Okubo [unpublished manuscript, 1988]. These values assigned to the friction model parameters:

$$\mu_0 = 0.6$$
$$a = 0.01$$
$$a_1 = 1 \times 10^{-6}\ \mathrm{m/s}$$
$$b = 0.015$$
$$b_1 = 1/\mathrm{s}$$
$$d_c = 1 \times 10^{-6}\ \mathrm{m}.$$

These values represent typical laboratory-measured values. The rupture calculations begin with slip initiation and quasistatic sliding on a patch which ultimately accelerates into dynamic rupture along the fault. The simulations continue through the fault instability with slip and fault extension under dynamic conditions, and, depending on fault initial conditions, end with rupture arrest. From the fault configurations following rupture arrest, fault restrengthening is expected to occur, but, in this discussion, subsequent ruptures or aftershocks are not included.

Rice and Tse [1986] present a nonlinear analysis of the sliding behavior of a single-degree-of-freedom, block and spring, system, including the effect of inertia, governed by a state variable friction model. Their analysis shows that two very different time scales are physically relevant during the quasistatic and the inertia-controlled stages of the problem. This aspect of the problem makes it infeasible to use a single modeling algorithm to completely simulate the behavior of the system. Rather, they present a modeling strategy based on assumptions appropriate to that time scale which is relevant and solve the full system of governing equations only in a transitional regime when both time scales are important.

With their discussion in mind, the simulations of full fault response presented in this paper are carried out in two stages. First, a quasistatic model is calculated to simulate the stable development of a nucleation fault patch. The quasistatic calculations are stopped when a specified maximum slip rate at any location on the fault is attained. Final values of fault traction, slip, slip rate, and state are saved and used as the initial conditions from which the dynamic calculation is started. Then a dynamic model is calculated to complete the simulation up to the point of rupture arrest.

The dynamic calculation starts from the final quasistatic fault configuration. If the specified v_{max} for stopping the quasistatic calculation is too small, the dynamic calculation does not produce crack extension. A range of v_{max} was observed to lead to rupture growth. One of the basic assumptions of the state variable friction constitutive formulation is that there is always some fault slip taking place. With the direct velocity-dependent term in (1), increases

Table 1. Initial dimensions of high stress patch.

model	L_0/R_c	Δx (cm)
ASPL8	1.33	12.5
ASPL10	1.67	12.5
ASP2RC	2.00	15.0
ASP3RC	3.00	25.0
ASP4RC	4.00	30.0

$\sigma = 10.0$ MPa (100 bars)

$v_S = 2.9$ km/s

$\nu = 0.25$

$G = 10^5$ MPa

in applied loading on the fault can be balanced by having the fault slip at a higher rate. Accelerating fault slip immediately prior to the onset of unstable slip is characteristic of faults governed by a state variable friction model. In the simulations which combine the quasistatic and dynamic models, this accelerating slip is included in the calculation as part of the rupture nucleation process. It establishes fault state at the onset of instability that is sufficiently different from the initially specified state.

It was mentioned earlier that both a slip weakening fault model and a state variable fault model predict critical fault dimensions for producing unstable fault slip. Based on a fracture mechanics approach, the critical slip weakening crack length L_c is derived from the work done at the tip of an extending crack [e. g., Andrews, 1976]. Analysis of the sliding stability of a one-degree-of-freedom sliding system governed by a state variable model results in a critical fault patch size R_c [Dieterich, 1986] , to distinguish it from the critical crack length, where R_c is given by

$$R_c = \frac{2 G d_c}{3 \sigma \xi} . \qquad (4)$$

Parameters G and d_c are as introduced above and normal stress σ is again specified to be 100 bars acting uniformly over the entire fault. Parameter ξ is determined by friction model coefficients $\xi = (b\text{-}a)/2.303$. While similar in nature to the critical crack length, the critical patch size is understood to include the effects of the sliding process over the entire patch and not just at the extreme ends of the slipping patch. The differences between L_c and R_c are discussed in more detail in Dieterich [1988].

The first nonuniform initial stress models calculated were set up with $R_c > L_0 > L_c$. The high stress fault patch accelerates but the slip rate does not reach the cutoff of 100 times a_1 before the fault decelerates. The instability condition is not met. If, on the other hand, L_0 is chosen such that $L_0 > R_c$, the central fault patch does indeed reach the maximum slip rate for the quasistatic calculation and the subsequent slip is unstable.

Shown in figure 5 are space-time perspective plots of fault slip, fault slip rate and, traction from the dynamic calculation of a crack model in which the initial size of the high-stress patch is three times that of the critical fault patch. The edge of the high stress patch is located at element 36, indicated by the arrow in the figure. The early stages of the dynamic calculation closely resemble the early stages of the calculation for the uniformly distributed initial stress. Once the critical fault patch is established, the rate of rupture extension quickly reaches the Rayleigh wave speed. When the rupture front encounters the edge of the high stress patch, the rupture velocity suddenly decreases but the slipping part of the fault continues to grow. As the rupture continues to decelerate, the peak fault slip rate decreases with position on the fault away from the edge of the high stress patch. The slipped patch extends to element

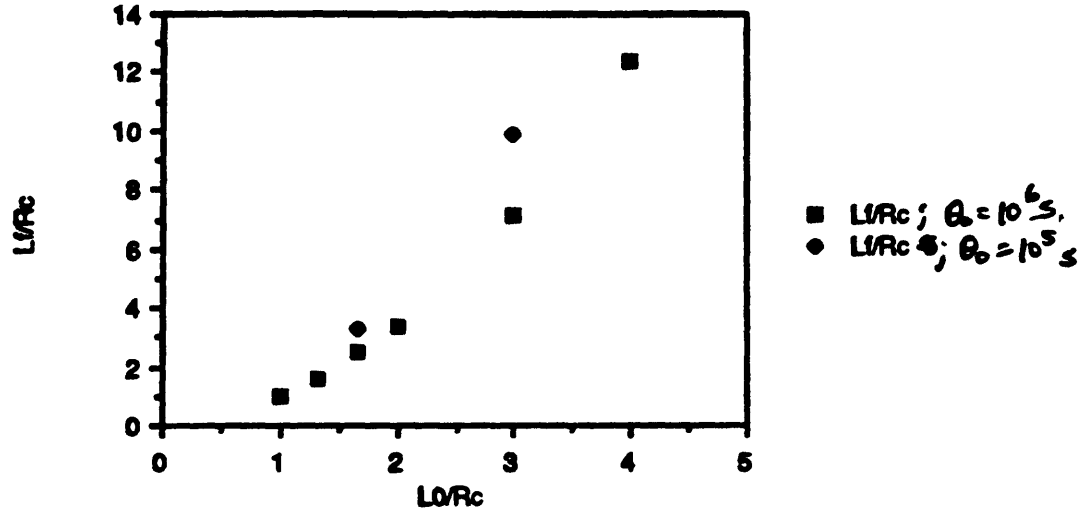

Figure 5. Final rupture length plotted as a function of starting size of high stress patch. Square symbols represent rupture models with $\theta_0 = 10^6$ s. Diamond symbols : $\theta_0 = 10^5$ s.

85, that is, the dynamic rupture propagates to a length L_f of 2.36 times L_0.

The rupture models listed in Table 1 contain features similar to those shown in figure 5 and described above. The total extents of the ruptures are measured and then L_f/R_c is plotted in figure 6 as a function of L_0/R_c . For the rupture models calculated from an initial θ value of 10^6 s, the overshoot data are fit well by a quadratic function. Rupture models ASPL10 and ASP3RC, recalculated with starting θ values of 10^5 s but otherwise with identical starting conditions as before, are shown in the figure as crosses. For the smaller value of θ, the overshoot of the ruptures is greater.

DISCUSSION

Rupture models of the failure of a high stress patch surrounded by a region of zero stress drop feature an overshoot, or penetration of the slip surface, into the region of zero stress drop. figure 6 suggests that the final fault extent L_f is proportional to the square of the initial high stress patch size L_0. A means of understanding this scaling is provided by a simple energy balance argument for the rupture geometry pictured schematically in figure 7.

Shown in the figure are the initial patch size, the final patch size, and a hypothetical distribution of slip in the fault after rupture arrest. Of the strain energy change associated with relieving the stress on the high stress patch, the available energy is that component which is not lost to frictional heating of the fault surfaces. This available energy E_a is given by

$$E_a = \frac{1}{2}\int_{-L_f}^{L_f} T(x)\,u(x)\,dx \tag{5}$$

where $T(x)$ and $u(x)$ are the distributions of the stress drop and fault offset over the fault. For the case shown in the figure with constant asperity stress drop T_a over the interval $-L_0 < x < L_0$, E_a reduces to

$$E_a = \frac{1}{2}T_a\int_{-L_0}^{L_0} u(x)\,dx \tag{6}$$

Slip $u(x)$ is related to average stress drop over the entire slip surface by

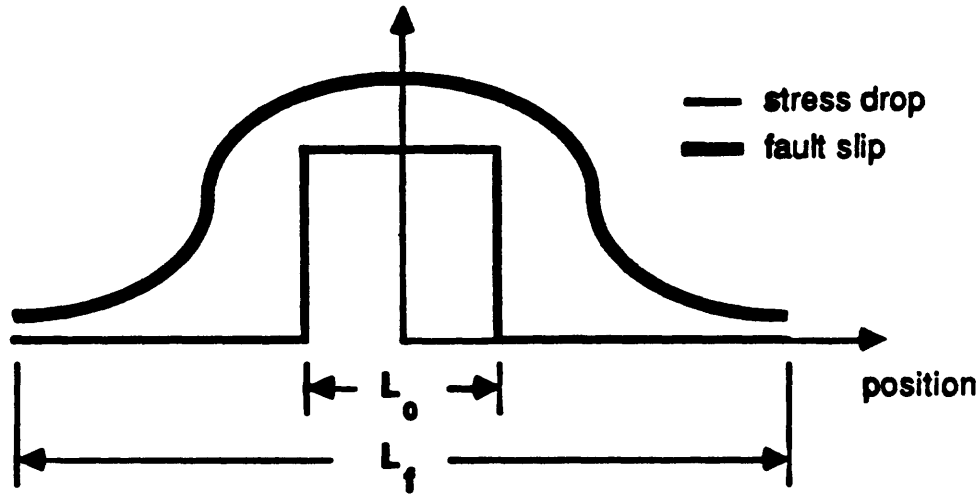

Figure 6. Hypothetical fault slip and initial stress distribution for asperity rupture models.

$$u(x) = \frac{(1-\nu)}{G} T_a \frac{L_0}{L_f} \left(L_f^2 - x^2\right)^{\frac{1}{2}}, \tag{7}$$

where ν is Poisson's ratio. E_a in equation (6) can be approximated by

$$E_a \approx \frac{(1-\nu) T_a^2 L_0^2}{G} \tag{8}$$

Energy is absorbed at the crack tips in the process of creating freshly faulted surfaces is given by the integral of the fracture energy over the rupture length. Recalling the similarity between a slip weakening model and a state variable model at high slip rates, an approximate expression for the fracture energy $\mathcal{G}$ of the rupture process is given by

$$\mathcal{G} = \frac{1}{2}(T_p - T_r)\, d_r \tag{9}$$

Stress parameters T_p and T_r are identified with friction model expressions $\sigma \mu_{max}(\theta)$ and $\sigma \mu_0$, respectively. For the state evolution law given in equation (2), critical slip weakening displacement is roughly approximated by 10 d_c . The total energy absorbed in creating the fault surfaces is simply the integral of (9) over the total rupture length, or

$$E_F = \int_{-L_f}^{L_f} \mathcal{G}\, dx$$

$$E_F = (T_p - T_r)\, d_r L_f. \tag{10}$$

Balancing this work against the available energy E_a , a quadratic relationship between L_0 and L_f is established. Using the definitions of R_c and strength parameter s, this result can be stated in terms of the proportionality

$$L_f \propto \frac{L_0^2}{(1+s) R_c}. \tag{11}$$

The model calculations confirm this proportionality, varying both L_0 and **s**. The seismic efficiency characterizes the partitioning of the available energy between the fracture energy component and the radiated seismic energy component. Without an *a priori* means of assigning a value to the seismic efficiency for cracks with variable rupture speed, the relationship between L_0 and L_f is preferably left as proportionality (11).

CONCLUSIONS

A laboratory-motivated frictional constitutive relation of the kind proposed by Dieterich and Ruina has been incorporated into a numerical model of dynamic rupture. A complete faulting cycle of stable rupture nucleation and dynamic rupture propagation is simulated. The simulation is achieved by calculating the fault response in two stages, using the same state variable friction law in both sets of calculations. First, rupture nucleation is simulated for the fault under conditions of quasistatic equilibrium. When slip rate at any position on the fault reaches a specified maximum slip rate, the numerical dynamic rupture model is started. In this stage of the calculation, the full equations of motion, including inertia, are solved following the complete state variable friction model. Following this procedure, rupture nucleation is achieved in a natural way and the complete solution, including elastodynamic radiation, is determined during the dynamic rupture. Within the context of the state variable formulation, physically reasonable distributions of fault traction and fault state are determined both leading up to dynamic rupture and following rupture arrest.

Different rupture models are calculated for the rupture of a high stress patch surrounded by a region of zero stress drop. In these calculations, not only are the rupture nucleation processes simulated realistically, but the rupture arrest is also achieved naturally without specifying the final fault rupture dimensions or using artificially high fault strengths to limit the extent of rupture. Some features of dynamic frictional sliding, for example, the peak shear stress S_{max} or the slip weakeninglike behavior at the onset of instability, can be viewed within the framework of fracture mechanics. In turn, these can be used to establish a scaling relationship between the initial and final dimensions of a seismological asperity. The calculations establish that the final size of the asperity rupture is proportional to the square of the initial asperity size, consistent with a scaling relationship derived from energy balance arguments.

Because of the rate dependence of the frictional response at lower fault slip rates, rupture nucleation processes occurring at lower slip rates are not completely characterized by engineering fracture analysis of the stress field surrounding the tip of the extending fault. Rupture nucleation with a state variable friction model differs from that following a rate-independent slip weakening model, requiring a different interpretation of critical fault dimension. The calculations are consistent with predictions of a critical rupture nucleation patch size derived from frictional stability analyses, rather than with a critical fault length

that is derived from crack tip energy balance arguments.

With the development of techniques to gather and analyze high-quality seismological data has come the impetus to understand details of the earthquake rupture process. Much attention is being placed on the non-uniformity of the rupture process regarding, for example, the variability of rupture velocity during an earthquake or the development of large earthquakes from smaller ruptures or sub-events. Models of the spontaneous development and growth of the rupture based on the stress field and fault constitutive response do not require making *a priori* assumptions of the rupture behavior that are required in strictly kinematic modeling efforts. Use of the physically reasonable, laboratory-motivated friction law can lead to the identification of physically reasonable distributions of non-uniform fault properties. The state variable frictional fault constitutive relation used in these calculations is still the object of extensive laboratory research in a number of different laboratories. While the physical processes that control the friction model parameters are not fully understood, aspects of the fault response can be interpreted in terms of the model parameters.

REFERENCES

Andrews, D. J., Rupture velocity of plane-strain shear cracks, *J. Geophys. Res., 81*, 5679-5687, 1976.

Andrews, D. J., Dynamic plane-strain shear rupture with a slip-weakening friction law calculated by a boundary integral method, *Bull. Seismol. Soc. Am., 75*, 1-21, 1985.

Barenblatt, G. I., The formation of equilibrium cracks during brittle fracture. General ideas and hypotheses: Axially symmetric cracks, *Appl. Math. Mech.*, 23, 622-636, 1959.

Cao, T., and K. Aki, Seismicity simulation with a rate- and state-dependent friction law, *Pure Appl. Geophys., 124*, 487-513, 1986.

Day, S. M., Three-dimensional simulation of spontaneous rupture: The effect of nonuniform prestress, *Bull. Seismol. Soc. Am., 72*, 1881-1902, 1982.

Dieterich, J. H., Time-dependent friction in rocks, *J. Geophys. Res., 77*, 3690-3697, 1972.

Dieterich, J. H., Time dependent friction and the mechanics of stick-slip, *Pure Appl. Geophys., 116*, 790-806, 1978.

Dieterich, J. H., Modeling of rock friction 1. Experimental results and constitutive equations, *J. Geophys. Res.*, *84*, 2161-2168, 1979a.

Dieterich, J. H., Modeling of rock friction 2. Simulation of preseismic slip, *J. Geophys. Res.*, *84*, 2169-2175, 1979b.

Dieterich, J. H., Constitutive properties of faults with simulated gouge, in *Mechanical Behavior of Crustal Rocks*, Geophysical Monograph, *24*, American Geophysical Union, eds. N. L. Carter, M. Friedman, J. M. Logan and D. W. Stearns, 103-120, 1981.

Dieterich, J. H., A model for the nucleation of earthquake slip, in *Earthquake Source Mechanics*, Geophysical Monograph, *37* (Maurice Ewing Volume *6*), 37-47, eds. S. Das, J. Boatwright, and C. H. Scholz, American Geophysical Union, Washington, D. C., 1986.

Gu, J.-C., J. R. Rice, A. L. Ruina, and S. T. Tse, Slip motion and stability of a single degree of freedom elastic system with rate and state dependent friction, *J. Mech. Phys. Solids*, *32*, 167-196, 1984.

Ida, Y., Cohesive force across the tip of a longitudinal shear crack and Griffith's specific surface energy, *J. Geophys. Res.*, *77*, 3796-3805, 1972.

Ida, Y., The maximum acceleration of seismic ground motion, *Bull. Seismol. Soc. Am.*, *63*, 959-968, 1973.

Mavko, G. M., Simulation of earthquakes and creep events on a spatially variable model (abstract), *EOS*, Trans., American Geophysical Union, *61*, 1120, 1980.

Okubo, P. G., and J. H. Dieterich, Effects of physical fault properties on frictional instabilities produced on simulated faults, *J. Geophys. Res.*, *89*, 5815-5827, 1984.

Okubo, P. G., and J. H. Dieterich, State variable fault constitutive relations for dynamic slip, in *Earthquake Source Mechanics*, Geophysical Monograph, *37* (Maurice Ewing Volume *6*), 25-35 eds. S. Das, J. Boatwright, and C. H. Scholz, American Geophysical Union, Washington, D. C., 1986.

Palmer, A. C., and J. R. Rice, The growth of slip surfaces in the progressive failure of over-consolidated clay, *Proc. R. Soc. London, A332*, 527-548, 1973.

Rice, J. R., The mechanics of earthquake rupture, *Physics of the Earth's Interior* (Proceedings of the International School of Physics 'Enrico Fermi', Course 78, 1979),555-649, ed. A. M. Dziewonski and E. Boschi, North Holland, Amsterdam, 1980.

Rice, J. R., Constitutive relations for fault slip and earthquake instabilities, *Pageoph., 121*, 443-475, 1983.

Rice, J. R., and S. T. Tse, Dynamic motion of a single degree of freedom system following a rate- and state-dependent friction law, *J. Geophys. Res., 91*, 521-530, 1986.

Rudnicki, J. W., and H. Kanamori, Effects of fault interaction on moment, stress drops and strain energy release, *J. Geophys. Res., 86*, 1785-1793, 1981.

Ruina, A. L., Friction laws and instabilities: A quasistatic analysis of some dry frictional behavior, Ph. D. thesis, Brown Univ., Providence, R. I., 1980.

Ruina, A. L., Slip instability and state variable friction laws, *J. Geophys. Res., 88*, 10359-10370, 1983.

Tse, S. T., and J. R. Rice, Crustal earthquake instability in relation to the depth variation of frictional slip properties, *J. Geophys. Res., 91*, 9452-9472, 1986.

Tullis, T. E., and J. D. Weeks, Constitutive behavior and stability of frictional sliding of granite, *Pure Appl. Geophys., 124*, 383-414, 1986.

THE GEOLOGIC AND SEISMIC EXPRESSION OF THE CALAVERAS FAULT, CENTRAL CALIFORNIA: A LACK OF COINCIDENCE

David H. Oppenheimer, U.S. Geological Survey, 345 Middlefield Road – MS 977, Menlo Park, CA, 94025

Fault segmentation can often be recognized from offsets and bends observed from the mapped surface expression of faults. Frequently, these observations are corroborated by hypocentral patterns which develop over time and during aftershock sequences (Bakun, 1980). However, at two locales southeast of the San Francisco Bay the geologically mapped trace of the Calaveras fault departs from the extrapolation of seismic patterns to the surface. The first locale is the region of the Calaveras fault which ruptured during the 1984 M6.2 Morgan Hill earthquake (Figure 1) (Cockerham and Eaton, 1987; Oppenheimer *et al.*, 1988). The rupture surface is clearly defined by the aftershock activity and shows that this segment of the Calaveras fault is a near vertical plane. However, the mapped surface expression of the fault is offset southwest of the seismic expression of the fault from the point of rupture initiation at the northern end of San Felipe Valley to the southeast end of Anderson Lake. Since there was no unequivocable surface rupture for this earthquake (Harms *et al.*, 1987), it is not possible to establish that the mapped fault represents an active strand of the Calaveras fault. Conversely, there is no surface expression of faulting above the seismically determined fault trace that might support the accuracy of the aftershock locations.

The second locale is the juncture of the Calaveras and Hayward faults (Figure 2). This segment of the Calaveras fault is immediately north of the Morgan Hill segment shown in Figure 1. It too is near vertical and planar, but the seismicity and surface expression of the Calaveras fault are coincident. The Hayward fault is southwest of and parallel to the Calaveras fault and is mapped as far south as the Morgan Hill epicenter, but there is no evidence in the geologic surface expression of the two faults that they actually join. However, the earthquake locations shown in Figure 2 clearly demonstrate that the Hayward fault splays from the Calaveras fault. It is notable that the seismicity departs from the mapped trace of the Hayward approximately 40 km north of the southernmost

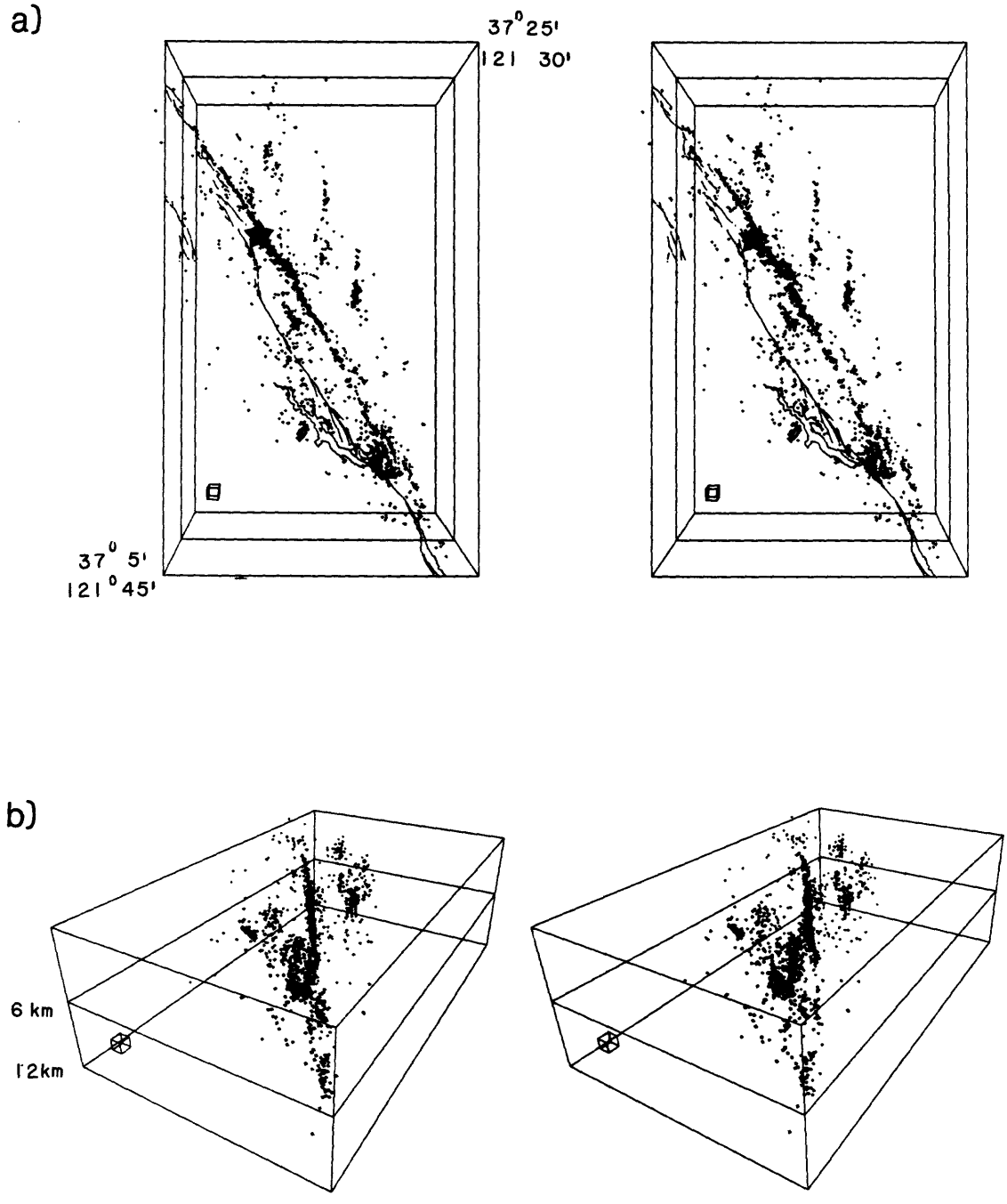

Figure 1. Stereoscopic views of Morgan Hill aftershocks for period 4/24/84 – 9/30/84. Cube with 1-km dimension is shown for scale at southwest corner. (a) View from directly above. Calaveras fault trace at surface connects Coyote Lake at southeast corner to northwest corner of figure. Southern terminus of Hayward fault is shown along left margin southwest of Calaveras. Anderson Lake is shown in south-central portion of figure. Morgan Hill mainshock epicenter indicated by star at 37°18′ latitude), (b) Oblique view from the southeast along strike of Calaveras fault.

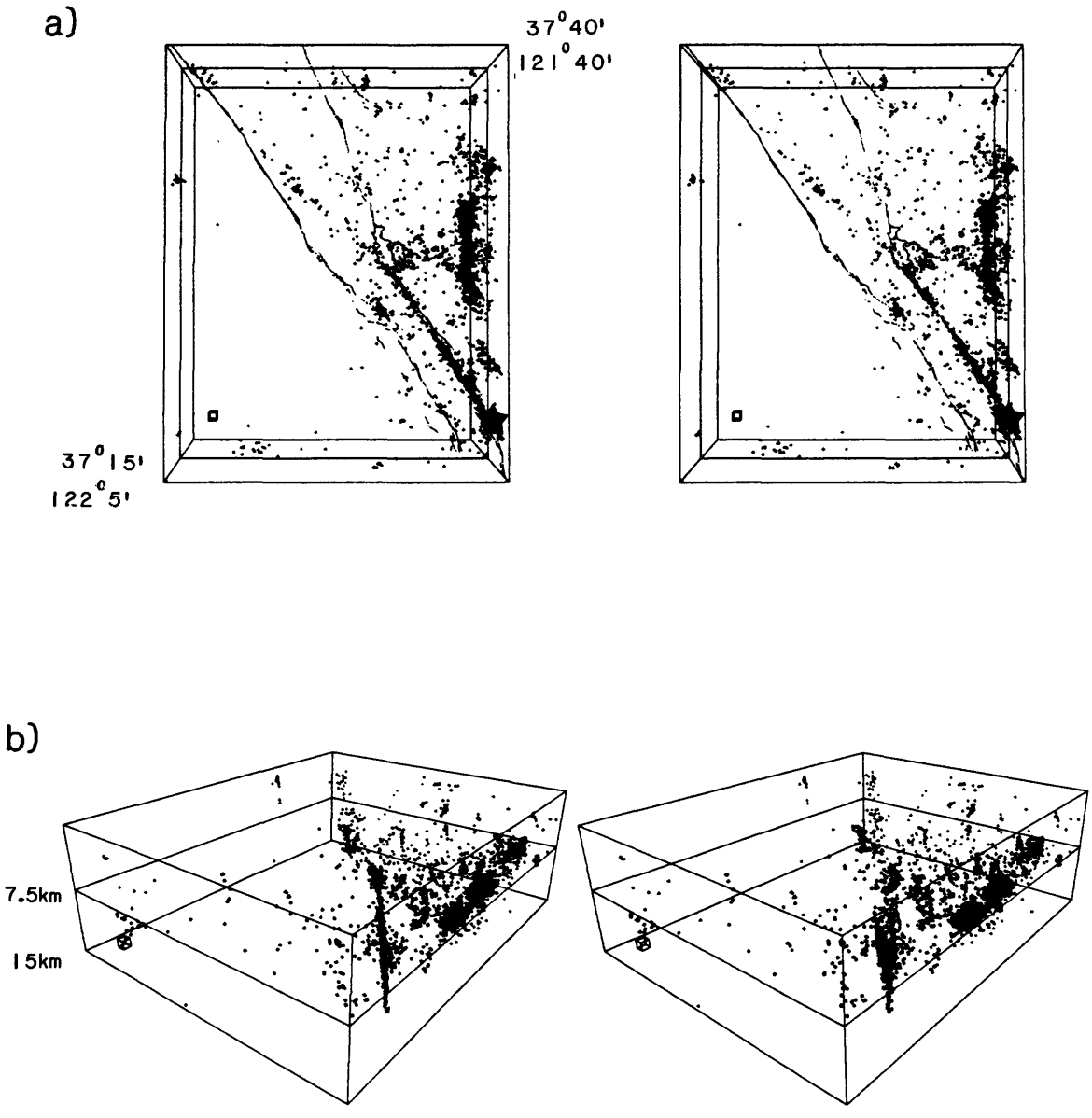

Figure 2. Stereoscopic views of seismicity at juncture of Hayward and Calaveras faults for period 6/01/84 – 12/31/86. Cube with 1-km dimension is shown for scale at southwest corner. (a) View from directly above. Calaveras fault trace runs from southeast corner, through Calaveras Reservoir to top-center of figure. Hayward fault trace is southwest of Calaveras, running from southeast corner to northwest corner. Morgan Hill mainshock epicenter indicated by star at southeast corner. (b) Oblique view from the southeast along strike of Calaveras fault.

extent of the mapped fault and approximately 10 km north of an active creep site. Unlike the Morgan Hill segment, the seismicity linking the Calaveras and Hayward faults can be associated with the Mission fault, but there is no reported Holocene movement or creep on the Mission fault.

Inherent in any discussion of earthquake locations is the problem of systematic mislocation due to unmodeled velocity variations. This problem does not appear to be significant in this region, for the following reasons: 1) Seismicity locates beneath the mapped traces of the Calaveras and Hayward faults immediately beyond the regions where the discrepancies are noted, suggesting that the velocity model is appropriate. 2) Were the hypocenters to be severely mislocated, the mislocation would probably manifest itself as a constant offset. However, the relative hypocentral pattern does not mimic the offsets observed in the surface expression of the faults in the above areas. 3) Three-dimensional velocity modelling in the Morgan Hill region by Michael (1988) yields hypocentral locations similar to the locations presented here.

These observations indicate that the seismic expression of a fault may not necessarily coincide with the surface expression of a fault. If the seismic data are correctly located, then it is difficult to explain the absence of significant surface rupture above the hypocenters, the presence of pronounced fault features at the surface without any corresponding seismicity below, and the presence of aseismic creep off the "seismic" fault. The apparent contradiction may in fact reflect a deformation process that has not been widely recognized. Simpson (1986) has demonstrated through dislocation modeling that fault bends and offsets at the surface, such as along the San Andreas fault at Parkfield, may reflect three-dimensional warps in the fault plane that arise from the end effects of a locked fault. If the crust is not perfectly elastic, the warp does not completely disappear at the time of the mainshock. Instead, a portion of the strain accumulates in the form of a permanent offset. A similar phenomena may exist along the Calaveras fault, suggesting a possible mechanical decoupling of the shallow crust above 2km, the minimum depth of earthquake occurrence. Whatever the explanation, these observations indicate that caution should be exercised

when predicting the location and extent of rupture solely on the evidence provided by the geologic expression of faults.

REFERENCES

Bakun, W. H. , Seismic activity on the southern Calaveras fault in central California, *Bull. Seism. Soc. Am., 70*, 1181–1197, 1980.

Cockerham, R. S., and J. P. Eaton, The earthquake and its aftershocks, April 24 through September 30, 1984, in The Morgan Hill, California Earthquake of April 24, 1984, *U.S. Geol. Surv. Bull. 1639*, 15–28, 1987.

Harms, K. K., M. M. Clark, M. J. Rymer, M. G. Bonilla, E. L. Harp, D. G. Herd, K. R. Lajoie, J. J. Lienkaemper, S. A. Mathieson, J. A. Perkins, R. E. Wallace, and J. I. Ziony, The search for surface faulting, in The Morgan Hill, California Earthquake of April 24, 1984, *U.S. Geol. Surv. Bull. 1639*, 61–68, 1987.

Michael, A. J., Effects of three-dimensional velocity structure on the seismicity of the 1984 Morgan Hill, CA aftershock sequence, *Bull. Seism. Soc. Am., 78*, 1199–1221, 1988.

Oppenheimer, D. H., P. A. Reasenberg, and R. W. Simpson, Fault plane solutions for the 1984 Morgan Hill, California, earthquake sequence: evidence for the state of stress on the Calaveras fault, *J. Geophys. Res., 93*, 9007–9026, 1988.

Simpson, R. W., Fault patterns and strain budgets, National Earthquake Hazards Reduction Program, summaries of Technical Reports volume XXII, *U.S. Geol. Surv., Open-File Rept. 87-63*, 446–451, 1986.

BEHAVIOR OF INDIVIDUAL FAULT SEGMENTS ALONG THE ELSINORE-LAGUNA SALADA FAULT ZONE, SOUTHERN CALIFORNIA AND NORTHERN BAJA CALIFORNIA: IMPLICATIONS FOR THE CHARACTERISTIC EARTHQUAKE MODEL

by

Thomas Rockwell
Department of Geology
San Diego State University
San Diego, CA 92182
(619) 265-4441

INTRODUCTION

The Elsinore fault zone of southern California is well-expressed on a regional scale as an alignment of major escarpments and mountains, fault line valleys, and juxtaposition of topographically high and low areas. On a more local scale, the fault is expressed geomorphically along most of its length as a series of offset and deflected drainages, scarps, sags, pressure ridges, shutter ridges, hillside valleys and benches, springs, and vegetation lineaments (Kennedy, 1977; Clark, 1982; Millman and Rockwell, 1986; Vaughan and Rockwell, 1986; Rockwell and Pinault, 1986). Field mapping of individual active strands, based on the above indicators of recent activity, suggests that the Elsinore fault can be broken into several discrete segments, each bounded by a major step or bend (Fig. 1). There is usually good geomorphic expression and continuity along the straight fault segments in between the steps. However, the expression of youthful faulting is commonly less well expressed in some of the areas of the steps or bends, suggesting complex strain release in those areas.

From the northwest to the southeast, the segments are: Whittier/Chino (60 km), Glen Ivy (22 km), Wildomar/Wolf Valley/Pala (55 km), Julian (80 km), and Coyote Mountains (60 km). South of the United States/Mexico international border, the fault zone continues as the Laguna Salada (38 km) and Chupamiertos (22 km) faults (Fig. 1), and at least two other unnamed faults that connect to the head of the Gulf of California. Three segments of the Elsinore fault zone may have broken in association with historical earthquakes: the February, 1892 earthquake (M7-7.5) which produced up to 5 m of dip slip and probably 1-2 m of right slip over at least 20 km of the Laguna Salada fault; the May, 1910 Temescal Valley earthquake (M6?)(Glen Ivy segment) which produced up to 30 cm of right-lateral slip; and the 1934 Chupamiertos(?) earthquake (M6.5)(presumably the Chupamiertos segment; not yet studied on the ground).

Paleoseismic evidence from three of these segments, the Glen Ivy, Coyote Mountains, and Laguna Salada segments, suggests that slip per event varies by a factor of about two where the fault is dominantly strike-slip, but is more consistent where the sense of slip is dominantly dip-slip. These data, as discussed below, generally support characteristic earthquakes but suggest that

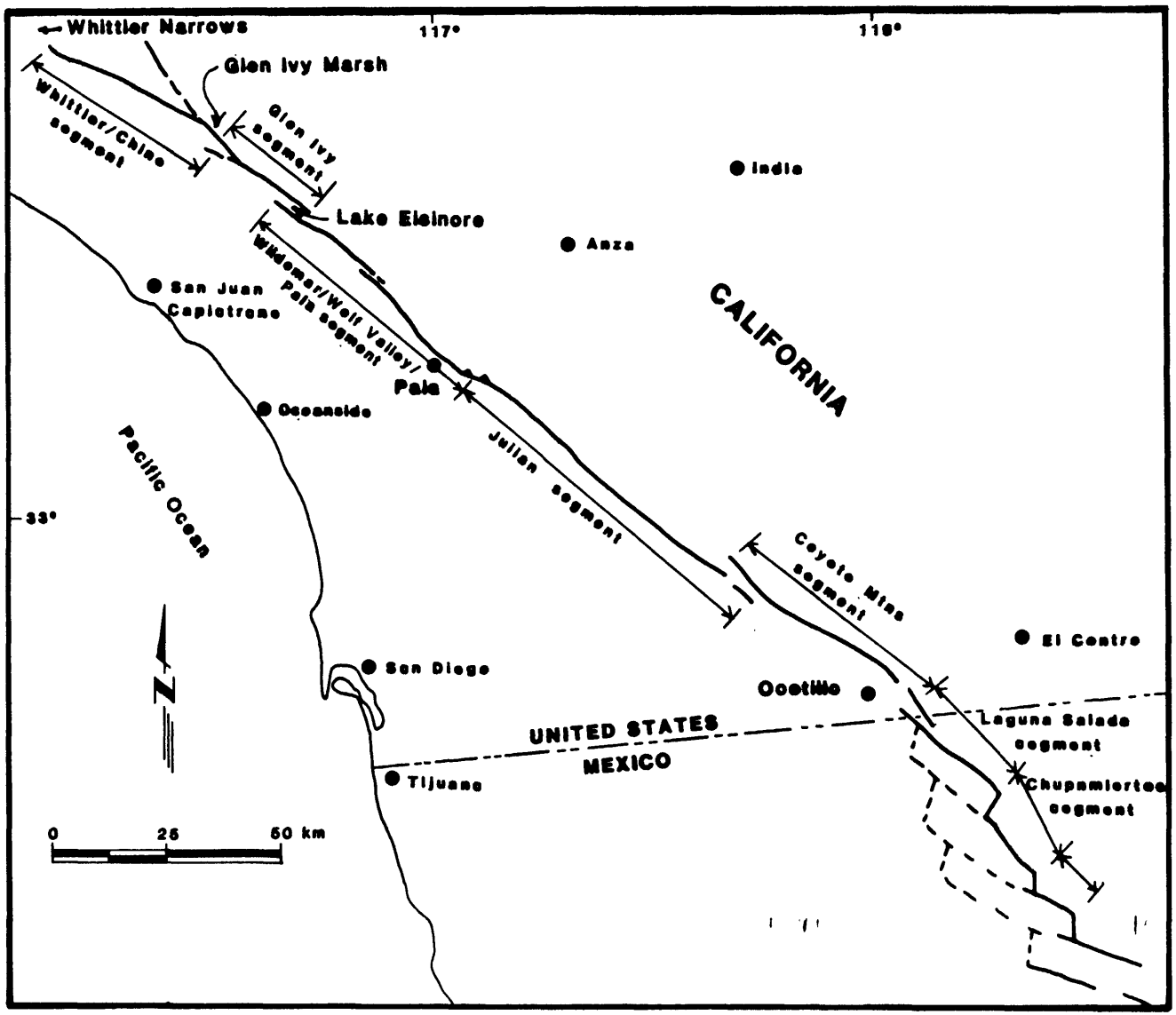

Figure 1. Map showing fault segments along the Elsinore fault zone.

strike-slip faults may be considerably more variable than dip-slip faults, perhaps due in part to the rupture of multiple segments in some earthquakes.

BEHAVIOR OF INDIVIDUAL FAULT SEGMENTS

Glen Ivy Segment

The Glen Ivy segment is a relatively short (22 km long) segment of the Elsinore fault between a releasing bend to the Whittier/Chino segment on the northwest and a right step across Lake Elsinore to the Wildomar segment on the southeast. Both the double bend and the step measure 3-4 km in dimension perpendicular to the fault and may provide an impediment to propagation of surface rupture (Sibson, 1985).

The paleoseismology of the Glen Ivy segment was studied at Glen Ivy Marsh (Rockwell and others, 1985; 1986), which is located in the releasing bend at the north end of the segment. The marsh resulted from subsidence between the right-lateral Glen Ivy North fault and the normal-slip Glen Ivy South fault, which is a direct result of the releasing bend (Millman and Rockwell, 1986; Rockwell and others, 1986)(Fig. 2). The location of the trenching study in a releasing bend suggests that the strata may record evidence of earthquakes from either or both the Glen Ivy and Whittier/Chino fault segments, however.

Glen Ivy Marsh has recorded at least five episodes of ground breakage since about 1000 A.D. (Rockwell and others; 1986), suggesting an average recurrence interval of about 200 years for the fault at that site. Below thousand year old strata, a buried soil is developed on extensively faulted mid-Holocene strata that date to about 5000 years B.P.; thus the pre-1000 A.D. rupture history is lost at this site (Fig. 3). The uppermost strata exposed in trenches also have a soil developed in them and thus represent a recent hiatus in deposition for the past one to several hundred years. The surface soil was broken by at least one earthquake, which is believed to have been the May 15, 1910 M6 Temescal Valley temblor, although active bioturbation in the upper 1 m may have obscured evidence from other post-1500 A.D. ruptures. Thus, the recurrence interval is probably a maximum value and could be shorter.

Lateral displacement associated with the 1910 earthquake and a circa 1300 A.D. event was studied by Brake and Rockwell (1987). The surface soil is broken in every exposure of the fault at Glen Ivy Marsh. Liquefaction of the soil and the development of soil fissures was associated with this most recent faulting event, establishing a seismic origin for the displacement. Glass and pottery was included within one of the liquefied fissure fillings (Rockwell and others, 1985; 1986).

During excavation of a fault-parallel exploratory trench, a cement flume was exposed that has both right-lateral and vertical offset at the fault (Fig. 4). The flume crosses the fault zone in an area of a small right step with a considerable vertical component of slip. The flume appears to be associated with an early historical artesian well and is affected by a subsidence cone adjacent to the fault which has amplified the apparent vertical component of slip. Thus, the precise amount of vertical

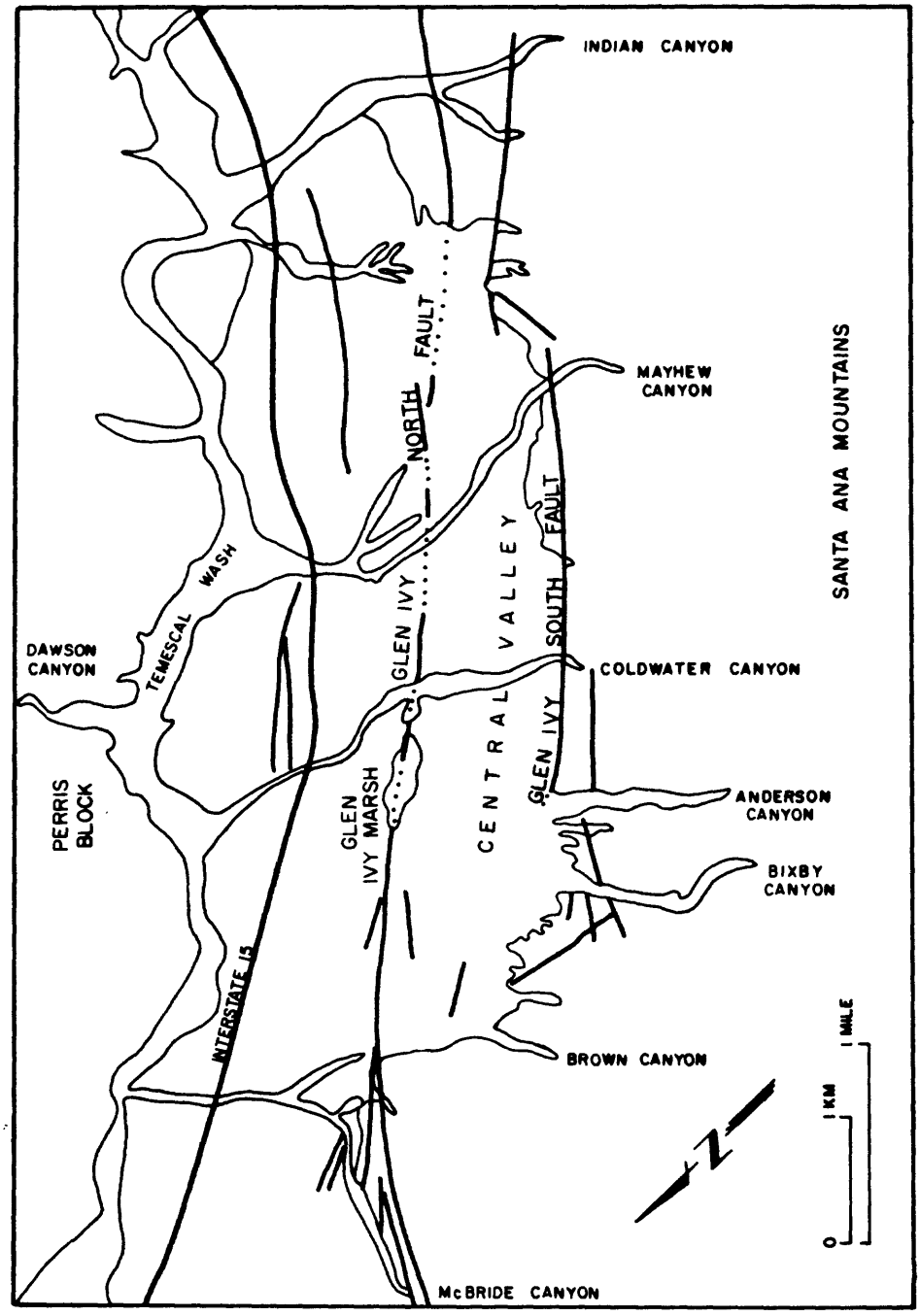

Figure 2. Generalized fault map of Temescal Valley.

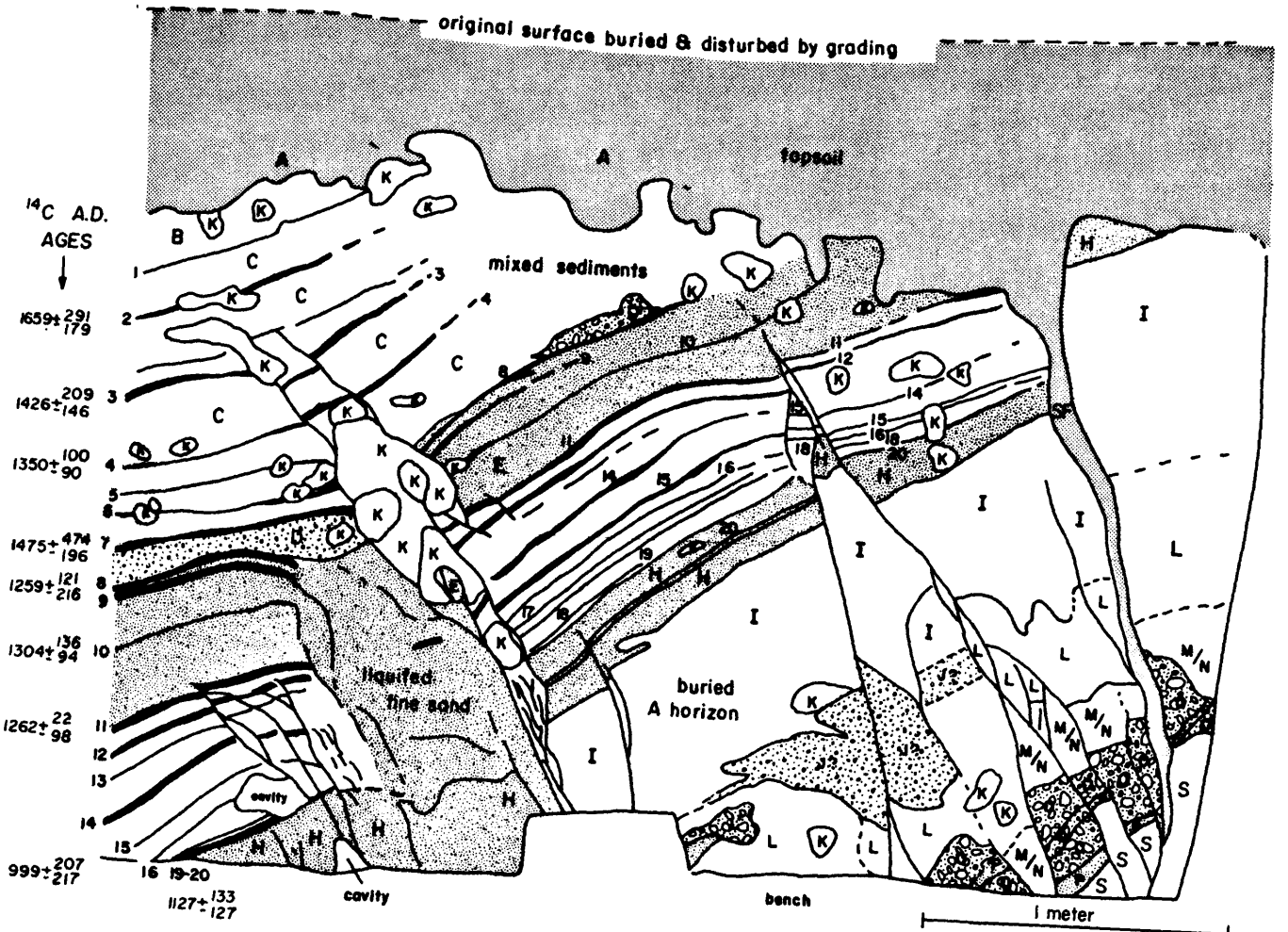

Figure 3. Log of trench face 00+90 cm in MT-1 across the Glen Ivy North fault (after Rockwell and others, 1986). Peats are numbered sequentially from youngest to oldest.

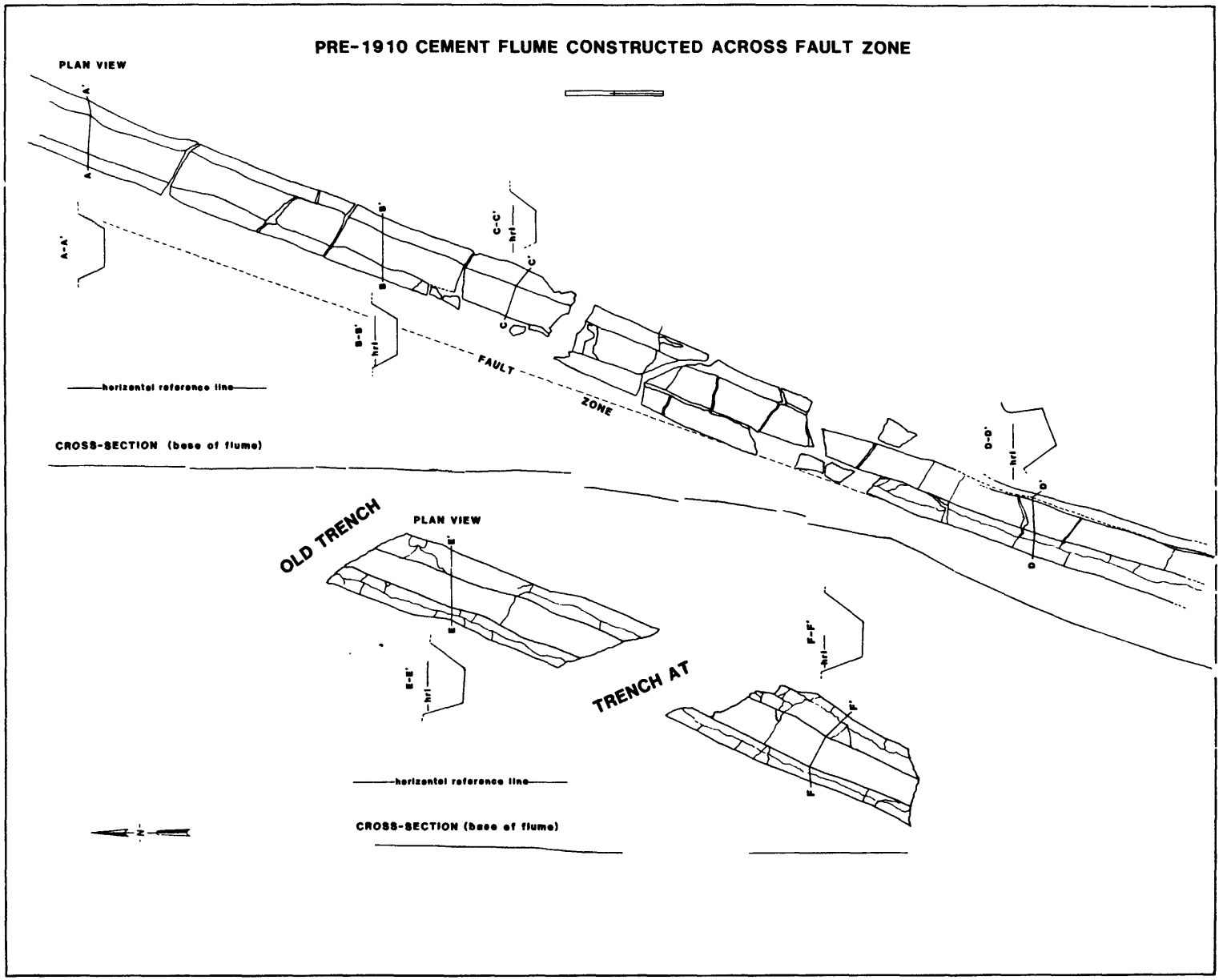

Figure 4. Map of displaced flume associated with the 1910 earthquake.

deformation has not yet been established but it is between 25 and 200 cm. The flume is laterally displaced about 22 cm along individual fault strands and an additional 10-15 cm by flume rotation (probably associated with plastic deformation of the underlying soil) resulting in about 35 cm of total lateral shear across a several-meter-wide fault zone. The flume is hand-molded cement and appears to date to the beginning of the Temescal Water Co. in the late 1880's or 1890's. Water company records suggest that the flume predates 1900-1901 when the main water pipe system was emplaced.

An earthquake in Temescal Valley on May 15, 1910 with an estimated magnitude of 6 (Toppozada and Parke, 1982) was the probable cause for the displacement of the cement flume. The epicenter, according to Toppozada and Parke, was located along the Elsinore fault zone between Lake Elsinore and Glen Ivy. Other historical features were sought to establish whether or not the 1910 earthquake produced ground rupture.

A terracota pipe, dating to 1914, was excavated that crossed the fault and that drained a well on the downthrown (SW) side of the fault. The pipe is broken within the fault zone and is displaced vertically between 75 and 100 cm but is clearly displaced right-laterally by no more than a few centimeters (Fig. 5). The area of subsidence appears to be local to the well since its affects are not apparent in other nearby trenches, and is interpreted to result from water withdrawal; thus a significant lateral component would not be expected. The apparent minor lateral displacement may be due to a lateral shift in the sediments during subsidence towards the west-northwest because the excavation is in an area of a minor right bend or step (releasing) in the fault zone. Alternatively, the right deflection may be tectonic slip that resulted from either afterslip from the 1910 earthquake or minor tectonic creep.

Another historic feature, a circa 1940's concrete pipe, crosses the fault in the same area as the terracota pipe and is also broken vertically by about 25-30 cm but displays no lateral deflection. This supports the water withdrawal subsidence hypothesis although some creep or afterslip cannot be ruled out. Clearly, the pre-1910 features are significantly right-laterally offset whereas post 1910 features are not. This strongly suggests that the May 15, 1910 earthquake sustained ground rupture with a lateral component of as much as 35 cm. The fault most likely ruptured the relatively straight 20-km-long section between Lake Elsinore and Glen Ivy. Such a rupture length is not inconsistent with its inferred magnitude (Toppozada and Parke, 1982) and with the amount of observed lateral displacement. The vertical displacement may have varied in the vicinity of Glen Ivy Marsh due to variations in structure along strike of the fault. Because of local withdrawal of water, the vertical, and possibly the lateral, components of slip may also have been amplified during the earthquake due to the added collapse of the soil in the vicinity of the wells. Thus, both the vertical and horizontal slip estimates should be considered maximum values.

A major event occurred about 1300 A.D. between the deposition of peats 8 (circa 1260 A.D.) and 7 (circa 1475 A.D.)

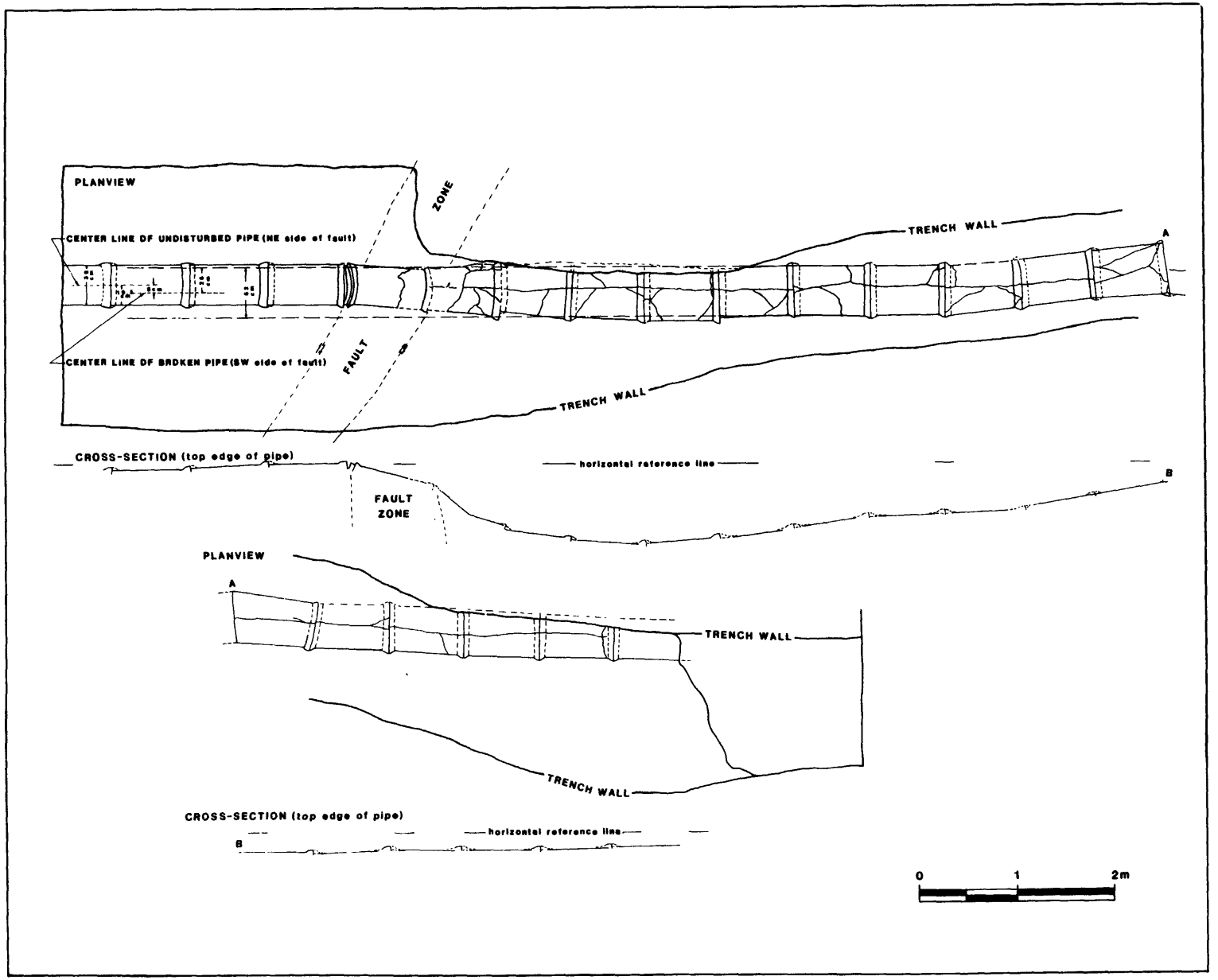

Figure 5. Map of terracota pipe (circa 1914) that is broken and vertically displaced across the fault, due primarily to subsidence.

(Fig. 3). Liquefaction, folding and faulting occurred in the main fault zone as well as along several subsiderary faults (Rockwell and others, 1986, Brake, 1987). In trench MT-1, Figure 3 shows results of a liquefaction and faulting event which breaks peat 8 but which is overlain by a sand channel not involved in the liquefaction.

Two fault splays off the main fault zone broke peats 8 and strata below, but do not break peat 7. This relationship is the same as in the main trench (MT-1) and indicates that these two faults formed as splays off of the main fault during this earthquake.

Differences in stratigraphic thickness of several units across the fault indicated a lateral component of movement. To establish the magnitude of lateral slip, the sediments overlying a particular peat horizon (that overlay gravelly sand) were removed by hand and the peat was peeled off to expose the underlying sand and channel morphology (Figs. 6 and 7). A total of about 50 cm of lateral slip is expressed across the two strands of this break, both as faulting and folding, and an indeterminant amount may have occurred on the main break of the fault. Thus, this slip value is a minimum for this earthquake. The brittle slip decreases towards the southwest and dies out in folding (Figs. 6 and 7).

From these data, the circa 1300 A.D. earthquake appears to have been larger than the 1910 earthquake. Total slip determination for this event was not possible, however.

Coyote Mountain Segment

Mapping along the Elsinore fault in the Coyote Mountains segment has located over 40 right-laterally offset fluvial channel and bar deposits, channel walls, debris flow deposits, and small landslide headscarps (Table 1 and Fig. 8) in Holocene drainages along a 1.5 km section of the fault (Rockwell and Pinault, 1986). The amount of right-lateral offset varies from about 1.5 m to over 20 m dependent upon the age of the displaced deposit or geomorphic feature. The measured offsets cluster into six distinct groupings, although three of these groups have very small populations. Nevertheless, two to three measurements are better than the usual one measurement afforded in many trenching projects. Preliminary analysis of soils developed in offset deposits in Alverson Canyon indicates that the deposits that are offset by greater amounts display progessively stronger soil development (Fig. 9)(all of these soils are very weak and have only minor secondary $CaCO_3$ accumulation but differences are apparent). These data suggest that the groupings represent discrete earthquake events with estimated displacement magnitudes ranging from about 0.9 to 1.85 m per event for this section of the fault, a factor of two variability in slip/event.

Laguna Salada Segment

The Laguna Salada fault has a nearly continuous expression of a very recent, large magnitude earthquake along a 20-25 km long section of the fault zone (Mueller and Rockwell, 1984; 1988 in press). Free faces in unconsolidated alluvium (Fig. 10)

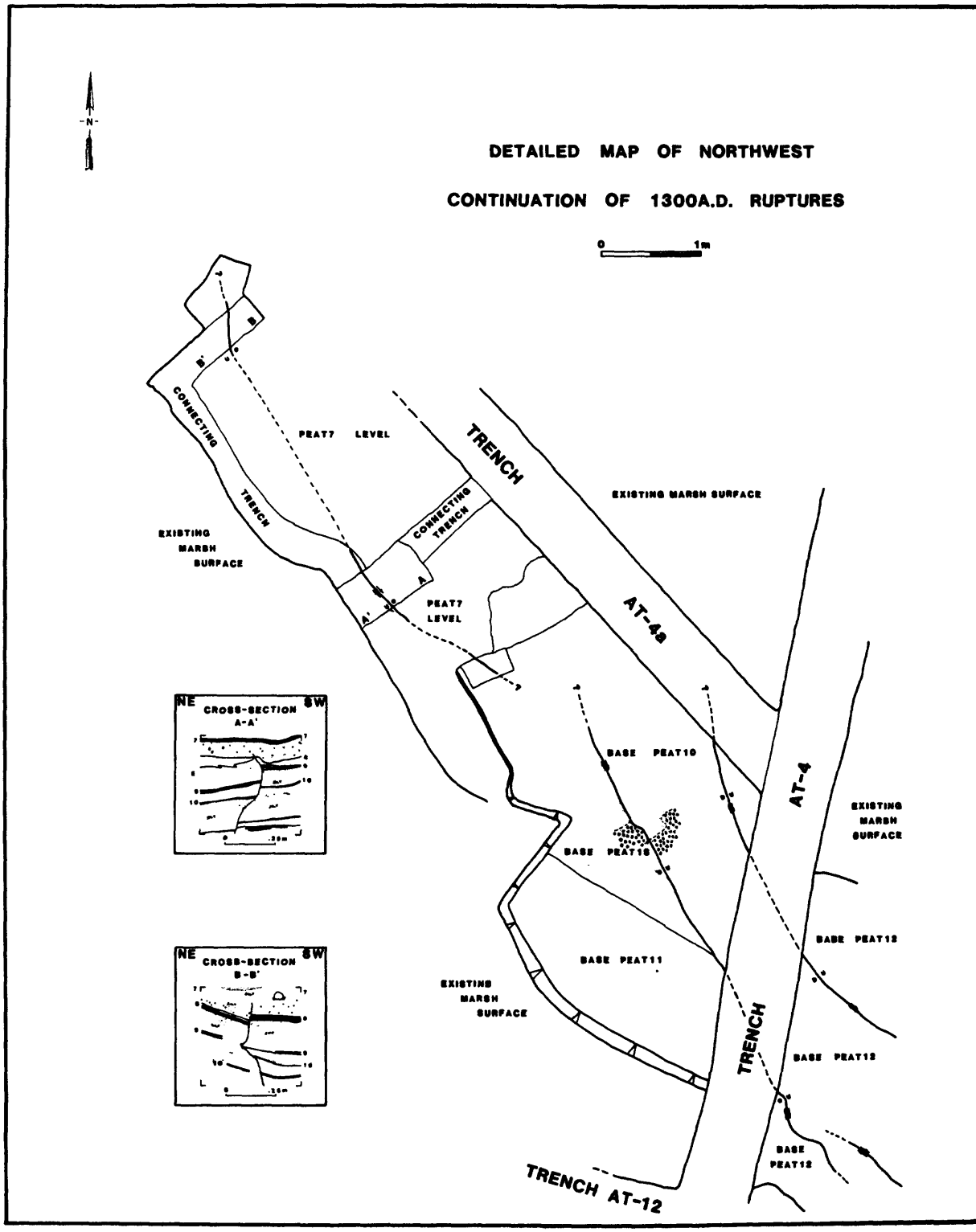

Figure 6. Map of secondary faults that developed in the circa 1300 A.D. earthquake. These faults splayed off of the main fault trace.

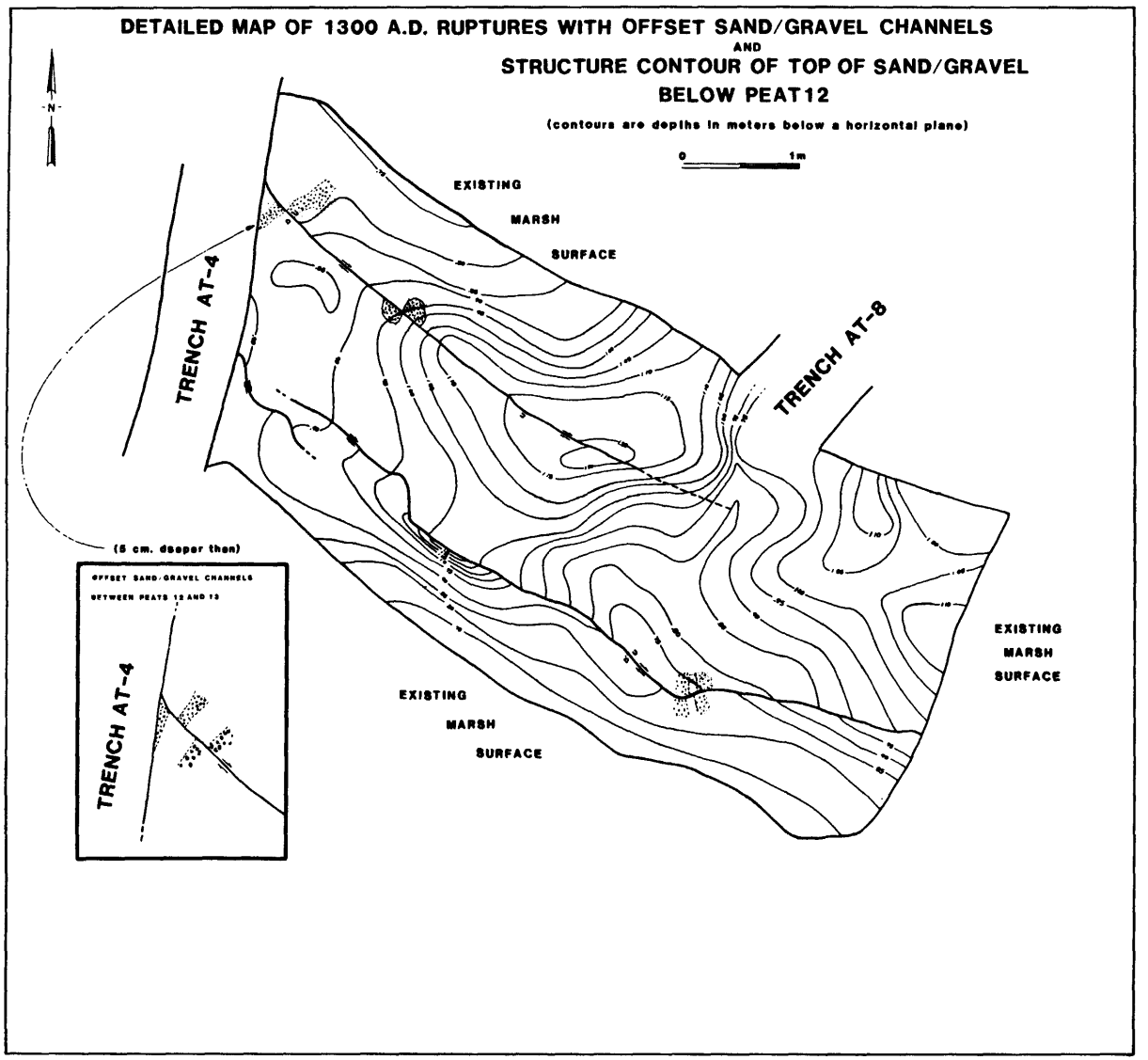

Figure 7. Structure contours of the folded peats that ewere deformed during the circa 1300 A.D. earthquake.

Table 1. Tabulation of amount of offset of geomorphic features and channel deposits as shown in Fig. 8 for a one kilometer reach of the fault. The errors stated represent the estimated maximum error for each offset when measured in the field. Many of these offsets represent an average of two or three measurements of discrete piercing points. The mean for each group is represented by $\bar{x}$, whereas the difference between successive means, which presumably represents an estimate of the slip for that event, is represented by Δu.

Group 1 (n=13)	Group 2 (n=12)	Group 3 (n=3)	Group 4 (n=7)	Group 5 (n=3)	Group 6 (n=2)	Group 7 (n=9)
1.4±0.2	2.9±0.5	3.9±0.5	5.2±0.2	6.7±0.5	8.5±0.3	11.4±2.0
1.7±0.4	2.7±0.3	3.5±0.5	5.0±0.3	7.1±0.5	8.9±1.0	17.0±2.0
1.4±0.2	2.8±0.3	3.3±0.3	5.3±1.0	7.1±0.2		19.0±1.0
1.4±0.2	2.6±1.0		5.4±0.3			20.0±2.0
1.6±0.3	2.5±0.3		5.0±0.2			22.0±2.0
1.5±0.2	2.6±0.3		5.0±0.5			23.0±1.0
1.4±0.3	2.7±0.3		5.2±0.3			38.0±2.0
1.4±0.2	2.3±0.3					40.0±2.0
1.4±0.2	2.7±0.5					41.0±3.0
1.5±0.3	2.7±0.5					
1.6±0.2	2.7±0.3					
1.4±0.2	3.0±0.5					
1.5±0.2						

$\bar{x}$ = 1.5 — 2.7 — 3.6 — 5.2 — 7.0 — 8.7 —

Δu = 0.8 — 1.1 — 1.6 — 1.8 — 1.7

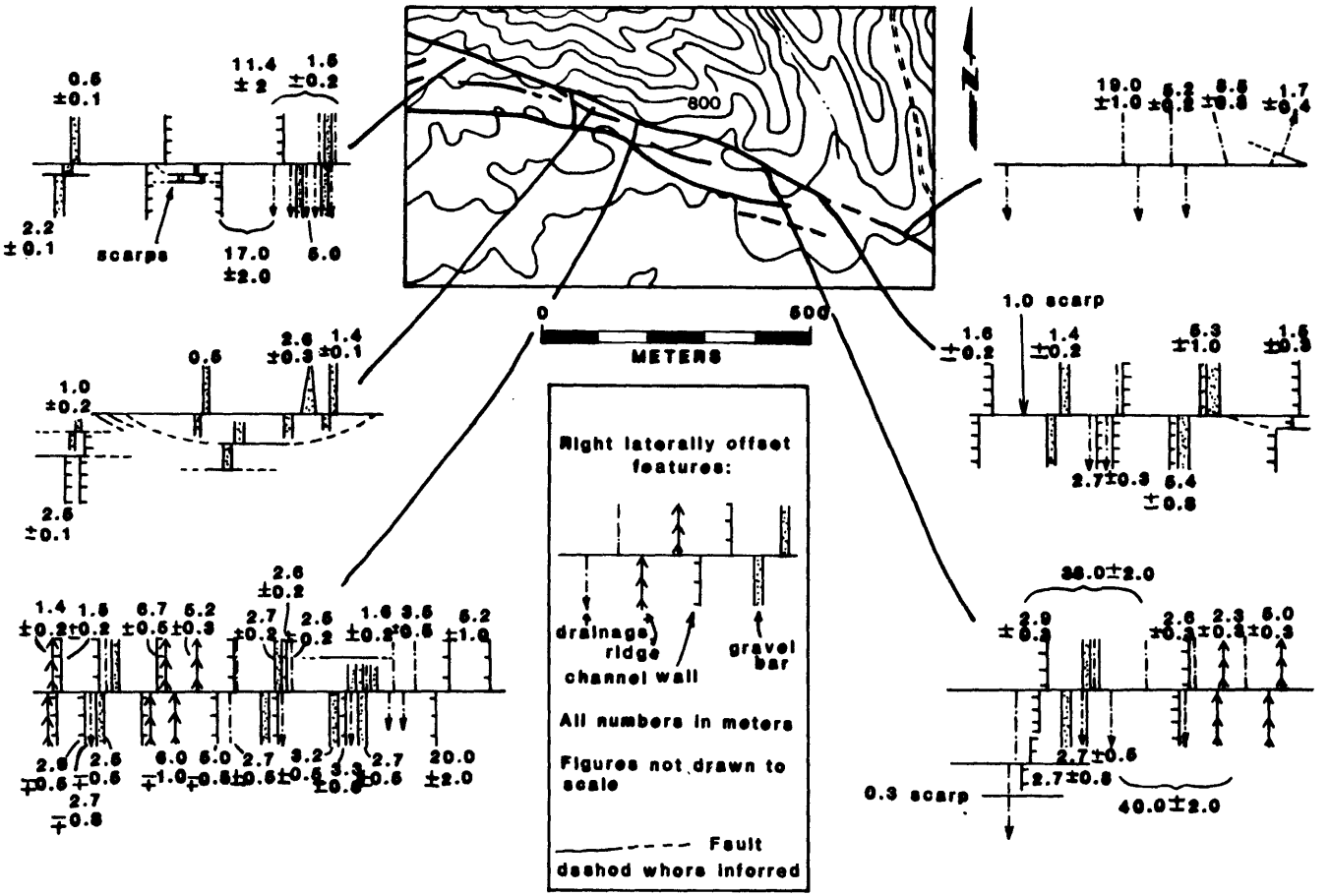

Figure 8. Diagrammatic sketch of right-laterally offset features along a 1 km long reach of the Elsinore fault near Alverson and Fossil Canyons in the southeastern Coyote Mountains (from Rockwell and Pinault, 1986). Only slip estimates from offset features that crossed only one active fault trace, or where multiple traces were closely spaced, were used.

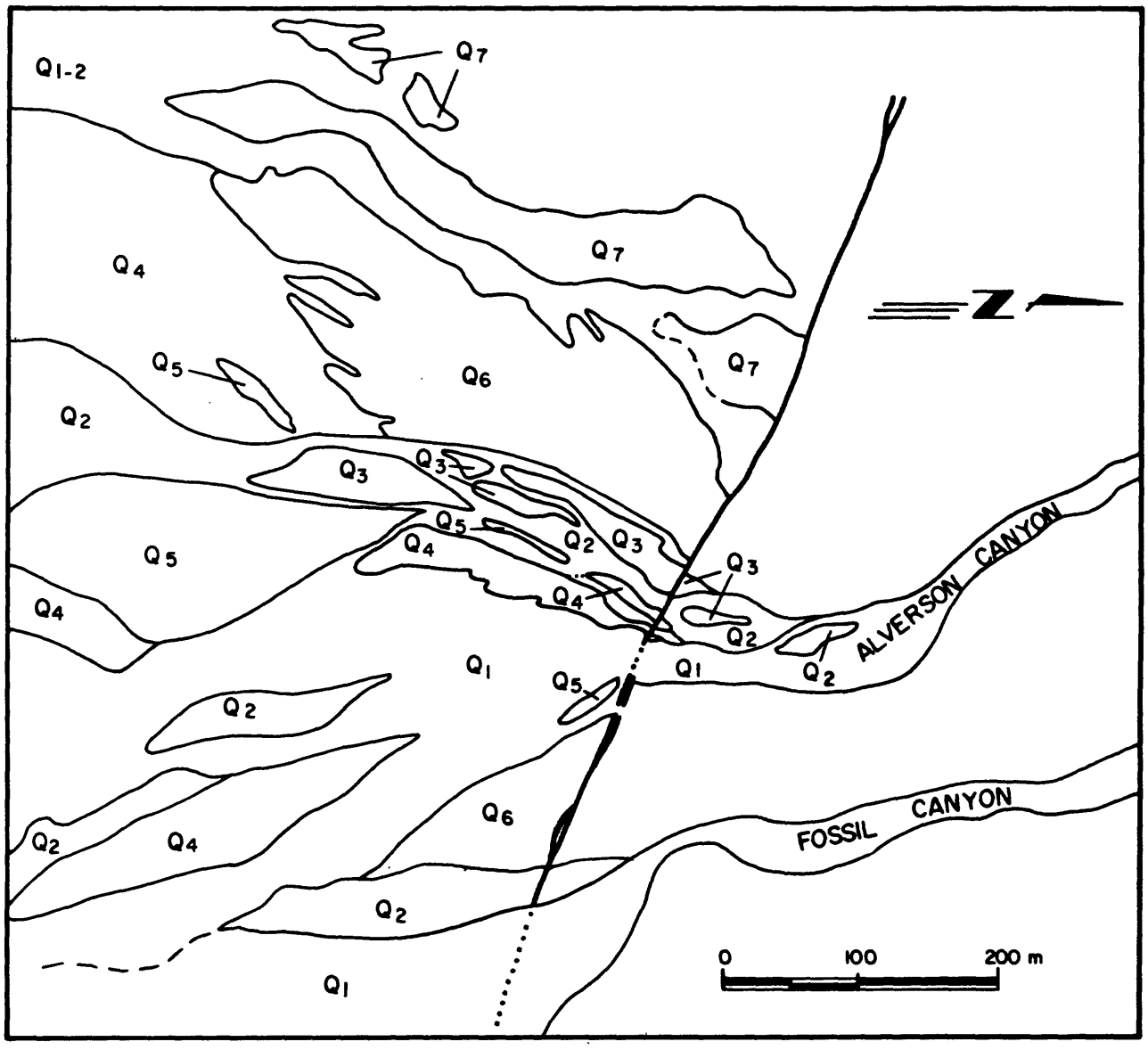

Figure 9. Map of Quaternary deposits that cross the Elsinore fault in the vicinity of Alverson and Fossil Canyons. Q1 deposits are not faulted. Q2 deposits are offset about 1.5 m, Q3 deposits are offset about 2.7 m, and Q4 deposits are offset about 5.2 m. The Q5 deposits are inferred to be offset 8 m whereas the Q6 deposits (Pleistocene) are offset between 60 and 120 m and the Q7 deposits are offset 150-200 m.

Figure 10. Free face on fault scarp along the Laguna Salada fault. Alluvium is early to middle Holocene in age.

attest to the recency of the last event. Strand (1980), without having seen any field evidence for a recent earthquake, placed the Feb. 23, 1892 earthquake on the Laguna Salada fault based on the isoseisms of shaking effects produced by this earthquake. The epicenter was placed a little to the west in an area of no known Holocene faulting by Topozzada and others (1983) due to reports of ground fissuring that could simply have been secondary shaking effects, and because shaking was less severe at Yuma than in San Diego. This second aspect is explained by Anderson and others (1988) as an attenuation effect. Based on the overwhelming evidence for a very recent earthquake along the Laguna Salada fault, Mueller and Rockwell (1988, in press) concurred with Strand (1980) that the 1892 earthquake most likely ruptured the Laguna Salada fault.

The rupture during this last event propogated around the intersection of the Laguna Salada and the Canon Rojo faults (Fig. 11); the Canon Rojo fault is a northeast trending normal fault that connects to the Chupamiertos fault to the southeast. The Canon Rojo fault, along with other north-northeast trending normal faults in the Laguna Salada basin, link a series of right-stepping dextral-oblique faults that form the western margin of the Sierra de los Cucapas (Mueller and Rockwell, 1988 in press). Thus, the last rupture appears to have terminated to the southeast at a major right step in the transfer of dextral slip.

Dip displacement during this last event ranges from about 2 m near its end points to a maximum of about 5 m near the intersection of the two faults. The dextral component is clearly demonstrated by mullions on the fault surface which are parallel to striae on the normal slip Canon Rojo fault, suggesting up to 2 m of right-lateral slip at the fault intersection. The magnitude of the vertical slip component along with burial of the downthrown block in many locations has obscured the geomorphic evidence for lateral slip.

The size of the two previous earthquakes are clearly apparent in several areas where the bedrock fault surface was exposed in the last event. Salt weathering (the fault is generally down wind from the playa/lake) of the fault surface has resulted in pitting and crystal disaggregation of the older (higher) exposures whereas the fault surface exposed during the last earthquake is still relatively fresh, suggesting that a considerable length of time (500-2000 years?) lapsed between events. In addition, the salt weathering has degraded the older fault surfaces such that the progressively older scarps are at lower slopes (Fig. 12). Profiling of the scarps suggests that the last three earthquakes had similar amounts of dip slip at several locations along the length of the last surface rupture (Mueller, 1984).

DISCUSSION

For the three segments studied, slip data exist for at least two or more earthquakes. Both the dominantly strike-slip Glen Ivy and Coyote Mountain segments display a considerable variation in the magnitude of slip at a point along the fault. The Glen

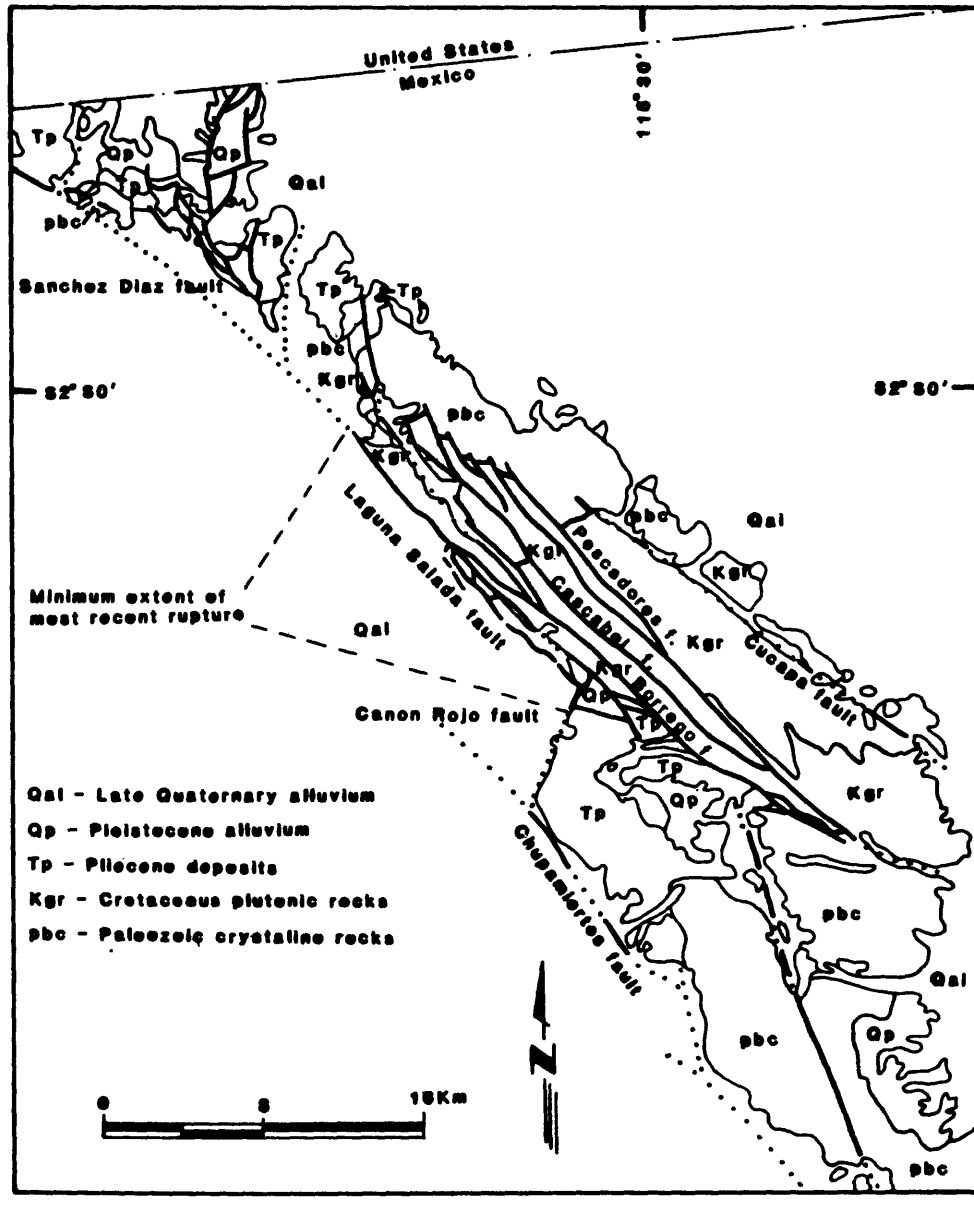

Figure 11. Generalized map of the Sierra de los Cucapas, bounded on the southwest by the Laguna Salada fault (after Gastil, 1971). Note the minimum rupture length of the 1892 earthquake as suggested by scarps with free faces in unconsolidated alluvium.

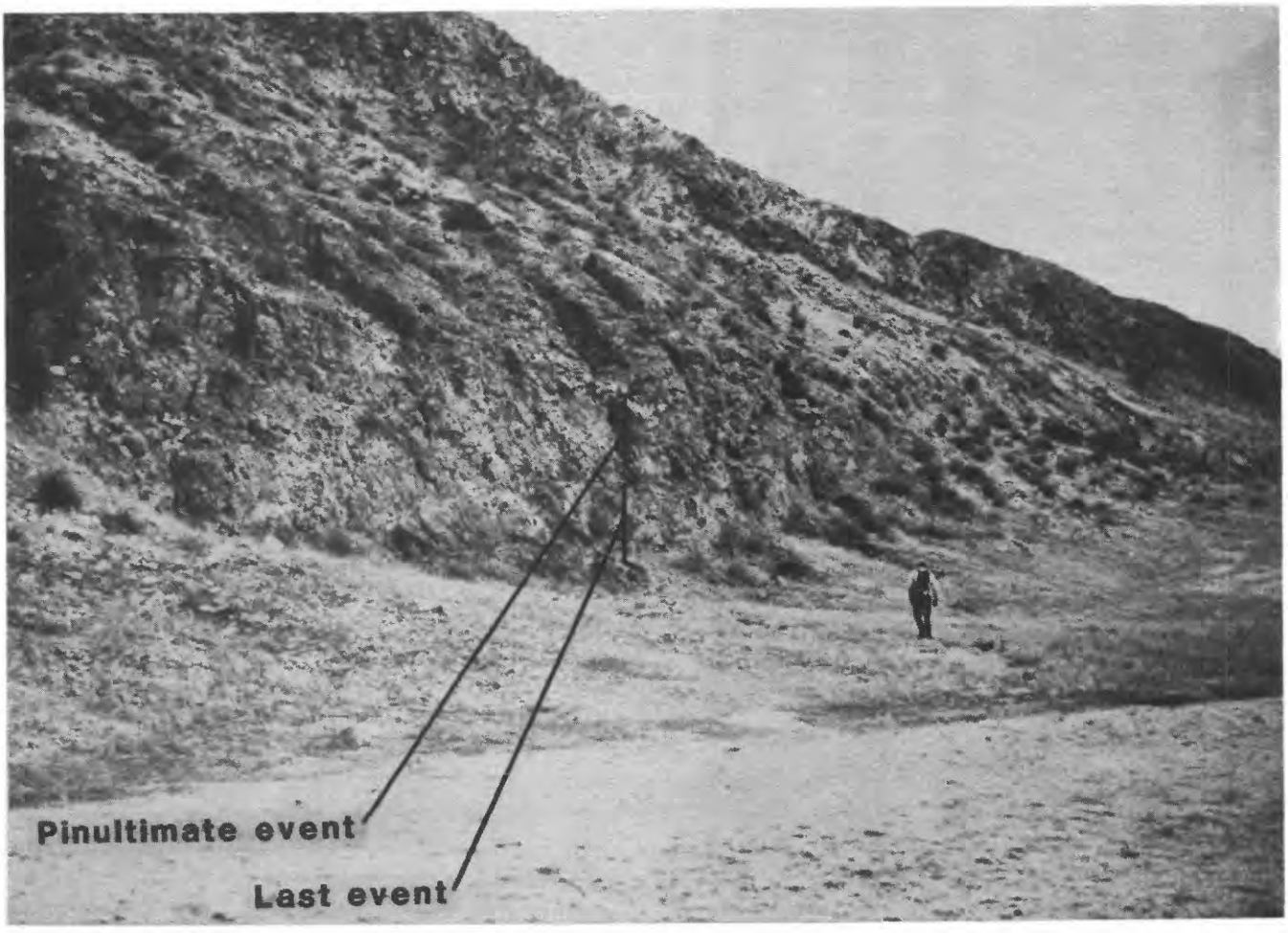

Figure 12. Fault scarps associated with the penultimate and most recent earthquakes along the Laguna Salada fault. Note similarity in scarp sizes.

Ivy study area falls within a major double bend, which could explain some of the variability, but the Coyote Mountain segment does not. These data are similar to the variations in the amount of slip inferred for the last two Superstition Hills earthquake (Lindvall and others, 1989 in press; Hudnut and Sieh, 1989 in press), assuming that afterslip continues as predicted for the 1987 earthquake. Similarly, there have been significant variations for the historical earthquakes along the dextral Cerro Prieto fault in northern Baja California (Anderson and Bodin, 1987). Conversely, the dominantly dip-slip Laguna Salada events suggest repeatability of similar sized earthquakes, similar to normal faults in the Great Basin (Schwartz and Coppersmith, 1984; Schwartz and Crone, 1985). The characteristic earthquake concept was initially developed from paleoseismic studies of normal faults along the Wasatch fault zone and other normal fault zones in the Great Basin (Schwartz and Coppersmith, 1984). From their studies, many events represented entire segments or entire faults that ruptured repeatedly, producing a mountain front with a similar topographic shape as the scarps from the most recent earthquakes (Wallace and Whitney, 1984). There appears to be considerably more variability, however, in slip at a point along a strike-slip fault. Part of this variation may be due to co-temporal rupture of adjacent fault segments to produce larger earthquakes with longer ruptures and greater amounts of slip.

ACKNOWLEDGEMENTS

I thank all of my students who have worked with me at various times along the Elsinore fault. In particular, I thank Tom Pinault, Karl Mueller, Doug Millman, Sharon Isaac, Pat Vaughan, and Rob McElwain who contributed extensively during completion of their theses. I also thank Mike Rymer for a thorough review which led to significant improvement of the presentation of this manuscript. This work was partially supported by U.S.G.S. Grant no. 14-08-0001-G1164.

REFERENCES CITED

Anderson, J.G. and Bodin, P., 1987, Earthquake recurrence models and historical seismicity in the Mexicali-Imperial Valley: Seis. Soc. Am. Bull., v. 77, no. 2, p. 562-578.

Anderson, J.G., Rockwell, T.K., and Agnew, D.C., 1988, Past and possible future earthquakes significant to the San Diego region: Earthquake Spectra, in press for December issue.

Brake, J.F. and Rockwell, T.K., 1987, Magnitude of slip from historical and prehistorical earthquakes on the Elsinore fault, Glen Ivy Marsh, southern California: Geological Society of America Abstracts with Programs, v. 19, no. 6.

Clark, M.M., 1982, Map showing recently active breaks along the Elsinore and associated faults, California, between Lake Henshaw and Mexico: U.S. Geological Survey Misc. Inv. Map I-1329, two sheets.

Kennedy, M., 1977, Recency and character of faulting along the Elsinore fault zone in southern Riverside County, California: Calif. Div. of Mines and Geology, Spec. Rpt. 131, 12 p.

Millman, D.E. and Rockwell, T.K. 1986, Neotectonics of the Elsinore fault in Temescal Valley, California: in (P. Ehlig, ed.) Neotectonics and faulting in southern California; Geol. Soc. of Amer. Guidebook for the Cord. Sect. Meeting in Los Angeles, p. 159-166.

Mueller, K.J., 1984, Neotectonics, alluvial history and soil chronology of the southwestern margin of the Sierra de los Cucapas, Baja California Norte: unpub. M.S. thesis, San Diego State Univ., 363 p.

Mueller, K.J. and Rockwell, T.K., 1984, Sense, recency and rates of faulting along the Laguna Salada and Canon Rojo faults, NE Baja California: Geol. Soc. Am. Abst. With Progs., p. 602.

Mueller, K.J. and Rockwell, T.K., 1988, Structural evolution of the western margin of the Sierra de los Cucapas, Baja California, Mexico: Amer. Assoc. Petr. Geol. Memoir, in press.

Pinault, C.T. and Rockwell, T.K., 1984, Rates and sense of Holocene faulting on the southern Elsinore fault: Further constraints on the distribution of slip between the Pacific and North American Plates: Geol. Soc. of Amer. Abstracts With Programs, v. 16, no. 6, p. 624.

Rockwell, T.K., Lamar, D.L., McElwain, R.S., and Millman, D.E., 1985, Late Holocene recurrent faulting on the Glen Ivy North strand of the Elsinore fault, southern California: Geol. Soc. of Am., Abstracts with Programs, m. 17, no. 4., p. 404.

Rockwell, T.K., McElwain, R.S., Millman, D.E. and Lamar, D.L., 1986, Recurrent late Holocene faulting on the Glen Ivy North strand of the Elsinore fault at Glen Ivy Marsh: in Guidebook and Volume on Neotectonics and Faulting in Southern California (P. Ehlig, ed.), Cordilleran Section, Geological Society of America, p. 167-176.

Rockwell, T.K. and Pinault, C.T., 1986, Holocene slip events on the southern Elsinore fault, Coyote Mountains, southern California: in (P. Ehlig, ed.) Neotectonics and faulting in southern California; Geol. Soc. Amer. Guidebook for the Cord. Sect. Meeting in Los Angeles, p. 193-196.

Schwartz, D.P. and Coppersmith, K.J., 1984, Fault behavior and characteristic earthquakes: Examples from the Wasatch and San Andreas faults: Jour. Geophys. Res., v. 89, p. 5681-5698.

Schwartz, D.P. and Crone, A.J., 1985, The 1983 Borah Peak earthquake: A calibration event for quantifying earthquake recurrence and fault behavior on Great Basin normal faults: in Proceedings of Workshop XXVIII on the Borah Peak, Idaho, Earthquake: U.S. Geological Survey Open File Report 85-290, p. 153-160.

Sibson, R.H., 1985, Stopping of earthquake ruptures at dilational fault jogs: Nature, v. 316, no. 6025, p. 248-251.

Strand, C.L., 1980, Pre-1900 earthquakes of Baja California and San Diego County: unpub. M.S thesis, San Diego State Univ., 320 p.

Toppozada, T.R., Real, C.R. and Parke, D.L., 1981, Preperation of isoseismal maps and summaries of reported effects for pre-1900 California earthquakes: Cal.Div. Mines and Geol. Open File Report 81-11 SAC, 181 p.

Toppozada, T. R. and D. L. Parke, 1982, Areas damaged by California Earthquakes, 1900-1949; California Division of Mines and Geology, Open-file Report 82-17, Sacramento, CA.

Vaughan, P. and Rockwell, T.K., 1986, Alluvial stratigraphy and neotectonics of the Elsinore fault zone at Agua Tibia Mountain, southern California: in (P. Ehlig, ed.) Neotectonics and faulting in southern California; Geol. Soc. of Amer. Guidebook for the Cord. Sect. Meeting in Los Angeles, p. 177-191.

Wallace, R.E. and Whitney, R.A., 1984, Late Quaternary history of the Stillwater seismic gap, Nevada: Seis. Soc. Am. Bull., v. 74, no.1, p. 301-314.

SURFACE RUPTURE IN A FAULT STEPOVER ON THE SUPERSTITION HILLS FAULT, CALIFORNIA

by

Michael J. Rymer
U.S. Geological Survey
Menlo Park, California 94025

ABSTRACT

A stepover in the central part of the Superstition Hills fault was reactivated during surface rupture associated with the November 1987 Superstition Hills earthquake. The stepover separates the north and Imler fault strands, which have at least 3 km of fault trace overlap. Earlier detailed studies of tectonic and triggered slips on the Superstition Hills fault following nearby earthquakes in 1951, 1968, 1979, and 1981 had not detected the presence of the stepover because rupture either stopped at or near the stepover or passed through the stepover. Plots of initial and postseismic displacements associated with the 1987 event show approximately equal amounts of slip on the north and Imler strands at 12 days after the earthquake and extrapolated for 1 day and the final slip. Slip plotted at 12 days after the main shock has a greater density of measurement sites and thus allows a more detailed look at the behavior of slip in the stepover. There is a gradual decrease in slip from near the center of either strand toward the stepover until the area of maximum slip crossover is reached, where a precipitous slip dropoff occurs on both strands. Observations at 546 days after the earthquake indicate that the area of maximum slip crossover had extended about 300 m to the northwest or that earlier observations were incomplete. The sum of displacements on the two strands in the area of slip crossover is less than adjacent slip highs on the individual strands. Minor splay, subsidiary, and bedding-plane thrust faults take up some of the missing slip, and deformation of strata enclosed between the north and Imler strands probably accounts for the rest.

Subsurface extent of the fault stepover is unclear. Aftershocks of the 1987 Superstition Hills earthquake greatly decrease in number near the stepover, which was also the stopping point for the high-frequency strong ground motion. However, like the surface ruptures that went past the stepover in 1968, 1979, 1981, and 1987, long-period waves associated with the 1987 earthquake extended well past the stepover. Both a change in basement lithologies and a 6° bend in the fault at the stepover may account for the decrease of aftershocks and end of radiated high-frequency strong ground motion, thus clouding the picture as to whether the stepover extends to hypocentral depths.

Study of the stepover in the Superstition Hills fault and the history of surface ruptures in the same area only partly support models of fault interaction in segment stepovers.

INTRODUCTION

Recent studies on the geometry of brittle failure, including earthquake rupture, have shown breakage to be arranged in discrete segments. Steps, jogs, or bends are located on or between segments and are sites of stress accumulation (Segall and Pollard, 1980). Such segmented failure is scale independent, ranging from microscopic (Bartlett *et al.*, 1981) to lengths of tens of kilometers (Vedder and Wallace, 1970; Barka and Kandinsky-Cade, 1988).

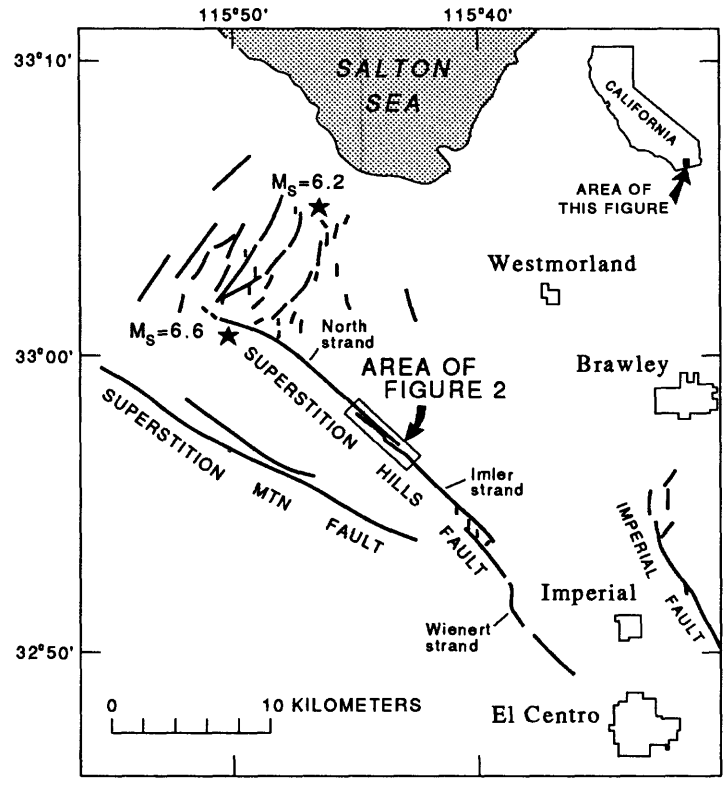

Figure 1.—Index map showing major faults and 1987 surface faulting in the Superstition Hills area. Epicenters of the November 24, 1987 earthquakes in the Superstition Hills are shown by stars.

Microearthquake investigations have shown local surface irregularities, that is, steps, jogs, or bends, mapped at the ground surface of fault zones to extend to hypocentral depths (Eaton *et al.*, 1970; Bakun *et al.*, 1980; Reasenberg and Ellsworth, 1982). Fault trace irregularities, therefore, imply potential sites of rupture nucleation or termination (Sibson, 1985, 1986; King and Nabelek, 1985) and thus are worthy of more detailed study.

In light of the potential importance of fault complexities, this paper addresses three aspects of a fault stepover along the Superstition Hills fault, southern California (Fig. 1). First, the history of five surface displacements is presented and compared: tectonic slip associated with a moderate earthquake on the Superstition Hills fault in 1951, three triggered slip events, and tectonic slip associated with the 1987 Superstition Hills earthquake. Second, the details of 1987 faulting within the fault stepover are described. Third, the distribution of aftershocks along the fault and possible subsurface extent of the stepover are discussed. The value of studying this stepover on the Superstition Hills fault is that with five documented surface-rupture events and details of fault complexities and locations of slip an evaluation of fault interaction in a segment stepover is allowed.

The fault stepover lies between 11 and 15 km southeast of the northwestern end of surface rupture associated with the M_S 6.6 November 24, 1987 earthquake on the Superstition Hills fault (Sharp *et al.*, in press, plate 1). The stepover, a dilational jog, is toward the right, along the predominantly right-lateral fault. The stepover separates

two fault strands, here referred to as the north and Imler strands. Separation distances between the two traces range from 60 to 280 m, with the shorter distance located near the area of maximum slip crossover (see below). Overlap of the two strands parallel to the fault is about 3.5 km, with the Imler strand segment extending 1.5 km past the area of maximum slip crossover (Fig. 2). The Superstition Hills fault has an azimuthal change of 6° at the fault stepover. The 6° bend was measured from the mean azimuth of 8-km-long sections of the north and Imler strands nearest the fault stepover as mapped by Sharp *et al.* (1989). A larger-scale fault stepover lies between the Imler and Wienert strands, near the southeast end of 1987 surface rupture on the Superstition Hills fault (Fig. 1), but that jog is not addressed in this report because less information is available.

The geologic setting of the Superstition Hills was described by Dibblee (1954, 1984) and Sharp *et al.* (1989). In brief, strata exposed in the area of the fault stepover on the Superstition Hills fault consist of poorly consolidated and highly deformed Pleistocene continental sediments, primarily silty and clayey lake deposits that contain local sand and gravelly sand units, collectively named the Brawley Formation by Dibblee (1954). These are locally covered by young lacustrine deposits and alluvium.

HISTORY OF SLIP

Mapped surface ruptures in and near the stepover on the Superstition Hills fault during the last four decades are plotted in Figure 2. Surface rupture was mapped by Joseph Ernst following tectonic slip probably associated with the January 24, 1951 Superstition Hills earthquake (M=5.6) (Fig. 2*A*; written commun., 1989; Allen *et al.*, 1965). Four other events that caused surface displacement are accurately recorded: three triggered and the 1987 tectonic slips. The three triggered-slip events along the fault were associated with the 1968 Borrego Mountain earthquake (Fig. 2*B*; Allen *et al.*, 1972), the 1979 Imperial Valley earthquake (Fig. 2*C*; Fuis, 1982), and the 1981 Westmorland earthquake (Fig. 2*D*; Sharp *et al.*, 1986). Epicenters of these three events were located 42 km northwest, 55 km southeast, and 18km northeast of the jog, respectively. Right slip during each of the triggered events was small in the area shown in Figure 2; the maxima were 0.9 cm in 1968, 1.0 cm in 1979, and 1.4 cm in 1981. The three triggered slips were discontinuous. Gaps in surface rupture reported after the events coincide, in part, with the location of loose sand or a thin hardened sand surface in stream channels that obscurred the minor displacements. The area of no surface rupture about 600 m northwest of the center of strips *B*, *C*, and *D* (Fig. 2) is where surface slip is inferred to have stepped over from one fault strand to the next, the area of maximum slip crossover. This site was also the southeastern limit of surface rupture mapped after the 1951 earthquake by Joseph Ernst (Fig. 2*A*), indicating that surface rupture in 1951 stopped at the fault stepover.

Surface rupture associated with the 1987 Superstition Hills earthquake in the area of the fault stepover, in contrast to the triggered slips, had significantly greater displacement and complexity (Figs. 2*E*, 3, 4*A*). The 1987 surface rupture, aside from its greater complexity, coincides with the traces mapped after the earlier tectonic and triggered slips. Minor variations in fault trace locations reported from one slip event to the next can be attributed to the various techniques used in mapping the surface rupture or to the various scales (and therefore accuracy of mapping) of aerial photos used in mapping. Another possible error source is the transfer method, where the topographic model is insufficient in detail. The 1987 rupture was large enough to maintain surface breakage in the loose sand or thin-crusted sands that had earlier obscurred the presence of the fault stepover. Highest

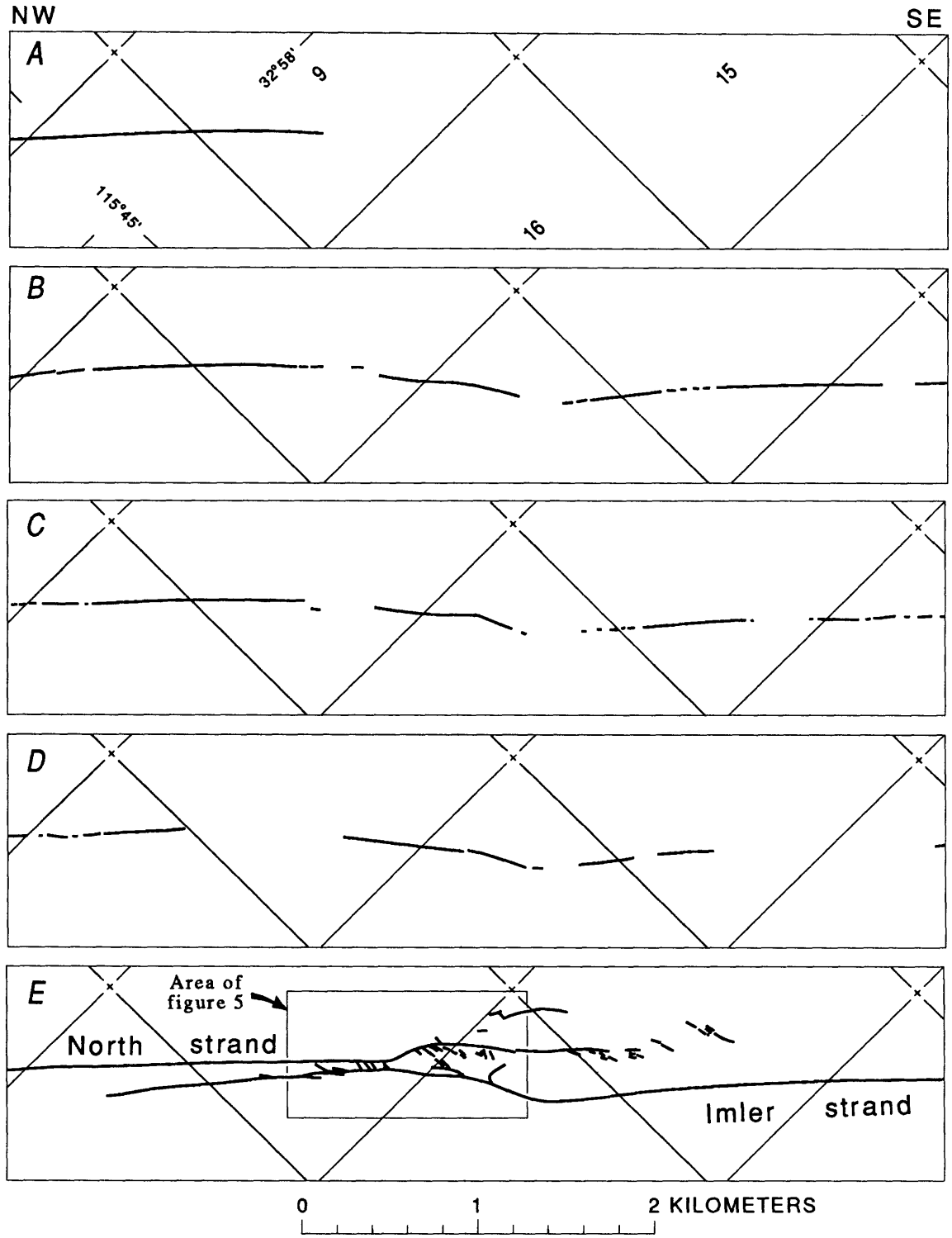

Figure 2.—Surface-rupture traces in the area of the right stepover (jog) on the Superstition Hills fault. *A* through *E* cover the same area and represent tectonic slip associated with the 1951 Superstition Hills earthquake (*A*, Joseph Ernst, written commun., 1989), triggered surface rupture associated with the 1968 Borrego Mountain earthquake (*B*, Allen *et al.*, 1972), the 1979 Imperial Valley earthquake (*C*, Fuis, 1982), and the 1981 Westmorland earthquake (*D*, Sharp *et al.*, 1986), and tectonic slip associated with the 1987 Superstition Hills earthquake (*E*, Sharp *et al.*, 1989). Section lines of land grid and section numbers 9, 15, and 16 are shown for reference.

values of right slip in the area of Figure 2 associated with the 1987 event are about 50 cm after 1 day and about 96 cm for final slip (Sharp *et al.*, 1989, Fig. 8; Boatwright *et al.*, 1989, Budding *et al.*, 1989).

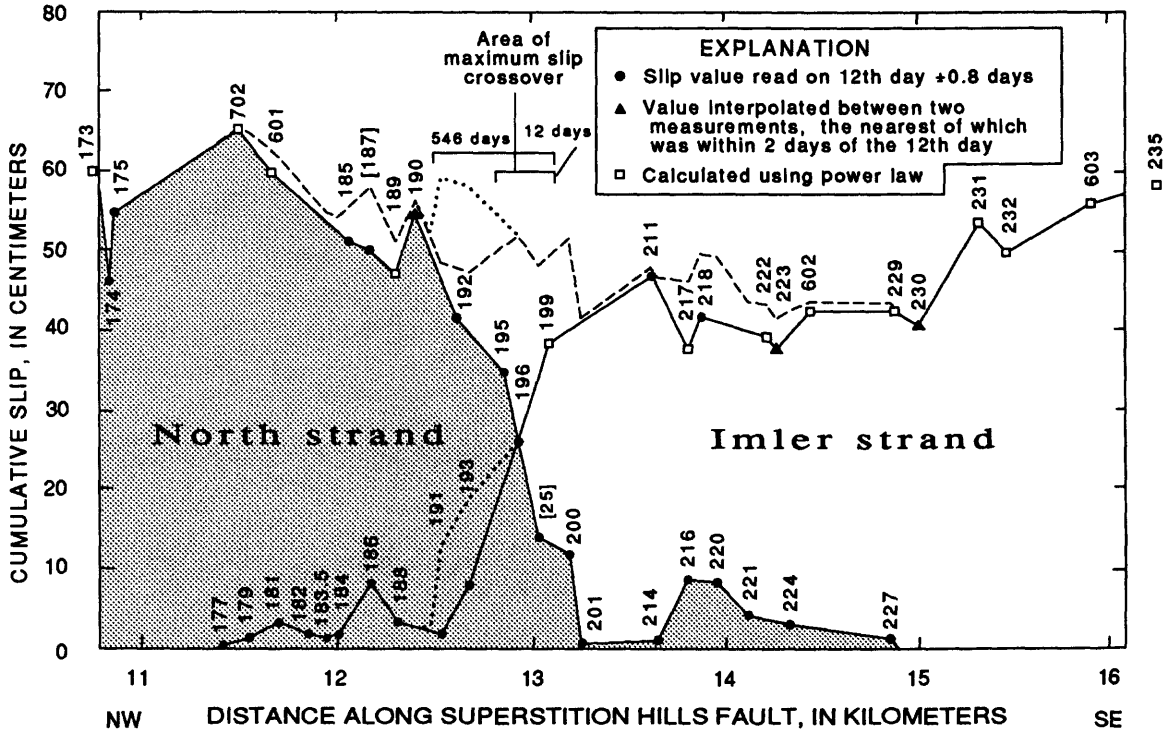

Figure 3.—Plots of right slip at 12 days after the earthquake versus distance along a 5.3-km-long section of the Superstition Hills fault (same section of fault as shown in Fig. 2). Separate plots are shown for the north and Imler strands. Displacements were measured on the twelfth day ± 0.8 days after the event or interpolated between two measurements on log-time plots, or calculated for the twelfth day after the earthquake using the power law of Sharp and Saxton (1989) and Boatwright *et al.* (1989). The change in slip caused by the ± 0.8 day difference in the time that measurements were made amounts to less than 2 cm of slip and commonly less than 1 cm. (For extrapolated slip amounts at 1 day and final slip see Fig. 4*A* and Sharp *et al.*, 1989; Budding *et al.*, 1989.) Dashed line represents approximate 12-day cumulative right slip summed for the north and Imler strands and the extensions of the strands beyond the area of maximum slip crossover. That is, the dashed line is the sum of the upper and lower plots in this figure. Dotted lines represent estimated slip values on splay faults near stations 191 and 193 on the Imler strand. The upper dotted line is the sum of the dashed and lower dotted lines. Distances along the fault are relative to a standard zero point used in all previous surface displacement investigations. Station numbers refer to sites listed in Sharp *et al.* (in press), except stations 25 and 187, shown in brackets, both of which had local fault complexity and whose displacements can only be considered a minimum. Errors estimated for slip measurements average about ± 3 cm.

Details of surface slip in the stepover area are shown in Figure 3, where right slip is plotted at 12 days after the November 24 main shock. The 12th day was the time that

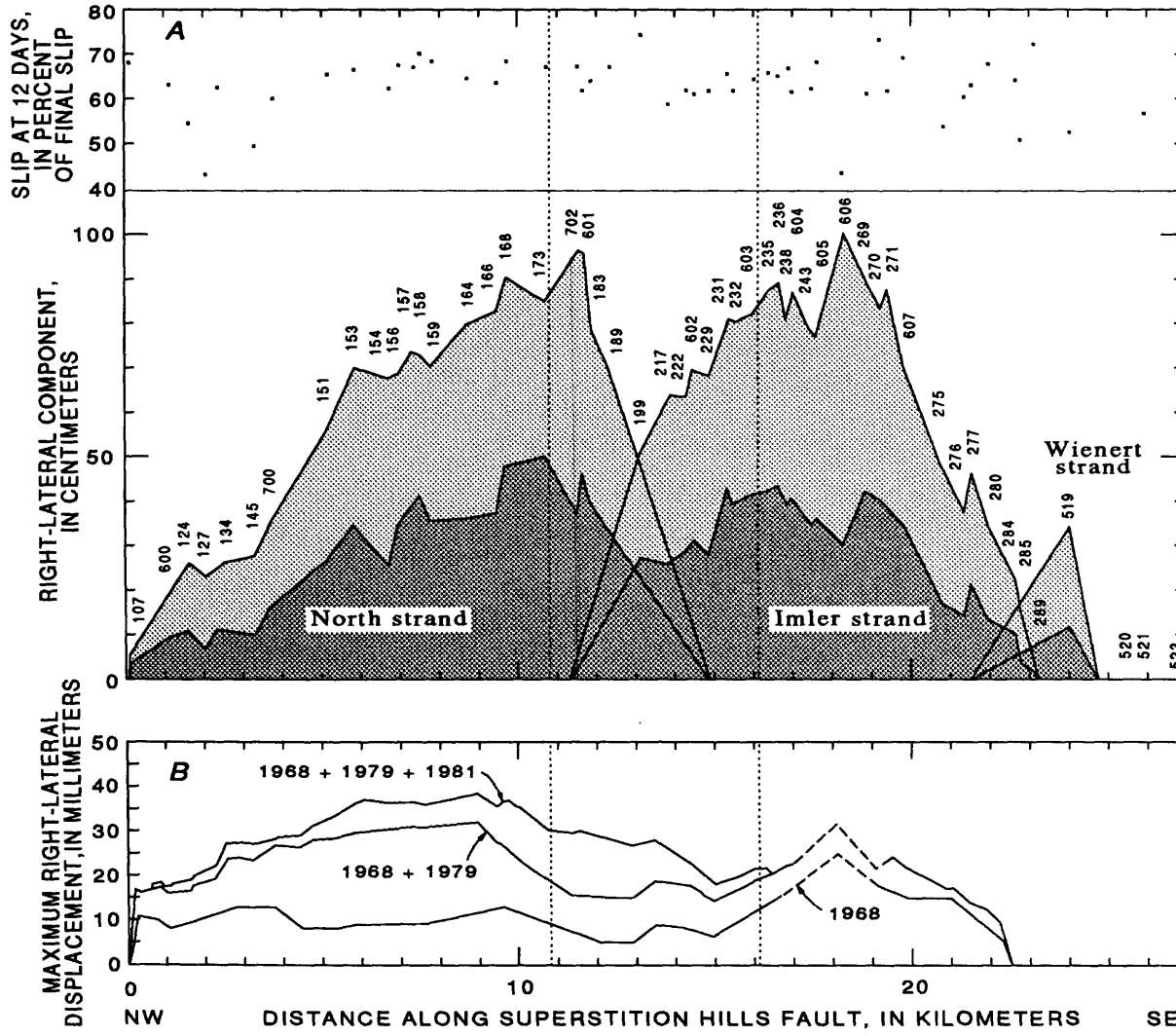

Figure 4.—Plots of measured right slip along the entire Superstition Hills fault. *A*, Extapolated right slip associated with the 1987 Superstition Hills earthquake for 1 day and final slip. (from Sharp *et al.*, 1989, Fig. 8.) Extrapolated right slip at 12 days after the main shock shown in percent of final slip at the top of *A*. Limits of area shown in Figures 2 and 3 shown by vertical dotted lines. *B*, Plots of cumulative right slip after the 1968 (Allen *et al.*, 1972), 1979 (Fuis, 1982), and 1981 (Sharp *et al.*, 1986) earthquakes. Most of Wienert strand not checked in 1968 and 1979. Note that *B* has 10 × greater vertical scale relative to *A*. Dashed lines represent uncertainty in displacement profiles near the Caltech geodetic network where slip was detected in 1968 (Allen *et al.*, 1972). Strand rupture ends are not shown in *B*. (From Sharp *et al.*, 1986.)

surface rupture in the fault stepover was mapped, and the day that many solitary slip measurements were made. Sites along most of the main traces of the north and Imler strands, in contrast, were measured repeatedly (see Sharp *et al.*, 1989, table 1), and for those sites the slip values at 12 days after the event were calculated using the power law described by Sharp and Saxton (1989) and Boatwright *et al.* (1989) or were interpolated

between measurements plotted linearly in log time. That the 12-day profile is a realistic model of final slip is shown by slip calculated at 12 days as a percentage of final slip in the top plot in Figure 4*A*. The percentages in the stepover area vary from 59along most of the fault. The relatively consistent percent slip values along the fault at 12 days suggests that the 12-day picture is a realistic model of final displacement. This assumption is based on the constancy of power-law variables in time as used in the calculations (for further discussion on the power law see Sharp and Saxton, 1989; Boatwright *et al.*, 1989; Budding *et al.*, 1989). Figure 3 shows the north and Imler strands decreasing in slip toward the stepover from regional maxima; for example, compare stations 173 and 235 in Figures 3 and 4*A*. Both strands decrease in displacement toward the crossover, where dropoffs in slip occur. Slip values on the individual strands past the area of maximum slip crossover are significantly lower than regional values and diminish to zero at the ends of the strands.

DETAILS OF 1987 FAULTING IN THE STEPOVER

Details of surface rupture in the stepover include splays from both north and Imler strands, bedding-plane thrusts, crossover faults, and breaks showing both right and left slip. Surface rupture details are shown in Figure 5, which is a larger-scale view of the central part of the stepover than that afforded in Figure 2. For stations not plotted in Figure 3, the amount of slip is shown.

Splay and crossover faults within the area of Figure 5 at 12 days after the earthquake were most conspicuous, and had the most slip, in three areas. These areas are (1) between stations 200 and 203 on the north strand and the splay fault (station 206) on the Imler strand, (2) near stations 195 and 197 on the north strand and 196 on the Imler strand (between the '*X*'s), and (3) the splay fault ('*Y*') between stations 191 and 193 on the Imler strand. In the more southeasterly of these areas faulting consisted of dispersed ruptures between the north strand and the splay fault off the Imler strand. Numerous subparallel surface breaks were present, all with right slip. This area coincides with slip crossover from one strand to another in a wide part of the fault stepover. Amounts of slip on these minor crossover faults was in the range of 4.7 cm (site 204) to approximately 2 to 3 cm. The slip crossover area in the narrow part of the stepover had nearly parallel surface traces and coincides with the area of maximum slip crossover at 12 days after the earthquake. Slip values on individual breaks in this area were estimated to be in the range of 2 to 5 cm. [Precise measurements were not made in the crossover area because of loose surface sand that made for imprecise fault-block matches.] Crossover on the splay fault between stations 191 and 193 was on one break that at each time of observation (at 1, 12, 175, and 546 days) did not connect with the north strand. Right slip on this splay at 12 days is estimated at less than 10 cm.

A visit to the fault stepover at 546 days after the earthquake showed a slightly different picture of crossover fault development than at 12 days. Most splay and crossover faults that had been mapped shortly after the earthquake were barely noticeable; rain, surface runoff, and windblown sand obscurred evidence of currently inactive or very slowly slipping fault breaks. However, crossover faults at three locations showed recent and more pronounced development than at 12 days. The three locations are labeled in Figure 5: three crossover faults between the '*X*'s, the splay fault '*Y*', and a newly mapped crossover fault '*Z*'. [Fault *Z* either developed after previous mapping or was overlooked.] It was not possible to measure the cumulative slip on these breaks because of poorly preserved fault-block matches. However, it now appears that afterslip expressed at the surface along the

Superstition Hills fault is crossing over from one fault strand to another on these labeled crossover faults.

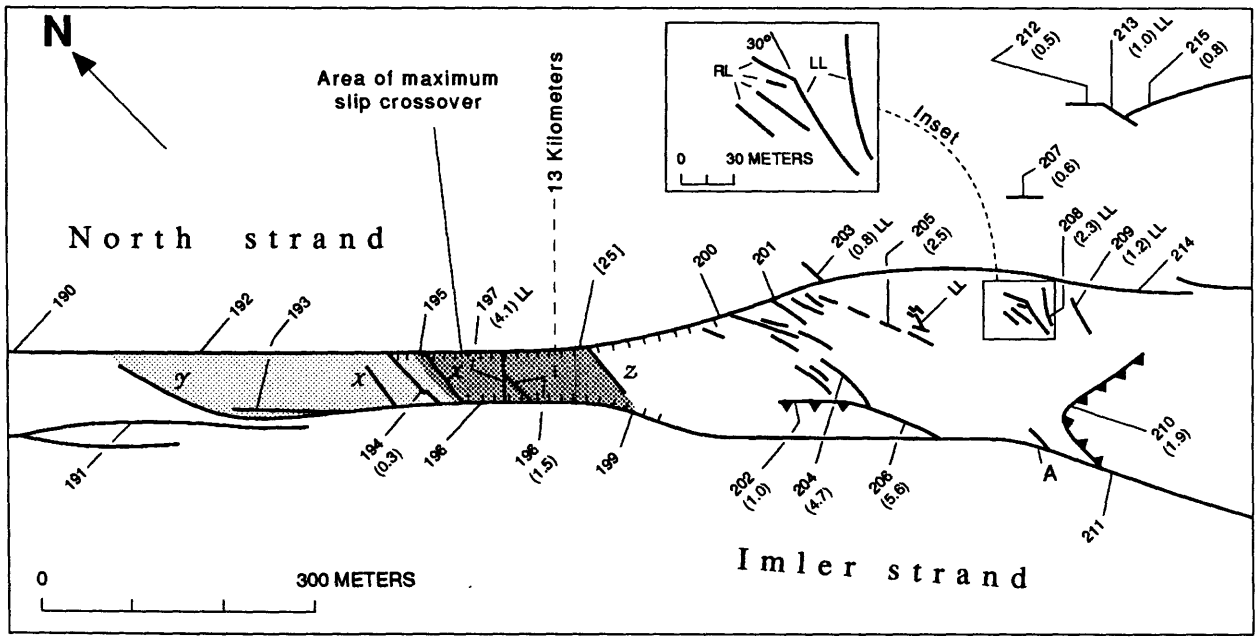

Figure 5.—Detailed map of surface faulting in right stepover (jog) in central part of the Superstition Hills fault. Map shows locations of fault complexities, that is, splays, bedding-plane thrusts, and left-lateral slips, between the north and Imler strands and to the northeast of the north strand. Site of maximum slip crossover between strands at 12 days is shown by coarse dot pattern. Fine dot pattern represents inferred area of maximum slip crossover at 546 days after the earthquake. Station numbers of Sharp *et al.* (1989) are shown for reference to displacement plots in Figure 3. Slip values for measurement sites not plotted in Figure 3, that is, between the two strands or northeast of the north strand, are shown in parentheses below station numbers; values are in centimeters. All faults with left-lateral slip are labeled 'LL', all other faults, except two bedding-plane thrusts, which are shown with teeth on the upper plate, are right lateral. Hachures along the north and Imler strands represent areas of marked vertical components of slip relative to the rest of the fault; hachures on downdropped side of fault. Splay faults labeled *X*, *Y*, and *Z* are discussed in the text. Inset shows geometric relations between right-lateral and left-lateral faults. Distance from the northwest end of the fault is shown by the 13 km mark. Site 'A' marks location of Figure 6.

An interesting feature that further reveals the nature of surface rupture in the fault stepover was the presence of left-lateral conjugate fault slip within the right-lateral Superstition Hills fault. Left slip is labeled for all such faults in Figure 5. Two of the sites are northeast of the north strand (near stations 203 and 213). Two other sites of left slip, and fault complexity, are within the stepover, near sites 208 and 209 (Fig. 5), and the site labeled 'LL', about 100 m northwest of site 208. In these two areas surface rupture was locally continuous from left slip to right slip. Changes in fault azimuth from left slip to right slip was about 30° (see inset, Fig. 5). A fifth site of left slip is at site 197, near where the north and Imler strands are closest together. This site is unique in that the left rupture is oriented normal to the north and Imler strands.

Another interesting feature in the stepover is the pattern of the vertical components of slip. Both the north and Imler strands had larger than average vertical components of slip within the stepover. Locations of large vertical components of slip on the north and Imler strands are shown by hachure marks in Figure 5 (similar features are not shown for the splay, bedding-plane thrust, and crossover faults). Vertical components of slip in the hachured areas along the Imler strand ranged from 19 to 21 percent of the strike-slip component; along the north strand they ranged from about 100 percent to more than 12 times the strike-slip component (site 200). The area where the vertical component of slip was larger than normal is where both strands have the greatest angle of convergence to the mean fault trend and in the area of maximum slip crossover.

The age of the stepover is unknown, but stratigraphic features allow qualitative estimates of the stepover's longevity. Sharp *et al.* (1989) suggest Pleistocene or older activity for the Superstition Hills fault. Figure 6 is a view of the Imler strand at site 'A' (Fig. 5) that shows contrasting lithologies and bedding orientations on opposite sides of the fault. Similar contrasts are present along the north strand within the stepover. The complexity of deformation and discordant bedding orientations within the stepover suggest a long period for development of this fault jog, but do not allow precise age estimates. Furthermore, it is unknown whether the jog preceeded or followed deposition of the Brawley Formation or if the jog developed during or much after initiation of faulting along the Superstition Hills fault.

SUBSURFACE DATA RELATED TO THE STEPOVER

I here discuss the aftershock distribution of the 1987 Superstition Hills earthquake and possible basement controls in relation to the fault stepover. This examination requires us to change scales and look at the Superstition Hills fault as a whole. The seismicity data are from the USGS-CIT southern California catalog for the period November 24 to December 31, 1987. The epicenters have not been relocated (see Magistrale *et al.*, 1989, for seismicity details related to the Superstition Hills earthquakes and aftershocks). Figure 7*A* is a plan view of the Superstition Hills fault and seismic activity. Aftershocks shown cluster about the northwest end of the north strand and extend approximately to the stepover between the north and Imler strands (Fig. 7*B*). Minor aftershock activity is located along the Imler strand with possible clustering near the fault stepover at the southeast end of the Imler strand. Figures 7*A* and *B* also show the top of basement rocks inferred from seismic refraction profiling by Fuis *et al.* (1982) and Kohler and Fuis (1986). In addition, Figure 7*A* shows the distribution of two kinds of basement rock types from Fuis *et al.* (1982). The two types of basement rocks are granitic and metasedimentary (greenschist facies). The granitic rocks are located primarily to the southwest in Figure 7*A* and include surface exposures northeast of the Superstition Mountain fault; greenschist-facies metasedimentary rocks are located toward the center of the Salton Trough (Muffler and White, 1969; Fuis *et al.*, 1982). Contours for the top of basement rocks in Figure 7*A* and *B* show gently decreasing elevation with increasing distance from granitic basement highs exposed near Superstition Mountain.

DISCUSSION AND CONCLUSIONS

Details of surface rupture and styles of slip within the fault stepover between the north and Imler strands of the Superstition Hills fault provide new understanding to the nature of fault segmentation. Closely spaced slip-measurement sites along fault traces after the 1987

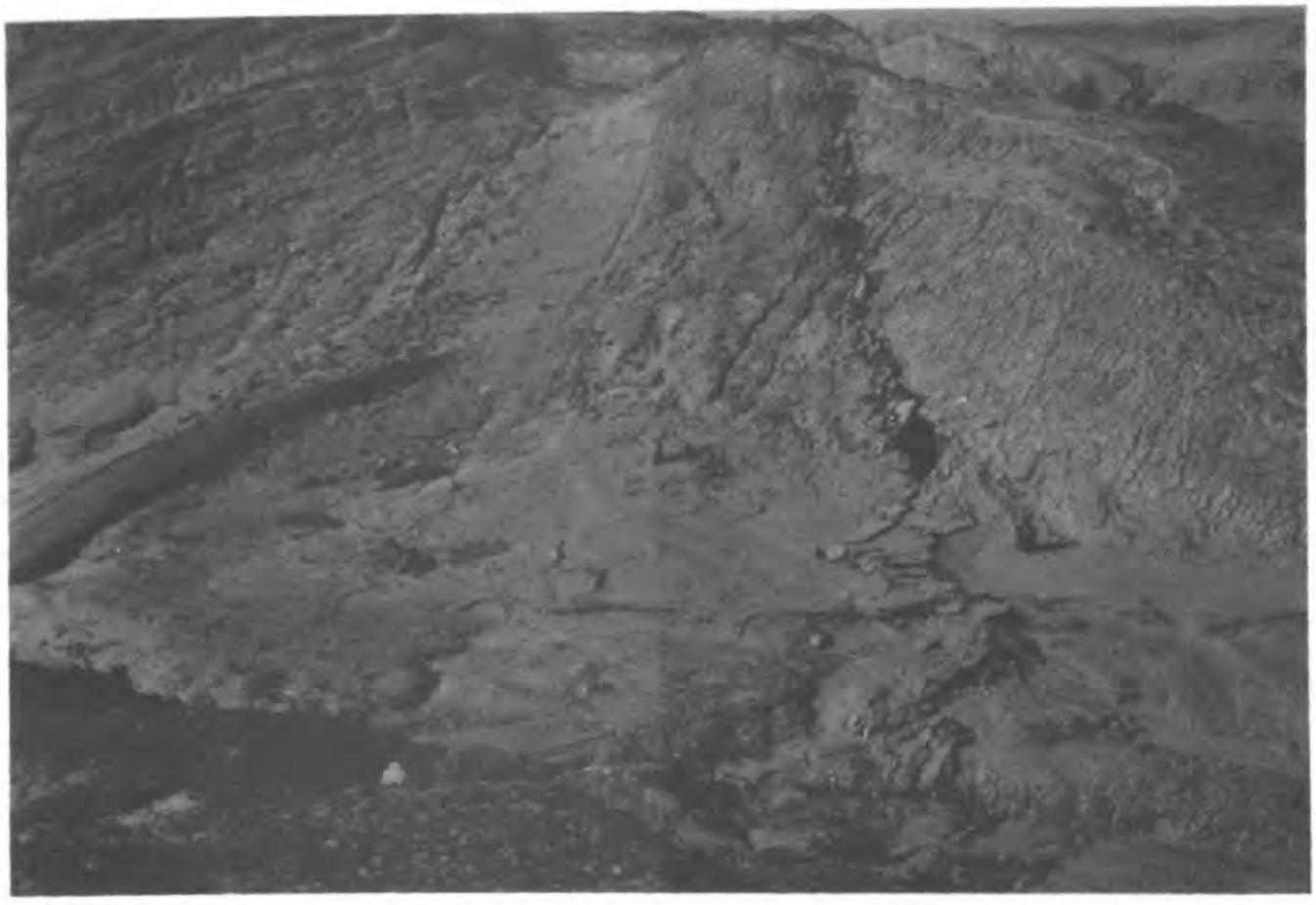

Figure 6.—Bedding discordance across the Imler strand (site A on Fig. 5). Contrasting lithologies on opposite sides of the fault suggest a substantial but unknown amount of displacement. Such discordance may indicate a great age for faulting in the stepover. Canteen at base of small hill on right side of view is 20 cm high.

earthquake showed the location of dominant slip transfer from one fault trace to the other, or the area of maximum slip crossover (Figs. 3, 4, 5). Qualitative observations of crossover faults within the stepover at 546 days after the earthquake suggest that either the area of maximum slip crossover extended about 300 m to the northwest (Fig. 5) or that earlier slip measurements were too sparse. The persistance of the area of maximum slip crossover as a site of slip transfer is suggested by the rupture traces observed after triggered slip events in 1968, 1979, and 1981 that did not show surface rupture on extensions of the strands past the area of maximum slip crossover (Fig. 2*B*, *C*, *D*). In fact, all four detailed studies, in 1968, 1979, 1981, and 1987, allow that slip crossover occurred at the same location. In addition, surface rupture mapped after the 1951 Superstition Hills earthquake by Joseph Ernst (written commun., 1989) showed rupture termination near the area of maximum slip crossover (Fig. 2*A*).

Slip was transferred from one strand to the other in the 1987 event via minor splay, subsidiary, crossover, and bedding-plane thrust faults (Figs. 3, 5), but the net slip on these minor faults was significantly less than the amount of displacement on the north and Imler strands (compare Figs. 3 and 5). Slip transfer from one strand to the other is

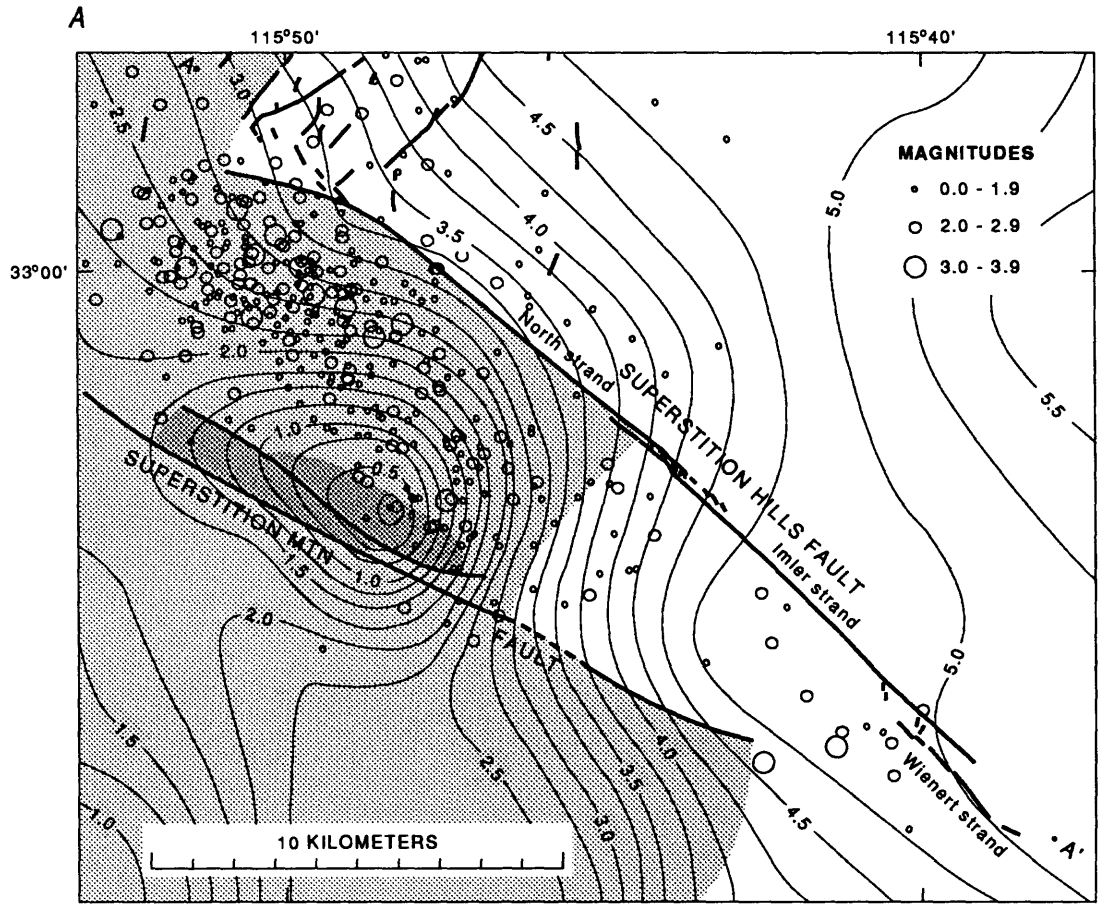

Figure 7.—Aftershocks and basement rocks along the Superstition Hills fault. Aftershocks shown were recorded on the USGS–CIT net from November 24 to December 31, 1987. *A*, Epicentral map of aftershocks plotted relative to surface traces of the Superstition Hills fault (only part of the traces of northeast-trending faults that ruptured in 1987, Fig. 1, are shown in this illustration). Contours (in kilometers below sea level) are top of basement as determined from seismic refraction profiling by Fuis *et al.* (1982) and Kohler and Fuis (1986). Fine dot pattern represents area of granitic basement from seismic refraction studies of Fuis *et al.* (1982); coarse dot pattern is surface exposure of granitic basement; unpatterned area represents metasediment (greenschist facies) basement. *B*, Cross-section from A to A' plotted parallel to the Superstition Hills fault. Projected hypocenters shown are from events located between 2 km northeast of the fault and 5 km southwest of the fault. Also shown is the profile of the top of basement rocks.

done, in large part, in the subsurface, probably taken up along minor crossover faults and in folding and downdrop within the stepover. The style of slip transfer and deformation agrees, in general, with modeling of fault segmentation by Segall and Pollard (1980) and Sibson (1986).

The history of surface-rupture events, in 1951, 1968, 1979, 1981, and 1987, along the Superstition Hills fault shows interesting points about the nature of the fault stepover. First, the 1951 tectonic slip event had surface rupture stop at or near the stepover, thus not

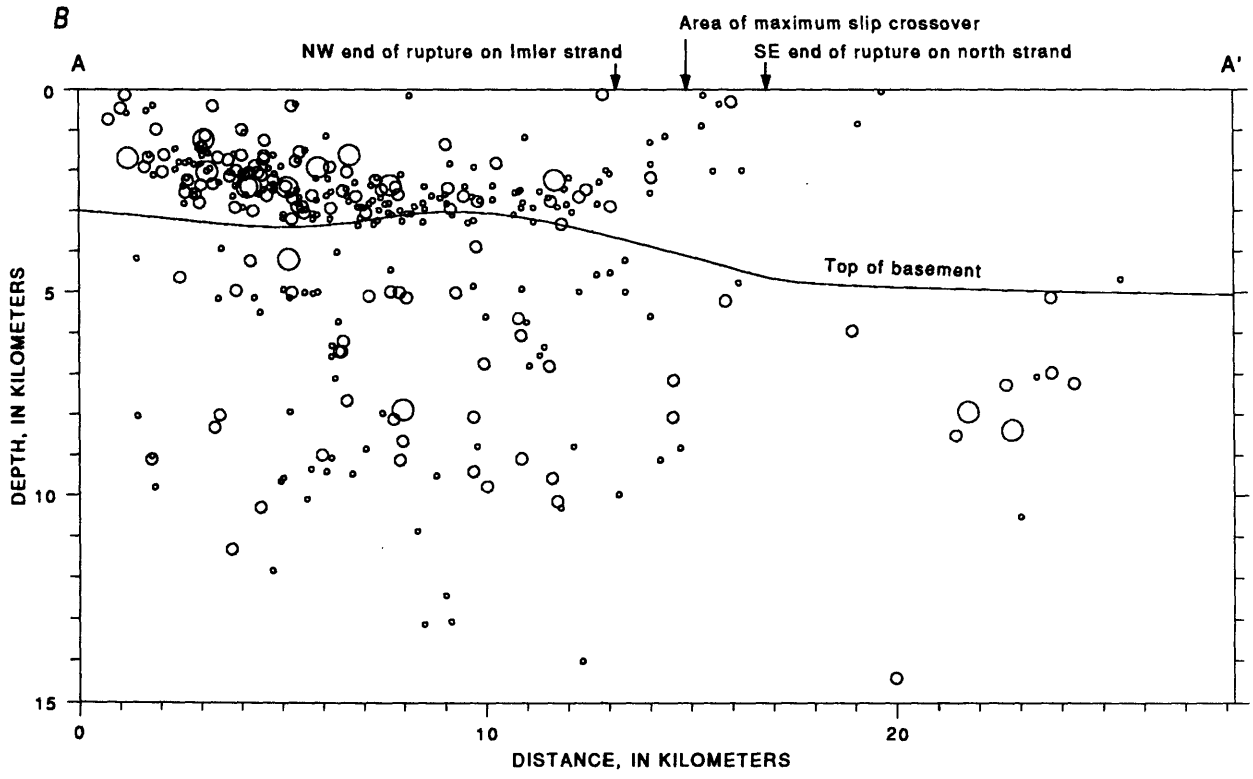

Figure 7.—Continued.

revealing the presence of the stepover. The triggered slip events, likewise, did not reveal the presence of the stepover because of their discontinuous surface traces and because the area of maximum slip crossover is only 60 m wide and is located in loose stream-channel sand or sand with a thin hardened crust. [It is possible that minor surface ruptures were present but not mapped on extensions of the fault strands during the triggered slip events.] A second point worth noting is that the cumulative slip maxima associated with the 1987 Superstition Hills earthquake are nearly equal on the north and Imler strands for 12 days and extrapolated for 1 day and the final slip (Figs. 3, 4*A*).

Another way of looking at the nearly equal slip highs on both strands is that the presence of the stepover reduced the net right slip there. And, like the view of nearly equal slip maxima on both strands, the reduced net slip can be viewed for 12 days and extrapolated for 1 day and the final slip. Triggered slips along the Superstition Hills fault in 1968 and 1979 also show a cumulative slip deficit in the stepover area (Fig. 4*B*). Triggered slip caused by the 1981 Westmorland earthquake, in contrast, reached a maximum in the area of the stepover (Fig. 4*B*).

Decreased slip in the central stepover may be accounted for by deformation within the stepover area, between the north and Imler strands. Minor slip on extensions of the strands beyond the area of maximum slip crossover do not significantly reduce the slip deficit; for example, the dashed and dotted lines in Figure 3 show approximate cumulative values of slip on the north and Imler strands and the fault extensions. The remaining slip deficit is still greater than slip amounts measured on splay, crossover, subsidiary, and bedding-plane thrust faults in the stepover (see Fig. 5). Deformation of strata between the north and Imler strands (see, for example, Fig. 6) may account for the remainder of

slip deficit.

Much less information exists with regard to the subsurface extent of the stepover. Aftershocks of the 1987 earthquake initiated near the northwest end of the Superstition Hills fault and extended southeastward to near the central stepover. Sparsely distributed aftershocks were also located along the Imler and Wienert strands with possible clustering of shocks near the stepover separating these strands (Fig. 7*A*, *B*; Magistrale *et al.*, 1989). Frankel and Wennerberg (1989) also show that radiation of high-frequency strong ground motion stopped near the central stepover. However, the pattern of aftershock propagation and high-frequency radiation of strong ground motion do not necessarily indicate deep extension of the fault stepover. The location of the stepover is approximately coincident with, and may be genetically related to, a boundary between granitic and greenschist-facies metasedimentary basement lithologies (Fig. 7*A*; Fuis *et al.*, 1982). A change in basement lithology and rheological properties below the stepover may account for the sparsness of the southeastward extension of aftershocks and high-frequency strong ground motion (Magistrale *et al.*, 1989; Frankel and Wennerberg, 1989). Also, Bent *et al.* (1989) show that radiation of long-period seismic waves initiated by the main shock extended past the central stepover, to the southeast end of 1987 rupture. The radiation of long-period waves would be less affected by a change in lithology and would be able to extend the length of the fault, as shown by Bent *et al.* (1989). Thus, the existing data are insufficient to satisfactorily address whether the fault stepover extends to hypocentral depths or not.

In summary, observations of the central stepover on the Superstition Hills fault only partly support models of fault interaction in segment stepovers. Fault segmentation models suggest that stepovers are possible sites of rupture nucleation or termination, and yet out of five surface-rupture events in the last four decades the central stepover on the Superstition Hills fault has had surface rupture stop at or near the site of maximum slip crossover only once, in 1951. The four most recent surface-rupture events, in 1968, 1979, 1981, and 1987, in contrast, had surface slip go past the stepover. The small 60-m-wide gap between the fault strands may account for slip going past the area of maximum slip crossover. And yet, the 1951 rupture apparently terminated at the stepover. Another point with regard to segmentation models is the style of slip crossover. Here, the 1987 rupture data possibly support segmentation models; slip partly is transferred from one strand to another on splay and crossover faults and partly in inferred and undocumented deformation of strata between the fault strands as in the models of Segall and Pollard (1980) and Sibson (1985, 1986). Slip at the surface in the crossover area at 12 days after the earthquake accounted for only part of the transferred slip. Surface slip in the crossover at 546 days may represent a greater proportion of total slip transfer, but this is not constrained. A final point with regard to segmentation models is the subsurface extent of the stepover. In order for fault rupture to nucleate or terminate at a stepover the stepover must extend to hypocentral depths. The subsurface extent of the central stepover on the Superstition Hills fault is uncertain. The pattern of aftershock propagation and high-frequency radiation of strong ground motion associated with the 1987 earthquake partly support a subsurface extent of the stepover, but the radiation of long-period waves past the stepover suggests that other factors may be involved. Other factors may be related to a change in basement lithology beneath the stepover, as mapped by Fuis *et al.* (1982) and Kohler and Fuis (1986), or a 6° bend in fault azimuth near the stepover.

ACKNOWLEDGMENTS

This paper was improved by informal discussions with U.S.G.S. colleagues A. Frankel

and G.S. Fuis, and H. Magistrale (Caltech). I thank M.G. Bonilla, C.S. Prentice, D.P. Schwartz, and R.V. Sharp (all at U.S.G.S.) for insightful and constructive comments on an earlier version of the paper. I am indebted to Joseph Ernst (Mission Resources) for supplying notes about surface rupture associated with the 1951 Superstition Hills earthquake. J.D. Bicknell (U.S.G.S.) helped find and measure surface rupture in the field.

REFERENCES CITED

Allen, C. R., St. Amand, P., Richter, C. F., and Nordquist, J. M., 1965, Relationship between seismicity and geologic structure in the southern California region: Seismological Society of America Bulletin, v. 55, p. 753–797.

Allen, C. R., Wyss, M., Brune, J. N., Grantz, A., and Wallace, R. E., 1972, Displacements on the Imperial, Superstition Hills, and San Andreas faults triggered by the Borrego Mountain earthquake, *in* The Borrego Mountain earthquake of April 9, 1968: U.S. Geological Survey Professional Paper 787, p. 87–104.

Bakun, W. H., Stewart, R. M., Bufe, C. G., and Marks, S. M., 1980, Implication of seismicity for failure of a section of the San Andreas fault: Seismological Society of America Bulletin, v. 70, p. 185–201.

Barka, A. A. and Kandinsky-Cade, K., 1988, Strike-slip fault geometry in Turkey and its influence on earthquake activity: Tectonics, v. 7, p. 663–684.

Bartlett, W. L., Friedman, M., and Logan, J. M., 1981, Experimental folding and faulting of rocks under confining pressure. Part IX. Wrench faults in limestone layers: Tectonophysics, v. 79, p. 255–277.

Bent, A. L., Helmberger, D. V., Stead, R. J., and Ho-Liu, P., 1989, Waveform modeling of the November 1987 Superstition Hills earthquakes: Seismological Society of America Bulletin, v. 79, 500–514.

Boatwright, J., Sharp, R. V., and Budding, K. E., 1989, Inverting measurements of surface slip along the Superstition Hills fault zone: Seismological Society of America Bulletin, v. 79, 411–423.

Budding, K. E., Boatwright, J., Sharp, R. V., and Saxton, J. L., 1989, Compilation and analysis of displacement measurements obtained on the Superstition Hills fault zone and nearby faults in Imperial Valley, California, following the earthquakes of November 24, 1989: U.S. Geological Survey Open-File Report 89-140, 90 p.

Dibblee, T. W., Jr., 1954, Geology of the Imperial Valley region, *in* Geology of southern California: California Division of Mines and Geology Bulletin 170, chapter 2, p. 21–28.

Dibblee, T. W., Jr., 1984, Stratigraphy and tectonics of the San Felipe Hills, Borrego Badlands, Superstition Hills, and vicinity, *in* Rigsby, C.A., ed., The Imperial basin—tectonics, sedimentation, and thermal aspects: Society of Economic Paleontologists and Mineralogists, Pacific Section, p. 31–44.

Eaton, J. P., O'Neill, M. E., and Murdock, J. N., 1970, Aftershocks of the 1966 Parkfield-Chalame, California, earthquake: A detailed study: Seismological Society of America Bulletin, v. 60, p. 1151–1197.

Frankel, A. and Wennerberg, L., 1989, Rupture process of the M_S 6.6 Superstition Hills earthquake determined from strong-motion recordings: Application of tomographic source inversion: Seismological Society of America Bulletin, v. 79, p. 515–541.

Fuis, G. S., 1982, Displacement on the Superstition Hills fault triggered by the 1979 Imperial Valley earthquake, *in* The Imperial Valley, California, earthquake of October 15, 1979: U.S. Geological Survey Professional Paper 1254, p. 145–154.

Fuis, G. S., Mooney, W. D., Healey, J. H., McMechan, G. A., and Lutter, W. J., 1982, Crustal structure of the Imperial Valley region, *in* The Imperial Valley, California, earthquake of October 15, 1979: U.S. Geological Survey Professional Paper 1254, p. 25–49.

King, G. and Nabelek, J., 1985, Role of fault bends in the initiation and termination of earthquake rupture: Science, v. 228, p. 984–987.

Kohler, W. M. and Fuis, G. S., 1986, Travel-time, time-term, and basement depth maps for the Imperial Valley region, California: Seismological Society of America Bulletin, v. 76, no. 5, p. 1289–1303.

Magistrale, H., Jones, L. M., and Kanamori, H., 1989, The Superstition Hills, California, earthquakes of 24 November, 1987: Seismological Society of America Bulletin, v. 79, p. 239–251.

Muffler, L. J. P., and White, D. E., 1969, Active metamorphism of upper Cenozoic sediments in the Salton Sea geothermal field and the Salton Trough, southeastern California: Geological Society of America Bulletin, v. 80, p. 157–181.

Reasenberg, P. A. and Ellsworth, W. L., 1982, Aftershocks of the Coyote Lake, California, earthquake of August 6, 1979: A detailed study: Journal of Geophysical Research, v. 87, p. 10,637–10,655.

Segall, P. and Pollard, D. D., 1980, Mechanics of discontinuous faults: Journal of Geophysical Research, v. 85, p. 4337–4350.

Sharp, R. V., and Saxton, J. L., 1989, Three-dimensional records of surface displacement on the Superstition Hills fault zone associated with the earthqauakes of 24 November 1987: Seismological Society of America Bulletin, v. 79, 376–389.

Sharp, R. V., Rymer, M. J., and Lienkaemper, J. J., 1986, Surface displacement on the Imperial and Superstition Hills faults triggered by the Westmorland, California, earthquake of 26 April 1981: Seismological Society of America Bulletin, v. 76, no. 4, p. 949–965.

Sharp, R. V., Budding, K., *et al.*, 1989, Surface faulting associated with the Superstition Hills earthquakes of November 24, 1987: Seismological Society of America Bulletin, v. 79, 252–281.

Sibson, R. H., 1985, Stopping of earthquake ruptures at dilational fault jogs: Nature, v. 316, p. 248–251.

Sibson, R. H., 1986, Rupture interaction with fault jogs, *in* Das, S., Boatwright, J., and Scholz, C. H., eds., Earthquake source mechanics: American Geophysical Union Geophysical Monograph 37, Maurice Ewing Volume 6, p. 157–167.

Vedder, J. G. and Wallace, R. E., 1970, Map showing recently active breaks along the San Andreas and related faults between Chalame Valley and Tejon Pass, California: U.S. Geological Survey Miscellaneous Field Investigations Map I-574, scale 1:24,000.

FAULT SEGMENTATION AND EARTHQUAKE OCCURRENCE IN THE STRIKE-SLIP SAN JACINTO FAULT ZONE, CALIFORNIA

by

Christopher O. Sanders
U.S. Geological Survey
Menlo Park, CA 94025

ABSTRACT

Based on geological and seismological data, twenty principal segments ranging in length from 7 to 35 km are identified in the 250-km-long San Jacinto fault zone. The discontinuities defining segment boundaries are steps, bends, branches, intersections, and steps in seismogenic zone depth. Rupture initiation or termination points of historic large earthquakes in the fault zone often coincide with segment boundaries. Of the seven or eight large earthquakes in the fault zone since 1899, all are less than *M* 7, consistent with the maximum segment lengths. These data suggest that characteristics of future large earthquakes in the fault zone may be estimated from knowledge of segment characteristics.

INTRODUCTION

Seismological and geological studies of strike-slip earthquakes have revealed that fault ruptures often begin and/or end near discontinuities (e.g. Allen, 1968; Lindh and Boore, 1974, 1981; Bakun and others, 1980; King and Nabelek, 1985; Sibson, 1985; Barka and Kadinsky-Cade, 1988). They also have revealed the complex nature of the fault rupture process and, thus, the nonuniform distribution of heterogeneities on the fault surface at many scales (e.g. Trifunac and Brune, 1970; Kanamori and Stewart, 1976). Fault heterogeneities are interpreted as spatial variations in fault strength and are called stuck patches, barriers, or asperities (Wesson and Ellsworth, 1973; Das and Aki, 1977; Kanamori, 1978). Two types of heterogeneities or discontinuities are recognized, geometrical and rheological (Aki, 1979); the geometrical heterogeneities are related to the geometry of the fault surface, and the rheological heterogeneities are related to spatial variations in fault zone properties such as rock type or fluid pressure. Geometrical heterogeneities have been the focus of many studies, largely because they are often expressed at the ground surface as fault discontinuities and are therefore observable. Rheological heterogeneities, rarely expressed at the ground surface, are less readily identified. None-the-less, study of both types of heterogeneity is important for understanding the complex nature of faulting and the relation of fault zone structure to earthquake occurrence. The ultimate goal is to gain insight to the processes of fault rupture initiation, propagation, and termination, and thereby improve our ability to forecast earthquake hazard.

Our desire is to identify major fault discontinuities at the ground surface and at depth, determine their depth extent, ascertain their effect on the local stress field, and establish their potential for affecting fault rupture. Because fault zone discontinuities bound fault segments with dimensions ranging from microscopic to the length of the fault zone we must limit our investigations to those discontinuities that are likely to be associated with fault ruptures of interest and whose characteristics can be determined within the precision of existing investigative techniques. These discontinuities are those that bound fault segments comparable in size to the rupture zones of major earthquakes. Previously, the existence of discontinuities in strike-slip fault zones has been demonstrated from mapping of the surface trace of fault zones (Wallace, 1973) and from plotting the distribution of earthquake hypocenters in cross section (Sibson, 1984). In addition, the mechanical properties of some classes of discontinuities have been determined from geometrical analysis (Segall and Pollard, 1980). However,

the importance of most discontinuities has not been clearly established; in some instances discontinuities seem to influence fault rupture, in other instances they do not (Knuepfer, 1988). For example, even though Wallace (1973) finds that the surface trace of the San Andreas fault zone is composed of segments with maximum lengths of 18 km, the historical great earthquakes in this fault zone each ruptured several hundred kilometers, or through several tens of these segments. Apparently, scale and other factors are involved. These observations suggest that our understanding of the properties of individual discontinuities and their effect on fault rupture is incomplete. Since fault rupture initiation, propagation, and termination are influenced by local values of shear stress and fault strength, to understand the relation between fault discontinuities and major fault rupture we must know the distribution of fault strength and shear stress in and around the discontinuities. To achieve this understanding we need information about individual discontinuities from geologic mapping, earthquake hypocenters, and geodetic measurements. In addition, we need knowledge of the history of fault rupture to determine the stress conditions near each discontinuity and on adjacent fault segments. The result should be an estimation of the effect of individual fault discontinuities on future fault ruptures.

In this paper, I present an interpretation of the segmentation of the San Jacinto fault zone in southern California. The right-slip San Jacinto fault zone provides a wealth of information about fault zone segmentation and fault rupture associated with earthquakes of M 6-7. Not only is the 250-km-long fault zone fragmented into about 20 principal geometrical and structural segments, but seven or possibly eight large earthquakes have occurred in the fault zone since 1899, and the locations of most of them are known quite well. In addition, precise hypocenters of most $M \geq 2$ earthquakes in the fault zone since 1976 are known, allowing comparison of background seismicity to segment locations. In this study, I will analyze the geological and seismological information about the San Jacinto fault zone and attempt to define significant fault discontinuities, determine how the discontinuities affected the historical fault ruptures, and assess their potential effects on future fault ruptures.

GEOLOGICAL SETTING

In southern California, the major crustal fractures which accomodate most of the motion between the Pacific and North American plates at about latitude 33° 50' N are the right-slip San Andreas and San Jacinto fault zones (Figure 1). The southern San Andreas fault zone has displacement of at least 165 km across it (Matti and others, 1985) and a late Pleistocene slip rate of 25 mm/yr (Weldon and Sieh, 1985). Historically, the southern San Andreas fault has been quiescent, except in the Banning Pass region where one or two earthquakes near M 6 have occurred (1948, M_L 6.5; 1986, M_L 5.9). The San Andreas fault northwest of the study area ruptured to produce a M_w 7.9 earthquake in 1857 (Sieh, 1978). The slip rates in and total displacements across the various segments of the San Jacinto fault zone are discussed below.

Total displacement

The total displacement across the San Jacinto fault zone has been measured along the Anza segment of the Clark fault (Figure 1). Here Sharp (1967) measured 24 km of dextral offset of Cretaceous intrusive rocks. In addition, Hill (1984) suggests about 5 km of dextral offset across the Hot Springs fault. Across the San Bernardino segment of the Claremont fault the apparent 25 km dextral offset of the Cucamonga and Banning faults may reflect the displacement documented across the Anza segment (Sharp, 1967). Southeast of the Anza segment, the fault zone is composed of dual principal traces, first the Clark and Buck Ridge faults, then the Clark and Coyote Creek faults, and finally, at the southeast end, the Superstition Mountain and Superstition Hills faults. The total dextral offset across the Buck Ridge fault is 6 km, across the Clark Valley and Santa Rosa segments of the Clark fault, 19 km, and across the Coyote Ridge segment of the Coyote Creek fault, 5 km (Sharp, 1967). The total displacement across the Borrego Mountain segment of the Coyote Creek fault and across the

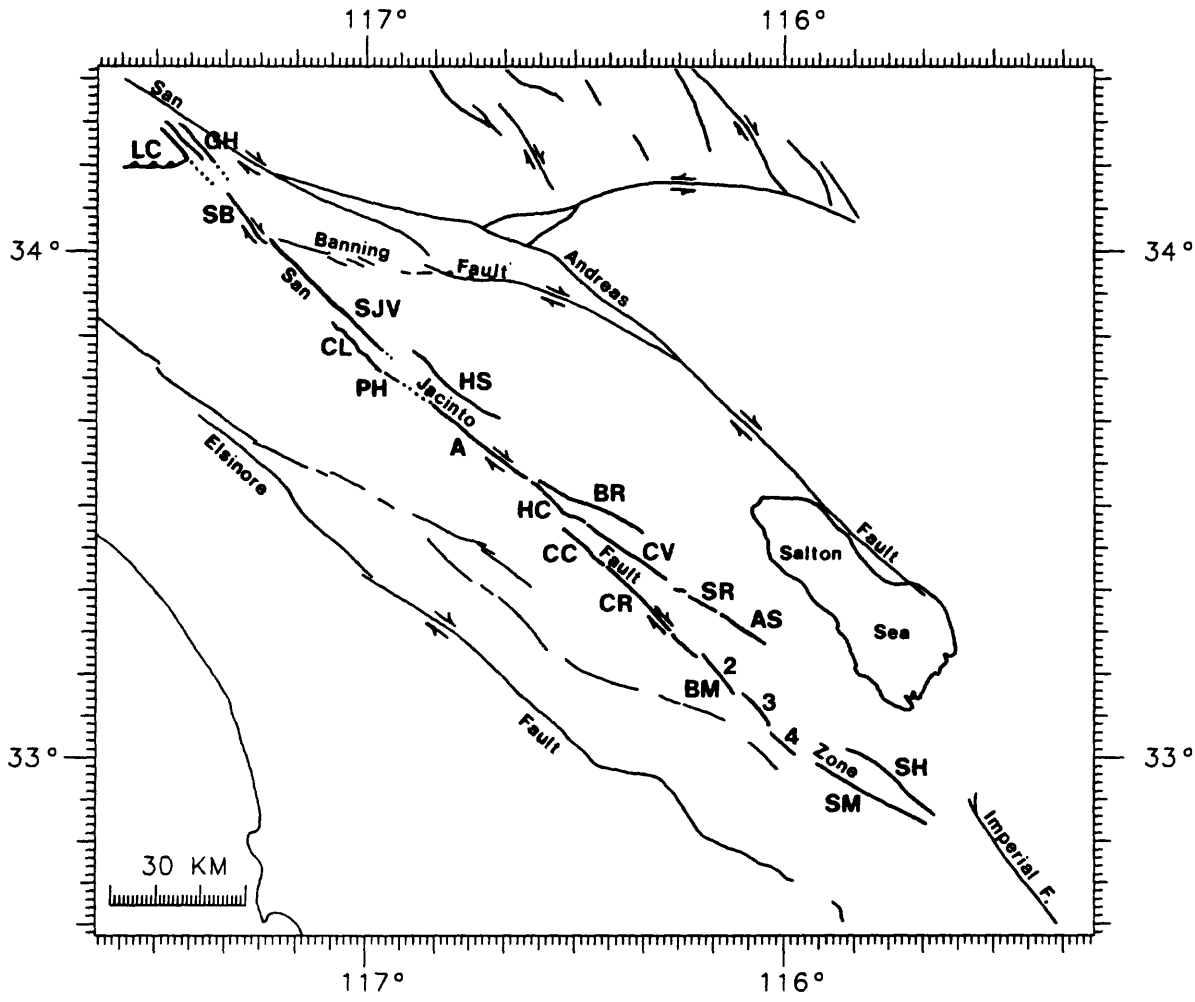

FIGURE 1 -- Map of the San Jacinto and other fault zones in southern California. The fault segments discussed in this paper are labeled with initials. LC: Lytle Creek fault; GH: Glen Helen fault; SB: San Bernardino segment, Claremont fault; SJV: San Jacinto Valley segment, Claremont fault; CL: Casa Loma fault; PH: Park Hill segment, Clark fault; HS: Hot Springs fault; A: Anza segment, Clark fault; HC: Horse Canyon segment, Clark fault; BR: Buck Ridge fault; CV: Clark Valley segment, Clark fault; SR: Santa Rosa segment, Clark fault; AS: Arroyo Salada segment, Clark fault; CC: Coyote Canyon segment, Coyote Creek fault; CR: Coyote Ridge segment, Coyote Creek fault; BM1-4: Borrego Mountain 1-4 segments, Coyote Creek fault; SM: Superstition Mountain fault; SH: Superstition Hills fault. Characteristics of these segments and the discontinuities that bound them are listed in Table 1.

Superstition Mountain and Superstition Hills faults is unknown.

Slip rate

The right-slip rate across the San Jacinto fault zone has been measured on the Anza segment of the Clark fault, where displaced 730 ka gravels indicate a minimum right slip rate of 8-12 mm/yr (Sharp, 1967, 1981). Also at this location, 29 to 4 ka ponded sediments and displaced fan deposits suggest a slip rate of 12-17 mm/yr (Merifield and others, 1987). These values represent the slip rate for the entire zone at this location, because the Clark fault is the only strand. Along the San Bernardino segment of the Claremont fault, offset alluvial deposits along one of two parallel fault strands suggest a minimum late Pleistocene right-slip rate of 5.4 mm/yr (Wesnousky and others, 1987). A maximum Pleistocene right-slip rate of 2.5 mm/yr has been measured on the Lytle Creek fault (Mezger and Weldon, 1983). The right-slip rate on the Borrego Mountain segments of the Coyote Creek fault is about 4 mm/yr since 400 ybp and 2 mm/yr between 400-6000 ybp (Sharp, 1981).

GEOMETRICAL FAULT ZONE DISCONTINUITIES AND THEIR MECHANICAL PROPERTIES

If we are to use knowledge of fault zone segmentation in a detailed manner to forecast characteristic effects of individual discontinuities we must consider the various physical processes at each discontinuity and their combined effect on fault strength. In general, discontinuities cause an increase or decrease in the effective strength of the fault locally. The determination of the specific effect of a discontinuity can be difficult, though, because factors such as the direction of overall block motion, the direction of individual rupture propagation, and the long-term versus short-term strain rate can have competing effects. These factors are not independent, because the block motion is associated with the long-term strain rate, and the rupture propagation is associated with the short-term strain rate. Because of the variable stress effects associated with these factors the influence of a discontinuity on the states of rupture initiation, propagation, and termination may be very different for each state.

In particular, the strain rate effect in the presence of pore fluids may be significant. The strength of a brittle fault is usually given by Coulomb's relation, $\tau = C + \mu(\sigma_n')$, where τ is the shear strength of the fault, C is the inherent cohesion of the rock, μ is the coefficient of static friction, and $\sigma_n' = \sigma_n - \sigma_f$ is the effective normal stress (normal stress minus fluid pressure; (Hubbert and Rubey, 1959)) on the fault plane. Since C and μ are relatively constant locally the strength of the fault is directly related to the values of the normal stress and the fluid pressure. For example, if normal stress increases but fluid pressure remains constant, then the effective normal stress increases and thus, fault strength increases. This situation would exist during the period of low strain rate associated with interseismic block motion, because the fluids would have time to diffuse into or out of the permeable fault zone, thereby minimizing excess fluid pressures. However, if the fluid pressure increased as well, due to rapid decrease in pore volume, then the increase in effective normal stress would be less; the effective normal stress could perhaps even decrease. In this case, fault strength could be lessened. The later situation could exist during fault rupture when local high strains occur temporarily. Thus, though we may estimate from geometrical analysis the effect of a discontinuity on dry fault strength, if we include fluids in the analysis the possible effects vary considerably.

The strain rate effects would have different influences on the individual states of rupture initiation, propagation, and termination. Rupture initiation would be influenced predominately by the effects associated with the long-term strain rates, whereas propagation and termination would be influenced by the effects of both the long- and short-term strain rates.

Most geometrical fault zone discontinuities are of two types, bends or steps, or variants thereof, such as branches and terminations. A third type, intersections, includes intersections with significant geological features. The effects these discontinuities have on the local stress fields can be deduced in part

from geometrical analysis; these effects are discussed below.

The perturbing effect of a fault bend on the local stress field is related to the directions of tectonic block motion and rupture propagation (Sibson, 1987) (Figure 2). In the long term, the fault bend area will be a site of increased or decreased effective fault-normal stress (tending to increase or decrease the strength of the fault plane) depending on the direction of the bend and the direction of block motion. In the short term, the effective normal stress will change depending on the direction of rupture propagation, the type of relative motion across the fault, and the influence of fluids. The overall effect will depend on the magnitudes of the block motion and rupture propagation effects.

The perturbing effect of a fault step on the local stress field depends on the direction of the block motion and the direction of the step (Segall and Pollard, 1980). These factors are important during both the interseismic and coseismic periods. In the long term, there will be an increase (compressional, restraining, antidilational) or a decrease (extensional, releasing, dilational) in the effective fault-normal stress in the step area, and thus an increase or decrease in fault strength (Figure 2). Segall and Pollard (1980) suggest that long-term fault displacement is hindered by a compressional step and enhanced by a releasing step. In the short term, the changes in fault-normal stress at the step due to fault rupture may be countered by equal or greater changes in fluid pressure, possibly leading to an effect on fault strength opposite to that of the long term. Sibson (1985) presents evidence indicating that fault rupture is impeded by releasing steps, possibly due to fluid interaction.

A fault branch is similar to a fault bend, though at a fault branch a discontinuity in slip rate exists, usually resulting in unequal stresses on the main fault and the branch fault. A fault termination can be thought of as one limb of a fault step, where displacement is not transfered to the adjacent limb but is rather distributed on minor faults over a wide zone.

The mechanical effects at an intersection discontinuity depend on the feature that intersects the fault zone. Along a strike-slip fault zone principal types of geometrical intersections include other strike-slip, normal, or thrust fault zones, or major folds; rheological intersections include significant local anomalies of crustal composition or properties.

IMPORTANCE OF THE RUPTURE HISTORY OF FAULT SEGMENTS

Knowledge of the time sequence and location of previous fault rupture is important in utilizing fault segmentation data in earthquake hazard study. Individual fault segments are bounded by discontinuities. Whether a discontinuity acts as a barrier to rupture propagation from one fault segment to the next or allows rupture to propagate through, triggering further fault rupture, depends not only on the geometrical structure of the discontinuity but also on the state of stress accumulation across the discontinuity. Rupture will have difficulty propagating into a low stress segment, because the stress concentrations near the rupture front will not increase the stress enough to overcome the strength of the fault. However, rupture may propagate more easily into an adjoining highly stressed segment where the additional stress concentration may trigger fault slip. Thus, the effectiveness of a discontinuity as a barrier is in large part contingent on the stresses on the adjoining segments, stresses that are related to the rupture history of the fault zone and the stress accumulation rate.

SEGMENTATION OF THE SAN JACINTO FAULT ZONE AND THE RELATION TO HISTORIC EARTHQUAKES

Detailed maps (Sharp, 1967, 1972, 1975; Clark, 1972; Matti and others, 1985) indicate that the 250-km-long San Jacinto fault zone is composed of multiple fault strands separated by major discontinuities. Most of these faults are further divided by other discontinuities into shorter segments. In total, about 20 fault segments are recognized (Figure 1, Table 1). The discontinuities, spaced from 7 to 35 km apart, are bends, branches, intersections, steps, or terminations. In addition, local changes in maximum earthquake depth along strike in the fault zone correspond with some segment boundaries,

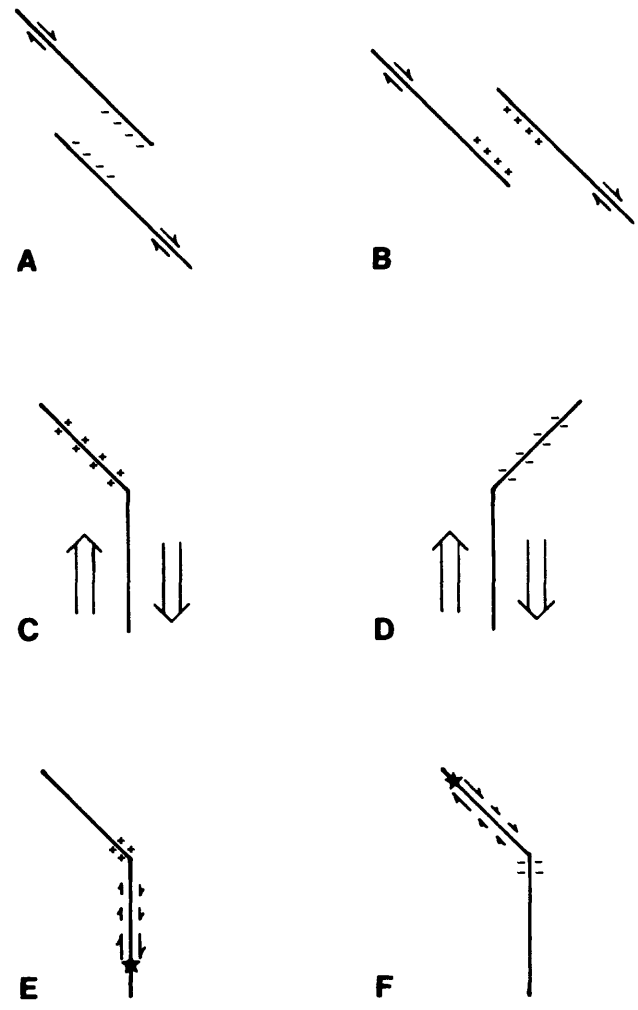

FIGURE 2 -- Characteristics of step and bend discontinuities in fault zones. *A*: extensional step; *B*: compressional step; *C*: compressional bend caused by block motion; *D*: extensional bend caused by block motion; *E*: compressional bend caused by rupture propagation; *F*: extensional bend caused by rupture propagation. At compressional discontinuities fault-normal stress increases, at extensional discontinuities fault-normal stress decreases.

TABLE 1. -- San Jacinto Fault Zone Segments

Segment Name	Length, km	NW boundary	SE boundary
Glen Helen, Lytle Creek - GH, LC	15	bends	steps and/or bends
San Bernardino - SB	15-20	steps and/or bends	intersection, 2 km left step,bend
San Jacinto Valley - SJV	35	intersection, 2 km left step, bend	5 km right step
Hot Springs - HS	25	4 km left step	4 km right step
Casa Loma - CL	15-20	5 km right step	15° bend
Park Hill - PH	10-15	15° bend	buried
Anza - A	25-30	buried	10° bend, branch
Buck Ridge - BR	27	branch	termination
Horse Canyon - HC	14	10° bend	1 km left step, 14° bend
Clark Valley - CV	22	1 km left step, 14° bend	bend, right step (?)
Santa Rosa - SR	12	bend, right step (?)	character change, intersection
Arroyo Salada - AS	12	character change, intersection	termination (?)
Coyote Canyon - CC	9	5 km right step	16° bend, character change
Coyote Ridge - CR	20	16° bend, character change	intersection
Borrego Mountain 1 - BM1	9	intersection	3 km left step
Borrego Mountain 2 - BM2	14	3 km left step	2 km left step
Borrego Mountain 3 - BM3	10	2 km left step	2 km right step, 10° bend
Borrego Mountain 4 - BM4	7	2 km right step, 10° bend	intersection, 10° bend
Superstition Mountain - SM	27	intersection, 10° bend	intersection
Superstition Hills - SH	25	intersection	buried

extending segment definition to the depth dimension.

Recent seismicity

The San Jacinto fault zone is one of the most seismically active fault zones in southern California (Allen and others, 1965). In general, recent seismicity in the fault zone occurs in distinct clusters; three predominate (Figure 3) (Sanders, 1986). The first is located at the step from the San Bernardino segment to the San Jacinto Valley segment where the Banning fault intersects (Figure 3a). The second occurs along the northwest Anza and southeast Hot Springs segments (Figure 3b). The third extends across the Horse Canyon-Clark Valley segment boundary and along the central Buck Ridge fault (Figure 3b). These clusters are defined not only by the number of small events but also by the sizes of the events, with many $M \geq 4$ earthquakes present. Earthquakes also occur along the Coyote Ridge segment (Figure 3b), at the southern end of the Arroyo Salada segment (Figure 3c), and along the northern end of the Superstition Mountain fault (Figure 3c). Some sections of the fault zone have relatively few earthquakes. These are the San Jacinto Valley, Casa Loma, and Park Hill segments, (Figure 3a), an 18 km section of fault zone spanning the boundary of the Anza and Horse Canyon segments (called the Anza Seismic Gap (Sanders and Kanamori, 1984)) (Figure 3b), and the Borrego Mountain 1-4 segments (Figure 3c).

Variations in maximum earthquake depths

An important type of rheological heterogeneity is the change at depth in the fault zone from stable to unstable sliding that affects the depth of the seismogenic regime. Sibson (1984) noted that because most large earthquakes nucleate near the base of the maximum seismogenic zone the variations in seismogenic depth along fault zones represent fault zone discontinuities that may affect fault rupture. Thus, identification of these discontinuities is important.

Distinct steps of several kilometers in the maximum depths of recent earthquakes are associated with three discontinuities, those between the Lytle Creek and San Bernardino, Coyote Ridge and Borrego Mountain 1, and Borrego Mountain 4 and Superstition Mountain segments (Figure 4a, b). The step at the discontinuity between the Coyote Ridge and Borrego Mountain 1 segments is also apparent in the combined aftershocks of the 1968 Borrego Mountain and 1969 Coyote Mountain earthquakes (Figure 4c). In each case, earthquakes are more abundant on the deeper side of the discontinuity.

Overall, the maximum depth of recent earthquake occurrence (indicative of the depth of the seismogenic fault) varies by a factor of two along strike in the fault zone, from about 21 km in the central and northwestern fault zone to about 12 km in the southeast fault zone. These variations in seismogenic depth along different fault segments may result in differences in characteristics of large earthquakes on these segments.

Large-scale segmentation of the San Jacinto and San Andreas fault zones

The segments of the San Jacinto fault zone can be grouped into four principal sections based on their overall trends and continuity. The intersections between these sections and the intersections at the northwest and southeast ends of the fault zone with the San Andreas and Imperial faults are the primary discontinuities in the fault zone. Fault rupture through these discontinuities may be considered unlikely.

The Claremont section in the northwest fault zone includes the Lytle Creek-Glen Helen, San Bernardino, and San Jacinto Valley segments and has a trend of N 45° W (Figure 1). The Clark section in the central fault zone includes the Park Hill, Anza, Horse Canyon, Clark Valley, Santa Rosa, and Arroyo Salada segments and has a trend of N 52° W. The Coyote Creek section in the central and southeastern fault zone includes the Coyote Canyon, Coyote Ridge, and Borrego Mountain 1-4

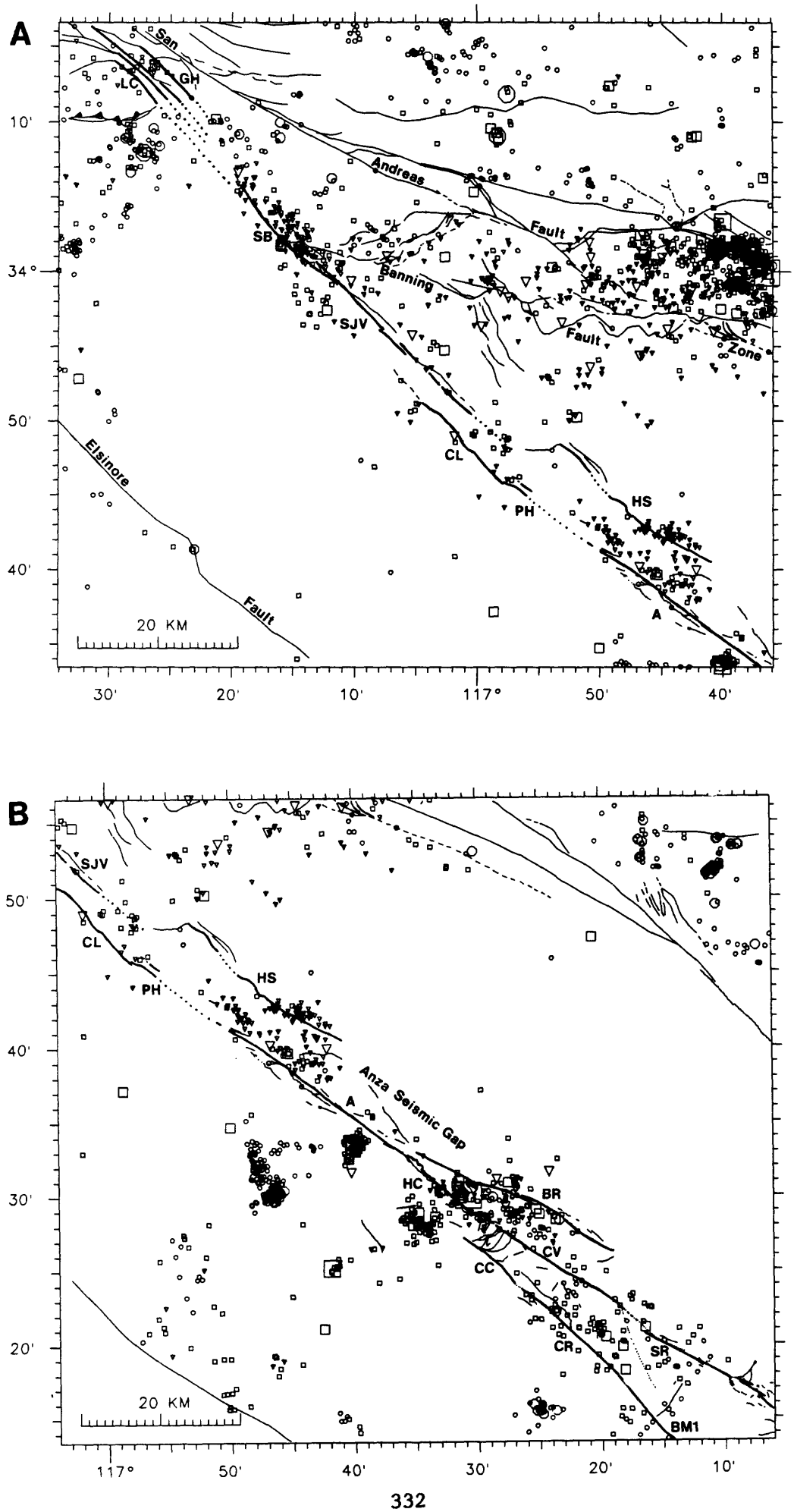

FIGURE 3 -- Maps of $M \geq 2$, location quality A earthquakes in the San Jacinto fault zone during the time period January 1978 through June 1987. *A*: northwest fault zone; *B*: central fault zone; *C*: southeast fault zone (interpreted subsurface structures (Fuis and others, 1982) are shown with dashed lines, ball on relatively downthrown block). The fault segments are labeled (see Table 1).

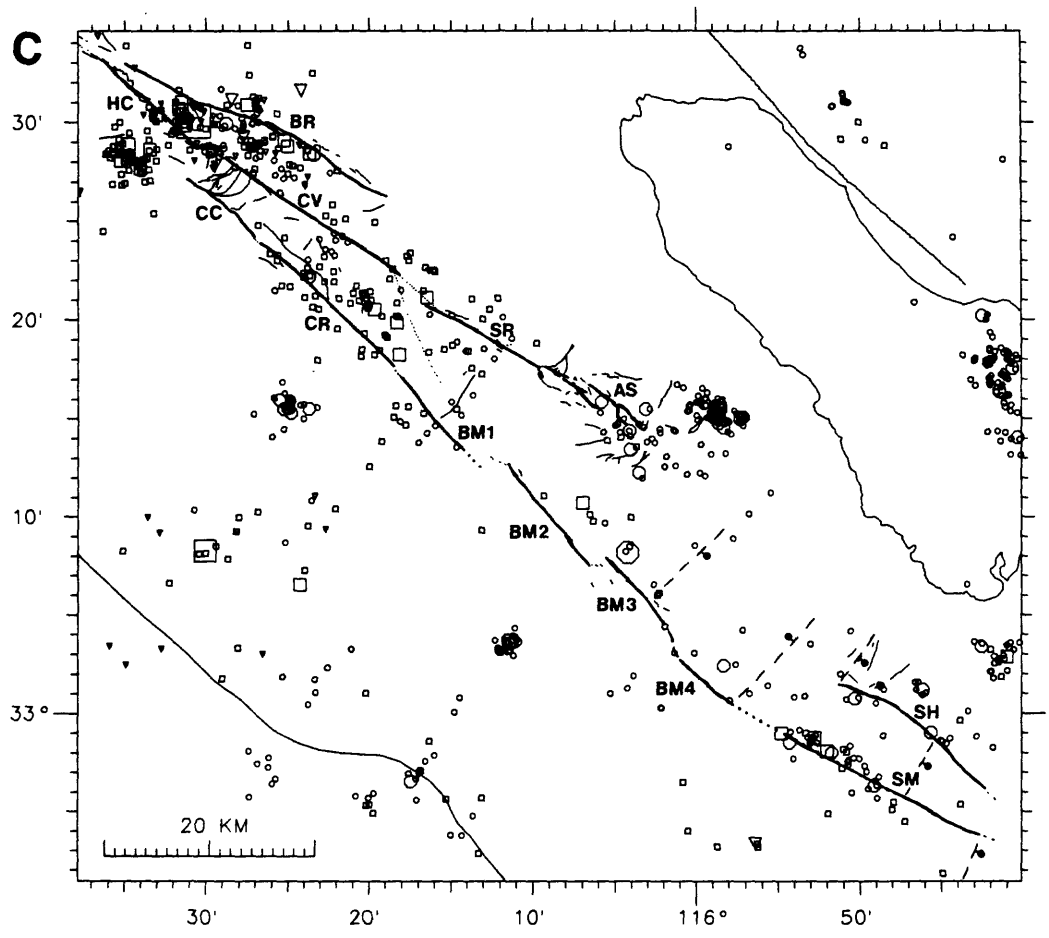
C
30'
20'
10'
33°
HC
BR
CV
CC
CR
SR
AS
BM1
BM2
BM3
BM4
SH
SM
20 KM
30'
20'
10'
116°
50'

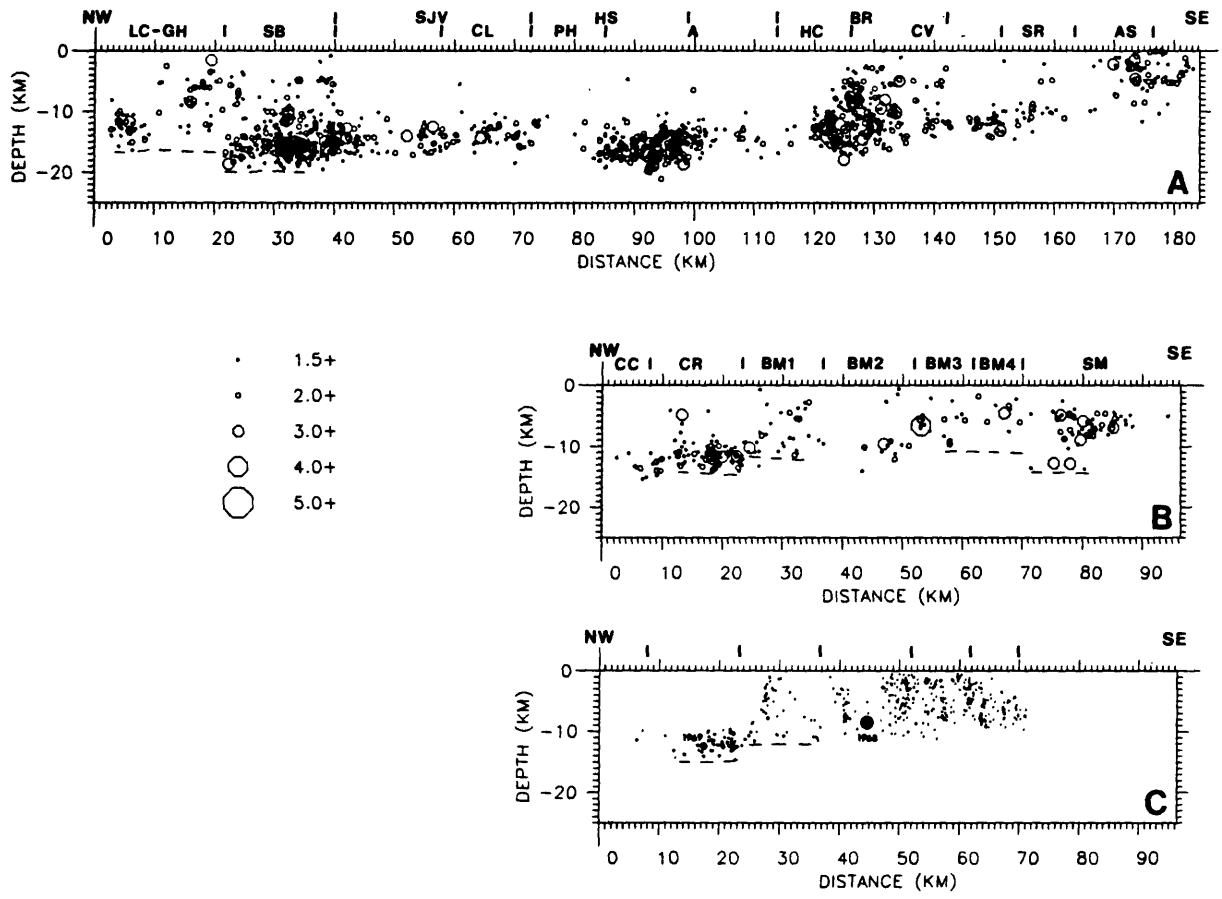

FIGURE 4 -- Vertical sections of earthquakes in the San Jacinto fault zone. *A*: section along the Claremont-Clark strands; *B*: section along the Coyote Creek-Superstition Mountain strands; *C*: same as *B* except with aftershocks of the 1968 Borrego Mountain and 1969 Coyote Mountain earthquakes (from Thatcher and Hamilton, 1973). Segment boundaries are marked along the top of each section. Note the vertical steps in the maximum depth of earthquake occurrence at three of the discontinuities. Shown are earthquakes with $M \geq 1.5$, location quality A which occurred during the time period January 1980 through June 1987.

segments and has a trend of N 45° W. The Superstition section in the southeastern fault zone includes the Superstition Mountain and Superstition Hills segments and has a trend of about N 60° W. At the intersections of the Claremont and Clark sections and the Clark and Coyote Creek sections major structural complexities have resulted, which can be related to the crustal block motion and the geometry of the intersection. Crustal block motion along the San Jacinto fault zone is probably about N 45° W, the same as that along the southern San Andreas fault. Thus, the Claremont and Coyote Creek sections are parallel to the motion, and the Clark and Superstition sections are oblique. At the intersection of the Coyote Creek and Clark sections convergence is manifested by the surficial thrust faults and the structurally high Coyote Ridge (Figure 6). At the intersection of the Claremont and Clark sections divergence is manifested by the subsiding basin between the San Jacinto Valley and Casa Loma segments (Figure 5).

It is worth noting that a major discontinuity in the San Andreas fault zone exists at its intersection with the San Jacinto fault zone (Figure 1). The San Jacinto fault zone is a branch of the San Andreas fault zone, and as such, the branch point represents a discontinuity in slip rate in the San Andreas fault zone. Northwest of the branch point the San Andreas fault zone is the primary plate boundary, and displacement across it occurs at about 34 mm/yr (Sieh and Jahns, 1984); southeast of the branch point the San Jacinto fault zone accomodates about a third of this slip. The M_w 7.9, 1857 rupture on the San Andreas fault (Sieh, 1978) had its southeast termination in the zone that defines this discontinuity.

Lytle Creek-Glen Helen

At the northwestern end of the San Jacinto fault zone the Lytle Creek, Glen Helen, and possibly other faults between these two, accommodate the right-lateral displacement (Figures 3a and 5). In addition, displacement is accommodated by the Cucamonga thrust fault at the southern front of the San Gabriel Mountains. The recent slip rate on the Cucamonga fault is measured at 5 mm/yr (Matti and others, 1985) and on the Lytle Creek fault at a site northwest of the Cucamonga fault at 2.5 mm/yr (maximum) (Mezger and Weldon, 1983). If the total slip rate on these faults equals the 12 mm/yr slip rate on the central section of the fault zone (Sharp, 1967; Merifield and others, 1987), then about 4.5 mm/yr must be accommodated by the Glen Helen and other faults. Also, by vector addition, the section of the Lytle Creek fault between the San Gabriel mountain front and the northwest end of the San Bernardino segment must accommodate 7.5 mm/yr of right slip and, therefore, is the principal strand of the San Jacinto fault zone northwest of the San Bernardino segment. This also indicates that the Lytle Creek fault is segmented by the discontinuity in slip rate at the intersection with the Cucamonga fault.

At their northwest ends in the San Gabriel Mountains the right-slip faults coalesce or bend abruptly west and become left-slip faults (Matti and others, 1985). No surface connection with the San Andreas fault has been found. Rupture on the Lytle Creek, Glen Helen, or other right-slip faults would terminate at these bends. To the southeast, these faults disappear at the mountain front beneath the young fluvial sediments of San Bernardino Valley. Fifteen kilometers further southwest the fault zone reappears at the surface as a single trace, the San Bernardino segment of the Claremont fault. This indicates that the discontinuity between the Lytle Creek-Glen Helen faults and the San Bernardino segment includes stepping and/or branching relationships. There is also a 3 km step in the maximum depth of earthquakes at this discontinuity (Figure 4), suggesting that the discontinuity extends the entire depth of the seismogenic zone.

San Bernardino

The discontinuity between the San Bernardino and San Jacinto Valley segments of the Claremont fault is a 2 km restraining step that is also the site of intersection with the Banning and Crafton Hills fault zones (Figures 3a). In addition, the San Bernardino segment has an orientation that is about 12° more northerly than either the San Jacinto Valley or Lytle Creek segments.

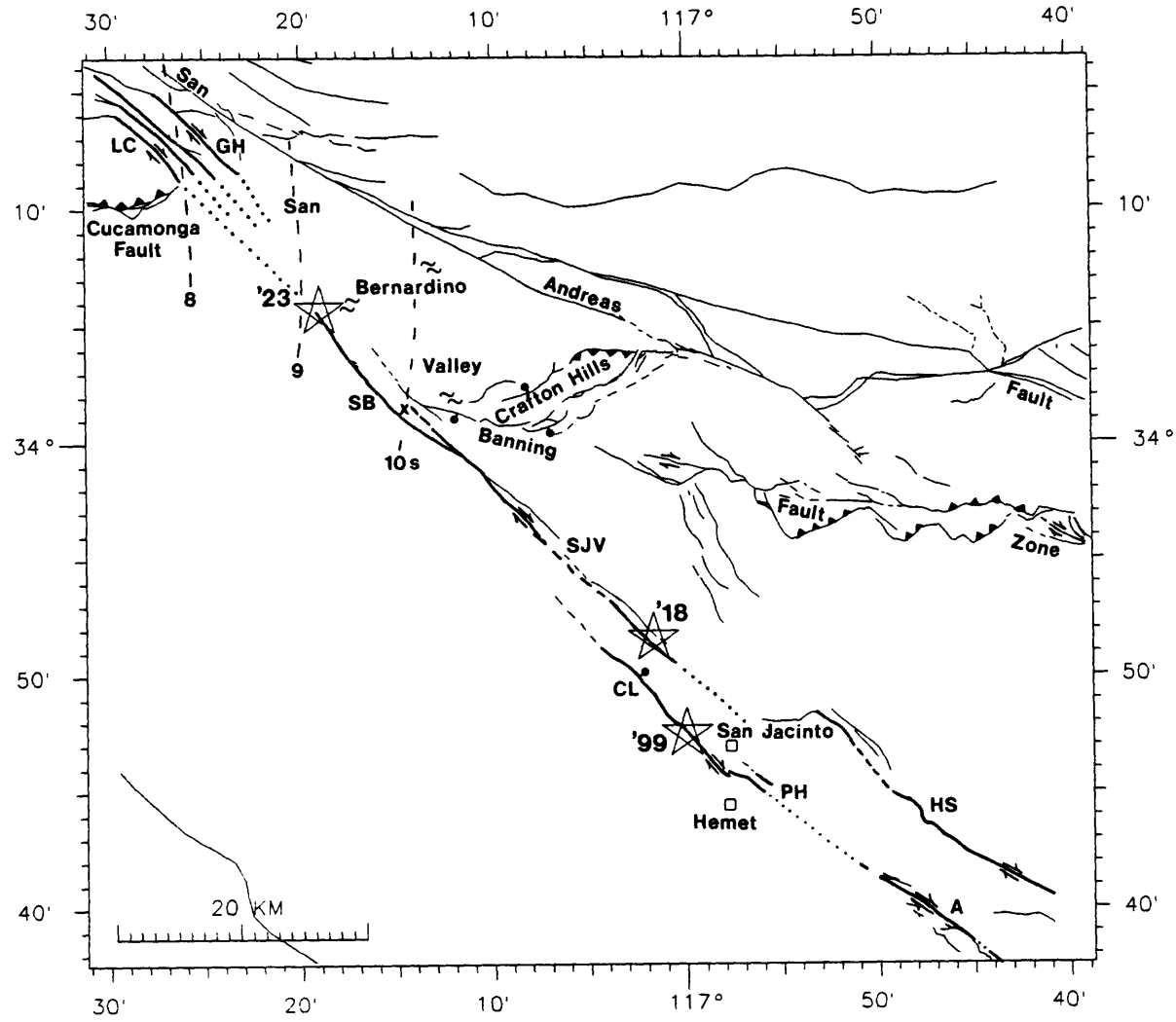

FIGURE 5 -- Map of historic large earthquakes in the northwest San Jacinto fault zone. Stars mark the interpreted locations of the 1899, 1918, and 1923 earthquakes. The San Jacinto fault zone segments are labeled (see Table 1). Dashed curves in the San Bernardino Valley area distances from Pasadena determined from S-P times. The reference is a well-located earthquake (2 October 1985, 2344 GMT) on the San Bernardino segment (marked by a cross) with an S-P time of 10.1 s at Pasadena. The aftershocks of the 1923 earthquake have S-P times at Pasadena of 8-10 s, average 9 s, and give longitudinal constraint to the mainshock location. Sites of greatest damage from the 1923 earthquake are marked with squiggles.

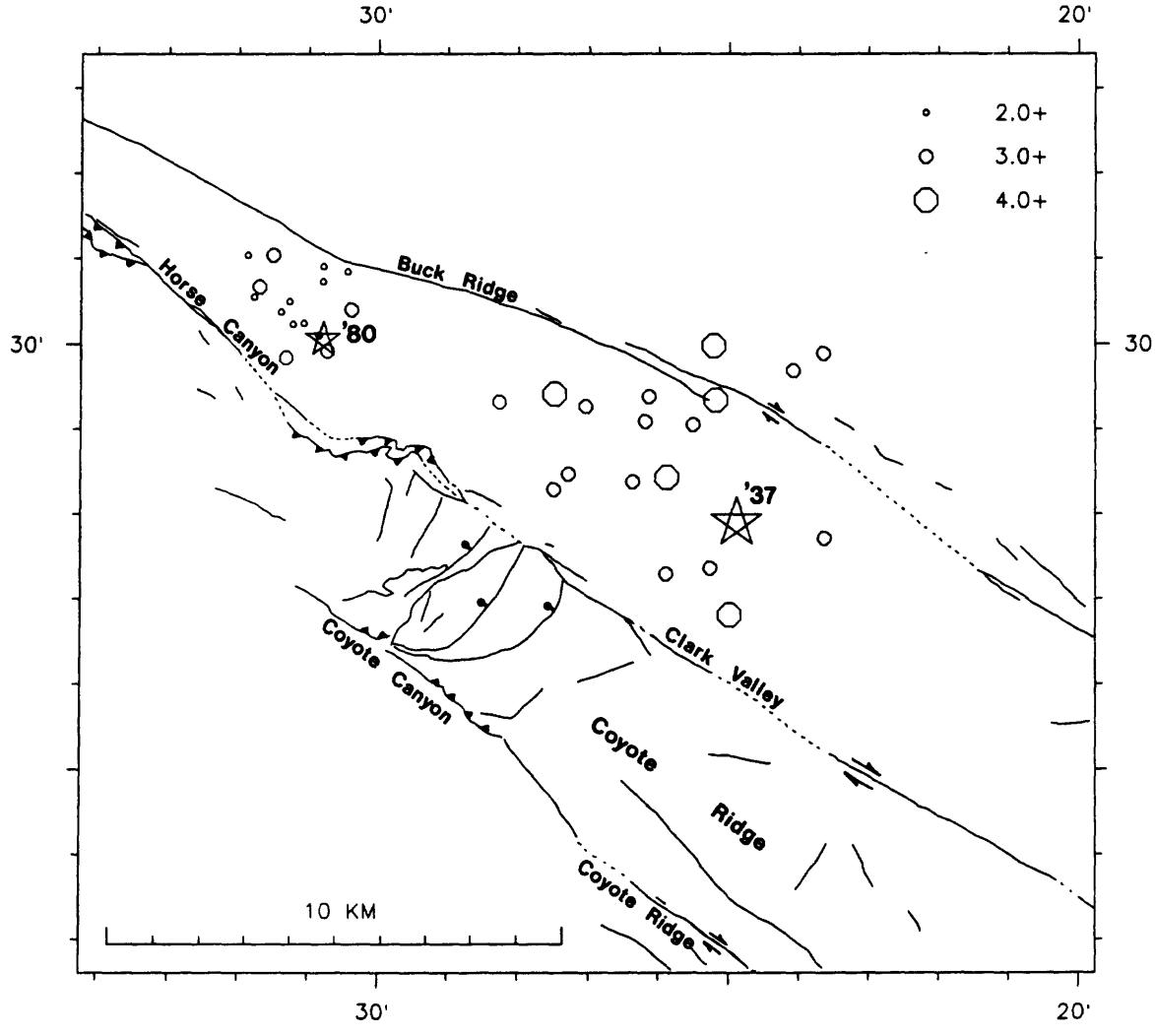

FIGURE 6 -- Map of epicenters of the 1937 (M_L 5.9) and 1980 (M_L 5.5) earthquakes and aftershocks. For the 1937 earthquake, 2 days of aftershocks of $M \geq 3$ are plotted, and for the 1980 earthquake, 2 days of aftershocks of $M \geq 2$ are plotted. The 1937 aftershocks indicate that rupture terminated at a 1 km restraining step between the Clark Valley and Horse Canyon segments. The 1937 and 1980 rupture initiations may have been influenced by discontinuities in the Buck Ridge fault.

The July 22, 1923 earthquake (M_L 6¼ (Richter, 1958); M_o 1 x 10^{25} dyne-cm (Hanks and others, 1975)) was strongly felt in the San Bernardino Valley (Figure 5). $S-P$ times of numerous aftershocks recorded in Pasadena range from 8 to 10 s (average 9 s) (Sanders and Kanamori, 1984), and when compared with the $S-P$ time of a recent, well-located earthquake in the San Bernardino Valley region, these times constrain the longitude of the epicenter to between 117° 14' and 27' (Figure 5). Intensities were greatest in the central and southern San Bernardino Valley (Laughlin and others, 1923). Together these data favor a hypocenter for this earthquake on the San Bernardino segment, though this is not proven. The seismogenic zone is relatively deep in this section of the fault zone (Figure 4), thus the 1923 hypocenter may have been deep as well. A deep hypocenter coupled with a relatively small seismic moment (Thatcher and others, 1975) could account for the lack of a more pronounced zone of damage near the fault at the surface. Shaking was undoubtedly enhanced in the regions of the valley where fluvial sediments have accumulated.

The concentration of recent earthquakes on the San Bernardino segment (Figures 3a and 4) indicates that stresses are large. This may be related to incomplete stress release due to the small moment of the 1923 earthquake (if it occurred here). It may also be indicative of the heterogeneous nature of local stresses and fault strength near the intersection with the Banning fault zone. Recent earthquakes have been as large as M_L 4.8.

San Jacinto Valley and Casa Loma

The discontinuity between the San Jacinto Valley and Casa Loma segments is a 5 km releasing step (Figure 5). The San Jacinto Valley, which has accumulated about 2.5 km of sediments since the Pliocene (Fett, 1968), lies in the subsiding basin between these faults.

Two of the largest historic earthquakes in the San Jacinto fault zone may have been located on these segments; these occurred in December 25, 1899 (M_S 6.4 (Abe, 1988)) and April 21, 1918 (M_S 6.9 (B. Ellsworth, pers. comm., 1988); M_o 15 x 10^{25} dyne-cm (Hanks and others, 1975)). Both of these earthquakes were most strongly felt in the towns of San Jacinto and Hemet, suggesting that the epicenters were located nearby (see discussion and references in Sanders and Kanamori, 1984) (Figure 5). No definite fault ruptures were reported from investigations at the time, though Allen and others (1965) report fresh-appearing scarps (age presumably late Holocene to historic) along the San Jacinto fault zone near Hemet. The fault segments near these towns are the San Jacinto Valley, Casa Loma, Park Hill, and Hot Springs segments. Lack of evidence for Holocene fault movement at the surface (Sharp, 1967; Hill, 1984) suggests that these earthquakes did not occur on the Hot Springs fault. Since the town of San Jacinto is located atop a sedimentary basin between the right stepping Casa Loma and San Jacinto Valley segments one interpretation of the apparently similar locations of the 1899 and 1918 earthquakes is that each was caused by rupture of one of the bounding faults (Sanders and Kanamori, 1984). The 30-km-long San Jacinto Valley segment and the 15-km-long Casa Loma segment are of sufficient length to have produced earthquakes of these magnitudes. In any event, segmentation of the fault zone may have been important in allowing both of these large earthquakes to be located so near each other.

The number of recent earthquakes on these segments is relatively small (Figures 3a and 4). This may be related to relatively lower stresses due to the stress release during the 1899 and 1918 earthquakes.

Hot Springs

The discontinuity between the San Jacinto Valley and Hot Springs segments is a 5 km restraining step (Figure 5). The Hot Springs fault itself is segmented by a 10° internal bend that separates a northwestern section with an irregular trace from a southeastern section with a more linear trace. The Hot Springs segment does not show evidence of recent faulting at the surface (Sharp, 1967; Hill,

1984), though small earthquakes occur deep on the southeastern linear section (Figure 3b). This segment does not appear to be a active member of the San Jacinto fault zone at present.

Park Hill

The discontinuity between the Casa Loma and Park Hill segments is a 15° bend (Figure 3a). The intersection of the Park Hill and Anza segments is covered by sediments, but the Park Hill segment may well be a continuation of the Anza segment with little or no discontinuity between the two. It is possible that either the 1899 or 1918 earthquake occurred on or ruptured into the Park Hill segment. Recent earthquakes are scarse on this segment, suggesting possible historical stress release.

Anza

The discontinuity at the northwest end of the Anza segment of the Clark fault is not clearly visible. It is very likely that most of the displacement on the Anza segment continues through the Park Hill segment to the Casa Loma segment. This is supported by the presence of the deep subsiding basin between the Casa Loma and San Jacinto Valley segments, which would not exist if considerable displacement were not transferred from the Casa Loma to the San Jacinto Valley segment. Thus, the effective northwest end of the Anza segment may be the bend at the northwest end of the Park Hill segment. However, minor faults suggest that some slip may transfer directly from the Anza segment to the San Jacinto Valley segment, in which case there may be a discontinuity in slip rate between the Anza and Park Hill segments. The discontinuity at the southeast end of the Anza segment includes a 10° bend to the Horse Canyon segment and the branching of the Buck Ridge fault.

One of the principal clusters of recent earthquakes in the fault zone is located in the northwest half of the Anza segment (Figure 3b). These earthquakes occur to 20 km depth, indicating a relatively deep seismogenic zone (Figure 4). The southeastern half of the segment is relatively aseismic and is part of the Anza seismic gap (Sanders and Kanamori, 1984).

Buck Ridge

The Buck Ridge fault branches from the San Jacinto fault zone near the intersection of the Anza and Horse Canyon segments (Figure 1). Holocene scarps indicate that this fault is an active member of the fault zone (Sharp, 1967). If the relative total displacements on the Buck Ridge and Clark faults indicate the current relative slip rates, then the Buck Ridge fault accounts for one-fifth of the slip rate in this part of the fault zone. The Buck Ridge fault is itself segmented by small ½ km steps and a 17° bend (Figure 6). Recent small earthquakes have occurred near the central part of this segment (Figure 3b), though their locations do not define a fault plane and appear to distributed between the Buck Ridge and Clark faults (Sanders and Kanamori, 1984; Sanders, 1986).

Horse Canyon

The Horse Canyon segment is a major restraint to fault rupture between the Anza and Clark Valley segments. It is capable of producing earthquakes at least as large as M_L 5.5 (Figure 6), and may be capable of initiating rupture propagation into adjoining segments. The Horse Canyon segment is expressed at the surface along much of its length by shallow thrust faults, which indicate a component of convergence across the segment. A 1 km restraining step and 14° bend to the Clark Valley segment is located at the southeast end of this segment. A focal mechanism from a M 3 earthquake in the step reveals right slip on a N 70° W trending fault plane, suggesting that the step may extend to at least 9 km depth (Sanders, 1986). On February 25, 1980 an M_L 5.5 earthquake occurred 2 km northwest of this step and rupture propagated 3 km further northwest (Given, 1983, Sanders and Kanamori, 1984).

Interaction of this earthquake with the Buck Ridge fault may have occurred, because the epicenter lies near an 11° bend in the Buck Ridge fault.

The northwestern part of the Horse Canyon segment is relatively aseismic (part of the Anza seismic gap) (Figure 3b). The southeastern part of the segment, though, has had numerous recent earthquakes, including the 1980 M_L 5.5 White Wash earthquake (Figures 3b and 6). These earthquakes may be related to the high stresses at the northwest end of the 1937 earthquake rupture (Figure 6), and may indicate the potential for rupture further northwest into the Anza segment.

Clark Valley

The Clark Valley segment is bounded on its northwest end by a 1 km step and 14° bend to the Horse Canyon segment. Its southeast end is hidden in sediments, but may be an extensional step to the Santa Rosa segment, because a broad alluvial valley is present and forms an embayment into the mountainous terrain. Also there is a 4° difference in trend between the Clark Valley and Santa Rosa segments.

The March 25, 1937 Buck Ridge earthquake (M_L 5.9 (Sanders and others, 1986); M_o 0.3 x 10^{25} dyne-cm (Hanks and others, 1975)) mainshock and aftershock epicenters are located between the surface traces of the Clark Valley and Buck Ridge segments (Sanders and others, 1986), which are subparallel and about 5 km apart here (Figure 6). It is not clear from these locations which fault ruptured to produce the 1937 earthquake. Because both faults are active and lie so close to each other the earthquake was possibly influenced by the stress conditions on each fault. The mainshock epicenter is near a step discontinuity in the Buck Ridge fault. The aftershocks indicate that rupture propagated predominately 6 km northwest and terminated at the restraining step between the Clark Valley and Horse Canyon segments.

Recent earthquakes occur along all of the Clark Valley segment, but most cluster near the northwestern end (Figure 3b). This cluster is in part spatially coincident with the 1937 rupture zone (Figure 6) and may indicate incomplete stress release (Das and Aki, 1977) during the earthquake. Because the 1937 earthquake had a small moment Thatcher and others (1975) suggested incomplete rupture of the fault plane.

Santa Rosa

At the southeast end of the Santa Rosa segment the fault branches into the numerous splays of the Arroyo Salada segment. The southeast discontinuity is also an intersection with the southeast end of the Santa Rosa Mountain structural block. Some recent small earthquakes have occurred on this segment (Figure 3c).

Arroyo Salada

The Clark fault is not recognized southeast of the southeast end of the Santa Rosa segment as a single, throughgoing fault (Sharp, 1967). Instead, the fault zone here (the Arroyo Salada segment) is expressed at the surface by discontinuous, short fault traces in Quaternary sediments (R. V. Sharp, unpublished map) (Figure 7). However, structural relations suggest that in the subsurface the fault may be more continuous. The piercing point of the Santa Rosa mylonite, near the southeastern end of the Santa Rosa segment, was used by Sharp (1967) to measure 19 km of offset across this portion of the fault zone (Figure 8). Because an extensional basin has not developed southwest of the Santa Rosa segment due to the right-lateral displacement, conservation of mass requires that significant slip must have occurred on an extension of the fault southeast of the piercing point. The 1954 Arroyo Salada earthquake is evidence of this extension of the fault (Figure 7).

The discontinuity between the Santa Rosa and Arroyo Salada segments coincides with the southeast

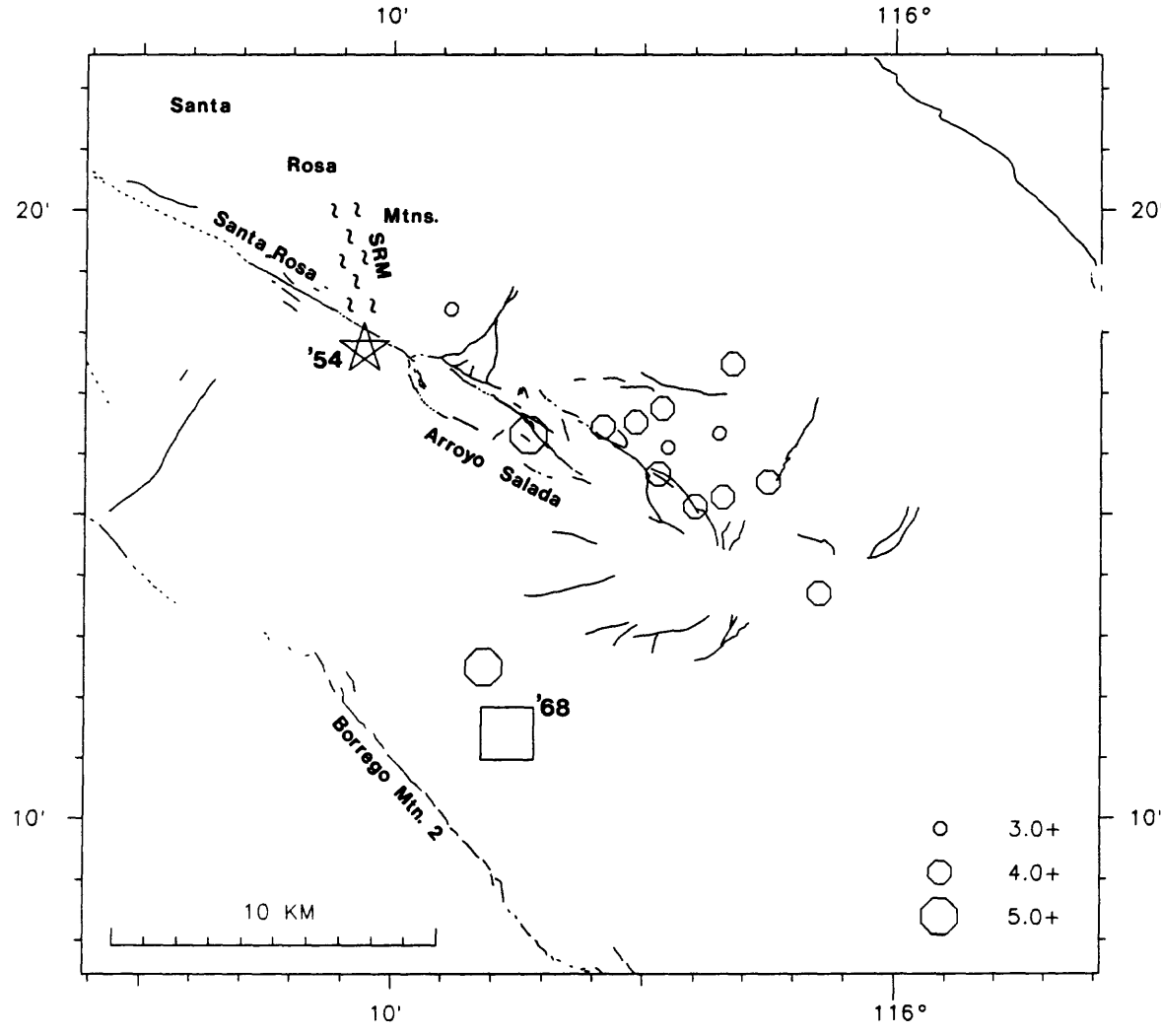

FIGURE 7 -- Map of epicenters of the 1954 (M_L 6.2) Arroyo Salada earthquake anad aftershocks. Aftershocks of $M \geq 3.9$ are shown. The 1968 Borrego Mountain mainshock epicenter is plotted also. The 1954 rupture initiated at the discontinuity between the Santa Rosa and Arroyo Salada segments and propagated southeast on the Arroyo Salada segment. This discontinuity is characterized by a change from a single, relatively continuous fault strand of the Santa Rosa segment to multiple, discontinuous fault strands of the Arroyo Salada segment. This discontinuity is also an intersection with the topographic break between the Santa Rosa Mountains and the Salton Trough; this break may have a structural origin. The largest aftershock of the 1954 earthquake occurred near the initiation point of the 1968 earthquake, suggesting a region of localized stess concentration even though a discontinuity is not evident at the surface. SRM, Santa Rosa Mylonite.

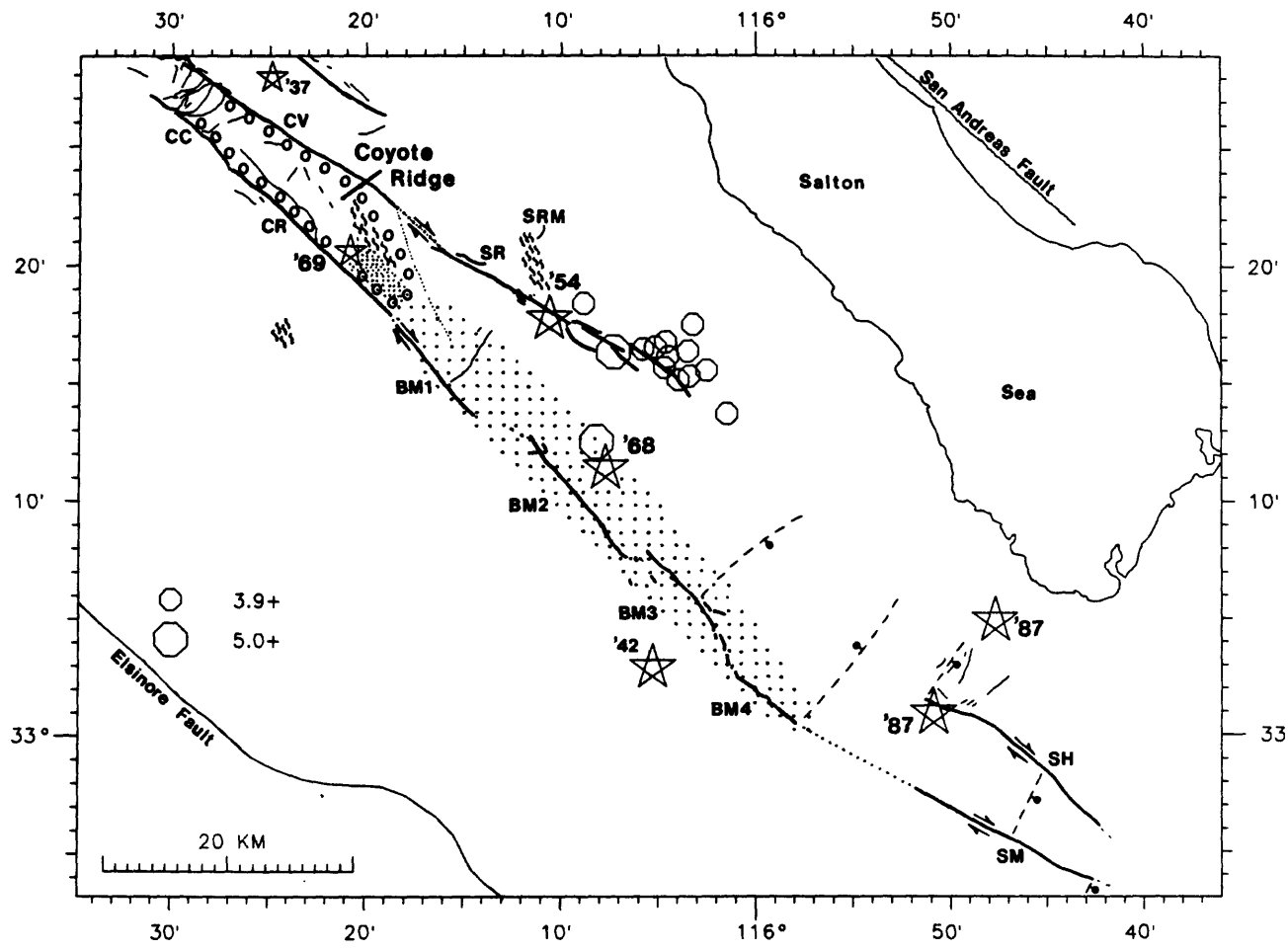

FIGURE 8 -- Map of the southeastern San Jacinto fault zone showing the epicenters of large historic earthquakes, rupture zones of the 1954, 1968 (broad stippling), 1969 (tight stippling), and 1987 earthquakes, and other significant features. Subsurface structures interpreted from seismic refraction data (Fuis and others, 1982) are shown with dashed lines, ball on relatively down-thrown block.

end of the Santa Rosa Mountains and the beginning of basin sediments. This topographic and lithologic transition may also be a structural transition and, thus, somehow related to the change in fault character at this location.

The March 19, 1954 Arroyo Salada earthquake (M_L 6.2 (Richter, 1958); M_o 4.4 x 10^{25} dyne-cm (Thatcher and Hanks, 1973)) occurred on the Arroyo Salada segment (Sanders and others, 1986). The mainshock epicenter lies at the discontinuity between the Santa Rosa and Arroyo Salada segments, and aftershocks indicate rupture propagation 12 km southeast (Figure 7).

Currently, earthquakes occur at the southeast end of the Arroyo Salada segment, while the northwest end of the segment is relatively aseismic (Figure 3c). This may indicate current low stress near the initiation of the 1954 rupture, and higher stress near the southeast end of the rupture (Figure 7). Recent earthquakes occur several km further southeast than the aftershocks of the 1954 earthquake indicating that the fault continues further southeast in the subsurface. The seismogenic zone is about 12 km deep along this segment (Figure 4).

Coyote Canyon

The Coyote Canyon segment of the Coyote Creek fault is a short segment characterized by an irregular surface trace and areas of shallow thrust faulting (Figure 6). The northwest end is a 5 km releasing step to the Horse Canyon segment of the Clark fault. The intrastep block, Coyote Ridge, has been uplifted however (Sharp, 1967), suggesting a component of convergence in this region of the fault zone (Sanders and Kanamori, 1984). The discontinuity at the southeastern end of the Coyote Canyon segment is a 16° bend and change in surface expression to the linear Coyote Ridge segment. Very few recent earthquakes have occurred on this segment (Figure 3c).

Coyote Ridge

The Coyote Ridge segment of the Coyote Creek fault forms the southwest edge of Coyote Ridge, and the segment ends to the southeast at the southeast termination of Coyote Ridge (Figure 8). The spatial relation of this discontinuity to the Santa Rosa mylonite and to the topographic relief at the southeastern end of the Coyote Ridge suggests that it is a displaced twin of the discontinuity at the southeastern end of the Santa Rosa segment of the Clark fault, and thus may be structural in nature. A distinct step in the maximum depth of earthquakes occurs at this discontinuity (Figure 4b, c).

The April 28, 1969 Coyote Mountain earthquake (M_L 5.8, M_o 0.5 x 10^{25} dyne-cm; (Thatcher and Hamilton, 1973)) occurred on this segment about one year after the 1968 Borrego Mountain earthquake on the segments to the southeast. The 1969 mainshock occurred about 10 km northwest of the end of the Borrego Mountain aftershock zone, and aftershocks indicate that the rupture extended southeast (Thatcher and Hamilton, 1973) and terminated at the segment boundary (Figure 8).

Numerous earthquakes have occurred recently on the Coyote Ridge segment, with a concentration in the same region as the 1969 fault rupture. These perhaps indicate incomplete stress release during the small-moment 1969 earthquake.

Borrego Mountain 1-4

The April 9, 1968 Borrego Mountain earthquake (M_L 6.8 (Kanamori and Jennings, 1978); M_o 8 x 10^{25} dyne-cm (Hanks and Wyss, 1972)) ruptured at least three and possibly four fault segments, the Borrego Mountain 1-4 segments (Figure 8). Surface rupture (Clark, 1972) terminated to the northwest at the end of the Borrego Mountain 2 segment, where a restraining step exists; however aftershocks (Hamilton, 1972; Allen and Nordquist, 1972) suggest subsurface rupture may have continued northwest on the Borrego Mountain 1 segment and terminated near the southern end of Coyote Ridge. Surface rupture and aftershocks associated with this earthquake terminated at the southeast end

of the Borrego Mountain 4 segment. There is a 10° bend between the Borrego Mountain 4 and Superstition Mountain segments that is restraining for this direction of rupture propagation. In addition, a step in the depth of the seismogenic zone occurs here (Figure 4), and a subsurface structural boundary between basement rocks and sediments may exist (Fuis and others, 1982; Magistrale and Kanamori, 1988).

Two of the internal boundaries of the Borrego Mountain segments are 2-3 km restraining steps, and the third is a 2 km releasing step. Fault rupture was able to propagate southeast through the 2 km restraining step between the Borrego Mountain 2 and 3 segments and the 2 km releasing step between the Borrego Mountain 3 and 4 segments, though surface displacement diminished considerably between the segments from about 400 mm on Borrego Mountain 2 to 200 mm on Borrego Mountain 3 to 75 mm on Borrego Mountain 4 (Clark, 1972). Sibson (1986) suggests that rupture propagation was hindered by the releasing step between Borrego Mountain segments 3 and 4. The mainshock epicenter (Allen and Nordquist, 1972) does not seem to coincide with a fault discontinuity, though it is recognized as an area of stress concentration as early as 1954 (Figure 7) (Sanders and others, 1986) and was the site of greatest fault displacement (Clark, 1972; Burdick and Mellman, 1976).

Few earthquakes have occurred on these segments recently (Figure 3c). The seismogenic zone is about 12 deep along these segments (Figure 4).

Superstition Mountain

The discontinuity at the southeast end of the Superstition Mountain segment may be subsurface structural intersection (Figure 8). Another subsurface structural intersection may occur near the south-central part of the segment and may influence earthquake occurrence; recent earthquakes on the segment do not occur southeast of this intersection (Figure 3c). Many small earthquakes have occurred on the north-central part of the segment recently; though the northwest and southeast ends are relatively aseismic (Figure 3c).

Superstition Hills

The discontinuity at the northwest end of the Superstition Hills fault may be a subsurface structural intersection (Figure 8) (Magistrale and Kanamori, 1988). Another subsurface structure may intersect near the central part of the fault, where a small releasing step occurs (M. Rymer, unpublished data). The aftershocks of the November 24, 1987 Superstition Hills earthquake (m_b 6.3) were limited to the region between these intersections (Magistrale and Kanamori, 1988). Surface rupture, however, occurred along the entire 25 km length of the fault (Budding and Sharp, 1988). The southeastern end of the fault is buried by sediments. There were few earthquakes on the fault between 1978 and 1987 (Figure 3c).

EARTHQUAKE POTENTIAL IN THE SAN JACINTO FAULT ZONE

The data presented in this paper suggest that segmentation of the San Jacinto fault zone has an influence on the characteristics of fault rupture in the fault zone. Thus, we may use this knowledge to assess the earthquake potential in the fault zone.

In general, the fragmented nature of the fault zone, with segment lengths from 7 to 35 km, and the history of large earthquakes in the fault zone with magnitudes of 6-7 suggest that future large earthquakes will also be of similar size. A magnitude 7.5 earthquake could occur if rupture were to cascade from one long segment into another long segment.

Presently, the segments that can be considered to have low potential for a large earthquake in the near future are in the southern third of the fault zone. These are the Arroyo Salada, Borrego Mountain 1-4, and Superstition Hills segments which ruptured during the 1954, 1968, and 1987 earthquakes,

respectively. In this region of the fault zone, the Superstition Mountain fault has potential for an earthquake similar to the Superstition Hills earthquake. A large earthquake has not occurred on the Superstition Mountain fault since at least 1892. The cluster of earthquakes near the north-central end of this segment may indicate stress concentration at the end of the 1968 fault rupture.

Most of the other segments in the fault zone should be considered to have potential for rupture, in particular those segments which have experienced low moment release historically. Thatcher and others (1975) recognized two seismic-slip gaps in the fault zone, one including the Anza, Horse Canyon, Clark Valley, Santa Rosa, Coyote Canyon, Coyote Ridge, and Buck Ridge segments in the central fault zone and one including the Lytle Creek-Glen Helen and San Bernardino segments in the northwest fault zone. The San Jacinto Valley, Casa Loma, and Park Hill segments may have ruptured to cause the 1899 and 1918 earthquakes, however enough time has passed since then for significant potential slip to have accumulated again. In the central fault zone, particular attention has been given to the Anza and Horse Canyon segments, parts of which form the Anza seismic gap (Figure 3b) (Sanders and Kanamori, 1984). It is likely that this stretch of fault zone has not ruptured since at least 1892. The 1937 and 1980 earthquakes and the concentrated seismicity at the southeast end of the Anza seismic gap suggest that stresses are high in that area and that rupture of the gap could initiate in the central Horse Canyon segment. Rupture could propagate northwest along the entire Anza segment and possibly into the Park Hill and Casa Loma segments, forming an earthquake of M 7. The San Jacinto Valley is a major step discontinuity in the fault zone, and it is unlikely that rupture would propagate through to the San Jacinto Valley segment. In the northeastern fault zone, the San Bernardino and Lytle Creek-Glen Helen segments have not ruptured since at least 1892, except possibly for the small-moment 1923 earthquake. Numerous recent earthquakes along the southern end of the San Bernardino segment suggest high stresses. Rupture of the San Bernardino segment may or may not propagate to the Lytle Creek or Glen Helen segments. Rupture from the San Bernardino segment to the San Jacinto Valley segment is possible.

SEGMENTATION, FAULT ZONE MATURITY, AND PRECURSORY SEISMICITY

The characteristics of earthquake occurrence may vary between fault zones with different amounts of total displacement. For example, the San Jacinto and southern San Andreas faults, though both major members of the Pacific-North American plate boundary with similar recent fault-parallel strain rates (King and Savage, 1983), have significant differences in earthquake occurrence historically. The San Jacinto fault zone is very active seismically, while the southern San Andreas fault zone is nearly aseismic. The total offset across the San Jacinto fault zone is about 25 km (Sharp, 1967), while offset across the southern San Andreas fault exceeds 160 km (Matti and others, 1985). This difference in total offset is reflected in the continuity of the fault zones; the San Jacinto fault zone is relatively discontinuous and is composed of numerous short segments (7-35 km), while the southern San Andreas fault is relatively continuous, essentially one long (70 km) segment extending from the south end of the Salton Sea to near the branch point of the Banning fault (Figure 1). Wesnousky (1988, also this volume) has documented that as total offset across a strike slip fault zone increases, average surface trace segment length increases as well. This suggests that irregularities become more widely spaced along a fault zone as total offset increases. Apparently, small-scale irregularities are smoothed out. Undoubtedly, the high rate of earthquake occurrence in the San Jacinto fault zone and the essentially aseismic nature of the southern San Andreas fault are related to the relative distributions of discontinuities. The numerous shorter wavelength irregularities in the San Jacinto fault zone cause small local stress concentrations, which result in abundant small to moderate sized earthquakes. The longer wavelength irregularities on the southern San Andreas fault, however, allow stresses to build evenly in the fault zone so that local concentrations are avoided, and rupture occurs only in large earthquakes. Thus, given the apparently broad distribution of asperity sizes in the San Jacinto fault zone, earthquakes precursory to major fault rupture may be likely. In the southern San Andreas fault zone,

however, the distribution of asperity sizes may preclude the occurrence of precursory earthquakes.

CONCLUSIONS

Twenty principal segments ranging in length from 7 to 35 km are identified in the 250-km-long San Jacinto fault zone. The characteristics of large earthquakes in the fault zone, each limited in size to less than *M* 7, and often limited in rupture extent by discontinuities, indicate that segmentation of this fault zone is important in influencing the size of earthquakes. The relatively short lengths of the segments of the San Jacinto fault zone suggest that most future earthquakes will be similarly limited in size.

Rupture initiation or termination points of historic large earthquakes in the fault zone often coincide with segment boundaries. The 1937 Buck Ridge earthquake terminated at a restraining step. The 1954 Arroyo Salada earthquake initiated at a change in surficial expression of the fault zone which may also be a structural intersection. The 1968 Borrego Mountain earthquake terminated to the northwest at either a restraining step or a structural intersection and seismogenic zone depth step. It terminated to the southeast at a restraining bend-seismogenic zone depth step-structural intersection. Rupture continued, however, through a restraining step and a releasing step. The 1969 Coyote Mountain earthquake terminated at a structure intersection and step in the seismogenic zone depth. The 1987 Superstition Hills earthquake initiated near a fault intersection and terminated to the northwest at a possible subsurface structure intersection. Rupture of future large earthquakes in the fault zone may be affected by segment boundaries as well.

Recent small earthquakes in the fault zone tend to cluster near segment boundaries that were stopping points for large historical earthquake rupture. If the clusters indicate high local stresses, then the adjoining segments that have not ruptured historically may have increased potential for large earthquakes.

Based on the historical rupture patterns, only three segments of the fault zone are considered to have low potential for large earthquakes in the near future; these are the Arroyo Salada, Borrego Mountain 1-4, and Superstition Hills fault segments. The remaining fault segments, which lie primarily in the northern half of the fault zone and, thus, near the most populous regions, must be considered to have potential for large earthquakes in the near future.

The relative earthquake hazard associated with these segments or groups of segments may be estimated from detailed consideration of their characteristics. Since a useful earthquake forecast includes the location, size, and time of the earthquake we can judge the effectiveness of segmentation analysis by how well it helps us determine these elements. Understanding of the lengths of fault segments in the fault zone will help constrain the sizes of the earthquakes to be expected. Knowledge of the history of large earthquake occurrence in the fault zone and the relation of fault rupture to fault segments allows the location of future earthquakes to be deduced (based on knowledge of strain accumulation in the fault zone). The time of future large earthquakes is more difficult to estimate from knowledge of segmentation; however, knowledge of stress effects near discontinuities coupled with knowledge of likely discontinuities to watch may help in recognizing precursory signals related to local stress accumulation.

REFERENCES

Abe, K., 1988, Magnitudes and origin times from Milne seismograph data: earthquakes in China and California, 1989-1912, *in* Lee, W. H. K., Meyers, H., and Shimazaki, K., eds., Historical Seismograms and Earthquakes of the World, Academic Press, pp. 37-50.

Aki, K., 1979, Characterization of barriers on an earthquake fault, J. Geophys. Res., v. 84, pp. 6140-6148.

Allen, C. R., 1968, The tectonic environments of seismically active and inactive areas along the San Andreas fault system, Stanford Univ. Publ. Geol. Sci., v. XI, pp. 70-82.

Allen, C. R., P. St. Amand, C. F. Richter, and J. M. Nordquist, 1965, Relationship between seismicity and geologic structure in the southern California region, Bull. Seis. Soc. Am., v. 55, pp. 753-797.

Allen, C. R., and J. M. Nordquist, 1972, Foreshock, main shock, and larger aftershocks of the Borrego Mountain earthquake, U. S. Geol. Surv. Prof. Pap. 787, pp. 16-23.

Bakun, W. H., R. M. Stewart, C. G. Bufe, and S. M. Marks, 1980, Implication of seismicity for failure of a section of the San Andreas fault, Bull. Seis. Soc. Am., v. 70, pp. 185-201.

Barka, A. A., and K. Kadinsky-Cade, 1988, Strike-slip fault geometry in Turkey and its influence on earthquake activity, Tectonics, v. 7, pp. 663-684.

Budding, K. E., and R. V. Sharp, 1988, Surface faulting associated with the Elmore Desert Ranch and Superstition Hills, California, earthquakes of 24 November 1987 [abs.], Seis. Res. Letts., v. 59, p. 49.

Burdick, L. J., and G. R. Mellman, 1976, Inversion of the body waves from the Borrego Mountain earthquake to the source mechanism, Bull. Seis. Soc. Am., v. 66, pp. 1485-1499.

Clark, M. M., 1972, Surface rupture along the Coyote Creek fault, U. S. Geol. Surv. Prof. Pap. 787, pp. 55-86.

Das, S., and K. Aki, 1977, Fault plane with barriers: a versatile earthquake model, J. Geophys. Res., v. 82, pp. 5658-5670.

Fett, D., 1968, Geophysical investigation of the San Jacinto Valley, Riverside County, California, M.A. Thesis, Univ. of Calif., Riverside, 50 p.

Fuis, G. S., W. D. Mooney, J. H. Healey, G. A. McMechan, and W. J. Lutter, 1982, Crustal structure of the Imperial Valley region, U. S. Geol. Surv. Prof. Pap. 1254, pp. 25-50.

Given, D. D., 1983, Seismicity and structure of the trifurcation in the San Jacinto fault zone, southern California, Masters Thesis, California State University, Los Angeles, 73 p.

Hamilton, R. M., 1972, Aftershocks of the Borrego Mountain earthquake from April 12 to June 12, 1968, U. S. Geol. Surv. Prof. Pap. 787, pp. 31-54.

Hanks, T. C., and M. Wyss, 1972, The use of body-wave spectra in the determination of seismic source parameters, Bull. Seis. Soc. Am., v. 62, pp. 561-589.

Hanks, T. C., J. A. Hileman, and W. Thatcher, 1975, Seismic moments of the larger earthquakes of the southern California region, Geol. Soc. Am. Bull., v. 86, pp. 1131-1139.

Hill, R. I., 1984, Petrology and petrogenesis of batholithic rocks, San Jacinto Mountains, southern California, Ph.D. Thesis, California Institute of Technology, 800 p.

Hubbert, M. K. and W. W. Rubey, 1959, Role of fluid pressure in the mechanics of overthrust faulting, Bull. Seism. Soc. Am., v. 70, pp. 115-205.

Kanamori, H., 1978, Use of seismic radiation to infer source parameters, U. S. Geol. Surv. Open-file Report 78-380, pp. 283-318.

Kanamori, H. and G. S. Stewart, 1976, Seismological aspects of the Guatemala earthquake of February 4, 1976, J. Geophys. Res., v. 83, pp. 3427-3434.

Kanamori, H., and P. C. Jennings, 1978, Determination of local magnitude, M_L, from strong-motion accelerograms, Bull. Seis. Soc. Am., v. 68, pp. 471-485.

King, G., and J. Nabelek, 1985, Role of fault bends in the initiation and termination of earthquake rupture, Science, v. 228, pp. 984-987.

King, N. E., and J. C. Savage, 1983, Strain rate profile across the Elsinore, San Jacinto, and San Andreas faults near Palm Springs, California, 1973-1981, Geophys. Res. Lett., v. 10, pp. 55-57.

Knuepfer, P. L. K., 1988, Implications of the characteristics of end-point of historical surface fault ruptures for the nature of fault segmentation, this volume.

Laughlin, H., R. Arnold, and W. S. W. Kew, 1923, Southern California earthquake of July 22, 1923, Bull. Seis. Soc. Am., v. 13, pp. 105-106.

Lindh, A. and D. M. Boore, 1974, The relation of the Parkfield foreshocks to the initiation and extent of rupture [abs.], Earthquake Notes, v. XLV, p. 54.

Lindh, A. G. and D. M. Boore, 1981, Control of rupture by fault geometry during the 1966 Parkfield earthquake, Bull. Seis. Soc. Am., v. 71, pp. 95-116.

Magistrale, H., and H. Kanamori, 1988, Superstition Hills earthquakes and basement structure of the western Imperial Valley [abs.], Seis. Res. Letts., v. 59, p. 48, 1988.

Matti, J. C., D. M. Morton, and B. F. Cox, 1985, Distribution and geologic relations of fault systems in the vicinity of the Central Transverse Ranges, southern California, U. S. Geol. Surv. Open-File Report 85-365, 23 p.

Merifield, P. M., T. K. Rockwell, and C. C. Loughman, 1987, Slip rate on the San Jacinto fault zone in the Anza seismic gap, southern California [abs.], Geol. Soc. Am. Abs. with Progs., v. 19, no. 6, pp. 431-432.

Mezger, L., and R. J. Weldon, 1983, Tectonic implications of the Quaternary history of lower Lytle Creek, southeast San Gabriel Mountains [abs.], Geol. Soc. Am. Abs. with Progs., v. 15, no. 5, p. 418.

Richter, C. F., 1958, Elementary Seismology, W. H. Freeman, San Francisco, 768 pp.

Sanders, C. O., 1986, Seismotectonics of the San Jacinto fault zone and the Anza seismic gap, Ph.D. Thesis, California Institute of Technology, Pasadena, 180 p.

Sanders, C. O. and H. Kanamori, 1984, A seismotectonic analysis of the Anza seismic gap, San Jacinto fault zone, southern California, J. Geophys. Res., v. 89, pp. 5873-5890.

Sanders, C., H. Magistrale, and H. Kanamori, 1986, Rupture patterns and pre-shocks of large earthquakes in the southern San Jacinto fault zone, Bull. Seis. Soc. Am., v. 76, pp. 1187-1206.

Segall, P., and D. D. Pollard, 1980, Mechanics of discontinuous faults, J. Geophys. Res., v. 85, pp. 4337-4350.

Sharp, R. V., 1967, San Jacinto fault zone in the Peninsular Ranges of southern California, Geol. Soc. Am. Bull., v. 78, pp. 705-730.

Sharp, R. V., 1972, Map of recently active breaks along the San Jacinto fault zone between the San Bernardino area and Borrego Valley, California, U. S. Geol. Surv. Misc. Geol. Invest. Map I-675.

Sharp, R. V., 1975, En echelon fault patterns of the San Jacinto fault zone, *in* Crowell, J. C. (ed.), San Andreas Fault in southern California, Spec. Rep. Calif. Div. Mines Geol. 118, pp. 147-154.

Sharp, R. V., 1981, Variable rates of Late Quaternary strike-slip on the San Jacinto fault zone, southern California, J. Geophys. Res., v. 86, pp. 1754-1762.

Sibson, R. H., 1984, Roughness at the base of the seismogenic zone: contributing factors, J. Geophys. Res., v. 89, pp. 5791-5799.

Sibson, R. H., 1985, Stopping of earthquake ruptures at dilational fault jogs, Nature, v. 316, pp. 248-251.

Sibson, R. H., 1986, Earthquakes and lineament infrastructure, Phil. Trans. R. Soc. Lond., v. 317, pp. 63-79.

Sibson, R. H., 1987, Effects of fault heterogeneity on rupture propagation, U. S. Geol. Surv. Open-File Rept. 87-673, pp. 362-373.

Sieh, K. E., 1978, Slip along the San Andreas fault associated with the great 1857 earthquake, Bull. Seis. Soc. Am., v. 68, pp. 1421-1448.

Sieh, K. E., and R. H. Jahns, 1984, Holocene activity of the San Andreas fault at Wallace Creek, California, Geol. Soc. Am. Bull., v. 95, pp. 883-896.

Thatcher, W., and R. M. Hamilton, 1973, Aftershocks and source characteristics of the 1969 Coyote Mountain earthquake, San Jacinto fault zone, California, Bull. Seis. Soc. Am., v. 63, pp. 647-661.

Thatcher, W., and T. C. Hanks, 1973, Source parameters of southern California earthquakes, J. Geophys. Res., v. 78, pp. 8547-8576.

Thatcher, W., J. A. Hileman, and T. C. Hanks, 1975, Seismic slip distribution along the San Jacinto fault zone, southern California and its implications, Geol. Soc. Am. Bull., v. 86, pp. 1140-1146.

Trifunac, M. D., and J. N. Brune, 1970, Complexity of energy release during the Imperial Valley, California, earthquake of 1940, Bull. Seis. Soc. Am., v. 60, pp. 137-160.

Wallace, R. E., 1973, Surface fracture patterns along the San Andreas fault, Stanford Univ. Publ. Geol. Sci., v. XIII, pp. 248-250.

Weldon, R. J. and K. E. Sieh, 1985, Holocene rate of slip and tentative recurrence interval for large earthquakes on the San Andreas fault in Cajon Pass, southern California, Geol. Soc. Am. Bull., v. 96, pp. 793-812.

Wesnousky, S. G., 1988, Seismological and structural evolution of strike-slip faults, Nature, v. 335, pp. 340-343.

Wesnousky, S. G., 1989, Earthquake size and the degree of fault trace complexity as a function of the total offset registered across major strike-slip faults in California, this volume.

Wesnousky, S. G., C. S. Prentice, and K. E. Sieh, 1987, Fault slip-rate determination on the northern segment of the San Jacinto fault, San Bernardino, California [abs.], EOS Trans. Amer. Geophys. Union, v. 68, p. 1506.

Wesson, R. L., and W. L. Ellsworth, 1973, Seismicity preceding moderate earthquakes in California, J. Geophys. Res., v. 78, pp. 8527-8545.

COMMENTS ON MODELS OF EARTHQUAKE RECURRENCE

C. H. Scholz
Lamont-Doherty Geological Obsevatory
and Dept. of Geological Sciences,
Columbia University, Palisades, N.Y., 10964

ABSTRACT

The recurrence of earthquakes on a given fault segment has been found to be quasi-periodic in the sense that the mean recurrence time is well-defined but there is a significant variation from the mean that is not a result of insufficient data. This variation appears to be intrinsic to the system and precludes accurate long range prediction. Various semi-empirical models that have been advanced to explain earthquake recurrence, and some of which may contain aperiodicity, are shown to be lacking in that they are not found to hold in all cases. A dynamic analysis of the earthquake loading-relaxation system also shows that these models generally lack rigor. A simple single degree of freedom system predicts strict periodicity, but because it is nonlinear chaotic behavior may be expected for some choices of parameters and friction functions. A simple four block model with heterogeneous friction and dynamic triggering exhibits a rich variety of behavior that resembles observed behavior in many aspects and points to some of the complexity that may occur in nature. These exercises indicate that in order to reduce the intrinsic uncertainty in recurrence time estimation a better understanding of the effects of initial conditions on earthquake rupture is needed.

INTRODUCTION

In a global study of the recurrence of large earthquakes that rupture a given section of fault or plate boundary, Nishenko and Buland (1987) found that the mean recurrence time is well-defined but that the earthquakes are not strictly periodic. They found that recurrence times may be described by a log normal distribution in which the standard deviation is a function of T, the recurrence time.

As an example, Sieh et al (1988) found that the last ten earthquakes on the San Andreas fault at Pallet Creek, California occurred with a mean recurrence time of 131± 1 yr, but that individual recurrence times ranged from 45 to 332 yr.

These studies show that earthquake recurrence is quasi-periodic, in that it has a well defined mean but also has a well-defined aperiodicity, or fluctuation from that mean. These fluctuations are not due to uncertainties in the determinations; Nishenko and Buland found that there is an intrinsic standard deviation $\sigma_D = 0.21$ in ln T, which is fundamental to the rupture process. As a practical matter, this means that there will always, regardless of the quality of data, be limitations on long range earthquake prediction, and that these limitations will grow with T.

It is easy to understand why the mean recurrence time is well-defined. Because earthquakes are a relaxation process, the strain energy in the system must be charged to some level above the relaxed state for an earthquake to occur, and since strain accumulation is slow, this puts a lower limit on recurrence time, and also means that it scales with the strain accumulation rate. Similarly, an upper limit on strain energy is a result of the finite strength of faults, and this sets an upper limit

on recurrence time, which will also scale with strain rate. Thus any relaxation model will predict that recurrence times will cluster around some mean that scales with the strain rate. A more important problem is to try to explain the intrinsic variability of the process, as expressed by σ_D. If this can be understood, it may be possible, in individual cases, to overcome this as a barrier to more precise long term prediction.

DISCUSSION OF PREVIOUS MODELS

When Reid (1910) discussed long range prediction, he espoused the principle that the next earthquake would happen when the strain released in the previous one had re-accumulated. This amounts to an assumption of constant fault strength. If the strain relaxed in an earthquake on a particular fault strand was also constant, then earthquakes on that strand would be perfectly periodic. Shimazaki and Nakata (1980), recognising that such strict periodicity does not occur, proposed two variations on Reid's model. In the first, called, "time-predictable", they assumed that the strength was constant but strain release was variable. In the second, called "size predictable", they assumed that strength was variable but that the base stress level, to which the stress was relaxed, was constant.

Empirical models based on observations of paleoseismicity introduce, as a variable, the length of fault that may be ruptured in a give eathquake (Sieh, 1981; Schwartz and Coppersmith, 1984). In the "variable slip" model, both the amount of slip in a given place and the length of the rupture may vary from earthquake to earthquake, but the net long term slip is uniform along the fault (or variable, as the case may be). In the "uniform slip" model, the latter two conditions hold but the slip at a given point is the same in each earthquake. Finally, in the "characteristic earthquake" model, the fault ruptures repeatedly in a series of "characteristic earthquakes", each identical, with the same slip distribution and length characteristic of the particular segment. In this last model, if the slip in a given earthquake is observed to vary along the fault, the long term slip rate must vary accordingly.

In order to discuss the question as to how well these models agree with observations, we need to examine cases where three or more earthquakes, of known slip, recurrence time, and length, have been known to have ruptured a single fault segment. There are only two such cases well enough documented for study: the Nankaido earthquakes of southwest Japan and the Parkfield earthquakes in central California.

The history of Nankaido earthquakes has been compiled by Ando (1975), and is shown in figure 1 as a plot of coastal uplift at Moroto Pt. for the last 1200 years. The actual uplift is known only for the three most recent events, the relevant data for which is given in table 1. An examination of the table shows simple proportionality between fault length and uplift, corresponding to a linear slip-length relationship found to be typical for large earthquakes (Scholz, 1982), so this same proportionality is used to estimate uplift for the events prior to 1707.

Table 1. Nankaido earthquake characteristics

	*1707	1854	1946	Ratio, last cycle/ previous cycle
Rupture Length, km	500	300	300	1.7
Uplift, Muroto Pt., m	1.8	1.2	1.15	1.5
Recurrence Interval, yr		147	92	1.6

* Refers to rupture of AB block, (see Ando, 1975)

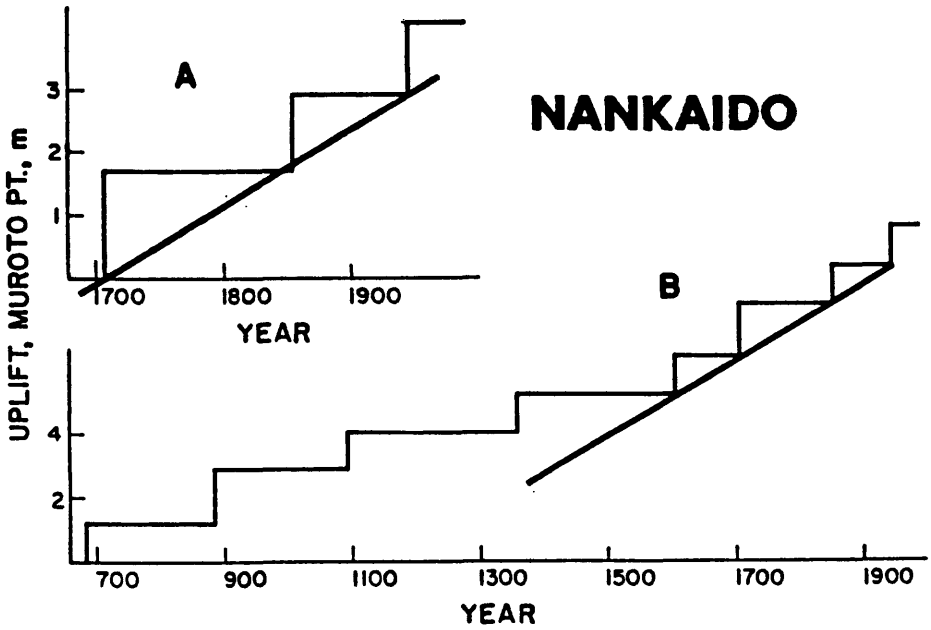

FIGURE 1. Slip history of Nankaido, Japan, earthquakes recorded as uplift at Muroto Point. In A the data as actually measured in the last three cycles. In B the data are extended back in time using Ando's (1975) history and a linear relation between slip and length. Heavy lines indicate constant long term slip rates, according to the time-predictable model.

A constant uplift rate line has been fit to the post-1605 data in fig. 1a, which it fits very well. Prior to that time there is a marked discrepancy, with the average recurrence time of the earthquakes being about twice that of later times. This is probably an artifact of the data base, indicating that the historic record before 1605 is incomplete, which would not be surprising since Japan was in a protracted state of civil war over much of that period. The last three earthquakes, for which the data are quite reliable, show a constant mean uplift (slip) rate but are decidedly aperiodic.Shimazaki

and Nakata (1980) showed that the recurrence of these earthquakes are consistent with the "time predictable" model, as indicated by the solid line in Fig. 1a.

The Parkfield segment of the San Andreas fault has been known to have ruptured six times in the last 130 years. These earthquakes occur almost periodically with a mean recurrence time of 22 years. However, a major exception was the earthquake of 1934, which occurred just 12 years after the previous event in 1922. These two events, plus the most recent earthquake, of 1966, were instrumentally recorded and found to be of identical size (within 25% in moment), hence the explanation of this aperiodicity cannot rest with either of the models suggested by Shimazaki and Nakata (Bakun and McEvilly, 1984). Since a significant fraction of the moment release in the Parkfield segment is accomplished by aseismic slip, it is possible that a time variation of the partition between aseismic and seismic slip may explain this discrepancy. Bakun and McEvilly presented a variety of such ad hoc models in an attempt to explain the 1934 earthquake, but no data is available to test them. Bakun and Lindh (1985) suggested a model in which there are two critical failure strengths.

A general observation of paleoseismic studies is that the slip in earthquakes observed at a given site tend to be characteristic of that site (Sieh, 1981; Schwartz and Coppersmith, 1984). Hence those authors have argued that the "uniform slip" or "characteristic earthquake" model are correct descriptions of earthquake recurrence. However the Nankaido case shows that both the amount of slip at a given place and the length of rupture may vary, so these models, while they may be adequate rules of thumb for certain faults or fault segments, do not provide any fundamental constraints of the physics of the process. Similarly, the Parkfield recurrence series does not agree with the "time predictable" model, so that, if we are unwilling to advance an ad hoc explanation for that case, we cannot treat that model as fundamental either. In any case, such models do not explain the physical bases for the assumptions that underly them. In the next section we explore, in a preliminary way, some physical models for recurrence and discuss how aperiodicity could arise.

COMMENTS ON PHYSICAL RECURRENCE MODELS

Dynamic Analysis

Models such as the time predictable and slip predictable ones are essentially kinematic; one does not know if they correspond to any real dynamic system with realistic friction properties. To examine the question of earthquake recurrence we need to look more closely at the dynamics of the entire system. Consider a simple model of the system to be that shown at the top of figure 2, in which a mass-slider restrained by a spring rides on a conveyor belt that moves at a constant velocity v_{pl}. The velocity of slip between the mass and belt is

$$\dot{s} = \dot{\xi} - v_{pl} \qquad (1)$$

where ξ is the departure from the unstretched position of the spring. A force diagram is shown in the middle of Figue 2, in which the force in the spring, $-k\xi$ is resisted by a friction force Φ. The friction force is assumed to be a function of slip velocity $\dot{s}$, in which a negative velocity

dependence (velocity weakening) is assumed at low velocities in order that an instability occurs, and positive (velocity strengthening) at high velocities, as shown in the lower part of the figure.

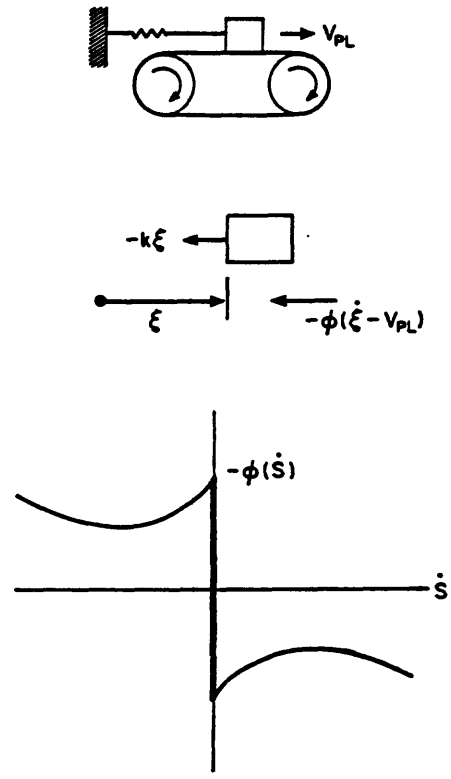

FIGURE 2. A one degree of freedom model of the loading-relaxation cycle. See text for description.

These friction characteristics agree with those observed in laboratory studies of rock friction (e.g. Blanpied et al., 1987). The friction force - $\Phi(\dot{s})$ rises to some critical value as the spring is extended at the rate v_{pl} and then slip begins, meeting at first a reduced resistance that leads to an instability if k is less than a critical value. The equation of motion of the block is

$$m\ddot{\xi} + \Phi\left(\dot{\xi} - v_{pl}\right) + k\,\xi = 0 \qquad (2)$$

This system is a classical one in nonlinear dynamics, being first introduced by Rayleigh (1877) to analyse the action of a bow on a stringed instrument, and its solution is often used as an example in standard texts on the subject (eg. Stoker, 1950). The phase portrait of the system is shown in figure 3. Dynamic analysis shows that the phase plane contains a focal point repellor (solid dot) within a periodic attractor (dark curve). Thus if the system starts from any initial state on the phase plane either inside or outside the attractor it will converge on it, as shown be the light

curves with arrows. Once on the attractor the system will stay on it and will cycle clockwise. Point 1 to 2 is the loading portion, when the block is stuck to the conveyor, and hence moves at v_{pl}. Point 2 is the point of critical friction where slip begins, and the loop during dynamic slip, from 2 back to 1, where locking re-occurs, depends only on the form of $\Phi(\dot{s})$ and the spring stiffness k. (the velocity scale during this loop is greatly supressed, for diagrammatic purposes). The stress-drop, from state 2 to 1, is constant. This is a typical example of a limit cycle, and it is strictly periodic. An analysis of this system using a single state variable friction law has been given by Rice and Tse (1986).

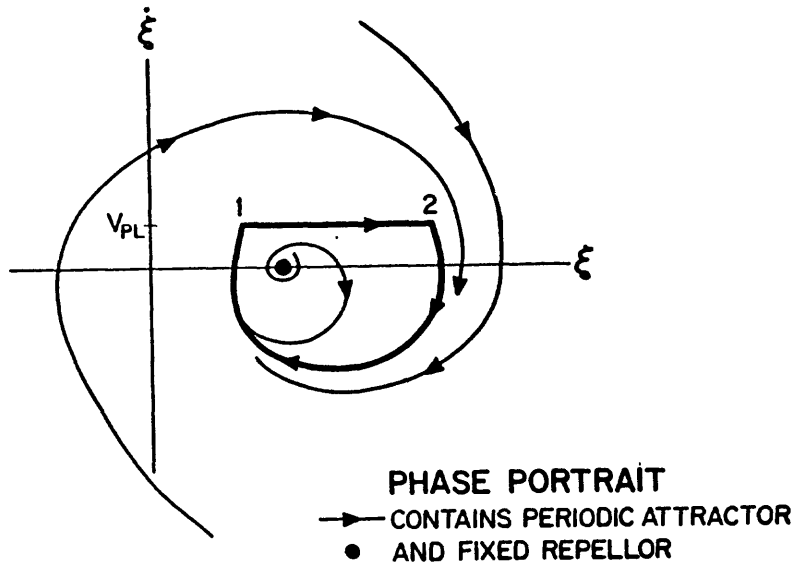

FIGURE 3. Phase portrait for the periodic solution to the dynamic system.

The observations reviewed in the previous section do not seem to support this simple model; indeed some important exceptions to exact periodicity have been noted. This should not be too surprising, however. This model system has only one degree of freedom and would only be expected to apply if the friction and loading rate is uniform over the fault. For an extended fault, this need not apply: many reasons may be cited for expecting that fault friction is spatially variable. In the case of spatially variable friction, the critical stress is only reached at one point in the quasi-static loading process (the hypocenter); the rest of the fault is ruptured by dynamic triggering.

A Coupled Model

Let us now try another simple model in which there is spatially varying friction with dynamic triggering. Consider a fault composed of segments in which each segment obeys a slip (or velocity) weakening friction criterion such as shown in figure 4. Each segment in the model has a different value of σ_y, the critical stress for sliding. The applied stress, σ_1, increases with tectonic loading. Assume that during dynamic slip the friction drops to a dynamic value that is a constant

fraction of the strength, i.e. $\sigma_f = \gamma\sigma_y$, and that no overshoot occurs so that the final stress equals σ_f.

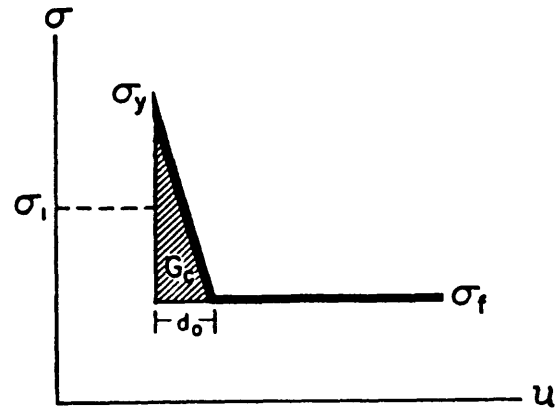

FIGURE 4. A simple slip-weakening friction law used in the coupled system.

Consider two adjacent segments, on designated ' and one ". There are two rupture criteria, a quasistatic on when a segment ' ruptures when $\sigma_1' = \sigma_y'$ and a dynamic one when slip on the ' segment is triggered by rupture of an adjacent " segment when

$$S' = \left(\frac{\sigma'_y - \sigma'_1}{\sigma''_1 - \sigma''_f} \right) < 1 \qquad (3)$$

where the critical S value chosen indicates a moderate triggering sensitivity (see Das and Aki, 1977; Andrews, 1985). Assume, as an example, a four segment fault with σ_y values 5,11,3, and 13, consecutively along the fault, and $\gamma = 0.8$. Start with $\sigma_1 = \sigma_f$ in all segments and load them at the same rate.

The result is shown in figure 5. Five different sized earthquakes are produced, and a complete cycle of the model, as shown, from one initial state to the same initial state, is a great deal longer than the recurrence time of a single event. Notice that the stronger segments act as "barriers" and resist slip most of the time, but when they rupture they act as "asperities" and trigger the adjoining segments. The long term slip is the same in all segments, and the slip in each segment tends to have a characteristic value, but this is not the "characteristic earthquake" model because earthquakes of different length are produced. It is close to the "uniform slip model", but not quite the same. Notice that the slip and recurrence time in the segment "5" alternates as 5,4. So the slip in this segment is not constant or periodic. This segment behaves, to a certain extent, like the "variable slip" model, but with only slight departures from its characteristic slip value.

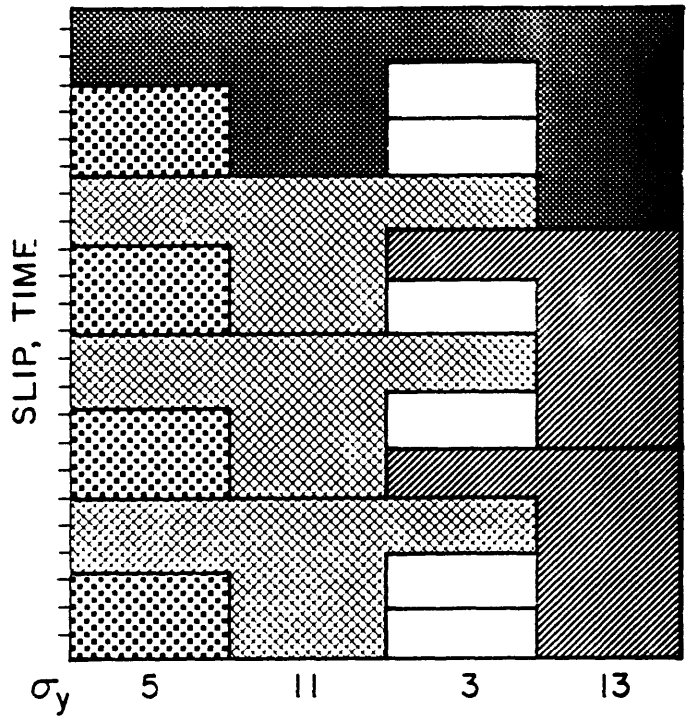

FIGURE 5. Results of one full cycle of the coupled model.

DISCUSSION

The geological data discussed by Sieh (1981) and Schwartz and Coppersmith (1984) seem consistent with the coupled model, but are not definitive one way or the other. Slip in each event is not determined better that about 20%, and the radiocarbon dating method cannot establish synchrony in rupture, so that the measurement precision is not sufficient to test the model. However what is demonstrated is that even a very simple heterogeneous fault model can produce a fairly rich behavior that on the whole is aperiodic and may be aperiodic even within a given homogeneous segment. Yet each segment can obey the dynamics of equation 2, with mild coupling between them. A physical model of this sort has been explored experimentally and numerically by Burridge and Knopoff (1967), and Cao and Aki (1984). A more thorough study of the stability of a two block model was made by Nussbaum and Ruina (1987).

Can this model explain the subtantial variation in slip and recurrence time demonstrated for the Nankaido earthquakes? This does not seem possible because in all three cases listed in table 1 the adjacent CD region also ruptured, so changes in triggering conditions did not occur. The coupled model, in which a region can be triggered prematurely to produce a smaller slip event, should follow the predictions of the slip predictable model, yet the Nankaido events seem to obey the time predictable model. In any case it does not seem likely that very great departures from periodicity can be produced by this mechanism, because that would require strong triggering (at

much higher critical values of S, eq. 3). The robustness of seismic gaps in surviving throughout much of their cycle indicates that they are not so easily triggered.

If we consider that the Nankaido case demonstrates slip variability of a greater degree than may be explained by the above, we may then ask the question: are either of the two proposed variable slip models, time-predictable and slip-predictable, consistent with the dynamic system of figure 2? The simple answer, if these models are interpreted in terms of the loading histories as shown by Shimazaki and Nakata, is that they are not. This is because this dynamic system is characterized by two fixed critical stresses, at states 1 and 2, whereas these models require variation in one or the other of these. However, the data in table 1 suggest another possibility. Notice that the ratio of the length of the 1707 event to the later ones is the same as that of the corresponding uplifts at Muroto Pt. and of the recurrence times. This indicates that the slip is proportional to fault length, which seems to be a general property of large earthquakes, as noted before. If we now interpret this with an L-model, discussed by Scholz (1982), we infer that these earthquakes had variable slip but the same stress-drop. This interpretation makes the time-predictable model consistent with the dynamic system of figure 2. The variation of slip arises from the variations of fault length, this being the equivalent of changing spring constants for different relaxations (which rescales the abscissa of fig. 3). Two fixed critical stresses are still present. The slip-predictable model, on the other hand, cannot be so rationalized to be compatable with this dynamic system, except to the limited extent allowed by dynamic triggering.

We may also consider the effect of variable loading rates, v_{pl}, as discussed by Thatcher (1984b). The effect of nonlinearity in the loading cycle discussed by him can be incorporated in the dynamic model by using a soft (nonlinear) spring. This distorts the shape of the attractor but does not change its periodic nature. This effect therefore makes extrapolation of geodetic data to determine the recurrence time more difficult, but otherwise does not change the basic behavior. Irregular transients in crustal deformation may also prematurely trigger earthquakes (Thatcher, 1982), but we don't consider these a general mechanism for the aperiodicity that seems to occur.

A rather more drastic possibility exists. For nonlinear equations such as 2 it is notoriously difficult to prove that the solution obtained is unique and that it characterizes the phase space for all choices of parameters. In many cases chaotic behavior occurs over some range of parameters, and this is both aperiodic and unpredictable. For example, in the case of the van der Pol equation, which is similar to equation 2 but with a different characteristic, it is known that forced periodic oscillations will produce chaotic behavior (Hubermann and Crutchfield, 1979). More to the point, Gu et al. (1984), in their study of the system of figure 2 with a two state variable friction law, observed chaotic behavior near the critical stiffness. This shows that, depending on the exact form of Φ, chaotic behavior is possible over some part of the phase space for this system. Since we do not actually know the correct form of Φ as it applies to the real case, this leaves open the possibility that earthquake recurrence is truly unpredictable in the strict sense.

Of course the orbits of strange attractors depart only gradually from one cycle to the next, so that if one knows the initial conditions one may be able to predict a single cycle reasonably well. However, the spatial heterogeniety of faults introduces many degrees of freedom, so that considerable uncertainty in the outcome should always be expected. Put a simpler way, if one has a good knowledge of the past rupturing history of a section of fault, one may be able to estimate the approximate time of the next rupture, but still not know how far, once initiated, that rupture will propagate.

This discussion has not taken us very far, but it does focus on one salient point. The intrinsic uncertainty in earthquake recurrence, denoted σ_D by Nishenko and Buland, probably reflects variations in initial conditions between different earthquakes, such as occurred in the coupled model we have explored. If we can learn more about the dependence of earthquakes on

their initial conditions we should be able to reduce this uncertainty considerably for individual cases.

ACKNOWLEDGEMENTS

This paper was written while the author was a visitor at the Geology Department of the Victoria University of Wellington, New Zealand, aupported by NSF grant INT 86-00401. I thank B. Raliegh and D. Simpson for helpful reviews. Lamont-Doherty Geological Observatory publication no. 4368.

REFERENCES CITED

Ando, M., 1975, Source mechanisms and tectonic significance of historic earthquakes along the Nankai trough, Japan: Tectonophysics, v. 27, p. 119-140.

Andrews, J., 1985, Dynamic plane strain shear rupture with a slip weakening friction law calculated with a boundary integral method: Bulletin of the Seismological Society of America, v. 75, p. 1-21.

Bakun, W.H. and McEvilly, T.V., 1984, Recurrence models and Parkfield, California, earthquakes: Journal of Geophysical Research, v. 89, p. 3051-3058.

Bakun, W.H. and Lindh, A., 1985, The Parkfield, California earthquake prediction experiment: Science, v. 229, p. 619-621.

Blanpied, M., Tullis, T., and Weeks, J., 1987, Frictional behavior of rock at low and high sliding velocity: Geophysical Review Letters, v. 14, p. 554-557.

Burridge, R. and Knopoff, L., 1967, Model and theoretical seismology: Bulletin of the Seismological Society of America, v. 57, p., 341-371.

Cao, T. and Aki, K., 1984, Seismicity simulation with a mass-spring model and a displacement hardening-softening friction law: Pageoph, v. 122, p. 10-23.

Das, S. and Aki, K., 1977, Fault plane with barriers: a versatile earthquake model: Journal of Geophysical Research, v. 82, p., 5658-5670.

Gu, J.-C., Rice, J.R., Ruina, A.L., and Tse, S.T., 1984, Slip motion and stability of a single degree of freedom elastic system with rate and state dependent friction: J. Mechanics and Physics of Solids, v. 32, p., 167-196.

Hobbs, B.E., 1988, Chaotic behavior of frictional shear instabilities: 2nd International Symposium of rockbursts and seismicity in mines, Minneapolis, June, 1988, in press.

Huberman, B.A. and Crutchfield, J.P., 1979, Chaotic states of anharmonic systems in periodic fields: Physical Review Letters, v. 43, p., 1743-1746.

Nishenko, S. and Buland, R., 1987, A generic recurrence interval distribution for earthquake forecasting, Bulletin of the Seismological Society of America: v. 77, p. 1382-1399.

Nussbaum, J., and Ruina, A., 1987, A two-degree-of-freedom earthquake model with static/dynamic friction: Pageoph, v. 125, p., 629-656.

Rayleigh, 1877, The Theory of Sound, Dover: New York.

Rice, J.R., and Tse, S.T., 1986, Dynamic motion of a single degree of freedom system following a rate and state dependent friction law: Journal of Geophysical Research, v. 91, p., 521-530.

Scholz, C.H., 1982, Scaling laws for large earthquakes: consequences for physical models, Bulletin of the Seismological Society of America, v. 72, p., 1-14.
Schwartz, D.P. and Coppersmith, K., 1984, Fault behavior and characteristic earthquakes: examples from the Wasatch and San Andreas faults: Journal of Geophysical Research, v. 89, p., 5681-5698.
Shimazaki, K., and Nakata, T., 1980, Time-predictable recurrence model for large earthquakes: Geophysical Research Letters, v., 7, p. 279-282.
Sieh, K., 1981, A review of geological evidence for recurrence times of large earthquakes, *in* Earthquake Prediction: an International Review, M. Ewing Ser. 8 (ed. D. Simpson and P. Richards), American Geophysical Union, Washington D.C., pp. 209-216.
Sieh, K., Stuiver, M., and Brillinger, D., 1988, A very precise chronology of earthquakes produced by the San Andreas fault in Southern California: preprint.
Stoker, J.J., 1950, Nonlinear Vibrations: Interscience, New York, 273 p.
Thatcher, W., 1982, Seismic triggering and earthquake prediction: Nature, v. 299, p. 12-13.
Thatcher, W., 1984, The earthquake deformation cycle, recurrence, and the time-predictable model: Journal of Geophysical Research, v. 89, p. 5674-5680.

Paleoseismicity, Persistence of Segments, and Temporal Clustering of Large Earthquakes -- Examples from the San Andreas, Wasatch, and Lost River Fault Zones

David P. Schwartz
U.S. Geological Survey
Menlo Park, CA 94025

INTRODUCTION

Faults are geometrically and mechanically segmented at a variety of scales. The rupture of fault lengths of tens to hundreds of kilometers represent the greatest hazard and results in sufficient surface deformation to allow fault behavior to be tracked through time. The ability to identify those parts of a fault that behave as independent seismogenic sources is an essential element in the evaluation of seismic hazards. Ideally, the repeated occurrence of moderate to large earthquakes along a fault zone could show the degree to which ruptures repeat spatially and with regard to slip distribution, adjacent segments rupture together, ruptures are arrested at or bypass apparent structural or geometric barriers, and subsegments rupture to produce events smaller than the expected maximum or characteristic earthquake. However, there are few shallow crustal faults that have had repeated historical surface faulting. Therefore, paleoseismic data, particularly the timing of past events, slip per event, and slip distribution along the length of a fault are critical for defining persistent rupture segments and segment boundaries and for modeling earthquake recurrence.

An important observation from paleoseismicity studies is that for many faults the amount of slip at a point on the fault is essentially the same during successive events. This led Schwartz and Coppersmith (1984) to suggest that major stress release on faults occurs as repetition of essentially the same size or characteristic event. An implication of repeated similar slip distribution is that the same fault length, or rupture segment, is involved. Paleoseismicity data from three recent and ongoing studies are summarized below. These provide new observations for addressing uncertainties, complexities, and variability in fault behavior, especially the persistence and nature of fault segments and their boundaries, and aspects of earthquake recurrence.

SEGMENTATION MODELS

Figures 1 and 2 show conceptual models of segmentation and slip distribution for strike-slip and normal faults, respectively. Figure 1 is for large earthquakes on strike-slip faults. It is inspired, in part, from observations that *a)* for many long surface ruptures, such as those in 1857 and 1906 on the San Andreas fault and in 1940 on the Imperial fault, coseismic slip varies along long lengths of fault and *b)* the amount of point-specific slip per event repeats. In *1a*, point-specific slip, rupture length, and earthquake magnitude are variable and there are no persistent segments. In *1b*, slip along a master segment (for example, 1857) repeats periodically. Regions of low slip in the large event define independent subsegments that fill in with smaller, more frequent earthquakes. The amount of slip during successive events could be similar or variable. Segment boundaries would be associated with locations of slip steps. This type of segmentation and the recurrence associated with it would be expressed paleoseismically by variability in the number and timing of events at points on a fault and by constant slip rate along its length. In *1c*, the slip distribution during a large event repeats itself in successive earthquakes. Overlap occurs toward the end of the segment. Lengths of fault with low slip do not define seismogenically independent segments. Displacement per event at any point along the fault is essentially constant. Paleoseismically, the timing of events is the same but slip rate would vary systematically along the fault. This variation is explained by off-fault deformation whereby the volume of crust surrounding the fault responds to a uniform deformation rate; however, some of the slip is partitioned into folds and other faults. Consequently, the slip rate is maintained across the volume but slip variability accumulates on individual structural elements. Figure *1d* expands on *1c*. Here, the slip distribution of two large events nucleating at A and B, and a zone of overlap, are shown. This is expressed paleoseismically by more frequent events in the overlap zone. These could be closely spaced in time, reflecting the close timing of events at A and B. In this case, the overlap zone is <u>not</u> an independent source of earthquakes, but is driven by the recurrence at nucleation sites A and B.

Figure 2 shows several possible segmentation models for normal faults. The amount of displacement per event for these can be tracked through time more easily than it can be for strike-slip faults, largely because scarp-derived colluvial wedges from individual earthquakes are generally well-preserved, easily recognizable, and provide, along with scarp profiles, information on the amount of coseismic slip. Typically, the amount of point-specific displacement repeats (Figure 3) and locations of low slip, especially near the ends of the rupture, do not fill in during subsequent events. Long-term slip rates vary systematically along the fault segment and are frequently lowest near segment boundaries (often coincident with the ends of ranges). In *2a* the repeated difference in timing of events along a fault zone is a strong basis for interpreting independent rupture segments and persistent segment boundaries. In *2b* and *2c* paleoseismic recurrence data would suggest similar behavior although the actual segmentation is different. In neither case is the segment boundary a permanent feature. In *2b*, the fault behaves primarily as a master segment with a subsegment that is also an independent seismic source. In *2c*, adjacent segments are independent but slip on one may trigger slip on the other, which later fails, possibly soon thereafter, as a separate source. A major difference is that in *2b* the fault is capable of producing larger earthquakes than in *2c*. In *2d*, segments are independent but closely coupled in

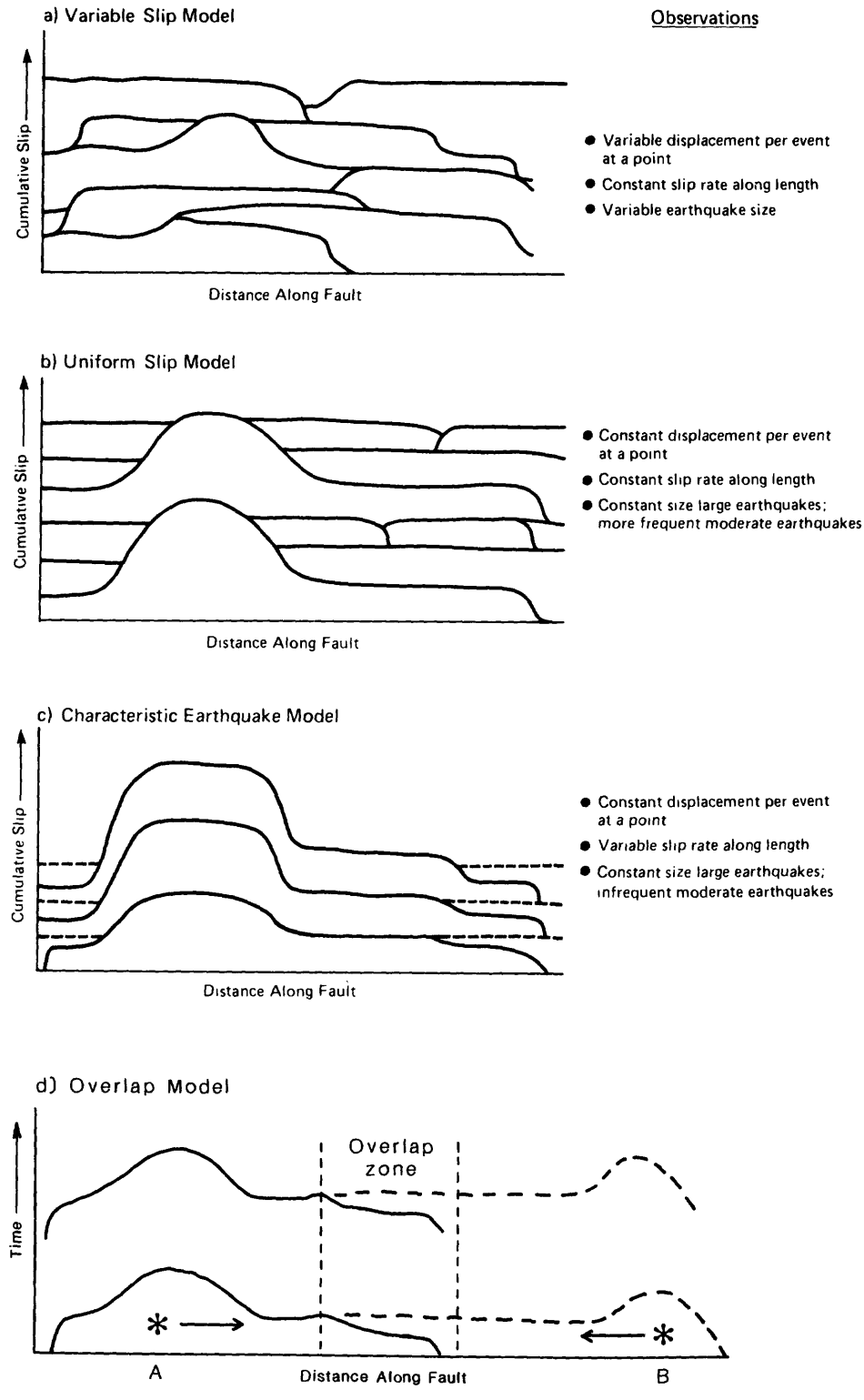

Figure 1. Conceptual segmentation - slip distribution - recurrence models for strike slip faults. *A* - *C* from Schwartz and Coppersmith (1984). *D* is expansion of *C*.

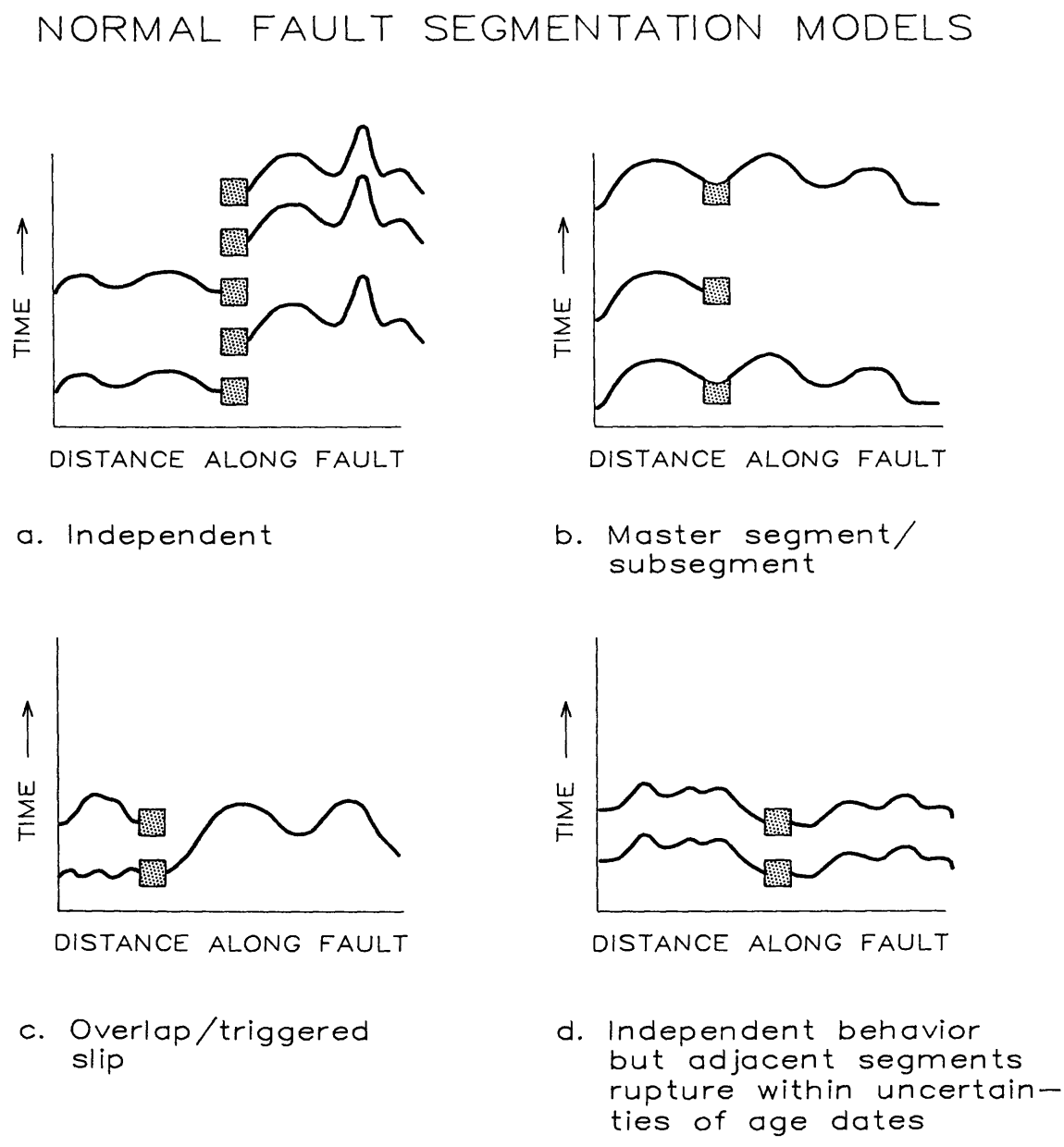

Figure 2. Segmentation models for normal faults. Curvilinear lines are hypothetical slip distributions during a single event. Stippled boxes are segment boundaries/barriers.

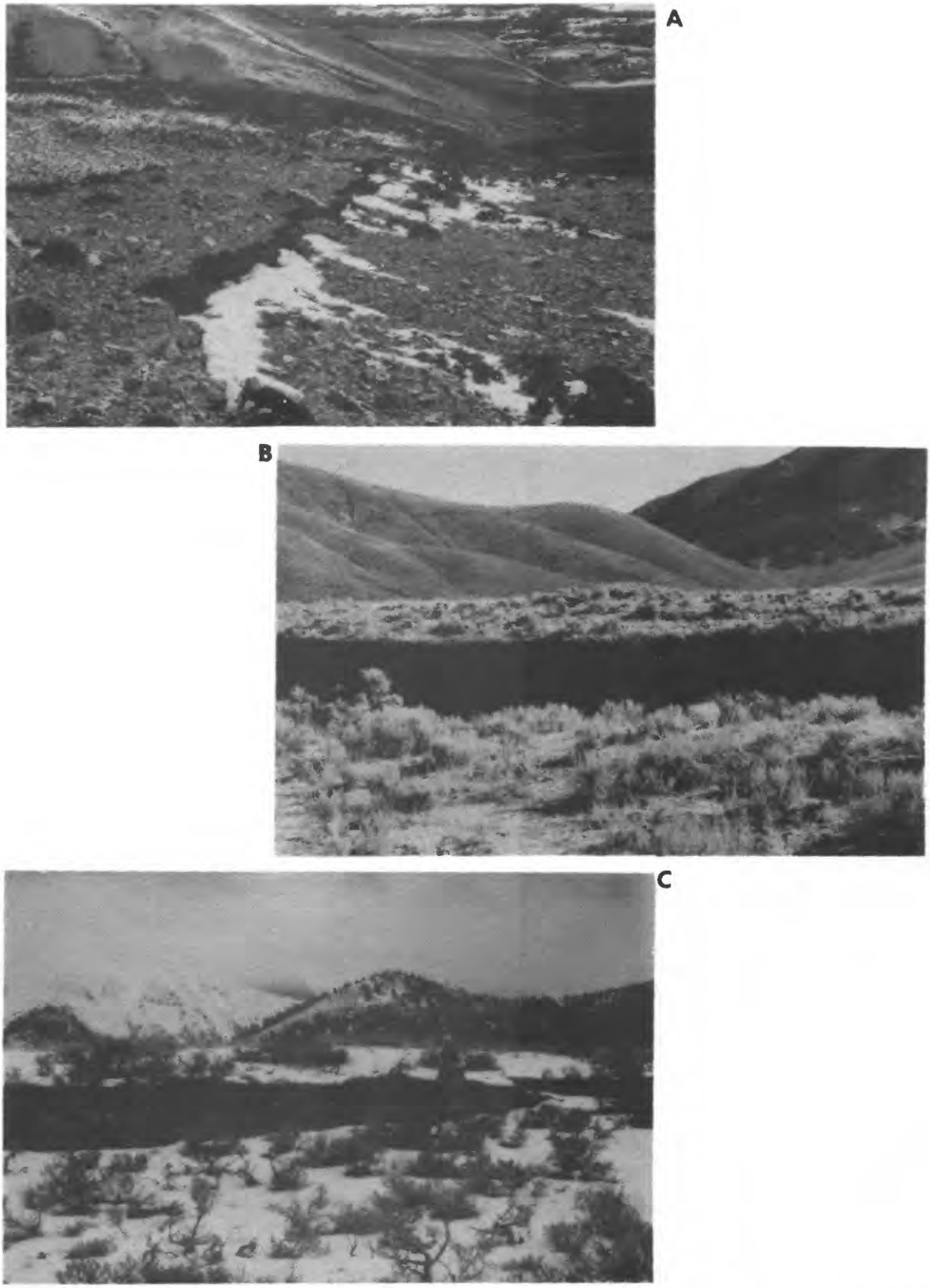

Figure 3. Photographs showing similarity in amount of surface faulting during 1983 Borah Peak earthquake and the prior event. *A)* Scarplet of about 25 cm is coincident with a minor break in slope defining pre-1983 displacement of same amount; *B)* 1.8-m-high scarp (in shadow) at Doublespring Pass Road with degraded scarp of about same height from pre-1983 event; *C)* 1.0-m-high scarp near Arentson with similar sized pre-1983 scarp (covered by snow) on top.

time, making distinction of separate events and independent segments difficult within the resolution of age-dating techniques. This could also result in overestimation of the size of a paleoearthquake.

SOUTH CENTRAL SAN ANDREAS FAULT

We are presently working to develop a better understanding of segmentation along the south central San Andreas fault. The 1857 surface faulting on the south central San Andreas fault extended from the vicinity of Parkfield to just north of Cajon Creek *(CC)*; it nucleated in the Parkfield-Carrizo Plain area (Sieh and Jahns, 1984) (Figure 4). The northern boundary of the rupture is the general transition zone from locked to creeping section; the southern boundary occurs within the general area of structural complexity associated with the confluence of the San Andreas and San Jacinto faults. Slip distribution estimated for the 1857 event on the basis of gully offsets (Sieh, 1978*a*) suggests that 9-10 m occurred in the Carrizo Plain, and 4-1/2 m occurred between Three Points *(TP)* and Cajon Creek *(CC)* on the section of the fault commonly referred to as the Mojave segment. The variable slip distribution has been used as the basis for dividing the 1857 rupture into three separate segments that are referred to as Cholame, Carrizo, and Mojave. Each has been assigned an independent behavior for probabilistic hazard analysis (Sykes and Nishenko, 1984; Working Group, 1988).

New dating of events raises intriguing questions about the nature of segmentation along the south central San Andreas. At Pallett Creek *(PC)* the event prior to 1857 (event X of Sieh, 1978*b*) now has a revised radiocarbon age of 1785±32 (Sieh and others, 1989). Dendrochronological studies on trees along the fault at Wrightwood *(W)* suggest an event in 1812 (Jacoby and others, 1988). Sieh and others (1989) correlate this with event X. The lateral extent of the 1812 rupture zone is unknown. Single-event pre-1857 stream offsets of at least 4-5 meters have been mapped between Lake Hughes and Cajon Creek (Sieh, 1978*a*; Sieh and Jahns, 1984). We have observed and are reevaluating these in the Littlerock and Leona Valley areas, which are located 35 km and 70 km, respectively, north of Wrightwood. If these offsets are from 1812, the large amount of displacement would be consistent with a rupture length of many tens to possibly a few hundred kilometers. Figure 4 shows two possible interpretations. In *4a* the 1812 event nucleates outside of the Mojave segment, possibly in the San Gorgonio Pass area (star) and extends an unknown distance north of Pallett Creek. The 1857 rupture overlaps it (stippled area). In this scenario the Mojave is not an independent rupture segment but rather a broad overlap zone between long rupture segments, as suggested by Schwartz and Coppersmith (1984) and implied by Sieh and Jahns (1984). In *4b* the 1812 event extends from Cajon Creek to Three Points, defining an independent segment along the low slip section of events such as the 1857 rupture. In this case the reach between Cajon Creek and San Gorgonio Pass is also a separate segment. Paleoseismic observations at Cajon Creek (Weldon and Sieh, 1985) suggest the elapsed time for this part of the fault could date back past 1812.

The final chapter remains to be written on San Andreas segmentation. The 1857 rupture segment should be considered a master segment that periodically slips to produce large 1857-type events. However, present data on historical surface faulting, paleoseismicity, fault

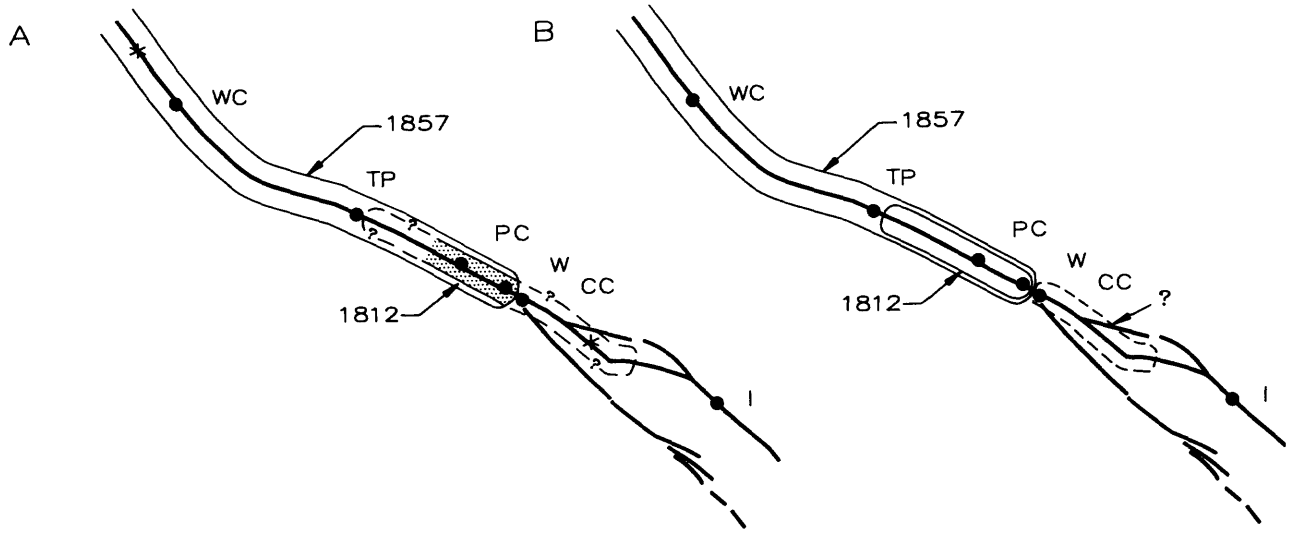

Figure 4. Alternative segmentation models for the south central San Andreas fault. *A)* 1857 and 1812 earthquakes nucleate outside of Mojave segment (stars) and the surface ruptures overlap; *B)* Mojave is an independent segment; San Bernardino (dashed line) also ruptures as an independent segment.

geometry and structural geology do not provide strong constraints on whether low slip sections of the 1857 rupture behave as independent seismic sources. A sequence of late Holocene slip rates along the length of the Mojave segment, better constraints on slip per event, and additional recurrence interval sites would go a long way toward resolving questions of the lateral extent of ruptures and persistence of segments. This is extremely important from a seismic hazards perspective because alternative segmentation models will strongly effect probabilistic hazards analysis.

Although the persistence of rupture segments remains in question, the available recurrence data provide a basis for some intriguing speculation on the large-scale behavior of the fault zone. Large events on adjacent segments in 1812 and 1857 and, jumping the central creeping section, 1906 have ruptured a major percentage of the fault zone in a short period of time. Sieh and others (1989) interpret the timing of earthquakes at Pallett Creek as clusters of two and three events separated by intervals of 200 to 350 years. Also, Prentice (1989) suggests that recurrence of large events along the 1906 rupture near Point Arena is about 200-400 years. These observations, if correct, suggest to me that recurrence on the San Andreas reflects temporal clustering controlled, in large part, by the longer recurrence of strong slip patches (sections with large surface offset such as the Carrizo Plain) that fail more or less sequentially during a short period of time. Superimposed on this broad framework would be localized variability at ends of long ruptures, at slip steps, or at zones of structural complexity.

WASATCH FAULT ZONE

Figure 5, which is based on published data and work in progress, shows the present version of a still-evolving understanding of segmentation and the space-time distribution of large magnitude (M 7 - 7-1/2) earthquakes on the Wasatch fault during the past 6000 years (see also Machette and others, this volume). The initial Wasatch segmentation model (Schwartz and Coppersmith, 1984) proposed five active, independent rupture segments. It was based on observed differences in the timing of events at points on the fault and on projecting these differences along strike to major geometric and structural changes (salients, *en echelon* steps, gaps in Holocene surface faulting, major changes in strike, intersections with transverse structures), which were interpreted as segment boundaries. Additional trenching (Personius in Machette and others, 1987) has resulted in division of the original Ogden segment into the Brigham City and Weber segments. There now appear to be six independent active rupture segments which, from south to north, are called Levan, Nephi, Provo, Salt Lake, Weber, and Brigham City.

Examination of the best estimate of the age of the most recent event shows that there are differences in timing between adjacent proposed segments. There are even greater differences when the timing of events prior to the most recent is compared. The paleoseismic observations of differences in timing of repeated earthquakes provide a strong basis for proposing a segmentation model for this fault zone.

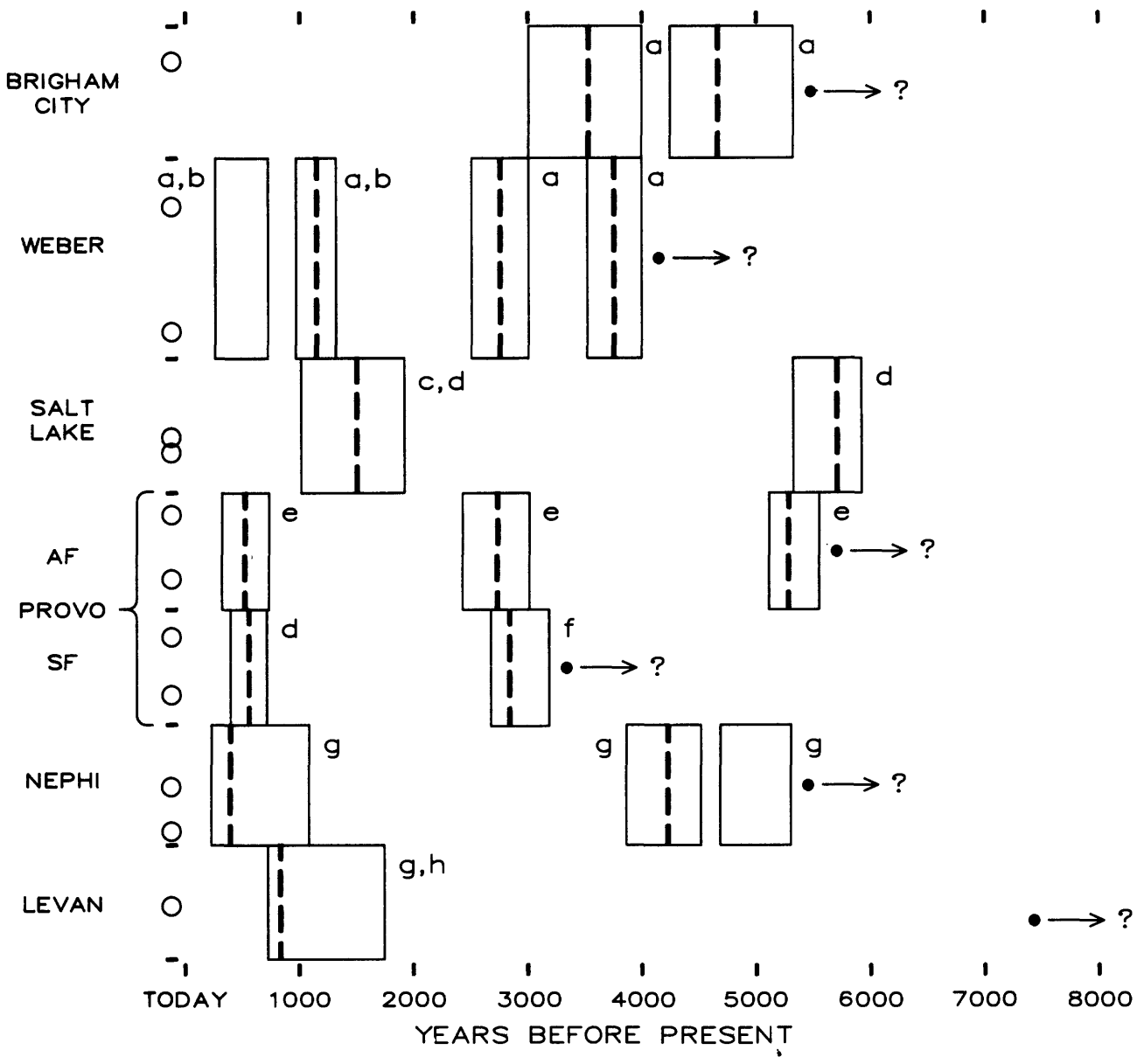

Sources of data: a. Machette and others (1987), modified in this report. b. Swan and others (1980), c. Lund and Schwartz (1986), d. Schwartz and others (1988), e. Forman and others (1989) f. Schwartz and Lund (unpublished field data) g. Schwartz and Coppersmith (1984), h. Jackson (1988)

Figure 5. Space-time diagram of large magnitude, scarp-forming earthquakes on the Wasatch fault zone during the past 6,000 years. Heavy dashed line is best estimate of timing of event. Box is uncertainty in date. Small circles along segment axis show locations of trenches. Arrow with query indicates that there is no additional information on timing of older events at that location.

The Provo segment has been a source of uncertainty. As age estimates change during field investigations, it has been interpreted as one segment, three segments, and then two segments. Figure 6 shows two subsegments named American Fork (AF) and Spanish Fork (SF). The timing of the most recent event is extremely close, 500 and 600 years respectively, and the uncertainties in the dates overlap. The same is true of the penultimate event. These could very well be the same earthquake. The preferred interpretation is to consider American Fork and Spanish Fork as comprising a single Provo segment, with the possibility that there are two independent segments having events that are very closely spaced in time.

Of particular interest is the temporal clustering of large earthquakes expressed by rupture of almost the entire fault zone between about 300 and 1500 years ago (Machette and others, 1988; Schwartz and others, 1988). The only segment that has not produced an event during the present cycle is Brigham City. It produced events about 3500 and 4700 years ago, similar to the other segments (especially Nephi). Within the framework of the Wasatch segmentation model and the present sequence of events, the Brigham City segment appears to be a leading candidate for the next large Wasatch earthquake.

LOST RIVER FAULT ZONE

Segmentation of the Lost River fault zone was initially discussed by Scott and others (1985) (see also Crone and Haller, this volume). Our present studies are focusing on details of timing and segmentation along the proposed Mackay, Thousand Springs, and Warm Spring segments (Schwartz and Crone, 1988), which define the active (post-late Pleistocene) northern part of the zone. Figure 6 summarizes data on timing of events. The Mackay segment did not rupture in 1983 but has been the source of two events during the past 12,000-15,000 years. In contrast, the Pass Creek segment, which is located immediately south, has not experienced any events in at least the past 30,000 years (Malde, 1987). Trench exposures at the south end of the Mackay segment indicate that only one event has occurred since deposition of both Glacier Peak (11,300 yr B.P.) and Mazama (6,845 yr B.P.) ashes. Preliminary radiocarbon dating of organic material from scarp-derived colluvium (Scott and others, 1985) and our scarp morphological modeling suggests the event is older than about 4300 years. A second event is pre-Glacier Peak. Mapping along the segment suggests this event occurred during or after deposition of 12,000-15,000-year-old Pinedale outwash deposits. These two events, and possibly a third of unknown age, are the only events associated with the scarp across an approximately 140,000-year-old outwash fan surface associated with Bull Lake glaciation.

The Thousand Springs segment ruptured in 1983. Slip distribution in 1983 faithfully reproduced the slip distribution of the pre-1983 event (Figure 3). Only one other event occurred along this segment during the past 12,000-15,000 years. Reconstruction and diffusion modeling of the pre-1983 scarp suggest the event occurred about 6000-8000 years ago (Hanks and Schwartz, 1987). The Thousand Spring-Mackay boundary is marked by a change in strike of the range front and and the intersection with major cross faults. The Warm Spring segment is north of a complex transverse structural feature called the Willow Creek hills, which is proposed as a barrier to the coseismic 1983 rupture (Crone and others, 1987). However, in 1983 the Warm

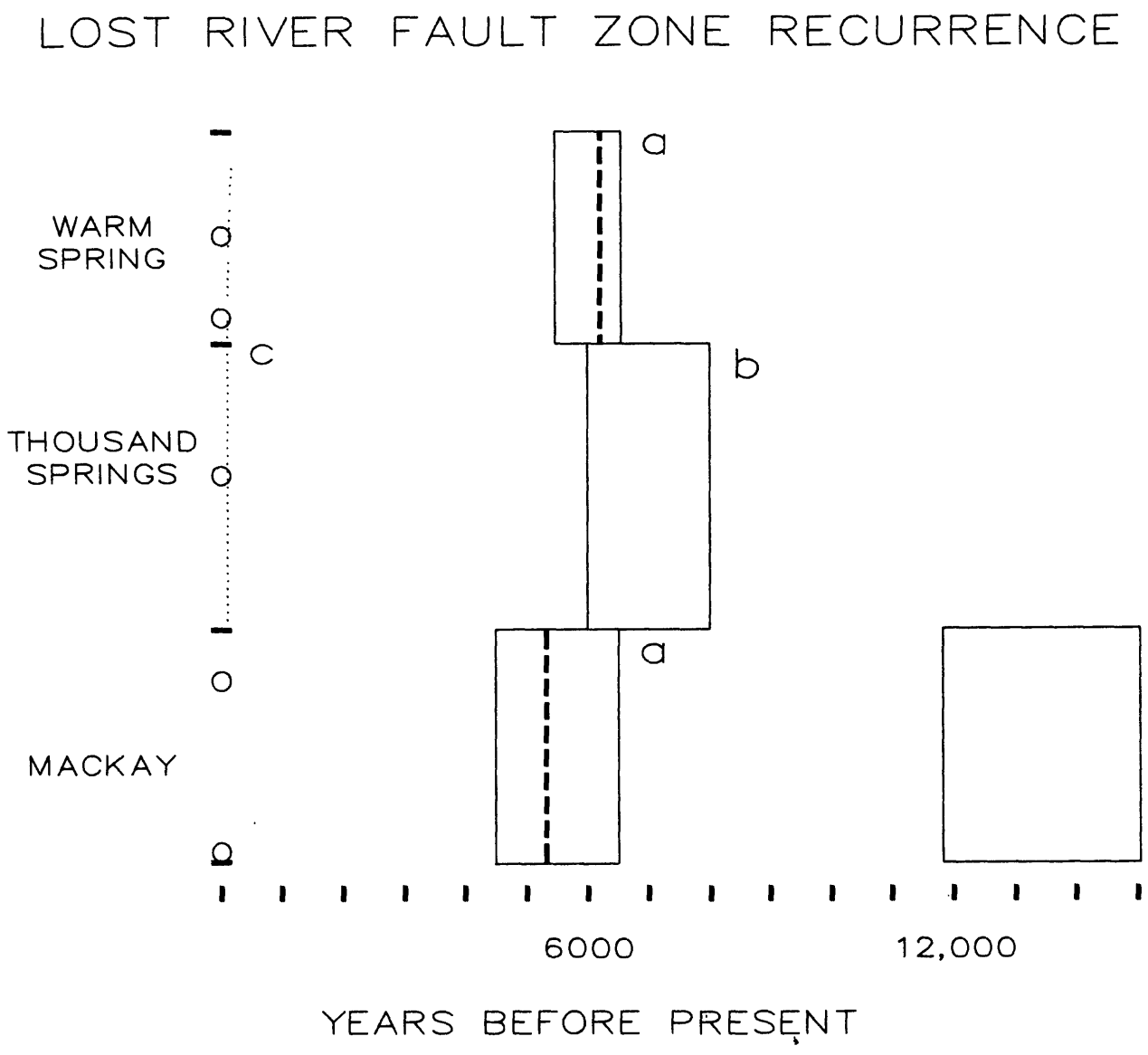

Figure 6. Space-time diagram for large magnitude scarp-forming earthquakes on the Lost River fault zone during the past 12,000-15,000 years. Heavy dashed line is best estimate of timing of event. Box is uncertainty in date. Small circles along segment axis show locations of trenches.

Spring segment did experience discontinuous surface rupture with displacements averaging 10-20 cm. This has been interpreted as shallow triggered slip that does not represent coseismic energy release (Crone and others, 1987). The small 1983 scarplets were coincident with older 1-1.5-m-high scarps in alluvial fans. Radiocarbon dating of in place burns in and near the base of scarp-derived colluvial wedges observed at two trench sites, and the degree of soil carbonate development indicate only one event prior to 1983 during the past 12,000-15,000 years; this paleoearthquake appears to have occurred shortly before 5500-6200 yr B.P. At present there is no information on timing of older events along the Thousand Springs and Warm Spring segments. The 1983 fault plane is clearly defined in the trenches and small (8 cm) displacements of units in the colluvial wedge from the pre-1983 earthquake are measurable. If these relationships were exposed without overall knowledge of the 1983 event, a reasonable interpretation would be that the Warm Spring segment produced two earthquakes of different size.

The timing of paleoearthquakes, the extent and slip distribution of 1983 surface faulting, and geometric changes in the range front coincident with transverse structures suggest that persistent boundaries separate the Mackay from adjacent segments. However, there is ambiguity concerning Warm Spring-Thousand Springs segmentation. The pre-1983 earthquake could have been somewhat larger and completely ruptured both segments as a master segment during a single event. This is within the constraints of present timing estimates. Alternatively, both segments may be independent seismogenic sources. In this case stress at the Warm Spring Hills barrier triggered shallow slip on the Warm Spring segment, which will produce a separate event at some future time.

The timing of paleoearthquakes on the Lost River fault zone provides information on several aspects of earthquake recurrence. On a long term basis parts of the fault zone have experienced long periods of both quiescence and activity. For example, the southern part of the zone (Pass Creek and Arco segments) has high degraded scarps that indicate a period of late Quaternary faulting but there have been no scarp-forming earthquakes during the past 30,000 years. The Mackay segment was essentially quiescent between about 140,000 and 15,000 years ago and now appears to be in an active phase. The long-term behavior of the Thousand Springs and Warm Spring segments has not yet been established but both are also active. The northern part of the Lost River fault zone is presently in an active cycle of behavior that is similar to the Wasatch with temporal clustering on adjacent segments. The most recent sequence occurred between 4500 and 8000 years ago, although the actual timing of events could have been considerably closer.

PERSISTENCE OF SEGMENTS AND TEMPORAL CLUSTERING

The examples from the in-progress studies described above indicate that paleoseismic information, particularly the timing of the most recent event and the several prior events along the length of a fault, can provide a strong basis on which to develop fault-specific segmentation models. Certainly for the Wasatch and Lost River fault zones, a very reasonable interpretation can be made for the persistence of independent rupture segments and their boundaries during

repeated earthquakes. Limited data, such as only one recurrence interval site on a long reach of a fault, large uncertainties in the timing of events, and similar timing of events leads to ambiguous interpretations and result in several possible segmentation models.

The closely timed ruptures of adjacent parts of major circum-Pacific subduction zones, the 1939-1966 earthquake sequence that has ruptured approximately 1000 km of the North Anatolia fault zone, and the 1904-1954 normal faulting sequence along the northern part of the Nevada seismic zone are historical examples of temporal clustering. One of the very exciting results from paleoseismic studies is that temporal clustering along adjacent, and often independent, segments can be deciphered in the geologic record. This certainly appears to be the case along the Wasatch and Lost River fault zones and, possibly, along the San Andreas fault. This type of behavior may be more common than previously recognized for shallow crustal faults and it has implications for understanding recurrence and seismic hazards evaluation. It raises the possibility that segments adjacent to historical ruptures may have a high potential to produce the next earthquakes, particularly if they can be shown to have elapsed times similar to the historical rupture segment. Focused studies to collect data on timing of past earthquakes for both the historical and adjacent segments could yield information on the degree to which failure of adjacent segments has, or has not, been closely coupled in time.

REFERENCES

Crone, A. J., Machette, M. N., Bonilla, M. G., Lienkaemper, J. J., Pierce, K. L., Scott, W. E., and Bucknam, R. C., 1987, Surface faulting accompanying the Borah Peak earthquake and segmentation of the Lost River fault, central Idaho: *Bulletin of the Seismological Society of America*, v. 77, no. 3, p. 739-770.

Forman, S. L., Machette, M. N., Jackson, M. R., and Mott, P., 1989, An evaluation of thermoluminescence dating of paleoearthquakes on the American Fork segment, Wasatch fault zone, Utah: *Journal of Geophysical Research*, v. 94, p. 1622-1630.

Hanks, T. C., and Schwartz, D. P., 1987, Morphologic dating of pre-1983 fault scarp on the Lost River fault at Doublespring Pass Road, Custer County, Idaho: *Bulletin of the Seismological Society of America, v. 77*, p. 837-846.

Jackson, M. E., 1988, Thermoluminescence dating of Holocene paleoseismic events on the Nephi and Levan segments, Wasatch fault zone, Utah: Boulder, University of Colorado, M. S. thesis, 149 p.

Jacoby, G., Sheppard, P., and Sieh, K., 1988, Irregular recurrence of large earthquakes along the San Andreas fault -- evidence from trees: *Science*, v. 241, p. 196-199.

Machette, M. N., Nelson, A. R., Personius, S. F., Schwartz, D. P., and Lund, W. R., 1988, The late Quaternary Wasatch fault zone, Evidence for segmentation, recent faulting, and clustering of earthquakes [abs.]: *Geological Society of America Abstracts with Programs*, no. 20, p. 177.

Malde, H. E., 1987, Qauternary faulting near Arco and Howe, Idaho: *Bulletin of the Seismological Society of America*, v. 87, p. 847-867.

Machette, M. N., Personius, S. F., and Nelson, A. R., 1987, Quaternary geology along the Wasatch fault zone -- Segmentation, recent investigations, and preliminary conclusions, in Gori, Paula and Hays, W. W., eds., assessment of regional earthquake hazards and risk along the Wasatch Front, Utah: *U.S. Geological Survey Open-File Report 87-585*, v. I, Chapter A., p. A1-A72.

Prentice, C. E., 1989, Earthquake geology of the San Andreas fault near Point Arena, California: Pasadena, California Institute of Technology, Ph.D. dissertation, 252 p.

Schwartz, D. P., and Coppersmith, K. J., 1984, Fault behavior and characteristic earthquakes -- Examples from the Wasatch and San Andreas fault zones: *Journal of Geophysical Research*, v. 89, no. B7, p. 5681-5698.

Schwartz, D. P., Lund, W. R., Mulvey, W. E., and Budding, K. E., 1988, New paleoseismicity data and implication for space-time clustering of large earthquakes on the Wasatch fault zone [abs.]: *Seismological Research Letters*, v. 59, no. 1, p. 15.

Schwartz, D. P., and Crone, A. J., 1988, Paleoseismicity of the Lost River fault zone, Idaho: Earthquake recurrence and segmentation [abs.]: *Geological Society of America Abstracts with Programs*, no. 20, p. 228.

Scott, W. E., Pierce, K. L., and Hait, M. H., Jr., 1985, Quaternary tectonic setting of the 1983 Borah Peak earthquake, central Idaho: *Bulletin of the Seismological Society of America*, v. 75, no. 4, p. 1053-1066.

Sieh, K., Stuiver, M., and Brillinger, D., 1989, A more precise chronology of earthquakes produced by the San Andreas fault in southern California: *Journal of Geophysical Research*, v. 94, p. 603-623.

Sieh, K., 1978a, Prehistoric large earthquakes produced by slip on the San Andreas fault at Pallett Creek, California: *Journal of Geophysical Research*, v. 83, p. 3907-3939.

Sieh, K., 1978b, Slip along the San Andreas fault associated with the great 1857 earthquake: *Bulletin of the Seismological Society of America*, v. 86, p. 1421-1428.

Sieh, K., and Jahns, R. H., 1984, Holocene activity of the San Andreas fault at Wallace Creek, California: *Geological Society of America Bulletin*, v. 95, p. 883-896.

Swan, F. H., III, Schwartz, D. P., and Cluff, L. S., 1980, Recurrence of moderate to large magnitude earthquakes produced by surface faulting on the Wasatch fault zone, Utah: *Bulletin of the Seismological Society of America*, v. 70, p. 1431-1462

Sykes, L., and Nishenko, S., 1984, Probabilities of occurrence of large plate rupturing earthquakes for the San Andreas, San Jacinto, and Imperial faults, California, 1983-2003: *Journal of Geophysical Research*, v. 89, p. 5905-5927.

Weldon, R., and Sieh, K., 1985, Holocene slip rate and tentative recurrence interval for large earthquakes on the San Andreas fault, Cajon Pass, southern California: *Geological Society of America Bulletin*, v. 96, p. 793-812.

Working Group on California earthquake Probabilities, 1988, Probabilities of large earthquakes occurring in California on the San Andreas fault: *U.S. Geological Survey Open-File Report 88-398*, 62 p.

STRUCTURAL DUPLEXING IN THE STRIKE-SLIP ENVIRONMENT

by

Mark T. Swanson
Department of Geosciences
University of Southern Maine
Gorham, Maine, 04038

ABSTRACT

The deformation of the offset-overlap zones between en echelon faults serves to accommodate continued displacements on segmented fault structures. For strike-slip faults this deformation takes the form of structural duplexing in contractional and extensional kinematic styles. The geometric configuration of this duplexing for individual ruptures within the upper crustal strike-slip seismogenic zone is found to vary from surface faulting down through the brittle-ductile transition, due to effects of depth and pressure and through the influence of preexisting vertical planar anisotropy. Dip-slip and oblique-slip structures dominate the surface and near-surface environments and give way to strike-slip structures at depth. Lens-duplexing dominates in the shallow to intermediate depth range associated with cataclastic fault rocks, while slab-duplexing dominates in the lower depth ranges associated with the mylonitic rocks of the brittle-ductile transition.

Introduction

En echelon segmentation is a common feature of strike-slip faults throughout the seismogenic zone at all scales and levels of exposure. The offset-overlap zone between the en echelon fault segments must deform

in order to accommodate slip transfer across the initial en echelon configuration. It is the continued displacements on these segments and the deformation of the intervening offset-overlap zones that lead to the evolution of a throughgoing structure. Thus, they must in some way control the propagation and termination of earthquake ruptures as well as the cumulative fault zone evolution. The style of this deformation, as the mechanism of strain accommodation between individual segments, is found to vary with depth through the upper crust from surface breaks down through the brittle-ductile transition. Examination of the various structural configurations preserved in active surface faulting and in exhumed cataclastic to mylonitic fault zones allows a reconstructed composite profile through this upper crustal strike-slip seismogenic zone.

Of particular interest is the style of structural development near the base of the seismogenic zone where larger earthquake ruptures commonly initiate (Sibson, 1983; 1984). The rapid coseismic slip associated with these ruptures leads to the production of pseudotachylyte, generally attributed to friction melting (Sibson, 1975) or to extreme cataclasis (Wenk, 1978) during displacement. Pseudotachylyte associated with distinctive paired parallel fault structures has been recognized in a number of localities (Grocott, 1981; Swanson, 1988). These pseudotachylyte-bearing structures are preserved along exhumed faults, particularly those from deeper levels of exposure, and suggest that they may represent the style of earthquake rupture at focal, or at least near-focal, depths within the seismogenic zone.

En Echelon Surface Faulting

Offset-overlap zones between en echelon surface faults typically develop structures that reflect the asymmetry of the offset segments and their sense of slip (Fig. 1a). The mechanisms of strain accommodation within these zones in the surface and near-surface environment are dominated by dip-slip and oblique-slip structures. Dextral strike-slip segments with right-stepping en echelon offsets

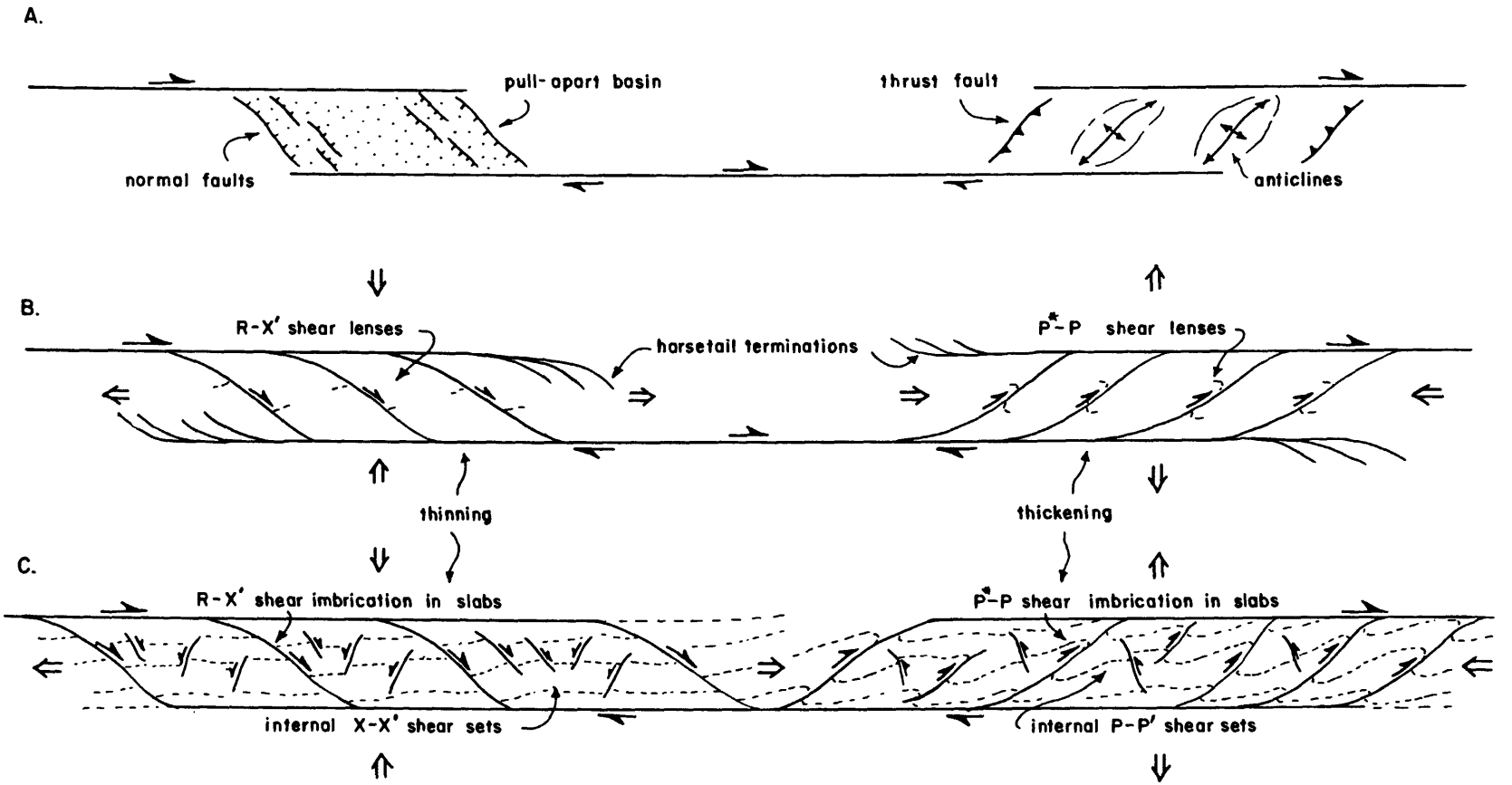

FIGURE 1. -- Structural mechanisms of strain accommodation between en echelon offset and offset-overlap zones for dextral strike-slip faults: (a.) Large-scale dip-slip features of the surface and near-surface environment; (b.) smaller-scale oblique-slip to strike-slip features at intermediate depths and (c.) smaller-scale strike-slip features within the dominant vertical fault-parallel mylonitic layering of the brittle-ductile transition.

(Fig. 1a, left) develop zones of extension that are reflected in local subsidence, normal faulting, and the formation of pull-apart basins. Left-stepping en echelon segments (Fig. 1a, right) develop contractional structures that include anticlinal ridges and thrust faults. Surface or near-surface dip-slip and oblique-slip structures tend to converge downwards and narrow to more discrete zones of strike-slip (Sylvester, 1988). The transition may be gradual or abrupt, with localized upper level detachments that splay off the main fault zone.

The local horizontal extension and contraction associated with the offset-overlap zones as expressed at the surface must be accommodated at greater depths by different structural mechanisms as a result of the change in principal stress directions. In segmented strike-slip faults at depth, therefore, the dominant mechanism of strain accommodation within the offset-overlap zones should eventually adjust to the change in principal stress directions. This horizontal plane-strain style of accommodation at depth takes the form of structural duplexing.

Duplexing at Depth

Duplexes in strike-slip faults (Woodcock & Fischer, 1986) as in thrust zones, are defined as blocks, lenses or slabs of host rock that are bound by sub-parallel slip surfaces and exhibit an internal deformation or imbrication that accommodates displacement. Strike-slip duplex structures are most typically developed at the offset-overlap zones between en echelon fault segments (Fig. 1b & c) associated with slip transfer during finite displacements (Swanson, 1988). The geometry of the en echelon segments and the failure mechanisms for the intervening "rock bridges" (Gamond, 1987) will ultimately lead to doubly-tapered lens (Fig. 1b) and slab (Fig. 1c) duplex configurations. Outward growth of the duplex structure as well as internal deformation of the decoupled lenses or slabs accommodates the total finite extension or contraction within the offset-overlap zone and allows continued slip along the main fault segments. The finite strain accommodation within these duplex zones is also reflected in the thinning and thickening (Fig. 1b & c) of the decoupled bridge areas as well.

Cataclastic fault structures in en echelon arrays should dominate the shallow to intermediate depths within the strike-slip seismogenic zone. Based on studies of the Two Lights dextral strike-slip faults in the chlorite-grade phyllitic quatrzites of the Cape Elizabeth Formation in southern Maine, en echelon fault segments typically develop low-angle P-type contractional linkages (Fig. 1b, right) or R-type extensional linkages (Fig. 1b, left) as lateral ramps or splays. Shear fracture terminology follows that of Logan et al. (1979) and Swanson (1988). Multiple ramps create asymmetric doubly-tapered imbricate lenses. Variations observed include stacked contractional duplexes, thinned extensional R-shear duplexes and locally, long, thin Y-slab duplexes (similar to Y gouge slivers described by Rutter et al., 1986). Extensional "horsetail" relays and terminations (after Granier, 1985) as oblique extension fractures abound, along with minor quartz-calcite cemented breccias.

Mylonitic fault fabrics should become dominate near the lower depths of the strike-slip seismogenic zone within the brittle-ductile transition. The development of mylonitic fabrics creates an effective vertical planar anisotropy that controls the orientations of the developing rupture surfaces. In studies of the Fort Foster Brittle Zone in the sillimanite-andalusite grade mylonitic Rye Formation of southernmost Maine (Swanson, 1988), pseudotachylyte-bearing fault structures (with some evidence of ductile redeformation) within the mylonitic host rocks were found to have developed a distinctive slab-duplex configuration (Fig. 1c). Slab-duplexes are interpreted as decoupled host rock slabs between long overlapping layer-parallel slip surfaces. Contractional duplexes (Fig. 1c, right) accommodate displacements through internal strain by the development of P-type ramp linkages, P-shear slab imbrication and conjugate P-P' shear structures as well as asymmetric folds and kinks that result in shortening and thickening of the host rock slabs. Extensional slab-duplexes (Fig. 1c, left) accommodate displacements through internal strain by the development of R-type ramp linkages and X-X' shear fractures in antithetic, synthetic and conjugate sets, extensional pseudotachylyte veining and localized breccias with pseudotachylyte matrix. Extensional "horsetail" fracture arrays and termination structures are conspicuously absent.

Discussion

Microseismicity patterns (Bakun et al. 1980) suggest that the offset fault segmentation found at the surface does, in some cases, extend to the base of the seismogenic zone. Field evidence suggests that extreme overlap of en echelon segments may be a dominant characteristic of focal-depth ruptures. This is, in part, attributed to the effect of a controlling vertical mylonitic anisotropy in host rocks at the base of the seismogenic zone, within the brittle-ductile transition.

The hypothesized variation with depth for the structural mechanisms of strain accommodation in these offset-overlap zones associated with fault segmentation is illustrated in Figure 2. The three-dimensional view shows a possible physical and mechanical relationship between surface faulting and structural duplexing at depth. This model for earthquake ruptures in the seismogenic zone is based on earlier models proposed by Sibson (1983; 1986) and recent experimental studies by Naylor et al. (1986). The sand box experiments by Naylor et al. (1986) suggest that the en echelon segmentation found at the surface decreases in spacing or offset in converging to a single basement fault plane as constrained by their models. This would imply that segmented ruptures initiating at the base of the seismogenic zone within the brittle-ductile transition would propagate upward in outwardly flaring trajectories away from the focus. The overall configuration for the intervening host rock that represents the offset-overlap zone is a vertical helicoidal slab that narrows and lengthens with depth.

The initial en echelon fault ruptures skip past the offset or offset-overlap zones during propagation. The intact vertical rock slabs between overlapping en echelon segment ends that survive the initial propagating ruptures represent the barriers (Aki, 1979; Das & Aki, 1977) of recent earthquake source zone models. Further displacement increments are accommodated by the progressive inelastic deformation of the surviving barriers left between the en echelon segments as asperities (Lay & Kanamori, 1980). This deformation results in the growth of lens and slab duplex structures leading to a linking through-going rupture. Contractional duplexes develop into binding

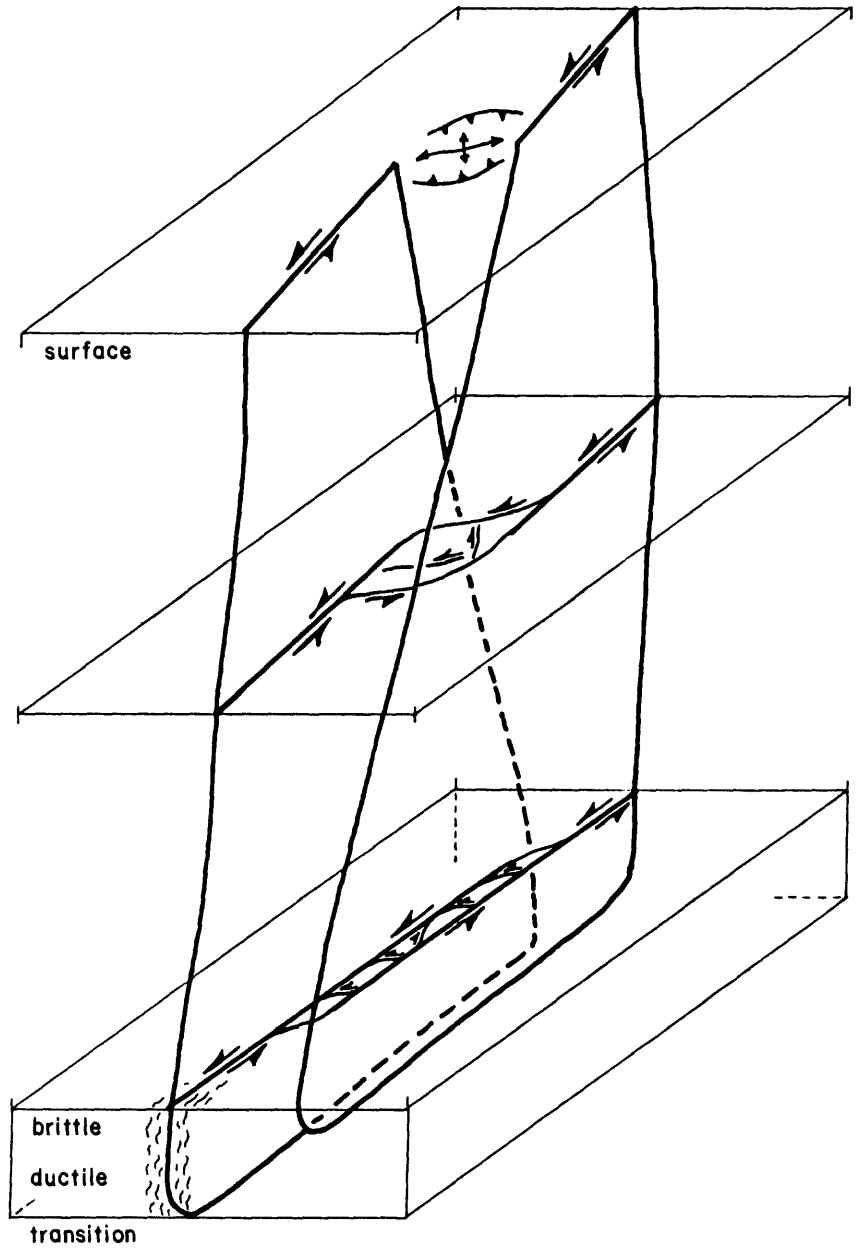

FIGURE 2. -- Proposed relationship between surface en echelon fault geometries and the lens and slab duplex geometries at depth. En echelon ruptures initiating at depth within the slab-duplex domain propagate upward and outward into the typical en echelon surface geometry. Continued displacements are accommodated by deformation within the offset-overlap zones by different structural mechanisms at different depths within the crust.

asperities that may lead to future catastrophic ruptures. Extensional duplexes on the other hand, form dilational jogs (Sibson, 1985) and often play a role in the termination of the propagating ruptures by distributing rupture energy as diffuse extensional fracturing. The formation of these initial barriers and their evolution as duplexes may control the initiation, propagation and termination of earthquake ruptures on segmented strike-slip fault structures.

Conclusions

Continued displacement and strain accommodation on segmented en echelon strike-slip faults at depth develop linking structures that evolve as duplexes in contractional and extensional kinematic styles. Duplex geometry varies from lens to slab configurations with the influence of preexisting anisotropy. Slab duplexes between overlapping layer-parallel fault segments appear to dominate within the preexisting vertical mylonitic anisotropy expected at focal depths of larger ruptures in the vicinity of the brittle-ductile transition.

Acknowledgements:

Research for this project was conducted under the United States Geological Survey's National Earthquake Hazards Reduction Program, Grant # 14-08-0001-G1395 . Released time from academic duties was provided by the University of Southern Maine.

References cited:

Aki, K., 1979, Characterization of barriers on an earthquake fault: Journal of Geophysical Research, v. 84, p. 6140-6148.

Bakun, W. H., Stewart, R. M., Bufe, C. G. and Marks, S. M., 1980, Implication of seismicity for failure of a section of the San Andreas fault: Bulletin of the Seismological Society of America, v. 70, p. 185-201.

Das, S. and Aki, K., 1977, Fault planes with barriers: a versatile earthquake model: Journal of Geophysical Research, v. 85, p. 4337-4350.

Gamond, J. F., 1987, Bridge structures as sense of displacement criteria in brittle fault zones: Journal of Structural Geology, v. 9, p. 602-620.

Granier, T., 1985, Origin, damping and pattern of development of faults in granite: Tectonics, v. 4, p. 721-737.

Grocott, J., 1981, Fracture geometry of pseudotachylyte generation zones: a study of shear fractures formed during seismic events: Journal of Structural Geology, v. 3, p. 169-178.

Lay, T. and Kanamori, H., 1980, An asperity model of great earthquake sequences:in Simpson, D.W. and Richards, P. G. (eds.), Earthquake Prediction - An International Review, American Geophysical Union, Washington, D.C., p. 579-592.

Logan, J. M., Friedman, M., Higgs, N., Dengo, C. and Shimamoto, T., 1979, Experimental studies of simulated gouge and their application to studies of natural fault zones: U.S. Geological Survey, Open-File Report 79-1239, p. 305-343.

Naylor, M. A., Mandle, C. and Sijpesteijn, Ch.K., 1986, Fault geometries in basement induced wrench faulting under different initial stress states: Journal of Structural Geology, v. 8, p. 737-752.

Rutter, E.F., Maddock, R.H., Hall, S.H. and S.H. White, 1986, Comparative microstructures of natural and experimentally produced clay-bearing fault gouges: Pure and Applied Geophysics, v. 124, p. 3-30.

Sibson, R. H., 1975, Generation of pseudotachylyte by ancient seismic faulting: Geophysical Journal of the Royal Astronomical Society of London, v. 133, p. 191-213.

Sibson, R. H., 1983, Continental fault structure and the shallow earthquake source: Journal of the Geological Society of London, v. 140, p. 741-767.

Sibson, R. H., 1984, Roughness at the base of the seismogenic zone: contributing factors: Journal of Geophysical Research, v. 89, p. 5791-5799.

Sibson, R. H., 1986, Brecciation processes in fault zones: inferences from earthquake rupturing: Pure and Applied Geophysics, v. 124, p. 159-175.

Swanson, M.T., 1988, Pseudotachylyte-bearing strike-slip duplex structures in the Fort Foster brittle zone, S. Maine: Journal of Structural Geology, v. 10, in press.

Sylvester, A.G., 1988, Strike-slip faults, Geological Society of America Bulletin, v. 100, p.1666-1703.

Wenk, H. R., 1978, Are pseudotachylytes products of fracture or fusion?: Geology, v. 6, p. 507-511.

Woodcock, N. H. and Fisher, M., 1986, Strike-slip duplexes: Journal of Structural Geology, v. 8, p. 725-735.

EARTHQUAKE FAULT SLIP ESTIMATION FROM GEOLOGIC, GEODETIC AND SEISMOLOGIC OBSERVATIONS: IMPLICATIONS FOR EARTHQUAKE MECHANICS AND FAULT SEGMENTATION

by

Wayne Thatcher and Manuel G. Bonilla

U.S. Geological Survey, Menlo Park, CA 94025

The spatial distribution of coseismic fault slip provides clues to the mechanics of earthquake strain release and sheds light on the nature and importance of fault segmentation in controlling the strain release process. Although the true slip distribution is not accessible to direct observation, several methods can be applied to recover informative features of its spatial pattern. Figure 1 illustrates this schematically, showing how geologic, geodetic, and seismologic observations sample different aspects of the coseismic slip distribution. Each approach produces a pattern of slip that is in varying degrees a filtered and biased version of the true slip, and the advantages and limitations of each method thus deserve careful attention in examining the results that follow.

When sufficiently numerous, fault slip (geologic) data can provide a very detailed picture of surface slip distribution along the fault rupture (figure 1, top). However, this pattern is seldom wholly representative of the slippage on the fault at seismogenic depths and even surface values will be biased where the fault zone is complex or coseismic deformation is distributed over a zone wider than that spanned by an offset feature.

Geodetic slip estimates are usually free of these shortcomings but are at best a rather coarse spatial averaging of fault slip in the zone of principal strain release (figure 1, middle). Furthermore, geodetic estimates are subject to the usual vagaries of network distribution relative to the coseismic rupture and this factor, along with measurement uncertainty, limits the precision and spatial resolution of derived slip estimates.

Seismic measurements of sufficient number and quality can in principle supply details of two dimensional slip distribution not provided by either geologic or geodetic methods. However, even for earthquakes with both near-source and distant seismic recordings from a range of source-receiver azimuths there is as yet a significant degree of nonuniqueness in the derived slip estimates. In the more common condition of less-than-complete observations, only large-scale features of the pattern of seismic moment release on the rupture plane are reliably obtained (figure 1, bottom).

The purpose of this paper is to examine case histories of earthquakes for which seismic slip has been estimated by one or more of the methods illustrated in figure 1 and to extract any significant generalizations that are indicated by these results.

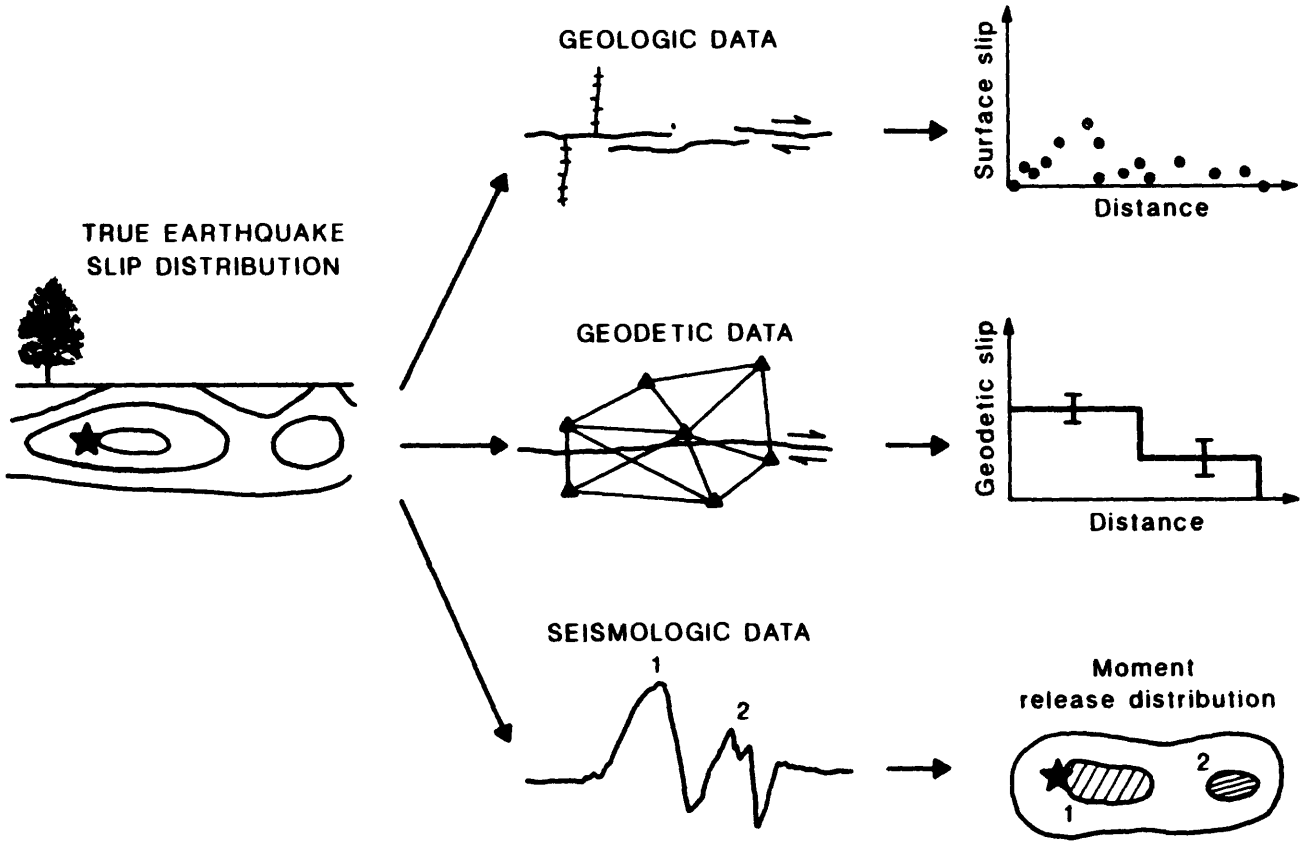

FIGURE 1. Three methods of earthquake slip estimation. True slip distribution is shown on cross-section at left. Geologic observations of offset features at the fault trace (center frame, top) provide information for plotting surface slip versus distance along fault (top right). Repeat geodetic measurements of angles, baseline lengths, or elevation changes for networks located near surface rupture (center frame, middle) provide data from which average fault slip at seismogenic depths can be estimated for various segments of fault and plotted versus distance along the fault (middle right, straight lines with error bars on each determination). Seismograms (center frame, bottom) can be analyzed to locate regions of concentrated seismic moment release; frame at bottom right schematically shows aftershock zone, with two regions of high moment release determined from seismograms and indicated by diagonal ruling within aftershock zone.

GEOLOGIC DATA

To date we have examined surface slip and faulting patterns for 22 earthquakes from active regions around the world. The events range from M_w 6.0 to 8.1 and have fault lengths from 15 km to 460 km. Fifteen of the shocks show predominantly strike-slip faulting and the remaining events have either normal or reverse slip. Representative features are summarized in figures 2, 3, and 4. Each figure has the same format, showing surface slip plotted against distance along the fault. A map view of the surface rupture is plotted at the same scale as the graph, a star locates the mainshock epicenter, and the geodetic slip estimates (when available) are indicated by straight lines with one standard deviation error bars.

Whenever surface slip determinations are sufficiently closely spaced we have observed considerable irregularity in slip magnitude over distances of a few kilometers or less. Occasionally these variations are systematic, pointing to a single cause such as local fault geometry. More commonly the origin of these local variations is unknown. Where observations are numerous such short wavelength fluctuations in surface slip can, for this study, be identified as noise and discarded. However, where data distribution is sparse, unrepresentative sampling of this local noise can introduce significant bias into the long wavelength variations in surface slip that are the main focus of this study.

For those cases in which such aliasing is not a problem and where fault zone complexity introduces no additional biases, the surface slip data for many earthquakes we have examined show notable variations over length scales of $\sim$10 km and greater. Figures 2, 3, and 4 illustrate this, showing that surface slip profiles are typically highly irregular and bear little resemblance to the smooth elliptical slip distributions predicted by models of uniform stress release across planar cracks that are occasionally still used to represent seismic faulting. Often, as for the 1940 El Centro and 1968 Dasht-e Bayaz earthquakes (see figures 3 and 4), this irregularity is characterized by regions of locally high slip on a rupture that otherwise shows considerably smaller slip amplitudes. We have found no simple relation between the locations of these high slip regions and fault geometry. For example, note the linearity and relative simplicity of the Imperial fault in the region where 1940 surface slip increases to more than 6 meters (figure 3). Similar features are documented for the 1976 Guatemala earthquake [*Bucknam et al.*, 1978] and for the great California earthquakes of 1857 and 1906 [*Sieh*, 1978; *Lawson*, 1908].

Surface slip profiles often reveal the effects of fault segmentation, with the magnitude of slip being a maximum near the center of each segment and dying off towards both ends. This feature is illustrated well by the 1968 Borrego Mountain earthquake (figure 2) and is also seen in the offset profiles for the 1915 Pleasant Valley (Nevada) and 1891 Mino-Owari (Japan) earthquakes [*Wallace*, 1984; *Matsuda*, 1974]. For those earthquakes that involve failure of only one or a few identifiable segments the surface slip patterns are sometimes simpler than those shown for the majority of the larger events. For example, the 1968 Meckering and 1987 Superstition Hills earthquakes [*Gordon and Lewis*, 1980; *P. Williams and H. Magistrale*, unpublished manuscript 1988] have surface slip profiles that are roughly

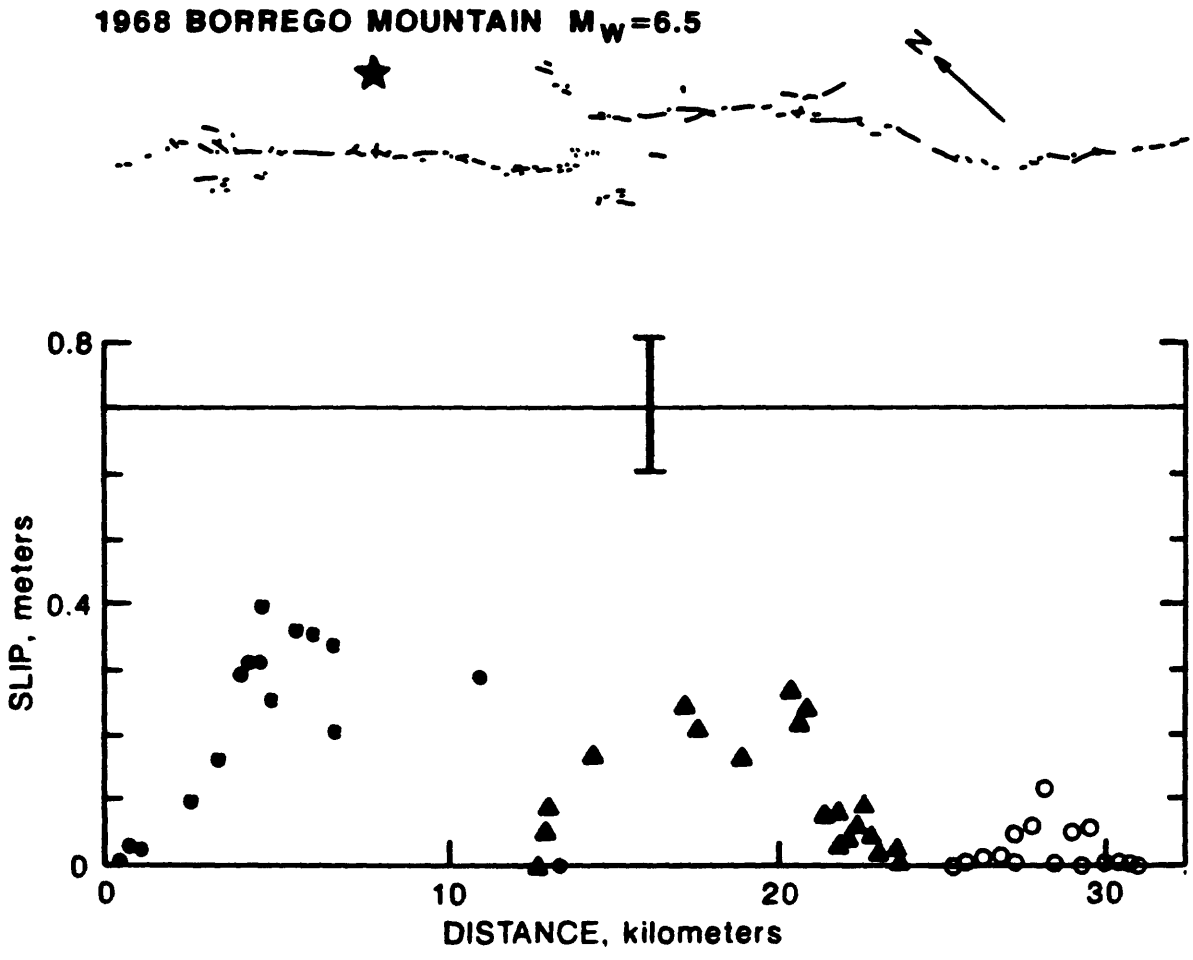

FIGURE 2. 1968 Borrego Mountain earthquake. Surface slip distribution versus distance along fault strike. Map view of surface faulting is shown at top of figure at the same scale. North arrow indicates map orientation. Offset symbols are keyed to three main segments of surface rupture. Geologic data are from *Clark* [1972]. Star locates mainshock epicenter, the initiation point of seismic rupture [*Allen and Nordquist*, 1972]. Geodetic estimate of fault slip [*Snay et al.*, 1983] is indicated by straight line with one standard deviation error bar.

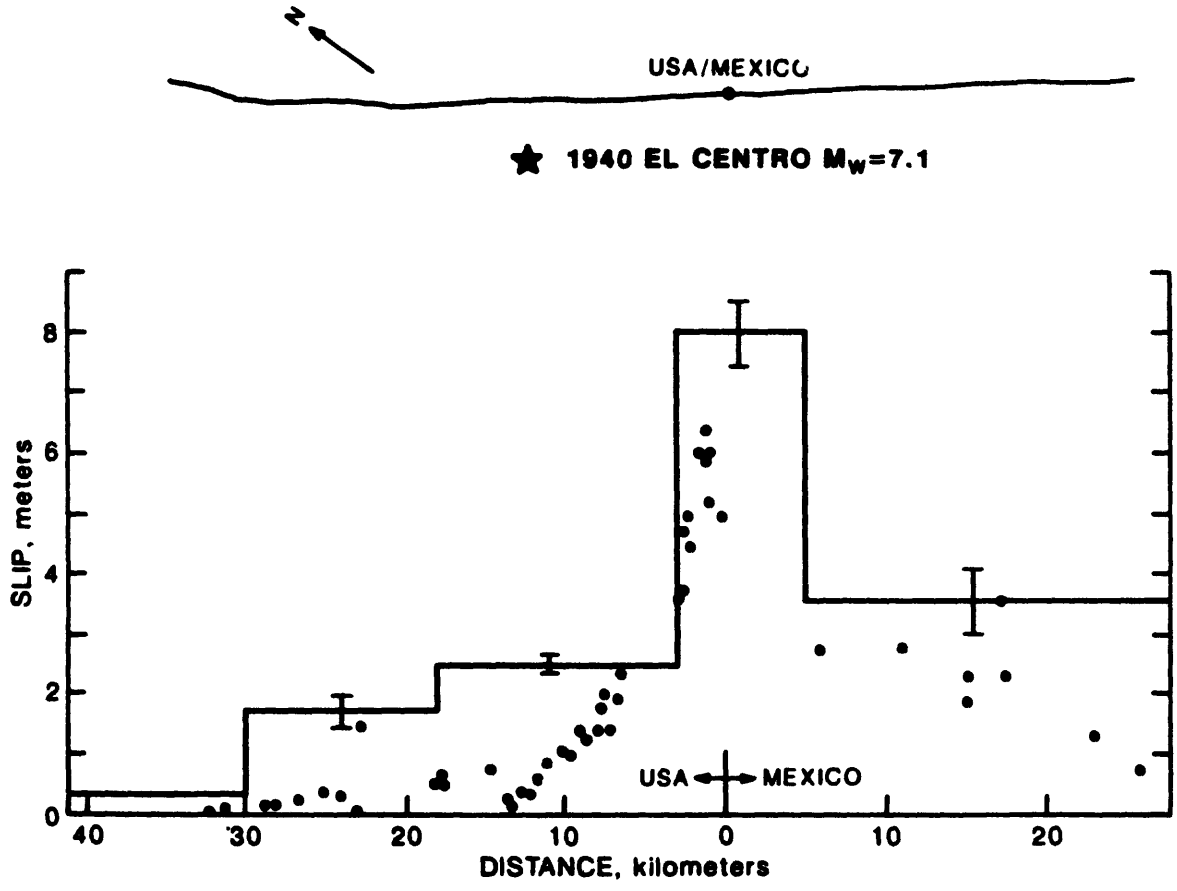

FIGURE 3. 1940 El Centro earthquake. Surface slip distribution versus distance along fault strike. Map view of surface faulting is shown at top of figure at the same scale, with north arrow indicating map orientation. Geologic data from *Sharp* [1982]. Star locates mainshock epicenter, initiation point of seismic rupture [*Richter*, 1958]. Geodetic estimates of fault slip are indicated by straight lines with one standard deviation error bars [*Zhang and Thatcher*, 1988, unpublished manuscript].

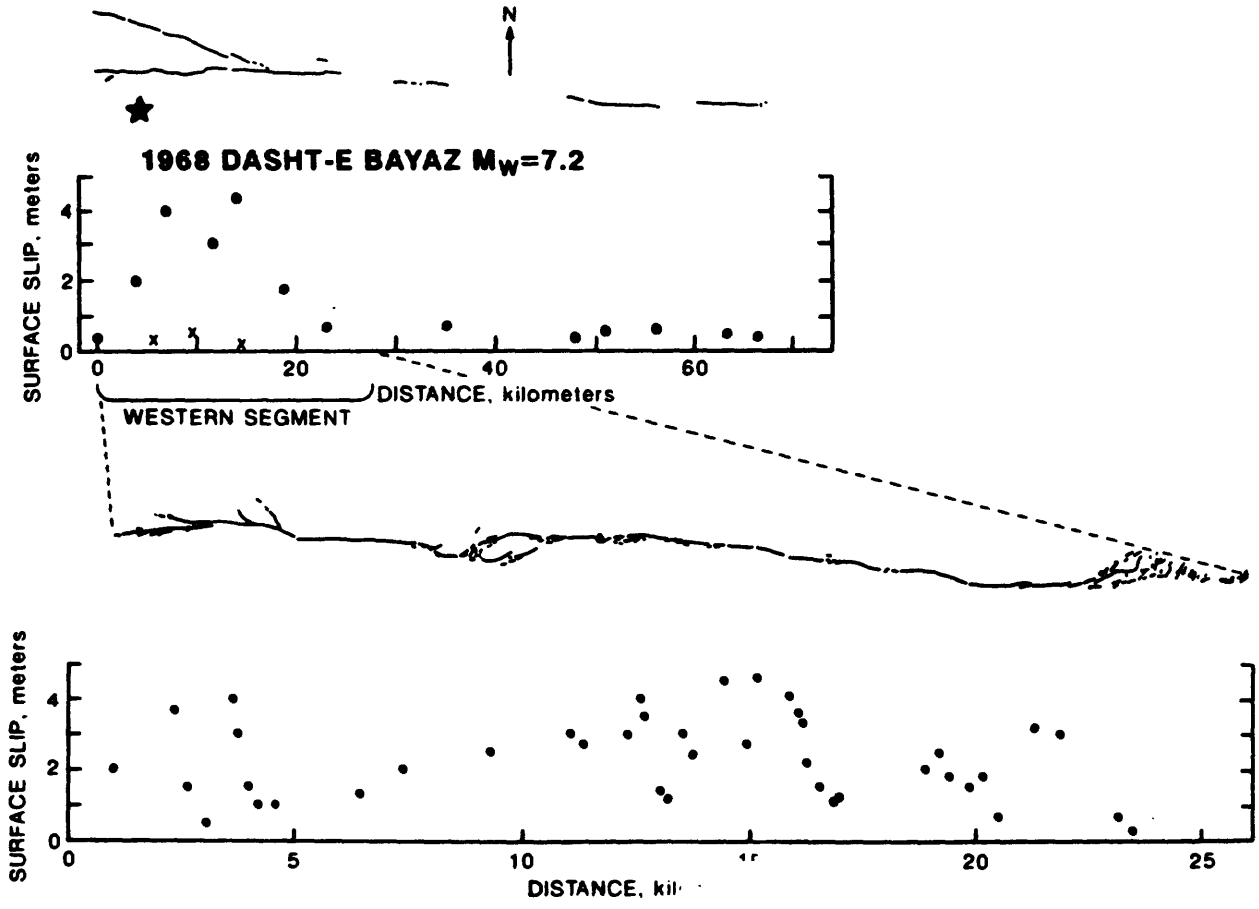

FIGURE 4. 1968 Dasht-e Bayaz (Iran) earthquake. Top frame of figure shows surface faulting map, north arrow indicating map orientation, and slip distribution along fault for entire 80-km-long rupture (crosses show surface slip on northwestern segment). Star locates mainshock epicenter, initiation point of seismic rupture. Bottom frame shows detailed map of surface faulting and slip along westernmost 25 km of the 1968 rupture. All data from *Ambraseys and Tchalenko* [1969].

symmetric, with maxima near the center of the rupture and relatively uniform decreases in slip amplitude towards the ends of the zone of surface faulting.

We have also noted some systematic features in the location of the mainshock epicenter along the zone of surface faulting. First, as many other studies have shown, we find that the mainshock epicenter, the initiation point of seismic rupture, is preferentially located towards the ends of the zone of surface faulting – in only four of the earthquakes studied here did the mainshock nucleate within the central 50 percent of the surface rupture. Furthermore, there is a tendency for the mainshock to locate in or near the region of maximum surface slip, although this is by no means a universal feature. For example, while the 1968 Borrego Mountain and 1968 Dasht–e Bayaz epicenters are, within location uncertainties, inside the maximum slip zone, the 1940 epicenter is not. Other events fall into one or the other of these classes, although significant epicentral uncertainty degrades the strength of the test of this hypothesis for many of the events examined here. We shall return to this issue when discussing seismologic observations, where the evidence is more conclusive.

GEODETIC DATA

Ten of the earthquakes with surface faulting and slip distributions also have geodetic estimates of fault slip reliable enough to afford a comparison between the two methods. Figures 2 and 3 show specific examples, and a summary of all the comparisons is presented in figure 5. Each independent estimate of geodetic slip is shown by a vertical block. Error bars are small, generally less than 10% of each slip estimate, and are omitted in the figure. Surface slip (solid dots give maximum slip, crosses are average values) is compared with each independent geodetic estimate. Histogram shows ratio of maximum surface slip to geodetic slip (in percent) plotted against number of examples that occur in 20 percent increments for 0% to 100% and for ratios greater than 100%.

The comparisons illustrate that in cases where the geologic data are sufficiently numerous (*e.g.*, 1906 San Francisco, 1940 El Centro), the surface slip distributions are qualitatively similar to those indicated by the geodetic estimates. However, even the maximum slip is usually less than the geodetically estimated slip at seismogenic depths. The ratio shows considerable dispersion but its average is about 80%. Both the large scatter among surface slip observations and their biases relative to the geodetic determinations of slip underline a truth of which Quaternary fault geologists are acutely aware, that it is a rare fault locality where either total event slip or long–term slip rate can be reliably obtained.

SEISMOLOGICAL DATA

During the past five years broad–band seismic recordings from large earthquakes have found increasing use in delineating those regions of the earthquake rupture surface where seismic moment or energy release are concentrated [*e.g.*, *Ruff and Kanamori*, 1983; *Kikuchi and Kanamori*, 1982; *Kikuchi and Fukao*, 1987]. Although the dimensions of these zones are seldom constrained well enough to reliably convert moment release into fault slip, the

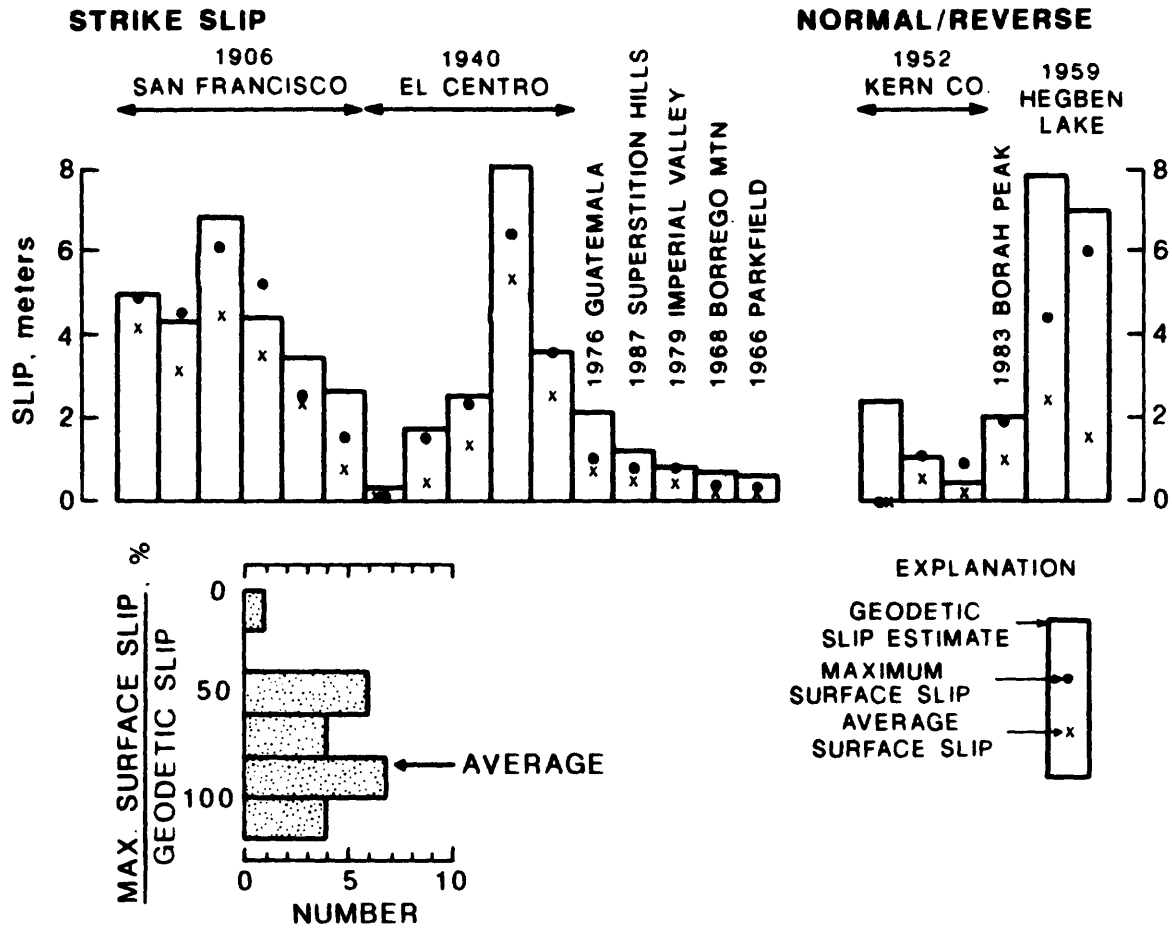

FIGURE 5. Geodetically-estimated slip (bars) compared with maximum surface slip (solid dots) and arithmetic average of reported surface slip (crosses) for strike slip (left) and normal or reverse faulting earthquakes (right). Note slip estimates on more than one fault section for 1906 San Francisco, 1940 El Centro, 1952 Kern County, and 1959 Hebgen Lake earthquakes. Bottom of figure shows histogram of ratio of maximum surface slip and geodetically-estimated slip, plotted as a percent, in twenty percent increments from 0 to 100% and for ratios greater than 100%.

results provide at least qualitative indications of two-dimensional slip distribution. All practitioners in this field have commented on the high degree of spatial heterogeneity in moment release revealed by their results, and the patterns shown are reminiscent of the long wavelength irregularity in slip distribution seen in the geologic and geodetic results discussed here.

Thus far in our review of the seismologic data we have examined analyses done for 16 earthquakes, all but one with $M_w \geq 7.5$, the great majority of these being great shallow focus underthrust events. The results of over a dozen separate studies by L. Ruff, M. Kikuchi, H. Kanamori and their coworkers of 14 of these events are summarized in greatly simplified cartoon fashion in figure 6. For each earthquake the aftershock zone is outlined in map view (north is towards the top of the figure), with the regions of high moment release shown by diagonal ruling and the mainshock epicenter indicated by a star. For the underthrust events the trench axis is shown as a line with teeth on the overthrust lithospheric plate. In this study we have followed convention and assumed that aftershock zones delimit the regions of coseismic fault slip. Although this may in some instances lead to overestimates of the true extent of the earthquake rupture plane, we do not think this bias is very great.

The most striking feature of figure 6 is the generally small area of the zone or zones of high moment release relative to the entire rupture plane. Equally notable is the usual location of mainshock epicenter either inside or immediately adjacent to one of these zones. The 1979 Colombia and 1977 Sumba Sea earthquakes are exceptions to this general rule, and for several other events (1968 Tokachi-oki, 1976 Mindinao, 1976 Guatemala) the regions of high moment release comprise such a large proportion of the aftershock zone that the rule is only weakly confirmed. Nonetheless, the coincidence of mainshock epicenter with zones of high moment release is striking. Figure 7 summarizes the evidence favoring systematic mainshock location relative to both maximum surface slip region (geologic data) and zones of concentrated moment release (seismologic results). Clearly the geologic observations only suggestively support such a systematic localization of mainshock epicenter, while the seismologic evidence is much stronger. Although our study has focussed on shallow crustal earthquakes it may be noteworthy that for 14 of 18 intermediate- and deep-focus events analyzed by *Fukao and Kikuchi* [1987] the mainshock also lay within the zone of high moment release.

IMPLICATIONS

Earthquake slip distributions obtained by all three methods examined here are typically highly irregular, with maximum slippage often localized in one or a few restricted regions that together comprise only a small proportion of the entire rupture plane. This complexity does, however, contain some systematic elements, since rupture has a tendency to initiate towards the ends of the zones of seismic faulting and near or within regions of high coseismic slippage. Although this latter feature is an assumption or consequence of several simple models of uniformly propagating earthquake rupture, it is a perhaps somewhat surprising property of complex ruptures of the type illustrated here. For

ZONES OF CONCENTRATED MOMENT RELEASE FOR MAJOR EARTHQUAKES

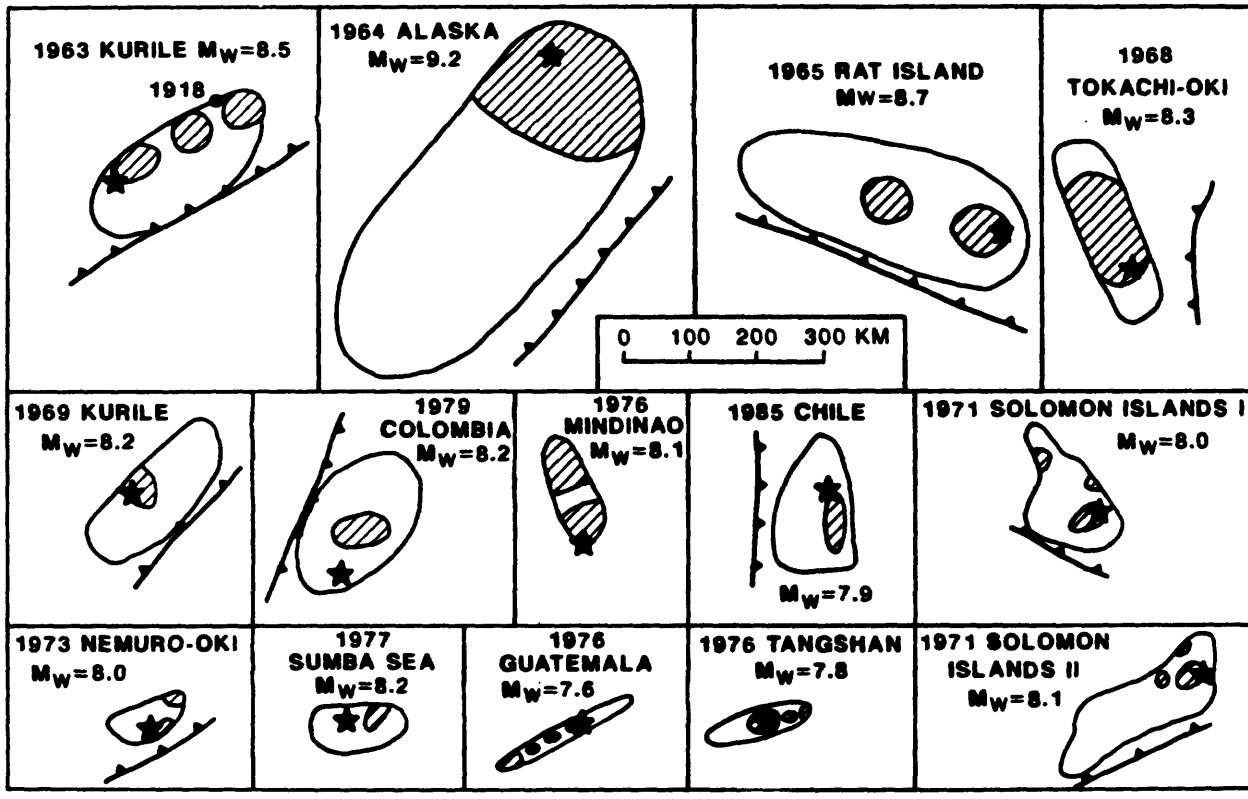

FIGURE 6. Schematic map-view summaries of aftershock zones (solid line) and regions of high seismic moment release (diagonal ruling) for 14 major earthquakes. Star locates mainshock epicenter, initiation point of seismic rupture. For interplate underthrust earthquakes, trench axis is shown, with teeth on overthrust lithospheric plate. North is towards top of figure for each map. In the 1963 Kurile earthquake zone (top left) the epicentral location of the most recent preceding great earthquake, which occurred in 1918, is shown for reference.

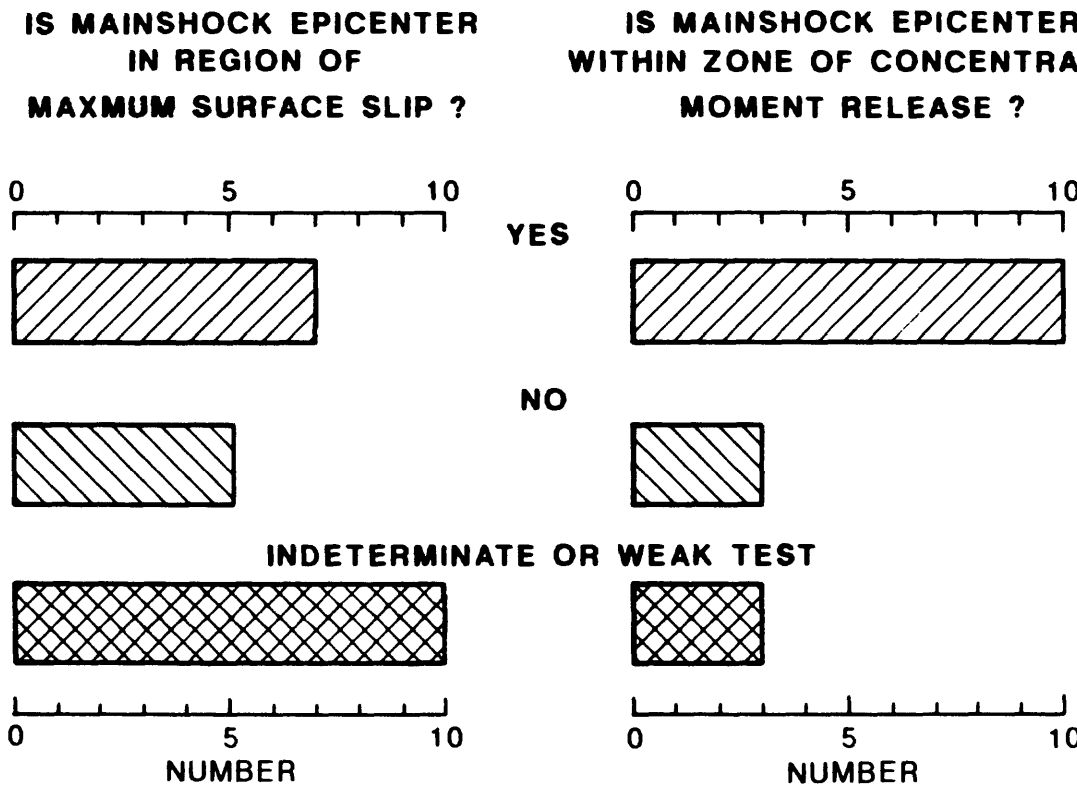

FIGURE 7. Summary of geologic and seismic observations that constrain the location of mainshock epicenter relative to (a) maximum surface slip region and (b) regions of high seismic moment release.

example, at one extreme, it has suggested that large–scale seismic failure might be triggered by a small shock randomly located on the rupture plane [*Brune*, 1979]. On the other hand, the generalizations we argue for here hint at some considerable order in the earthquake preparation process that has perhaps not hitherto been sufficiently appreciated, and our results provide observational evidence that seismic faulting may indeed be controlled by the physical properties of very localized regions of the rupture zone where slip nucleates ('asperities').

The ultimate significance of these observations depends to a considerable extent on an issue not addressed in this study, the degree to which large earthquakes repeatedly rupturing the same fault segment have similar slip distributions. Some historical and paleoseismic data suggest strong repeatability from event to event, as for example in the rupture zone of the 1966 Parkfield earthquake, along parts of the 1857 San Andreas rupture, and for several prehistoric Wasatch fault (Utah) events [*Bakun and McEvilly*, 1984; *Sieh*, 1978; *Schwartz and Coppersmith*, 1984]. In contrast, observations from a number of subduction zones indicate notable variability from one event to the next, both in the inferred slip and in the along strike extent of the source region. Examples include the 1906 and 1979 Colombia earthquakes [*Kanamori and McNally*, 1982], the 1985 and earlier Valpariaso (Chile) events [*Christensen and Ruff*, 1986], the 1894 and 1973 Nemuro–oki (Japan) shocks [*Abe*, 1977] and the 1957 Aleutian and 1986 Andreanof Islands earthquakes [*Huang and Kanamori*, 1986]. The currently available evidence bearing on this matter is thus equivocal and may suggest a range of behavior.

However, if recurrent earthquakes on the same segment of fault retain even grossly similar characteristics from event to event then the observations reported here have obvious implications for earthquake prediction research and for the issues that are the principal focus of this workshop. The tendency for rupture to initiate near regions of maximum slip suggests that it is this maximum value that controls the recurrence characteristics for the segment. Provided the regions of high slip and/or concentrated moment release can be identified from historical data or paleoseismic investigation, geologic studies and intensified monitoring might then be especially concentrated in areas that comprise only a small portion of the entire earthquake source region and yet may well lie near the eventual location of rupture initiation.

REFERENCES

Abe, K., 1977, Some problems in the prediction of the Nemuro-oki earthquake, *J. Phys. Earth*, Suppl. Issue, **25**, p. 261–271.

Allen, C.R., and Nordquist, J.M., 1972, Foreshock, mainshock, and larger aftershocks of the Borrego Mountain earthquake, *U.S. Geol. Survey Prof. Paper 787*, p. 16–23.

Ambraseys, N.N., and Tchalenko, J., 1969, The Dasht-e Bayaz earthquake of August 31, 1968 in Iran, *Bull. Seismol. Soc. Amer.*, **59**, p. 1751–1792.

Bakun, W.H., and McEvilly, T.V., 1984, Recurrence models and the Parkfield, California, earthquakes, *J. Geophys. Res.*, **89**, p. 3051–3058.

Brune, J.N., 1979, Implications of earthquake triggering and rupture propagation for earthquake prediction based on premonitory phenomena, *J. Geophys. Res.* **84**, p. 2195–2198.

Bucknam, R.C., Plafker, G., and Sharp, R.V., 1978, Fault movement (afterslip) following Guatemala earthquake of February 4, 1976, *Geology*, **6**, p. 170–173.

Christensen, D.H. and Ruff, L.J., 1986, Rupture process of the March 3, 1985 Chilean earthquake, *Geophys. Res. Lett.*, **13**, p. 721–724.

Clark, M.M., 1972, Surface rupture along the Coyote Creek fault, *U.S. Geol. Survey Prof. Paper 787*, p. 55–86.

Fukao, Y., and Kikuchi, M., 1987, Source retrieval for mantle earthquakes by iterative deconvolution of long-period P-waves, *Tectonophys.*, **144**, p. 249–269.

Gordon, F.R., Lewis, J.D., 1980, The Meckering and Calingiri earthquakes, October 1968 and March 1970, *Geol. Survey W. Australia, Bull. 126*, 229 pp.

Huang, L., and Kanamori, H., 1986, On the May 7, 1986 Andreanof Islands earthquake source parameters, *Geophys. Res. Lett.*, **13**, p. 1426–1429.

Kanamori, H., and McNally, K., 1982, Variable rupture mode of the subduction zone along the Ecuador–Colombia coast, *Bull. Seismol. Soc. Amer.*, **72**, p. 1241–1254.

Kikuchi, M. and Fukao, Y., 1987, Inversion of long-period P-waves from great earthquakes along subduction zones, *Tectonophys.*, **144**, p. 231–247.

Kikuchi, M., and Kanamori, H., 1982, Inversion of complex body waves, *Bull. Seismol. Soc. Amer.*, **72**, p. 491–506.

Lawson, A.C. (Chairman), 1908, The California Earthquake of April 18, 1906, Report of the State Earthquake Investigation Commission, 2 vol., 641 pp., Carnegie Institution of Washington, Washington, D.C.

Matsuda, T., 1974 (in Japanese), Surface faults associated with Nobi (Mino-Owari) earthquake of 1891, Japan, *Spec. Rep. Earthq. Res. Inst.*, **13**, p. 85–126.

Richter, C.F., 1958, Elementary Seismology, Freeman, San Francisco, 768 pp.

Ruff, L. and Kanamori, H., 1983, The rupture process and asperity distribution of three great earthquakes from long-period diffracted P-waves, *Phys. Earth Planet. Int.*, **31**, p. 203–230.

Schwartz, D.P., and Coppersmith, K.J., 1984, Fault behavior and characteristic earthquakes, examples from the Wasatch and San Andreas fault zones, *J. Geophys. Res.*, **89**, p. 5681–5698.

Sharp, R.V., 1982, Comparison of 1979 surface faulting with earlier displacements in the Imperial Valley, in *The Imperial Valley, California, Earthquake of October 15, 1979, U.S. Geol. Surv. Prof. Paper 1254*, p. 213–221.

Sieh, K., 1978, Slip along the San Andreas fault associated with the great 1857 earthquake, *Bull. Seismol. Soc. Amer.*, **68**, p. 1421–1448.

Snay, R.A., Cline, M.W., and Timmerman, E.L., 1983, Regional deformation of the earth model for the San Diego region, California, *J. Geophys. Res.*, **88**, p. 5009–5024.

Wallace, R.E., 1984, Faulting related to the 1915 earthquakes in Pleasant Valley, Nevada, *U.S. Geol. Surv. Prof. Paper 1274-A*, p. A1–A33.

Zhang, Y., Thatcher, W., 1988. Coseismic deformation accompanying the May 8, 1940 Imperial Valley, California earthquake, to be submitted to *J. Geophys. Res.*.

FAULT-PLANE SEGMENTATION IN BRITTLE CRUST AND ANISTROPY IN LOADING SYSTEM

by

Robert E. Wallace
U.S. Geological Survey
Menlo Park, CA 94025

ABSTRACT

Lengths of fault segments are strongly influenced by the thickness of the brittle layer of the crust. The maximum length of fault segments in plan or map view approximates the down-dip dimensions of the fault-plane segments. In addition to segmentation in the prefractured, brittle upper crust -- the response system -- anisotropy in the loading system below may govern which segment of a fault, or which set of faults, is activated. Various degrees of decoupling between the brittle response system above, and the brittle-ductile loading system below are likely.

Segmentation in the Brittle Crust

Lengths of fault segments appear to be strongly influenced by the thickness of the brittle layer of the crust. The maximum length of fault segments in plan or map view approximates the down-dip dimension of the fault-plane segments through the brittle part of the crust. The greatest depth of microseismicity is assumed to represent the depth of brittle behavior.

For strike-slip faults, such as the San Andreas fault, the fault plane is nearly vertical and the down-dip dimension equals the thickness of the brittle crust. The maximum length of segments and down-dip dimension both approximate 10-15 km (Fig. 1, and Wallace, R.E., 1973). The census of segment lengths was derived by measuring the lengths of fault strands shown on strip maps prepared by the staff of the U.S. Geological Survey (Brown, R.D., Jr., 1970, Brown, R.D., Jr., and Wolfe, E.W., 1972, Vedder, J.G., and Wallace, R.E., 1970, Ross, D.C., 1969). The elements mapped are the traces of the most recent displacements of the ground surface. Characteristic patterns of these surface fractures are shown in Wallace (1973).

In large earthquakes, many adjacent and overlapping fault segments display surface displacement. An implication is that if each segment represents a distinct rupture event, a large earthquake is made up of a set of such events very closely spaced in time. What controls the extent or number of segments that break during a single large earthquake is unknown, but later in this paper I suggest that anisotropy in the loading system below the prefactured upper crust is a significant control.

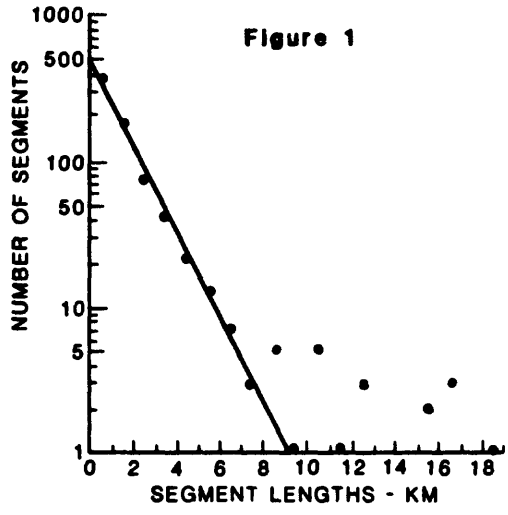

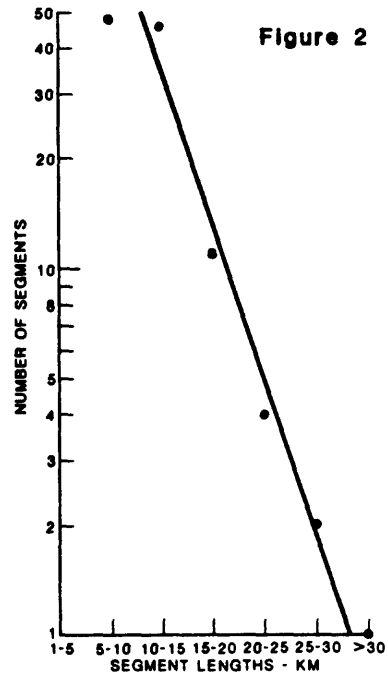

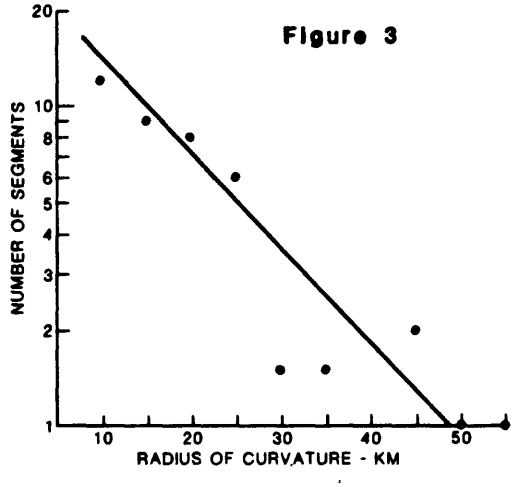

Figure 1.--Census of fault segments of different lengths along the San Andreas fault, California. Points represent number of segments in increments 0.09-.9 km, 1-1.9 km, etc. (from Wallace, R.E., 1973).

Figure 2.--Census of range-front fault segments in The Basin and Range province, north-central Nevada. Points represent number of segments in increments 5-10 km, 10-15 km, etc.

Figure 3.--Census showing radius of curvature of nearly-circular arcuate segments of range-front faults in the Basin and Range province, north-central Nevada. Points represent number of radii of approximately 10 km, 15 km, 20 km, etc.

In north-central Nevada, a census of segments larger than about 1 km of range-bounding faults was made in the Lovelock, McDermitt, Millett, Tonopah and Winnemucca two-degree quadrangle topographic maps (scale 1:250,000). For this study a first approximation was made by considering range fronts that topographically are linear or arcuate to be fault controlled, and no further classification by age or type of fault was made. The maximum length of segments approximates 30 to 35 km (Fig. 2). Such segment lengths approximate the down-dip dimension along planes dipping between 45 and 60 degrees, a common dip of normal faults, through a brittle crust about 25 km thick.

Considering the maximum depth of microseismicity to represent the thickness of the brittle crust, a few events, indeed, have been recorded at depths between 20 and 28 km (Smith and Ryall, 1980). A more significant cutoff, however, appears to be in the 13 to 15 km range.

Several geometric relations should be considered in comparing down-dip dimensions to segment lengths. Instead of fault planes continuing to depth at uniform dips of 45 to 60 degrees, they may flatten with depth in a listric style. A listric fault extending to a depth of 15 km, for example, would be 23 km along a cross section having a circular arc. The fault planes, conceivably, may gradually decrease in dip to approach a subhorizontal plane of decoupling asymptotically. Given such geometry, the down-dip dimension through a 15-km thick brittle zone could be as large as the 30-35 km maximum segment length observed.

Many of the range-front faults, as well as of the range crests, are arcuate in plan and may be arcuate in cross section as well (Moore, 1960). Moore also noted that in the Basin and Range province the preponderance of ranges that are tilted east are convex east in plan, and similarly those ranges that are tilted west are convex west. Further data on the three-dimensional configurations of range-bounding faults could be significant to the present problem.

Apropos of the arcuate nature of many faults, in the four quadrangles on which the present study focused, the radii of curvature of range-front fault segments that are arcs of circles in plan, are generally less than 30 km, although a few are between 50 and 55 km (Fig. 3). Commonly, the arcuate segments subtend between 40 and 50 degrees of arc, and are about 25 km long.

The Response System, the Loading System and Coupling Between Them

In the previous section, segmentation is considered only in the prefractured, brittle part of the crust, what may be referred to as the "response system." The "loading system" below the brittle upper crust also seems to be partitioned into zones, patches and segments; it is anisotropic. The loading system may itself be layered into a brittle-

ductile upper zone and a deeper, rheid or ductile zone. Sibson (1982, 1984) discusses transitions with depth as well as roughness at the base of the seismogenic zone; both factors influence the coupling of the loading system to the response system. A model is suggested as follows:

1. Elastic response system: This is made up of the brittle, upper part of the crust in which earthquakes are primarily generated. In the western United States this zone is between 10 and 20 km thick. This upper crust is highly fractured, and for a single loading event may be considered particulate or prefractured. The distribution of faults activated by a single loading event depends largely on the shape and size of the zone of loading, and to a lesser extent on the orientation and fracture mechanics of the upper crust.

2. Anelastic loading system: This is perhaps made up of two zones, an upper brittle-ductile zone in which inhomogeneities are abundant, and a deeper more-nearly homogeneous ductile zone. Localizations of strain relate to the distribution of heat, ductility, shear zones, kink zones, etc.

3. Zones of decoupling: Between the response and loading systems some degree of decoupling is likely. Zones of decoupling relate primarily to vertical transitions between zones of different behavior. For example, zones of decoupling develop along gravity-driven, low-angle thrust faults, and may develop above zones of extension in ductile materials. Decoupling undoubtedly is not uniform everywhere.

An excellent example of a deep zone causing the reactivation of faults in a prefractured crust, is provided by the set of surface faults produced during the earthquakes of October 2, 1915, in Pleasant Valley, Nevada (Fig. 4, and Wallace, R.E., 1984). There, four fault segments were reactivated in a belt six km wide by 60 km long. Only those segments of the earlier faults that extended into or through the 6 by 60 km belt were broken in 1915, even though some of the faults extend far beyond the belt. The four segments display an en echelon pattern suggestive of left-lateral slip, whereas slickensides and other evidence shows that the strain was extensional and normal to the trend of the 60-km long belt. The 6 by 60 km belt is interpreted to represent a deep, linear structure, not obvious at the surface except through its effect on the prefractured zone above.

The relation of a prefractured brittle crust to an underlying zone of localized extension in the loading system is shown in figure 5. The slip directions imposed on the existing faults may be different from those characteristic of the formative period of the faults.

I suggest that although the details of segmentation may be controlled by the geometry of the original fractures, the gross features, for example, how many adjacent segments, or what part of a fault set will be reactivated, depends on the shape and size of the loading patch below the brittle crust. This idea is illustrated in figure 6. If the loading patch

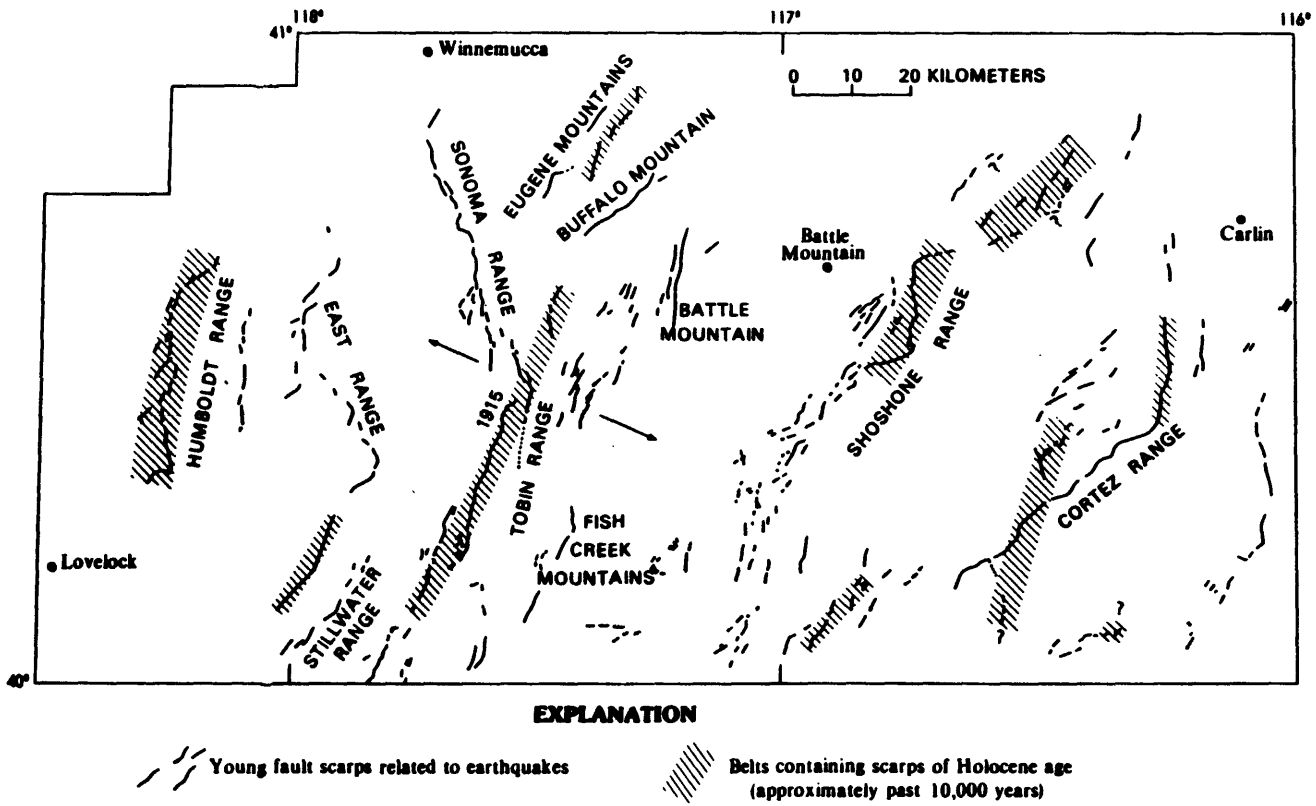

Figure 4.--Faults in north-central Nevada, showing reactivation of faults in belts that cut across the preexisting pattern of faults. For example, four fault segments were reactivated in 1915 in a belt 6 by 60 km even though some faults extend beyond that belt (from Wallace, R.E., 1984).

Figure 5

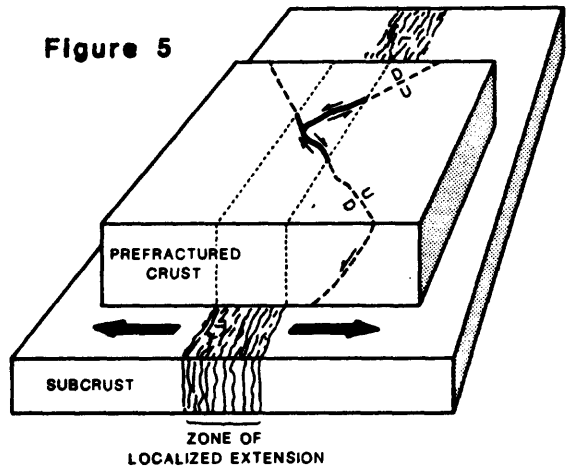

Figure 6

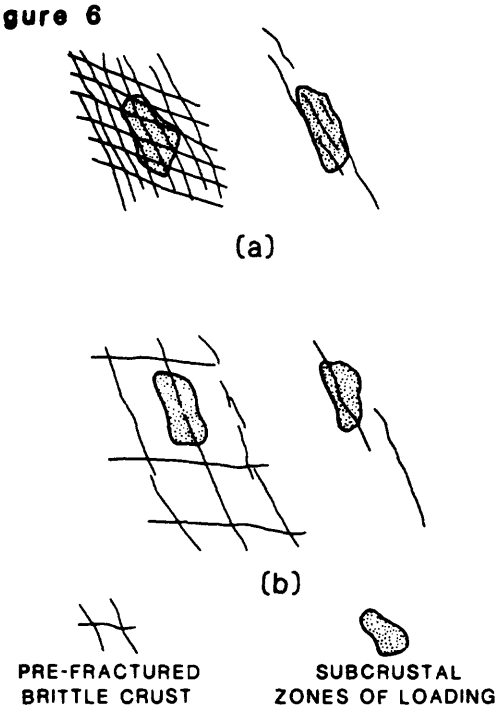

Figure 5.--Diagram showing how a zone of localized extension in the subcrust may reactivate segments in a prefractured upper crust, as appears to have happened in the 1915 Pleasant Valley earthquake, Nevada.

Figure 6--Diagram to show how size and shape of a loading patch below a prefractured upper crust may reactivate a part of one fault or several faults. a. Loading patch is relatively large with respect to the texture of the existing fracture pattern so that several segments are reactivated. b. Loading patch is relatively small with respect to the texture of the existing fracture pattern so that only parts of individual faults are reactivated.

is small compared to the texture of the prefractured upper crust, a single fault or segment of a single fault may be all that is reactivated. If the loading patch is large compared to the texture of the set of fractures, several segments may be reactivated, including some faults and segments that are not ideally oriented to the stress system.

The inhomogeneities in the loading system are difficult to assess. Regional gravity and magnetic studies provide evidence of the types and distribution of potential inhomogeneities in the deeper loading system. Maps by Hildenbrand and others (1984) reveal many anomalies that must relate to inhomogeneities in the deeper crust, and these may have a bearing on the anistropy of the loading system. For example, in the map showing residual Bouguer gravity of wavelengths less than 1,000 km, a rectangular area about 150 km by 100 km in northwestern Nevada shows a striking high. This gravity high coincides with an area of extensive basin development, and is interpreted by Wallace (1984) as an area of relatively rapid extension as compared to surrounding regions. The central Nevada seismic belt lies along the southeastern margin of this area, and the extension direction displayed in the 1915 event is approximately normal to the long axis of this large, rectangular zone of extension.

Discussion and Conclusions

For most large earthquakes, the upper part of the crust to depths of 10 to 20 km, should be considered part of a response system, characteristically brittle and prefractured. The thickness of this brittle zone has considerable influence on the maximum length of surface segments of faults.

Loading of the brittle upper crust is imposed from below through materials that increase in ductility with depth. Inhomogeneities in this material below the brittle crust may load the existing faults above in a variety of patterns, sometimes and in some places reactivating only one fault, or at other times and in other places reactivating a set of faults, even some that are disconnected.

Various degrees of coupling and decoupling between the loading system and the response system must exist. Evaluation of this factor is extremely important, but would seem to be a very difficult problem to address.

REFERENCES CITED

Brown, R.D., Jr., 1970, Map showing recently active breaks along the San Andreas and related faults between the northern Gabilan Range and Cholame Valley, California: U.S. Geological Survey Miscellaneous Geologic Investigations Map I-575, scale 1:62,500.

Brown, R.D., Jr., and Wolfe, E.W., 1972, Map showing recently active breaks along the San Andreas fault between Point Delgada and Bolinas Bay, California: U.S. Geological Survey Miscellaneous Geologic Investigations Map I-692, scale 1:24,000.

Hildenbrand, T.G., Simpson, R.W., Godson, R.H., and Kane, M.F., 1984, Digital colored residual and regional Bouguer gravity maps of the conterminous United States with cutoff wavelengths of 250 km and 1,000 km: U.S. Geological Survey Geophysical Investigations Map, GP-953-A, Scale 1:7,500,000.

Moore, J.G., 1960, Curvature of normal faults in the Basin and Range province of the western United States: U.S. Geological Survey Research, 1960--Short Papers in the Geological Sciences, p. B409-B411.

Ross, D.C., 1969, Map showing recently active breaks along the San Andreas fault between Tejon Pass and Cajon Pass, southern California: U.S. Geological Survey Miscellaneous Geologic Investigations Map I-553, scale 1:24,000.

Sibson, R.H., 1982, Fault zone models, heat flow, and the depth distribution of earthquakes in the continental crust of the United States: Seismological Society of America Bulletin, v. 72, no. 1, p. 151-163.

---1984, Roughness at the base of the seismogenic zone: contributing factors: Journal of Geophysical Research, v. 89, no. B7, p. 5791-5799.

Smith, G.M., and Ryall, F.D., 1980, Bulletin of the Seismological Laboratory for the period Jan. 1, 1975 to December 31, 1979: Mackay School of Mines, University of Nevada, Reno, p. 1-84.

Vedder, J.G., and Wallace, R.E., 1970, Map showing recently active breaks along the San Andreas and related faults between Cholame Valley and Tejon Pass, California: U.S. Geological Survey Miscellaneous Geologic Investigations Map I-574, scale 1:24,000.

Wallace, R.E., 1973, Surface fracture patterns along the San Andreas fault: in Kovach, R.L., and Nur, Amos, eds., Proceedings of the conference on tectonic problems of the San Andreas fault system: Geological Sciences, Vol. XI, School of Earth Sciences, Stanford Universitv, Stanford, Calif., p. 248-250.

---1984, Faulting related to the 1915 earthquakes in Pleasant Valley, Nevada: U.S. Geological Survey Professional Paper 1274-A, p. A1-A33.

---1984, Patterns and timing of Late Quaternary in the Great Basin province and relation to some regional tectonic features: Journal of Geophysical Research, v. 89, no. B7, p. 5763-5769.

SEISMICITY AND THE STRUCTURAL EVOLUTION OF STRIKE-SLIP FAULTS

Steven G. Wesnousky
Center For Earthquake Research and Information
Memphis State University
Memphis, TN, 38152

ABSTRACT

The mapped traces of strike-slip faults are commonly characterized by discontinuities that appear as steps in map-view. My survey of major fault zones in California and Turkey indicates that the number of steps per unit length along the trace of strike-slip faults is a smoothly decreasing function of cumulative geologic offset. The observation is consistent with previously published laboratory models which suggest that, during the initial stages of development, strike-slip faults are characterized by a zone of discrete en echelon fault segments and that, with continued offset, the separate fault segments ultimately coalesce to produce a single, throughgoing strand. When coupled with a growing body of evidence which indicates steps in fault traces work to impede or arrest the propagation of earthquake ruptures, the apparent smoothing of the fault trace with displacement may be further interpreted to indicate that the distribution of strength properties on a fault plane is spatially heterogeneous, and that the degree of heterogeneity is a function of cumulative offset. A consequence of this structural evolution is that faults may undergo a seismological evolution as well, whereby the maximum size and relative frequency distribution of earthquakes of different size on a fault is also a function of cumulative offset.

INTRODUCTION

An earthquake in California or other region of similar tectonic style does not generally rupture the whole length of the fault on which it occurs but, rather, only a fraction of the entire fault length. As well, sufficient observations now exist to indicate that the endpoints of strike-slip earthquake ruptures are commonly associated with step-like discontinuities along mapped fault traces (e.g. Segall and Pollard, 1980; Sibson, 1985, 1986; Barka and Hancock, 1982; Barka and Kadinsky-Cade, 1988). Stress concentrations will occur along a fault at step-like discontinuities when slip occurs along the fault during an earthquake (Segall and Pollard, 1980). Such discontinuities are commonly referred to as releasing- or restraining-steps depending on whether the stress concentration is extensional or compressional in nature, respectively, and the severity of the stress concentration will generally be

a function of the size l_s of the step (Figure 1; Crowell, 1974a,b, Segall and Pollard, 1980). The stress concentrations at steps may be sufficient to impede or stop the propagation of an earthquake rupture and, on that basis, investigators have attributed a causal association to the observed coincidence between the endpoints of earthquake ruptures and the location of steps along mapped fault traces (Segall and Pollard, 1980; Barka and Kadinsky-Cade, 1988; Barka and Hancock, 1982; Sibson, 1985, 1986). In turn, laboratory models and scattered field observations have been the basis to suggest that, during the initial stages of development, strike-slip faults are characterized by a zone of discrete fault segments, each of which is separated from the next segment by a step, and that, with continued displacement, the individual fault segments ultimately coalesce to accomodate displacements along a principal and throughgoing fault (Figure 2, Wilcox et al, 1973; Harding, 1974, 1976, Withjack and Jamison, 1986). The few observations available thus point to a close connection between the seismological and structural evolution of fault zones and provide the impetus here to examine whether or not there exists a systematic relationship between frequency of occurrence of step-like discontinuities, the maximum size of earthquakes, and the total geologic offset registered along the trace of active strike-slip faults.

OBSERVATIONS

Strike-slip fault zones and earthquakes in California are the principal basis for my observations. It is for this region that relatively comprehensive data are available concerning the surface trace and the total geologic offset of active faults. As well, I will draw upon observations regarding the much studied North Anatolian fault in Turkey. In this section then, data concerning the total geologic offset, the extent of surface rupture during historical earthquakes, and the location of step-like discontinuities along each of the fault zones are briefly reviewed. Due to the scale of available maps, attention is limited to steps in fault trace characterized by $l_s \geq$ 1km. The sum of observations provides the groundwork for later discussion of the structural and seismological evolution of strike-slip fault zones.

The Newport-Inglewood, Elsinore, San Jacinto, Garlock, Calaveras-Green Valley, Hayward-Maacama, and San Andreas are the major strike-slip fault zones in California (Figure 3). Data concerning the total geologic offset, the sites of historical earthquake ruptures, and the location of step-like discontinuities along each of the fault zones are pictured in Figures 4 and 5, summarized in Table 1, and briefly reviewed in the following paragraphs.

It is generally accepted that right-slip of 250 km or more has been accomodated by the San Andreas fault since early Miocene (Crowell, 1962; Grantz and Dickinson, 1968; Hill, 1981). The total length of the fault where exposed onshore is about 1000 km. Though profoundly bent, the trace of the San Andreas is continuous except for a complex, ill-defined restraining step near the San Gorgonio Pass fault zone and a 1-km releasing step at Parkfield (Figure 4). Surface ruptures during the 1857 (M=7.9) Ft. Tejon earthquake extended southward from near the 1-km step near Parkfield for a distance of 360-400 km to a point near Cajon Pass (Figure 4, Sieh, 1978). As well, the 1906 San Francisco earthquake produced surface ruptures extending northward to offshore Pt. Arena from a point near San Juan Bautista (Figure 4; Lawson, 1908).

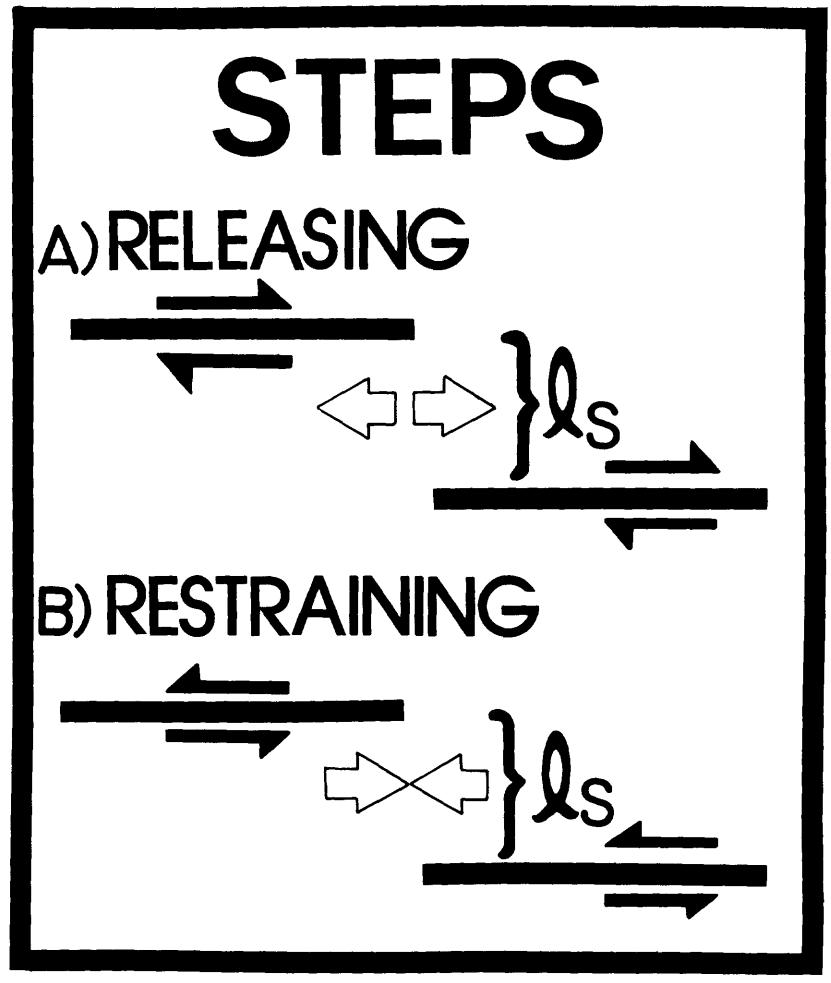

Figure 1. Map-view illustration of a) right-lateral and b) left-lateral faults, each characterized by a step of dimension l_s in the fault trace. Stress concentrations (open arrows) will occur within steps along the fault trace when slip occurs along a fault during an earthquake. Such discontinuities are commonly referred to as a) releasing or b) restraining steps depending on whether the stress concentration resulting from slip is extensional ($\Leftarrow\Rightarrow$) or compressional ($\Rightarrow\Leftarrow$) in nature. The sense of stress concentration is a function of the sense of the displacement vector (solid half-arrows) relative to the direction of the step, either to the right or left as viewed along strike of the fault.

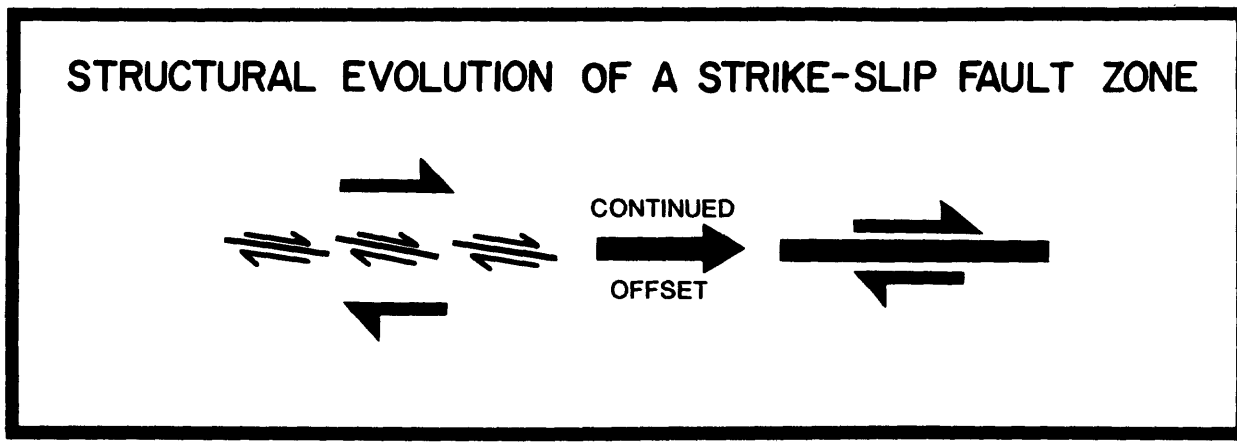

Figure 2. Laboratory observations coupled with scattered field observations suggest that, during the initial stages of development, strike-slip faults, when observed in map-view, are characterized by a zone of discrete en echelon fault segments which, when taken together, form a fault zone, and that, with continued offset through time, the fault segments ultimately coalesce to accommodate displacements along a principal and throughgoing fault.

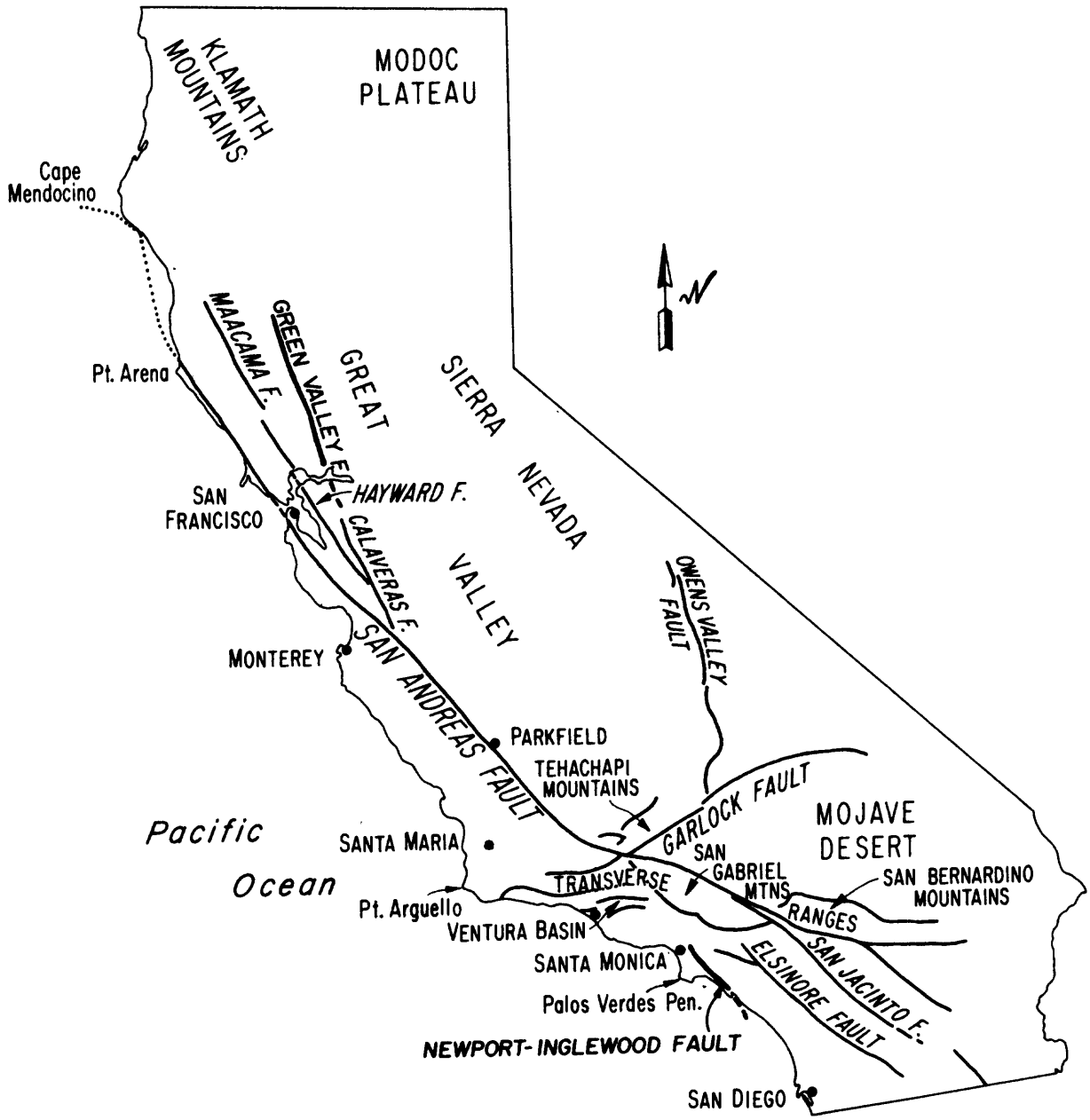

Figure 3. Major fault zones discussed in text of this study are shown in this map of California.

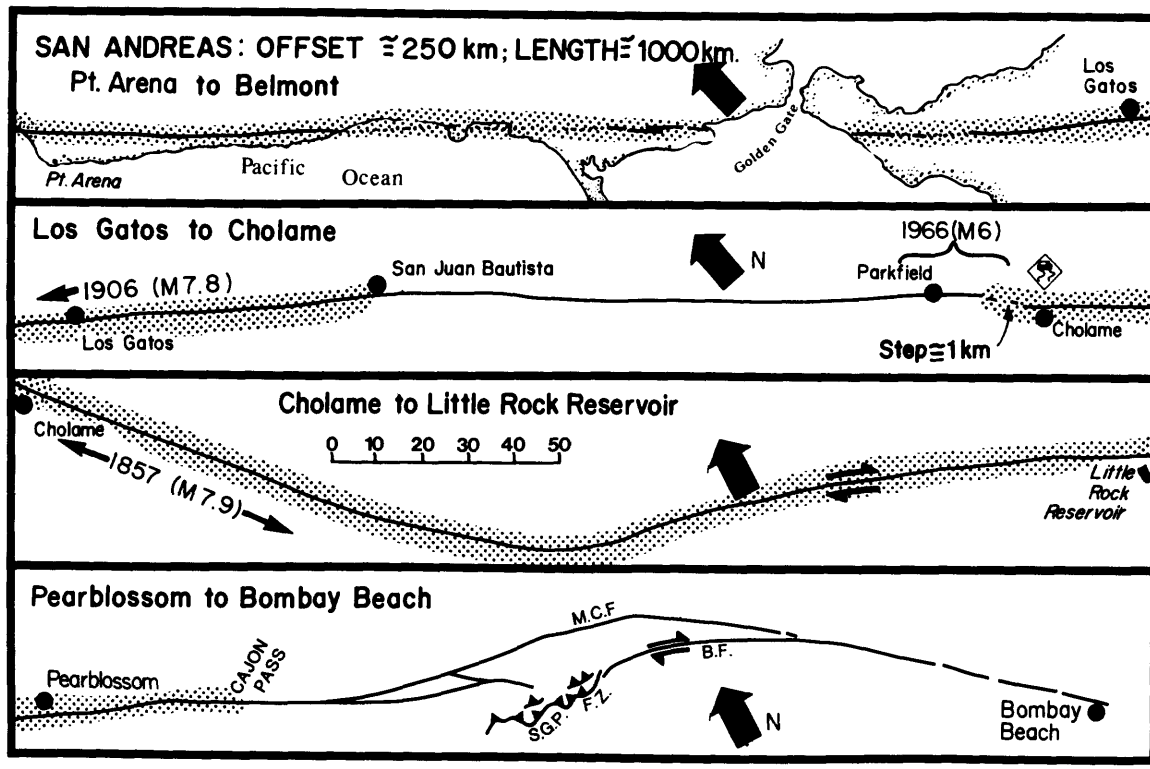

Figure 4. Strip map of San Andreas fault, California. Strips progress northwest to southeast from top to bottom of figure, respectively. Large ($M \sim 7.9$) earthquakes in 1906 and 1857 produced surface ruptures (stippled pattern) extending to the northwest of Belmont and southeast of Parkfield, respectively. A small ($M \sim 6$) earthquake broke the segment of the fault between Parkfield and Cholame in 1966. The trace of the fault is relatively smooth but for a 1km releasing step near Parkfield and a complex restraining bend which encompasses the Banning fault (B.F.), Mission Creek Faults (M.C.F.) and the San Gorgonio Pass Fault Zone (S.G.P.F.Z.). Right-lateral offset indicated by half sided arrows. Primary references for figure are Clark (1984), Hope (1969), Ross (1969), Vedder and Wallace (1970), Brown (1970), Brown and Wolfe (1972), and Matti et al (1985).

Table 1. Earthquake and Fault Data						
#	Fault	Total Offset (km)	Total Fault Length (km)	Historical Maximum Magnitude	# of Steps	Steps/ Length (km^{-1})
1	Newport-Inglewood	1-10	60	6.3	4	.066
2	Whittier-Elsinore	10-40	330	7	3	.009
3	San Jacinto	25	230	6.5-6.8	5	.022
4	Garlock	64	240	—	1	.004
5	Calaveras	24	220	6.2-6.6	4	.018
6	San Andreas	$\geq$250	1000	7.9	2	.002
7	Hayward	?	200	6.8	3	.015
8	N. Anatolian	25-45	980	8	12	.012

Cumulative left-lateral offset on the Garlock fault (Figure 5a) is 64 km, as evidenced by the separation of a Mesozoic dike swarm (Smith, 1962). A releasing step of 3-4 km along the fault trace occurs at Fremont Valley. Except for another small 1/2 km restraining step near the eastern end of the fault zone, the remainder of the Garlock trace is relatively smooth (Clark, 1973). Thus, the 240 km trace of the Garlock fault consists of 2 principal segments which are separated by the releasing step at Fremont Valley. The Garlock has not been the site of any large historical earthquakes.

The Whittier-Elsinore fault zone, including the Laguna-Salada strand, strikes northwest for about 330 km from south of the U.S.-Mexico border to north of Lake Elsinore (Figure 5b). Lamar and Rockwell (1986) summarize studies concerning the age and offset of the Whittier-Elsinore fault zone. Apparent offset of Paleocene facies across the Whittier-Elsinore fault suggests 30-40 km of right-slip near Lake Elsinore (Lamar, 1961; Yerkes and Campbell, 1971; Sage, 1973). However, Weber (1977) estimates that the total right-slip along the Elsinore fault in the same area is about 9 to 11 km., based on the distribution of older basement rocks. Woodford et al. (1972) similarly believe that large post-Cretaceous strike-slip on the Whittier-Elsinore fault zone is precluded by the distribution of distinctive Upper Cretaceous and Paleocene strata on opposite sides of the fault zone. Farther to the southeast, Mueller (1984) constrains total slip to no more than 35 to 40 km based on the size and geometry of pullapart basins developed along the Laguna Salada fault zone. Maximum total offset along the Elsinore fault thus appears limited to between 10 km and 40 km, and may vary along fault strike. The 330 km length of the fault zone is interrupted by 3 steps, each with an effective step length $l_s \simeq 3$ km (Figure 5b). Geological evidence in conjunction with reported isoseismal data have been used to strongly suggest that offsets of 5 m or more observed along a stretch of the Laguna Salada fault were produced by a magnitude 7 or larger earthquake on Feb 24, 1892 (Toppozada et al., 1981; Strand, 1980; Mueller, 1984; Mueller and Rockwell, 1984; Anderson et al., 1988).

The Calaveras-Green Valley fault zone strikes northward and approximately parallel to the San Andreas fault starting from a point east of Monterey (Figures 3 and 5c). I am aware of only one study regarding the total offset of this fault zone. Kintzer et al. (1977) report that a Middle Miocene shoreline exposed near Calaveras Reservoir may be offset in a right-lateral sense for a distance of 24 km across the Calaveras fault zone. The 220 km length of the mapped fault zone is broken by 4 distinct steps of $l_s \geq 1$ km. The largest recent earthquakes to occur on the fault were the 1979 Coyote Lake (M=5.9) and 1984 Morgan Hill (M=6.2) events (Bakun et al., 1984; Reasenberg and Ellsworth, 1982). Although significant surface ruptures were not observed for either event, aftershock studies show rupture lengths for each were on order of 25 km (Figure 5d). The 1984 earthquake was apparently preceded by a larger magnitude 6.6 earthquake in 1911 (Bakun et al., 1984), which is the largest historical earthquake attributed to slip along this fault zone.

The Hayward-Maacama fault branches from the Calaveras a few kilometers north of Calaveras Reservoir (Figure 5c). I am aware of no data bearing directly on the total offset of the Hayward-Maacama fault zone, though the discontinuous trace and weak geomorphic expression of the fault have been used as evidence to suggest a relatively recent inititiation for the fault zone (Herd, *pers. comm*, Herd, 1978, Herd and Helley, 1977, and Pampeyan et al., 1981). The 200 km length of the fault characterized by strike-slip offset is interrupted

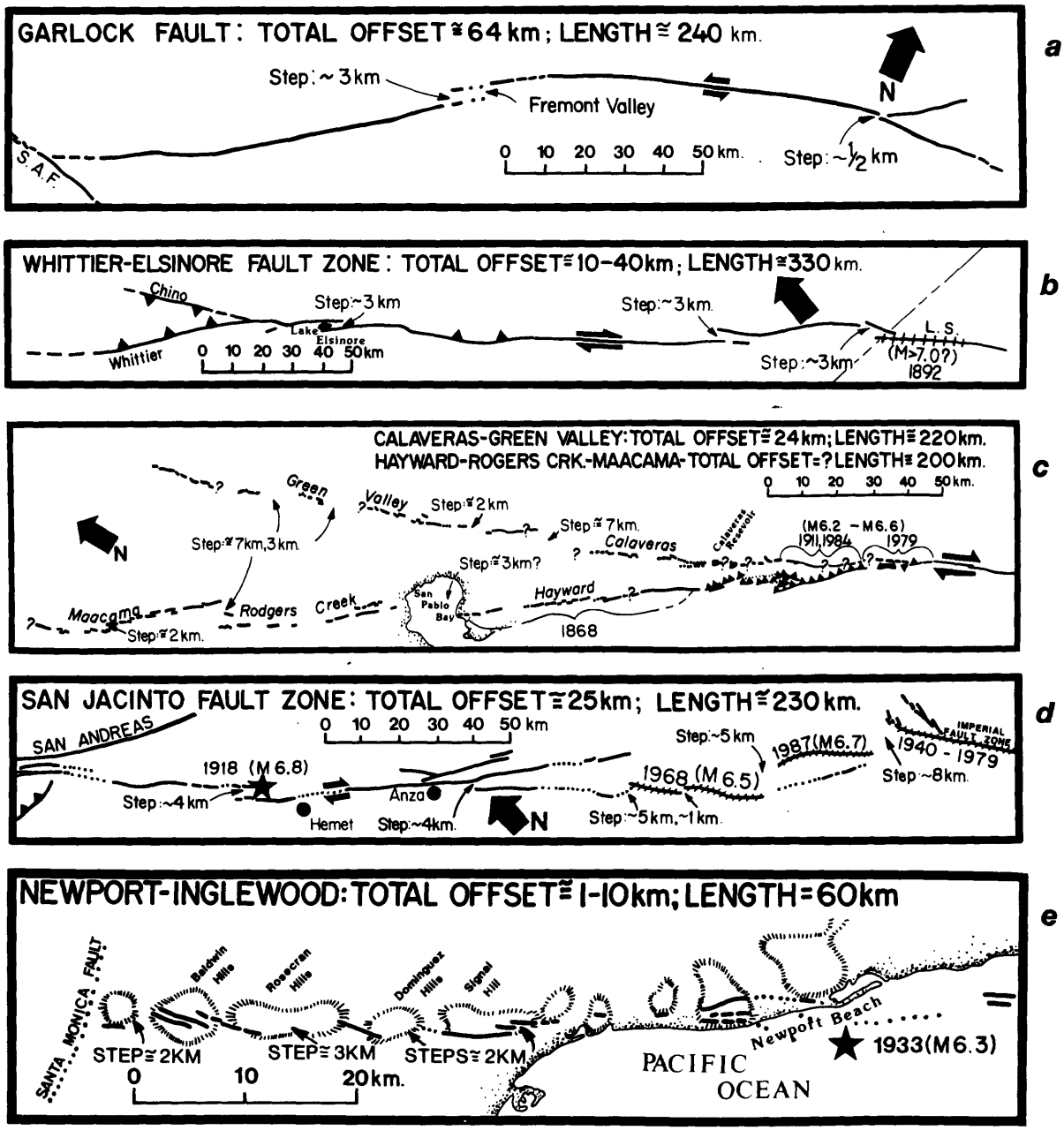

Figure 5. Mapped traces of the a) Garlock, b) Whittier-Elsinore, c) Calaveras-Green Valley and Hayward-Rogers Greek-Maacam, d) San Jacinto, and e)Newport-Inglewood fault zones. Figures are adapted from Clark (1973), Anderson et al. (1988), Herd (1988), Sharp (1975) and Barrows (1974), respectively. Steps in fault trace greater than about 1 km are annotated. The extent of rupture during the 1911, 1979, 1984 and 1868 earthquakes along the Calaveras and Hayward fault systems are bracketed. Hachured segments of the San Jacinto and Imperial faults produced surface rupture in 1940, 1968, 1979 and 1987 along and near the Superstition Hills (S.H.) and Superstition Mountains (S.M.) strands of the fault zone. The Laguna Salada fault (L.S.) ruptured in a large earthquake in 1892. Star marks epicenter of 1933 Long Beach earthquake. Half-sided arrows indicate sense of displacement along faults.

by 3 steps with l_s greater than 1 km (Figure 5c). An approximately 60 km segment of the fault zone ruptured in a magnitude 6.8 earthquake in 1868 (Figure 5c; Toppozada et al., 1981). There are also reports that a similar sized event ruptured the same segment of the fault in 1836, though evidence for the actual location of the 1836 event is scant (Toppozada et al., 1981).

The San Jacinto fault zone splays and strikes southeastward from the San Andreas fault for a distance of about 230 km (Figures 3 and 5d). Cumulative right-lateral movement across the San Jacinto is interpreted to be about 25 km and may have all taken place since Pliocene time (Sharp, 1967). North of the Imperial fault, the San Jacinto is interrupted by 4 or 5 steps of $l_s \geq 1$ km, depending on whether the Superstition Hills or Superstition Mountain fault segments is interpreted to be the active continuation of the San Jacinto fault (Figure 5d). The recent 1968 Borrego Mountain (M=6.5) and 1987 Superstition Hills (M=6.7) earthquakes produced surface ruptures about 24 and 30 km in length, respectively (Clark, 1972; Kahle et al., 1988). A magnitude 6.8 earthquake also reportedly occurred north of Anza in 1918, but evidence of surface rupture is lacking (Sanders and Kanamori, 1984).

The Newport-Inglewood fault zone strikes southward from near the Baldwin Hills and is expressed topographically by an aligned series of low hills that rise as much as 120 m above the adjacent plains (Figure 5e). Structurally, the fault zone near the surface is a series of discontinuous north- to northwest striking faults and northwest- to west-trending folds (Barrows, 1974). Evaluations of total right-lateral displacement along the fault zone range from 200 meters near the Baldwin Hills to a maximum of 10 km near Huntington Beach (Barrows, 1974). The fault zone is about 60 km long where evident onshore and broken by at least 4 prominent steps (Figure 5e). The 1933 Long Beach earthquake (M=6.3) epicenter is located off Newport Beach (Figure 5e; Richter, 1958). Aftershocks for the 1933 event apparently concentrated along a 30 km stretch of the fault zone between Signal Hill and the epicenter (Benioff, 1938; Richter, 1958).

Relatively detailed information regarding the character of the mapped fault trace, the extent of historical earthquake ruptures, and the cumulative geologic offset also exists for the North Anatolian fault zone in Turkey and is summarized in Table 1. The fault zone strikes easterly across Turkey for a distance of about 1000 km (Figure 6a). An extensive review of recent literature and presentation of new geological observations by Barka and Gulen (1988) indicates displacement initiated along the North Anatolian fault in the late Miocene to early Pliocene and ranges between 25 and 35 km. The fault zone recently ruptured in a westwardly-migrating sequence of large magnitude 7 to 8 earthquakes between the years 1939 and 1967 (Figures 6; Ambraseys, 1970, 1975). Recently, Barka and Kadinsky-Cade (1988) compared details of fault trace geometry to the extent of historical surface ruptures along the North Anatolian fault zone. They concluded that fault geometry strongly controlled the extent of the earthquake ruptures, noting that the endpoints of the Anatolian earthquakes commonly ended at large releasing steps along the fault zone. Figure 6, adapted directly from their map, shows all steps with $l_s \geq 1$ km and the extent of surface ruptures during large historical earthquakes in 1939, 1942, 1943, 1944, and 1967. The 1000 km length of the fault trace in Figure 6 is broken by 12 steps of $l_s \geq 1$ km. Though the endpoints of the historical ruptures commonly end near steps, it is also

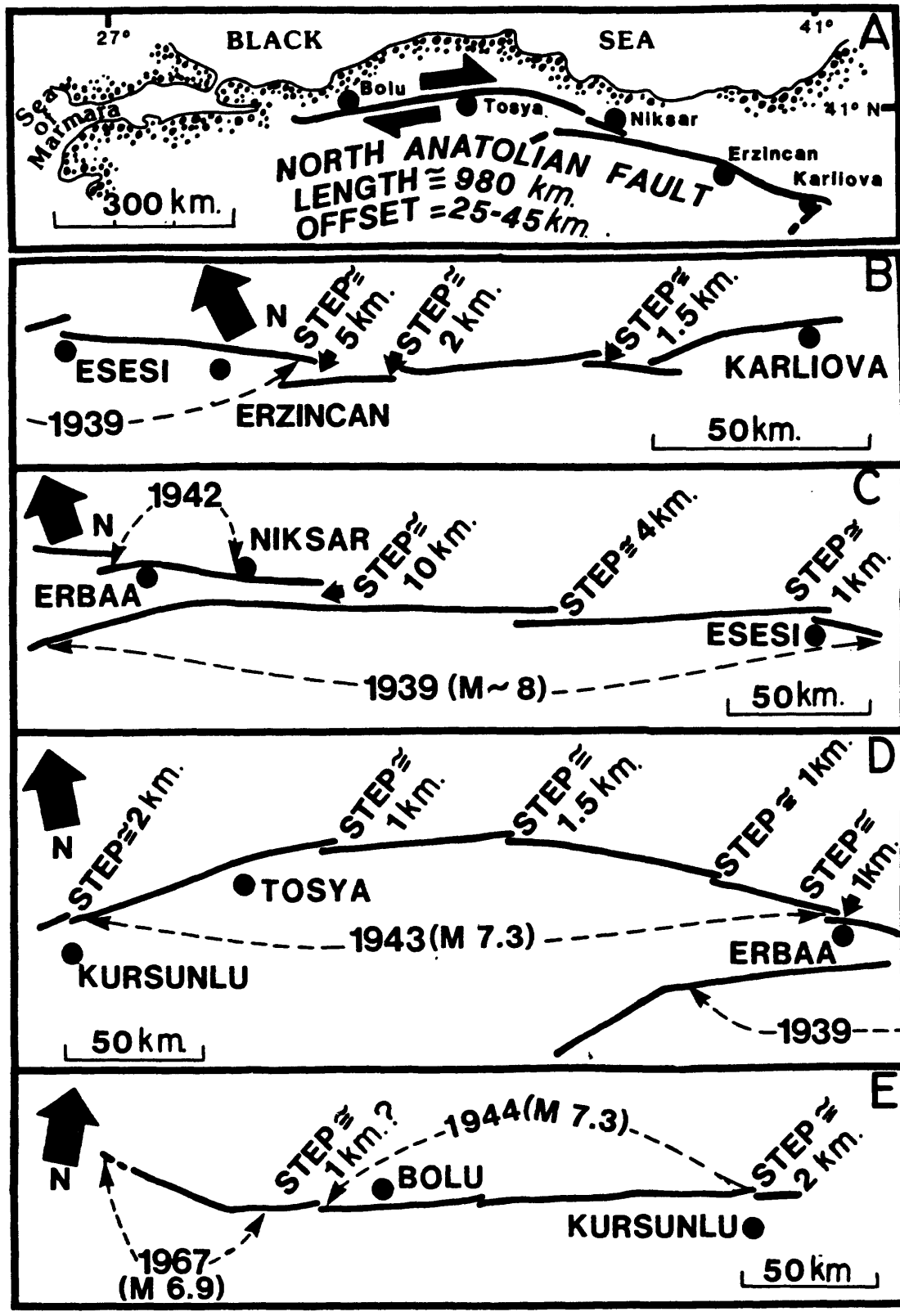

Figure 6. a) The North Anatolian fault shows right-lateral movement and strikes westward across Turkey from a point near Karliova to west of Bolu. Larger scale and overlapping strip maps of the fault are taken from Barka and Kadinsky-Cade (1988) (b–e) and show location of steps greater than about 1km in size. The extent of rupture along strike of the fault (dashed arrows) is shown for large and recent earthquakes of 1939, 1942, 1943, and 1944.

evident that the 1939 Ercincan and 1943 Tosya earthquakes ruptured through a number of steps in the fault trace.

DISCUSSION

A plot of the rupture lengths of large California and Anatolian earthquakes versus the values of l_s for each step in fault trace observed at both the endpoints and within the respective earthquake rupture zones is shown in Figure 7. In addition, I also have included observations regarding the well-documented great 1891 Nobi earthquake of Japan (Matsuda, 1974). The figure graphically summarizes the above observations regarding the relationship of the size and location of steps along strike-slip fault traces to the length and location of earthquake ruptures. Hence, for example, Figure 7 shows that the 1939 Anatolian earthquake produced about 320 km of surface rupture and that the endpoints of the rupture are associated with steps of 10 and 15 km, respectively. As well, the figure shows that the same rupture propagated through steps of 1 and 4 km. Hence, the steps located within the 1939 rupture zone are smaller than the steps associated with the termination of the rupture. A similar pattern is found upon observing the other earthquakes in Figure 7. Specifically, steps associated with the endpoints of ruptures are commonly the largest discontinuities registered along the length of the respective fault zones. The trend, admittedly, is not without exception. The 1943 Anatolian earthquake is a case in point, where a step interior to the rupture zone is larger than a similar step observed at the endpoint of the rupture. As well, it is apparent that the endpoints of all ruptures are not marked by steps in mapped fault traces, as evidenced by the southern limit of the 1857 earthquake (Figure 4). Nonetheless, the observations are certainly sufficient to argue that the association of steps with the endpoints of earthquakes is not merely coincidence. Rather, the stress concentrations resulting from the discontinuities appear to play a principal and causal role in limiting the extent of earthquake ruptures.

The data in Figure 7 also illustrate the inherent difficulty in predicting whether a particular step along a fault zone will ultimately mark the end of an earthquake rupture. For example, it may be observed over the entire range of rupture lengths that steps as small as 1 km are associated with the endpoints of many of the ruptures. In contrast, similar and larger size steps are completely ruptured during the occurrence of other earthquakes. Hence, there is no simple relationship between the final length of an earthquake rupture and the size of steps associated with the endpoints of the rupture, which should not be a surprise, since many factors will likely play a role in determining the relative resistance of a particular step to a propagating rupture. Fundamental, of course, will be the level of the stress which drives the earthquake or, more specifically, the deviatoric stress concentration which exists at the front of a propagating earthquake rupture. If the driving stress varies between different earthquakes, which is in part suggested by several compilations of static stress drop data (e.g. Kanamori and Anderson, 1975; Scholz, 1982; Scholz et al., 1986; Kanamori and Allen, 1986), then the relative resistance to rupture of a given size step may vary between earthquakes. Indeed, if it is assumed that the resistance to rupture propagation posed by a step is solely a function of the step length l_s, then the data in Figure 7, which indicate that a 1 km step may or may not mark the endpoint of a rupture, are most simply interpreted to suggest that the driving stress varies significantly between

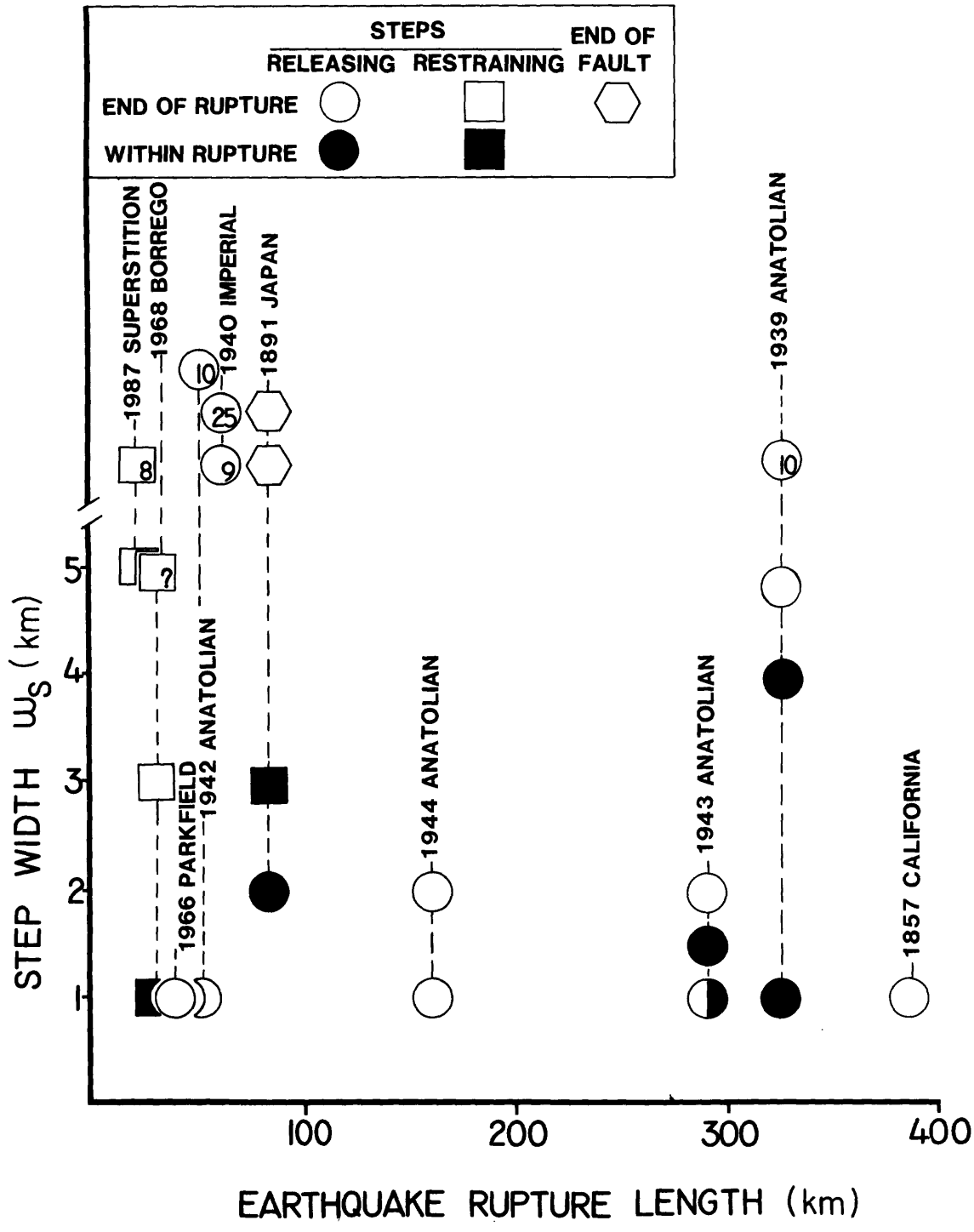

Figure 7. Earthquake rupture length versus the size l_s of steps in mapped fault trace observed at the endpoints (open symbols) and within (solid symbols) the rupture zone of large Anatolian and California earthquakes. Hence, for example, the 1939 Anatolian earthquake produced about 320 km of surface rupture and the endpoints of the rupture are marked by releasing steps (circles) of 10 km and 15 km, respectively. As well, the same rupture propagated through steps of 1 and 4 km. In contrast, steps within and at the endpoints of the 1968 Borrego earthquake are restraining (squares) in nature. Half-filled symbol indicates that similar sized steps occurred both within and at the endpoint of an earthquake rupture.

large earthquakes. However, little confidence can be placed in such an assumption. Steps observed only in map view may not extend completely through the seismogenic layer and, as well, other associated discontinuities such as bends may modify the stress concentration associated with a step in fault trace (Barka and Kadinsky-Cade, 1988). Moreover, it has been previously pointed out that the sense of a step, either releasing or restraining, and local hydrologic conditions may strongly control the relative resistance of a specific step to a propagating rupture (Segall and Pollard, 1980; Sibson, 1985, 1986). Consequently, available data are insufficient to determine whether it is variations in the driving stress or local geological and hydrological conditions which ultimately lead to the arrest of an earthquake rupture by a specific step. Hence, while the data are too few and the variables apparently too many to yet confidently predict if a particular step will mark the endpoint of an earthquake rupture, the observations that the endpoints of ruptures are commonly marked by steps in the fault trace and that the steps at the endpoints of ruptures are commonly larger than similar steps observed within the respective ruptures lends strong credence to the hypothesis that geometric discontinuities along fault strike work to limit the extent of strike-slip of earthquake ruptures.

A number of recent studies have attempted to explain characteristics of the spatial, temporal, and size distribution of earthquakes along faults by assuming an arbitrary or fractal distribution of strength properties along fault planes (e.g. Lay et al., 1981 Andrews, 1980; Aki, 1981; Scholz and Aviles, 1986; Smalley et al, 1985). In turn, observations summarized thus far suggest that the geometrical complexity of fault traces may be used to gauge, in a general sense, the heterogeneity of strength properties along fault planes. Toward that end, the number of steps ($l_s \geq 1$ km) per unit length of a fault zone provides a simple, quantitative measure of fault trace complexity. The complexity of fault trace measured in this manner is listed for each fault zone in Table 1 and plotted as a function of fault length in Figure 8. It may be observed that fault trace complexity varies by nearly 2 orders of magnitude between the individual faults. This variability is of interest for, by inference, it indicates that the distribution of strength properties along fault planes is not self-similar between all strike-slip faults. This simple observation, however, though of interest, provides no physical insight to the process which produces these differences.

Physical insight to the processes which produce the varying degree of fault trace complexity between faults is gained when fault trace complexity is plotted versus cumulative geologic offset (Figure 9). It is seen in Figure 9 that fault trace complexity is a smoothly decreasing function of cumulative geologic offset. The observation supports the idea that fault zones are characterized by a discontinuous trace during the initial stages of development and that increasing displacement along such faults works to remove discontinuities along the fault trace, effectively smoothing the fault plane. Moreover, when coupled with the growing body of evidence which indicates that steps in fault traces work to impede or arrest the propagation of earthquake ruptures, the apparent smoothing of the fault trace with displacement may be further interpreted to indicate that the distribution of strength properties on a fault plane is spatially heterogeneous, and that the degree of heterogeneity is a function of cumulative offset. A consequence of this structural evolution is that faults may undergo a seismological evolution as well, whereby, the size distribution and relative frequency of occurrence of earthquakes of different size on a fault is also a function

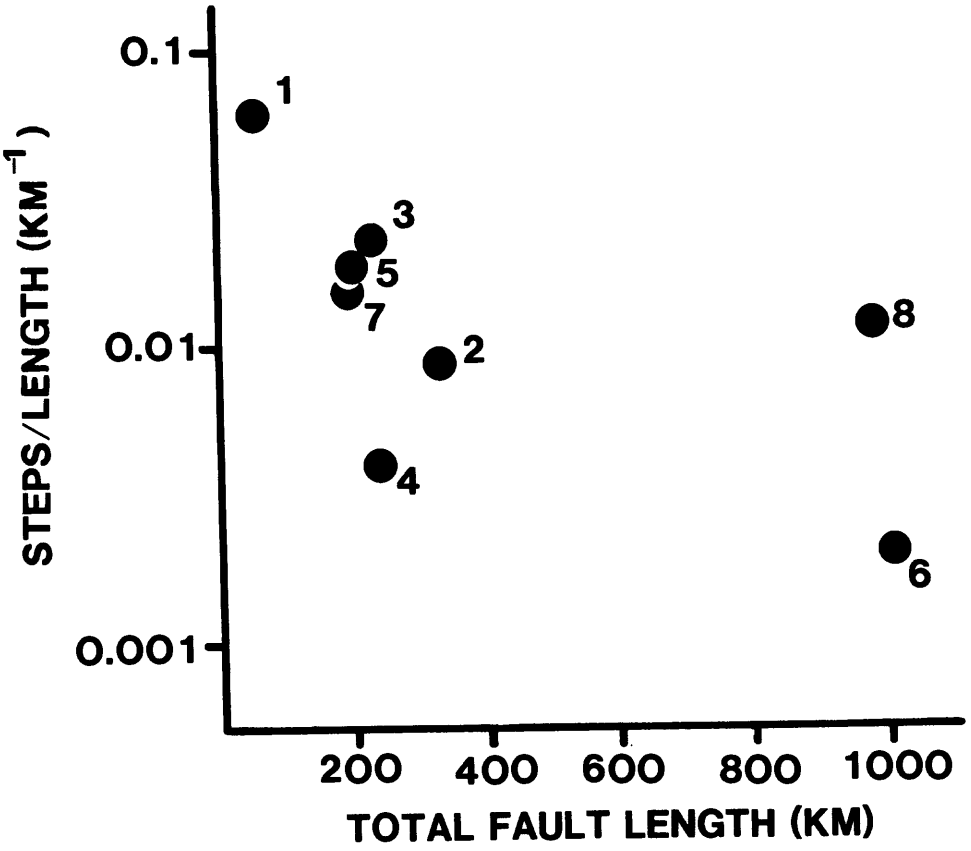

Figure 8. Total fault length versus steps ($l_s \geq 1km$) per unit length of fault trace for California and Antolian fault zones listed in Table 1.

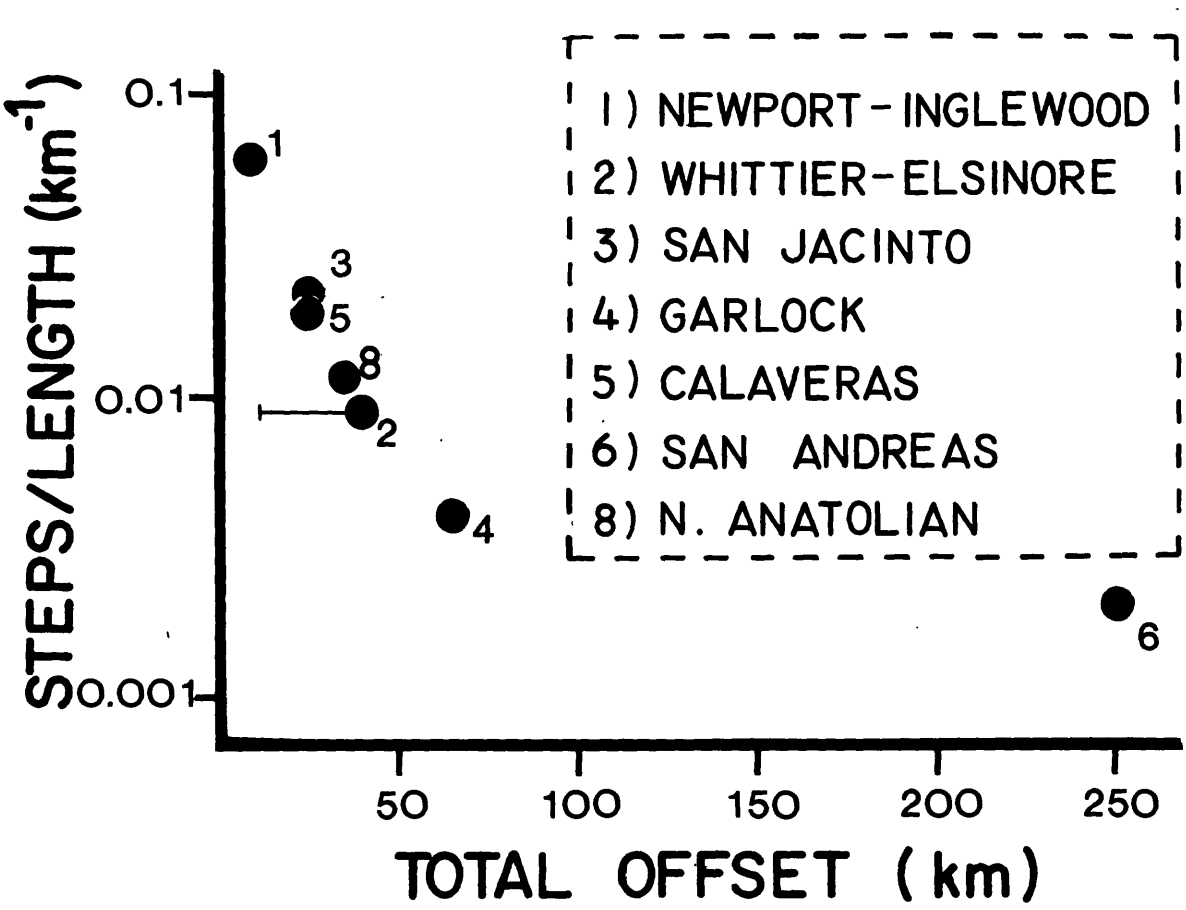

Figure 9. Steps ($l_s \geq 1km$) per unit length of fault trace versus cumulative geologic offset on California and Anatolian faults listed in Table 1.

of cumulative geologic offset. It is beyond the scope of this paper to examine in detail properties of the earthquake frequency distribution along each fault. But, for example, it might be expected that the degree of fault trace complexity plays a controlling role in determining the maximum size earthquake on a fault. In that regard, the data in Figure 10, a plot of the maximum-magnitude earthquake versus cumulative geologic offset across the fault on which the earthquake occurred, suggest that seismological maturation, when viewed as the capability to produce earthquakes of magnitude 7 or greater, occurs at or before 25 km of offset.

CONCLUSIONS

Observations of major fault zones in California and Turkey suggest that the number of step-like discontinuities per unit length along the trace of strike-slip faults is a smoothly decreasing function of the cumulative geologic offset. The observation is consistent with laboratory models which have been used to suggest that, during the initial stages of development, strike-slip faults are characterized by a zone of discrete en echelon fault segments, and that, with continued displacement, the individual fault segments ultimately coalesce to produce a single, throughgoing strand. When coupled with a growing body of evidence that indicates steps in fault traces work to impede or arrest the propagation of earthquake ruptures, the observations further suggest that the distribution of strength properties on a fault plane is spatially heterogeneous, and that the degree of heterogeneity is a function of the cumulative geologic offset along a fault. As a result, it is reasonable to then expect that the size and and relative frequency of occurrence of earthquakes of different size on strike-slip faults be a function of total offset.

Acknowledgements

A. Barka and A. Johnston reviewed the manuscript and A. Barka, T. Rockwell, and D. Herd kindly provided preprints of unpublished papers and maps, respectively, and Tanya George drafted the figures. This material is based upon work supported by the National Science Foundation under Grant No. EAR-86-18314.

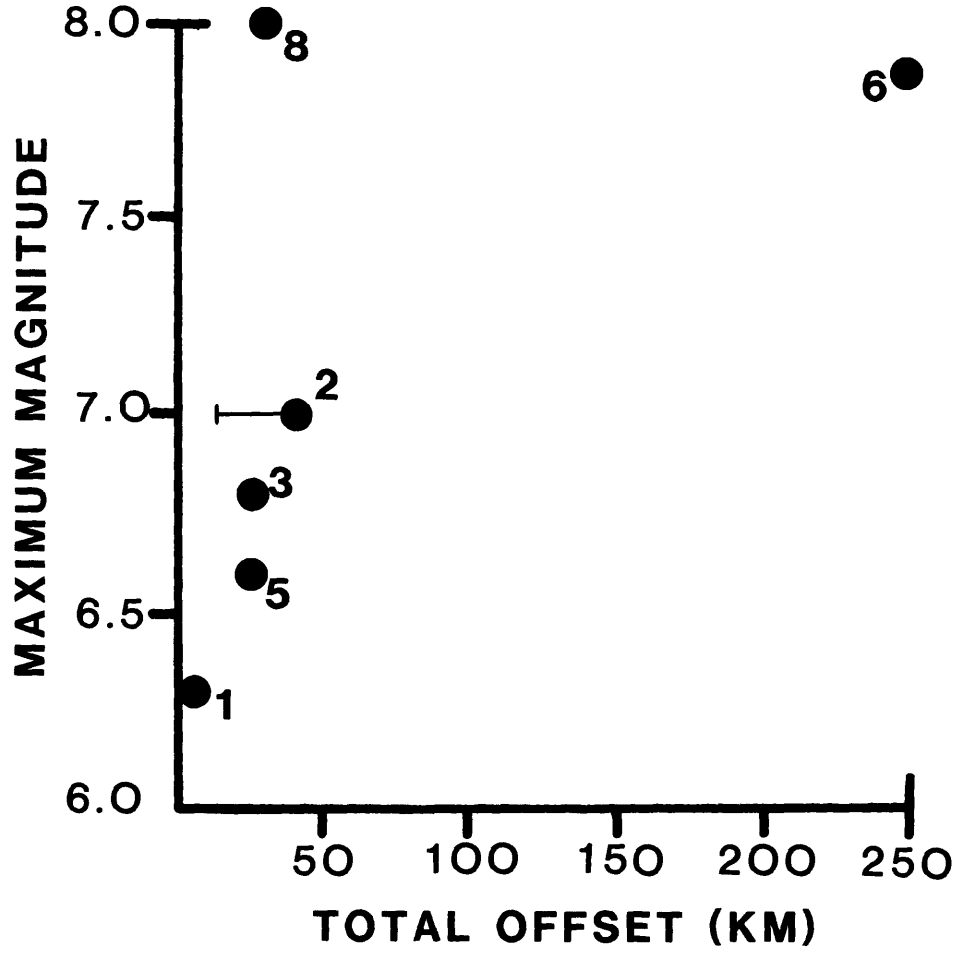

Figure 10. Maximum magnitude of earthquake historically observed along the California and Anatolian faults listed in Table 1 versus cumulative geologic offset across the respective faults.

REFERENCES

Aki, K., A probabilistic synthesis of precursory phenomena, in Earthquake Prediction, edited by D. Simpson, and P. Richards, Maurice Ewing Series 4, p. 56,574, AGU, Washington, D.C.

Ambraseys, N. N., 1970, Some characteristic features of the North Anatolian fault zone: Tectonophysics 9, 143-165.

Ambraseys, N. N., 1975, Studies in historical seismicity and tectonics, *in* Geodynamics of Today: Royal Society of London, p. 9-16.

Anderson, J. G., Rockwell, T., and Agnew, D., 1988, A study of seismic hazard of San Diego submitted to: Earthquake Spectra.

Andrews, D. J., A Stochastic fault model, 1, Static Case, J. Geophy. Res., v. 85, p. 3867-3877, 1980.

Bakun, W. H., Clark, M. M., Cockerham, R. S., Ellsworth, W. L., Lindh, A. G., Prescott, W. H., Shakal, A. F., and Spudich, P., 1984, The 1984 Morgan Hill, California, earthquake: Science, v. 225, p. 288-291.

Barka, A. A. and Kadinsky-Cade, 1988, Strike-slip fault geometry in Turkey and its influence on earthquake activity, in press: Tectonics.

Barka, A. A. and Gulen, L. 1988, New constraints on age and total offset of the north Anatolian fault zone: Implications for tectonics of the eastern Meditteranean region, *in* Spec. Publ. Middle East. Techn. Univ.: 1987 Meloh Tokay Geology Symposium, Ankara, Turkey (in press).

Barka, A. A. and Hancock, P. L., 1982, Relationship between fault geometry and some earthquake epicenters within the North Anatolian fault zone, *in* Multidisciplinary Approach to Earthquake Prediction: p.137-142, edited by A.M. Isikara and A. Vogel, Friedr. Vieweg and Sohn, Federal Republic of Germany.

Barrows, A.G., 1974, A review of the geology and earthquake history of the Newport-Inglewood structural zone, southern California: Spec. Rep. Calif. Div. Mines Geol., v. 114, 115 p.

Brown, R.D. 1970, Map showing recently active breaks along the San Andreas and related faults between the northern Gabilan Range and Cholame Valley, California: U.S.G.S. Misc. Geologic Invest. Map, v. I-575.

Brown, R.D. Jr., and Wolfe, E.W., 1972, Map showing recently active breaks along the San Andreas fault between Point Delgada and Bolinas Bay, California: U.S.G.S. Misc. Geol. Invest. Map, v. I-692.

Clark, M.M., 1972, Surface rupture along the Coyote Creek fault, The Borrego Mountain earthquake of April 9, 1968: U.S.Geol. Surv. Prof. Pap., v. 787, p. 55-86.

Clark, M.M., 1973, Map showing recently active breaks along the Garlock and associated faults, California: U.S.G.S. Misc. Geol. Invest. Map v. 74.

Clark, M.M., 1984, Map showing recently active breaks along the San Andreas fault and associated faults between Salton Sea and Whitewater River-Mission Creek, California: U.S.G.S. Misc. Field Invest. Map, v. I-1483.

Crowell, J. C., 1962, Displacement along the San Andreas Fault, California: Geological Society of America Special Pap., v. 7, 61 p.

Crowell, J. C., 1974a, Origin of Cenozoic basins in souther California *in* Dott, R. H., and Shavers, R. H., eds., Modern and ancient geosynclinal sedimentation: Society of Economic Paleontologists and Mineralogists Special paper, v. 22, p. 190-204.

Crowell, J. C., 1974b, Sedimentation along the San Andreas fault, California *in* Dott, R. H., and Shaver, R. H., eds., Modern and ancient geosynclinal sedimentation: Society of Economic Paleontologists and Mineralogists Special Publication, v. 19, p. 292-303.

Dibblee, T. W., Jr., 1977, Strike-slip tectonics of the San Andreas fault and its role in Cenozoic basin evolvement *in* Late Mesozoic and Cenozoic sedimentation and tectonics in California: San Joaquin Geological Society, p. 26-38.

Grantz, A., and Dickinson, W. R., 1968, Indicated cumulative offsets along t he San Andreas fault in California Coast Ranges *in* Dickinson, W. R. and Grantz, A., eds., Proceedings of Conference on Geologic problems of San Andreas fault system: Stanford University Publication XI, P. 117-120.

Harding, T. P., 1974, Petroleum traps associated with wrench faults: The American Association of Petroleum Geologists Bulletin, v. 58, p. 1290-1304.

Harding, T. P., 1976, Tectonic significance and hydrocarbon trapping consequences of sequential folding synchronous with San Andreas Faulting, San Joaquin Valley, California: The American Association of Petroleum Geologists Bulletin, v. 60, p. 356-378.

Herd, D. G., and Helley, E. J., 1977, Faults with Quaternary displacement northwestern San Francisco Bay region, California: U. S. geol. Surv. Misc. Field Stud. Map, v. MF-818, 1977 p.

Herd, D. G., 1979, Neotectonic framework of central California and its implications to microzonation of the San Francisco Bay region: U. S. Geol. Surv. Circ., v. 807, 3-12, 1979.

Herd, D. G., 1988, Map of active traces of Hayward-Maacama and Calaveras-Rogers Creek-Green Valley fault zones at 1:250,000 scale (unpublished map).

Hill, M. L., 1981, San Andreas fault: History of concepts: Geological Society of America Bulletin, v. 92, p. 112-131.

Hope, R. A., 1969, Map showing recently active break along the San Andreas and related faults between Cajon Pass and Salton Sea: U. S. G. S. Open-file Rept., p. 691-30.

Kahle, J. E., Wills, C. J., Hart, E. W., Treiman, J. A., Greenwood, R. B., and Kaumeyer, R. S., 1988, Surface rupture Superstition Hills earthquakes of November 23 and 24, 1987, California Geology.

Kanamori, H., and Allen, C. R., 1986, Earthquake repeat time and average stress drop *in* Earthquake Source Mechanics: Geophys. Monogr., v. 37, edited by Das, S., Boatwright, J., Scholz, C. H., 157-167, Washington, D. C.

Kanamori, H., and Anderson, D. L., 1975, Theoretical basis of some empirical relations in seismology: bull. Seism. Soc. Amer., V. 65, p. 1073-1095.

Kintzer, F. C., and Brooks, J. C., and Cummings, J. C., 1977, An offset Miocene Shoreline: implications for Calaveras fault movement: Geol. Soc. Am. Abstracts with programs, v. 9, p. 65.

Lamar, D. L. and Rockwell, T. K., 1986, An overview of the tectonics of the Elsinore fault zone *in* Neotectonics and Faulting in Southern California, complied by Ehlig, Perry L: Geological Society of America, Cordilleran section, Los Angeles, California, p., 149-158.

Lamar, D. L., 1961, Structural evolution of the norther margin of the Los Angeles basin: Ph.D. thesis, Univ. Calif., Los Angeles, 142 p.

Lawson, A. C., et al., 1908, The California earthquake of April 18, 1906 *in* Report of the State Earthquake Investigation Commission, Vol. 1-2, 451 pp., Carnegie Institution of Washington, Washington, D. C., 1908.

Lay, T., and Kanamori, H., 1981, an asperity model of great earthquake sequences *in* Earthquake Prediction: an International Review edited by Simpson, D., and Richards, P.: pp. 579-592, AGU, Washington, D.C.

Matsuda, T., 1974, Surface faults associated with Nobi (Mino-Owari) earthquake of 1891, Japan, Spec. Bull. Earthquake Res. Inst., Univ. Tokyo, 14, 23-36.

Matti, J. C., Morton, D. M., and Cox, B. F., 1985, Distribution and geologic relations of fault systems in the vicinity of the Central Transverse ranges, southern California: U. S. G. S. Open-file Rept. 85-365, pp. 23.

Mueller, K. J., 1984, Neotectonics, alluvial history and soil chronology of the southwestern margin of the sierra de los Cucapas, Baja Balifornia Norte, unpublished M.S. thesis, San Diego State University, 363 p.

Mueller, K. J., and Rockwell, T. K., 1984, Basin development and fault kinematics of the Laguna Salada rhombochasm, Baja California Norte, Geol Soc., Am., Abstracts with programs, v. 16, p. 602.

Pampeyan, E. H., Harsh, P. W., and Coakley, J. M., 1981, Recent breaks along Maacama fault zone, Laytonville to Hopland, California: U. S. Geol Surv. Map, v. MF-1217.

Reasenberg, P., and Ellsworth, W. L., 1982, Aftershocks of the Coyote Lake, California, earthquake of August 6, 1979: A detailed study: J. Geophys. Res., v. 91, 10637-10655.

Richter, C. F., 1958: Elementary Seismology, 768 pp., W. H. Freeman, New York.

Ross, D. C., 1969, Map showing recently active breaks along the San Andreas fault between Tejon Pass and Cajon Pass, southern California: U. S. G. S. Misc. field. Invest. Map, v. I-553.

Sage, O. G., JR., 1973, Paleocene geography of the Los Angeles region, *in* Proceedings of conference on tectonic problems of San Andreas fault system, Stanford Univ. Publ., v. XIII, p. 348-357.

Sanders, C. O. and Kanamori, H., 1984, A seismotectonic analysis of the Anza seismic gap, San Jacinto fault zone, souther California: J. Geophy. Res., v. 89, p. 5873-5890.

Scholz, C. H., 1982, Scaling laws for large earthquakes: Consequences for physical models: Bull. Seism. Soc. Amer., v. 72, p. 1-14.

Scholz, C. H., and, Aviles, C. A., 1986, The fractal geometry of faults and faulting *in* Earthquake Source Mechanics: Geophys. Monogr., v. 37, edited by Das, S., Boatwright, J., and Scholz, C. H., p. 147-155, Washington, D. C.

Scholz, C. H., Aviles, C. A., and Wesnousky, S. G., 1986, Scaling differences between large interplate and intraplate earthquakes: Bull. Seism. Soc. Amer., v. 76, p. 65-70.

Segall, P., and Pollard, D. D., 1980, Mechanics of discontinuous faults: J. Geophys. Res., v. 85, p. 4337-4350.

Sharp, R. V., 1967, San Jacinto fault zone in the peninsular Ranges of southern California: Geological Society of America Bulletin, v. 78, p. 705-730.

Sharp, R. V., 1975, En echelon fault patterns of the San Jacinto fault zone, southern California, Bull.Calif. Div. Mines Geol, v. 196, p. 187-194.

Sibson, R. H., 1985, Stopping of earthquake ruptures at dilational fault jogs: Nature, v. 316, p. 248-251, 1985.

Sibson, R. H., 1986, Rupture interactions with fault jogs *in* Earthquake Source Mechanics, Geopys. Monogr.: v. 37, edited by Das, S., Boatwright, J., and Scholz, C. H., 157-167,Washington, D.C.

Sieh, K. E., 1978, Slip along the san Andreas fault associated with the great 1857 earthquake: Bull. Seismol. Soc. Am., v. 68, p. 1421-1448.

Smalley, R., Turcotte, D., and Solla, S., 1985, A renormalization group approach to the stick-slip behavior of faults: J. Geophys. Res., v. 90, p. 1894-1900.

Smith, G. I., 1962, Large lateral displacement on Garlock fault, California, as measured from offset dike swarm: Bull. Am. Assoc. Petrol. Geol., v. 46, p. 85-104.

Strand, C. L., 1980, Pre-1900 earthquakes of Baja California and San Diego County, M.S. Thesis, San Diego State University, San Diego, CA.

Toppozada, T. R., Real, C. R., and Parke, D. L., 1981, Preparation of isoseismal maps and summaries of reported effects for pre-1900 California earthquakes: Calif. Div. Mines Geol. Open File rep. 81-11 SAC, 182 pp.

Vedder, J. B., and Wallace, R. E., 1970, Map showing recently active breaks along the San Andreas and related faults between Cholame Valley and Tejon Pass, California: U.S.G.S. Misc. Geol. Invest. Map, v. I-574.

Weber, F. H., Jr., 1977, Seismic hazards related to geologic factors, Elsinore and Chino fault zones, northwestern Riverside county, California: Calif. Div. Mines and Geology, Open-File Report, v. 77-4, Los Angeles, 96 p.

Wilcox, R. E., Harding, T. P., and Seely, D. R., 1973, Basic Wrench Tectonics: The American Association of Petroleum Geologists Bulletin, v. 57, p. 74-96.

Withjack, M. O., and Jamison, W. R., 1986, Deformation produced by oblique rifting: Tectonophysics, v. 126, p. 99-124.

Woodford, A. O., McCulloch, T. H., and Schoelhamer, J. E., 1972, Paleographic significance of metatuff boulders in middle Tertiary strata, Santa Ana mountains, California: Bull. Geol. Soc. Amer., v. 82, p. 3421-3448.

Yerkes, R. F., and Campbell, R. H., 1971, Cenozoic evolution of the Santa Monica Mountains-Los Angeles Basin area: U. S. Geological Survey, open file report.

PERSISTENT SEGMENT BOUNDARIES ON BASIN-RANGE NORMAL FAULTS

by

Russell L. Wheeler

U.S. Geological Survey

ABSTRACT

Boundaries between segments of a normal fault are parts of the fault that are not completely broken by the main rupture zones of most large earthquakes. The amount of slip tapers to zero at each end of each rupture zone, so that a segment boundary which persists through many earthquakes accumulates a slip deficit compared to the accumulated slip along segment interiors. This slip deficit results in less structural relief across the fault at the boundary. The lesser relief is expressed as a transverse bedrock ridge, with or without a footwall salient. Rupture-zone ends and bedrock ridges identify four persistent segment boundaries on large, historic, surface-breaking rupture zones of the Basin-Range, and at least four more persistent boundaries on the Wasatch fault zone.

INTRODUCTION

This report explains and illustrates a method to identify persistent segment boundaries on normal faults. The method is applied to normal faults in the area of Basin and Range structure (here called Basin-Range), including parts of Idaho, Montana, and northern New Mexico.

Segments of a normal fault are fault sections that usually rupture independently of each other during large earthquakes. Independence implies that the rupturing of one segment does not induce the rupturing of an adjacent segment. The fault section that breaks during a large rupture (rupture zone) can span a segment or can break only part of a segment. In either case the rupture zone has two ends. If the rupture process is unilateral the rupture-zone end near the hypocenter is the starting end (initiation point) and the other end is the stopping end (termination point). If the rupture process is bilateral both ends are stopping ends. In general we can distinguish unilateral and bilateral propagation only for earthquakes of the last several decades, so most of the following discussion does not distinguish starting and stopping ends.

Segments can be identified by locating the ends of rupture zones produced by individual large earthquakes. We have assumed that segments usually rupture independently. This assumption implies that most large ruptures will not cross segment boundaries. Therefore, a segment boundary is defined as a part of a fault where at least 2 (preferably successive) rupture zones have ends. This definition is consistent with most other uses of the term segment, because these other uses imply that some aspect of faulting is repeated (the term single-earthquake segment is self-contradictory).

A contagion effect, whereby rupture of one segment induces rupture of another nearby segment (Perkins, 1987), can mimic a segment boundary where none exists. A large rupture on an unsegmented fault loads an adjacent unbroken part of the fault, which induces a second rupture on the loaded part. This second rupture propagates away from the first rupture zone. Thus, the starting end of the second rupture zone coincides with one end of the first rupture zone. Such coincidence mimics a segment boundary between the two rupture zones. To avoid this error, use only rupture zones on the same segment to identify a segment boundary (Wheeler, 1987).

Geometrical, petrological, and structural considerations suggest that segment boundaries on normal faults persist differently (Wheeler, 1987). At one extreme, persistent boundaries control most large, nearby ruptures during much of the evolution of a fault. At the other extreme, nonpersistent segment boundaries control only a few successive ruptures during a short part of the fault's evolution but none before or after these few (Wheeler and Krystinik, 1987). Determining a boundary's persistence is crucial to estimating the liklihood that the boundary will control the next large, nearby rupture. Such estimates can affect seismic-hazard assessments, as described later.

Direct determination of boundary persistence is impractical for normal faults of the Basin-Range because recurrence intervals of hundreds to thousands of years for individual segments preclude observing repeated ruptures. Consequently, even along the intensely studied Wasatch fault zone, paleoseismologists have been able to study no more than the last four surface breaks on any segment; study of the last two or three surface breaks is most common (Schwartz and Coppersmith, 1984; Machette and others, 1987, this volume; Schwartz, this volume). Accordingly, we must determine the persistence of a segment boundary indirectly.

We start with normal faults that have ruptured historically because for historical ruptures we know the lateral extent of the surface-rupture zones that formed during a single earthquake or earthquake sequence. We consider faults that have not ruptured historically later because they present more difficulties--we cannot yet distinguish prehistoric fault scarps that formed within minutes in a single earthquake from scarps that formed in several smaller earthquakes separated by decades.

HISTORICAL RUPTURES

The vertical component of slip tapers to zero at each end of a rupture zone (fig. 1). (The following analysis deals with vertical displacement of the top surface of bedrock, so horizontal components of slip are ignored.) The taper of vertical slip produces a slip deficit at the ends of the rupture zone. Therefore, a segment boundary that persists through many earthquakes builds up a cumulative slip deficit compared with the accumulated slip in the interiors of adjacent segments (Wheeler, 1987). This slip deficit results in less structural relief across the fault at the boundary. The lesser relief is expressed as a transverse bedrock ridge between basins in the hanging wall, with or without a footwall salient (a projection of the footwall into the hanging wall) (Wheeler and Krystinik, 1987). Geologic and topographic maps show footwall salients and exposed bedrock ridges. Gravity maps show buried

bedrock ridges as gravity saddles between gravity lows that identify hanging-wall basins that are filled with low-density sediments (Zoback, 1983; Mabey, 1987; Wheeler and Krystinik, 1987, 1988; Crone and Haller, this volume). Thus, persistent boundaries can be recognized on segments that have ruptured only once historically, if an end of the rupture zone coincides with a cumulative slip deficit on the fault.

Figure 1F shows that a persistent boundary must produce a bedrock ridge. However, the converse is less certain--a bedrock ridge indicates only that few large ruptures throughout the history of the fault zone have broken through the ridge to produce large, continuous ruptures in and beyond the ridge. In fact, the ridge must break occasionally or the fault would end there. Even if large, continuous scarps of a segment are bounded by a bedrock ridge, small, discontinuous scarps can form in or beyond the ridge (fig. 1E). Also, figure 2B shows that two separate earthquakes that occur close together in time can form large, continuous scarps of indistinguishable ages on both sides of a bedrock ridge. Thus, a bedrock ridge by itself, without paleoseismological evidence from one or more individual rupture zones, only limits the extent of large, continuous scarps of most large ruptures.

FIGURE 1.--Long profiles showing normalized vertical separations along large, historic, surface-rupture zones of the Basin-Range. Each profile is normalized to its maximum separation (vertical axes) and to the mapped length of tectonic surface breaks (horizontal axes). Normalizing removes systematic differences between profiles caused by different scarp-height corrections. A, 1915 Pleasant Valley, Nevada (Wallace, 1984). Separations are scarp heights corrected for erosion (Wallace, 1980). B, 1954 Fairview Peak, Nevada (Slemmons, 1957). Separations are uncorrected scarp heights. C, 1954 Dixie Valley, Nevada (Slemmons, 1957). Separations are uncorrected scarp heights. D, 1959 Hebgen Lake, Montana (Myers and Hamilton, 1964; Witkind, 1964). Separations are scarp heights corrected for antithetic faulting and backtilting within several meters of scarps, but not for erosion. E, 1983 Borah Peak, Idaho (Crone and others, 1987). Separations are net vertical tectonic displacements; scarp heights are corrected for erosion, antithetic faulting, and backtilting. The gap in surface breaks at about 60 percent of the surface-rupture zone's length is at the Willow Creek Hills segment boundary (fig. 2A). F, Summary of five preceding profiles. Profiles are smoothed individually by dividing each profile's length into 10-percent increments and calculating the median separation for each increment. Thus, each increment has 4-5 median separations--one for each earthquake (Dixie Valley, Fairview Peak, and Hebgen Lake rupture zones lack data in some increments). Next, the smoothed profiles are combined. Dots connected by heavy line show medians of the 4-5 median separations in each increment, with dots at centers of increments. Light lines show envelope of the median separations. Therefore, heavy line represents a typical long profile from a large Basin-Range earthquake, with site-to-site and earthquake-to-earthquake variations reduced by smoothing.

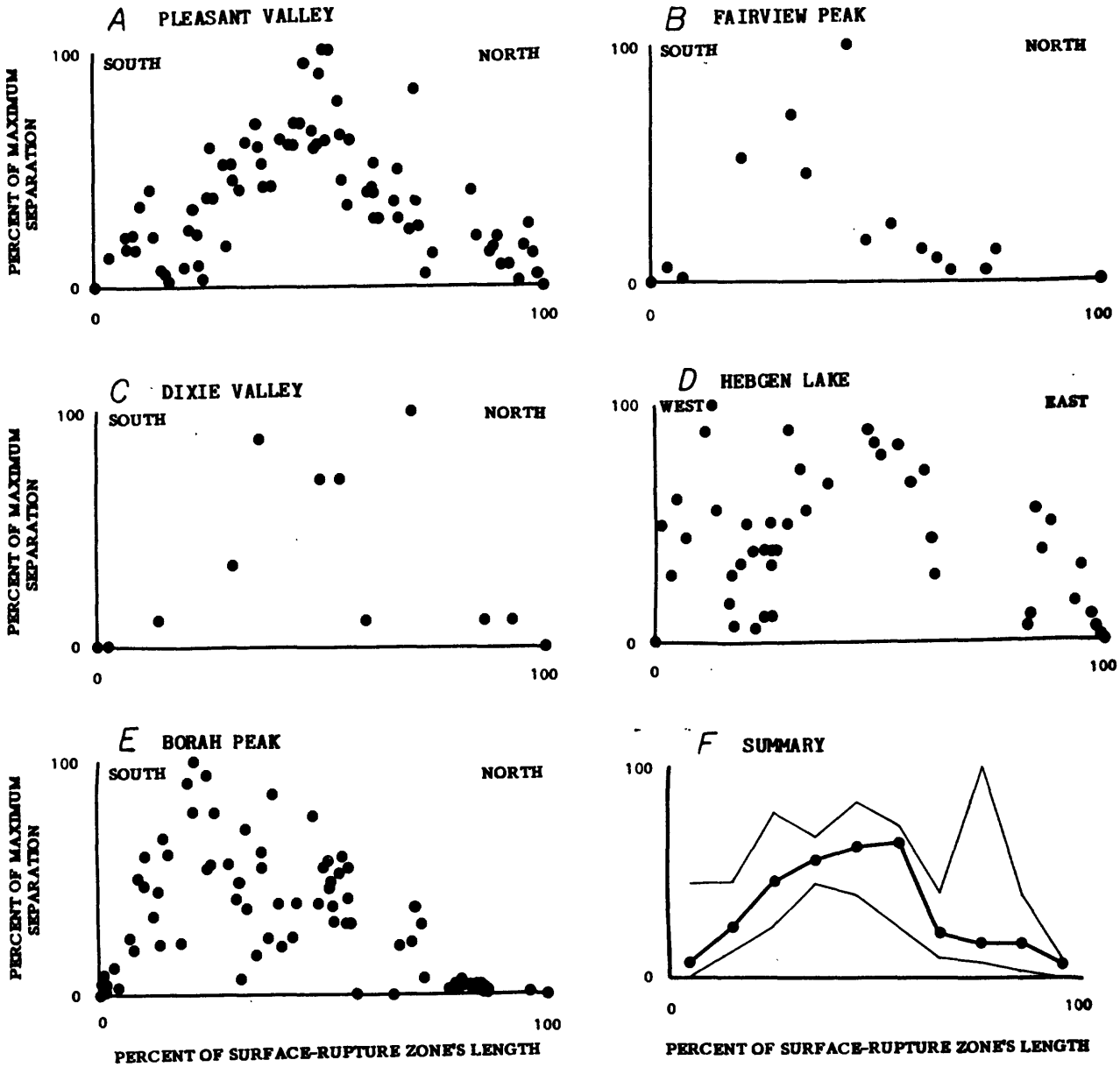
A PLEASANT VALLEY
B FAIRVIEW PEAK
C DIXIE VALLEY
D HEBGEN LAKE
E BORAH PEAK
F SUMMARY
SOUTH
NORTH
WEST
EAST
100
0
PERCENT OF MAXIMUM SEPARATION
PERCENT OF SURFACE-RUPTURE ZONE'S LENGTH

FIGURE 1

A bedrock ridge whose crest is now deeply buried by sediments might identify a segment boundary that was persistent early in the history of a normal fault, but which no longer controls ruptures. The Wasatch fault zone has possible examples (R.L. Wheeler and M.N. Machette, unpublished results). Thus, historical or paleoseismological evidence of the behavior of the last surface rupture to approach the boundary can determine whether the boundary remains persistent.

Four large surface ruptures have occurred on Basin-Range normal faults in historical time (figs. 2A-D). Rupture-zone ends and bedrock ridges identify four persistent segment boundaries on three of these surface-rupture zones (figs. 2A-C). Wheeler and Krystinik (1987) named and described these boundaries and explained how each satisfies the conditions given earlier for identifying a persistent segment boundary.

Wheeler and Krystinik (1987) concluded that the 1959 Hebgen Lake, Montana, earthquake (fig. 2D; Myers and Hamilton, 1964) ruptured a fault whose geometry is still evolving, so to identify boundaries there would be premature.

The Elkhorn Creek Segment Boundary, Idaho

This boundary is at the starting end of the 1983 Borah Peak rupture zone (fig. 2A; Crone and others, 1987). The boundary is at a buried, fault-bounded, bedrock ridge that is identified by a gravity saddle. The youngest pre-1983 scarps on the adjacent Mackay and Thousand Springs segments are of early(?)-middle Holocene age (Crone and Haller, this volume), but no large, continuous scarps of similar age are known in the boundary. Thus, the segment-spanning 1983 rupture zone, perhaps one pre-1983 rupture zone of unknown length, and many of the prehistoric rupture zones that produced the northwest side of the bedrock ridge all spanned part or all of the Thousand Springs segment, and the large, continuous scarps of their surface-rupture zones ended at the boundary.

The Willow Creek Hills Boundary, Idaho

This boundary is marked by an exposed bedrock ridge at the stopping end of the main Borah Peak rupture zone (fig. 2A; Crone and others, 1987). The youngest pre-1983 scarps on the adjacent Thousand Springs and Warm Spring segments have overlapping age ranges (Schwartz and Crone, 1988), but similar-

FIGURE 2.--Persistent segment boundaries (open arrows) on four historical surface-rupture zones and the Wasatch fault zone of the Basin-Range. Solid lines show historical (in A - D) and prehistoric (in E) surface breaks; bar and ball on downthrown sides. A, WSS, Warm Spring segment; TSS, Thousand Springs segment; MS, Mackay segment. Dotted line, prehistoric fault scarp along MS. Fault traces after Crone and Machette (1984). B, Fault traces after Slemmons (1957). C, Northernmost group of scarps is in bedrock of China Mountain, over a pass to the east of Pleasant Valley. Fault traces after Wallace (1984). D, Fault traces after Myers and Hamilton (1964, plate 2). E, Fault traces after Machette and others (1987).

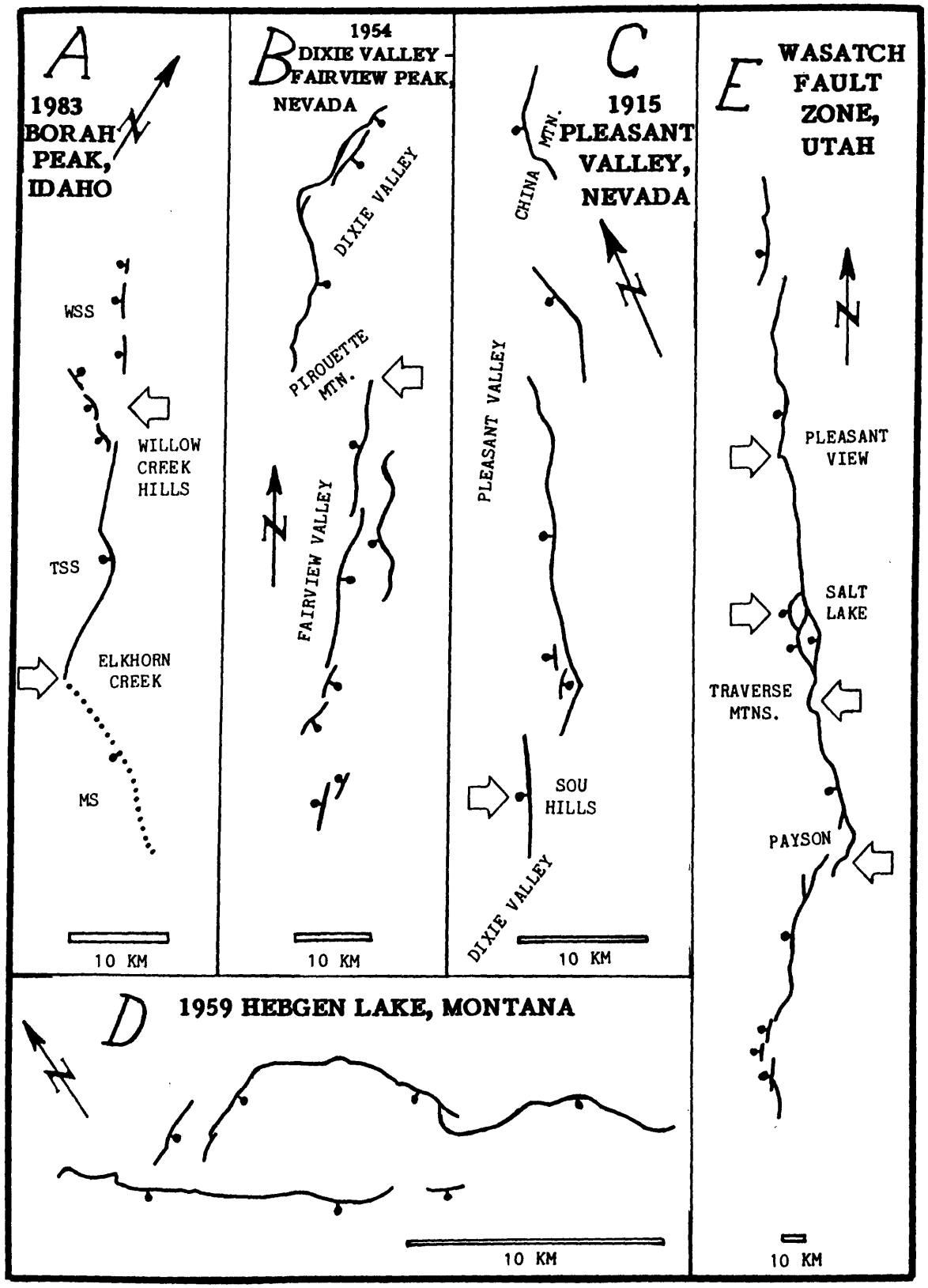
A
1983
BORAH
PEAK,
IDAHO
WSS
WILLOW
CREEK
HILLS
TSS
ELKHORN
CREEK
MS
10 KM
B
1954
DIXIE VALLEY -
FAIRVIEW PEAK,
NEVADA
DIXIE VALLEY
PIROUETTE
MTN.
FAIRVIEW VALLEY
10 KM
C
1915
PLEASANT
VALLEY,
NEVADA
CHINA
MTN.
PLEASANT VALLEY
SOU
HILLS
DIXIE VALLEY
10 KM
E
WASATCH
FAULT
ZONE,
UTAH
PLEASANT
VIEW
SALT
LAKE
TRAVERSE
MTNS.
PAYSON
10 KM
D
1959 HEBGEN LAKE, MONTANA
10 KM

FIGURE 2

age scarps are not found along the fault in the Willow Creek Hills boundary. Thus, the pre-1983 scarps on the Warm Spring and Thousand Springs segments could represent either (1) two different rupture zones, each of which ruptured one of the segments and both of which stopped at the boundary, or (2) a single earthquake that ruptured two segments (Schwartz and Crone, 1988). In either case large, continuous scarps of the 1983 rupture zone and many of the prehistoric rupture zones that produced the southeast side of the bedrock ridge spanned part or all of the Thousand Springs segment and ended at the Willow Creek Hills boundary.

The Pirouette Mountain Boundary, Nevada

This boundary separates the rupture zones of the 1954 Dixie Valley and Fairview Peak earthquakes (fig. 2B; Slemmons, 1957; Doser, 1986). Faults on the west side of Dixie Valley and the east side of Fairview Valley broke four minutes apart. The Pirouette Mountain boundary is at a partly exposed bedrock ridge that coincides with a gravity saddle. All scarps of the Dixie Valley rupture zone are north of the boundary. The largest, most continuous scarps of the Fairview Peak rupture zone are south of the boundary, although this rupture also produced discontinuous scarps in the bedrock within the boundary. Thus, both the north and south sides of the boundary are marked by the coincident ends of a 1954 rupture zone and of the large, continuous scarps of many of the prehistoric rupture zones that formed the bedrock ridge.

The 1903 Wonder earthquake, smaller than the 1954 earthquakes, aids recognition of the Pirouette Mountain boundary as a structure separate from the segments in either Dixie Valley or Fairview Valley. Most surface breaks from the Wonder earthquake were confined to the boundary itself (Slemmons and others, 1959). Therefore, the Pirouette Mountain boundary can rupture separately from faults in Dixie Valley or Fairview Valley.

The Sou Hills Boundary, Nevada

This boundary is at the south end of the 1915 Pleasant Valley rupture zone (fig. 2C; Wallace, 1984; Fonseca, 1988). The exposed bedrock ridge that forms the Sou Hills coincides with a gravity saddle. From the heights and morphologies of prehistoric scarps in the Sou Hills and Pleasant Valley, Fonseca (1988) suggested that the youngest, large, pre-1915 rupture zone in Pleasant Valley also ended at the Sou Hills boundary. Thus, the large, continuous scarps of the 1915 rupture zone, perhaps of the youngest pre-1915 rupture zone, and of many of the older rupture zones had ends at the Sou Hills segment boundary.

PREHISTORIC RUPTURES

A procedure similar to the one used for historical ruptures can identify persistent segment boundaries on a fault that has not broken historically. A persistent boundary has a cumulative slip deficit. The boundary probably still persists if a single Holocene or late Pleistocene rupture zone satisfies two conditions: (1) the rupture zone spanned a segment adjacent to the boundary, and (2) the rupture zone did not cross the boundary. We cannot observe whether all scarps attributed to the prehistoric rupture zone formed in the same earthquake sequence, but we must infer this coevality by

correlating the scarps. A convincing demonstration that the correlated scarps satisfy the first condition includes showing that vertical separations on several correlated scarps are largest in the middle of the segment and smallest at both ends (for example, Fonseca, 1988, fig. 11). A convincing demonstration that the scarps satisfy the second condition includes showing that the correlated scarps on one segment differ in age from scarps on adjacent segments. Preferably the scarp correlations and age comparisons will be based on isotopic or radiogenic age estimates from trenches or natural exposures.

Five factors can complicate attempts to show that a single prehistoric rupture zone satisfies both conditions. First, prehistoric fault scarps are incompletely preserved, so their extents can be hard to determine. Second, correlating scarps that are several kilometers apart is uncertain because the morphology of a scarp can vary with its azimuthal orientation and the material in which it formed. Third, even if orientation and material are accounted for, the estimation of scarp age from scarp morphology remains uncertain because data points scatter around the regression line that is fitted to morphological data (for example, Pierce and Colman, 1986), or because of geological uncertainties in diffusion modeling (for example, Hanks and Schwartz, 1987). Fourth, even where the inferred faulting history is based on radiogenic or isotopic age estimates, the history contains uncertainties because dating methods have inherent analytical imprecisions and geological uncertainties (Machette and others, this volume; Schwartz, this volume). Fifth, the primary rupture of a segment can trigger the formation of small scarps in a segment boundary or on another segment beyond the boundary (the leaky boundaries of Crone and Haller, this volume). Such small scarps can mask the true end of the primary rupture. For example, small scarps formed and aftershocks occurred in the Warm Spring segment northwest of the main rupture zone of the 1983 Borah Peak earthquake (Crone and others, 1987; Richins and others, 1987). These aftershocks radiated little energy compared to the main shock that ruptured the Thousand Springs segment; probably formation of the small scarps also radiated little energy. Thus, neither aftershocks nor small scarps indicate that the primary rupture crossed the Willow Creek Hills boundary into the Warm Spring segment. In fact, geodetic and body-wave modeling and geological evidence show that the primary rupture was restricted to the Thousand Springs segment (Barrientos and others, 1987; Doser and Smith, 1985; Crone and Machette, 1984).

Several workers used the two conditions listed earlier and related criteria to identify segment boundaries on prehistoric rupture zones in the Basin-Range. Wheeler and Krystinik (1987) identified the Pleasant View, Salt Lake, Traverse Mountains, and Payson persistent boundaries on the Wasatch fault zone in Utah (fig. 2E). Machette and others (1987, this volume) presented evidence of other persistent segment boundaries on the Wasatch fault zone. Crone and Haller (this volume) identified persistent boundaries on the Lost River, Beaverhead, Lemhi, and Red Rock faults of east-central Idaho and southwestern Montana.

LA JENCIA FAULT

The preceding ideas can guide preliminary interpretation of other faults that are less well understood than those discussed earlier. The La Jencia fault in New Mexico is an example (fig. 3). Machette (1986, in press) divided the fault into six segments. However, he did this in and before 1982, before "segment" acquired its present connotation of repeated rupture behavior. Machette used "segment" as a synonym for "rupture zone" (M.N. Machette, oral commun., 1988). In the following discussion I distinguish the two terms.

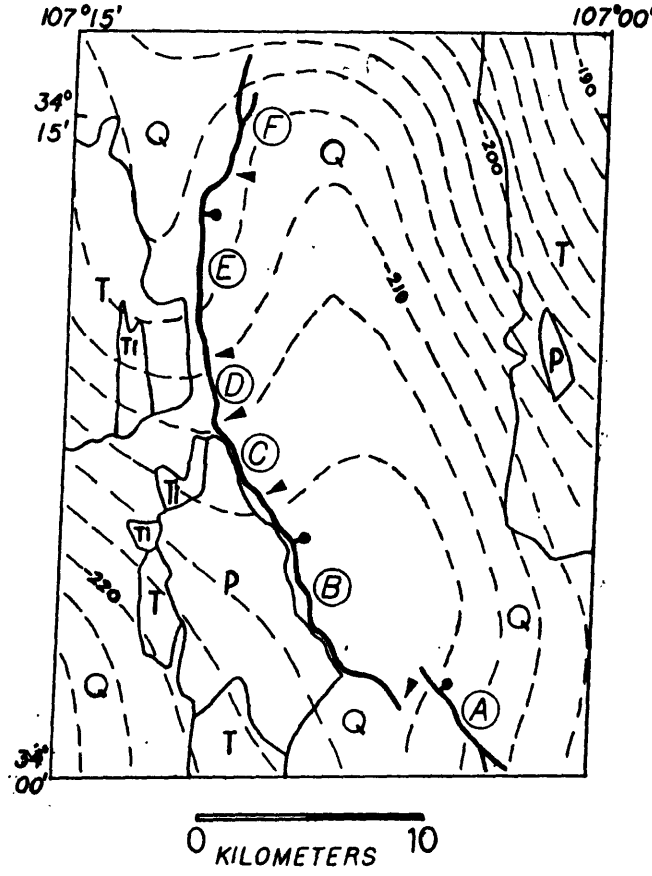

FIGURE 3.--La Jencia fault, New Mexico. Heavy line shows fault trace; bar and ball on downthrown side. Circled letters identify "segments" (rupture zones) of Machette (1986, in press), with boundaries at solid darts. Thin solid lines represent contacts between Paleozoic and Precambrian rocks (P), Tertiary sedimentary and extrusive igneous rocks (T), Oligocene intrusive igneous rocks (Ti), and Cenozoic (mostly Quaternary) basin-filling sediments (Q). Thin dashed lines show isogals, with 2 milligal contour interval. Simplified and compiled from Dane and Bachman (1965), Machette (1978, 1986), and Keller (1983).

Near the middle of the La Jencia fault the ends of late Quaternary scarps satisfy the two persistency conditions listed earlier and define both boundaries of Machette's (1986) rupture zone D. Rupture zone D could be a segment in the sense of this report. However, rupture zone D is unusually short--4 km compared to 11-57 km for the 32 segments of the Wasatch, Lost River, Beaverhead, Lemhi, and Red Rock faults. D last ruptured 33 ± 6 ka. D is bounded by longer rupture zones that broke more recently but not at 33 ka (Machette, 1986, table 1). The short length and location between two longer, separate rupture zones make D resemble the short 1903 rupture zone in the Pirouette Mountain boundary between the longer 1954 Dixie Valley and Fairview Peak rupture zones (fig. 2B). Perhaps rupture zone D is a segment boundary, not a segment.

Other evidence supports this suggestion. Geologic (Dane and Bachman, 1965; Chapin, 1971, and oral commun., 1988; Machette, 1978), Bouguer gravity (Keller, 1983), and aeromagnetic (Cordell, 1983) maps show that structural relief is much greater on the La Jencia fault southeast of rupture zone D than northwest of it. The footwall exposes Precambrian and Paleozoic rocks southeast of D, compared with Tertiary rocks northwest of D. The entire hanging wall of the La Jencia fault is a basin filled with young sediments, and southeast of rupture zone D the hanging wall coincides with gravity and aeromagnetic lows. These lows indicate that the hanging wall basin is deeper along the southeastern part of the fault than along the northwestern part. Thus, southeast of rupture zone D the footwall block is structurally higher and the hanging wall block is structurally lower than northwest of D.

However, the cited maps show no evidence of a transverse bedrock ridge at rupture zone D (fig. 3). The available information cannot discriminate clearly between three overlapping hypotheses about segmentation of the La Jencia fault. (1) Perhaps the fault has six segments as shown in figure 3, but most of the boundaries between the segments are nonpersistent. If so, these segments would be much shorter than segments of other normal faults in the Basin-Range. This discrepancy makes this first hypothesis less likely than the next two. (2) Perhaps rupture zone D is a persistent boundary similar to those described earlier on other faults, but the present geologic mapping and gravity data lack sufficient detail to detect a transverse bedrock ridge. If so, the La Jencia fault has two segments, one comprising rupture zones A-C and the other comprising E and F (fig. 3). The distinct ages of the scarps of rupture zones A-F mean that the two segments would have broken piecemeal instead of as units (Machette, 1986, table 1). This second hypothesis is less likely than the third one, because probably the contour interval and station density of the gravity data (Keller, 1983) would have revealed a buried bedrock ridge at D if one were present there. (3) Perhaps the fault southeast of rupture zone D ruptures more often, or with greater slip per rupture, or both, compared with the fault northwest of D. In the latter case rupture zone D would be a persistent boundary of a kind not previously recognized, and again D would divide the fault into two segments that have ruptured piecemeal.

In any case, the unusually short rupture-zone lengths of 4-8 km (Machette, 1986) suggest that the La Jencia fault might rupture differently than the other normal faults mentioned previously, which have much longer

surface ruptures. Menges (1987) suggested some similarly short rupture zones on the western range-front fault of the Sangre de Christo Mountains of northern New Mexico.

IMPLICATION FOR HAZARD ASSESSMENT

Modeling calculations show that whether a normal fault is segmented or not need not have a large direct effect on probabilistic-hazard maps (Youngs and others, 1987; P.C. Thenhaus, oral and written communs., 1987). However, a persistent segment boundary can affect the geographic extent of strong ground motion. Strong motion is most likely to occur near the energy-radiating parts of the rupture zone, with local variations caused by lobate radiation patterns, directivity, asperities, and site effects. If a persistent segment boundary limits the area of energy-radiating rupture then it will also limit the area that is most likely to undergo strong shaking. If geologic and seismologic data identify a segment as likely to be the next to break, and if this segment is delimited by persistent boundaries, then segmentation of the fault will have an indirect impact on probabilistic-hazard maps of the area.

CONCLUSIONS

A persistent segment boundary on a normal fault produces a cumulative slip deficit, and the geological and geophysical expressions of the deficit identify the boundary. A persistent boundary that controlled the rupture of the last large earthquake near the boundary is likely to control the next such rupture. Such control can limit the area of expected strong ground motion.

ACKNOWLEDGEMENTS

I thank M.N. Machette for discussions and suggestions. Suggestions by A.J. Crone, D.C. Schnabel, and D.P. Schwartz improved the manuscript greatly.

REFERENCES CITED

Barrientos, S.E., Stein, R.S., and Ward, S.N., 1987, Comparison of the 1959 Hebgen Lake, Montana and the 1983 Borah Peak, Idaho, earthquakes from geodetic observations: Bulletin of the Seismological Society of America, v. 77, p. 784-808.

Chapin, C.E., 1971, The Rio Grande rift, Part I--Modifications and additions, in James, J.L., ed., Guidebook of the San Luis Basin, Colorado: New Mexico Geological Society 22nd Field Conference Guidebook, p. 191-201.

Cordell, Lindrith, 1983, Composite residual total intensity aeromagnetic map of the Socorro region, New Mexico, in Chapin, C.E., and Callender, J.F., eds., Socorro region II: New Mexico Geological Society 34th Field Conference Guidebook, p. 97.

Crone, A.J., and Machette, M.N., 1984, Surface faulting accompanying the Borah Peak earthquake, central Idaho: Geology, v. 12, p. 664-667.

Crone, A.J., Machette, M.N., Bonilla, M.G., Lienkaemper, J.J., Pierce, K.L., Scott, W.E., and Bucknam, R.C., 1987, Surface faulting accompanying the Borah Peak earthquake and segmentation of the Lost River fault, central Idaho: Bulletin of the Seismological Society of America, v. 77, p. 739-770, 3 folded plates.

Dane, C.H., and Bachman, G.O., 1965, Geologic map of New Mexico: U.S. Geological Survey and New Mexico Bureau of Mines and Mineral Resources, 2 sheets, scale 1:500,000.

Doser, D.I., 1986, Earthquake processes in the Rainbow Mountain-Fairview Peak-Dixie Valley, Nevada, region 1954-1959: Journal of Geophysical Research, v. 91, no. B12, p. 12,572-12,586.

Doser, D.I., and Smith, R.B., 1985, Source parameters of the 28 October 1983 Borah Peak, Idaho, earthquake from body wave analysis: Bulletin of the Seismological Society of America, v. 75, p. 1041-1051.

Fonseca, Julia, 1988, The Sou Hills--A barrier to faulting in the central Nevada seismic belt: Journal of Geophysical Research, v. 93, no. B1, p. 475-489.

Hanks, T.C., and Schwartz, D.P., 1987, Morphologic dating of the pre-1983 fault scarp on the Lost River fault at Doublespring Pass Road, Custer County, Idaho: Bulletin of the Seismological Society of America, v. 77, p. 837-846.

Keller, G.R., 1983, Bouguer gravity anomaly map of the Socorro region, in Chapin, C.E., and Callender, J.F., eds., Socorro region II: New Mexico Geological Society 34th Field Conference Guidebook, p. 96.

Mabey, D.R., 1987, Subsurface geology along the Wasatch Front, in Gori, P.L., and Hays, W.W., eds., Assessment of regional earthquake hazards and risk along the Wasatch Front, Utah: U.S. Geological Survey Open-File Report 87-585, volume I, p. C1-C39.

Machette, M.N., 1978, Preliminary geologic map of the Socorro 1° x 2° quadrangle, central New Mexico: U.S. Geological Survey Open-File Report 78-607, scale 1:250,000.

_____1986, History of Quaternary offset and paleoseismicity along the La Jencia fault, central Rio Grande rift, New Mexico: Bulletin of the Seismological Society of America, v. 76, p. 259-272.

_____in press, Quaternary movement along the La Jencia fault, central New Mexico: U.S. Geological Survey Professional Paper.

Machette, M.N., Personius, S.F., and Nelson, A.R., 1987, Quaternary geology along the Wasatch fault zone--Segmentation, recent investigations, and preliminary conclusions, in Gori, P.L., and Hays, W.W., eds., Assessment of regional earthquake hazards and risk along the Wasatch Front, Utah: U.S. Geological Survey Open-File Report 87-585, v. I, p. A1-A72.

Menges, C.M., 1987, Temporal and spatial segmentation of Pliocene-Quaternary fault-rupture along the western Sangre de Christo mountain front, northern New Mexico, in Crone, A.J., and Omdahl, E.M., eds., Proceedings of Conference XXXIX--Directions in Paleoseismology: U.S. Geological Survey Open-File Report 87-673, p. 203-222.

Myers, W.B., and Hamilton, Warren, 1964, Deformation accompanying the Hebgen Lake earthquake of August 17, 1959--The Hebgen Lake, Montana, earthquake of August 17, 1959: U.S. Geological Survey Professional Paper 435-I, p. 55-98, 2 folded plates.

Perkins, D.M., 1987, Contagious fault rupture, probabilistic hazard, and contagion observability, in Crone, A.J., and Omdahl, E.M., eds., Proceedings of Conference XXXIX--Directions in paleoseismology: U.S. Geological Survey Open-File Report 87-673, p. 428-439.

Pierce, K.L., and Colman, S.M., 1986, Effect of height and orientation (microclimate) on geomorphic degradation rates and processes, late-glacial terrace scarps in central Idaho: Geological Society of America Bulletin, v. 97, p. 869-885.

Richins, W.D., Pechmann, J.C., Smith, R.B., Langer, C.J., Goter, S.K., Zollweg, J.E., and King, J.J., 1987, The 1983 Borah Peak, Idaho, earthquake and its aftershocks: Bulletin of the Seismological Society of America, v. 77, p. 694-723.

Schwartz, D.P., and Coppersmith, K.J., 1984, Fault behavior and characteristic earthquakes--Examples from the Wasatch and San Andreas fault zones: Journal of Geophysical Research, v. 89, no. B7, p. 5681-5698.

Schwartz, D.P., and Crone, A.J., 1988, Paleoseismicity of the Lost River fault zone, Idaho--Earthquake recurrence and segmentation: Geological Society of America Abstracts with Programs, v. 20, no. 3, p. 228.

Slemmons, D.B., 1957, Geological effects of the Dixie Valley-Fairview Peak, Nevada, earthquakes of December 16, 1954: Bulletin of the Seismological Society of America, v. 47, p. 353-375, 1 folded plate.

Slemmons, D.B., Steinbrugge, K.V., Tocher, Don, Oakeshott, G.B., and Gianella, V.P., 1959, Wonder, Nevada, earthquake of 1903: Bulletin of the Seismological Society of America, v. 49, p. 251-265, 2 folded plates.

Wallace, R.E., 1980, Nomograms for estimating components of fault displacement from measured height of fault scarp: Association of Engineering Geologists Bulletin, v. 17, p. 39-45.

_____1984, Fault scarps formed during the earthquakes of October 2, 1915, in Pleasant Valley, Nevada, and some tectonic implications: U.S. Geological Survey Professional Paper 1274-A, p. A1-A33, 1 folded plate.

Wheeler, R.L., 1987, Boundaries between segments of normal faults--Criteria for recognition and interpretation, in Crone, A.J., and Omdahl, E.M., eds., Proceedings of Conference XXXIX--Directions in paleoseismology: U.S. Geological Survey Open-File Report 87-673, p. 385-398.

Wheeler, R.L., and Krystinik, K.B, 1987, Persistent and nonpersistent segmentation of the Wasatch fault zone, Utah--Statistical analysis for evaluation of seismic hazard, in Gori, P.L., and Hays, W.W., eds., Assessment of regional earthquake hazards and risk along the Wasatch Front, Utah: U.S. Geological Survey Open-File Report 87-585, v. I, p. B1-B124.

_____1988, Segmentation of the Wasatch fault zone, Utah--Summaries, analyses, and interpretations of geological and geophysical data: U.S. Geological Survey Bulletin 1827, 47 p.

Witkind, I.J., 1964, Reactivated faults north of Hebgen Lake--The Hebgen Lake, Montana, earthquake of August 17, 1959: U.S. Geological Survey Professional Paper 435-G, p. 37-50, 1 folded plate.

Youngs, R.R., Swan, F.H., Power, M.S., Schwartz, D.P., and Green, R.K., 1987, Probabilistic analysis of earthquake ground shaking hazard along the Wasatch Front, Utah, in Gori, P.L., and Hays, W.W., eds., Assessment of regional earthquake hazards and risk along the Wasatch Front, Utah: U.S. Geological Survey Open-File Report 87-585, v. II, p. M1-M110.

Zoback, M.L., 1983, Structure and Cenozoic tectonism along the Wasatch fault zone, Utah, in Miller, D.M., Todd, V.R., and Howard, K.A., eds., Tectonics and stratigraphy of the eastern Great Basin: Geological Society of America Memoir 157, p. 3-27.

CONFERENCES TO DATE

Conference I	Abnormal Animal Behavior Prior to Earthquakes, I Not Open-Filed
Conference II	Experimental Studies of Rock Friction with Application to Earthquake Prediction Not Open-Filed
Conference III	Fault Mechanics and Its Relation to Earthquake Predition Open-File No. 78-380
Conference IV	Use of Volunteers in the Earthquake Hazards Reduction Program Open-File No. 78-336
Conference V	Communicating Earthquake Hazard Reduction Information Open-File No. 78-933
Conference VI	Methodology for Identifying Seismic Gaps and Soon-to-Break Gaps Open-File No. 78-943
Conference VII	Stress amd Strain Measurements Related to Earthquake Prediction Open-File No. 79-370
Conference VIII	Analysis of Actual Fault Zones in Bedrock Open-File No. 79-1239
Conference IX	Magnitude of Deviatoric Stresses in the Earth's Crust and Upper Mantle Open-File No. 80-625
Conference X	Earthquake Hazards Along the Wasatch and Sierra-Nevada Frontal Fault Zones Open-File No. 80-801
Conference XI	Abnormal Animal Behavior Prior to Earthquakes, II Open-File No. 80-453
Conference XII	Earthquake Prediction Information Open-File No. 80-843
Conference XIII	Evaluation of Regional Seismic Hazards and Risk Open-File No. 81-437
Conference XIV	Earthquake Hazards of the Puget Sound Region, Washington Open-File No. 82-19
Conference XV	A Workshop on "Preparing for and Responding to a Damaging Earthquake in the Eastern United States" Open-File No. 82-220
Conference XVI	The Dynamic Characteristics of Faulting Inferred from Recording of Strong Ground Motion Open-File No. 82-591
Conference XVII	Hydraulic Fracturing Stress Measurements Open-File No. 82-1075
Conference XVIII	A Workshop on "Continuing Actions to Reduce Losses from Earthquakes in the Mississippi Valley Area" Open-File No. 83-157
Conference XIX	Active Tectonic and Magmatic Processes Beneath Long Valley Open-File No. 84-939

Conference XX	A Workshop on "The 1886 Charleston, South Carolina, Earthquake and its Implications for Today" Open-File No. 83-843
Conference XXI	A Workshop on "Continuing Actions to Reduce Potential Losses from Future Earthquakes in the Northeastern United States" Open-File No. 83-844
Conference XXII	A Workshop on "Site-Specific Effects of Soil and Rock on Ground Motion and the Implications for Earthquake-Resistant Design" Open-File No. 83-845
Conference XXIII	A Workshop on "Continuing Actions to Reduce Potential Losses from Future Earthquakes in Arkansas and Nearby States" Open-File No. 83-846
Conference XXIV	A Workshop on "Geologic Hazards in Puerto Rico" Open-File No. 84-761
Conference XXV	A Workshop on "Earthquake Hazards in the Virgin Islands Region" Open-File No. 84-762
Conference XXVI	A Workshop on "Evaluation of the Regional and Urban Earthquake Hazards in Utah" Open-File No. 84-763
Conference XXVII	Mechanics of the May 2, 1983 Coalinga Earthquake Open-File No. 85-44
Conference XXVIII	A Workshop on "The Borah Peak, Idaho, Earthquake" Open-File No. 85-290
Conference XXIX	A Workshop on "Continuing Actions to Reduce Potential Losses from Future Earthquakes in New York and Nearby States" Open-File No. 85-386
Conference XXX	A Workshop on "Reducing Potential Losses from Earthquake Hazards in Puerto Rico" Open-File No. 85-731
Conference XXXI	A Workshop on "Evaluation of Regional and Urban Earthquake Hazards and Risk in Alaska" Open-File No. 86-79
Conference XXXII	A Workshop on "Future Directions in Evaluating Earthquake Hazards of Southern California" Open-File No. 86-401
Conference XXXIII	A Workshop on "Earthquake Hazards in the Puget Sound, Washington Area" Open-File No. 86-253
Conference XXXIV	A Workshop on "Probabilistic Earthquake-Hazards Assessments" Open-File No. 86-185
Conference XXXV	A Workshop on "Earth Science Considerations for Earthquake Hazards Reduction in the Central United States" Open-File No. 86-425

Conference XXXVI	A Workshop on "Assessment of Geologic Hazards and Risk in Puerto Rico" Open-File No. 87-007
Conference XXXVII	A Workshop on "Earthquake Hazards Along the Wasatch, Utah" Open-File No. 87-154
Conference XXXVIII	A Workshop on "Physical & Observational Basis for Intermediate Term Earthquake Prediction" Open-File 87-154
Conference XXXIX	Directions in Paeloseismology Open-File No. 87-673
Conference XL	A Workshop on "The U.S. Geological Survey's Role in Hazares Warnings" Open File No. 87-269
Conference XLI	A Review of the Earthquake Research Applications in the National Earthquake Hazard Reduction Program: 1977-1987 Open-File No. 88-13-A
Conference XLII	A Workshop on "Evaluation of Earthquake Hazards and Risk in the Puget Sound and Portland Areas" Open File No. 88-541
Conference XLIII	A Workshop on "Earthquake Risk: Information Needs of the Insurance Industry" Open-File No. 88-669
Conference XLIV	A Workshop on "Geological, Geoophysical, and Tectonic Settings of the Cascade Range" Open-File No. 89-178
Conference XLV	A Workshop on "Fault Segmentation and Controls of Rupture Initiation and Termination" Open-File No. 89-315

For information on ordering the above publications, please contact:

U.S. Geological Survey
Books and Open-File Reports Service Section
Building 41, Box 25425
Federal Center
Denver, Colorado 80225

☆U.S. GOVERNMENT PRINTING OFFICE: 1989-688-214 19219